

# **Click hydrogel as a regenerative approach to vocal fold reconstruction**

Mika Brown

Department of Biological and Biomedical Engineering

McGill University, Montréal, Canada

August 2024

A thesis submitted to McGill University in partial fulfillment  
of the requirements for the degree of Doctor of Philosophy

©Mika Brown 2024

## Abstract

Severe vocal fold (VF) disorders lead to difficulty in speaking, swallowing or aspiration pneumonia. Injectable biomaterials are available in clinics but require periodic reinjections as they are absorbed by surrounding tissue and do not have the capacity to stimulate functional tissue regeneration. Designing an injectable VF biomaterial that repairs defects in one treatment could reduce the burden of multiple treatments.

To achieve an effective VF biomaterial, key considerations include mimicking mechanical properties to support function while stimulating VF-specific regeneration and degradation at a rate that matches functional tissue repair. Decellularized extracellular matrix (dECM) is a material derived from tissue by the removal of cells, leaving behind the network of proteins, proteoglycans, and glycosaminoglycans that provide the tissue structure. Hydrogels made from dECM retain innate bioactive molecules that are expected to facilitate the growth of new matrix and blood vessels. Tissue-specific dECM sources have been proposed for regenerative targets but VF dECM lacks scalability due to the small organ size. dECM biomaterials synthesized from soft tissue also degrade rapidly and fail to replicate the mechanical properties of native tissue.

In this thesis, we proposed a novel composite dECM-alginate hydrogel fabricated using click chemistry that retained the innate regenerative properties of dECM while achieving VF-like viscoelasticity with controllable degradation profiles. dECM tissue source was considered through the comparison of VF-specific dECM and clinically available small intestinal submucosa (SIS) dECM in terms of both tissue specificity and scale-up feasibility for the first time.

First, we compared VF dECM to SIS dECM through a lens of proteomics and neo-ECM deposition. We discerned that SIS dECM possesses a reasonably similar proteomic profile and regenerative capacity to VF dECM with reduced inter-sample variability, supporting the use of SIS dECM as a promising alternative dECM source in VF regeneration.

We then developed the click dECM-alginate hydrogel using tetrazine ligation. The bioorthogonal nature of click tetrazine ligation allows in situ gelation with minimal cell toxicity as the reaction proceeds with high selectivity, without side reactions with molecules found in

cell and tissue, or formation of toxic side products. The click dECM-alginate hydrogels were comprehensively evaluated with respect to the mechanical properties, degradation profile, cytotoxicity, and vasculogenesis. We found that click dECM hydrogels from both VF dECM and SIS dECM better mimic the properties of native VF, exhibit slowed degradation, and better maintain their microstructure in comparison to standard dECM hydrogels. We showed that click dECM-alginate hydrogels resist contraction by human vocal fold fibroblasts and provide a favorable environment for vasculogenesis without growth factor supplementation.

We further assessed the biocompatibility of click dECM-alginate hydrogels in a subcutaneous rat model. An initial strong immune response induced the formation of fibrous capsules around the click dECM hydrogels on day 7. However, by day 21 the fibrous capsule was no longer in evidence and collagenous ECM was observed. The local immune response in terms of macrophage and B cell behaviors were shown to be comparable for both VF dECM and SIS dECM derived hydrogels.

Overall, click tetrazine ligation of dECM with the slower degrading polymer alginate can improve the mechanical stability and tunability of dECM hydrogels while retaining biocompatibility and stimulating capillary formation. Click dECM-alginate hydrogels may support permanent tissue restoration that would reduce the burden of repeated treatments on the medical system.

## Résumé

Des conditions graves des cordes vocales (CV) entraînent des difficultés à parler, à avaler ou une pneumonie par aspiration. Les biomatériaux injectables sont disponibles en clinique mais nécessitent des rejets périodiques parce qu'ils sont absorbés par les tissus environnants et n'ont pas la capacité de stimuler la régénération fonctionnelle des tissus. Concevoir un biomatériau CV injectable qui répare les défauts en un seul traitement pourrait réduire le fardeau de plusieurs traitements.

Pour obtenir un biomatériau CV efficace, les principales considérations incluent l'imitation des propriétés mécaniques pour soutenir la fonction tout en stimulant la régénération et la dégradation spécifiques au VF à un rythme correspondant à la réparation fonctionnelle des tissus. La matrice extracellulaire décellulaire (MECD) est un matériau dérivé du tissu par l'élimination de cellules, laissant derrière lui le réseau de protéines, de protéoglycanes et de glycosaminoglycanes qui fournissent la structure du tissu. Les hydrogels fabriqués à partir de MECD conservent des molécules bioactives innées qui devraient faciliter la croissance de nouvelles matrices et de nouveaux vaisseaux sanguins. Des sources de MECD spécifiques aux tissus ont été proposées pour les cibles régénératives, mais le MECD CV manque d'évolutivité en raison de la petite taille de l'organe. Les biomatériaux MECD synthétisés à partir de tissus mous se dégradent également rapidement et ne parviennent pas à reproduire les propriétés mécaniques des tissus natifs.

Dans cette thèse, nous avons proposé un nouvel hydrogel composite MECD-alginate fabriqué à l'aide de la chimie click qui conservait les propriétés régénératrices innées du dECM tout en obtenant une viscoélasticité de type CV avec des profils de dégradation contrôlables. La source tissulaire MECD a été prise en compte pour la première fois en comparant pour la première fois le MECD spécifique à la CV et le MECD de la sous-muqueuse de l'intestin grêle (SIS) cliniquement disponible en termes de spécificité tissulaire et de faisabilité de mise à l'échelle.

Tout d'abord, nous avons comparé le MECD CV au MECD SIS à travers le prisme de la protéomique et du dépôt néo-MEC. Nous avons discerné que MECD SIS possède un profil protéomique et une capacité de régénération raisonnablement similaires à ceux de MECD CV avec une variabilité inter-échantillons réduite, ce qui soutient l'utilisation de MECD SIS comme source alternative prometteuse de MECD dans la régénération de CV.



Nous avons ensuite développé l'hydrogel MECD-alginate en utilisant la ligature de la tétrazine. La nature bioorthogonale de la ligature tétrazine click permet une gélification in situ avec une toxicité cellulaire minimale car la réaction se déroule avec une sélectivité élevée, sans réactions secondaires avec les molécules présentes dans les cellules et les tissus, ni formation de produits secondaires toxiques. Les hydrogels MECD-alginate ont été évalués de manière approfondie en ce qui concerne les propriétés mécaniques, le profil de dégradation, la cytotoxicité et la vasculogénèse. Nous avons constaté que les hydrogels MECD click de MECD CV et MECD CV imitent mieux les propriétés du CV natif, présentent une dégradation ralentie et maintiennent mieux leur microstructure par rapport aux hydrogels MECD standard. Nous avons montré que les hydrogels MECD-alginate résistent à la contraction des fibroblastes des cordes vocales humaines et fournissent un environnement favorable à la vasculogénèse sans supplémentation en facteurs de croissance.

Nous avons en outre évalué la biocompatibilité des hydrogels MECD-alginate dans un modèle sous-cutané de rat. Une forte réponse immunitaire initiale a induit la formation de capsules fibreuses autour des hydrogels MECD click au jour 7. Cependant, au jour 21, la capsule fibreuse n'était plus visible et une MEC collagène a été observée. Il a été démontré que la réponse immunitaire locale en termes de comportement des macrophages et des cellules B est comparable pour les hydrogels dérivés de MECD CV et de MECD SIS.

Dans l'ensemble, la ligature click tétrazine du MECD avec l'alginate polymère à dégradation plus lente peut améliorer la stabilité mécanique et l'accordabilité des hydrogels MECD tout en conservant la biocompatibilité et en stimulant la formation capillaire. Les hydrogels MECD-alginate peuvent prendre en charge la restauration permanente des tissus, ce qui réduirait le fardeau des traitements répétés sur le système médical.

## Acknowledgements

The completion of this thesis has been the greatest challenge of my life and would not have been possible without the support and guidance of my supervisors, Nicole Li-Jessen and Maryam Tabrizian through the ups and downs. It's been a long journey, and I've appreciated the chances to develop my technical and analytical skills along the way. Thank you for saying yes all the times I took vacation right after an international conference – on my own behalf, and that of my wallet.

Thanks to all the members of both the VUA and Biomat'X labs for advice and companionship and putting up with my whining over the years, especially Patrick, Mike, and Alex. Ling Li was an invaluable help in training me for cell culture and providing invaluable advice whenever I knocked on her office door, even when she was swamped with work.

Guangyu Bao trained me on the rheometer and AFM, and responded patiently to several panicked emails, and Zhen Yang handled the delicate Instron Machine. Lorne Taylor was a great help in running mass spectroscopy and for his guidance in data analysis, along with Shirley Zhu, who handled complex programming for data analysis as an undergrad. Hideaki Okuyama helped greatly by handling the rats for my animal work even though I was too squeamish to be there for the sacrifice, and for training me on how to handle the samples.

Over at the ABIF, I would like to thank Joel for his patient and priceless assistance in teaching me the ins and outs of ImageJ, Phil for all the times he fixed a buggy microscope, and both for training me on the microscopes I practically lived at last year. Thanks to Kelly, Jeanne, David, and Weawkamol, at the Facility for Electron Microscopy for training me on the equipment. At the Magnetic Resonance Facility, Tara Sprules and Robin Stein helped greatly with my NMR samples and data interpretation, and I greatly appreciate how Alexandre Arnold at UQAM stepped in to help with sample analysis when the solid state NMR at McGill was down. Thanks also to Jianyu Li, Tom Durcan, and David Rudko for their feedback and guidance on my committee over the years, and to Pina Sorrini, for listening.

I would also like to thank my parents for their support and understanding throughout my grad school experience, and all the times they braved Quebec winters to visit me. Grandma Pat, for making sure in her will that her grandkids would be able to afford an education. My best friends, Giulia and Christine, for all the long hours keeping me company during lockdown and after. I

love you, and I can't wait to see the adventures the future has in store for us. My cats, Artemis and Athena, have been the most necessary and adorable emotional support. Thanks for all the cuddles, and even the troubles. Finally, Alice, for helping me see the world differently and be ready for what comes next.

## Thesis Organization

This thesis is written and presented in a manuscript-based style divided into seven chapters, as follows.

**Chapter 1. Introduction:** A brief introduction to the thesis presenting the research motivations, rationale, and objectives of the study at a high level.

**Chapter 2. Trends in Injectable Biomaterials for Vocal Fold Regeneration and Long-Term Augmentation:** A review of literature in the field of injectables for vocal fold tissue engineering, describing the state of the art and emerging techniques for improved biomaterial design.

**Chapter 3. Decellularized extracellular matrix: New promising and challenging biomaterials for regenerative medicine:** A comprehensive review of literature in the field of decellularized extracellular matrix biomaterials focusing primarily on hydrogels, electrospun scaffolds, and bioprinted scaffolds. Tissue-specific material design approaches suitable for application to different organs and tissues are systematically addressed. Advantages and limitations of existing decellularized extracellular matrix biomaterials are discussed, and future directions are proposed.

**Chapter 4. Unraveling the Relevance of Tissue-Specific Decellularized Extracellular Matrix Hydrogels for Vocal Fold Regenerative Biomaterials: A Comprehensive Proteomic and In Vitro Study:** An evaluation of the importance of tissue-specificity as opposed to scale-up viability in the use of decellularized extracellular matrix for vocal fold applications through the lens of proteomic analysis and *in vitro* functional assays.

**Chapter 5. The Puzzle of Complete Regeneration: Click Decellularized Extracellular Matrix Hydrogels for Vocal Fold Tissue Regeneration:** Development of a composite, injectable decellularized extracellular matrix and alginate hydrogel using click chemistry capable of mimicking tissue mechanical properties, improved stability, and tissue integration.

**Chapter 6. Discussion:** Discussion of key findings, limitations, and future directions for the biomaterials developed and characterized in this thesis.

**Chapter 7. Conclusion:** Final conclusions and remarks.

## Contributions to Original Knowledge

The body of work presented in this thesis includes two main original contributions in the field of tissue engineering.

1. *We postulated that the use of dECM from an alternative soft tissue source could solve challenges with scale up and batch-to-batch inconsistencies characteristic of tissue-specific vocal fold dECM.* In contrast to prior literature on tissue-specificity, this material comparison takes into account both functionality and practical considerations for biomaterial fabrication. This work presents a strategy for selecting optimal dECM for applications beyond the vocal folds.

This work was published in *Advanced NanoBiomed Research* in 2023:

Mika Brown, Shirley Zhu, Lorne Taylor, Maryam Tabrizian\*, and Nicole YK Li-Jessen\*. "Unraveling the Relevance of Tissue-Specific Decellularized Extracellular Matrix Hydrogels for Vocal Fold Regenerative Biomaterials: A Comprehensive Proteomic and In Vitro Study." *Advanced NanoBiomed Research* 3, no. 4 (2023): 2200095. \*Co-Senior Authors

2. *We developed a new composite dECM hydrogel that utilizes click chemistry to increase dECM hydrogel stability and mimic the mechanical properties of native tissue while maintaining ECM-like structure and biocompatibility.* This hydrogel first gels through fibrillogenesis, resulting in the ECM-like microstructure characteristic of dECM hydrogels, and is subsequently reinforced by click crosslinking with alginate within the existing hydrogel structure. This composite material fabrication technique opens new avenues for biomimicking injectable biomaterial fabrication with biocompatible *in situ* crosslinking and shows great promise for translation to regenerative applications.

This work is in preparation for submission to *Biomaterials*:

Mika Brown, Hideaki Okuyama, Ling Li, Jianyu Li, Zhen Yang, Maryam Tabrizian\*, Nicole YK Li-Jessen\*. "The Puzzle of Complete Regeneration: Click Decellularized Extracellular Matrix Hydrogels for Vocal Fold Tissue Regeneration." *Biomaterials*. (In Preparation) (2024).

\*Co-Senior Authors

## Contributions of Authors

The completion of this thesis would not have been possible without the collaboration and support of colleagues and collaborators with a wide range of expertise. This section describes the scientific contributions of authors for each chapter contained in this thesis. All research work was conceived and designed in collaboration with my PhD advisors and mentors, Prof. Nicole Li-Jessen and Prof. Maryam Tabrizian. Their input was essential to the ideas and research design for the project presented in this thesis. For all manuscripts, Profs. Li-Jessen and Tabrizian provided feedback on research techniques, data interpretation, and manuscript editing.

**In Chapter 2, work including initial conceptualization, literature investigation, and manuscript writing was done by myself.** Hideaki Okuyama and Masaru Yamashita provided valuable feedback from a clinical standpoint, particularly regarding future directions for vocal fold injectables.

This work has been accepted for publication in *Tissue Engineering Part B: Reviews* in 2024: Mika Brown, Hideaki Okuyama, Masaru Yamashita, Maryam Tabrizian, Nicole YK Li-Jessen. "Trends in Injectable Biomaterials for Vocal Fold Regeneration and Long-Term Augmentation." *Tissue Engineering Part B: Reviews*. (2024).

**In Chapter 3, work including initial conceptualization, literature investigation, and manuscript writing was done by myself.** Jianyu Li and Christopher Moraes provided valuable feedback on the presentation and interpretation of the literature reviewed in this article.

This work was published in *Biomaterials* in 2022.

Mika Brown, Jianyu Li, Christopher Moraes, Maryam Tabrizian, and Nicole YK Li-Jessen. "Decellularized extracellular matrix: New promising and challenging biomaterials for regenerative medicine." *Biomaterials* 289 (2022): 121786.

**In Chapter 4, most of the work involving conceptualization, practical research and analysis, data interpretation, and manuscript writing was done by myself.** Lorne Taylor performed mass spectroscopy on tissue and dECM samples and provided invaluable guidance on proteomic data analysis and interpretation. Shirley Zhu performed software analysis of proteomic data gathered using mass spectroscopy and generated associated figures.

This work was published in *Advanced NanoBiomed Research* in 2023.

Mika Brown, Shirley Zhu, Lorne Taylor, Maryam Tabrizian, and Nicole YK Li-Jessen. "Unraveling the Relevance of Tissue-Specific Decellularized Extracellular Matrix Hydrogels for Vocal Fold Regenerative Biomaterials: A Comprehensive Proteomic and In Vitro Study." *Advanced NanoBiomed Research* 3, no. 4 (2023): 2200095.

**In Chapter 5, most of the work involving material design and characterization, data analysis and interpretation, and manuscript writing was done by myself.** Nuclear magnetic resonance testing was performed by Tara Sprules and Robin Stein at the McGill Magnetic Resonance Facility and Alexandre Arnold at UQAM. Zhen Yang aided in experimental design and operated equipment for the compression testing experiment. Jianyu Li provided feedback on mechanical data interpretation within the manuscript. Ling Li provided training, support and feedback for cell culture experiments, and also advised on protocol medication techniques for cryosection staining protocol modification. Hideaki Okuyama helped design and carry out *in vivo* studies, notably performing all direct handling of live animals and preservation of tissue explants. He also provided training and helped me optimize protocols for immunofluorescence staining of cryosections.

This work is in preparation for submission to *Biomaterials*:

Mika Brown, Hideaki Okuyama, Ling Li, Jianyu Li, Zhen Yang, Maryam Tabrizian, Nicole YK Li-Jessen. "The Puzzle of Complete Tissue Regeneration: Click Decellularized Extracellular Matrix Hydrogels for Vocal Fold Tissue Engineering." *Biomaterials*. (In Preparation) (2024).

## Table of Contents

Abstract .....	1
Résumé.....	3
Acknowledgements.....	5
Thesis Organization .....	7
Contributions to Original Knowledge.....	8
Contributions of Authors.....	9
Table of Contents .....	11
Abbreviations.....	16
Chapter 1. Introduction .....	19
1.1 Thesis Motivation. ....	19
1.2. Thesis Rationale.....	19
1.3. Thesis Objectives .....	20
Preface to Chapter 2.....	22
Chapter 2. Trends in Injectable Biomaterials for Vocal Fold Regeneration and Long-Term Augmentation.....	23
2.1. Introduction.....	23
2.2. Overview of Existing VF Biomaterials Used in Clinics .....	26
2.3. Choosing Polymers for Vocal Fold Injectables.....	29
2.3.1. Natural Materials .....	29
2.3.2. Synthetic Materials .....	31
2.4. Enhancing Bioactivity of Injectable VF Biomaterials .....	33
2.4.1. Conjugation with Bioactive Motifs.....	33
2.4.2. Encapsulation of Growth Factors.....	34
2.4.3. Cell Delivery .....	34



2.5. Modulating the Mechanical, Physical, and Degradation Properties of VF Biomaterials .....	37
2.5.1. Composite VF Biomaterials .....	37
2.5.2. Conventional Crosslinking of VF Biomaterials .....	40
2.5.3. Bioorthogonal Click Chemistry in VF Biomaterials .....	42
2.6. Discussion and Future Prospects .....	46
2.7. References .....	48
Preface to Chapter 3 .....	59
Chapter 3. Decellularized extracellular matrix: New promising and challenging biomaterials for regenerative medicine. ....	60
3.1. Introduction .....	60
3.2. Progress in key tissue types in dECM TE .....	64
3.2.1. Cardiac dECM TE .....	64
3.2.2. Cartilage dECM TE .....	75
3.2.3. Neural tissue engineering .....	81
3.2.4. Adipose dECM TE .....	90
3.2.5. Muscle dECM TE .....	95
3.2.6. Liver dECM TE .....	100
3.2.7. Bone dECM TE .....	106
3.2.8. Skin tissue engineering .....	111
3.2.9. Lung dECM TE .....	118
3.3. Progress in dECM TE of other tissue types .....	122
3.3.1. Gastrointestinal dECM TE .....	122
3.3.2. Corneal dECM TE .....	125
3.3.3. Kidney dECM TE .....	128
3.3.5. Vocal fold dECM TE .....	137

3.4. Future prospects in dECM biomaterials for TE .....	140
3.4.2. Missing links in tissue-specific dECM biomaterial design .....	141
3.5. Conclusions.....	148
3.5. References.....	150
Preface to Chapter 4.....	176
Chapter 4. Unraveling the Relevance of Tissue-Specific Decellularized Extracellular Matrix Hydrogels for Vocal Fold Regenerative Biomaterials: A Comprehensive Proteomic and In Vitro Study .....	177
4.1. Introduction.....	178
4.2. Results.....	180
4.2.1. Efficacy of Decellularization Protocols for Porcine Vocal Folds .....	180
4.2.2. Hydrogel Formation and Characterization.....	181
4.2.3. Protein Identification, Gene Ontology Enrichment, and Analysis.....	183
4.2.4. Quantitative Comparison of Key Vocal Fold ECM Components by Tissue Source .....	197
4.2.5 Viability and Cytotoxicity of Human Vocal Fold Fibroblasts.....	199
4.2.6 Deposition of Neo-ECM by HVFF on dECM Hydrogels .....	200
4.3. Discussion.....	201
4.3.1 Proteomic Insights into Tissue Specificity.....	201
4.3.2. Validation of Proteomic Analyses through ECM Component Quantification .....	205
4.3.3. In vitro Validation of Neo-ECM Production by dECM Hydrogels .....	206
4.3.4. Future Directions .....	207
4.4. Conclusions.....	208
4.5. Experimental Section .....	208
4.6. References.....	219
Preface to Chapter 5.....	227

Chapter 5. The Puzzle of Complete Tissue Regeneration: Click Decellularized Extracellular Matrix Hydrogels for Vocal Fold Tissue Engineering .....	229
5.1. Introduction.....	230
5.2. Results.....	233
5.2.1. Click Chemistry Enables the Synthesis of dECM Hydrogels.....	233
5.2.2. Click dECM Hydrogels Mimic the Mechanical Properties of Native Vocal Folds .....	234
5.2.3. Click Chemistry with Alginate Improves the Stability of dECM Hydrogels .....	237
5.2.4 Click dECM Hydrogels Stimulate Vasculogenesis over dECM-only Hydrogels.	240
5.2.5 Click dECM hydrogels form an initial fibrous capsule followed by integrating into surrounding tissue over time .....	243
5.2.6. Click dECM hydrogels induce an elevated macrophage response with an M2 response predominating in SIS-Alg hydrogels .....	247
5.2.7. Click dECM hydrogels recruit B cells in the initial immune response that decrease in density over time.....	251
5.3. Discussion.....	253
5.3.1. Fibrillogenesis followed by bioorthogonal click tetrazine ligation produces hydrogels with ECM-like structure.....	253
5.3.2 Tissue-mimicking mechanical property correlates with functional regeneration.	254
5.3.3. Resistance to contractility may correspond to improved reliability of injectables .....	256
5.3.4. Click dECM hydrogel stability and cellular infiltration .....	256
5.3.5. Click dECM-Alg hydrogels are biocompatible with SIS-Alg exhibiting M2 Polarization .....	257
5.3.6. Conclusions.....	259
5.4. Methods.....	260
5.4.1. Production of Powder ECM from Small Intestinal Submucosa .....	260

5.4.2. Decellularization of Porcine Vocal Folds.....	260
5.4.3. Functionalization of Decellularized Extracellular Matrices .....	260
5.4.4. Functionalization of Alginate.....	261
5.4.5. Fabrication of Click dECM-Alg Hydrogels.....	262
5.4.6. Turbidimetric Gelation Kinetics and Tetrazine Ligation Reaction Kinetics.....	262
5.4.7. Rheological Analysis .....	262
5.4.8. Atomic Force Microscopy.....	263
5.4.9. Compression Testing.....	263
5.4.10. Hydrogel Stability, and Degradation.....	263
5.4.11. Cell Culture .....	264
5.4.12. Human Vocal Fold Fibroblast Viability and Morphology.....	264
5.4.13. Human Umbilical Vein Endothelial Cell Viability and Network Formation Analyses.....	265
5.4.14 Evaluation of the Local Fibrotic and Immune Response in Subcutaneous Rat Model .....	265
5.4.15 Histology and Immunohistochemistry .....	266
5.4.16 Statistical Analysis .....	266
5.5. Supplementary Information .....	268
5.6. References.....	284
Chapter 6. Discussion .....	293
6.1. Tissue Specificity and Choice of Tissue Source .....	293
6.2. Mechanical Property Mimicry .....	296
6.3. Sufficiency of dECM-based Regeneration .....	298
6.4. Future Prospectives.....	300
6.4.1. Harnessing the Potential of Click Chemistry: Hydrogel Optimization .....	300
6.4.2. Translation to the Clinic for VF Applications.....	302

6.4.3. Personalized Medicine: Stem Cell-derived dECM .....	303
Chapter 7. Conclusions .....	305
References .....	306

## Abbreviations

$\alpha$ -SMA – Alpha smooth muscle actin

Alb - Albumin

Alg – Alginate

AFM – Atomic Force Microscopy

ASC – Adipose Stem Cell

bFGF – Basic fibroblast growth factor

BBV – Bio-Blood Vessel

BSA – Bovine serum albumin

CM – Cardiomyocytes

CNS – Central Nervous System

Col – Collagen

CVD – Cardiovascular Disease

DAT – Decellularized Adipose Tissue

dECM – Decellularized extracellular matrix

DMEM – Dulbecco's modified Eagle medium

ECM – Extracellular matrix

EDC – 1-ethyl-3-(3-dimethylaminopropyl) carbodiimide hydrochloride

EGM-2 – Endothelial Growth Medium 2

EPSC - Excitatory Post Synaptic Current

FGF-2 – Fibroblast growth factor 2

GDPH - Glycerol-3-phosphate dehydrogenase

GelMA – Methacrylated gelatin

HGF – Hepatocyte growth factor

HP – Heparin Polaxamer

Huh7, HepG2 – Human hepatocarcinoma cell

HUVEC – Human umbilical vein endothelial cell

HVFF – Human vocal fold fibroblasts

IEDDACs – Inverse electron demand Diels-Alder cycloadditions

iPSC – Induced pluripotent stem cells

MCS – Methacrylated Chondroitin Sulfate

MSC – Mesenchymal Stem Cell

MTz – Methyltetrazine

Nb – Norbornene

NHS – N-hydroxysuccinimide

NMR – Nuclear magnetic resonance

OCT – Optical coherence tomography

PBS – Phosphate Buffered Saline

PCL – (Poly)  $\epsilon$ -caprolactone

PEG – Polyethylene glycol

PEGDA – Polyethylene glycol diacrylate

PEUU – Polyester urethane urea

PDGF – Platelet-derived growth factor

PFA – Paraformaldehyde

PLGA – Poly(lactic-co-glycolic acid)

PLA – Polylactic acid

PLLA – Poly(L-lactic acid)

PNI – Peripheral Nerve Injury

RGD – Arginylglycylaspartic acid

SC – Schwann Cell

SCI – Spinal Cord Injury

SEM – Scanning Electron Microscopy

SIS – Small intestinal submucosa

SM – Skeletal Muscle

SPAACs – Strain promoted azide-alkyne cycloadditions

TCO – Trans cyclooctene

TE – Tissue Engineering

Tz – Tetrazine

TGF- $\beta$  – Transforming growth factor beta

UBM – Urinary bladder matrix

USC – Urine-derived stem cells

VEGF – Vascular endothelial growth factor

VEGFR – Vascular endothelial growth factor receptor

VF – Vocal fold

VML – Volumetric muscle loss

# Chapter 1. Introduction

## *1.1 Thesis Motivation.*

As many as 1 in 13 adults annually experience a form of vocal fold (VF) disorder or dysfunction in the United States, with 10% seeking treatment.<sup>1</sup> Common risk factors of disordered voice include voice overuse in the workplace, history of smoking, respiratory infection, and surgical resection.<sup>2</sup> In 2012, the direct costs of treatment for laryngeal disorders in the United States, excluding additional patient costs due to leave from work, were estimated at \$5 billion a year.<sup>3</sup>

Injectable biomaterials are a viable treatment option for severe VF conditions that can be performed at relatively low cost in outpatient settings.<sup>4,5</sup> Existing injectables such as hyaluronan or calcium hydroxyapatite-based fillers are injected to the thyroarytenoid muscle or paraglottic space and restore function by bringing impaired VF closer to the midline of the glottal gap. However, these fillers only temporarily improve VF function as they are absorbed by surrounding tissue without stimulating tissue deposition or remodeling.<sup>6</sup> Patients require repeated injections or subsequent surgeries that lead to substantial time and financial costs.

An improved injectable VF biomaterial design is warranted to permanently restore VF function in one treatment. These biomaterials should mimic VF mechanical properties to effectively maintain VF function while stimulating tissue deposition and remodeling and degrade at a rate comparable to tissue repair. Designing biomaterials with the end goal of permanent voice restoration would reduce the burden of repeated treatments on the medical system and increasing quality of life for patients.

## *1.2. Thesis Rationale*

This thesis proposed to develop a novel, VF-mimicking injectable hydrogel utilizing decellularized extracellular matrix (dECM) and click chemistry to induce tissue regeneration for long-term augmentation of disordered VF.

dECM was proposed to promote tissue regeneration due to its innate regenerative functionality and ability to imitate the VF microenvironmental niche. Decellularization is the process of removing cells from host tissue while retaining extracellular matrix (ECM) for use as a regenerative biomaterial. Cell removal from ECM serves to minimize adverse immune



responses to foreign tissue while retaining the microstructure and bioactive proteins, glycosaminoglycans, and small molecules that promote cell-matrix interactions for functional regeneration.<sup>7,8</sup>

Tissue-specific sources of dECM have been repeatedly found to provide substantial benefits for regeneration of the target tissue.<sup>9-11</sup> However, manufacturing VF-specific dECM biomaterials at the commercial scale is almost impossible because only minute amounts of matrix can be derived from the small VF. To address this critical scalability challenge, we proposed that dECM from small intestinal submucosa (SIS), a larger volume soft connective tissue with extensive mechanical activity and extant clinical uses, would be an effective substitute for tissue-specific VF dECM in VF regeneration.<sup>12-15</sup> Meanwhile, critical drawbacks of using dECM hydrogels for VF applications are rapid degradation and low mechanical properties compared to native VF as mechanical function is required for the development of the specific VF structure.<sup>11,16-23</sup>

To enhance *in situ* gelation and mechanical mimicry of VF, click chemistry was proposed for its high yield, stereospecific nature in biological applications.<sup>24</sup> Specifically, click tetrazine ligation is a chemical reaction between a tetrazine and a strained alkene with non-toxic nitrogen gas as the only side product.<sup>25,26</sup> There are no chemical groups found naturally *in vivo* with which a side reaction may occur, and no catalyst is required, making this ligation a favorable reaction for *in situ* crosslinking of injectable biomaterials. In this thesis, we postulated that the use of click chemistry to crosslink dECM and alginate, a highly tunable polymer, to achieve VF-like mechanical properties, would facilitate improved regenerative outcomes and long-term restoration of VF functionality.

### *1.3. Thesis Objectives*

The overarching goal of this project was to develop a VF-mimicking and regenerative injectable hydrogel for VF regeneration utilizing dECM and click chemistry. Effectively, the click composite hydrogel was intended to supplement the innate regenerative capacity of dECM with VF-mimicking mechanical properties and a regulated degradation rate. Two aims were proposed in this thesis, as follows.

***Aim 1: To compare the proteomic composition of SIS, VF dECM, and Native VF and predict their applicability to tissue regeneration.*** Mass spectrometry-based proteomics and *in vitro*

functional regenerative outcomes based on neo-ECM deposition were used to compare the applicability of dECM hydrogels prepared from VF and SIS dECM to VF applications.

***Aim 2. To develop and characterize the mechanical and biological properties of injectable VF-mimicking click dECM hydrogels.*** Following the development of click dECM hydrogels, a series of tests were performed to evaluate their mechanical properties, impact on cell behavior, and biocompatibility for applicability as VF injectable biomaterials.

***Aim 2.1: To fabricate and characterize the mechanical properties of injectable click dECM hydrogels.*** Click dECM-alginate composite hydrogels were fabricated from both VF dECM and SIS dECM sources. Functionalization of dECM and alginate was characterized by nuclear magnetic resonance (NMR) and gel formation was characterized by turbidimetric assay. The mechanical properties of the click dECM-alginate hydrogel were characterized using rheology, atomic force microscopy (AFM), and compression testing and were compared to native VF and standard VF and SIS dECM-only hydrogels.

***Aim 2.2. To evaluate the stability and cellular response to injectable click dECM hydrogels in vitro.*** Stability of dECM hydrogels was assessed by *in vitro* degradation assays, scanning electron microscopy (SEM), and evaluation of cell viability and contraction in human VF fibroblasts. Also, the vasculogenic capacity of the hydrogels was evaluated with encapsulated human endothelial cells using fluorescent staining.

***Aim 2.3. To evaluate the biocompatibility of injectable click dECM hydrogels in vivo.*** The effects of the click dECM hydrogel on immune response and tissue integration were evaluated in a rat subcutaneous model. Histological staining was performed to evaluate hydrogel retention, foreign body response, and scaffold-tissue integration. Immunofluorescence staining was performed to investigate the immune cell response with respect to the recruitment of macrophages and B cells as well as macrophage subtype polarization.

Overall, we expected that SIS would share a comparable proteomic profile with VF dECM, and that SIS and VF dECM-based click dECM hydrogels would achieve reasonably comparable proteomic profiles, mechanical properties, cellular activity, and biocompatibility. Considering these expected outcomes, we conjectured that the click SIS dECM hydrogel would be a viable material with scale-up feasibility in VF regenerative biomaterials.

## Preface to Chapter 2

Injectable biomaterials are commonly used to augment impaired vocal fold (VF) function, a minimally invasive treatment methodology that can be performed in a doctor's office. However, existing injectable VF biomaterials only provide temporary augmentation, degrading rapidly without regenerating tissue, which leads to repeated injections. Innovative tissue engineering techniques show promise to better mimic native tissue, facilitate wound healing, and lead to permanent restoration of VF function.

In chapter 2, we review VF anatomy, VF dysfunctions that commonly require treatment with injectables, and the state of the art of injectable VF biomaterials. Trends in VF biomaterials currently under investigation intended to stimulate regeneration, achieve mechanical mimicry, and tube biodegradation are assessed for their advantages and limitations. Particular focus is given to strategies for improving bioactivity and the promise of composite biomaterials and click chemistry in the fabrication of in situ gelling VF injectables. Finally, we discuss future prospects for development of VF injectables including biomaterial requirements for intracordal versus intramuscular injection.

This work has been accepted for publication as a review paper in *Tissue Engineering Part B: Reviews* in 2024:

Mika Brown, Hideaki Okuyama, Masaru Yamashita, Maryam Tabrizian, Nicole YK Li-Jessen. "Trends in Injectable Biomaterials for Vocal Fold Regeneration and Long-Term Augmentation." *Tissue Engineering Part B: Reviews*. (2024).

## Chapter 2. Trends in Injectable Biomaterials for Vocal Fold Regeneration and Long-Term Augmentation

### *Abstract*

Human vocal folds (VF), a pair of small, soft tissues in the larynx, have a layered mucosal structure with unique mechanical strength to support high-level tissue deformation by phonation. Severe pathological changes to VF have causes including surgery, trauma, age-related atrophy, and radiation, and lead to partial or complete communication loss and difficulty in breathing and swallowing. VF glottal insufficiency requires injectable VF biomaterials such as hyaluronan, calcium hydroxyapatite, and autologous fat to augment VF functions. Although these biomaterials provide an effective short-term solution, significant variations in patient response and requirements of repeat reinjection remain notable challenges in clinical practice. Tissue engineering strategies have been actively explored in the search of an injectable biomaterial that possesses the capacity to match native tissue's material properties while promoting permanent tissue regeneration. This review aims to assess the current status of biomaterial development in VF tissue engineering. The focus will be on examining state-of-the-art techniques including modification with bioactive molecules, cell encapsulation, composite materials, as well as, *in situ* crosslinking with click chemistry. We will discuss potential opportunities that can further leverage these engineering techniques in the advancement of VF injectable biomaterials.

### *Impact Statement*

Injectable VF biomaterials augment tissue function through minimally invasive procedures, yet there remains a need for long-term VF reparation. This article reviews cutting-edge research in VF biomaterial development to propose safe and effective tissue engineering strategies for improving regenerative outcomes. Special focus is paid to methods to enhance bioactivity and achieve tissue-mimicking mechanical properties, longer *in situ* stability, and inherent biomaterial bioactivity.

### *2.1. Introduction*

Human vocal folds (VF) have distinct layers of submucosal connective tissue sandwiched between the laryngeal epithelium and the thyroarytenoid muscle and anchored by the arytenoid

cartilage (**Figure 1A**).<sup>1</sup> During phonation, the VF stretch longitudinally between 5-15 mm, while the superficial lamina propria (LP) oscillates with up to 0.5 mm amplitude.<sup>1,2</sup> These three layers are the superficial, intermediate, and deep LP (**Figure 1B**). Advanced imaging studies using multiphoton microscopy and optical coherence tomography found a continuous transition between LP layers, further elucidating the intricate organization of VF extracellular matrix (ECM) and microvasculature, which requires tissue-specific regenerative solutions.<sup>3-7</sup>

The ECM structure plays an important role in supporting phonation.<sup>2,8,9</sup> Collagens are the primary constituents of VF ECM, contributing 40-50% of total protein.<sup>10</sup> Collagen I fibers form the overarching structural network, regulate cell distribution, and recruit cells for wound healing.<sup>10,11</sup> Collagen III and elastin bundles contribute to VF resilience, tensile strength, and viscoelasticity. Hyaluronan is an abundant glycosaminoglycan that helps regulate wound healing and dampens mechanical stress from high frequency phonatory oscillation.<sup>11,12</sup>

VF atrophy, sulcus, scarring, and unilateral paralysis/paresis are candidates for injection laryngoplasty, where a biomaterial is injected to augment VF function and closure.<sup>13-16</sup> Age-associated VF atrophy is characterized by tissue bowing and reduced viscoelasticity that may impact LP or muscle.<sup>17-21</sup> Sulcus vocalis is related to fibrotic alterations characterized by groove formation and epithelium invading the superficial LP.<sup>22</sup> VF scarring is generally caused by surgical interventions, radiation, or trauma, where healthy LP is replaced by excessive fibrous collagen deposition.<sup>12,17</sup> VF paralysis/paresis is unilateral or bilateral VF immobilization caused by injury to the recurrent laryngeal nerve from cervical or thoracic surgical intervention, tumor formation, trauma, radiation, and chronic inflammation.<sup>23-26</sup> Bilateral VF paralysis may require reinnervation or airway bypass surgeries. However, unilateral VF paralysis and paresis account for up to 75% of injection laryngoplasty treatments.<sup>27-29</sup>

Injection laryngoplasty is performed in operating rooms or doctor's offices (**Figure 1C**).<sup>30-32</sup> In-office injection laryngoplasty offers relatively low risk and cost as well as immediate testing of glottal function. The materials are injected into the lateral aspect of the thyroarytenoid muscle, or the paraglottic space.<sup>32-35</sup> Material placement is critical to treatment outcomes. Superficial injection causes improper biomaterial localization, tissue stiffening, and impeded vibration.<sup>36-38</sup> While there is interest in developing regenerative biomaterials and delivery techniques for the superficial LP, intramucosal injections are limited to free drug formulations such as steroids

and growth factors.<sup>36,39-41</sup>

In this article, the primary goal is to assess the successes and limitations of current VF injectable biomaterials and review the state-of-the-art of VF biomaterials under development. We also evaluate advanced tissue engineering techniques that can help stimulate regeneration, mimic mechanical properties, and control material degradation towards permanent VF augmentation.

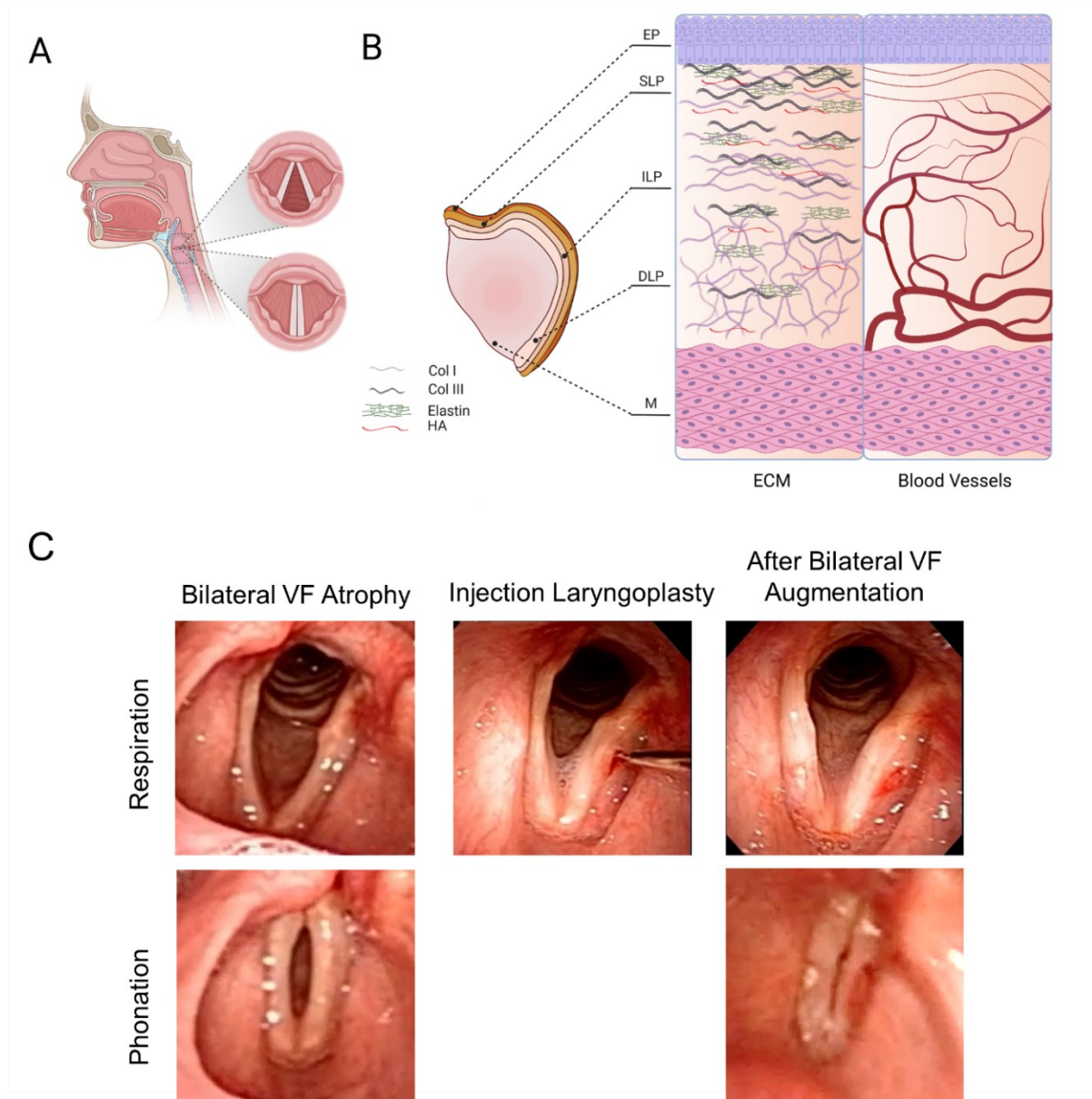


**Figure 1.** Vocal Fold (VF) Anatomy and Injection Laryngoplasty. A) Vocal folds are housed in the larynx. B) Vocal fold is composed of epithelium (EP), superficial lamina propria (SLP),

intermediate lamina propria (ILP), deep lamina propria (DLP), and muscle (M) with rich extracellular matrix and vasculature. C) Laryngoscopic images of injection laryngoplasty with Atelo-Collagen to VF with bilateral atrophy during respiration (top row) and phonation (bottom row). A and B Created with BioRender.com.

## *2.2. Overview of Existing VF Biomaterials Used in Clinics*

The first injectable VF biomaterial, Teflon, caused severe granuloma 5-10 years following injection and removal caused tissue morbidity.<sup>42</sup> Also, collagen (Zyplast®) and gelatin-based (Gelfoam®) injectables were used for VF augmentation for nearly 20 years but have been discontinued due to short-term efficacy and chance of allergic reaction to bovine collagen.<sup>43,44</sup> Atelocollagen, a similar bovine collagen material, continues to be used in Japan.<sup>45</sup> Cymetra™ is a discontinued micronized decellularized dermal matrix sourced from human cadavers that lasted six weeks to six months and reduced the risk of allergic reaction, decreased foreign body response, and improved voice outcomes compared to bovine collagen.<sup>46,47</sup>

These examples emphasize the need for long term safety evaluations and follow-up.<sup>42</sup> At present, common biomaterials for injection laryngoplasty include hyaluronan, calcium hydroxyapatite with carboxymethylcellulose, autologous fat, and silk-hyaluronan (**Table 1**).<sup>48</sup>

Restylane® and Juvederm® are produced from hyaluronan microparticles and reduce excess collagen I deposition as well as augment the glottal wave and voice quality.<sup>49,50</sup> These hyaluronan-based products are approved as dermal fillers but are used off-label for voice applications.<sup>48</sup> Treatment with HA-based products may improve phonation quality for at least six months.<sup>51</sup>

Calcium hydroxylapatite microparticles are a bioceramic injectable filler suspended in a carboxymethylcellulose gel.<sup>47,51</sup> Calcium hydroxyapatite, marketed as Radiesse® and Prolaryn Plus®, is FDA approved for Injection laryngoplasty. The residence time of calcium hydroxylapatite is relatively long, up to 24 months.<sup>47,51</sup> However, calcium hydroxylapatite injection outcomes may be variable, and cause deposits in the superficial LP and deleterious foreign body response.<sup>52,53</sup> VF stiffening, impaired mucosal wave, edema, and hypervascularity were also reported with calcium hydroxylapatite.<sup>48,52-54</sup>

A significant limitation of the aforementioned injectables is a lack of capacity to remodel

tissue.<sup>13,55,56</sup> In contrast, autologous fat and silk-hyaluronan show potential to stimulate tissue deposition for long-term efficacy.

Autologous fat grafts contain stem and endothelial cells that contribute to tissue remodeling and vascularization.<sup>55-57</sup> About 30-40% excess volume is commonly used to offset resorption, but optimal volume is difficult to predict as resorption varies from 20-60%.<sup>58-60</sup> Overinjection of autologous fat can alter VF shape and mechanics, cause dysphonia, and require surgery to remove the excess.<sup>57-59</sup> Autologous fat may also induce acute and chronic inflammation, necrosis, and fibrosis.<sup>55-57</sup>

Silk microparticles in a crosslinked hyaluronan carrier are new-FDA approved injection laryngoplasty biomaterials.<sup>33,61,62</sup> The silk microparticles incorporate bioactive properties to promote cellular infiltration and tissue remodeling.<sup>33,62-65</sup> Silk-hyaluronan improves control over degradation, wherein the hyaluronan degrades more rapidly while silk microparticles are retained for up to 18 months.<sup>63</sup> While the remodeling effects are promising, about 32% of patients in a large clinical study required additional injection laryngoplasty procedures after a median of 106 days.<sup>33,62</sup> Serious complications including edema, dyspnea, and difficulty swallowing were reported with low incidence.<sup>62,64</sup>

There remains an unfilled need for a minimally invasive, injectable VF biomaterial that effectively restores tissue structure and functions to reduce the requirement for repeated treatments. Tissue engineering strategies are required for injectable VF biomaterials with more permanent efficacy. In the following, we review options for biomaterial composition, enhancing bioactivity with biomaterial functionalization and encapsulation of growth factors and cells, and control of mechanical and degradation properties through composite materials and crosslinking.

**Table 1. Common VF Injectable Biomaterials**

Biomaterial Type	Commercial Name(s)	Status	Advantages	Disadvantages
Autologous Fat	N/A	Off-Label Use	- Longer-lasting results - Tissue remodeling capacity	- Unpredictable deleterious outcomes - Frequent resorption



			- VF-like mechanical properties	- Risk of overinjection - Variation and difficulty of preparation
Calcium hydroxylapatite	Radiesse®, Prolaryn Plus®, Renú Voice®	FDA Approved	- Up to 24-month residence time - FDA approved for VF applications	- Tissue stiffening - Potential for impaired VF function - Potential for migration out of target tissue - Potential or deleterious foreign body response
Collagen	Zyplast®, Atelo-collagen	Zyplast discontinued, Atelo-collagen used in Japan	- Low swelling	- Risk of allergic reaction - Gluteraldehyde cytotoxicity - Frequent reinjection
Decellularized human dermis	Cymetra™	Discontinued	- Reduced foreign body response - Improved voice quality	- Discontinued for poor ease of use
Gelatin	Gelfoam®	Infrequent Use	- Tissue tolerance - Early alternative to permanent medialization	- Pressurized injection through large-gauge needle - Short term use (2-8 weeks)
Hyaluronan	Juvederm®, Restylane®	Off-Label Use	- Reduces excess collagen I deposition - Improves voice quality	- Variable degradation time - Frequent reinjection

Hyaluronan-Silk	Silk Voice®	FDA Approved	<ul style="list-style-type: none"> <li>- Evidence of tissue remodeling</li> <li>- VF-like mechanical properties</li> <li>- FDA approved for VF applications</li> </ul>	<ul style="list-style-type: none"> <li>- Frequent reinjection</li> </ul>
Teflon	Teflon/Polytef Paste	Discontinued	<ul style="list-style-type: none"> <li>- Long-term injectable treatment</li> </ul>	<ul style="list-style-type: none"> <li>- Delayed inflammatory complications, particularly granuloma</li> <li>- Tissue morbidity upon removal</li> </ul>

### 2.3. Choosing Polymers for Vocal Fold Injectables

Injectable VF biomaterials are fabricated from polymers derived from natural sources or synthesized in laboratories, each of which carry advantages and limitations (**Table 2**). Selecting polymers for VF injectables relies on desired properties, including bioactivity, cell response, structure, mechanics, and biodegradability.

#### 2.3.1. Natural Materials

Natural polymers are selected for biocompatibility, bioactivity, porous ECM-like structure, or immunomodulatory capacity.<sup>66,67</sup> On the other hand, natural polymers have high variability, and may lack mechanical tunability or degrade before achieving permanent effect unless crosslinked or in composite.<sup>66,68</sup> In addition to those in clinical VF biomaterials, other natural polymers including alginate, chitosan, gelatin, and decellularized extracellular matrix (dECM) are under active investigation for favorable regenerative, mechanical, and degradation properties.

Collagen and gelatin are used in VF biomaterials for their capacity to promote cell adhesion, migration and proliferation.<sup>66,69-71</sup> However, collagen-based hydrogels exhibit rapid degradation and poor mechanical and structural stability.<sup>66,69</sup> Despite the discontinuation of existing collagen and gelatin VF injectables, crosslinked and composite collagen and gelatin

formulations are under investigation.<sup>68,72,73</sup>

Hyaluronan and silk-based biomaterials are under development to improve treatment duration and remodeling capacity.<sup>74-76</sup> Hyaluronan provides a damping function within the VF, regulates cell function, and modulates inflammation with reduced immunogenicity compared to collagens.<sup>44,77</sup> Silk fibroin has well-established biocompatibility due to its use in sutures with highly tunable mechanical and structural properties.<sup>69,70</sup> However, biomedical grade silk fibroin is expensive, depends on nonstandardized hand processing and environmental conditions, and is sold in unstable aqueous solution.<sup>78</sup> Production variability leads to differences in bioactivity, degradation, and mechanical properties.<sup>78</sup>

Sodium alginate is a biocompatible, antibacterial polysaccharide derived from brown seaweed that degrades into glucose-like monosaccharides that can be safely metabolized.<sup>66,69,79,80</sup> Alginate lacks innate cell adhesion sites, but its bioactivity and mechanical properties are highly tunable through variable molecular weight, chemical modification, and crosslinking.<sup>80</sup> In VF injectables, alginate is under investigation for cell and growth factor delivery, and as a composite to provide improved mechanics and durability to regenerative biomaterials.<sup>74,76,79,81</sup>

Chitosan is a biocompatible, antimicrobial polysaccharide derived from the exoskeletons of arthropods with low immunogenicity.<sup>66</sup> In VF applications, chitosan has been shown to reduce fibroblast proliferation and excess collagen deposition.<sup>82</sup> However, chitosan has a high swelling ratio, lacks elasticity, and is unstable at neutral pH, limitations that may be circumvented by crosslinking and use in composites.<sup>71,79,83,84</sup>

dECM is produced by removing cells from tissue. Its composition of ECM proteins, glycosaminoglycans, and other regenerative molecules helps stimulate innate wound healing processes.<sup>41,85,86</sup> VF-specific dECM has high batch to batch variability and poor scalability, but commercial sources from larger organs such as small intestinal submucosa (SIS) show regenerative potential in the VF.<sup>87,88</sup> Both VF and SIS dECMs have been shown to downregulate fibrotic genes, reduce excess collagen I deposition, and stimulate LP restoration, though these hydrogels possessed weak mechanical properties.<sup>86-90</sup> dECM also has potential to stimulate other VF-relevant processes including recruitment of endogenous stem cells, angiogenesis, and formation of tissue-specific structures.<sup>41,91-93</sup>

### 2.3.2. Synthetic Materials

Synthetic polymers have standardized fabrication processes and high tunability. However, synthetic polymers do not possess innate bioactivity and may integrate poorly with surrounding tissue or produce toxic byproducts.<sup>66</sup> Also, polymer synthesis may involve toxic materials, and require extensive purification.<sup>94,95</sup> Synthetic polymers under investigation for VF applications include polyethylene glycol (PEG), poly  $\epsilon$ -caprolactone (PCL), and polyurethane (PU).<sup>79,96-98</sup>

PEG is a non-immunogenic, amphiphilic polymer comprised of ethylene oxide monomers that degrades slowly through oxidative degradation.<sup>99-101</sup> PEG has extensive chemical modification capacity for modulating bioactivity, degradation, and mechanical properties.<sup>96,97,99</sup> However, some patients exhibit pseudoallergy to PEG, and PEG derivatives used at high concentrations or functionalized with molecules like acrylates may cause cytotoxicity.<sup>100,101</sup>

PCL possesses favorable viscoelasticity at physiological temperature and is biodegradable over 2-3 years, though its hydrophobicity limits cell adhesion and proliferation.<sup>102,103</sup> The mechanical properties of PCL are high compared to soft tissues, but may be tuned by using composites.<sup>103</sup> In rabbits with VF paralysis, PCL microspheres in a Pluronic F127 carrier augmented VF function for 12 months.<sup>98,102</sup>

PU has been used as a composite material for injectable VF biomaterials.<sup>104</sup> PU are flexible and durable block co-polymers that can be synthesized with hydrolytic or enzymatic degradability depending on linkages between its constituent monomers.<sup>105</sup> PU degradation products and impurities retained after synthesis may be cytotoxic, though safer methodologies are under development.<sup>105-107</sup>

**Table 2. Advantages and Disadvantages of VF Biomaterials Under Investigation**

Biomaterial	Advantages	Disadvantages
Alginate[79-81] <sup>27-29</sup>	<ul style="list-style-type: none"><li>- VF-like mechanical properties</li><li>- Readily modifiable with bioactive molecules</li><li>- Antimicrobial</li></ul>	<ul style="list-style-type: none"><li>- No innate cell adhesion sites</li><li>- Ionic crosslinking is heterogenous and uncontrollable</li><li>- Ion leaching causes loss of stability</li></ul>

Collagen/Gelatin[10, 46, 72]	<ul style="list-style-type: none"> <li>- Predominates structure of ECM</li> <li>- Stimulates cell recruitment, migration, and proliferation</li> </ul>	<ul style="list-style-type: none"> <li>- Some types carry high risk of allergic reaction</li> <li>- High contractility</li> <li>- Rapid degradation</li> </ul>
Chitosan[79] <sup>27</sup>	<ul style="list-style-type: none"> <li>- Stimulates ECM deposition</li> <li>- Low immunogenicity</li> <li>- Antimicrobial</li> <li>- Reduces fibroblast proliferation and excess collagen deposition</li> </ul>	<ul style="list-style-type: none"> <li>- High swelling</li> <li>- Unstable at neutral pH</li> </ul>
Decellularized extracellular matrix (dECM) [41, 85, 92]	<ul style="list-style-type: none"> <li>- Consists of innately regenerative ECM components</li> <li>- Stimulates native wound healing</li> <li>- Anti-fibrotic</li> <li>- Can be VF-specific</li> </ul>	<ul style="list-style-type: none"> <li>- Rapid degradation</li> <li>- Processing damages mechanical properties</li> <li>- Methods of producing can cause different immune and cell responses</li> </ul>
Hyaluronan[72, 121]	<ul style="list-style-type: none"> <li>- Sustained growth factor release</li> <li>- Improves vibration</li> <li>- VF-like viscoelasticity</li> <li>- Reduces deposition of fibrotic ECM molecules</li> </ul>	<ul style="list-style-type: none"> <li>- Rapid degradation</li> <li>- Lack of remodeling effects</li> </ul>
Poly $\epsilon$ -Caprolactone[98, 102-103]	<ul style="list-style-type: none"> <li>- Viscoelastic</li> <li>- Hydrolytic degradation</li> <li>- Biocompatibility</li> </ul>	<ul style="list-style-type: none"> <li>- Hydrophobicity</li> <li>- High mechanical properties compared to VF</li> </ul>
Polyethylene glycol[99-101, 154]	<ul style="list-style-type: none"> <li>- Biocompatibility</li> <li>- Low immunogenicity</li> <li>- Readily modifiable and crosslinkable</li> <li>- Tunable degradation</li> </ul>	<ul style="list-style-type: none"> <li>- Lacks innate bioactivity</li> <li>- Potential for pseudoallergy</li> <li>- Derivatives may be cytotoxic</li> </ul>

Poly(lactic co-glycolic acid)[160-161] <sup>30,31</sup>	<ul style="list-style-type: none"> <li>- Hydrolytic degradation</li> <li>- Biocompatibility</li> </ul>	<ul style="list-style-type: none"> <li>- Hydrophobicity</li> <li>- Acidic degradation byproducts</li> </ul>
Polyurethane[105-107]	<ul style="list-style-type: none"> <li>- Design versatility</li> <li>- Durability</li> </ul>	<ul style="list-style-type: none"> <li>- Toxic impurities and degradation byproducts</li> </ul>
Silk Fibroin[33, 62, 64, 69-70]	<ul style="list-style-type: none"> <li>- Biocompatible</li> <li>- Mechanical tunability</li> <li>- Stimulates cellular infiltration and ECM remodeling</li> </ul>	<ul style="list-style-type: none"> <li>- Nonstandardized fabrication</li> <li>- Expensive</li> <li>- Stored in unstable aqueous solution</li> </ul>

#### 2.4. Enhancing Bioactivity of Injectable VF Biomaterials

To achieve an intricate balance between material degradation, neo-tissue growth and its remodeling, the bioactivity of injectable VF biomaterials may be enhanced by functionalization with bioactive motifs and encapsulating growth factors or cells within a bioactive material.

##### 2.4.1. Conjugation with Bioactive Motifs

Conjugating polymers with biomolecular motifs can increase bioactivity.<sup>96,98,108</sup> Conjugation is performed via crosslinking the functional groups of the bioactive molecule and the polymer.<sup>109,110</sup> For example, arginylglycylaspartic acid (RGD), a peptide found in fibronectin and laminin, is commonly used to enable cellular adhesion to polymers without innate adhesion sites.<sup>108-111</sup> Heparin, a glycosaminoglycan, is another common conjugation choice, used to attract and sequester growth factors released by surrounding cells, or control the release rate of encapsulated growth factors.<sup>96,98,112,113</sup>

Injectable microparticles for VF augmentation were produced from PEG functionalized with maleimide and thiol groups that crosslinked by thiol-Michael addition.<sup>108</sup> The PEG-maleimide backbone was modified with thiol-functionalized RGD. After injection to rabbit thyroarytenoid muscle in annealing polymer solution, exposure to visible light produced a microporous annealed particle (MAP) hydrogel.<sup>114</sup> RGD-conjugated PEG and the MAP structure provided a favorable environment for cellular adhesion, infiltration, and vascularization.<sup>108,114</sup>

The Heparin and RGD-conjugated MAP hydrogel is the first to demonstrate tissue remodeling with long-term VF augmentation in an animal model.<sup>96</sup> The RGD-conjugated MAP hydrogel

was further conjugated with thiolated heparin to sequester growth factors and improve tissue integration (**Figure 2A**).<sup>96</sup> MAP hydrogels and a Restylane® control were injected intramuscularly to a rabbit vocal fold paralysis model. After 14 months, all 6 rabbits treated with MAP maintained augmentation. The biomaterial was replaced by collagen-rich neo-tissue with distinctive morphology compared to surrounding muscle.

#### *2.4.2. Encapsulation of Growth Factors*

Growth factors are signaling cytokines secreted by cells that stimulate cellular activity, inflammation, and tissue remodeling.<sup>115</sup> Basic fibroblast growth factor (bFGF) and hepatocyte growth factor (HGF) are used clinically to treat VF scarring due to fibroblast modulation and anti-fibrotic activity.<sup>39,115</sup> Free growth factors have several limitations including instability, rapid inactivation, and poor targeting resulting in safety concerns including tumorigenesis.<sup>116,117</sup> Encapsulating growth factors in biomaterials for intramuscular injection may slow release and improve target site retention.<sup>74,98</sup>

Encapsulation in a VF injectable has been performed by calcium chloride crosslinking, trapping the HGF within the “egg-box” network of a hyaluronan-alginate hydrogel.<sup>74</sup> *In vitro*, HGF release was sustained over three weeks as the porous “egg-box” facilitated slow diffusion.<sup>74,118</sup> When the hydrogel was injected into injured VF LP, vibrational and viscoelastic properties improved compared to controls treated with HGF alone.

Growth factors may also be bound to injectable microspheres with growth factor binding sites.<sup>98,119</sup> Gelatin microspheres with bFGF have reduced scarring when injected to injured rabbit and canine VF LP.<sup>119,120</sup> Heparin-immobilized PCL microspheres with bound bFGF and HGF in a Pluronic F127 carrier showed ECM deposition and muscular regeneration 1 month after injection to a VF paralysis rabbit model, a regenerative effect that could not be achieved with PCL alone.<sup>98</sup>

#### *2.4.3. Cell Delivery*

Co-delivery of cells with a biomaterial may provide a synergistic effect on VF regeneration. In VF animal models, stem cells have been shown to remodel fibrotic tissue and restore mechanical function.<sup>121-123</sup> In a nonrandomized clinical study, patients received injections of autologous mesenchymal stem cells (MSCs) to the LP and muscle following surgical resection

of scarring.<sup>122</sup> Up to 75% of patients (N = 16) showed improved VF function. Encapsulating cells in a biomaterial improves cellular viability and retention in the target tissue and provides the cells with bioactive and mechanical cues to enhance VF augmentation.<sup>122,123</sup>

Encapsulation of stem cells in hyaluronan has improved retention in VF LP or muscle and reduced fibrosis in rat and rabbit models.<sup>121,124</sup> However, a hyaluronan-MSCs group performed comparably to MSCs alone in a preliminary clinical study.<sup>122</sup> Encapsulation in a biomaterial with remodeling capacity or longer-term stability improve outcomes.

Delivery of urine-derived stem cells (USCs) in a SIS dECM hydrogel was recently explored in a heat-injury rabbit VF LP model (**Figure 2B**).<sup>86</sup> SIS dECM-only, USC-only, and SIS-USC groups all demonstrated lower inflammatory marker expression (CD86, TNF- $\alpha$ ) and reduced collagen I/collagen III ratio compared to LP without treatment after two and eight weeks, respectively. The SIS dECM-only and USC-only groups induced comparable responses, while the SIS-USC group induced an enhance synergistic effect on VF regeneration.



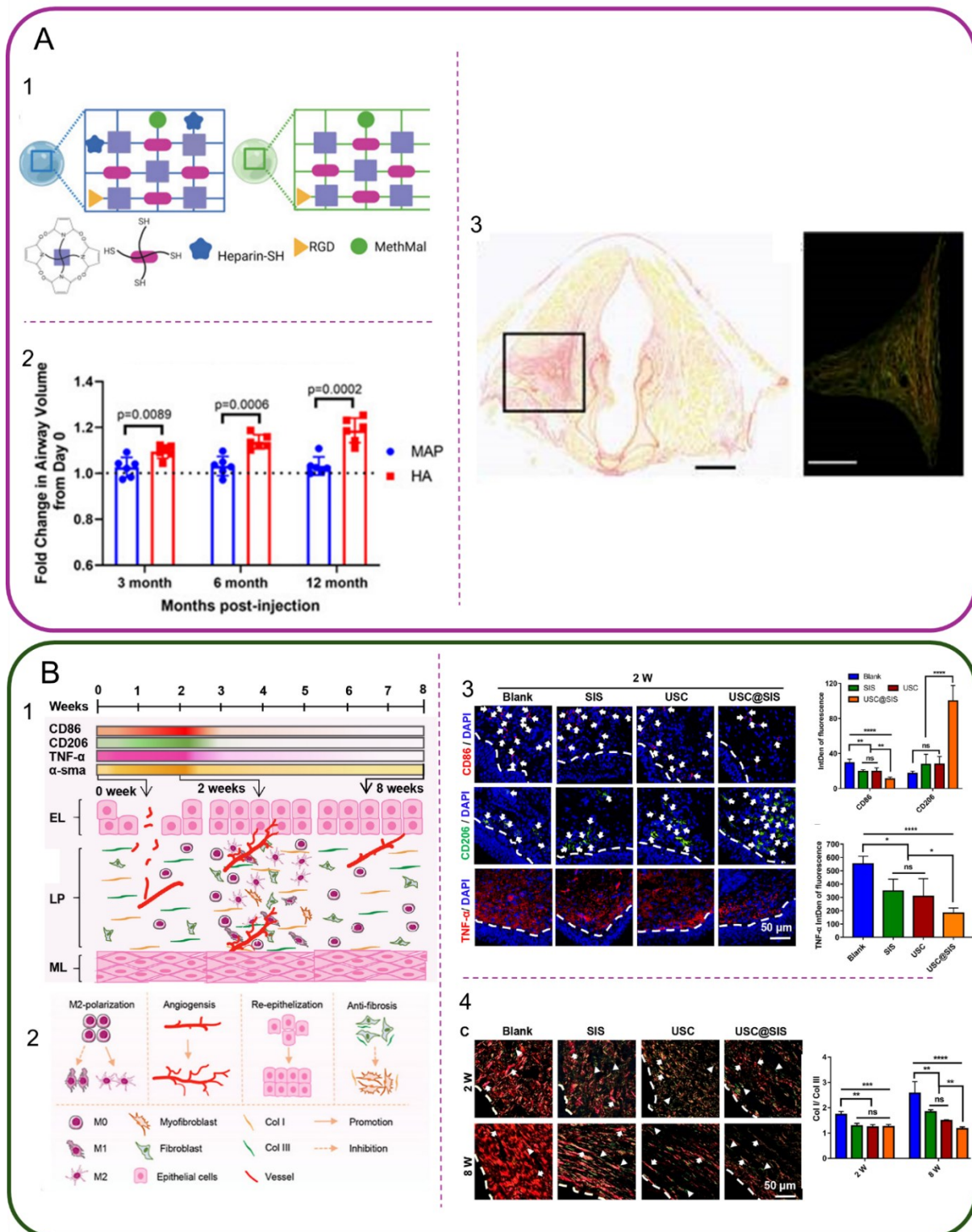


**Figure 2.** Regenerative Effects of Enhancing the Bioactivity of VF Injectable Biomaterials. A) RGD and Heparin-conjugated PEG-based MAP hydrogel. 1. MAP hydrogel structure

showing thiol-ether crosslinks, MethMal annealing, and conjugation with RGD and heparin within microparticles. **2.** Change in airway volume over 12 months. The MAP hydrogel maintained consistent augmentation while the airway volume increased with the hyaluronan control, indicating volume loss. **3.** Picosirius red staining of neo-tissue produced by MAP hydrogel after 12 months under brightfield (left) and polarized light (right). Black box outlines neo-tissue. **B)** SIS with encapsulated urinary stem cells in a rabbit model of VF injury promotes a regenerative immune response. **1.** Proposed regenerative timeline following biomaterial injection. **2.** Regenerative processes correlating to the proposed timeline. **3.** Immunofluorescence and quantified integrated density (IntDen) of inflammatory (CD68, TNF- $\alpha$ ) and anti-inflammatory (CD206) markers in excised rabbit VF. **4.** Immunofluorescence and quantified ratio of collagen I (red) to collagen III (green) in excised rabbit VF. \* $p < 0.05$ , \*\* $p < 0.01$ , \*\*\* $p < 0.001$ , \*\*\*\* $p < 0.0001$ , ns = not significant. Panel A is reproduced from Ref. <sup>32</sup> (Open Access: <https://creativecommons.org/licenses/by-nc-nd/4.0/>). Panel B is reproduced from Ref. <sup>33</sup> (Open Access: <https://creativecommons.org/licenses/by-nc-nd/4.0/>).

## 2.5. Modulating the Mechanical, Physical, and Degradation Properties of VF Biomaterials

Mimicking *in vivo* VF mechanical properties and degradation at a rate that matches regeneration are necessary for biodegradable materials to permanently augment VF function. Alongside biomolecular cues, the mechanical (stiffness, viscoelasticity) and physical (porosity, swelling) properties of a biomaterial help direct cells to generate neo-ECM characteristic of VF.<sup>125</sup> VF mimicry is complicated by its layered structure and varied thickness.<sup>3,126</sup> VF exhibit compressive moduli of 3.9-5.4 kPa on the medial LP surface, 2.7-3.2 kPa on the superior LP surface, and 1.3-2.7 kPa on the thyroarytenoid muscle.<sup>126</sup> A range representative of the muscle or LP is typically targeted in biomaterial design.

Degradation properties are also critical, as bioactive materials cannot achieve permanent VF augmentation if they degrade before tissue remodeling is complete.<sup>66</sup> Despite the bioactivity and VF-mimicking storage modulus of SilkVoice®, its stability varies, and reinjection are still frequently required.<sup>62,63</sup> The use of composite materials and chemical crosslinking can tune biomaterial properties to achieve VF mimicry and controlled degradation.

### 2.5.1. Composite VF Biomaterials

Natural, ECM-derived polymers with innate bioactivity may be combined with more stable polymers and the composition ratio and crosslinking method tuned to produce an injectable composite that better mimics human VF than either alone (**Table 3**).<sup>72,81</sup>

For instance, thiolated hyaluronan was crosslinked with PEG-diacrylate (PEGDA) to produce a hydrogel with tunable viscoelasticity for VF injection, and supplemented with collagen I collagen III to achieve a native-like structure.<sup>72</sup> Inclusion of collagens was necessary to retain encapsulated fibroblasts and increased the storage modulus from 0.16-0.21 kPa to 0.65-1kPa, within the 0.3-1.2k range of adult VF LP.<sup>72,127</sup> HA-PEGDA prevented the fibroblast-mediated contraction associated with collagen-only hydrogels. The inclusion of natural materials and a synthetic polymer improved tissue-mimicking and bioactivity.

The impact of material composition on mechanical properties is illustrated by the varied properties of calcium-crosslinked alginate microspheres in composite with poly-L-lysine or chitosan (**Figure 3A**).<sup>79</sup> The VF Young's modulus by nanoindentation ranges between 0.5-6 kPa, matching the Alginate-only (~3 kPa) and Alginate-poly-L-lysine (~2 kPa) microspheres but not alginate-chitosan (~12 kPa).<sup>79,128,129</sup> Low swelling ratios are favorable for stability and biological response predictability. Alginate-poly-L-lysine microspheres showed the lowest ratio at 9% after 48 h, while alginate-only microspheres swelled by 34%. Alginate-chitosan microspheres swelled by over 80%, contraindicating use due to risk of airway obstruction.

Alginate-chitosan hydrogels exhibited more favorable swelling characteristics when crosslinked with Schiff base and borate ester bonding and visible light methacrylate polymerization (**Figure 3B**).<sup>130</sup> Tuning the alginate-chitosan ratio revealed that a 1:1 ratio was most stable with a swelling ratio of ~26% after 48 h compared to 1:2 (~35%) and 2:1 (~45%) ratios. The 1:1 alginate-chitosan hydrogel retained the greatest mass by at least 1.5 times after a 28-day hydrolytic degradation test. Intramuscular injection of the 1:1 hydrogel in a VF paralysis rabbit model better maintained volume, exhibited a smaller glottal gap, and stimulated neo-ECM production after 12 weeks compared to a hyaluronan control.<sup>130</sup> In sum, composite biomaterials provide vast opportunities for tuning biomaterial properties to produce a synergistic effect on regeneration.

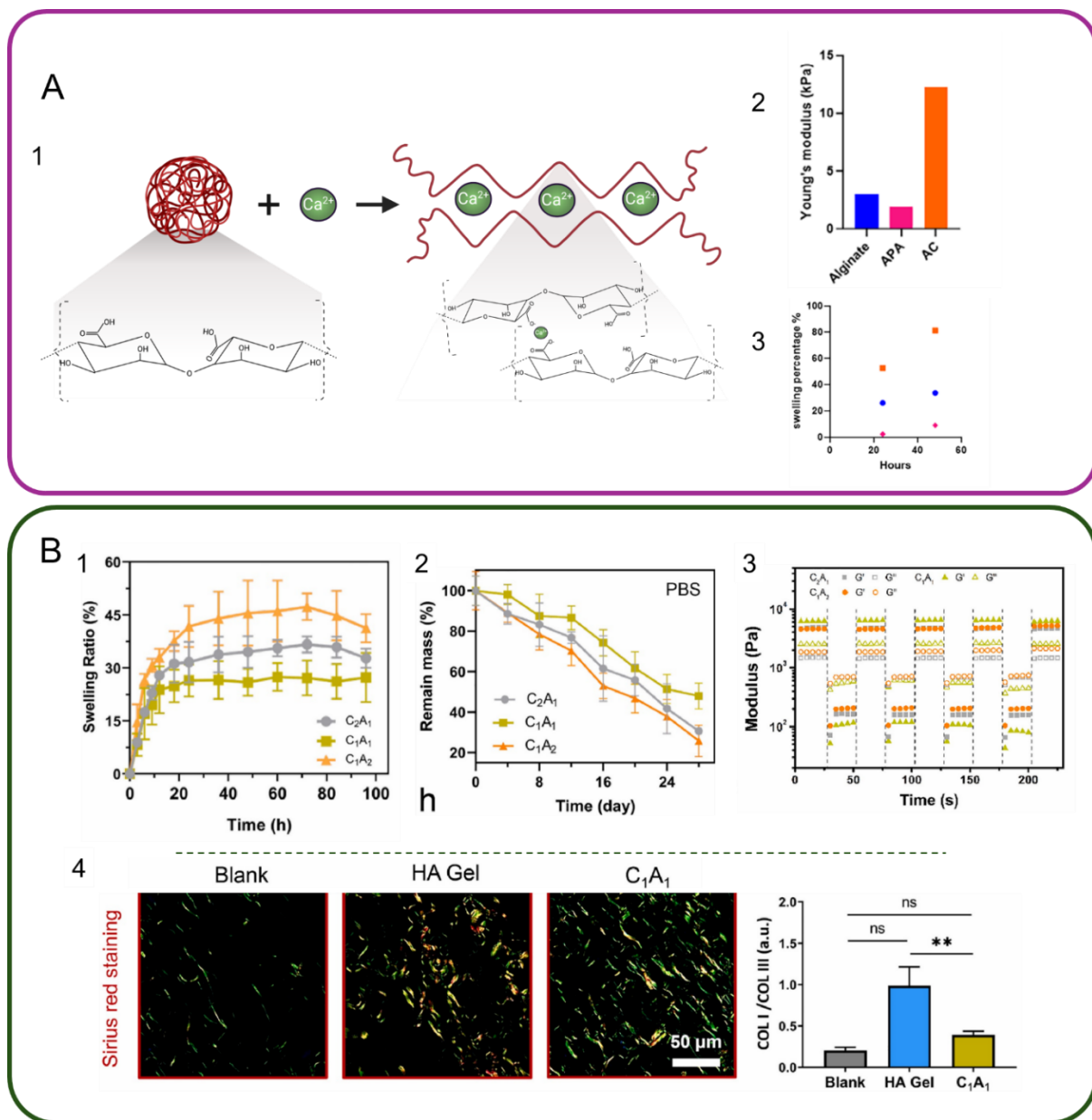


**Figure 3.** A) Alginate-based microspheres as injectable VF biomaterials. 1. Calcium Ion Crosslinking with “Egg-Box” Structure. Created with BioRender.com. 2. Young's modulus and 3. Swelling ratio of • alginate, • alginate-poly-L-lysine, and • alginate-chitosan microspheres. B) Alginate-chitosan VF injectable hydrogel with tunable mechanical and physical properties. 1. Swelling Ratio 2. Hydrolytic degradation and 3. Cyclic stress-relaxation between 300% and 1% strain at varying ratios (1:1, 2:1, 1:2) of alginate to chitosan. 4. Remodeling of Collagens I and III in response to the 1:1 alginate-chitosan hydrogel compared to hyaluronan and untreated injury controls. Panel A is reproduced from Ref [79]<sup>34</sup>. Panel B is reproduced from Ref [130]. (Open Access: <https://creativecommons.org/licenses/by-nc-nd/4.0/>).

### 2.5.2. Conventional Crosslinking of VF Biomaterials

Crosslinking method fundamentally impacts network structure, mechanical properties, and degradation rate of a biomaterial. Desirable properties for crosslinkers in VF injectables include reaction specificity, non-toxic byproducts, and capacity for safe in situ crosslinking.

Chemical and ionic crosslinking are used to fabricate VF injectables, such as 1,4-butanediol diclycidyl ether (BDDE) in Juvederm®, Restylane®, and SilkVoice®.<sup>131</sup> BDDE slows enzymatic degradation by obstructing hyaluronidase cleavage sites. Although BDDE is toxic, it is removed before patients are exposed.<sup>131</sup> However, BDDE-crosslinked hyaluronan degrades without repairing tissue, necessitating reinjection.

Dialdehydes such as glutaraldehyde and glyoxal react with amine groups and are used to strengthen mechanical properties and provide resistance to thermal and enzymatic degradation in collagen, gelatin, and glycol-chitosan VF injectables.<sup>83,119,132</sup> However, dialdehydes are cytotoxic at low concentrations and the reaction is difficult to control with multiple possible reaction products.<sup>43,133-136</sup>

Carbodiimide crosslinking with 1-Ethyl-3-(3-dimethylaminopropyl) carbodiimide (EDC) and N-hydroxysuccinimide (NHS) couples amine and carboxylic acid groups and is used to improve mechanical stability. EDC-NHS forms a favorable network structure for cellular integration but crosslinks DNA, proteins, and cell surface molecules and produces a toxic isourea byproduct.<sup>135-137</sup>

Genipin crosslinking is less cytotoxic and reacts specifically with primary amines, making it useful for controlling crosslinking density.<sup>138,139</sup> In VF applications, genipin-crosslinked gelatin hydrogels exhibited low swelling ratios, slow enzymatic degradation, and improved mechanical strength compared to carbodiimide-crosslinked hydrogels.<sup>68</sup> However, cytotoxicity and hinderance of cell infiltration in genipin-crosslinked biomaterials may increase at physiological temperature, and there is a shortage of clinical safety evaluation.<sup>138-141</sup>

Dialdehyde, carbodiimide, and genipin crosslinkers may be safe for microparticles that can be sufficiently purified prior to injection but are not recommended for *in situ* gelation to prevent cytotoxicity and crosslinking of ECM proteins in the native tissue (**Table 3**).<sup>136</sup>

Ionic crosslinking with calcium chloride, used to fabricate alginate and chitosan biomaterials,

is rapid and biocompatible.<sup>74,79,142</sup> However, limitations include rapid, uncontrollable crosslinking causing heterogenous bond distribution and difficulty of injection and ion leaching resulting in loss of structural stability.<sup>143</sup>

The side reactions, cytotoxicity, and heterogeneity inherent to conventional crosslinkers led to the development of bioorthogonal click chemistry, which may be more suitable for *in situ* gelling VF injectable applications.<sup>144</sup>

**Table 3. Advantages and Disadvantages of Conventional Crosslinkers**

Crosslinker	Advantages	Disadvantages
1,4-butanediol dicyclidyl ether[131]	<ul style="list-style-type: none"> <li>- Reliable for clinically approved <i>in situ</i> gelling materials</li> <li>- Excess removed prior to gel formation</li> <li>- Slows degradation rate compared to uncrosslinked hyaluronan</li> </ul>	<ul style="list-style-type: none"> <li>- Toxic in concentrations greater than 2 ppm</li> <li>- Reinjection required due to degradation</li> </ul>
Dialdehydes (glutaraldehyde, glyoxal)[43, 83, 119, 132-136]	<ul style="list-style-type: none"> <li>- High crosslinking efficiency</li> <li>- Soluble in water and organic solution</li> <li>- Mechanical tunability</li> <li>- Versatility with varied materials</li> <li>- Resistance to thermal and enzymatic degradation</li> </ul>	<ul style="list-style-type: none"> <li>- Toxic at low concentrations</li> <li>- Degrades by hydrolysis</li> <li>- Methods for reducing exposure may lower crosslinking efficiency</li> <li>- Unsuitable for <i>in situ</i> gelation due to protein crosslinking</li> </ul>
Genipin[136, 138-141]	<ul style="list-style-type: none"> <li>- Low cytotoxicity compared to other conventional crosslinkers</li> <li>- Mechanical tunability</li> <li>- Crosslinking specificity to primary amines</li> <li>- Low swelling ratio</li> <li>- Resistance to enzymatic</li> </ul>	<ul style="list-style-type: none"> <li>- Low cellular infiltration</li> <li>- Cytotoxicity increases at physiological temperature</li> <li>- Unsuitable for <i>in situ</i> gelation due to protein crosslinking</li> </ul>

degradation		
1-ethyl-3-(3-dimethylaminopropyl) carbodiimide hydrochloride (EDC)[135-136, 144]	<ul style="list-style-type: none"> <li>- Rapid gelation</li> <li>- Neutral reaction conditions</li> <li>- Forms favorable network structure for cellular attachment</li> </ul>	<ul style="list-style-type: none"> <li>- Rapid degradation</li> <li>- Toxic side products inhibit use in injectables</li> <li>- Unsuitable for in situ gelation due to protein crosslinking</li> </ul>

### 2.5.3. Bioorthogonal Click Chemistry in VF Biomaterials

Bioorthogonal click chemistry describes selective reactions that link molecules at high yield, do not require purification, and proceed safely *in vivo*.<sup>144-148</sup> Bioorthogonal click chemistries for *in situ* gelling VF injectables include Thiol-X, strain promoted azide-alkyne cycloaddition (SPAAC), and inverse electron demand Diels-Alder cycloaddition (IEDDAC) (**Table 4**).<sup>144,148</sup>

The MAP and HA-PEGDA hydrogels discussed previously were fabricated by the thiol-Michael thiol-X reaction.<sup>144,148-150</sup> The thiol-Michael reaction occurs through a thiol attacking an electron-deficient alkene, catalyzed by a base, primary amine, or phosphine.<sup>149</sup> A limitation is that catalysts may cause side reactions including disulfide bond formation, acrylate dimerization, and Aza-Michael addition.<sup>149,151</sup>

The light-catalyzed, radical-mediated thiol-ene reaction is a thiol-X without side reactions that proceeds between a thiol and an electron-rich alkene.<sup>152</sup> It has not yet been used to fabricate a VF injectable, but has been used to model the VF LP by reacting hyaluronan-norbornene of increasing concentrations (1-2.5%) with a UV-activated dithiol to produce three layers with differing stiffness. (**Figure 4A**).<sup>153</sup> A bench test showed that the scaffold could oscillate within the normal human speaking range (about 150Hz).<sup>153</sup> To prevent UV-induced tissue damage, VF injectables may be produced using visible light-catalyzed thiol-ene chemistry.<sup>152</sup>

SPAACs involve the reaction between strained ring cyclooctynes and aliphatic azides to form a triazole bond.<sup>154</sup> SPAACs do not require an external catalyst, but disadvantages include difficulty of cyclooctyne synthesis and low reaction yield.<sup>154</sup> A VF hydrogel was produced

from by SPAAC from four-arm PEG functionalized with azide and dibenzocyclooctyne (**Figure 4B**).<sup>97</sup> The storage modulus of the PEG hydrogel were low compared to native VF, less than 100 Pa. Nevertheless, the click PEG hydrogel showed increased stability compared to Radiesse® in a VF paralysis rabbit model after 16 weeks, albeit minimal cellular infiltration. Additionally, the PEG hydrogel remained within the thyroarytenoid muscle, while Radiesse® migrated to surrounding tissue and caused foreign body giant cell accumulation and vasculitis.<sup>97</sup>

IEDDACs are rapid reactions between dienes and alkenes or alkynes that forms a six-membered ring, do not require catalysts or react with moieties in tissue, and can occur at room and physiological temperatures.<sup>154-156</sup> IEDDACs have not yet been used for VF injectables, but have been used to model fibroblast differentiation during LP maturation.<sup>157,158</sup>

MSCs were first encapsulated in soft hydrogels formed by reaction between hyaluronan-tetrazine and a norbornene-functionalized MMP-degradable peptide, then stiffened by secondary reaction with hyaluronan-transcyclooctene after seven days (**Figure 4C**). Compared to hydrogels without secondary crosslinking, MSCs within the delayed-stiffening hydrogels upregulated expression of fibroblast (FAP, FSP1) and neo-ECM (collagen I, collagen III, fibronectin) markers matrix metalloproteinases, hyaluronan synthase 3, and regenerative growth factors (VEGF, HGF). To achieve delayed stiffening in an injectable biomaterial, a slow secondary crosslinker could be included in a rapidly gelling hydrogel. Overall, click chemistry shows great potential in VF tissue engineering for producing bioactive, injectable composites with tunable mechanical, physical, and degradation properties.

**Table 4. Advantages and Disadvantages of Click Crosslinking Methods**

Crosslinking Method	Advantages	Disadvantages	Vocal Fold Applications
Thiol-Michael[72, 75, 108, 149, 151]	<ul style="list-style-type: none"> <li>- Rapid reaction kinetics</li> <li>- High conversion rate</li> </ul>	<ul style="list-style-type: none"> <li>- Requires external catalyst</li> <li>- Potential for multiple products</li> <li>- Potential for heterogeneity and reduced stability</li> </ul>	<ul style="list-style-type: none"> <li>- RGD-conjugated PEG “MAP” hydrogel with tissue integration<sup>35</sup></li> <li>- HA-PEGDA hydrogel with collagens I and III<sup>34</sup></li> </ul>
Thiol-ene[152-	<ul style="list-style-type: none"> <li>- Rapid reaction</li> </ul>	<ul style="list-style-type: none"> <li>- UV light may</li> </ul>	<ul style="list-style-type: none"> <li>- Trilayered Hyaluronan <i>in</i></li> </ul>



153]	kinetics - Stable reactants - Potential for visible light catalyzation	induce toxicity - Ester bonds subject to hydrolysis	<i>vitro</i> model of the Lamina Propria* <sup>36</sup>
SPAAC[97, 154]	- Selectivity prevents reaction with biomolecules - No external catalyst	- Cyclooctene reactants are difficult to synthesize - Low reaction yield	- four arm PEG functionalized with azide and dibenzocyclooctyne <sup>37</sup>
IEDDAC[156-158]	- Crosslinks at room and physiological temperature - Selectivity prevents reaction with biomolecules - No external catalyst - Nitrogen gas only side product	- Typical alkenes may react slowly (norbornene) or lack aqueous stability (TCO)	- Core-Shell PCL-Hyaluronan <i>in vitro</i> model for modulating HVFF inflammatory response <sup>38</sup> - MSC differentiation into fibroblasts with delayed stiffening of Hyaluronan hydrogel by secondary click reaction <sup>39</sup>

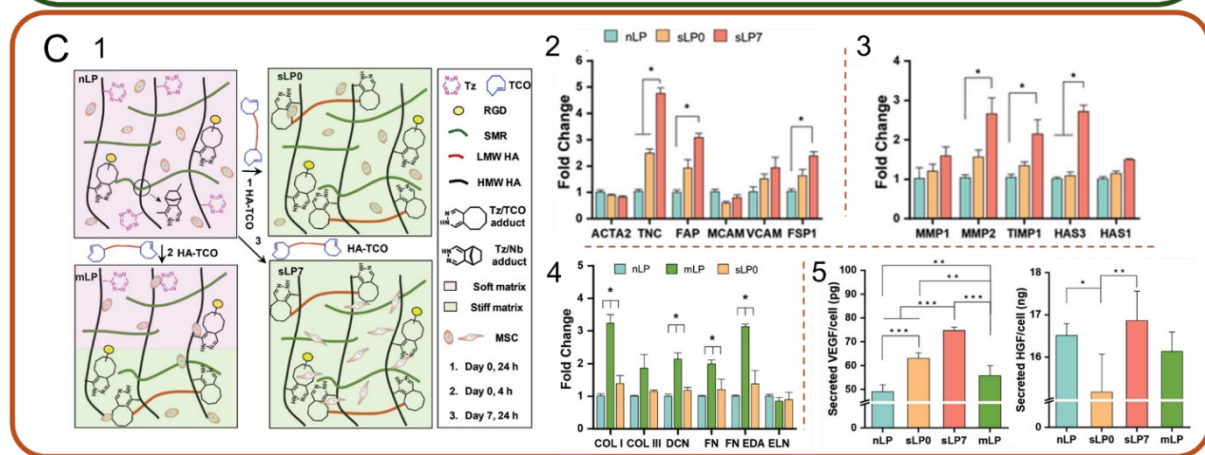
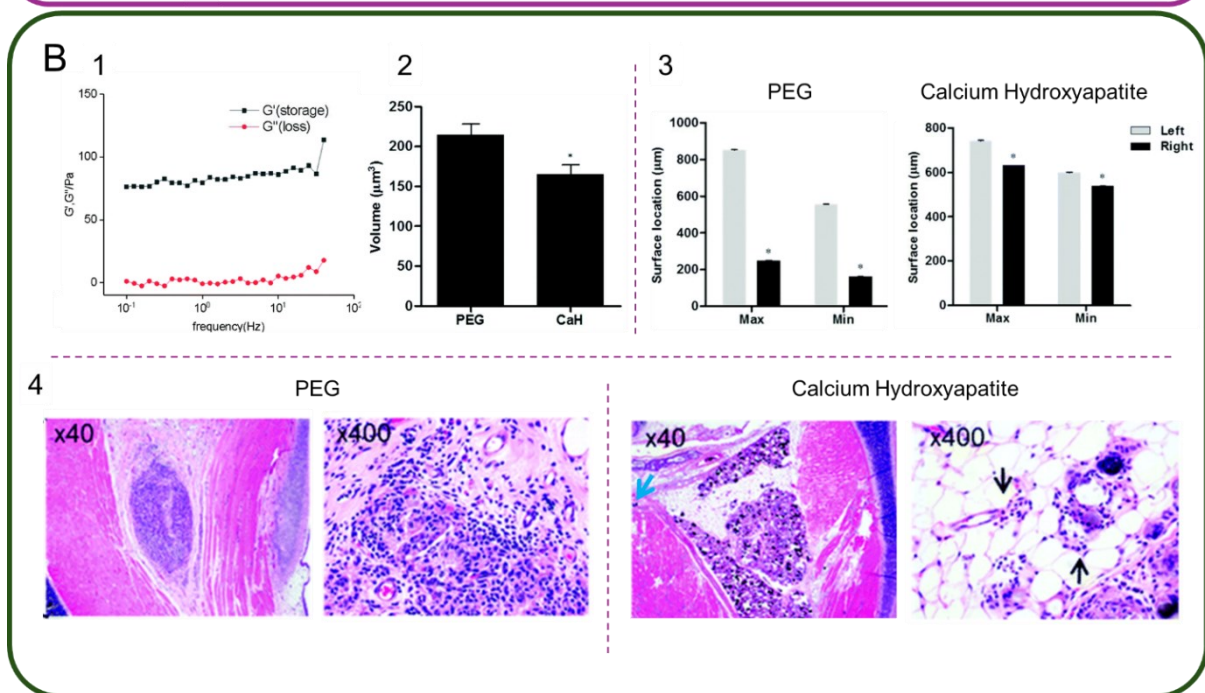
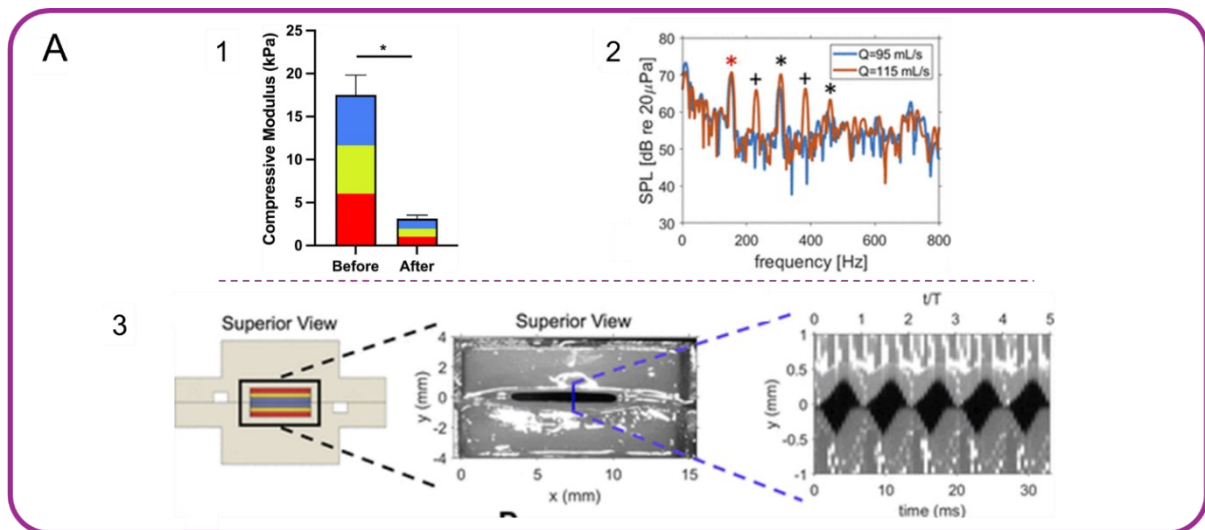


**Figure 4.** Click Chemistry in VF Tissue Engineering **A)** Tri-layer hyaluronan hydrogel produced by thiol-ene click chemistry vibrates to reproduce lamina propria structure. **1.** Compressive modulus of the tri-layer hydrogel is reduced by collagenase exposure. Red, yellow, and blue layers represent measurement of the composite, but do not have quantitative value within the figure. **2.** Sound pressure level and frequency for air flow at 95 and 115 mL/s. \* fundamental frequency \* harmonics. + subharmonics **3.** Vibration of trilayer hydrogels under airflow. \* $p < 0.05$ . **B)** Injectable PEG hydrogel fabricated by SPAAC for permanent VF augmentation. **1.** Storage and loss moduli of a Click 4% PEG hydrogel. **2.** Hydrogel volume 1 month after injection in mice. **3.** Location of VF at maximum and minimum amplitude of vibration. Lower values equate to more favorable results. **4.** Hemotoxylin and eosin staining of VF 16 weeks after injection. Blue arrow: Calcium-hydroxylapatite migrated to muscle tissue. Black arrows: vasculitis in adipose tissue. \* $p < 0.05$ . **C)** Hyaluronan hydrogels with delayed stiffening fabricated by IEDDAC for differentiation of MSCs into fibroblasts. **1.** Schematic representing hydrogel fabrication process for each crosslinking condition. nLP or “newborn lamina propria” is homogeneously crosslinked only with norbornene. sLP0 or “stiff lamina propria 0” is homogeneously crosslinked with added TCO on day 0. sLP7 or “stiff lamina propria 7” is homogeneously crosslinked with added TCO on day 7. mLP or “mature lamina propria” has a stiff top layer and soft bottom layer produced by stopping the TCO reaction after 4 hours. **2.** Expression of fibroblast gene markers by MSCs on Day 14. **3.** Expression of ECM remodeling enzyme gene markers by MSCs on Day 14. **4.** Expression of ECM gene markers by MSCs on day 14. **5.** Secretion of regenerative growth factors VEGF and HGF by MSCs on day 14. Panel A is reproduced from Ref[153]. Panel B is reproduced from Ref[97]. Panel C is reproduced from Ref[158]<sup>39</sup>.

## 2.6. Discussion and Future Prospects

Injection laryngoplasty provides a minimally invasive, relatively low-cost procedure. However, there remains a need for a reconstructive injectable biomaterial capable of permanently augmenting VF function. To achieve this goal, a balance is required between biodegradability and sufficient biomaterial longevity to stimulate VF repair. Neither biomaterials requiring reinjection nor non-degradable materials are ideal for long-term VF augmentation.

Standard injection laryngoplasty may be capable of permanently restoring VF function if a regenerative biomaterial is replaced with neo-ECM as it degrades, but cannot treat fibrotic conditions in the superficial LP.<sup>96</sup> Surgical techniques to preventing vibratory disruption in intramucosal biomaterial injection are under investigation alongside biomaterials with scar-

remodeling potential.<sup>39,82</sup> Ultrafast laser surgery has been proposed to aid with localization by sub-surface ablation, i.e. the precise removal of tissue to form a void within the LP.<sup>36,159</sup> When sub-surface ablation was performed in a preliminary canine study (N = 1), biomaterial localization was observed within the void indicating the surgical techniques may aid in retention at the target region by creating a defect for the injectable biomaterial to fill.<sup>159</sup>

Intramucosal injection with autologous fat has been tested clinically with variable outcomes.<sup>60</sup> Researchers have begun to explore the possibility of using dECM hydrogels to remodel scars in the LP, though these studies have not yet reached the clinical phase.<sup>41,86</sup> In future development of intramucosal biomaterials, it is critical to mimic the native mechanical and physical properties of the LP, as mechanical mismatch is one of the reasons superficial injection of existing VF biomaterials disrupts vibratory function.

The need for minimally invasive permanent VF restoration may be fulfilled by injectable VF biomaterials with improved stability that stimulate reconstruction. Promising results have been achieved *in vitro* and in animal models for VF-mimicking composites of mechanically tunable polymers and regenerative ECM-based proteins or polysaccharides. Bioorthogonal click chemistry can enable improved safety for *in situ* gelling crosslinked biomaterials and incorporate features such as delayed stiffening to stimulate cellular behavior toward wound healing. These advanced tissue engineering techniques will greatly improve the efficacy of minimally invasive intramucosal and injection laryngoplasty treatments.

### **Author contribution**

**Mika Brown:** Conceptualization (lead), Writing – Original Draft (lead), Hideaki Okuyama: Writing – Review and Editing (supporting). Masaru Yamashita: Writing – Review and Editing (supporting). Maryam Tabrizian: Supervision (supporting), Writing – Review and Editing (supporting). Nicole Y.K. Li-Jessen: Supervision (lead), Conceptualization (supporting), Writing – Review and Editing (lead).

### **Declaration of competing interest**

The authors declare that they have no known competing financial interests or personal relationships that could have appeared to influence the work reported in this paper.

### **Acknowledgements**

This review was supported by the National Sciences and Engineering Research Council of Canada (RGPIN-2018–03843, RGPIN-2024-04235 and ALLRP 548623-19), Canada Research Chair research stipend (M.T. and N.Y.K.L.-J.) and the National Institutes of Health (R01 DC-018577-01A1). The presented content is solely the responsibility of the authors and does not necessarily represent the official views of the above funding agencies.

## 2.7. References

1. Hirano M, Kakita Y, Ohmaru K, et al. Structure and Mechanical Properties of the Vocal Fold1 1A portion of this article was presented at the Vocal Fold Physiology Conference, Kurume, Japan, in January 1980. In: Speech and Language. (Lass NJ. ed.) Elsevier: 1982; pp. 271-297.
2. Miri AK. Mechanical Characterization of Vocal Fold Tissue: A Review Study. *Journal of Voice* 2014;28(6):657-667, doi:<https://doi.org/10.1016/j.jvoice.2014.03.001>
3. Benboujja F, Hartnick C. Quantitative evaluation of the human vocal fold extracellular matrix using multiphoton microscopy and optical coherence tomography. *Scientific Reports* 2021;11(1):2440, doi:10.1038/s41598-021-82157-9
4. Sato K. Blood Vessels of the Larynx and Vocal Fold. In: Functional Histoanatomy of the Human Larynx. (Sato K. ed.) Springer Singapore: Singapore; 2018; pp. 287-303.
5. Kolosova K, Gao Q, Tuznik M, et al. Characterizing Vocal Fold Injury Recovery in a Rabbit Model With Three-Dimensional Virtual Histology. *The Laryngoscope* 2021;131(7):1578-1587, doi:<https://doi.org/10.1002/lary.29028>
6. Kazarine A, Kolosova K, Gopal AA, et al. Multimodal virtual histology of rabbit vocal folds by nonlinear microscopy and nano computed tomography. *Biomed Opt Express* 2019;10(3):1151-1164, doi:10.1364/BOE.10.001151
7. Heris HK, Miri AK, Ghattamaneni NR, et al. Microstructural and mechanical characterization of scarred vocal folds. *J Biomech* 2015;48(4):708-711, doi:10.1016/j.jbiomech.2015.01.014
8. Muñoz-Pinto D, Whittaker P, Hahn MS. Lamina propria cellularity and collagen composition: an integrated assessment of structure in humans. *J Annals of Otolaryngology and Laryngology* 2009;118(4):299-306
9. Li NY, Heris HK, Mongeau L. Current Understanding and Future Directions for Vocal Fold Mechanobiology. *J Cytol Mol Biol* 2013;1(1):001, doi:10.13188/2325-4653.1000001
10. Hahn MS, Kobler JB, Zeitels SM, et al. Quantitative and comparative studies of the vocal fold extracellular matrix II: collagen. *Ann Otol Rhinol Laryngol* 2006;115(3):225-32, doi:10.1177/000348940611500311
11. Chen FM, Liu X. Advancing biomaterials of human origin for tissue engineering. *Progress in Polymer Science* 2016;53(86-168, doi:10.1016/j.progpolymsci.2015.02.004
12. Li L, Stiadle JM, Lau HK, et al. Tissue Engineering-Based Therapeutic Strategies for Vocal Fold Repair and Regeneration. *Biomaterials* 2016;108(91-110, doi:10.1016/j.biomaterials.2016.08.054
13. Švejsová A, Dršata J, Mejzlík J, et al. Injection laryngoplasty with hyaluronic acid for glottal insufficiency in unilateral vocal fold paralysis: a systematic review of the literature.

European Archives of Oto-Rhino-Laryngology 2022;279(11):5071-5079, doi:10.1007/s00405-022-07437-0

14. Bhatt NK, Garber D, Baertsch H, et al. Treatments for Age-related Vocal Atrophy: A Systematic Review. *The Laryngoscope* 2023;n/a(n/a), doi:<https://doi.org/10.1002/lary.30653>
15. Li R, Wong I, Zhang R, et al. 446. VOCAL FOLD AUGMENTATION REDUCES PNEUMONIA INCIDENCE IN PATIENTS WITH IATROGENIC RECURRENT LARYNGEAL NERVE PALSY AFTER ESOPHAGECTOMY. *Diseases of the Esophagus* 2023;36(Supplement\_2):doad052.235, doi:10.1093/dote/doad052.235
16. Rapoport SK, Alnouri G, Sataloff RT, et al. Acute vocal fold paresis and paralysis after COVID-19 infection: a case series. *J Annals of Otology, Rhinology and Laryngology* 2022;131(9):1032-1035
17. Hamilton NJI. The life-cycle and restoration of the human vocal fold. *Laryngoscope Investigative Otolaryngology* 2023;8(1):168-176, doi:<https://doi.org/10.1002/lio2.993>
18. Bruzzi C, Salsi D, Minghetti D, et al. Presbiphonia. *Acta bio-medica : Atenei Parmensis* 2017;88(1):6-10, doi:10.23750/abm.v88i1.5266
19. Baertsch HC, Bhatt NK, Giliberto JP, et al. Quantification of Vocal Fold Atrophy in Age-Related and Parkinson's Disease-Related Vocal Atrophy. *The Laryngoscope* 2023;133(6):1462-1469, doi:<https://doi.org/10.1002/lary.30394>
20. Almutawa D, Lagos-Villaseca A, Albathi M, et al. Geriatric Voice: Distinctive Clinical Profiles of Working Seniors in a Tertiary Laryngology Clinic. *Journal of Voice* 2024, doi:<https://doi.org/10.1016/j.jvoice.2023.12.018>
21. Sato K. Atrophy of the Vocal Fold. In: *Functional Histoanatomy of the Human Larynx*. (Sato K. ed.) Springer Singapore: Singapore; 2018; pp. 317-328.
22. Medeiros N, Castro MEM, van Lith-Bijl JT, et al. A Systematic Review on Surgical Treatments for Sulcus Vocalis and Vocal Fold Scar. *The Laryngoscope* 2022;132(4):822-830, doi:<https://doi.org/10.1002/lary.29665>
23. Alghonaim Y, Roskies M, Kost K, et al. Evaluating the timing of injection laryngoplasty for vocal fold paralysis in an attempt to avoid future type 1 thyroplasty. *Journal of otolaryngology - head & neck surgery = Le Journal d'oto-rhino-laryngologie et de chirurgie cervico-faciale* 2013;42(1):24, doi:10.1186/1916-0216-42-24
24. Prendes BL, Yung KC, Likhterov I, et al. Long-term effects of injection laryngoplasty with a temporary agent on voice quality and vocal fold position. *The Laryngoscope* 2012;122(10):2227-2233, doi:<https://doi.org/10.1002/lary.23473>
25. Bhatt NK, Pipkorn P, Paniello RCJAoO, Rhinology, et al. Association between upper respiratory infection and idiopathic unilateral vocal fold paralysis. 2018;127(10):667-671
26. Li-Jessen NY, Ridgway C. Neuroanatomy of voice and swallowing. *Neurologic and Neurodegenerative Diseases of the Larynx* 2020;21-40
27. Czesak MA, Osuch-Wójcikiewicz E, Niemczyk K. Methods of surgical treatment of bilateral vocal fold paralysis. *J Endokrynologia Polska* 2020;71(4):350-358
28. Shaili P. Vocal Cord Paralysis. In: *Updates on Laryngology*. (Balwant Singh G. ed.) IntechOpen: Rijeka; 2022; pp. Ch. 4.
29. Novakovic D, Nguyen DD, Chacon A, et al. Injection laryngoplasty as adjunct treatment method for muscle tension dysphonia: Preliminary findings. *Laryngoscope* 2020;130(4):980-985, doi:10.1002/lary.28205
30. Liu AQ, Ji Y, Hu A. Do patients regret having in-office vocal fold injections for glottic insufficiency? *Journal of Otolaryngology - Head & Neck Surgery* 2023;52(1):33, doi:10.1186/s40463-023-00643-8

31. Tam S, Sun H, Sarma S, et al. Medialization thyroplasty versus injection laryngoplasty: a cost minimization analysis. *Journal of Otolaryngology - Head & Neck Surgery* 2017;46(1):14, doi:10.1186/s40463-017-0191-5
32. Mallur PS, Rosen CA. Vocal fold Injection: Review of Indications, Techniques, and Materials for Augmentation. *Clinical experimental otorhinolaryngology* 2010;3(4):177
33. Gao WZ, Paoletti MF, Bensoussan Y, et al. Prospective >12 Months Outcomes After Vocal Fold Injection Medialization With Silk Microparticle-Hyaluronic Acid Material. *The Laryngoscope* 2023;n/a(n/a), doi:<https://doi.org/10.1002/lary.31039>
34. Gupta T, Ali Y, Sudan S, et al. Injection medialisation laryngoplasty: an alternative approach for challenging cases. *The Journal of Laryngology & Otology* 2023;137(12):1406-1408, doi:10.1017/S0022215123000038
35. Lasso JM, Poletti D, Scola B, et al. Injection laryngoplasty using autologous fat enriched with adipose-derived regenerative stem cells: a safe therapeutic option for the functional reconstruction of the glottal gap after unilateral vocal fold paralysis. *Stem Cells International* 2018;2018(1):8917913
36. Andrus L, Jeon H, Pawlowski M, et al. Ultrafast laser surgery probe for sub-surface ablation to enable biomaterial injection in vocal folds. *Scientific Reports* 2022;12(1):20554, doi:10.1038/s41598-022-24446-5
37. Umeno H, Tanaka H-i, Kurita T, et al. Long-Term Effects of Fat Injection Laryngoplasty in Relation to the Injected Fat Volume in Patients With Unilateral Vocal Fold Paralysis. *Journal of Voice* 2022, doi:<https://doi.org/10.1016/j.jvoice.2022.08.020>
38. Anderson TD, Sataloff RT. Complications of collagen injection of the vocal fold: report of several unusual cases and review of the literature. *Journal of Voice* 2004;18(3):392-397
39. Nozawa M, Takahashi S, Kanazawa T, et al. Intracordal injection therapy for vocal fold scarring: Steroid versus basic fibroblast growth factor. *Laryngoscope Investig Otolaryngol* 2022;7(5):1465-1473, doi:10.1002/lio2.881
40. Cates DJ, Simpson CB, Rosen CA. Awake Superficial Vocal Fold Injection. In: *Operative Techniques in Laryngology*. (Rosen CA, Simpson CB. eds.) Springer International Publishing: Cham; 2024; pp. 353-358.
41. Mora-Navarro C, Badileanu A, Gracioso Martins AM, et al. Porcine Vocal Fold Lamina Propria-Derived Biomaterials Modulate TGF- $\beta$ 1-Mediated Fibroblast Activation in Vitro. *Acs Biomater Sci Eng* 2020;6(3):1690-1703
42. Rosen CA, Simpson CB. Principles of Vocal Fold Augmentation. In: *Operative Techniques in Laryngology*. (Rosen CA, Simpson CB. eds.) Springer International Publishing: Cham; 2024; pp. 147-152.
43. Ryu CH, Kwon T-K, Kim H, et al. Guidelines for the management of unilateral vocal fold paralysis from the Korean society of laryngology, phoniatrics and logopedics. *J Clinical experimental otorhinolaryngology* 2020;13(4):340-360
44. Rowland Payne CME, Verner I, Cotofana S. Fillers and Soft Tissue Augmentation. In: *European Handbook of Dermatological Treatments*. (Katsambas AD, Lotti TM, Dessinioti C, et al. eds.) Springer International Publishing: Cham; 2023; pp. 1271-1305.
45. Matsuzaki H, Makiyama K. Collagen Injection for the Elderly with Dysphonia. *Aging Voice* 2017;67-74
46. Brake DA, Patel RR, Risser RM, et al. Treatment Outcomes of Type 1 Thyroplasty Using Gore-Tex® Following Injection Laryngoplasty. *J Annals of Otolaryngology*

Laryngology 2023;132(8):930-937

47. Bishop R, Mousset M, Althubaiti A, et al. Effect of injection laryngoplasty material on outcomes in pediatric vocal fold paralysis. *Translational pediatrics* 2022;11(7):1114-1121, doi:10.21037/tp-21-361
48. Kharidia KM, Bensoussan Y, Rosen CA, et al. Variations in Practices and Preferences of Vocal Fold Injection Materials: A National Survey. *J The Laryngoscope* 2023;133(5):1176-1183
49. Seo KK. Volumizing Fillers. In: *Facial Volumization with Fillers*. Springer: 2021; pp. 29-83.
50. Cheung HK, Han TT, Marecak DM, et al. Composite hydrogel scaffolds incorporating decellularized adipose tissue for soft tissue engineering with adipose-derived stem cells. *Biomaterials* 2014;35(6):1914-23, doi:10.1016/j.biomaterials.2013.11.067
51. Henriques DP, Martins RHG, Cataneo AJM. Efficacy of Injectable Laryngoplasty With Hyaluronic Acid and/or Calcium Hydroxyapatite in the Treatment of Glottic Incompetence. Systematic Review and Meta-analysis. *Journal of Voice* 2023, doi:<https://doi.org/10.1016/j.jvoice.2023.01.020>
52. Ting JY, Patel R, Halum SL. Managing Voice Impairment After Injection Laryngoplasty. *Journal of Voice* 2012;26(6):797-800, doi:<https://doi.org/10.1016/j.jvoice.2012.02.004>
53. DeFatta RA, Chowdhury FR, Sataloff RT. Complications of Injection Laryngoplasty Using Calcium Hydroxylapatite. *Journal of Voice* 2012;26(5):614-618, doi:<https://doi.org/10.1016/j.jvoice.2011.08.005>
54. Din-Lovinescu C, Talmor G, Gravina A, et al. Adverse events following injection laryngoplasty: An analysis of the MAUDE database. *American Journal of Otolaryngology* 2021;42(6):103092, doi:<https://doi.org/10.1016/j.amjoto.2021.103092>
55. Chang W-D, Chen S-H, Tsai M-H, et al. Autologous Fat Injection Laryngoplasty for Unilateral Vocal Fold Paralysis. 2021.
56. Lahav Y, Malka-Yosef L, Shapira-Galitz Y, et al. Vocal fold fat augmentation for atrophy, scarring, and unilateral paralysis: long-term functional outcomes. *J Otolaryngology–Head* 2021;164(3):631-638
57. Lin Y-H, Wang C-TJAoO, Rhinology, Laryngology. Salvage Treatments for Poor Voice Outcomes Following Autologous Fat Injection Laryngoplasty. 2022;00034894221140777
58. Prstačić R, Slipac J, Živković Ivanović T, et al. Autologous fat augmentation in the treatment of unilateral vocal fold paralysis—a 15-year experience in a single institution. *Acta Clinica Croatica* 2020;59(Supplement 1):32-37
59. Sanderson JD, Simpson CB. Laryngeal complications after lipoinjection for vocal fold augmentation. *Laryngoscope* 2009;119(8):1652-7, doi:10.1002/lary.20529
60. Lee B-J. Autologous Materials for Vocal Fold Augmentation. In: *Vocal Fold Injection*. (Lee B-J, Kwon T-K, Rosen CA. eds.) Springer Singapore: Singapore; 2021; pp. 79-85.
61. Carroll TL. Ideal Material Selection for Vocal Fold Augmentation. In: *Vocal Fold Injection*. (Lee B-J, Kwon T-K, Rosen CA. eds.) Springer Singapore: Singapore; 2021; pp. 73-78.
62. Dwyer CD, Kridgen S, Chiang S, et al. Silk-Hyaluronic Acid for Vocal Fold Augmentation: Safety Profile and Long-Term Voice Outcomes. *Journal of Voice* 2024, doi:<https://doi.org/10.1016/j.jvoice.2024.02.025>
63. Brown JE, Gulka CP, Giordano JEM, et al. Injectable Silk Protein Microparticle-based



- Fillers: A Novel Material for Potential Use in Glottic Insufficiency. *Journal of Voice* 2019;33(5):773-780, doi:<https://doi.org/10.1016/j.jvoice.2018.01.017>
64. Dwyer CD, Devore E, Kridgen S, et al. Preliminary Results on the Safety and Efficacy of Silk-Hyaluronic Acid for Treatment of Glottic Insufficiency. *Journal of Voice* 2022, doi:<https://doi.org/10.1016/j.jvoice.2022.11.009>
  65. Yu SE, DeVore EK, Carroll TL. Histologic Evaluation of Silk-Hyaluronic Acid After Human Vocal Fold Injection. *Journal of Voice* 2024, doi:<https://doi.org/10.1016/j.jvoice.2023.12.015>
  66. Prete S, Dattilo M, Patitucci F, et al. Natural and Synthetic Polymeric Biomaterials for Application in Wound Management. 2023.
  67. Vishwakarma A, Bhise NS, Evangelista MB, et al. Engineering Immunomodulatory Biomaterials To Tune the Inflammatory Response. *Trends in Biotechnology* 2016;34(6):470-482, doi:<https://doi.org/10.1016/j.tibtech.2016.03.009>
  68. Ng W-C, Lokanathan Y, Fauzi MB, et al. In vitro evaluation of genipin-crosslinked gelatin hydrogels for vocal fold injection. *Scientific Reports* 2023;13(1):5128, doi:10.1038/s41598-023-32080-y
  69. Khan MUA, Aslam MA, Abdullah MFB, et al. Recent perspective of polymeric biomaterial in tissue engineering—a review. *Materials Today Chemistry* 2023;34(101818)
  70. Chelu M, Musuc AM. Advanced Biomedical Applications of Multifunctional Natural and Synthetic Biomaterials. 2023.
  71. Akhtar A, Farzam Rad V, Moradi A-R, et al. Emerging polymeric biomaterials and manufacturing-based tissue engineering approaches for neuro regeneration-A critical review on recent effective approaches. *Smart Materials in Medicine* 2023;4(337-355, doi:<https://doi.org/10.1016/j.smaim.2022.11.007>
  72. Walimbe T, Calve S, Panitch A, et al. Incorporation of types I and III collagen in tunable hyaluronan hydrogels for vocal fold tissue engineering. *Acta Biomaterialia* 2019;87(97-107, doi:<https://doi.org/10.1016/j.actbio.2019.01.058>
  73. Hiwatashi N, Hirano S, Mizuta M, et al. The efficacy of a novel collagen–gelatin scaffold with basic fibroblast growth factor for the treatment of vocal fold scar. *Journal of tissue engineering and regenerative medicine* 2017;11(5):1598-1609
  74. Choi J-S, Heang Oh S, Kim Y-M, et al. Hyaluronic Acid/Alginate Hydrogel Containing Hepatocyte Growth Factor and Promotion of Vocal Fold Wound Healing. *Tissue Engineering and Regenerative Medicine* 2020;17(5):651-658, doi:10.1007/s13770-020-00280-6
  75. King RE, Lau HK, Zhang H, et al. Biocompatibility and Viscoelastic Properties of Injectable Resilin-Like Polypeptide and Hyaluronan Hybrid Hydrogels in Rabbit Vocal Folds. *Regenerative Engineering and Translational Medicine* 2019;5(4):373-386, doi:10.1007/s40883-019-00094-6
  76. Kim S, Lee H-Y, Lee HR, et al. Liquid-type plasma-controlled in situ crosslinking of silk-alginate injectable gel displayed better bioactivities and mechanical properties. *Materials Today Bio* 2022;15(100321, doi:<https://doi.org/10.1016/j.mtbio.2022.100321>
  77. Gaston J, Thibeault SL. Hyaluronic acid hydrogels for vocal fold wound healing. *Biomatter* 2013;3(1):e23799
  78. Bucciarelli A, Motta A. Use of Bombyx mori silk fibroin in tissue engineering: From cocoons to medical devices, challenges, and future perspectives. *Biomaterials Advances* 2022;139(212982, doi:<https://doi.org/10.1016/j.bioadv.2022.212982>
  79. Reyes Valenzuela A, Bao G, Vikstrom A, et al. Polymeric microspheres containing human vocal fold fibroblasts for vocal fold regeneration. *J The Laryngoscope*

2021;131(8):1828-1834

80. Deng Y, Shavandi A, Okoro OV, et al. Alginate modification via click chemistry for biomedical applications. *Carbohydrate Polymers* 2021;270(118360, doi:<https://doi.org/10.1016/j.carbpol.2021.118360>
81. Kim YM, Oh SH, Choi JS, et al. Adipose-derived stem cell-containing hyaluronic acid/alginate hydrogel improves vocal fold wound healing. *The Laryngoscope* 2014;124(3):E64-E72
82. Bouhabel S, Park S, Kolosova K, et al. Functional Analysis of Injectable Substance Treatment on Surgically Injured Rabbit Vocal Folds. *Journal of Voice* 2023;37(6):829-839, doi:<https://doi.org/10.1016/j.jvoice.2021.06.001>
83. Coburn PT, Herbay AC, Berrini M, et al. An in vitro assessment of the response of THP-1 macrophages to varying stiffness of a glycol-chitosan hydrogel for vocal fold tissue engineering applications. *Journal of Biomedical Materials Research Part A* 2021;109(8):1337-1352
84. Ravanbakhsh H, Bao G, Latifi N, et al. Carbon nanotube composite hydrogels for vocal fold tissue engineering: Biocompatibility, rheology, and porosity. *Materials Science and Engineering: C* 2019;103(109861, doi:<https://doi.org/10.1016/j.msec.2019.109861>
85. Brown M, Li J, Moraes C, et al. Decellularized extracellular matrix: New promising and challenging biomaterials for regenerative medicine. *Biomaterials* 2022;289(121786
86. Hu J-J, Lei X-X, Jiang Y-L, et al. Scarless vocal fold regeneration by urine-derived stem cells and small intestinal submucosa hydrogel composites through enhancement of M2 macrophage Polarization, neovascularization and Re-epithelialization. *Smart Materials in Medicine* 2022;3(339-351
87. Brown M, Zhu S, Taylor L, et al. Unraveling the Relevance of Tissue-Specific Decellularized Extracellular Matrix Hydrogels for Vocal Fold Regenerative Biomaterials: A Comprehensive Proteomic and In Vitro Study. *Advanced NanoBiomed Research* 2023;3(4):2200095
88. Pitman MJ, Kurita T, Powell ME, et al. Vibratory function and healing outcomes after small intestinal submucosa biomaterial implantation for chronic vocal fold scar. *The Laryngoscope* 2018;128(4):901-908, doi:<https://doi.org/10.1002/lary.26883>
89. Xu CC, Mau T. A tissue-specific, injectable acellular gel for the treatment of chronic vocal fold scarring. *Acta Biomaterialia* 2019, doi:10.1016/j.actbio.2019.08.025
90. Pitman MJ, Cabin JA, Jacob CE. Small Intestinal Submucosa Implantation for the Possible Treatment of Vocal Fold Scar, Sulcus, and Superficial Lamina Propria Atrophy. *Ann Otol Rhinol Laryngol* 2016;125(2):137-44, doi:10.1177/0003489415601685
91. Spang MT, Middleton R, Diaz M, et al. Intravascularly infused extracellular matrix as a biomaterial for targeting and treating inflamed tissues. *Nature Biomedical Engineering* 2023;7(2):94-109, doi:10.1038/s41551-022-00964-5
92. Wang T, Huang Q, Rao Z, et al. Injectable decellularized extracellular matrix hydrogel promotes salivary gland regeneration via endogenous stem cell recruitment and suppression of fibrogenesis. *Acta Biomaterialia* 2023;169(256-272, doi:<https://doi.org/10.1016/j.actbio.2023.08.003>
93. Diaz MD, Kandell RM, Wu JR, et al. Infusible Extracellular Matrix Biomaterial Promotes Vascular Integrity and Modulates the Inflammatory Response in Acute Traumatic Brain Injury. *Advanced Healthcare Materials* 2023;n/a(n/a):2300782, doi:<https://doi.org/10.1002/adhm.202300782>
94. Rahmani F, Atabaki R, Behrouzi S, et al. The recent advancement in the PLGA-based

- thermo-sensitive hydrogel for smart drug delivery. *International Journal of Pharmaceutics* 2023;631(122484, doi:<https://doi.org/10.1016/j.ijpharm.2022.122484>)
95. Fruijtier-Pöloth C. Safety assessment on polyethylene glycols (PEGs) and their derivatives as used in cosmetic products. *Toxicology* 2005;214(1-2):1-38
  96. Pruett LJ, Kenny HL, Swift WM, et al. De novo tissue formation using custom microporous annealed particle hydrogel provides long-term vocal fold augmentation. *NPJ Regenerative Medicine* 2023;8(1):10
  97. Kwon S, Choi H, Park C, et al. In vivo vocal fold augmentation using an injectable polyethylene glycol hydrogel based on click chemistry. *Biomaterials Science* 2021;9(1):108-115, doi:[10.1039/D0BM01155J](https://doi.org/10.1039/D0BM01155J)
  98. Choi YH, Ahn H-J, Park MR, et al. Dual growth factor-immobilized bioactive injection material for enhanced treatment of glottal insufficiency. *Acta Biomaterialia* 2019;86(269-279, doi:<https://doi.org/10.1016/j.actbio.2018.12.047>)
  99. Kroger SM, Hill L, Jain E, et al. Design of Hydrolytically Degradable Polyethylene Glycol Crosslinkers for Facile Control of Hydrogel Degradation. *Macromolecular Bioscience* 2020;20(10):2000085, doi:<https://doi.org/10.1002/mabi.202000085>
  100. Ibrahim M, Ramadan E, Elsadek NE, et al. Polyethylene glycol (PEG): The nature, immunogenicity, and role in the hypersensitivity of PEGylated products. *Journal of Controlled Release* 2022;351(215-230, doi:<https://doi.org/10.1016/j.jconrel.2022.09.031>)
  101. Shi D, Beasock D, Fessler A, et al. To PEGylate or not to PEGylate: Immunological properties of nanomedicine's most popular component, polyethylene glycol and its alternatives. *Advanced Drug Delivery Reviews* 2022;180(114079, doi:<https://doi.org/10.1016/j.addr.2021.114079>)
  102. Kwon SK, Kim H-B, Song J-J, et al. Vocal Fold Augmentation with Injectable Polycaprolactone Microspheres/Pluronic F127 Hydrogel: Long-Term In Vivo Study for the Treatment of Glottal Insufficiency. *PLOS ONE* 2014;9(1):e85512, doi:[10.1371/journal.pone.0085512](https://doi.org/10.1371/journal.pone.0085512)
  103. Raina N, Pahwa R, Khosla JK, et al. Polycaprolactone-based materials in wound healing applications. *Polymer Bulletin* 2021;1-23
  104. Hu J-J, Wang M, Lei X-X, et al. Scarless healing of injured vocal folds using an injectable hyaluronic acid-waterborne polyurethane hybrid hydrogel to tune inflammation and collagen deposition. *ACS Applied Materials & Interfaces* 2022;14(38):42827-42840
  105. Calleros EL, Simonovsky FI, Garty S, et al. Crosslinked, biodegradable polyurethanes for precision-porous biomaterials: Synthesis and properties. *Journal of Applied Polymer Science* 2020;137(25):48943
  106. van Minnen B, Stegenga B, van Leeuwen MBM, et al. A long-term in vitro biocompatibility study of a biodegradable polyurethane and its degradation products. *Journal of Biomedical Materials Research Part A* 2006;76A(2):377-385, doi:<https://doi.org/10.1002/jbm.a.30531>
  107. Singh S, Kumar Paswan K, Kumar A, et al. Recent Advancements in Polyurethane-based Tissue Engineering. *ACS Applied Bio Materials* 2023;6(2):327-348, doi:[10.1021/acsabm.2c00788](https://doi.org/10.1021/acsabm.2c00788)
  108. Pruett L, Koehn H, Martz T, et al. Development of a microporous annealed particle hydrogel for long-term vocal fold augmentation. *The Laryngoscope* 2020;130(10):2432-2441
  109. Hansson A, Hashom N, Falson F, et al. In vitro evaluation of an RGD-functionalized chitosan derivative for enhanced cell adhesion. *Carbohydrate Polymers* 2012;90(4):1494-1500, doi:<https://doi.org/10.1016/j.carbpol.2012.07.020>

110. Bidarra SJ, Barrias CC, Fonseca KB, et al. Injectable in situ crosslinkable RGD-modified alginate matrix for endothelial cells delivery. *Biomaterials* 2011;32(31):7897-7904, doi:<https://doi.org/10.1016/j.biomaterials.2011.07.013>
111. Causa F, Battista E, Della Moglie R, et al. Surface investigation on biomimetic materials to control cell adhesion: the case of RGD conjugation on PCL. *Langmuir* 2010;26(12):9875-9884
112. Ho Y-C, Mi F-L, Sung H-W, et al. Heparin-functionalized chitosan–alginate scaffolds for controlled release of growth factor. *International Journal of Pharmaceutics* 2009;376(1):69-75, doi:<https://doi.org/10.1016/j.ijpharm.2009.04.048>
113. Princz M, Sheardown H. Heparin-modified dendrimer cross-linked collagen matrices for the delivery of basic fibroblast growth factor (FGF-2). *Journal of Biomaterials Science, Polymer Edition* 2008;19(9):1201-1218
114. Truong NF, Kurt E, Tahmizyan N, et al. Microporous annealed particle hydrogel stiffness, void space size, and adhesion properties impact cell proliferation, cell spreading, and gene transfer. *Acta Biomater* 2019;94(160-172, doi:10.1016/j.actbio.2019.02.054
115. Xu H, Fan GK. The role of cytokines in modulating vocal fold fibrosis: a contemporary review. *The Laryngoscope* 2021;131(1):139-145
116. Ban MJ, Lee SC, Park JH, et al. Regenerative efficacy of fibroblast growth factor for the treatment of aged vocal fold: from animal model to clinical application. *Clinical Otolaryngology* 2021;46(1):131-137
117. Teixeira SP, Domingues RM, Shevchuk M, et al. Biomaterials for sequestration of growth factors and modulation of cell behavior. *Advanced Functional Materials* 2020;30(44):1909011
118. Hirano S, Bless D, Heisey D, et al. Roles of Hepatocyte Growth Factor and Transforming Growth Factor  $\beta$ 1 in Production of Extracellular Matrix by Canine Vocal Fold Fibroblasts. *The Laryngoscope* 2003;113(1):144-148, doi:<https://doi.org/10.1097/00005537-200301000-00027>
119. Imaizumi M, Nakamura R, Nakaegawa Y, et al. Regenerative potential of basic fibroblast growth factor contained in biodegradable gelatin hydrogel microspheres applied following vocal fold injury: Early effect on tissue repair in a rabbit model. *Brazilian Journal of Otorhinolaryngology* 2021;87(274-282
120. Kobayashi T, Mizuta M, Hiwatashi N, et al. Drug delivery system of basic fibroblast growth factor using gelatin hydrogel for restoration of acute vocal fold scar. *Auris Nasus Larynx* 2017;44(1):86-92
121. Hertegård S, Nagubothu SR, Malmström E, et al. Hyaluronan hydrogels for the local delivery of mesenchymal stromal cells to the injured vocal fold. *Stem Cells Development* 2019;28(17):1177-1190
122. Hertegård S, Nagubothu SR, Malmström E, et al. Treatment of vocal fold scarring with autologous bone marrow-derived human mesenchymal stromal cells—first phase I/II human clinical study. *Stem cell research & therapy* 2020;11(1-11
123. Svistushkin M, Shpichka A, Bikmulina P, et al. Vocal fold restoration after scarring: biocompatibility and efficacy of an MSC-based bioequivalent. *Stem Cell Research & Therapy* 2023;14(1):303
124. Imaizumi M, Li-Jessen NY, Sato Y, et al. Retention of human-induced pluripotent stem cells (hiPS) with injectable HA hydrogels for vocal fold engineering. *Annals of Otology, Rhinology & Laryngology* 2017;126(4):304-314
125. Yi B, Xu Q, Liu W. An overview of substrate stiffness guided cellular response and its

- applications in tissue regeneration. *Bioactive Materials* 2022;15(82-102, doi:<https://doi.org/10.1016/j.bioactmat.2021.12.005>
126. Chhetri DK, Zhang Z, Neubauer J. Measurement of Young's Modulus of Vocal Folds by Indentation. *Journal of Voice* 2011;25(1):1-7, doi:<https://doi.org/10.1016/j.jvoice.2009.09.005>
  127. Teller SS, Farran AJ, Xiao L, et al. High-frequency viscoelastic shear properties of vocal fold tissues: implications for vocal fold tissue engineering. *Tissue Engineering Part A* 2012;18(19-20):2008-2019
  128. Heris HK, Miri AK, Tripathy U, et al. Indentation of poroviscoelastic vocal fold tissue using an atomic force microscope. *J Mech Behav Biomed Mater* 2013;28(383-92, doi:10.1016/j.jmbbm.2013.05.026
  129. Miri AK, Heris HK, Mongeau L, et al. Nanoscale viscoelasticity of extracellular matrix proteins in soft tissues: A multiscale approach. *J Mech Behav Biomed Mater* 2014;30(196-204, doi:10.1016/j.jmbbm.2013.10.022
  130. Zou C-Y, Hu J-J, Lu D, et al. A self-fused hydrogel for the treatment of glottic insufficiency through outstanding durability, extracellular matrix-inducing bioactivity and function preservation. *Bioactive Materials* 2023;24(54-68, doi:<https://doi.org/10.1016/j.bioactmat.2022.12.006>
  131. Faivre J, Pigweh AI, Iehl J, et al. Crosslinking hyaluronic acid soft-tissue fillers: Current status and perspectives from an industrial point of view. *Expert Review of Medical Devices* 2021;18(12):1175-1187
  132. Wang C-T, Liao L-J, Huang T-W, et al. Preliminary report of vocal fold augmentation with cross-linked porcine collagen. *Otolaryngology--Head and Neck Surgery* 2012;146(4):606-610
  133. Abay A, Simionato G, Chachanidze R, et al. Glutaraldehyde – A Subtle Tool in the Investigation of Healthy and Pathologic Red Blood Cells. *Frontiers in physiology* 2019;10(
  134. McKenzie A. Glutaraldehyde: A review of its fixative effects on nucleic acids, proteins, lipids, and carbohydrates. 2019;
  135. Adamiak K, Sionkowska A. Current methods of collagen cross-linking: Review. *International Journal of Biological Macromolecules* 2020;161(550-560, doi:<https://doi.org/10.1016/j.ijbiomac.2020.06.075>
  136. Sapuła P, Bialik-Wąs K, Malarz K. Are Natural Compounds a Promising Alternative to Synthetic Cross-Linking Agents in the Preparation of Hydrogels? 2023.
  137. Moshnikova AB, Afanasyev VN, Proussakova OV, et al. Cytotoxic activity of 1-ethyl-3-(3-dimethylaminopropyl)-carbodiimide is underlain by DNA interchain cross-linking. *Cellular and Molecular Life Sciences CMLS* 2006;63(2):229-234, doi:10.1007/s00018-005-5383-x
  138. Yu Y, Xu S, Li S, et al. Genipin-cross-linked hydrogels based on biomaterials for drug delivery: A review. *Biomaterials science* 2021;9(5):1583-1597
  139. Wang Z, Liu H, Luo W, et al. Regeneration of skeletal system with genipin crosslinked biomaterials. *Journal of Tissue Engineering* 2020;11(2041731420974861
  140. Somers P, De Somer F, Cornelissen M, et al. Genipin blues: an alternative non-toxic crosslinker for heart valves? *J Journal of Heart Valve Disease* 2008;17(6):682
  141. Kawamura T, Yunoki S, Ohyabu Y, et al. Crosslinking Efficacy and Cytotoxicity of Genipin and Its Activated Form Prepared by Warming It in a Phosphate Buffer: A Comparative Study. 2021.
  142. Choi YH, Kim SH, Kim IG, et al. Injectable basic fibroblast growth factor-loaded

- alginate/hyaluronic acid hydrogel for rejuvenation of geriatric larynx. *Acta Biomaterialia* 2019;89(104-114, doi:<https://doi.org/10.1016/j.actbio.2019.03.005>
143. Zhang J, Ke J, Zhu Y, et al. Influence of divalent cations on the biofouling behaviors of alginate hydrogels. 2019;15(1):015003
  144. Hermanson GT. Chapter 17 - Chemoselective Ligation; Bioorthogonal Reagents. In: *Bioconjugate Techniques* (Third Edition). (Hermanson GT. ed.) Academic Press: Boston; 2013; pp. 757-785.
  145. Anseth KS, Klok H-A. Click chemistry in biomaterials, nanomedicine, and drug delivery. ACS Publications: 2016.
  146. Xu ZH, Bratlie KM. Click Chemistry and Material Selection for in Situ Fabrication of Hydrogels in Tissue Engineering Applications. *Acs Biomater Sci Eng* 2018;4(7):2276-2291, doi:10.1021/acsbiomaterials.8b00230
  147. Hermanson GT. Chapter 3 - The Reactions of Bioconjugation. In: *Bioconjugate Techniques* (Third Edition). (Hermanson GT. ed.) Academic Press: Boston; 2013; pp. 229-258.
  148. Reddy N, Reddy R, Jiang Q. Crosslinking biopolymers for biomedical applications. *Trends Biotechnol* 2015;33(6):362-9, doi:10.1016/j.tibtech.2015.03.008
  149. Chatani S, Gong T, Earle BA, et al. Visible-Light Initiated Thiol-Michael Addition Photopolymerization Reactions. *ACS Macro Letters* 2014;3(4):315-318, doi:10.1021/mz500132j
  150. Pruett LJ, Kenny HL, Swift WM, et al. De novo tissue formation using custom microporous annealed particle hydrogel provides long-term vocal fold augmentation. *NPJ Regen Med* 2023;8(1):10, doi:10.1038/s41536-023-00281-8
  151. Zhang D, Dumont M-J, Cherestes A. An efficient strategy for the synthesis of 5-hydroxymethylfurfural derivative based poly ( $\beta$ -thioether ester) via thiol-Michael addition polymerization. *J RSC advances* 2016;6(86):83466-83470
  152. Pirola V, Benassi A, Doria F. Lights on 2,5-diaryl tetrazoles: applications and limits of a versatile photoclick reaction. *Photochemical & Photobiological Sciences* 2022;21(5):879-898, doi:10.1007/s43630-022-00173-8
  153. Tindell RK, McPhail MJ, Myers CE, et al. Trilayered Hydrogel Scaffold for Vocal Fold Tissue Engineering. *Biomacromolecules* 2022;23(11):4469-4480, doi:10.1021/acs.biomac.1c01149
  154. Mueller E, Poulin I, Bodnaryk WJ, et al. Click Chemistry Hydrogels for Extrusion Bioprinting: Progress, Challenges, and Opportunities. *Biomacromolecules* 2022;23(3):619-640, doi:10.1021/acs.biomac.1c01105
  155. Desai RM, Koshy ST, Hilderbrand SA, et al. Versatile click alginate hydrogels crosslinked via tetrazine-norbornene chemistry. *Biomaterials* 2015;50(30-37
  156. Mayer SV, Murnauer A, von Wrisberg MK, et al. Photo-Induced and Rapid Labeling of Tetrazine-Bearing Proteins via Cyclopropanone-Caged Bicyclononynes. *Angew Chem Int Ed Engl* 2019, doi:10.1002/anie.201908209
  157. Ravikrishnan A, Zhang H, Fox JM, et al. Core-Shell Microfibers via Bioorthogonal Layer-by-Layer Assembly. *ACS Macro Letters* 2020;9(9):1369-1375, doi:10.1021/acsmacrolett.0c00515
  158. Zou X, Zhang H, Benson JM, et al. Modeling the Maturation of the Vocal Fold Lamina Propria Using a Bioorthogonally Tunable Hydrogel Platform. *Advanced Healthcare Materials* 2023;n/a(n/a):2301701, doi:<https://doi.org/10.1002/adhm.202301701>
  159. Andrus L, Camli B, Mau T, et al. Ultrafast Laser Microlaryngeal Surgery for In Vivo Subepithelial Void Creation in Canine Vocal Folds. *Laryngoscope* 2023;133(11):3042-3048,

doi:10.1002/lary.30713

160. Oleksy, M., K. Dynarowicz, and D. Aebisher *Advances in Biodegradable Polymers and Biomaterials for Medical Applications—A Review*. *Molecules*, 2023. **28**, DOI: 10.3390/molecules28176213.

161. Lee, J.H., et al., *Evaluation of the poly (lactic-co-glycolic acid)/pluronic F127 for injection laryngoplasty in rabbits*. *Otolaryngology--Head and Neck Surgery*, 2014. **151**(5): p. 830-835.

## Preface to Chapter 3

Decellularized extracellular matrix (dECM) biomaterials show robust potential for tissue engineering applications due to their innate regenerative capacity. This potential is derived from the complex mixture of proteins, glycosaminoglycans, and bioactive small molecules that comprise dECM. A notable challenge in the development of dECM biomaterials is to reproduce the physicochemical properties of native tissue, which vary from tissue to tissue. A wide variety of techniques have been used in dECM biomaterial development, creating a need for comprehensive assessment of the current state of technology and how diverse strategies may be applied to achieve effective regenerative outcomes.

In Chapter 3, we review literature in the field of decellularized extracellular matrix biomaterials focusing primarily on hydrogels, electrospun scaffolds, and bioprinted scaffolds. This review acts as a comprehensive look into the use of dECM biomaterials in various tissues. The unique requirements for application in each organ and tissue are emphasized, and promising methodologies for achieving these specifications are highlighted. Tissue-specific material design approaches suitable for application to different organs and tissues are systematically addressed. We discuss advantages and limitations of dECM biomaterials currently under investigation and discuss how innovative methodologies may be incorporated into dECM biomaterial design to improve regenerative efficacy.

This work was published in *Biomaterials* in 2022.

Mika Brown, Jianyu Li, Christopher Moraes, Maryam Tabrizian, and Nicole YK Li-Jessen. "Decellularized extracellular matrix: New promising and challenging biomaterials for regenerative medicine." *Biomaterials* 289 (2022): 121786.



## **Chapter 3. Decellularized extracellular matrix: New promising and challenging biomaterials for regenerative medicine.**

### *Abstract*

Extracellular matrix is rich in biomolecules including structural proteins, glycosaminoglycans, and small molecules that are important for the maintenance and repair of tissue. Decellularized extracellular matrix (dECM) is expected to retain these key biomolecules and makes it a promising biomaterial candidate for regenerative medicine applications. To date, dECM-particle based biomaterials have been developed to engineer over 15 tissue types or organs, with the ultimate goal of mimicking specific biological and physical properties of the native tissue. The most common scaffold types are injectable hydrogels, electrospun scaffolds and bioprinted scaffolds. The purpose of this review paper is to highlight key challenges, fabrication methods and progress made for each tissue type, along with the discussion of other elements that are integral to push dECM biomaterials towards effective and specialized tissue repair.

### *3.1. Introduction*

The native tissue niche is made up of multiple cell types surrounded by extracellular matrix (ECM). The ECM provides a structural and supportive network as well as presents a plethora of extracellular signaling molecules to the residing cells.<sup>1</sup> The molecular interaction between ECM and cells are intricate and reciprocal, enabling the regulation of various processes involved in tissue homeostasis and wound healing such as cell growth, migration, differentiation, and neo-ECM production. One imperative challenge in tissue engineering (TE) has been to accurately reproduce the physicochemical properties, or complex biological and physical features of native ECM for functional tissue repair in regenerative medicine. These physicochemical properties include surface structure, pore size, mechanical properties, biocompatibility and cellular adhesion, and biodegradability.<sup>2</sup>

Biomaterials produced from decellularized ECM (dECM) have the potential to support specialized cell types and trigger the innate regenerative process by providing a microenvironment close to the native target tissue.<sup>3</sup> During decellularization, cells and immunogenic molecules are largely removed while most structural proteins [e.g., collagen, elastin, fibronectin etc.] and macromolecules [e.g., proteoglycans, glycosaminoglycans (GAGs) etc.] are mostly preserved.<sup>4</sup>

Urinary bladder matrix (UBM) and small intestinal submucosa (SIS) are common dECM biomaterials approved by the Food and Drug Administration to fabricate regenerative biomaterials with proven outcomes in defected skin, muscle, and gastrointestinal tissues.<sup>5-14</sup>

Initially, decellularized organs or dECM sheets were designed for total organ or tissue replacement and regeneration.<sup>15,16</sup> However, the decellularization process can significantly diminish the structural stability and mechanical properties of whole decellularized organs or dECM sheets. These changes lead to an environment that less accurately matches the native tissue's physicochemical properties, suboptimal cell-matrix interactions, and healing outcomes.<sup>4,17-19</sup> Recent research efforts have expanded from replacing the defected tissue with whole dECM organs to producing biomaterials from micronized dECM particles or powders followed by reconstituting them into various forms of biomaterials such as hydrogels, electrospun scaffolds, and bioprinted scaffolds.<sup>17,20-22</sup> In the fabrication process, the properties and structure of these biomaterials can be designed to fill irregular defects and match native tissue physicochemical properties, particularly the mechanics.

In this article, we reviewed more than 300 original research papers on dECM-particle based biomaterials published in peer-reviewed journals between January 2012 and December 2021 (**Figure 1**). The final literature search was performed in July 2022 with combinations of the search terms “decellularized extracellular matrix”, “hydrogels”, “electrospun”, “bioprint”, and “biomaterial” in the databases Scopus®, Web of Science®, and Google Scholar®. dECM biomaterials such as ECM sheets and whole organ scaffolds that did not undergo homogenization into particles were excluded from this review. The number of dECM particle-derived biomaterial articles significantly grew from 7 papers in 5 tissue types in 2012 to 93 papers in 19 tissue types in 2021.

The most common dECM-particle biomaterials were injectable hydrogels (N = 162/305; ~53%) followed by bioprinted scaffolds (N = 61; ~20%), and electrospun scaffolds (N = 46; 15%) (**Figure 1-2**). The fabrication of injectable dECM hydrogels is mostly based on pepsin solubilization.<sup>23,24</sup> For clinical administration, injectable dECM hydrogels are favourable as they are less invasive and adapt to more irregular shapes than implanted scaffolds.<sup>25</sup> dECM particles are first suspended in a solution of pepsin and hydrochloric acid. Once solubilized, the pH is neutralized to

physiological level and the dECM-particle forms a hydrogel at physiological temperature. dECM-based hydrogels also retain growth factors and bioactive signaling cues of native ECM, they also possess high water content similar to natural tissue. Chemical or physical crosslinking is frequently required to improve the gelation kinetics and mechanics of dECM hydrogels.<sup>26</sup>

Electrospinning dECM is conducted by applying high voltage to a metallic needle containing a solubilized dECM solution.<sup>17</sup> Microfibers are drawn through the needle's tip and deposited onto a collector, on which the fibers are layered into a scaffold of the desired shape and architecture. A key advantage of electrospun scaffolds is that the layered microfibers can be designed to approximate the architecture of ECM networks. For instance, electrospinning can be used to systematically manipulate the diameter and distribution of ECM fibers to induce cell-specific functions such as adhesion and migration.<sup>27</sup>

dECM bioink is generally prepared through pepsin solubilization and can be printed in conjunction with cells and a synthetic polymer bioink.<sup>28,29</sup> The dECM bioink can be deposited drop by drop following a pattern that matches the dimensions and structure of a defect or organ. Bioprinted scaffolds can be designed, or patterned, to replicate the varying characteristics of layered ECM structures, mostly with extrusion-based and laser-assisted bioprinters. For instance, bioprinted dECM scaffolds can include layers with differential mechanical properties and tissue-specific cells.<sup>30</sup> This feature represents a unique advantage for enabling complex cellularity and ECM structure, promoting tissue vascularization, and repairing large defects.

In sum, dECM-based biomaterials can be developed to produce tissue-specific physical and chemical cues that help promote the body's intrinsic capacity for self-repair and regeneration.<sup>19,31,32</sup> Of the 19 tissue types identified, the TE application of dECM-particle biomaterials is more developed in 9 specific tissues (cardiac, cartilage, neural, adipose, muscle, liver, bone, skin, and lung), in which more than 15 research articles and across 3 biomaterial types were identified in literature. Their corresponding design challenges, goals and progress, as well as future prospects in each tissue application are presented in detailed herein. For other certain tissue types (gastrointestinal, ocular, kidney, pancreas, and vocal folds), the application of dECM-particle biomaterials started to gain traction, with at least 4 articles published to date. The recent progress of dECM-based TE in these tissues are summarized in brief. Lastly, we discuss the future

directions of dECM-based biomaterials with respect to goal of achieving tissue-specific functional tissue repair and regeneration in a reproducible and scalable manner.

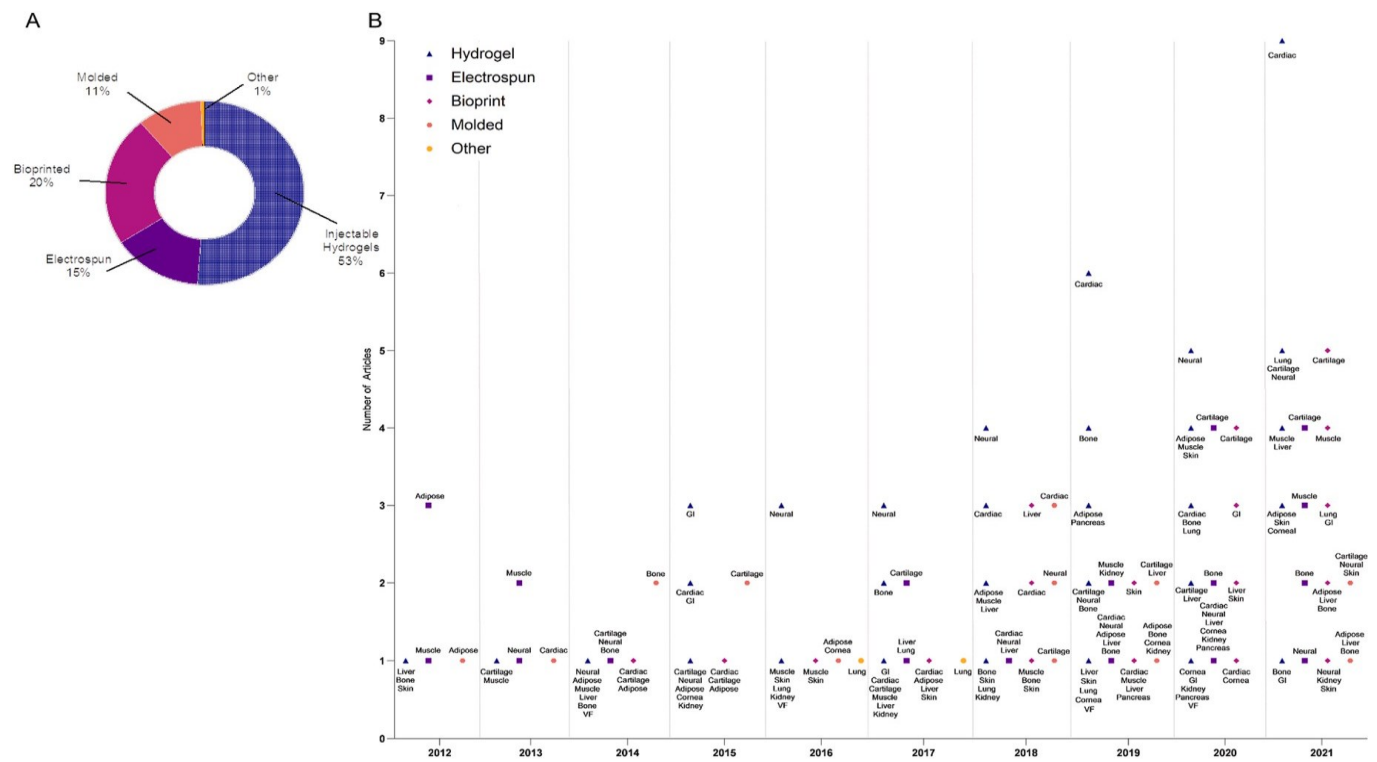


**Figure 1.** Summary of Articles Published Between January 2012 and June 2021 for each dECM Biomaterial Type. A. Number of dECM-particle original research articles published for each fabrication method. B. Number of dECM-particle original research articles of each tissue type across individual year. Abbreviations: Gastrointestinal (GI), Vocal Fold (VF).

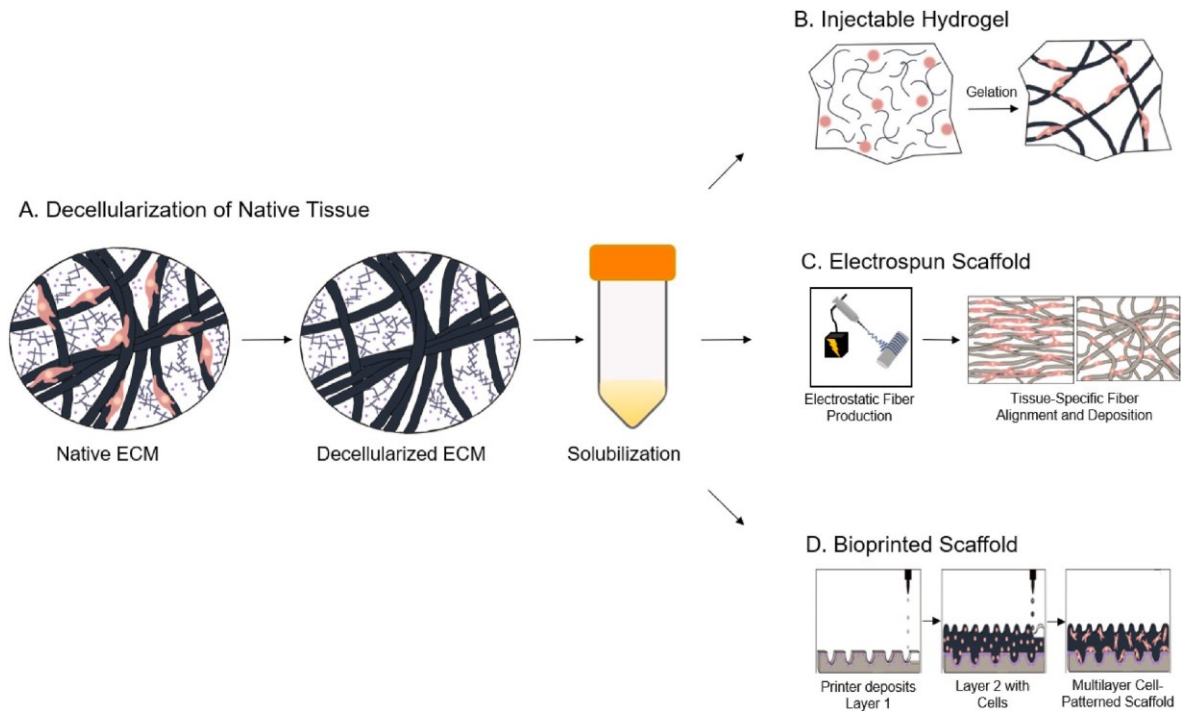


**Figure 2. Three Common dECM Biomaterial Types.** **A.** Native tissue is first decellularized with surfactants, acids, alcohols, nucleases, or salts and solubilized with pepsin. **B.** Injectable Hydrogels. Pre-gels can be injected to fill irregular tissue defects. During gelation, dECM fibers form an ECM-like network for cells to attach. **C.** Electrospun Scaffolds. Polymer fibers can be electrostatically deposited to match ECM fiber alignments of the target tissues for the maturation of cell phenotypes and the adaptation of native cell morphology. **D.** Bioprinted Scaffolds. A pre-gel can be patterned with or without cells to match the native 3D tissue microstructure. Bioprinting is particularly useful for tissues with multiple layers or zones, cell types, and functional features such as glands and ducts.

### 3.2. Progress in key tissue types in dECM TE

#### 3.2.1. Cardiac dECM TE

The heart is composed of cardiac muscle, valves, and blood vessels, wherein the myocardium is the thickest muscular layer that withstands its rapid, repeated contraction and electrical conduction (**Figure 3A**).<sup>33</sup> Cardiovascular diseases (CVD) such as myocardial infarction led to the rapid death of hundreds of millions of cardiac muscle cells, or cardiomyocytes (CM). As CM are terminally

differentiated, they do not divide and expand. Human hearts thus have minimal intrinsic regeneration capacity.<sup>34,35</sup> Heart transplants and implanted devices are therapeutic options for end-stage heart diseases. However, transplant rejection or the side effects of immunosuppression (e.g., malignancy, infection etc.) can cause secondary heart failure.<sup>36</sup>

Cardiac TE seeks to enhance the survival and retention of stem cells in situ by providing biodegradable, vascularized patches with the elasticity, conductivity, and contractility of cardiac muscle to replicate the native CM niche.<sup>37-39</sup> Due to the limited proliferation capacity of CM, cell availability is an ongoing challenge in cardiac TE. Stem cell therapies have shown some promise in stimulating functional CM regeneration. However, most cells are lost to the bloodstream after injection. Existing patches have a high risk of inflammation and largely fail to support sufficient contractility and conductivity for CM function.<sup>40,41</sup> Chronic heart failure is also documented in these treatments, typically resulting in death within five years.<sup>41</sup>

Cardiac-specific dECM biomaterials are designed to replicate cardiac mechanics and provide cues at precise timepoints for stem cell differentiation into CM and functional cardiac tissue reconstruction.<sup>34,42</sup> CM differentiation is indicated by gene markers such as MYH6, MYH7, SAC, GATA4, Hand1 and Hand2.<sup>42,43</sup> One physiological target for cardiac dECM biomaterials is to recapitulate the shear modulus (7–42 kPa), electrical conduction velocity (29–45 cm/s) and contractile force (9–12 mN/mm<sup>2</sup>) as in human hearts.<sup>44-47</sup> Another target is to promote capillary genesis through the release of native angiogenic growth factors.<sup>48,49</sup> Cardiac dECM biomaterials have thus far focused on patches and injectable hydrogels, and bioprinted scaffolds to repair and revascularize cardiac tissue (**Table 1**).

#### *3.2.1.1. Injectable hydrogels in cardiac dECM TE*

In cardiac TE, the primary goal of injectable dECM hydrogels is to stimulate CM differentiation from stem cells and revascularize ischemic cardiac tissue. SIS is already clinically applied to the repair of ischemic cardiac tissue.<sup>49</sup> When human umbilical vein ECs (HUVECs) and fibroblasts were co-cultured on SIS hydrogels and Col I controls, the formation of capillaries were observed only on SIS hydrogels after 7 days.<sup>49</sup> When injected subcutaneously in rats, the SIS gels generated a greater capillary density (165–305/mm<sup>2</sup>) after 7 days compared to Col I (4–32/mm<sup>2</sup>).

As SIS is not identical to cardiac tissue, dECM hydrogels derived from cardiac tissues were also

evaluated for their cardiomyogenic capacity. CM differentiation from ASCs was compared in cardiac dECM hydrogels or cardiac inductive cocktail with significant upregulation of CM markers over the cocktail in ASC cultures.<sup>42</sup> In a rat study, initial blood vessel formation was increased three-fold in cardiac dECM hydrogels over Col I 3 days after subcutaneous injection.<sup>50</sup>

However, cardiac dECM hydrogels had poor mechanical tunability and closed and disconnected pores, which limited cell-scaffold integration.<sup>40</sup> Subsequent cardiac dECM hydrogels were modified to replicate cardiac mechanics. For example, chitosan was added to a dECM hydrogel to improve pore size and connectivity.<sup>40</sup> Compared to a gelatin-chitosan control, the dECM-chitosan hydrogel exhibited improved conduction velocity (9–17 vs 3–12 cm/s) and contractile force (0.65–0.92 vs 0.46–0.72 mN/mm<sup>2</sup>), yet remained well below native CMs. Another composite of cardiac dECM-alginate was developed with improved long-term mechanical stability.<sup>41</sup> Over 28 days, the compressive modulus was better preserved in the dECM-alginate composite (at ~29 kPa) than the alginate-only controls (reduced to ~15 kPa).

PEG was also used to fabricate cardiac dECM composite hydrogels.<sup>51</sup> Hydrogel mechanics were tuned by PEG type (Star PEG-NHS, star PEG acrylate) and crosslinking method (EDAC and radical polymerization). Radical polymerization induced rapid gelation (4 min) compared to EDAC and dECM alone (30 min). Also, these cardiac dECM-PEG hydrogels were shown with highly tunable mechanics in viscoelastic moduli, gelation kinetics and degradation rate while maintaining CM viability.<sup>51</sup> The higher gelation rate could also prevent CM loss to the bloodstream. Additionally, only hydrogels fabricated from star PEG acrylate achieved higher shear moduli, tunable up to 719 Pa, than dECM alone (5–30 Pa). However, the material mechanics were still below the favorable range (7–42 kPa) for physiological CM function.<sup>47,51</sup>

In another study, electrically conductive gold and laponite nanoparticles were incorporated into dECM hydrogels to enhance differentiation into CM (**Figure 3B**).<sup>43</sup> Laponite increased pore interconnectivity for CM infiltration, while gold enhanced CM survival. After 48 h, over 90% of CMs survived on the composites and had begun forming aligned sarcomere structures. Further testing beyond 48 h would provide a more effective illustration of conductivity's impact on cardiomyogenesis. Together, these studies indicate that composite cardiac dECM hydrogels could improve both mechanical tunability and CM activity for functional cardiac hydrogels.

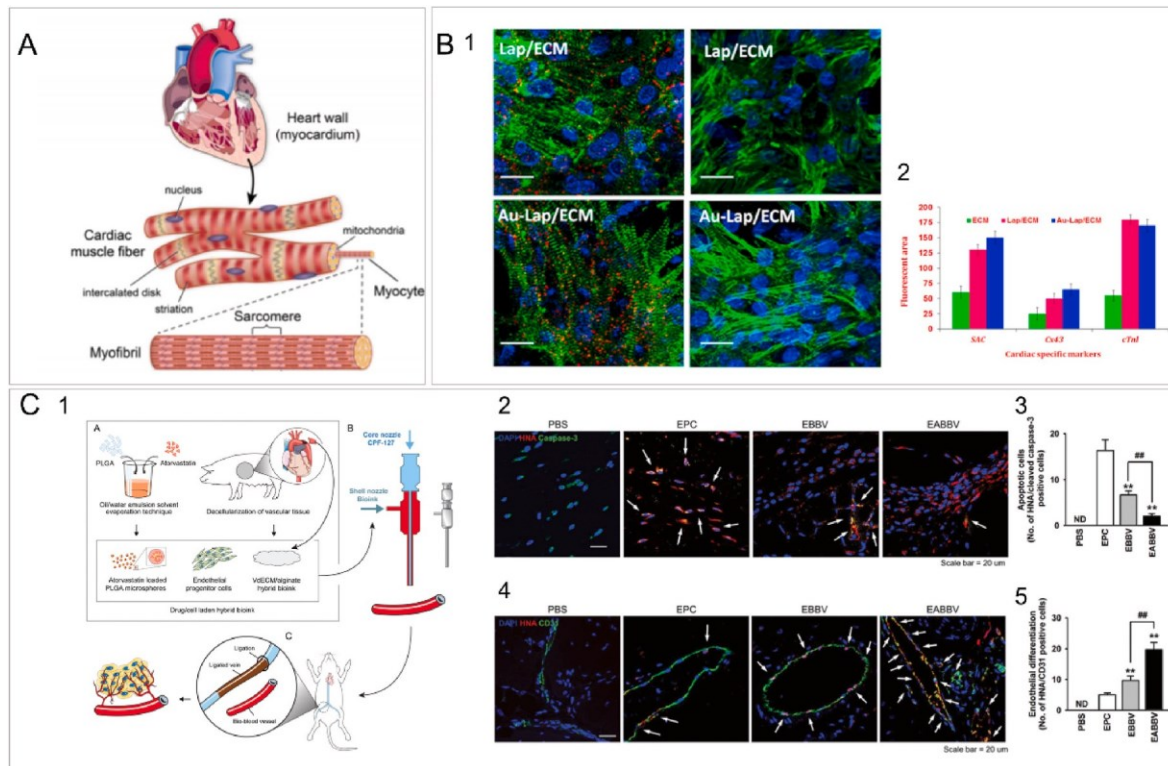


**Figure 3. Highlights of dECM Research in Cardiac TE.** **A.** Anatomy of the Heart's Myocardium. **B.** Injectable dECM hydrogels with Electrically Conductive Gold and Laponite Nanoparticles Enhance CM differentiation. **1.** Formation of aligned sarcomere structures by CM in culture. **2.** Expression of cardiac-specific markers within the sarcomere structures. **C.** Bioprinted BBV Stimulates Cardiac Differentiation in a Mouse Model. **1.** Schematic describing the fabrication and implantation of the BBV. **2.** Staining of Apoptotic cells in ischemic hindlimb tissue implanted with PBS, EPCs, EPC-laden BBV (EBBV), or EPC-laden BBV with loaded with atorvastatin (EABBV). **3.** Quantification of apoptotic cells. **4.** Fluorescence of EC-marker CD31 in ischemic hindlimb tissue implanted with PBS, EPCs, EBBV, or EABBV. **5.** Quantitative expression of CD31. Panel A. is reproduced from Ref. <sup>52</sup>; Panel B. is reproduced from Ref. <sup>43</sup>; Panel C. is reproduced from Ref. <sup>29</sup> with permissions.

### 3.2.1.2. Bioprinted scaffolds in cardiac dECM TE

Bioprinted cardiac dECM patches were designed to replicate the environmental niche of CMs and stimulate vascularization. <sup>24,44</sup> In Pati and Cho's proof-of-concept work, cardiac dECM bioink was printed without a polymer framework. <sup>28</sup> Myoblasts, CM precursors, upregulated markers of CM maturity when encapsulated in cardiac dECM bioink compared to a Col I control. Their



subsequent work was to fabricate disk-shaped cardiac patches, printed in a crosshatch structure from dECM and PCL bioinks.<sup>44</sup> When mesenchymal stromal cells (MSCs) and cardiac progenitor cells were printed in the scaffold, both cell types showed enhanced cell-cell interaction, differentiation, and maturation in vitro. Further, in a rat myocardial infarction model, the patches stimulated vascularization and functional cardiac reconstruction with reduced fibrosis compared to a Col I-PCL bioink.

The Bio-blood-vessel (BBV), another bioprinted dECM scaffold, was proposed as a low-risk vascular graft (Figure 3C).<sup>29</sup> BBV was an aortic dECM-alginate composite that encapsulated endothelial progenitor cells (EPCs) and the proangiogenic drug atorvastatin. The idea behind incorporating both dECM and atorvastatin was to improve nutrient delivery along with EPC differentiation. In a mouse hind limb ischemia model, the BBVs, which had tubular shapes similar to capillaries, provided an effective niche for stem cell differentiation in cardiac TE.

#### *3.2.1.3. Future prospects*

Tissue mechanics are crucial to the structure and function of the heart and blood vessels, yet many studies have not addressed this vital design element.<sup>37</sup> The impact of factors such as dECM biomaterial stiffness, elasticity, and conductivity on CM differentiation and tissue reconstruction should be addressed in comparison to native cardiac tissues. Laponite is considered a favorable composite material for enhancing dECM conductivity due to its biocompatibility in comparison to other conductive materials.<sup>24,53</sup> However, experiments with longer-time points are still needed to confirm scaffold support of viable CMs.<sup>41</sup>

Cardiac dECM biomaterials could go beyond cardiac patches and hydrogels and potentially act as a temporary stent for reconstruction of damaged vessels. Patches are mostly for repairing a small region of cardiac tissue. Instead, a bioprinted aortic model was designed as a 1:1 perfusable replica of the human aorta.<sup>54</sup> This first bioprinted aortic dECM model showed favorable survivability of aortic smooth muscle cells. However, mechanical failure of the aortic model occurred at a deformation of approximately half the elastic limit of native tissue. Drug-eluting cardiac stents composed of biodegradable polymers such as PLLA are commonly used in clinical settings but may lead to persistent inflammation and thrombosis following depletion of anti-proliferative, pro-endothelialization drugs and production of inflammatory degradation products.<sup>55,56</sup> An effective temporary stent is expected to match the mechanical properties of the aorta and prevent a repeat

failure of the vessel, while supporting arterial functions and cardiac tissue repair.<sup>57</sup> Temporary stents from bioprinted dECM materials may fulfill the aforesaid expectations given their capacity of tunable mechanical properties, modulating anti-inflammatory immune functions and stimulating native tissue repair.

Crosslinking protocols should be carefully selected when designing dECM composites to replicate cardiac mechanics. For example, EDAC and radical polymerization can both be cytotoxic at high crosslinker concentration.<sup>35,58</sup> These effects can be minimized by protocol design, but the potential cytotoxicity of fabrication methods should be thoroughly evaluated. These steps could lead to effective cardiac patches and angiogenic scaffolds with long-term efficacy.

**Table 1. Summary of dECM Particles in Cardiac Tissue Engineering.** Structural characterization includes SEM, FTIR, Raman, NMR, crosslinking efficiency, porosity, and swelling ratio. Mechanical characterization includes AFM, rheology, tensile testing, compressive testing, and electrical conductivity. Biological characterization includes in vitro studies, gene and protein assays, histology, and degradation kinetics. NU = Not Used. NA = Not Applicable. ND = Not Described.

Author/Year	Tissue Type	Decellularization Method			Homogenization Method		Material Composition			Fabrication Method	Characterization Method			
		Chemical Decellularization Solutions	Enzymatic Digestion	Protocol Length (Total Hours)	Mechanical Method	Solubilization	dECM only	Synthetic Addition	Natural Addition		Structural	Mechanical	Biological	Animal Model
Pok 2013 <sup>40</sup>	Porcine heart	dECM from	NA	NA	NA	NA			Chitosan	Molded	✓	✓	✓	
Pati 2014 <sup>28</sup>	Porcine adipose, cartilage, and heart	Christman Lab 0.5% or 1% SDS, Isopropanol, 0.1% Peracetic acid, 4% Ethanol, 1% Triton X-100	50 U/mL DNase, 1 U/mL RNase, 0.025% Trypsin	60–100	Mortar and Pestle	Pepsin		PCL		Scaffold Bioprinted Scaffold		✓	✓	
Grover 2015 <sup>51</sup>	Porcine heart	1% SDS	NU	120	Wiley Mini Mill	Pepsin		PEG		Injectable Hydrogel	✓	✓	✓	
Wang 2015 <sup>49</sup>	Porcine SIS	1:1 Methanol and chloroform, 0.05% EDTA, 0.5% SDS, 0.1% Peracetic acid, 20% Ethanol	0.05% Trypsin	28.5	Wiley Mini Mill	Pepsin	✓			Injectable Hydrogel	✓	✓	✓	✓
Claudio-Rizo 2017 <sup>18</sup>	Bovine heart, SIS, and tendon	100% Ethanol, 1% Triton X-100, 0.5% EDTA	0.5 mg/mL DNase, 2.5 mg/mL RNase	27–45	Mortar and Pestle	Pepsin	✓			Injectable Hydrogel	✓	✓	✓	
Jang 2017 <sup>44</sup>	Porcine heart	1% SDS, Triton X-100, 0.1% Peracetic Acid, 4% Ethanol	NU	125	Mortar and Pestle	Pepsin		PCL		Bioprinted Scaffold			✓	✓
Baghalishahi 2018 <sup>42</sup>	Rat heart	1% SDS, 1% Triton X-100	NU	76	ND	Pepsin	✓			Injectable Hydrogel	✓		✓	
Becker 2018 <sup>34</sup>	Human heart and amniotic membrane	0.1% EDTA, 0.5% or 1% SDS	NU	5–8	Precellys Ceramic kit and Minily's homogenizer	Pepsin	✓		Dual-ECM	Molded Scaffold	✓	✓	✓	
Bejleri 2018 <sup>37</sup>	Porcine ventricle	1% SDS	NU	120	ND Milling Method	Pepsin			GelMA	Bioprinted Scaffold		✓	✓	✓
Fujita 2018 <sup>35</sup>	Goat ventricle	1% SDS, 1% Triton X-100	NU	218	ND	Pepsin	✓			Molded Scaffold		✓	✓	
Gao 2018 <sup>29</sup>	Porcine aorta	0.3% SDS, 3% Triton X-100	NU	72	Mincing	Pepsin		PLGA	Alginate	Bioprinted Scaffold		✓	✓	✓
Hernandez 2018 <sup>59</sup>	Porcine lung, heart, and skeletal muscle	0.1% or 1% SDS	NU	ND	ND	Pepsin			Extracellular vesicles, microRNA	Injectable Hydrogel			✓	
Kim 2018 <sup>48</sup>	Rat heart, mouse liver, kidney, lung, and skin	0.01% and 1% SDS, 1% Triton X-100	NU	56–84	SPEX 6775	Pepsin		PCL		Electrospun Scaffold	✓	✓	✓	✓
Seo 2018 <sup>50</sup>	Rat heart	100% Ethanol, Liquid CO <sub>2</sub> , 1 M NaCl	2000 KU DNase	126	SPEX SamplePrep	Pepsin			Collagen	Injectable Hydrogel	✓		✓	

**Table 1** (continued)

Author/Year	Tissue Type	Decellularization Method			Homogenization Method		Material Composition			Fabrication Method	Characterization Method			
		Chemical Decellularization Solutions	Enzymatic Digestion	Protocol Length (Total Hours)	Mechanical Method	Solubilization	dECM only	Synthetic Addition	Natural Addition		Structural	Mechanical	Biological	Animal Model
Ventura 2018 <sup>60</sup>	Porcine skin	SDS, Triton X-100	NU	ND	ND	Pepsin	✓			Molded Scaffold	✓		✓	✓
Bai 2019 <sup>61</sup>	Rat heart	1% SDS, 1% Triton X-100	NU	102.5	ND	Pepsin	✓		Alginate	Injectable Hydrogel			✓	
Curley 2019 <sup>41</sup>	Porcine heart	0.16% Trizma hydrochloride, 0.05% and 0.6% EDTA, 0.05% Sodium azide, 3% Triton X-100, 4% Sodium deoxycholate, 0.1% Peracetic acid, 4% Ethanol	0.02% Trypsin	10	SPEX 6770	NU	✓			Injectable Hydrogel		✓	✓	
Das 2019 <sup>24</sup>	Porcine heart	1% SDS, 1% Triton X-100, Isopropanol, 0.1% Peracetic acid, 4% Ethanol	NU	151	Mortar and Pestle		✓			Bioprinted Scaffold		✓	✓	
Fu 2019 <sup>62</sup>	Porcine aorta	1% Triton X-100	NU	96	ND	Pepsin	✓			Injectable Hydrogel	✓		✓	✓
Qiao 2019 <sup>63</sup>	Rat and porcine heart	1% SDS	NU	72	ND	Pepsin	✓			Injectable Hydrogel	✓	✓	✓	✓
Reid 2019 <sup>64</sup>	Bovine aorta	0.5% SDS	NU	36	Retsch PM100	NU		PCL		Electrospun Scaffold	✓	✓	✓	
Roshanbinfar2019 <sup>65</sup>	Sheep pericardium	0.02% EDTA, 3% Triton X-100	0.05% Trypsin	26	Lyophilization	Pepsin		Carbon nanotubes		Injectable Hydrogel	✓	✓	✓	
Zhang 2019 <sup>43</sup>	Rat heart	1% SDS	NU	54	ND	Pepsin		Laponite clay and gold nanoparticles		Injectable Hydrogel	✓		✓	
Liguori 2020 <sup>66</sup>	Porcine heart	6 M NaCl, 70% Ethanol, 1% SDS, 1% Triton X-100	0.05% Trypsin, DNase	75	Commercial blender	Pepsin	✓			Injectable Hydrogel		✓	✓	
Rajabi 2020 <sup>67</sup>	Sheep skeletal muscle, cardiac muscle, aorta, and liver, Porcine SIS, human umbilical cord	0.5% SDS, 1% Triton X-100	NU	37-139	Mortar and Pestle	Pepsin	✓			Injectable Hydrogel			✓	



**Table 1** (continued )

Author/Year	Tissue Type	Decellularization Method			Homogenization Method		Material Composition			Biomaterial Type	Characterization Method			
		Chemical Decellularization Solutions	Enzymatic Digestion	Protocol Length (Total Hours)	Mechanical Method	Solubilization	dECM only	Synthetic Addition	Natural Addition		Structural	Mechanical	Biological	Animal Model
Reid 2020 <sup>68</sup>	Bovine heart and aorta	0.5% SDS	NU	36	Retsch PM100	NU	✓			Electrospun Scaffold	✓	✓	✓	
Bai 2021 <sup>61</sup>	Rat heart	1% SDS, 1% Triton X-100	NU	102.5	ND	Pepsin	✓			Injectable Hydrogel			✓	✓
Basara 2021 <sup>69</sup>	Human heart	1% SDS, 1% Triton X-100, Isopropanol	NU	25.5	ND	Pepsin			GelMA	Bioprinted Scaffold	✓	✓	✓	
Bejleri 2021 <sup>70</sup>	Porcine heart	1% SDS	NU	96–120	ND Milling Method	Pepsin			GelMA	Bioprinted Scaffold				✓
Diaz 2021 <sup>71</sup>	Porcine heart	SDS	NU	ND	ND Milling Method	Pepsin	✓			Injectable Hydrogel	✓			✓
Du 2021 <sup>72</sup>	Human fibroblast derived	0.25% Triton X-100	0.25 %	1–2	NU	NU			Collagen	Injectable Hydrogel			✓	✓
Ercan 2021 <sup>73</sup>	Bovine heart	0.45% and 1.8% NaCl, 1 SDS, 0.1% Peracetic acid, 4% ethanol	Trypsin, 50 U/mL DNase, 2.5 µL/mL RNase	102	Retsch MM400	Pepsin	✓			Injectable Hydrogel	✓	✓	✓	✓
Gomez-Cid 2021 <sup>74</sup>	Porcine heart	1% SDS, 1% Peracetic acid	NU	120–144	Mincing	Pepsin		PEG		Injectable Hydrogel	✓	✓	✓	✓
Guan 2021 <sup>75</sup>	Porcine spleen	1% SDS	NU	96	ND	Pepsin	✓			Bioprinted Scaffold	✓	✓	✓	✓
Kang 2021 <sup>76</sup>	Porcine heart, liver, and colon	1% SDS, 1% Triton X-100, Isopropanol, 0.1% Peracetic acid, 4% ethanol	NU	142	ND	Pepsin	✓			Bioprinted Scaffold		✓	✓	
Kim 2021 <sup>77</sup>	Porcine heart and cornea	1% SDS, 1% Triton X-100, 0.1% Peracetic acid, 4% Ethanol	NU	145	ND	Pepsin	✓			Bioprinted Scaffold	✓	✓	✓	
Kobayashi 2021 <sup>78</sup>	Porcine UBM and SIS	0.05% EDTA, 3% Triton X-100, 4% Sodium Deoxycholate, 0.1% Peracetic acid, 4% Ethanol, 0.1 M Citric Acid	0.02% Trypsin, 400 U/mL Dnase	333	IKA Tube Mill	Pepsin	✓			Injectable Hydrogel	✓	✓	✓	

**Table 1** (continued )

Author/Year	Tissue Type	Decellularization Method			Homogenization Method		Material Composition			Fabrication Method	Characterization Method			
		Chemical Decellularization Solutions	Enzymatic Digestion	Protocol Length (Total Hours)	Mechanical Method	Solubilization	ECM only	Synthetic Addition	Natural Addition		Structural	Mechanical	Biological	Animal Model
Liguori 2021 <sup>79</sup>	Porcine heart	6 M NaCl, 70% Ethanol, 1% SDS, 1% Triton X-100	0.05% Trypsin, DNase	75	ND Milling Method	Pepsin	✓			Injectable Hydrogel			✓	
Mousavi 2021 <sup>80</sup>	Porcine heart	1% SDS, 1% Triton X-100	NU	144-193	Amin Asia Panavar Fars Cryomill	Pepsin		Graphene oxide	Alginate	Injectable Hydrogel		✓	✓	
Nishiguchi 2021 <sup>81</sup>	Porcine UBM, heart, liver, pancreas, SIS	0.1% Peracetic acid, 4% Ethanol	300 U/mL DNase	ND	Osaka Chemical Lab	Pepsin		PEG		Injectable Hydrogel	✓	✓	✓	
Shin 2021 <sup>82</sup>	Porcine heart	1% SDS, 1% Triton X-100	NU	147	ND	Pepsin		Laponite clay and PEGDA		Bioprinted Scaffold	✓	✓	✓ ✓	
Tsui 2021 <sup>83</sup>	Porcine heart	1% SDS, 1% Triton X-100, 0.1% Peracetic acid 4% Ethanol	NU	109	ND	Urea		Graphene Oxide		Molded Scaffold	✓	✓	✓	✓
Wang 2021 <sup>84</sup>	Porcine heart	1% SDS, 1% Triton X-100	NU	ND	ND Milling Method	Pepsin	✓			Injectable Hydrogel			✓	
Zhu 2021 <sup>85</sup>	Porcine heart	1% SDS, 1% Triton X-100	NU	96-120	ND Milling Method	Pepsin	✓			Injectable Hydrogel			✓	✓

### 3.2.2. Cartilage dECM TE

Healthy articular cartilage possesses dense ECM with a zone-based structure with various stiffness, tensile strength, and fiber orientation.<sup>86</sup> Load bearing articular cartilages, such as the meniscus and the annulus fibrosus are commonly torn in sports injuries or impacted by osteoarthritis.<sup>87,88</sup> As articular cartilage has a sparse cell population and minimal vascularization, its intrinsic regenerative capacity is relatively limited. Current treatments for articular cartilage damage such as orthopedic surgical procedures may lead to iatrogenic cartilage degradation and osteoarthritis over time.<sup>87,88</sup>

Cartilage TE aims to regenerate the variable structure of cartilage zones to effectively distribute loads without reinjury.<sup>86</sup> The superficial zone has high tensile strength and densely packed Col II fibers organized parallel to the neighboring bone. The intermediate zone is a transition region with randomly organized Col II fibers. In the deep zone, Col II fibers are less dense and perpendicular to bone. Two commercial products for meniscus TE have been tested in Europe: Actifit® (polyurethane) and CMI® (gluteraldehyde crosslinked Col I), with satisfactory short-term benefits for cartilage restoration.<sup>89</sup> However, the long-term efficacy of Actifit® and CMI® is questionable because neither integrate effectively with neighboring cartilage, possess sufficient loading capacity for high stress regions, nor replicate the zone-based structure of articular cartilage.<sup>86</sup>

Cartilage dECM is expected to stimulate chondrocytes to produce neocartilage ECM, or chondrogenesis and has the potential to be incorporated into scaffolds with the three-zone structure for long-term weight bearing.<sup>20</sup> Chondrogenesis is characterized by expression of Col II, IX and XI. The bulk mechanical properties of cartilage dECM biomaterials aim to reach those of the native meniscus, 72–132 MPa for Young's modulus, 100–400 kPa for compressive modulus and 12–21 MPa for yielding stress, with varied local mechanical properties across zones.<sup>86,87,89,90</sup> Injectable hydrogels and electrospun scaffolds have been explored for dECM TE in repair of articular cartilage (**Table 2**).

#### 3.2.2.1. Injectable hydrogels in cartilage dECM-TE

Solubilization methodology and composite formulations have been investigated to optimize the fabrication of injectable dECM hydrogels with structural and mechanical relevance to articular cartilage. For instance, pepsin-solubilized cartilage dECM did not show any comparative advantage for enhancing chondrogenic differentiation of MSCs over a less bioactive methacrylated



gelatin hydrogel (GelMA).<sup>91,92</sup> One hypothesis was that pepsin might have removed the intrinsic chondrogenic components during decellularization. A subsequent in vitro study compared pepsin solubilisation with urea extraction for inducing chondrogenic differentiation. Urea extracted cartilage dECM hydrogels significantly enhanced MSC differentiation into chondrocytes over pepsin solubilized dECM.<sup>91,93</sup> Urea extraction may therefore be preferable to pepsin for preparing cartilage dECM hydrogels.

The mechanical properties of articular cartilage are limitedly recapitulated by cartilage dECM hydrogels. The compressive modulus of cartilage dECM hydrogels was around 280 Pa, well below the mechanical requirements of the meniscus (100–400 kPa).<sup>87</sup> One dECM composite formulation was derived from the nucleus pulposus of the AF together with chitosan and the crosslinker genipin.<sup>88</sup> Nucleus pulposus was selected because it is innately gelatinous and withstands high compressive forces. Chitosan was chosen for its mechanical tunability. Although this hydrogel was reported to enhance the production of Col II in annulus fibrosus-derived stem cells in vitro, no mechanical evaluation was performed to confirm the functionality of this composite.

Another cartilage dECM composite hydrogel consisted of Wharton's Jelly and silk fibroin.<sup>94</sup> Wharton's Jelly is a gelatinous connective tissue from umbilical cord blood vessels that is compositionally similar to cartilage but can be easily decellularized by centrifugation. Silk fibroin is a biodegradable polymer with the capacity to release bioactive molecules from dECM over time, enabling tunable delivery of molecules to stimulate cartilage regeneration.<sup>94</sup> The Wharton's Jelly and silk fibroin hydrogel was shown to enhance the proliferation of endometrial stem cells over silk fibroin alone. This composite also possessed more stable, solid-like storage and loss moduli than silk fibroin, which may be more representative of articular cartilage.

#### *3.2.2.2. Electrospun scaffolds in cartilage dECM-TE*

Electrospinning techniques can help generate an organized microstructure that is favorable for the regeneration of articular cartilage.<sup>17,89</sup> For instance, an electrospun scaffold of polyhydroxyalkanoate coated with cartilage dECM stimulated cellular adhesion, chondrogenic differentiation, and chondrocyte-like morphology by ASCs.<sup>17</sup> Another electrospinning study investigated dECM-PCL mixtures with varying dECM concentrations (0–80%) spun in either random or aligned patterns to replicate the mechanics of the native meniscus.<sup>89</sup> The viability of chondrocytes was highest at 20% dECM. The Young's modulus, tensile modulus and yield stress

of all mixtures were within the range of the human meniscus. These mechanical properties were also higher for aligned scaffolds than random patterns across all dECM-PCL concentrations<sup>89</sup> This is characteristic of the mechanics in the aligned, superficial vs random, intermediate zones of articular cartilage.<sup>86</sup> Layering the aligned and random scaffolds together could replicate the zone-based cartilage microstructure.

### *3.2.2.3. Future prospects*

Several shortcomings remain with dECM biomaterials for cartilage TE. For example, recent papers continue to use pepsin, despite evidence that it impairs mechanics and eliminates chondrogenic factors from cartilage dECM. While urea improves chondrogenic differentiation over pepsin, the mechanisms behind this effect are not yet clear. Proteomic analysis could help elucidate the influence of solubilization method on the retention of ECM-bound proteins in the decellularized products to help optimize the dECM preparation process for cartilage biomaterials. While several papers claimed to match the bulk mechanics of articular cartilage, these structures cannot yet account for differences in load-bearing requirements across its layers. Development of multilayer dECM scaffolds could provide cues to encapsulated cells and the surrounding environment to replicate these zones. Bioprinted dECM has been proposed to produce multilayered architecture with zone specific cellular cues.<sup>28,95</sup> In addition to Young's modulus and strength, other mechanical properties of cartilage such as fracture toughness and adhesion cannot be fully recapitulated with existing dECM-based biomaterials. Particularly, demand exists for strategies to enhance the adhesion or integration between the dECM implants and the target tissue, which is a recognized challenge in the field of cartilage TE.<sup>96</sup> To this end, recent advances in engineering tough hydrogel adhesion highlight opportunities to enhance the efficacy of dECM biomaterials.<sup>97,98</sup>

In conjunction with multilayered bioprinted scaffolds, cartilage dECM could be used to induce region-specific stem cell differentiation. That is, chondrogenesis would occur where a scaffold bordered cartilage, while osteogenesis would occur when receiving signals from bordering bone.<sup>99</sup> Together, multilayer scaffolds with zone specific mechanics and bioactive cues could collectively contribute to the representative regeneration of the meniscus, the annulus fibrosus, and other types of articular cartilage.

**Table 2 Summary of dECM Particles in Cartilage Tissue Engineering.** Structural characterization includes SEM, FTIR, Raman, NMR, crosslinking efficiency, porosity, and swelling ratio. Mechanical characterization includes AFM, rheology, tensile testing, compressive testing, and electrical conductivity. Biological characterization includes in vitro studies, gene and protein assays, histology, and degradation kinetics.

Author/Year	Tissue Type	Decellularization Method			Homogenization Method		Material Composition			Type	Biomaterial Characterization Method			
		Chemical Decellularization Solutions	Enzymatic Digestion	Protocol Length (Total Hours)	Mechanical Method	Solubilization	dECM only	Synthetic Addition	Natural Addition		Structural	Mechanical	Biological	Animal Model
Kwon 2013 <sup>100</sup>	Porcine articular cartilage	1% SDS	DNase	26	SPEX 6700	Pepsin	✓			Injectable Hydrogel	✓		✓	✓
Garrigues 2014 <sup>101</sup>	Porcine articular cartilage	ND	ND	ND	SPEX 6750	NU		PCL		Electrospun Scaffold	✓	✓	✓	
Pati 2014 <sup>28</sup>	Porcine adipose, cartilage, and heart	0.5% or 1% SDS, Isopropanol, 0.1% Peracetic acid, 4% Ethanol, 1% Triton X-100	50 U/mL DNase, 1 U/mL RNase, 0.025% Trypsin	60–100	Mortar and Pestle	Pepsin		PCL		Bioprinted Scaffold		✓	✓	
Sutherland 2015 <sup>20</sup>	Porcine cartilage	Hypertonic salt solution, 0.01% Triton X-100, 1% sodium lauroylsarcosine	0.0625 KU/mL Benzonase	ND	BioSpec Cryomill and SPEX SamplePrep	Pepsin	✓			Molded Scaffold	✓		✓	
Sutherland 2015 <sup>102</sup>	Porcine cartilage	Hypertonic salt solution, 0.01% Triton X-100, 1% sodium lauroylsarcosine solution,	0.0625 KU/mL Benzonase	ND	BioSpec Cryomill and SPEX SamplePrep	Pepsin		PLGA		Molded Scaffold	✓	✓	✓	
Wu 2015 <sup>87</sup>	Porcine meniscus	1% SDS, 0.1% EDTA	NU	110	ND	Pepsin	✓			Injectable Hydrogel		✓	✓	
Gao 2017 <sup>89</sup>	Porcine meniscus	Hydrogen peroxide	NU	ND	Tissue disintegrator	Pepsin		PCL		Electrospun Scaffold	✓	✓	✓	
Masaeli 2017 <sup>17</sup>	Human nasal septum cartilage and adipose	2% SDS, 0.02% EDTA, 1% Triton X-100	0.5 mg/mL DNase, 50 µg/mL RNase	6–26	Retsch	NU		PHA		Injectable Hydrogel	✓		✓	
Rothrauff 2017 <sup>91</sup>	Bovine tendon and cartilage	5 mM EDTA, 1% Triton X-100	200 U/mL DNase, 50 U/mL RNase	52	SPEX 8670	Pepsin or Urea			GelMa	Injectable Hydrogel			✓	
Liu 2018 <sup>88</sup>	Rabbit annulus fibrosis	1% Triton X-100	50 U/mL DNase, 1 U/mL RNase, 0.025% Trypsin	108	Mortar and Pestle	Acetic acid			Chitosan	Injectable Hydrogel	✓		✓	
Browe 2019 <sup>103</sup>	Porcine cartilage	0.2 M NaOH, 0.9 M and 5 M NaCl	NU	24	AC-Cryomill	Pepsin	✓			Molded Scaffold	✓	✓	✓	✓
Lindberg 2019 <sup>104</sup>	Equine vitreous humor	70%, 80%, and 100% Ethanol	NU	ND	NU	Pepsin	✓			Injectable Hydrogel		✓	✓	
Townsend 2019 <sup>105</sup>	Porcine cartilage	Hypertonic salt solution, 0.01% Triton X-100, 1% sodium lauroylsarcosine	0.0625 KU/mL Benzonase	ND	BioSpec cryomill and SPEX SamplePrep	Pepsin		Borate glass		Injectable Hydrogel		✓	✓	✓

**Table 2** (continued)

Author/Year	Tissue Type	Decellularization Method			Homogenization Method		Material Composition			Biomaterial Type	Characterization Method			
		Chemical Decellularization Solutions	Enzymatic Digestion	Protocol Length (Total Hours)	Mechanical Method	Solubilization	dECM only	Synthetic Addition	Natural Addition		Structural	Mechanical	Biological	Animal Model
Bhattacharjee 2020 <sup>106</sup>	Human placenta	Normal saline, 0.5 M NaOH	NU	ND	ND	Pepsin	✓			Injectable Hydrogel	✓	✓	✓	
Bordbar 2020 <sup>107</sup>	Sheep cartilage	5 or 10% SDS 10% EDTA	NU	20	Moulinex Grinder	Pepsin	✓			Injectable Hydrogel	✓	✓	✓	
Chen 2020 <sup>108</sup>	Bovine cartilage	1 M NaOH	NU	4	ND	NU			Gelatin	Electrospun and Bioprinted Scaffold	✓	✓	✓	
Feng 2020 <sup>109</sup>	Porcine auricular cartilage	1% SDS	NU	144	JX-NNJ Minigrinder	Pepsin		PCL		Electrospun Scaffold	✓	✓	✓	✓
Ibsirlioglu 2020 <sup>110</sup>	Human adipose	NU	0.1% Collagenase	ND	ND	Collagenase	✓			Injectable Hydrogel	✓		✓	
Kim 2020 <sup>111</sup>	Bovine cartilage	1% Triton X-100	50 U/mL DNase, 1 U/mL RNase, 0.025% Trypsin	102	ND	Pepsin		PCL		Electrospun Scaffold	✓		✓	✓
Visscher 2020 <sup>112</sup>	Porcine cartilage	1% Triton X-100	200 U/mL DNase	51	SPEX 6870	Pepsin	✓			Bioprinted Scaffold		✓	✓	
Xu 2020 <sup>113</sup>	Crow cartilage	1 M NaOH	NU	4	ND grinder and high-speed homogenizer	Pepsin			HA	Injectable Hydrogel	✓	✓	✓	
Yu 2020 <sup>114</sup>	Bovine nucleus pulposus	1% SDS, 0.1% EDTA,	NU	54	ND	Pepsin	✓			Injectable Hydrogel	✓		✓	
Zhang 2020 <sup>115</sup>	Goat cartilage	1% Triton X-100	50 U/mL DNase, 1 U/mL RNase	60	ND	Pepsin		PEG	Silk fibroin	Bioprinted Scaffold	✓	✓	✓	
Zhu 2020 <sup>116</sup>	Porcine cartilage	1% Triton X-100	200 U/mL DNase	51	Mortar and Pestle	Pepsin		PEGDA		Bioprinted Scaffold		✓	✓	✓
Antich 2021 <sup>117</sup>	MSC-derived	0.25% Triton X-100 1 mM Ammonium, hydroxide	50 U/mL DNase, 50 mg/mL RNase	2	Mortar and Pestle	Pepsin	✓			Injectable Hydrogel	✓	✓	✓	✓
Chae 2021 <sup>118</sup>	Porcine meniscus	3% Sodium deoxycholate, 0.1% Peracetic acid, 40% Ethanol	0.25% Trypsin							Bioprinted Scaffold			✓	✓
Jeyakumar 2021 <sup>119</sup>	Bovine cartilage	Hypertonic salt solution, 0.01% Triton X-100, 1% sodium lauroylsarcosine	0.0625 KU/ mL Benzonase	ND	SPEX SamplePrep	Pepsin			Silk fibroin	Molded Scaffold		✓	✓	✓
Kuang 2021 <sup>120</sup>	Rabbit nucleus pulposus	1% Triton X-100	0.25% Trypsin, 50 U/mL DNase, 1 U/mL RNase	60	Mortar and Pestle	Acetic acid			Chitosan	Injectable Hydrogel			✓	
Li 2021 <sup>121</sup>	Porcine meniscus	NU Gradient Centrifugation	NU	ND	NU	Pepsin		PLLA-CL		Electrospun Scaffold			✓	✓

**Table 2** (*continued*)

Author/Year	Tissue Type	Decellularization Method			Homogenization Method		Material Composition			Biomaterial Type	Characterization Method			
		Chemical Decellularization Solutions	Enzymatic Digestion	Protocol Length (Total Hours)	Mechanical Method	Solubilization	dECM only	Synthetic Addition	Natural Addition		Structural	Mechanical	Biological	Animal Model
Masaeli 2021 <sup>122</sup>	Human cartilage	2% Sodium deoxycholate, 0.02% EDTA	50 µg/mL RNase, 0.5 mg/mL DNase	8	Amin Asia Panavar Fars Cryomill	NU		PHB and PBVH		Electrospun Scaffold				✓
Peng 2021 <sup>123</sup>	Bovine annulus fibrosus and nucleus pulposus	1% SDS, 2% Triton X-100	NU	144	Wiley Mini Mill	Pepsin				Molded Scaffold		✓	✓	✓
Ravari 2021 <sup>124</sup>	Human cartilage	10 mM Tris-HCl, 1 % Triton X-100	50 U/mL DNase, Trypsin	48	Spex Sampleprep 8000D	Pepsin			Chitosan	Electrospun Scaffold and Injectable Hydrogel	✓	✓	✓	
Setayeshmehr2021 <sup>125</sup>	Bovine cartilage	Hypertonic salt solution 0.01% Triton X-100, 1% sodium lauroylsarcosine	0.0625 KU/mL Benzonase	ND	SPEX SamplePrep	Pepsin		PVA		Bioprinted Scaffold		✓	✓	
Shojarazavi 2021 <sup>126</sup>	Human cartilage	1% Triton X-100	Trypsin/ EDTA	84	Amin Asia Panavar Fars Cryomill	Pepsin			Alginate and Silk Fibroin	Injectable Hydrogel	✓	✓	✓	
Tian 2021 <sup>127</sup>	Porcine Cartilage	1% Triton X-100	50 U/mL DNase, 1 U/mL RNase	24+	ND	Pepsin				Molded Scaffold			✓	✓
Xia 2021 <sup>128</sup>	Bovine cartilage	1% SDS, 0.1% EDTA	NU	132	SPEX 6770	Acetic acid		PCL		Electrospun Scaffold	✓	✓	✓	
Yi 2021 <sup>129</sup>	Porcine Temporomandibular Disk	1% Triton X-100	50 U/mL DNase, 1 U/mL RNase	148	NU	Pepsin		PCL, polyurethane, and polydopamine		Bioprinted Scaffold		✓	✓	✓
Zhang 2021 <sup>130</sup>	Bovine cartilage	Hypertonic salt solution, 0.01% Triton X-100, 1% sodium lauroylsarcosine	0.0625 KU/mL Benzonase	ND	SPEX SamplePrep	Pepsin			Silk fibroin	Bioprinted Scaffold	✓		✓	

### 3.2.3. Neural tissue engineering

The central nervous system (CNS) consists of the brain and spinal cord, with branching peripheral nerves.<sup>131</sup> **(Figure 4A)** Together, the nervous system generates and carries signals to control the body's motor and sensory functions. Neural damage such as stroke, spinal cord injuries (SCI), and peripheral nerve injury (PNI) can lead to a range of symptoms such as chronic pain, paralysis, and death. No surgical method has yet succeeded in repairing spinal nerve and brain tissues damaged by SCI or stroke, respectively.<sup>132</sup> For example, decompressive surgery may help stabilize SCI. However, progressive cavitation, in which fluid-filled cysts and glial scars form and expand from the original injury site, can lead to further SCI deterioration and permanent disability.<sup>133</sup> Although peripheral nerves self-regenerate to certain degrees, severe PNI often require intervention.<sup>131</sup> Autologous nerve grafting is the gold standard for the management of PNI. However, nerve grafting is limited by autologous nerve supply and the risk of nerve damage at the harvest site.<sup>134</sup>

To use neural TE in the treatment of stroke, SCI, and PNI, strategies aim to design biomaterials that help guide axonal regeneration and remyelination, prevent cavitation, improve electrical signal conduction, and enhance the survival rate of transplanted cells.<sup>135,136</sup> Whole decellularized transplants have shown lowered immunogenicity in repairing PNI but limited functional recovery.<sup>134</sup> Injection of autologous Schwann cells (SCs) or stem cell-derived neural cells have been shown to promote neural regeneration and motor capacity in clinical trials, but with low cell survival rates.<sup>135-137</sup> At present, neural dECM biomaterials are partially successful for PNI, but no significant clinical benefits have yet been observed when tested for injuries in the CNS.<sup>138</sup>

Biomaterials are proposed to provide physical and biochemical cues to address low survival rates of transplanted cells in neural tissue regeneration.<sup>135,137,138</sup> Neural dECM biomaterials may guide neurite and axon growth, stimulate SC axonal remyelination, and stem cell differentiation into neurons.<sup>136,137,139</sup> SC remyelination is indicated by expression of S100 and MBP as well as morphological wrapping around axons and neurites.<sup>134</sup> Neural differentiation is associated with expression of  $\beta$ III-tubulin, SNAIL1, and GDNF as well as the outgrowth of neurofilaments.<sup>131,137,139</sup> Functional targets of neural dECM TE are to increase the neuronal response to electrophysiological stimulation and improve limb mobility.<sup>134</sup> Injectable

hydrogels, electrospun, and bioprinted scaffolds have been applied to neural dECM TE (**Table 3**).

#### *3.2.3.1. Injectable hydrogels in neural dECM TE*

Injectable dECM hydrogels were proposed to stimulate neural tissue regeneration by promoting cell infiltration and differentiation, neurite outgrowth, and axon growth and remyelination. Cellular infiltration is a preliminary requirement for repairing necrotic tissue in stroke cavities.

UBM hydrogels were tested for the ability to promote cell infiltration in rats after middle cerebral artery occlusion.<sup>132,140</sup> Hydrogels were injected into the stroke cavity while injection of PBS was used as a control. After 24 h, brain phenotype cells including neural progenitor cells, microglia, and astrocytes as well as M2 reconstructive macrophages were found to infiltrate from peripheral brain structures into the hydrogel. However, no control such as Col I hydrogels were included to confirm the efficacy of the dECM hydrogel.

For neuronal differentiation, hydrogels composed of spinal cord, bone, or dentine dECM were fabricated to evaluate the importance of dECM specificity. MSCs were cultured on aforesaid respective hydrogels and their differentiation into neural-lineage cells were tracked for 14 days.<sup>137</sup> MSCs showed elevated neural marker expression in spinal cord dECM hydrogels, but not on bone or dentine dECM hydrogels. The use of neural tissue-derived dECM may therefore be favorable for the differentiation of MSC into neural cells.<sup>137</sup>

In addition to cell differentiation, neurite growth and axon remyelination are required for functional nerve regeneration. dECM hydrogels from spinal cord or sciatic nerve were compared to Matrigel and Col I hydrogel controls for PNI regeneration in vitro.<sup>141</sup> Mass spectrometry was performed to compare the abundance of proteins retained in spinal cord and sciatic nerve dECM. The two dECM sources contained some overlapping proteins associated with axon regeneration such as Laminin  $\beta 2$  and  $\gamma 1$ . Other proteins related to axon growth and remyelination including Laminin  $\beta 1$  and clusterin were unique to the spinal cord. On the other hand, Col IV  $\alpha 1$  and  $\alpha 2$ , proteins associated with axon growth and synapse formation, were unique to the sciatic nerve. Moreover, when dorsal root ganglia neurons and SCs were cultured on the hydrogels, axon remyelination was more significant in the sciatic nerve dECM hydrogel compared to spinal cord dECM, Col I, and Matrigel.<sup>141</sup> (**Figure 4B**) The quantity of SCs wrapped around neurites growing from dorsal root ganglia and MBP expression were enhanced

on sciatic nerve dECM after 7 days. On the other hand, synapse formation was observed in dorsal root ganglia cultured on spinal cord dECM hydrogels. The amplitude of excitatory post-synaptic current were higher in the spinal cord dECM group (1200–1700 pA) compared to the sciatic nerve (290–480 pA). All in all, sciatic nerve dECM hydrogels may better promote axon remyelination by SCs, while spinal cord dECM hydrogels may better promote synapse formation between neurons.

To further investigate *in vivo* axon regeneration, a SCI rat model was tested with sciatic nerve dECM hydrogels with encapsulated SCs.<sup>135</sup> Compared to the Matrigel control, rats treated with sciatic nerve dECM hydrogel showed twice as many transplanted SC wrapped around axons after 8 weeks. The animals also showed greater recovery of hindpaw mobility compared to the Matrigel control at 4 weeks. However, recovery of hindpaw mobility did not show signs of full recovery at the end point of the study, i.e., 8 weeks. At that point, the dECM hydrogels were shown to degrade completely, which may lead to cavitation hampering full regeneration of the spinal cord. In another SCI rat study, small cysts in spinal cords were observed in groups treated with either spinal cord or sciatic nerve dECM hydrogels. Increases in cyst size is a symptom of cavitation. The cysts were found 4 weeks after injection and increased in size by 8 weeks when the dECM was fully degraded.<sup>142</sup> All in all, the neural-derived dECM hydrogel could promote axon remyelination, but functional SCI recovery was limited as cavitation proceeded after premature dECM degradation.

To enhance functional SCI recovery, Xu et al. fabricated a spinal cord dECM hydrogel with encapsulated exogenous FGF-2, a neuroregenerative growth factor.<sup>133</sup> Heparin poloxamer (HP) was mixed with spinal cord dECM and FGF-2 to produce an uncrosslinked composite. HP was hypothesized to preserve the activity of growth factors and could also slow the degradation rate of proteins in the composite.<sup>133,143</sup> In a rat SCI model, animals were treated with free FGF-2, dECM-HP hydrogels with or without FGF-2.<sup>133</sup> For the dECM-HP-FGF-2 composite group, animals recovered motility to the degree of an uninjured control 28 days after injection. Animals exhibited better bridging between broken axons and greater neurofilament protein expression. Instead, rats treated with free FGF-2 did not recover full motility of their hind legs. These results indicated the composite may help prevent cavitation by enhancing SCI regeneration over a longer time period prior to degradation of the dECM hydrogel.



#### 3.2.3.2. *Electrospun scaffolds in neural dECM TE*

Combining dECM with electrospun polymers has been proposed to stimulate axon elongation and remyelination along a nerve conduit, i.e., a tube-shape scaffold, to bridge the gaps between neurons in PNI. An electrospun composite scaffold from cauda-equina nerve dECM and PLGA was designed for PNI regeneration with either random or aligned fiber orientation.<sup>144</sup> SCs cultured on aligned scaffolds extended parallel to the fibers, which can help guide axon regeneration. In contrast, SCs on randomly aligned scaffolds were arbitrarily oriented, which limits the growth of axons. SCs on a PLGA-only control were round and flat. When seeded on the dECM/PLGA composite, SCs developed bipolar extensions and spindle-shapes, as in native neural tissue. Further, when dorsal root ganglia were seeded on the scaffolds, neurite outgrowth was significantly greater on the composite (700–1000  $\mu\text{m}$ ) compared to the PLGA-only controls (200–400  $\mu\text{m}$ ).

An aligned electrospun PLLA nerve conduit was also developed with a coated layer of sciatic nerve dECM.<sup>136</sup> (**Figure 4C**) When dorsal root ganglia were co-cultured with SCs on the dECM-PLLA scaffold, neurite outgrowth and SC migration were enhanced over the PLLA-only control. The dECM-PLLA scaffold also enhanced axon growth ( $\sim 2.1$  mm) from dorsal root ganglia over the PLLA control ( $\sim 1.6$  mm) and a dECM-coated glass slide ( $\sim 1$  mm). Results of these electrospun dECM studies showed that nerve-like conduits can guide nerve regeneration for PNI treatment.

#### 3.2.3.3. *Future prospects*

Challenges remain for the application of dECM to neural TE. Existing studies focused on the early impact of dECM on neural cell differentiation, neurite outgrowth, or axon remyelination. However, effective treatments for SCI or stroke also require continuous ECM remodeling to replace scars and cavities with functional neural tissue. A specific composition of neural dECM is required to promote regeneration of healthy, specialized neural tissue architecture, such as striated brain tissue and perineuronal nets, at desirable time points for complete regeneration. For example, neural ECM contains a higher ratio of carbohydrates to fibrous proteins than other ECMs. The high concentration of chondroitin sulfate proteoglycans in neural ECM, for example, is involved in regulating the beginning and end phases of neural regeneration. Assessing the impact of dECM on the ECM composition and organization could show whether dECM biomaterials effectively remodel injured neural tissue to be representative of the healthy

brain or nerves.

Another challenge is to minimize cavitation associated with premature dECM degradation. The natural rate of axon elongation is approximately 1 mm per day.<sup>145</sup> Depending on the size of the neuronal gap, a scaffold may need to stay in situ ranging from 2 weeks to several months to completely bridge the gap. Crosslinking dECM fibers with a polymer can be used to optimize the degradation rate of hydrogels to better match the time necessary for tissue regeneration. Polymers such as HP can help to both slow the degradation rate and preserve the activity of growth factors and proteins. Co-electrospinning dECM with the polymer can also preserve the dECM over a longer period by reducing exposure to ECM-degrading enzymes.

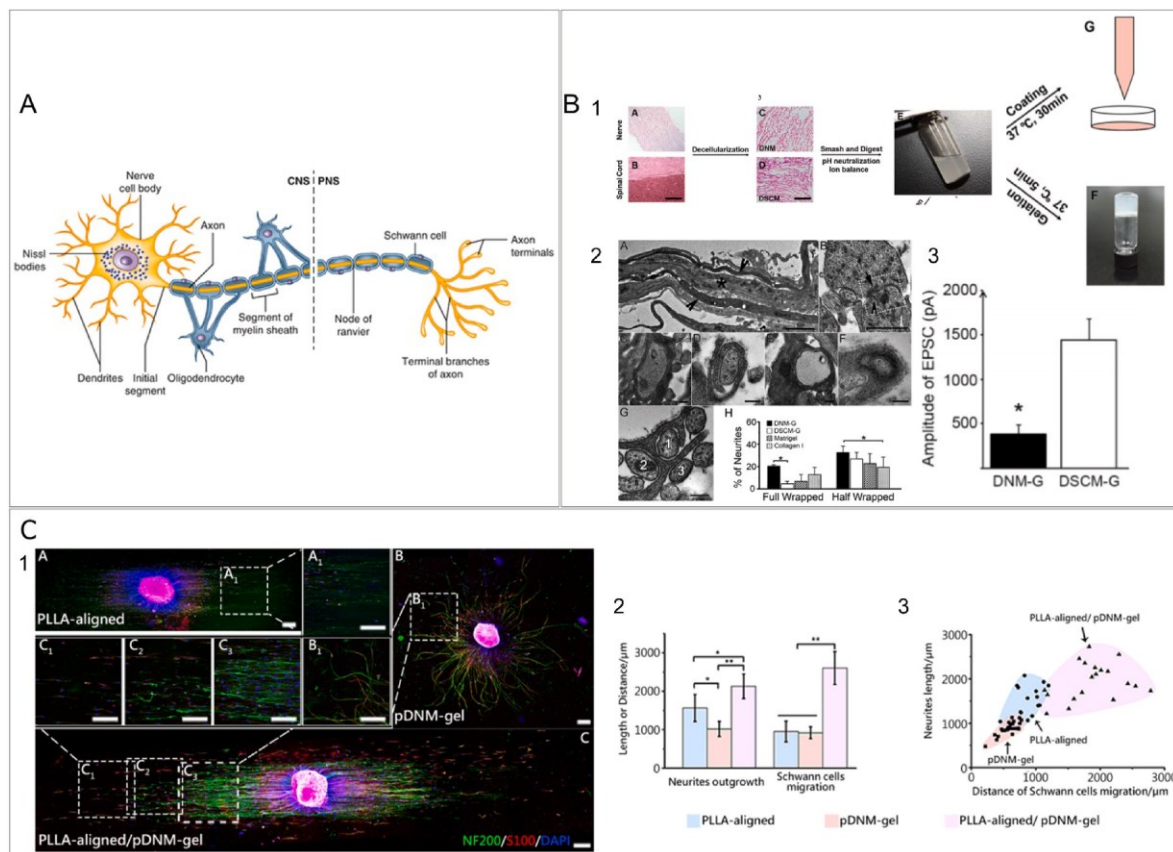


**Figure 4. Highlights of dECM Research in Nerve TE.** A. Neuron Anatomy within the CNS and PNS. B. dECM hydrogels from Sciatic Nerve and Spinal Cord Promote Axon Remyelination 1. Schematic describing production of nerve dECM hydrogel. 2. Imaging of Schwann cells wrapping around dorsal root ganglia after 14 days of culture in dECM hydrogels. A. Longitudinal image of neurite in sciatic nerve dECM. Arrows indicate Schwann cell. B. Synapse formed during culture (box) including a synaptic vessel (arrowhead). C–F. Cross sections of neurites with Schwann cells in different stages of wrapping. G. Comparison of wrapped(1), partially wrapped (2), and unwrapped(3) neurites H. Quantitative percent of fully or half-wrapped neurites in sciatic nerve dECM, spinal cord dECM, and Matrigel and Col I controls. 3. Excitatory Post Synaptic Current (EPSC) of neurites cultured in sciatic nerve or spinal cord dECM. The response of neurites in spinal cord dECM was significantly enhanced. C. Electrospun dECM-PLLA nerve conduits for promoting neurite outgrowth and remyelination. 1. Confocal imaging of dorsal root ganglia (pink) with neurite outgrowth (green) and Schwann cells (red), and showing the nuclei of each cell (blue). Imaging performed after 7 days of culture on: A. PLLA-only, B. A dECM-coated glass slide, C.

dECM-PLLA. Scale bar = 200  $\mu\text{m}$ . Boxes with subscripts (i.e., a1) show regions of interest at higher magnification. 2. Quantification of the distance of neurite outgrowth on each scaffold. 3. Length of neurite outgrowth versus distance of Schwann cell migration on each scaffold. Panel A. is reproduced from Ref. <sup>146</sup>; Panel B. is reproduced from Ref. <sup>141</sup>; Panel C. is reproduced from Ref. <sup>136</sup>with permissions.

**Table 3 Summary of dECM Particles in Neural Tissue Engineering.** Structural characterization includes SEM, FTIR, Raman, NMR, crosslinking efficiency, porosity, and swelling ratio. Mechanical characterization includes AFM, rheology, tensile testing, compressive testing, and electrical conductivity. Biological characterization includes in vitro studies, gene and protein assays, histology, and degradation kinetics.

Author/Year	Tissue Type	Decellularization Method			Homogenization Method		Material Composition			Biomaterial Type Characterization Method				
		Chemical Decellularization Solutions (Surfactants, Salts, Acids, Bases)	Enzymatic Digestion	Protocol Length (Total Hours)	Mechanical Method	Solubilization	dECM only	Synthetic Addition	Natural Addition		Structural	Mechanical	Biological	Animal Model
Baiguera 2013 <sup>147</sup>	Rat brain	1% Triton X-100, 4% Sodium deoxycholate, 1 M NaCl	200 KU DNase	24	ND Mechanical Milling	Acetic acid			Gelatin	Electrospun Scaffold	✓		✓	
Medberry 2014 <sup>148</sup>	Porcine brain, spinal cord, and UBM	0.05% EDTA, 3% Triton X-100, 1 M Sucrose, 4% Sodium deoxycholate, 0.1% Peracetic acid, 4% Ethanol	0.02% Trypsin	21.5	ND	Pepsin	✓			Injectable Hydrogel	✓	✓	✓	
Wen 2014 <sup>144</sup>	Porcine cauda equina	3% Triton X-100, 4% Sodium deoxycholate	NU	4	Ultra-Turrax	NU		PLGA		Electrospun Scaffold	✓		✓	
Massensini 2015 <sup>140</sup>	Porcine UBM	0.1% Peracetic acid, 4% Ethanol	NU	2	ND	Pepsin	✓			Injectable Hydrogel		✓		✓
Ghuman 2016 <sup>132</sup>	Porcine UBM	0.1% Peracetic acid, 4% Ethanol	NU	2	ND	Pepsin	✓			Injectable Hydrogel		✓		✓
Tukmachev 2016 <sup>142</sup>	Porcine UBM	0.1% Peracetic acid, 4% Ethanol	NU	2	ND	Pepsin	✓			Injectable Hydrogel			✓	✓
Viswanath 2016 <sup>137</sup>	Porcine spinal cord, bovine bone, human dentine	0.5 M HCl, 0.025% EDTA	0.05% Trypsin	49	Carver Press	Pepsin	✓			Injectable Hydrogel	✓	✓	✓	
Ghuman 2017 <sup>149</sup>	Porcine UBM	0.1% Peracetic acid, 4% Ethanol	NU	2	ND	Pepsin	✓			Injectable Hydrogel		✓		✓
Koci 2017 <sup>13</sup>	Human umbilical cord, porcine UBM, spinal cord, and brain	0.05% EDTA, 0.1% Peracetic acid, 4% Ethanol	0.02% Trypsin	52	ND	Pepsin	✓			Injectable Hydrogel	✓	✓		
Prest 2017 <sup>150</sup>	Canine UBM and sciatic nerve	3% Triton X-100, 0.05% EDTA, 1 M Sucrose, 0.1% Peracetic acid, 4% Ethanol	0.02% Trypsin	3.25	ND	Pepsin	✓			Injectable Hydrogel	✓		✓	✓
Cerqueira 2018 <sup>135</sup>	Rat sciatic nerve	0.6 mM sulfobetaine-10, 0.14% Triton X-100	200 µL Chondroitinase ABC	ND	Microscissors	Pepsin	✓			Injectable Hydrogel	✓		✓	✓
Chen 2018 <sup>131</sup>	Rat sciatic nerve	0.5% Triton X-100, 1 M NaCl, 1% SDS, 0.1% Peracetic acid, 4% Ethanol	NU	55	ND	Pepsin		PCL		Injectable Hydrogel	✓		✓	
Lin 2018 <sup>134</sup>	Porcine sciatic nerve	3% Triton X-100, 4% Sodium deoxycholate	NU	36	Wiley Mini Mill	Pepsin		PLC-co-poly(trimethylene carbonate) PEG	HA	Electrospun Scaffold	✓	✓	✓	✓
Thompson 2018 <sup>151</sup>	Embryonic stem cell-derived astrocytes	125 mM sulfobetaine-10, 0.16 mM sulfobetaine-16, 0.14% Triton X-200, 50 mM Trehalose	NU	68.5	ND	ND				Injectable Hydrogel			✓	✓
Xu 2018 <sup>133</sup>	Rat spinal cord	1% Triton X-100, 4% Sodium deoxycholate, 0.1% Peracetic acid, 4% Ethanol	NU	96	NU	Acetic acid and pepsin		Poloxamer	Heparin	Injectable Hydrogel	✓	✓	✓	✓
Zou 2018 <sup>141</sup>	Porcine sciatic nerve and spinal cord	3% Triton X-100, 4% Sodium deoxycholate, 4% Ethanol	NU	ND	ND	Pepsin	✓			Injectable Hydrogel	✓	✓	✓	

**Table 3** (continued)

Author/Year	Tissue Type	Decellularization Method			Homogenization Method		Material Composition			Biomaterial Type Characterization Method				
		Chemical Decellularization Solutions (Surfactants, Salts, Acids, Bases)	Enzymatic Digestion	Protocol Length (Total Hours)	Mechanical Method	Solubilization	dECM only	Synthetic Addition	Natural Addition		Structural	Mechanical	Biological	Animal Model
Chen 2019 <sup>136</sup>	Porcine sciatic nerve	3% Triton X-100, 4% Sodium deoxycholate, 1:2 Ethanol and dichloromethane	NU	ND	Wiley Mini Mill	Pepsin		PLLA		Injectable Hydrogel	✓		✓	
Tatic 2019 <sup>152</sup>	Porcine spinal cord, bovine bone	0.05% EDTA, 3% Triton X-100, 1 M Sucrose, .1% Peracetic acid, 4% Ethanol	0.02% Trypsin	21.25	ND	Pepsin	✓			Injectable Hydrogel		✓	✓	
Vyborny2019 <sup>153</sup>	Human umbilical cord	0.05% EDTA, 0.1% Peracetic acid, 4% Ethanol	0.02% Trypsin	4	Wiley Mini Mill	Pepsin	✓			Injectable Hydrogel		✓	✓	
Hong 2020 <sup>154</sup>	Porcine brain	3% Triton x-100, 1 M Sucrose, 4% Sodium Deoxycholate, 0.1% Peracetic acid, 4% Ethanol	0.02% Trypsin	5.25	SPEX SamplePrep	Pepsin			Collagen	Injectable Hydrogel	✓	✓	✓	✓
Xu 2020 <sup>155</sup>	Porcine sciatic nerve	3% Triton X-100, 4% Sodium deoxycholate, 1:2 Ethanol, and dichloromethane	NU	ND	Wiley Mini Mill	Pepsin		PLLA		Injectable Hydrogel	✓		✓	✓
Qiu 2020 <sup>156</sup>	Canine sciatic nerve	4% Triton X-100, 4% Sodium deoxycholate	NU	36	Wiley Mini Mill	Pepsin			Whole sciatic nerve dECM	Injectable Hydrogel	✓			✓
Rao 2020 <sup>157</sup>	Porcine Brain	3% Triton x-100, 1 M Sucrose, 4% Sodium Deoxycholate, 0.1% Peracetic acid, 4% Ethanol	0.02% Trypsin	5.25	SPEX SamplePrep	Pepsin			Collagen	Injectable Hydrogel	✓	✓	✓	
Seo 2020 <sup>158</sup>	Porcine spinal cord and peripheral nerve	3% Triton X-100, 4% Sodium deoxycholate, 1:2 Ethanol and dichloromethane, 4% Ethanol	NU	ND	ND	Pepsin	✓			Injectable Hydrogel	✓		✓	✓
Ghuman2021 <sup>159</sup>	Porcine UBM	0.1% Peracetic acid, 4% Ethanol	NU	ND	ND	Pepsin		PEGDA		Injectable Hydrogel				✓
Kong 2021 <sup>160</sup>	Porcine spinal cord and skeletal muscle	0.5% SDS, 25 mM EDTA, 3% Triton X-100, Isopropanol, 0.1% Peracetic acid 10% Ethanol	50 U/mL DNase	104	ND	Pepsin	✓			Bioprinted Scaffold	✓	✓	✓	✓
Li 2021 <sup>161</sup>	Porcine peripheral nerve	3% Triton X-100, 4% Sodium deoxycholate	NU	36	ND Pulverization	Pepsin				Injectable Hydrogel	✓	✓	✓	✓
Ozudogru2021 <sup>162</sup>	Bovine spinal cord	3% Triton x-100, 1 M Sucrose, 4% Sodium deoxycholate, 0.1% Peracetic acid, 4% Ethanol	0.02% Trypsin	5.25	T-18 Basic Ultra TURRAX	Pepsin	✓			Injectable Hydrogel	✓	✓	✓	
Simsa 2021 <sup>163</sup>	Porcine brain	1% Sodium deoxycholate	40 U/mL DNase	197	Wiley Mini Mill	Pepsin	✓			Injectable Hydrogel	✓	✓	✓	
Zhang 2021 <sup>164</sup>	Porcine sciatic nerve	0.5% Triton X-100, 4% Sodium Deoxycholate	4% DNase, RNase	40.5	ND	NU			Chitosan	Molded Scaffold	✓		✓	✓

#### 3.2.4. Adipose dECM TE

Adipose tissue is a loosely structured connective tissue that contains multipotent adipose stem cells and extensive vasculature, granting adipose tissue a high innate wound healing capacity.<sup>189</sup> Autologous adipose grafts are often used to fill soft tissue cavities in reconstructive and cosmetic plastic surgeries such as facial reconstruction, scar repair, breast augmentation, and treating atrophy or diabetic wounds.<sup>21,170,173,189</sup> Adipose grafts are obtained by liposuction, a relatively non-invasive procedure, and have negligible rates of rejection and infection, a distinct advantage over silicone and other synthetic soft tissue fillers. However, the efficacy of autologous adipose grafts varies between patients due to unpredictable absorption of the graft (30–70%) by surrounding tissue.<sup>170,173,189,190</sup> More severe side effects such as necrosis and fibrotic ECM remodeling were also reported with adipose grafts.<sup>170,173,189,190</sup>

Adipose-based therapeutic strategies are proposed for long-term repair of soft tissue defects, without the need for reinjection. One strategy is to directly inject autologous adipose stem cells (ASCs) to stimulate the formation of neo-adipose tissue i.e., adipogenesis.<sup>169,170</sup> However, ASC therapy has historically been limited by lack of cellular retention in the target site. Additionally, the standard 2D culture method for ASCs does not replicate the native stem cell niche, reducing their capacity for proliferation and differentiation.<sup>21</sup>

Adipose dECM has the innate potential to stimulate adipogenic differentiation of ASCs and adipogenesis, making it a leading candidate for adipose TE scaffolds and ASC culture expansion. Adipose dECM TE has focused on characterizing and optimizing the adipogenic potential of dECM. Adipogenesis is indicated using adipogenic marker genes (PPAR $\gamma$ , LPL, C/EBP $\alpha$ , Col IV), the activity of the enzyme glycerol-3-phosphate dehydrogenase (GPDH), and intracellular lipid accretion.<sup>169,170</sup> One mechanical target for replicating native adipose is the Young's modulus, 0.5–5.6 kPa.<sup>191</sup> Decellularized adipose tissue has been developed into injectable hydrogels, electrosprayed microcarriers, and bioprinted scaffolds (**Table 4**).

##### 3.2.4.1. Injectable hydrogels in adipose dECM TE

Flynn and coworkers have contributed substantial knowledge to adipose dECM TE through their decellularized adipose tissue (DAT) hydrogels.<sup>1, 3</sup> The DAT hydrogels were notably produced without solubilization of DAT microparticles by photocrosslinking with methacrylated chondroitin sulfate (MCS) after injection.<sup>169,170</sup> The intact microparticles theoretically retained a

greater quantity of adipogenic biomolecules than solubilized dECM. After 14 days of culture, adipogenic marker expression, adhesion, and proliferation was heightened only where encapsulated ASCs attached to the DAT particles.<sup>170</sup> The impact of available particle size on ASC proliferation was also of interest. Using large diameter (~275  $\mu\text{m}$ ) and small diameter (38  $\mu\text{m}$ ) DAT particles with concentrations chosen to provide identical surface areas, more ASC rapid proliferation occurred in the hydrogels containing the larger, more disperse particles. The more tightly packed, smaller particles provided greater incidence for cell-cell interactions and therefore enabled greater adipogenic marker expression. Investigating ASC response to DAT particles with varied size, concentration, and patterned distribution could illuminate the role of DAT in mediating ASC behavior and help develop a reliable hydrogel for either ASC culture or adipose TE.

#### *3.2.4.2. Electrospun scaffolds in adipose dECM TE*

In addition to injectable hydrogels, the Flynn lab developed microcarriers derived from adipose dECM, or DAT microcarriers for improving ASC expansion in suspension or in plastic surgery.<sup>21,167</sup> DAT microcarriers were hypothesized to possess biological cues present in the native ASC niche and create greater surface area than present in static 2D culture. The initial phase of DAT microcarrier development used photocrosslinking to stabilize DAT-alginate air-jet droplets pumped through a syringe needle.<sup>167</sup> These DAT microcarriers demonstrated greater adipogenic marker expression, GPDH activity, and lipid accumulation compared to gelatin-alginate controls both in vitro and in a 28-day subcutaneous injection rat study.<sup>168</sup> Later DAT microcarrier iterations overcame the need for stabilization by crosslinking with alginate, and enabled control over porosity and particle size.<sup>21</sup>

Electrospraying DAT microcarriers into liquid nitrogen did not require photochemical crosslinking, and reduced particle size by half (~425  $\mu\text{m}$ ).<sup>21</sup> The Young's modulus of the DAT microcarriers was 0.5–1 kPa, within the range of native adipose tissue. Additionally,  $\alpha$ -amylase, an enzyme that digest collagen at its carbohydrate groups, was used to solubilize the dECM rather than pepsin, which enabled homogeneous suspension of dECM for electrospraying. When compared to gelatin microcarriers, ASCs cultured on DAT microcarriers demonstrated a multifold increase in proliferation and adhesion and more uniform adipogenic differentiation.

#### *3.2.4.3. Bioprinted scaffolds in adipose dECM TE*

Pati and Cho pioneered bioinks derived from adipose dECM for creating spatially organized cell-patterned scaffolds.<sup>28</sup> In their first study, ASCs were encapsulated in an adipose bioink and printed



layer-by-layer into a poly( $\epsilon$ -caprolactone) (PCL) framework. Differentiation of ASCs into adipose cells was enhanced for scaffolds fabricated from the dECM bioink compared to a Collagen I (Col I) bioink control, as verified by immunohistochemistry for adipogenic factors. When printed into a flexible, dome-shaped scaffold, the adipose bioink demonstrated the capacity to differentiate ASCs into adipose-lineage cells in basal media without adipogenic supplementation.<sup>171</sup> When implanted in vivo, the dome-shaped scaffold stimulated constructive remodeling, integration, and regeneration of adipose tissue in mice without significant inflammation and fibrosis.

A composite of the adipose bioink with alginate was also tested as a bioactive coating for 3D printed PCL scaffolds.<sup>172</sup> The dECM-alginate composite demonstrated tunable release of encapsulated enzymes. When implanted in rats, vascularized adipose tissue regenerated greater than 40% surface area compared to a PCL control. The authors speculated that spatially patterned adipose bioprinted scaffolds might circumvent the necrotic side-effects associated with conventional adipose tissue replacement methods.<sup>171</sup> This could potentially be achieved by tuning pore size to facilitate cellular integration with the surrounding tissue.

#### *3.2.4.4. Future prospects*

In dECM adipose TE, significant variability in the age, gender, and body mass index of adipose tissue donors is often noted even in the same study.<sup>174</sup> Recruiting donors from more homogeneous groups could reduce variability and improve the ability of researchers to ascertain their results. Also, modified adipose dECM such as composite biomaterials may help decrease resorption and improve integration with surrounding tissue. Resorption will still need to be addressed for adipose dECM scaffolds in a more systematic and comprehensive manner. Degradation and resorption studies should be performed along with standard histological analysis of regenerated adipose to ensure a specific formulation represents an improvement over existing treatments. Lastly, the mechanical properties of adipose dECM formulations should be more extensively analyzed to determine whether scaffolds have sufficient porosity to provide the material with adequate viscoelasticity and material-host integration to guide non-fibrotic soft tissue wound healing. While current results appear promising, more defined methodology is necessary for the development of stable, regenerative materials for adipose dECM TE.

**Table 4. Summary of dECM particles in Adipose Tissue Engineering.** Structural characterization includes SEM, FTIR, Raman, NMR, crosslinking efficiency, porosity, and swelling ratio. Mechanical characterization includes AFM, rheology, tensile testing, compressive testing, and electrical conductivity. Biological characterization includes in vitro studies, gene and protein assays, histology, and degradation kinetics.

Author/Year	Tissue Type	Decellularization Method			Homogenization Method		Material Composition			Biomaterial Type	Characterization Method			
		Chemical Decellularization Solutions (Surfactants, Salts, Acids, Bases)	Enzymatic Digestion	Protocol Length (Total Hours)	Mechanical Method	Solubilization	dECM only	Synthetic Addition	Natural Addition		Structural	Mechanical	Biological	Animal Model
Choi 2012 <sup>165</sup>	Human adipose	1 M NaCl, 0.5 SDS	0.2% DNase, 200 µg/mL RNase	28	Blender	NU	✓			Molded Scaffold		✓	✓	✓
Francis 2012 <sup>166</sup>	Human adipose	0.5 M acetic acid	NU	97	Mortar and Pestle or Blender	Pepsin		Polydioxanone		Electrospun Scaffold	✓		✓	
Turner 2012 <sup>167</sup>	Human adipose	70% Ethanol, 0.5 M acetic acid	NU	0.5	NU	Pepsin			Alginate	Electrospun Scaffold	✓		✓	
Turner 2012 <sup>168</sup>	Human adipose	70% Ethanol, 0.5 M acetic acid	NU	0.5	NU	Pepsin			Alginate	Electrospun Scaffold			✓	✓
Cheung 2014 <sup>169</sup>	Human adipose	70% Ethanol, 0.5 M acetic acid	NU	0.5	Sartorius Stedim Mikro-Dismembrator	NU			MCS, methacrylated glycol chitosan	Injectable Hydrogel		✓	✓	✓
Pati 2014 <sup>28</sup>	Porcine adipose, cartilage, and heart	0.5% or 1% SDS, Isopropanol, 0.1% Peracetic acid, 4% Ethanol, 1% Triton X-100	50 U/mL DNase, 1 U/mL RNase, 0.025% Trypsin	60–100	Mortar and Pestle	Pepsin		PCL		Bioprinted Scaffold		✓	✓	
Brown 2015 <sup>170</sup>	Human adipose	0.1% EDTA, Isopropanol	0.25% Trypsin, 15 KU Dnase, 125 mg Rnase, 2 KU Lipase VI-S	53+	Sartorius Stedim Mikro-Dismembrator	NU			MCS	Injectable Hydrogel	✓		✓	
Pati 2015 <sup>171</sup>	Human adipose	0.5% SDS, Isopropanol, 0.1% Peracetic acid, 4% Ethanol	NU	100	Mortar and Pestle	Pepsin		PCL		Bioprinted Scaffold		✓	✓	✓
Yu 2016 <sup>21</sup>	Human adipose	0.1% EDTA, Isopropanol	0.25% Trypsin, 15 KU Dnase, 125 mg Rnase, 2 KU Lipase VI-S	53+	Retsch MM400	α-amylase	✓			Electrospun Scaffold	✓	✓	✓	
Rijal 2017 <sup>172</sup>	Porcine mammary adipose	0.5% SDS, Isopropanol	NU	72	NU	Pepsin		PCL		Bioprinted Scaffold	✓		✓	✓
Zhao 2018 <sup>173</sup>	Human adipose	1 M NaCl, 1% Triton X-100, Isopropanol	100 U/mL DNase, 100 µg/mL Rnase	50	Retsch MM400	Pepsin	✓			Injectable Hydrogel	✓		✓	✓
Zhu 2018 <sup>25</sup>	Porcine UBM	0.1% Peracetic acid, 4% Ethanol	NU	3	Wiley Mini Mill	Pepsin		polyNIPAAm		Injectable Hydrogel	✓	✓	✓	✓
Porcine van Dongen 2019 <sup>174</sup>	Human adipose	50% and 96% Ethanol, 0.05 mM EDTA, 0.5% SDS	30 µg/mL DNase	46	Ultra-Turrax	Pepsin	✓			Injectable Hydrogel		✓	✓	
Lin 2019 <sup>175</sup>	Human adipose	0.1% EDTA, Isopropanol, 0.1% Peracetic acid,	0.05% Trypsin Benzonase	47	ND	ND	✓			Molded Scaffold	✓	✓	✓	✓
Martin 2019 <sup>176</sup>	Human adipose	5 mM EDTA, Isopropanol	0.25% Trypsin	44.5	NU	α-amylase	✓			Electrospun Scaffold	✓	✓	✓	✓

**Table 4** (Continued)

Author/Year	Tissue Type	Decellularization Method			Homogenization Method		Material Composition			Biomaterial Type	Characterization Method			
		Chemical Decellularization Solutions (Surfactants, Salts, Acids, Bases)	Enzymatic Digestion	Protocol Length (Total Hours)	Mechanical Method	Solubilization	dECM only	Synthetic Addition	Natural Addition		Structural	Mechanical	Biological	Animal Model
Mohiuddin 2019 <sup>177</sup>	Human adipose	0.5 M and 1 M NaCl, Isopropanol, 1% Triton X-100	0.25% Trypsin	249	ND Milling Method	Pepsin	✓			Injectable Hydrogel	✓		✓	✓
Shridhar 2019 <sup>178</sup>	Human adipose	0.1% EDTA, Isopropanol	0.25% Trypsin, 15 KU Dnase, 125 mg Rnase, 2 KU Lipase VI-S	53+	Retsch MM400	NU			MCS	Injectable Hydrogel		✓	✓	
Getova2020 <sup>179</sup>	Human adipose	50% and 96% Ethanol, 0.05 mM EDTA, 0.5% SDS	30 µg/mL DNase	46	Ultra-Turrax	Pepsin	✓			Injectable Hydrogel			✓	
Mohiuddin 2020 <sup>180</sup>	Human adipose	0.5 M and 1 M NaCl, Isopropanol, 1% Triton X-100	0.25% Trypsin	249	ND Milling Method	Pepsin	✓			Injectable Hydrogel	✓		✓	
Nguyen 2020 <sup>181</sup>	Human adipose	Isopropanol, 0.1% SDS	NU	54	Omni Bead Ruptor	ND	✓			Injectable Hydrogel			✓	✓
Nyambat 2020 <sup>182</sup>	Rabbit adipose	1 M NaCl, 5 mM and 25 mM EDTA, 0.5% SDS	NU	50	ND	Pepsin	✓			Injectable Hydrogel	✓	✓	✓	
Chen 2021 <sup>183</sup>	Human adipose	0.1% EDTA, Isopropanol	0.25% Trypsin	64.5	ND	Pepsin	✓			Injectable Hydrogel	✓	✓	✓	✓
Cho 2021 <sup>184</sup>	Human adipose porcine aorta	0.5% SDS, Isopropanol, 0.1% and 3%, Triton X-100, 0.1% Peracetic acid, 4% Ethanol	NU	100	NU	Pepsin		PCL		Bioprinted Scaffold		✓	✓	✓
Leclerc 2021 <sup>185</sup>	Human adipose	5 mM EDTA, Isopropanol	0.25% Trypsin	44.5	NU	α-amylase	✓			Molded Scaffold			✓	✓
Lee 2021 <sup>186</sup>	Human adipose	0.5% SDS, Isopropanol	NU	172	SPEX SamplePrep	Pepsin		PLCL	Collagen	Bioprinted Scaffold	✓	✓		✓
Liu 2021 <sup>187</sup>	Porcine adipose	0.5% SDS, Isopropanol	NU	NU		6	NU	✓		Injectable Hydrogel			✓	✓
Pu 2021 <sup>188</sup>	Human adipose	0.1% EDTA, Isopropanol	0.25% Trypsin, 15 KU DNase, 125 mg RNase, 2 KU Lipase VI-S	53+		KZ-II	Pepsin	✓		Injectable Hydrogel			✓	

### 3.2.5. Muscle dECM TE

Skeletal muscles are the striated muscles linked to the skeleton by tendons that help control voluntary movement as part of the musculoskeletal system.<sup>220</sup> The striated fibers are sarcomeres, repeated actin-myosin units that control muscle contraction and mobility. The musculoskeletal system has an effective innate wound healing process. However, orthopaedic trauma, surgical excision, and degenerative muscular diseases result in volumetric muscle loss (VML) and functional impairment beyond the regenerative threshold.<sup>204</sup> The standard treatment for VML, or the loss of greater than 10% of muscle mass, is autologous muscle grafts.<sup>204,205</sup> These grafts are not fully successful, as the muscle does not completely regain its pre-injury structure and function.

Replicating directionally dependent striations and vascular network remain major challenges in skeletal muscle biomaterials. In a clinical trial, patients treated with whole decellularized skeletal muscle regained only partial mobility at the site of VML.<sup>221</sup> Strategies in skeletal muscle TE have focused on improving retention and function of stem cell-derived myoblasts to reproduce the striations and vasculature of skeletal muscle.<sup>195,197,200,221</sup> Survival of stem cell-derived myoblasts has been suboptimal in existing biomaterials and did not efficiently undergo myogenesis, due to the absence of a striated guiding structure and native biomolecular cues.<sup>200</sup>

Biomaterials produced from skeletal muscle dECM (SM-dECM) are designed to replicate the striated structure of native muscle and stimulate myogenesis and vasculogenesis.<sup>200,204</sup> Mechanical targets include the tensile strength around  $163 \pm 76$  kPa and elastic modulus  $\sim 12$  kPa as in native muscle.<sup>204,222</sup> In successful myogenesis, differentiation is followed by the formation of striated myotubes that express myosin heavy chains in banded patterns.<sup>197</sup> Another target is vasculogenesis of arterioles and capillaries alongside muscle fibers that withstand the tensile muscle stretch.<sup>200</sup> In muscle dECM TE, injectable hydrogels have been applied to revascularization, and electrospun and bioprinted scaffolds to striated skeletal muscle (**Table 5**).

#### 3.2.5.1. Injectable hydrogels in muscle dECM TE

SM-dECM hydrogels were proposed to create a myogenic and angiogenic nanofibrous environment through fibrillogenesis and cell-matrix signaling.<sup>194,200</sup> In a rat hind limb ischemia model, animals injected with the SM-dECM hydrogel increased myoblast recruitment as well as capillary and arteriole density compared to those a Col I hydrogel.<sup>194</sup> SM-dECM also stimulated neo-ECM production with greater morphological similarity to striated muscle than umbilical cord

dECM by day 10, indicating a possible tissue specific effect.<sup>199</sup>

In comparison to a Col I control hydrogel in vitro, the myoblasts encapsulated in SM-dECM showed a significant increase in mature myocyte marker expression.<sup>200</sup> When myoblasts were cultured with SM fibroblasts within SM-dECM, contractile myotube formation was observed, but not in co-culture with Col I hydrogel or myoblasts alone. When SM-dECM-encapsulated myoblasts were injected into defected anterior tibialis in mice, greater myoblast retention, survival, and differentiation to myocytes were observed compared to Col I. Further, myoblast survival and capillary density were enhanced when myoblasts and fibroblasts were co-delivered to the animals.

#### *3.2.5.2. Electrospun scaffolds in muscle dECM TE*

Electrospinning SM-dECM biomaterials can create tissue constructs for full thickness defect regeneration across layered muscles and control fiber orientation.<sup>205</sup> A sandwich structure dECM-PEUU composite was generated by wet electrospinning. First, PEUU was electrospun with concurrent electrospraying of PBS to create a fiber-rich outer layer.<sup>195</sup> This first step was followed by a layer of PEUU electrosprayed with dECM slurry, then a final layer like the first, i.e., PEUU/PBS. The tensile modulus of the sandwich scaffold (200–300 kPa) was found comparable to native SM (85–250 kPa). When equivalent thickness ( $2.45 \pm 0.09$  mm) sandwich scaffolds and single layer dECM-PEUU controls were implanted in an abdominal wall defect rat model, hernias were found in five of seven rats after eight weeks after the implantation of the single-layer control, but not in those implanted with the sandwich scaffold.

In an in vitro study, composites of dECM-PCL, and a PCL-only control were electrospun in either aligned or random patterns to determine the importance of fiber orientation in satellite cell mediated SM regeneration.<sup>205</sup> The highest density of myocyte precursors was identified on the aligned dECM-PCL scaffold, indicating improved cellular adhesion and proliferation. The satellite cells on aligned dECM-PCL composite adopted the spindle morphology of skeletal muscle that elongated unidirectionally along the fibers. Additionally, myocyte differentiation and myotube formation significantly increased after 4 days on the aligned dECM-PCL scaffold.

Smoak et al. developed an alternative electrospinning method to enhance the mechanical stability of SM-dECM-only scaffolds.<sup>204</sup> These scaffolds were fabricated using either random or aligned patterning and crosslinked with glutaraldehyde. The tensile modulus of crosslinked aligned scaffolds (~850 kPa) was significantly higher than the native SM. The tensile modulus of

uncrosslinked aligned dECM (~213 kPa) and crosslinked random dECM scaffolds (~185 kPa) were within the range of native SM. Uncrosslinked random scaffolds (~44 kPa) were lower but not significantly different from native SM. Myoblasts culture on aligned, crosslinked dECM scaffolds produced the greatest number of myotubes.<sup>216</sup>

#### *3.2.5.3. Bioprinted scaffolds in muscle dECM TE*

Bioprinted SM-dECM was proposed to replicate the architectural and biomolecular cues for striated muscle regeneration.<sup>197</sup> To ensure mechanical stability, pre-gels of dECM and a Col I control with encapsulated myoblasts were printed onto PCL supports under high pressure (50 kPa). After 7 days of culture, the Young's modulus of the dECM scaffold was higher (8–10 kPa) than the Col I control (2–6 kPa). After 14 days of culture, the dECM scaffold's Young's modulus reached up to ~15 kPa, which was significantly higher than the Col I control (4–6 kPa) and comparable to that of native muscle (~12 kPa). The improved mechanical properties might be due to myoblast maturation into longitudinally elongated myocytes. Myogenic gene expression and formation of contractile, striated myotubes was enhanced in dECM compared to the Col I control.

#### *3.2.5.4. Future prospects*

Research gaps remain in the design and evaluation of SM-dECM biomaterials for regenerating SM. For instance, quantitative evaluation of contractility has been limited for SM-dECM biomaterials. Increased compound muscle action potential and contractility was observed in a rat VML model when a bioprinted methacrylated dECM scaffold with encapsulated ASCs that were cultured under stimulation by an electrical field, demonstrating contractility is a critical measure of SM function.<sup>212</sup> One quantitative method for measuring contractility in vitro is measuring the contractile force in response to electrical signals.<sup>223</sup>

Additionally, VML defects can occupy thick regions of muscle, yet the majority of skeletal muscle dECM biomaterials are relatively thin as those of electrospun meshes. Layered scaffolds like Takanari's sandwich could be adapted to produce thicker skeletal muscle scaffolds to fill the void for VML defects. Also, Takanari's sandwich technique facilitated cell-scaffold integration, which is important for multi-layer scaffolds.

**Table 5 Summary of dECM Particles in Muscle Tissue Engineering.** Structural characterization includes SEM, FTIR, Raman, NMR, crosslinking efficiency, porosity, and swelling ratio. Mechanical characterization includes AFM, rheology, tensile testing, compressive testing, and electrical conductivity. Biological characterization includes in vitro studies, gene and protein assays, histology, and degradation kinetics.

Author/Year	Tissue Type	Decellularization Method			Homogenization Method		Material Composition			Biomaterial Type	Characterization Method			
		Chemical Decellularization Solutions	Enzymatic Digestion	Protocol Length (Total Hours)	Mechanical Method	Solubilization	dECM only	Synthetic Addition	Natural Addition		Structural	Mechanical	Biological	Animal Model
Hong 2012 <sup>192</sup>	Porcine dermis	3% Triton X-100, 4% Sodium Deoxycholate, 0.1% Peracetic acid, 4% Ethanol	0.02% Trypsin	103	Commercial Blender	NU		PEUU		Electrospun Scaffold	✓	✓		✓
Chainani 2013 <sup>193</sup>	Porcine skeletal muscle	ND	ND	ND	ND Freezer Mill	NU		PCL		Electrospun Scaffold	✓	✓	✓	
DeQuach 2013 <sup>194</sup>	Porcine skeletal muscle	1% SDS, Isopropanol, 0.001% Triton X-100	NU	146.75	Wiley Mini Mill	Pepsin	✓			Injectable Hydrogel	✓	✓	✓	✓
Takanari 2013 <sup>195</sup>	Porcine dermis	3% Triton X-100, 4% Sodium Deoxycholate, 0.1% Peracetic acid, 4% Ethanol	0.02% Trypsin	103	Commercial Blender	NU		PEUU		Electrospun Scaffold	✓	✓	✓	✓
Farnebo 2014 <sup>196</sup>	Human tendon	0.1% EDTA, 0.1% SDS	NU	28	Wiley Mini Mill	Pepsin	✓			Injectable Hydrogel	✓	✓	✓	✓
Choi 2016 <sup>197</sup>	Porcine skeletal muscle	1% SDS, Isopropanol, 0.001% Triton X-100	NU	146.75	Wiley Mini Mill	Pepsin		PCL		Bioprinted Scaffold		✓	✓	
Fu 2016 <sup>198</sup>	Porcine skeletal muscle	0.1% EDTA, 0.5% and 1% Triton X-100, 0.2% sodium deoxycholate	0.2% Trypsin	27	ND Ball Mill	Pepsin	✓			Injectable Hydrogel	✓	✓	✓	✓
Ungerleider 2016 <sup>199</sup>	Porcine skeletal muscle and umbilical cord	1% SDS, Isopropanol, 0.001% Triton X-100	40 U/mL DNase, 1 U/mL RNase	146~242	Wiley Mini Mill	Pepsin	✓			Injectable Hydrogel				✓
Rao 2017 <sup>200</sup>	Porcine skeletal muscle	1% SDS, Isopropanol, 0.001% Triton X-100	NU	146.75	Wiley Mini Mill	Pepsin	✓			Injectable Hydrogel	✓	✓	✓	✓
Hernandez 2018 <sup>59</sup>	Porcine lung, myocardium, and skeletal muscle	0.1% or 1% SDS	NU	ND	ND	Pepsin			Extracellular vesicles, microRNA(encapsulated)	Injectable Hydrogel			✓	
Toprakhisar 2018 <sup>201</sup>	Bovine tendon	1.5 M NaCl, 0.05% EDTA, 2% SDS	0.05% Trypsin	289.5	Commercial Blender	Pepsin	✓			Bioprinted Scaffold	✓	✓	✓	
Choi 2019 <sup>202</sup>	Rabbit skeletal muscle	SDS, 1% Triton X-100	DNase	122	ND	Pepsin		PLLA		Injectable Hydrogel		✓	✓	
Lee 2019 <sup>203</sup>	Porcine skeletal muscle	0.5% SDS, Isopropanol, 0.1% Peracetic acid, 4% Ethanol	NU	100	ND	Pepsin		PLGA		Electrospun Scaffold	✓	✓	✓	
Smoak 2019 <sup>204</sup>	Rabbit skeletal muscle	0.05% EDTA, 1% Triton X-100, 1.5 M NaCl	0.025% Trypsin	18.5	ND Tissue Homogenizer	NU	✓			Electrospun Scaffold		✓	✓	
Patel 2019 <sup>205</sup>	Bovine skeletal muscle	0.5% Triton X-100, 47.6 mM Ammonium hydroxide	NU	96	ND	Pepsin		PCL		Electrospun Scaffold	✓	✓	✓	
Hernandez 2020 <sup>206</sup>	Porcine skeletal muscle	1% SDS, Isopropanol	NU	144	Wiley Mini Mill	Pepsin		✓		Injectable Hydrogel		✓	✓	✓

**Table 5** (*continued*)

Author/Year	Tissue Type	Decellularization Method			Homogenization Method		Material Composition			Biomaterial Type	Characterization Method			
		Chemical Decellularization Solutions	Enzymatic Digestion	Protocol Length (Total Hours)	Mechanical Method	Solubilization	dECM only	Synthetic Addition	Natural Addition		Structural	Mechanical	Biological	Animal Model
Lee 2020 <sup>207</sup>	Rabbit skeletal muscle	1% SDS, Triton X-100	DNase	122	NU	Pepsin		PLLA		Injectable Hydrogel	✓	✓	✓	
Moreno-Manzano 2020 <sup>208</sup>	Porcine UBM	1% SDS, 0.5% Triton X-100, 0.05% Ammonia, hydroxide	NU	120	NU	Pepsin	✓			Injectable Hydrogel	✓	✓	✓	
Raj 2020 <sup>209</sup>	Porcine gallbladder	NU	NU	24	SPEX 6770	Pepsin		PEGDA		Injectable Hydrogel	✓	✓	✓	
Rajabi 2020 <sup>67</sup>	Sheep skeletal muscle, cardiac muscle, aorta, and liver, Porcine SIS, human umbilical cord	0.5% SDS, 1% Triton X-100	NU	37–139	Mortar and Pestle	Pepsin	✓			Injectable Hydrogel			✓	
Boso 2021 <sup>210</sup>	Porcine muscle	4% Sodium deoxycholate, 1 M NaCl	2000 kU DNase	124	ND Milling Method	Pepsin	✓			Injectable Hydrogel	✓	✓	✓	✓
Chae 2021 <sup>118</sup>	Porcine tendon and bone	2% Triton X-100, 25 mM EDTA, 0.1% Peracetic Acid, 40% Ethanol	0.5% Trypsin, 50 U/mL DNase	129	ND Pulverization	Pepsin	✓			Bioprinted Scaffold		✓	✓	✓
Gaffney 2021 <sup>211</sup>	Porcine skeletal muscle and tendon	0.5% Sodium deoxycholate, 1% Triton X-100, 0.0% Peracetic acid, 4% Ethanol	0.2% Trypsin	29.5	Fisher Scientific Sonic Dismembrator 120	Pepsin	✓			Injectable Hydrogel		✓	✓	
Kim 2021 <sup>212</sup>	Porcine skeletal muscle	1% SDS, 1% Triton X-100	DNase	100	NU	Pepsin				Bioprinted Scaffold			✓	✓
Lee 2021 <sup>213</sup>	Porcine skeletal muscle	1% SDS, 1% Triton X-100	DNase	123	NU	Pepsin	✓			Bioprinted Scaffold		✓	✓	✓
Liu 2021 <sup>214</sup>	Human amniotic membrane	1% Triton X-100, 0.02% EDTA	0.25% Trypsin, 50 U/mL DNase	30	ND	NU		PCL	Silk fibroin	Electrospun Scaffold	✓	✓	✓	✓
Ning 2021 <sup>215</sup>	Maquacue tendons	NU	150 IU/mL DNase, 100 µg/mL RNase	12	Retsch MM400	Pepsin	✓			Injectable Hydrogel	✓		✓	
Smoak 2021 <sup>216</sup>	Rabbit skeletal muscle	1% Triton X-100, 0.05% EDTA, 1.5 M NaCl	0.025% Trypsin	18	ND	NU	✓			Electrospun Scaffold	✓	✓	✓	
Yang 2021 <sup>217</sup>	Human amniotic membrane	75% alcohol, 1% Triton X-100	1000 U/L Lipase, 1000 U/L DNase	ND	Retch MM 400	Pepsin		PCL		Electrospun Scaffold	✓	✓	✓	
Zhao 2021 <sup>218</sup>	Porcine tendon	EDTA, 0.5% SDS, 0.5% Triton X-100, 0.1% Peracetic acid, 4% Ethanol	0.25% Trypsin	100	Retsch Cryomill	Pepsin	✓			Bioprinted Scaffold	✓	✓	✓	
Zhu 2021 <sup>219</sup>	Rat skeletal muscle	1% SDS, 0.2% Sodium deoxycholate, 0.5 and 1% Triton X-100, 0.1% EDTA	0.2% Trypsin, 9 × 10 <sup>6</sup> U/L DNase, 6 × 10 <sup>7</sup> U/ L RNase	266	ND	Pepsin	✓			Injectable Hydrogel	✓		✓	
Ning 2021 <sup>215</sup>	Maquacue tendons	NU	150 IU/mL DNase, 100 µg/mL	12	Retsch MM400	Pepsin	✓			Injectable Hydrogel	✓		✓	



### 3.2.6. Liver dECM TE

Hepatocytes are the primary functional cells of the liver parenchyma.<sup>22</sup> Hepatocytes are organized into vascularized lobules that also contain ducts of the biliary tree which transports bile through the liver for detoxification.<sup>224</sup> **(Figure 5A)** Hepatic cirrhosis is a progressive liver disease associated with chronic alcohol consumption, hepatitis, cystic fibrosis and hepatotoxic drugs.<sup>224</sup> In cirrhosis, the parenchyma of the liver is progressively replaced by scarred and fibrotic tissues. Transplants are the only solution for late-stage liver diseases such as severe cirrhosis. Even if a suitable donor is found, liver transplants have life-long, high-cost health complications.

In liver TE, design strategies aim to produce biomaterials for the culture of functional hepatocytes and to model disease progression and drug response throughout the liver parenchyma including vasculature and biliary ducts.<sup>225</sup> Progress in liver TE has been hampered because the challenge of inducing fully mature hepatocytes in standard 2D or 3D culture methods.<sup>22</sup> Although 3D Col I scaffolds improved hepatocyte survival for up to 3 weeks over 2D culture, hepatocytes still did not fully mature.<sup>225</sup> As such, existing in vitro models for the human liver are under-representative due to the use of immature hepatocytes and the lack of biliary ducts and vasculature.

Liver dECM biomaterials have the potential to provide the matrix cues necessary for functional hepatocyte culture and structurally organized liver tissue regeneration.<sup>226,227</sup> A mechanical target for liver dECM TE is the physiological stiffness of the hepatocyte niche, represented by the macro (10–15 MPa) and microscale (0.6–6 kPa) Young's modulus and  $G'$  (10–40 kPa).<sup>22,228,229</sup> Hepatocyte maturation is indicated by expression of genes in the Cytochrome P450 family, E-cadherin, fibronectin, and Col IV as well as albumin (Alb) secretion and drug metabolism. Functional targets for biliary duct generation include the formation of a branching network of specialized epithelial cells, i.e., cholangiocytes expressing HNF1 $\beta$ , SOX9, CK19, and ZO-1. Injectable hydrogels, electrospun scaffolds, and bioprinted scaffolds have been produced for liver TE applications (**Table 6**).

#### 3.2.6.1. Injectable hydrogels in liver dECM TE

Liver dECM hydrogels were initially tested as platforms for 3D hepatocyte culture.<sup>230</sup> Primary hepatocytes encapsulated within dECM enhanced Alb secretion over the Col I control over 7 days. When human hepatocarcinoma cells (Huh7), HUVECs, and MSCs were encapsulated in liver dECM, the cells self-organized into liver organoids in the dECM group and Col I control.<sup>231</sup> Huh7

upregulated hepatocyte markers in dECM compared to Col I. When a liver dECM hydrogel was implanted in a 70% partial hepatectomy rat model with encapsulated hepatocytes, the number of viable hepatocyte clusters was also significantly higher for dECM vs Col I after 1 week.<sup>226</sup> However, the viscoelastic properties of liver dECM ( $G' = 1570.5$  Pa) were much lower than the native liver ( $G' = 10\text{--}40$  kPa), limiting the organoid's structural mimicking of the liver.<sup>231</sup> While liver dECM hydrogels promoted hepatocyte function over single ECM components like Col I, the mechanical properties of the hydrogels would need to be enhanced to match those in the human hepatic niche.

#### *3.2.6.2. Electrospun scaffolds in liver dECM TE*

Electrospun dECM-polymer scaffolds could present biomolecular cues along electrospun fibrils with mechanics representative of the liver.<sup>22</sup> Electrospun scaffolds have a high surface to volume ratio, increasing the surface area available for the display of biomolecular cues within a stable polymer-supported structure.<sup>228</sup> To determine whether liver dECM created a more specific niche than single proteins, a liver dECM-PLA scaffold was compared to composites of PLA with Col I, laminin, and fibronectin.<sup>22</sup> The dECM scaffold possessed the highest macroscale Young's modulus (17–20 MPa) of any scaffold. The authors claimed this increased stiffness created a more favorable hepatocyte environment, though all were close to the average for non-fibrotic liver.<sup>22,229</sup>

Primary hepatocytes cultured on dECM-PLA increased hepatocyte marker expression after 16 days compared to single-ECM components and the PLA-only control.<sup>22</sup> On a dECM-PCL-gelatin scaffold, metabolic activity and Alb secretion increased per cell in compared to gelatin-PCL controls over 7 days. However, other markers such as Col IV and mitochondrial activity were downregulated on dECM-PLA and dECM-PCL-gelatin scaffolds, suggesting that hepatocytes did not fully mature in both scaffolds. As such, electrospun dECM scaffolds might have created a more mechanically relevant and bioactive environment than single-ECM components, but have yet to completely replicate the hepatic niche.

#### *3.2.6.3. Bioprinted scaffolds in liver dECM TE*

Bioprinting hepatocytes within a liver dECM scaffold could guide hepatocyte maturation by mimicking the structure and mechanics of the liver.<sup>232,233</sup> When encapsulated in a photocrosslinked and bioprinted dECM-GelMa scaffold, hepatocytes derived from iPSCs formed spheroids in 7 days.<sup>232</sup> The iPSC-derived hepatocytes in dECM-GelMa reached a more mature state than in a Col I control and remained viable at densities comparable to the native liver for 28

days. Liver dECM-GelMA was also used to study cirrhosis progression to hepatocellular carcinoma by culturing HepG2 cells on scaffolds patterned with stiff “cirrhotic” regions.<sup>224</sup> **(Figure 5B)** The scaffold Young’s modulus was modulated to model HepG2 activity on soft (0.5 kPa), healthy (5 kPa) and cirrhotic (10 kPa) regions. On cirrhotic regions, HepG2 migrated into surrounding regions and upregulated the metastatic marker TWIST1 indicating that stiffness may play a role in liver cancer progression.

Bioprinting has also been proposed to stimulate biliary duct formation.<sup>227,234</sup> In a liver dECM hydrogel, encapsulated cholangiocytes self-organized into branching, duct-like tubes, and expressed mature cholangiocyte markers. Such self-organized branching was not observed in the Col I control group. The liver dECM pre-gel was then bioprinted with sacrificial Pluronic F-127 **(Figure 5C)**. The sacrificial material provided the mechanical conditions for bioprinting dECM without a permanent polymer composite. After gelation, the Pluronic F-127 was removed and the dECM hydrogel was left in the shape of a branching biliary tree. When hepatocytes were seeded after 7 days, distinct duct and hepatocyte regions were observed within the co-culture. This liver function model could be used to study interactions between hepatocytes and cholangiocytes or develop an in vitro liver model that recapitulates each unique structural feature of the liver.

#### *3.2.6.4. Future perspectives*

Liver dECM poses an advantage over single ECM component methods for supporting hepatocyte culture and maturation. However, liver dECM models could be advanced by incorporating more complex liver structures and cell types. For instance, the co-culture organoid model used cancer cell lines for hepatocytes and did not assess MSC differentiation or tubule formation by HUVECs. As immortalized hepatocytes are not viable for use in humans, stem-cell derived hepatocytes together with liver dECM biomaterials could present a plausible option for clinical application to liver replacement.<sup>232</sup> Vascularization with endothelial cells could lead to improved oxygen delivery to cells and increase the potential culture length. Additionally, hepatoblasts are a major structural element of the biliary tree, forming a bilayer that is essential for signaling between the biliary ducts and vasculature.<sup>227</sup> Expanding structurally patterned co-culture of hepatocytes and these other types of liver cells from the hepatocyte-cholangiocyte platform could improve liver models. The cell-cell interplay would better represent vascularized healthy tissue, disease progression, and drug response.<sup>22</sup> These techniques could lead to more physiologically relevant liver dECM biomaterials for liver models and TE.

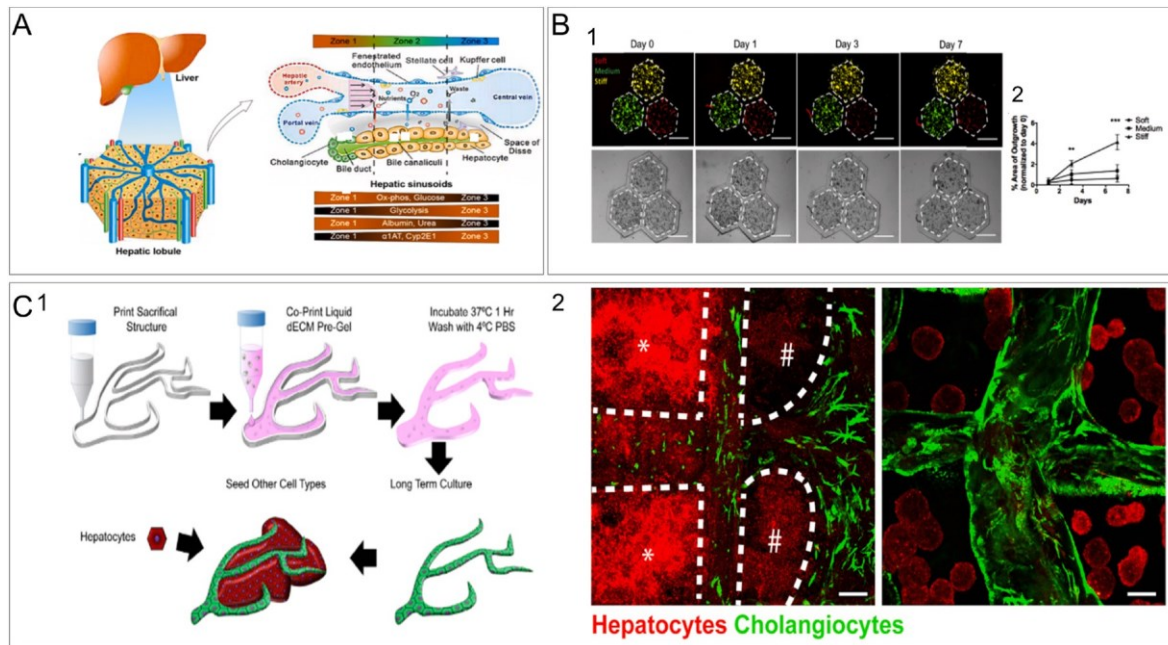


**Figure 5. Highlights of dECM Research in Liver TE.** A. Anatomy of the liver, showing the structure, cell types, and concentration of key small molecules by location. B. Bioprinted dECM Liver Stiffness Model. Hep2 cells cultured on stiff, cirrhotic-like tissue showed the greatest potential for migration and outgrowth, characteristic of malignant liver cancer. 1. Migration of Hep2 cells was tracked over 7 days of culture on stiff (yellow), medium (green) and soft (red) 2. Percent area of HepG2 migration out from stiff, medium, and soft scaffolds over 7 days. C. Bioprinted bile duct and hepatocyte construct, demonstrating the potential to reconstruct the liver parenchyma through bioprinting. 1. A Pluronic F-127 sacrificial structure was printed. A liver dECM pre-gel with encapsulated cholangiocytes was then printed into the Pluronic F-127 framework. After 1 h at 37 °C, the structure had gelled. Washing at 4 °C removed the sacrificial structure. Hepatocytes were seeded surrounding the bioprinted bile ducts after 7 days. 2. Hepatocytes (red) were either seeded after gel formation (left) and co-cultured with cholangiocytes (green) for 7 days, or seeded after 7 days of cholangiocyte-only culture (right). Low hepatocyte density was found in regions marked #. Dotted lines mark the boundary of the dECM scaffold<sup>234</sup>ld. Seeding after 7 days of cholangiocyte-only culture enabled the formation of sharply delineated bile-ducts and hepatocyte regions. Panel A. is reproduced from Ref. <sup>235</sup> (Open Access: <https://creativecommons.org/licenses/by/4.0/>); Panel B. is reproduced from Ref. <sup>224</sup>; Panel C. is reproduced from Ref. <sup>234</sup> with permissions.

**Table 6. Summary of dECM Particles in Liver Tissue Engineering.** Structural characterization includes SEM, FTIR, Raman, NMR, crosslinking efficiency, porosity, and swelling ratio. Mechanical characterization includes AFM, rheology, tensile testing, compressive testing, and electrical conductivity. Biological characterization includes in vitro studies, gene and protein assays, histology, and degradation kinetics.

Author/ Year	Tissue Type	Decellularization Method			Homogenization Method		Material Composition			Biomaterial Type	Characterization Method			
		Chemical Decellularization Solutions (Surfactants, Salts, Acids, Bases)	Enzymatic Digestion	Protocol Length (Total Hours)	Mechanical Method	Solubilization	dECM only	Synthetic Addition	Natural Addition		Structural	Mechanical	Biological	Animal Model
Skardal 2012 <sup>225</sup>	Porcine liver	2% Triton X-100	NU	216	ND Freezer Mill	Pepsin			Collagen, HA, HA	Injectable conjugated Heparin Hydrogel			✓	
Lee 2014 <sup>230</sup>	Rat liver	1% Triton X-100, 0.1% Ammonium hydroxide	NU	4.5	Mincing	Pepsin	✓			Injectable Hydrogel	✓	✓	✓	✓
Bao 2017 <sup>236</sup>	Rat liver	1% Triton X-100, 0.1% Ammonium hydroxide	NU	4.5	Wiley Mini Mill	Pepsin	✓			Injectable Hydrogel	✓		✓	
Lee 2017 <sup>233</sup>	Porcine liver	0.5% Triton X-100, 1% SDS, 0.1% Peracetic acid	NU	14	ND Milling Method	Pepsin		PCL		Bioprinted Scaffold		✓	✓	
Saheli 2017 <sup>231</sup>	Porcine liver	0.5% SDS	NU	92.5	ND Milling Method	Pepsin	✓			Injectable Hydrogel	✓	✓	✓	
Bual 2018 <sup>228</sup>	Porcine liver	1% Triton X-100	NU	168	ND Milling Method	Pepsin		PCL		Electrospun Scaffold	✓	✓	✓	
Hiller 2018 <sup>237</sup>	Human lung	0.1% SDS	350 IU/mL DNase	6	ND Milling Method	Pepsin			Gelatin, alginate	Bioprinted Scaffold		✓	✓	
Ijima 2018 <sup>238</sup>	Porcine liver	1% Triton X-100	NU	ND	Lyophilization	Pepsin	✓			Injectable Hydrogel	✓	✓	✓	
Lewis 2018 <sup>227</sup>	Porcine liver	0.1% SDS, 70% Ethanol	NU	32	ND Milling Method	Pepsin	✓			Injectable Hydrogel	✓	✓	✓	
Lewis 2018 <sup>234</sup>	Porcine liver	0.1% SDS, 70% Ethanol	NU	32	ND Milling Method	Pepsin	✓			Injectable Hydrogel	✓	✓	✓	
Ma 2018 <sup>224</sup>	Porcine liver	1% SDS	NU	87	Retsch MM400	Pepsin			GelMA	Bioprinted Scaffold	✓	✓	✓	
Grant 2019 <sup>22</sup>	Porcine liver	0.5% SDS	NU	28	Retsch PM100	NU		PLLA		Electrospun Scaffold	✓	✓	✓	
Ijima 2019 <sup>226</sup>	Porcine liver	1% Triton X-100	NU	ND	ND	Pepsin	✓			Injectable Hydrogel			✓	✓
Lee 2019 <sup>239</sup>	Porcine heart, liver, kidney, muscle, and intestine	1% Triton X-100, 1% Ammonium hydroxide, 1% SDS	NU	96	NU	Pepsin	✓			Injectable Hydrogel		✓	✓	✓
Vafaei 2019 <sup>240</sup>	Mouses adipose	2:1, 1:1, 1:2 Chloroform and methanol, Isopropanol	0.25% Trypsin	144	Mortar and Pestle	Pepsin			Glutaryl PE	Injectable Hydrogel			✓	
Yu 2019 <sup>232</sup>	Porcine liver and heart	0.5% SDS	NU	51.5	Retsch MM400	Pepsin			GelMA	Bioprinted Scaffold	✓	✓	✓	
Ahmed 2020 <sup>241</sup>	Rat liver	1% Triton X-100	0.1% DNase	ND	ND Milling Method	Pepsin	✓			Injectable Hydrogel	✓		✓	
Hussein 2020 <sup>242</sup>	Rat liver	0.1% SDS, 0.1% Peracetic acid		4	ND	Pepsin	✓			Injectable Hydrogel	✓		✓	
Kim 2020 <sup>243</sup>	Porcine liver	1% Triton X-100, 0.1% Ammonium hydroxide	NU	12	SPEX 6870D	Pepsin			Gelatin, HA	Bioprinted Scaffold	✓	✓	✓	
Mao 2020 <sup>244</sup>	Porcine liver	1% Triton X-100, 2% SDS	0.025% Trypsin	72.5	ND Milling Method	Pepsin			GelMA	Bioprinted Scaffold	✓	✓	✓	
Asadi 2021 <sup>245</sup>	Rat liver	0.5% SDS, 1.5% Triton X-100	NU	157	ND Milling Method	Acetic Acid	✓			Injectable Hydrogel	✓		✓	
Chen 2021 <sup>246</sup>	Porcine liver	1% SDS, % Triton X-100	NU	132	NU	Pepsin	✓			Injectable Hydrogel			✓	
Choi 2021 <sup>247</sup>	Porcine axillary lymph node and cardiac muscle	0.1% or 1% SDS	NU	55–91	ND	Pepsin	✓			Injectable Hydrogel	✓		✓	✓

**Table 6** (continued)

Author/ Year	Tissue Type	Decellularization Method			Homogenization Method		Material Composition			Biomaterial Type	Characterization Method			
		Chemical Decellularization Solutions (Surfactants, Salts, Acids, Bases)	Enzymatic Digestion	Protocol Length (Total Hours)	Mechanical Method	Solubilization	dECM only	Synthetic Addition	Natural Addition		Structural	Mechanical	Biological	Animal Model
Janani 2021 <sup>248</sup>	Porcine liver	1% Triton X-100, 0.1% Ammonium hydroxide	NU	12	ND	Pepsin			Silk Fibroin	Molded Scaffold	✓		✓	✓
Jeong 2021 <sup>249</sup>	Porcine liver	1% Triton X-100, 0.1% Ammonium	NU	50	ND	Pepsin	✓			Bioprinted Scaffold	✓	✓	✓	
Kang 2021 <sup>76</sup>	Porcine heart, liver, and colon	1 M NaCl, 1% Triton x- 100, 0.1% Peracetic acid	NU	49.5	ND	Pepsin	✓			Bioprinted Scaffold		✓	✓	
Li 2021 <sup>250</sup>	Rat liver	1% SDS, Triton X-100	NU	22.5	ND	Pepsin	✓			Injectable Hydrogel	✓		✓	✓

### 3.2.7. Bone dECM TE

Bone has dense ECM and bound minerals such as hydroxyapatite, with a porous and mesh-like structure.<sup>270</sup> Bone defects result from traumatic injuries, craniectomies, and degenerative musculoskeletal diseases.<sup>251,254</sup> Critical size bone defects cannot be fully repaired by the host's innate wound healing process. At present, critical size bone defects are frequently treated with bone allografts.<sup>105</sup> However, allografts are difficult to process and sterilize as they are restricted by the amount of bone that can be safely removed from a donor and in shaping bone to the defect requirements.<sup>253</sup> Also, allografts possess limited regenerative capacity and high fracture risk at the defect site.<sup>251,254</sup> For example, cranioplasty with allografts often requires a long recovery time with long-term side effects ranging from headaches to reduced dexterity.

In bone TE, design strategies aim to produce bioactive materials that induce MSC differentiation into osteoblasts, which are responsible for the generation of new bone, or osteogenesis.<sup>252</sup> Mechanical integrity of both the biomaterial and regenerated tissue is essential to prevent reinjury. Demineralized bone matrix particles (DBM) have been used to fill bone defects and stimulate osteoblast differentiation.<sup>251</sup> However, DBM efficacy varies significantly because demineralization reduces the structural integrity of remaining ECM components and retains inflammatory foreign DNA.

Instead of DBM, bone dECM can potentially stimulate osteogenesis and be readily shaped to meet defect requirements without the risks presented by foreign DNA.<sup>253</sup> Osteogenesis is indicated by osteogenic markers (osteocalcin, RunX2, Col I, OPN), alkaline phosphatase (ALP) activity, and calcium deposition.<sup>258</sup> Bone dECM TE also aims to match relevant mechanical properties with respect to native bone such as the storage modulus ( $G'$ , 8–11 GPa) and macroscale Young's modulus (2–10 GPa).<sup>271,272</sup> A variety of bone dECM injectable hydrogels, electrospun, and bioprinted scaffolds have been designed to promote bone repair (**Table 7**).

#### 3.2.7.1. Injectable hydrogels in bone dECM TE

The osteogenic capacity of bone dECM has been demonstrated with replicability.<sup>251,254,256</sup> However, bone dECM hydrogels possessed low  $G'$  (~150 Pa at 6 mg/mL) compared to bone (8–11 GPa).<sup>251</sup> Composites of bone dECM and polymers were proposed to improve hydrogel mechanics. For example, a bone dECM-alginate hydrogel combined the mechanical tunability of alginate and bioactivity of dECM into a stable scaffold, though its Young's modulus (3.4 MPa)

remained lower than native bone, though cellular activity may stiffen the scaffold over time.<sup>254</sup>

Carbodiimide crosslinking with GAGs (for instance, HA and chondroitin sulfate) without pepsin solubilization are indicated for improved mechanics and increased osteogenic capacity, indicating non-enzymatic methods for dECM hydrogel preparation aid in cell-matrix cue preservation.<sup>23,26</sup> In particular GAG-ECM hydrogels enhanced osteogenic differentiation of ASCs without pepsin solubilization and increased the maximum  $G'$  to 1–10 kPa.

The GAG-ECM hydrogels were prepared from porcine bone, cartilage, adipose, lung and spleen to investigate the impact of tissue specificity on osteogenic differentiation.<sup>26</sup> Bone dECM displayed the greatest osteogenic capacity, while cartilage and adipose performed more robustly than lung or spleen. These results indicated that tissue source could be a determining factor in scaffold efficacy for inducing osteogenesis.

#### *3.2.7.2. Electrospun scaffolds in bone dECM TE*

The nanostructural architecture of bone can be imitated by electrospinning polymeric nanofibers, i.e., PCL.<sup>258</sup> The addition of dECM was predicted to promote osteogenesis to overcome the major shortcoming in polymer-only electrospun scaffolds. In one study, the PCL scaffolds were coated with dECM. The expression of osteogenic genes was enhanced in ASCs cultured in the PCL-dECM scaffolds compared to PCL-only scaffolds.<sup>252</sup> The coating may have limited the tunability of dECM degradation and bioactive stability.

Compared to the coating method, electrospinning dECM and PCL within the same solution was predicted to integrate the biological cues of dECM into the PCL framework with greater availability and stability.<sup>258</sup> This dECM was derived from co-culture of MSCs and HUVECs. The addition of dECM from co-culture did not significantly change  $G'$  from PCL (~12 MPa), while scaffolds containing dECM from MSC monoculture possessed a significantly lower  $G'$  (~8.6 MPa). ALP activity and osteogenic marker expression were enhanced in scaffolds containing dECM after 14 days. A comparative study of electrospun dECM-coated scaffolds versus integrated dECM-PCL scaffolds in mechanical properties and cellular behavior could provide vital information towards the development of bioactive electrospun scaffolds for bone TE.

#### *3.2.7.3. Bioprinted scaffolds in bone dECM TE*

A bone dECM bioink has also been developed with the goal of replicating the bone microenvironment through controlled patterning.<sup>257</sup> This bioink was used in composite with PCL



and an osteoconductive ceramic, beta-tricalcium phosphate ( $\beta$ -TCP). The incorporation of bone dECM into the PCL- $\beta$ -TCP composite was found to enhance cellular attachment and osteogenic marker expressions in pre-osteoblastic C3T3-E1 cells. The combination of dECM and  $\beta$ -TCP maximized osteogenic marker expression in pre-osteoblastic C3T3-E1 cells. When implanted in a rabbit cranial defect, bone dECM absorbed surrounding bone marrow into the scaffold, creating a pro-regenerative environment. Overall, this tri-component composite displayed a synergistic effect on osteogenesis when compared to scaffolds containing only dECM or  $\beta$ -TCP with PCL.

#### *3.2.7.4. Future prospects*

Bone dECM biomaterials show potential, yet numerous variables remain to be addressed for eventual clinical applications. Thus far, the evidence suggests that bone dECM biomaterials are effective in enhancing osteogenesis for bone TE. Several studies suggested incorporation of osteogenic additives (i.e.,  $\beta$ -TCP). Further investigation is needed to evaluate the risk of extraneous bone growth. It is vital to address whether the cues provided by dECM prevent these osteogenic additives from being transported to other regions.

Multiple studies noted the suboptimal mechanical strength of dECM biomaterials compared to bone, even in composite with tunable polymers. Some studies did not perform mechanical testing despite its importance to the integrity of the repaired bone tissue. In future work, parameters that signify a biomaterial meets the mechanical requirements for bone TE should be outlined and mechanical tuning should be performed to meet those parameters.

**Table 7. Summary of dECM Particles in Bone Tissue Engineering.** Structural characterization includes SEM, FTIR, Raman, NMR, crosslinking efficiency, porosity, and swelling ratio. Mechanical characterization includes AFM, rheology, tensile testing, compressive testing, and electrical conductivity. Biological characterization includes in vitro studies, gene and protein assays, histology, and degradation kinetics.

Author/Year	Tissue Type	Decellularization Method			Homogenization Method		Material Composition			Biomaterial Type	Characterization Method			
		Chemical Decellularization Solutions	Enzymatic Digestion	Protocol Length (Total Hours)	Mechanical Method	Solubilization	dECM only	Synthetic Addition	Natural Addition		Structural	Mechanical	Biological	Animal Model
Sawkins 2012 <sup>251</sup>	Bovine bone	0.5 N HCl, 1:1 Chloroform and methanol, 0.02%EDTA	0.05% Trypsin	73	Liquid Nitrogen Fragmentation	Pepsin	✓			Injectable Hydrogel	✓	✓	✓	
Gibson 2014 <sup>252</sup>	Porcine bone, cartilage, adipose, liver, spleen, lung, human bone	3% Peracetic acid, 1% Triton X-100	600 U/mL DNase	39	SPEX 6770	Pepsin		PCL		Electrospun Scaffold	✓		✓	
Ni 2015 <sup>253</sup>	Human bone	3% Hydrogen peroxide	NU	ND	ND	NU		PEG-PCL-PEG		Injectable Hydrogel	✓		✓	✓
Smith 2014 <sup>254</sup>	Bovine bone	0.5 N HCl, 1:1 Chloroform, and methanol, 0.02%EDTA	0.05% Trypsin	73	Liquid Nitrogen Fragmentation	Pepsin		PLGA	Alginate	Injectable Hydrogel		✓	✓	✓
Smith 2014 <sup>255</sup>	Bovine bone	0.5 N HCl, 1:1 Chloroform and methanol, 0.02%EDTA	0.05% Trypsin	73	Liquid Nitrogen Fragmentation	Pepsin		PLGA	Alginate	Injectable Hydrogel		✓	✓	✓
Alom 2017 <sup>256</sup>	Bovine bone	0.5 N HCl, 1:1 Chloroform and methanol, 0.02%EDTA	0.05% Trypsin	73	Coffee grinder	Pepsin	✓			Injectable Hydrogel			✓	
Beachley 2017 <sup>26</sup>	Porcine bone, adipose, liver, spleen, lung	0.5 N HCl, 3% Peracetic acid, 1% Triton X-100	600 U/mL DNase	39	SPEX 6770	NU		PEG	CS, HA	Injectable Hydrogel		✓	✓	✓
Kim 2018 <sup>257</sup>	Porcine bone	0.5 N HCl, 1:1 Chloroform and methanol, 0.02% EDTA	0.05% Trypsin	73	Meat grinder	Pepsin		PCL		Bioprinted Scaffold		✓	✓	✓
Kusuma 2018 <sup>23</sup>	MSC-derived	0.5% Triton X-100, 20 mM Ammonium hydroxide	100 U/mL DNase	1	NU	Pepsin, urea, or acetic acid	✓			Injectable Hydrogel			✓	
Basiri 2019 <sup>94</sup>	Human umbilical cord, Wharton's Jelly	NU	NU	16	NU	NU			Silk fibroin	Injectable Hydrogel	✓	✓	✓	
Carvalho 2019 <sup>258</sup>	MSC and HUVEC-derived	0.5% Triton X-100, 20 mM Ammonium hydroxide	NU	0.1	Lyophilization	NU		PCL		Electrospun Scaffold	✓	✓	✓	
Mohiuddin2019 <sup>259</sup>	Human adipose	0.5 M and 1 M NaCl, Isopropanol, 1% Triton X-100	0.25% Trypsin	249	ND Milling Method	Pepsin	✓			Injectable Hydrogel				✓

Table 7 (Continued)

Author/Year	Tissue Type	Decellularization Method			Homogenization Method		Material Composition			Biomaterial Type	Characterization Method			
		Chemical Decellularization Solutions	Enzymatic Digestion	Protocol Length (Total Hours)	Mechanical Method	Solubilization	dECM only	Synthetic Addition	Natural Addition		Structural	Mechanical	Biological	Animal Model
Shridhar 2019 <sup>178</sup>	Bovine bone and human adipose	5 mM EDTA, 23% Formic acid, Isopropanol	DNase, RNase	57	Retsch	Proteinase K			MCS	Injectable Hydrogel	✓		✓	
Wu 2019 <sup>260</sup>	Porcine bone	10% Formic acid, 3% Peracetic acid, 1% Triton X-100, 2 mM EDTA	600 U/mL DNase	172	SPEX 6670	Pepsin	✓			Injectable Hydrogel	✓	✓	✓	✓
Black 2020 <sup>261</sup>	Bovine bone	0.5 N HCl, 1:1 Chloroform and methanol, 0.02% EDTA	0.05% Trypsin	73	Coffee grinder	Pepsin	✓			Injectable Hydrogel			✓	✓
Choi 2020 <sup>262</sup>	Porcine bone	dECM from T&R Biofab	NA	NA	ND Milling Method	NU	✓			Electrospun Scaffold	✓	✓	✓	
Junka 2020 <sup>263</sup>	Osteoblast and endothelial cell-derived	125 mM SB-10, 0.14% Sodium deoxycholate, 0.6 mM SB-16	NU	96	NU	NU		PCL		Electrospun Scaffold	✓	✓	✓	✓
Luciana 2020 <sup>264</sup>	Bovine bone	0.5 N HCl, 1:1 Chloroform and methanol, 0.02% EDTA	0.05% Trypsin	73	Liquid Nitrogen Fragmentation	Pepsin		Barium titanite		Injectable Hydrogel	✓	✓	✓	
Obregon- Miano 2020 <sup>265</sup>	Porcine bone	0.5 N HCl, 1:1 Chloroform and methanol, 0.02% EDTA	0.05% Trypsin	73	Liquid Nitrogen Fragmentation and Commercial grinder	Pepsin		PEGDA		Injectable Hydrogel		✓	✓	
Datta 2021 <sup>266</sup>	Porcine bone	0.02% EDTA	0.05% Trypsin	48	ND	Pepsin			Collagen and oleoyl chitosan	Injectable Hydrogel	✓	✓	✓	✓
Dong 2021 <sup>267</sup>	Porcine bone	1% Triton X-100, Methanol, 12% EDTA	DNase	242	ND	Pepsin		PCL		Electrospun Scaffold	✓	✓	✓	✓
Kim 2021 <sup>268</sup>	MSC-derived	0.1% Triton X- 100	NU	1	NU	Pepin		PEG diacrylate		Molded Scaffold	✓	✓	✓	✓
Parthiban 2021 <sup>269</sup>	Bovine bone	0.5 N HCl, 1:1 Chloroform and methanol, 0.02% EDTA	0.05% Trypsin	73	SPEX 6700	Pepsin	✓			Bioprinted Scaffold	✓		✓	
Zhang 2021 <sup>130</sup>	Goat bone and cartilage	0.5 N HCl, 1:1 Chloroform and methanol, 0.02% EDTA, 1% Triton X-100	50 U/mL DNase, 1 U/mL RNase	87	ND	Pepsin			Silk Fibroin	Bioprinted Scaffold	✓	✓	✓	✓

### 3.2.8. Skin tissue engineering

Healthy skin has extensive vasculature, hair follicles, and sweat glands.<sup>30,273</sup> (**Figure 6A-B**) The epidermal barrier layers have high levels of keratin, while the dermis conducts extensive biomolecular signaling and produces the elastin, Col I, and Col III that grant the skin its viscoelasticity. While the skin has a robust wound healing system against everyday insult, severe injuries such as full-thickness third or fourth degree burns or diabetic wounds are beyond the skin's capacity for self-regeneration.<sup>273,274</sup> Skin autografts are the standard treatment, though these are not an option for extensive burns due to skin availability and are less effective for diabetic wounds.<sup>273</sup> Decellularized grafts are widely used and have improved diabetic wound healing and increased survival for patients with extensive third-degree burns.<sup>30,273</sup> However, currently available dermal replacements often require a second procedure to replace the epidermis.

Ongoing research efforts in skin TE aim to produce biomaterials that replicate the epidermal and dermal layers for full thickness skin replacement in a single procedure.<sup>273</sup> Design strategies have focused on producing architectural features and cell patterning through 3D bioprinting, as well as studying the wound healing process in in vitro models.<sup>30,273</sup> However, the efficacy of existing biomaterials for skin TE is limited by the lack of diverse cell types and cues for producing vasculature, sweat glands, and hair follicles.

The biomolecular cues contained in skin dECM have the potential to regenerate the functional features of skin when patterned with varied skin cells and architecture.<sup>30</sup> The goal is to enhance the expression of genes involved in skin regeneration processes such as hair follicle development, ECM organization, and skin barrier development.<sup>275</sup> For example, keratinocytes are expected to express involucrin, keratin 10 and KGF1.<sup>30</sup> Targets for epidermis restoration are thickness between 75 and 150  $\mu\text{m}$ , trans-epithelial resistance of about 5500  $\Omega$ , and reduced water permeability.<sup>30</sup> The regenerated dermis is expected to restore the capillary network. Injectable hydrogels and bioprinted scaffolds are under development in contemporary skin dECM TE (**Table 8**).

#### 3.2.8.1. Injectable hydrogels in skin dECM TE

dECM hydrogels have been tested to stimulate diabetic wound healing. Skin dECM was isolated from thrombospondin-2 knockout mice to fabricate a skin dECM hydrogel, which was hypothesized to stimulate angiogenesis because thrombospondin-2 knockout enhances EC and

fibroblast migration.<sup>274</sup> In a diabetic mouse model, the knockout skin dECM hydrogel promoted cell infiltration 20–100  $\mu\text{m}$  deeper into the hydrogel compared to wild type skin dECM and a knockout-wild type mixture 5 days after injection. A higher number of blood vessels also formed in the knockout hydrogel, along with increased expression of CD31 and  $\alpha$ -SMA, indicating lumen formation and vessel stabilization, respectively. Initial results supported the use of knockout skin dECM hydrogel for revascularization in diabetic wounds.

Another skin dECM hydrogel for diabetic wound healing focused on hair follicle and sweat gland regeneration.<sup>276</sup> In a rat diabetic wound model, wounds covered with hydrogels that contained skin dECM, sacchachitin, or their composite closed the wound and formed an epithelial layer within 14 days (**Figure 6C**). Sacchachitin has a chemotactic effect on cells that may aid wound healing together with dECM. Wounds treated with HA or chitosan hydrogels closed in 16 days. The formation of an extensive network of capillaries in wounds treated with dECM-sacchachitin after 8 days, whereas capillaries were only found on day 14 in other groups, likely enabled more efficient oxygen delivery to cells, facilitating diabetic wound regeneration. Additionally, hair follicles, sweat glands, and neo-ECM were morphologically mature in the dECM-SC hydrogel by day 14 compared to other formulations. The combination of dECM and sacchachitin accelerated the wound healing process and contributed to a more complete regenerative effect on diabetic wounds.

#### 3.2.8.2. Bioprinted scaffolds for skin dECM TE

Bioprinted dECM scaffolds were proposed to stimulate skin regeneration using patterned architecture representative of the native skin. Kim et al. developed a skin-derived dECM bioink that might better resemble the skin's heterogeneous microstructure and bioactivity, compared to previously developed, homogeneous bioinks.<sup>30</sup> (**Figure 6D**) In particular, skin dECM or Col I were patterned into a dermal layer containing skin fibroblasts and an epidermal layer containing keratinocytes. After 10 days of culture in a liquid-air interface model, the skin dECM scaffold showed greater stability with little contraction (7.8%). Also, the thickness of the epidermal layer reached about 98  $\mu\text{m}$ , which is close to that of the native human epidermis. In contrast, the Col I scaffold controls showed about 47% retraction, with a thinner epidermal layer ( $\sim 22 \mu\text{m}$ ) after 10 days of culture. In addition, the epidermal section of the dECM scaffold demonstrated stronger expression of early (keratin 10) and late stage (involucrin) stratification markers compared to the Col I scaffold. The skin dECM scaffold also enhanced epidermal function over the Col I scaffold,

with higher TEER (2000–4500 vs 750–1100) and decreased permeability (70% vs 53%). Results suggested that the skin dECM scaffold could help promote the regeneration of a functional, stratified epidermis.

Kim et al.'s group also developed the skin dECM bioink as a printable skin patch for more efficient skin wound healing. ASCs alone or together with endothelial progenitor cells were encapsulated in the patch. The patch was applied to full-thickness excision skin wounds in mice.<sup>30</sup> Compared to ASC-only or cell free dECM patches, the patch with both ASC and endothelial progenitor cells accelerated healing of the full thickness wound over a 21-day period. The key factor in this accelerated healing was that the presence of endothelial progenitor cells promoted early vascularization. Early vascularization simultaneously provided an increased oxygen supply to cells in the patch and stimulated cell recruitment to aid in remodeling of injured tissue. Bioprinting skin dECM provides unique opportunities for accelerating skin regeneration by pre-patterning the skin's layers, blood vessels, and glands into one material.

#### *3.2.8.3. Future prospects*

Skin dECM has made significant strides towards regenerating functional skin tissue. A key step toward complete skin regeneration is ensuring that each type of skin microarchitecture develops in the neo-tissue. Methods for regenerating the epidermis or hair follicles have been investigated in isolation. Ideally, these techniques should be combined as skin TE moves forward. For instance, skin tissue development could be more completely replicated in vitro by co-encapsulating different cell types in the regions of a layered skin dECM construct. Both epidermal and hair follicle regeneration could be evaluated in the same construct by encapsulating keratinocytes in the epidermal region, and fibroblasts and dermal papilla cells in the dermal region.

Likewise, bioprinted skin dECM scaffolds have produced a stratified epidermis on a simple, fibroblast-laden dermis. Bioprinting techniques could be used to pre-pattern hair follicles and sweat glands within a skin dECM scaffold. Stem cells patterned along with these architectural features could aid in the development of functional glands. Advanced biomaterial strategies such as mechanically active wound dressings could be integrated for faster, better skin healing.<sup>277</sup> With several clinically approved products in use, skin dECM biomaterials have proven efficacy in skin regeneration. However, ongoing work is necessary to completely regenerate each functional feature of the skin.

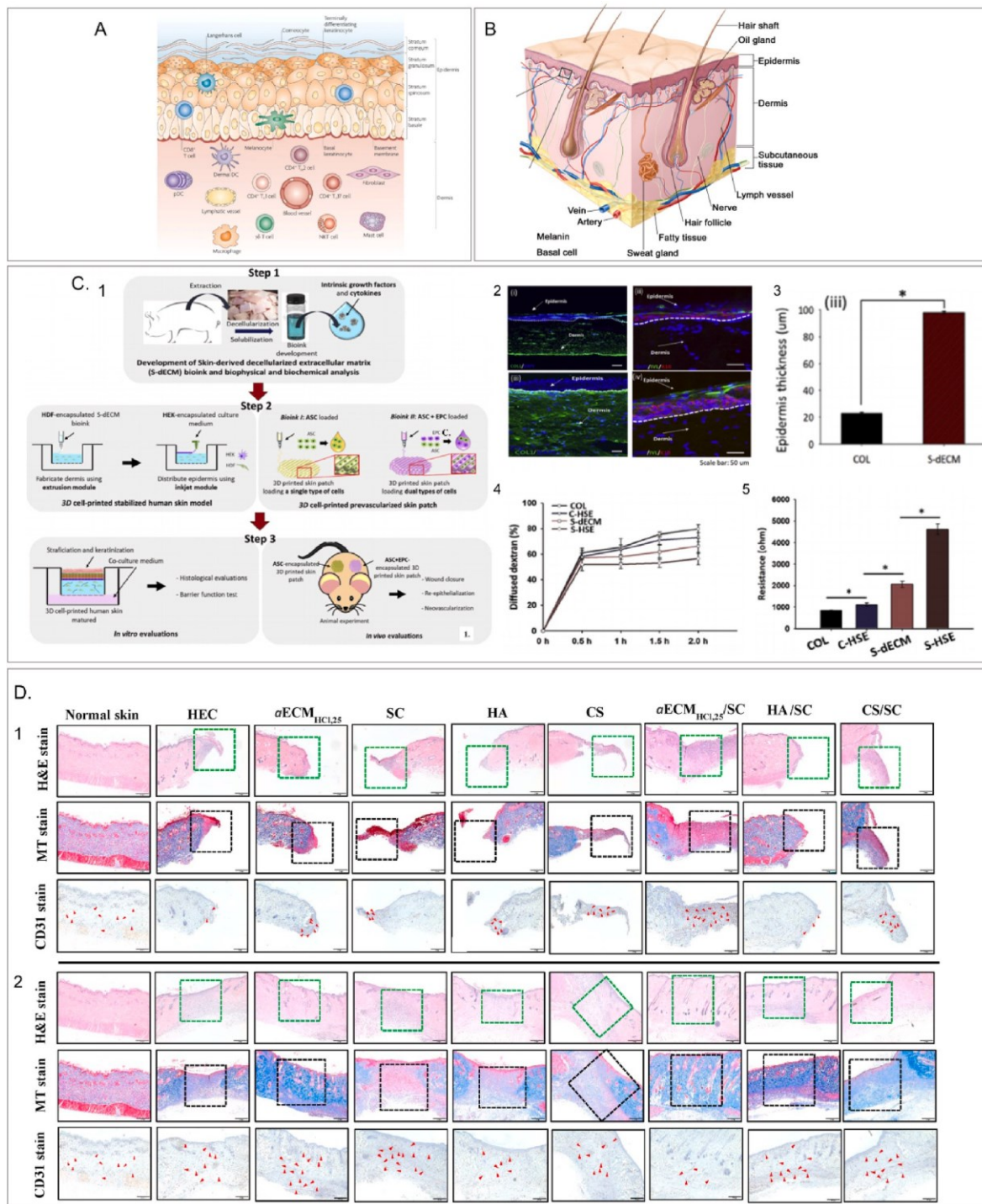


**Figure 6. Highlights of dECM Research in Skin TE.** A. Anatomy of Skin Including Cells in the Epidermal and Dermal layers B. Schematic Representation of Normal Skin Including Hair Follicles and Glands. Masson's Trichrome shows hair follicle formation while CD 31 shows blood vessel formation. Normal skin control. Injectables tested from left to right were: Hydroxyethyl

cellulose (HEC), dECM-only, sacchachitin-only, HA-only, CS-only, dECM-sacchachitin, HA-sacchachitin, and CS-sacchachitin. C. dECM Bioink Replicating the Epidermal and Dermal Layers of the Skin 1. Flow diagram of skin bioink production and the in vitro and in vivo models used in the study 2. Human keratinocytes cultured in the epidermal layer and human dermal fibroblasts in the dermal layer of Col (top) or dECM (bottom) encapsulated bioprinted constructs (HSE) with: 3. Epidermal thickness 4. Water permeability and 5. Electrical resistance. D. dECM-Sacchachitin Hydrogel for Promoting Regeneration of Skin Structures. Histological staining by H&E, Masson's Trichrome (MT), and CD 31 after 1. 8 days and 2. 14 days in a rat skin wound model. Panel A. is reproduced from Ref. <sup>278</sup>; Panel B. is reproduced from the National Cancer Institute; Panel C is reproduced from Ref. <sup>30</sup>; Panel D. is reproduced from Ref. <sup>276</sup> with permissions.



**Table 8. Summary of dECM Particles in Skin Tissue Engineering.** Structural characterization includes SEM, FTIR, Raman, NMR, crosslinking efficiency, porosity, and swelling ratio. Mechanical characterization includes AFM, rheology, tensile testing, compressive testing, and electrical conductivity. Biological characterization includes in vitro studies, gene and protein assays, histology, and degradation kinetics.

Author/Year	Tissue Type	Decellularization Method			Homogenization Method		Material Composition			Biomaterial Type	Characterization Method			
		Chemical Decellularization Solutions	Enzymatic Digestion	Protocol Length (Total Hours)	Mechanical Method	Solubilization	dECM only	Synthetic Addition	Natural Addition		Structural	Mechanical	Biological	Animal Model
Wolf 2012 <sup>279</sup>	Porcine dermis and UBM	70% Ethanol, 3% Hydrogen peroxide, 1% Triton X-100, 0.26% EDTA, 0.1% Peracetic acid, 4% Ethanol	0.25% Trypsin	40.25	Wiley Mini Mill	Pepsin	✓			Injectable Hydrogel	✓	✓	✓	✓
Wolf 2014 <sup>280</sup>	Porcine dermis	70% Ethanol, 3% Hydrogen peroxide, 1% Triton X-100, 0.26% EDTA, 0.1% Peracetic acid, 4% Ethanol	0.25% Trypsin	40.25	ND	Pepsin		Polypropylene		Injectable Hydrogel	✓	✓		✓
Lee 2016 <sup>281</sup>	Human foreskin	25 mM Ammonia	NU	20	ND Freezer mill	NU		PCL		Bioprinted Scaffold	✓	✓	✓	
Ahn 2017 <sup>282</sup>	Porcine skin	70% Ethanol, 3% Hydrogen peroxide, 1% Triton X-100, 0.26% EDTA, 0.1% Peracetic acid, 4% Ethanol	0.25% Trypsin	40.25	ND	Pepsin	✓			Bioprinted Scaffold	✓	✓	✓	
Kim 2018 <sup>30</sup>	Murine skin	70% Ethanol, 3% Hydrogen peroxide, 1% Triton X-100, 0.26% EDTA, 0.1% Peracetic acid, 4% Ethanol	0.25% Trypsin	40.25	ND	Pepsin	✓			Injectable Hydrogel	✓	✓	✓	
Morris 2018 <sup>274</sup>	Porcine skin	70% Ethanol, 3% Hydrogen peroxide, 1% Triton X-100, 0.26% EDTA, 0.1% Peracetic acid, 4% Ethanol	0.25% Trypsin	40.25	ND	Pepsin	✓			Bioprinted Scaffold		✓	✓	✓
Shi 2019 <sup>283</sup>	Porcine dermis	70% Ethanol, 3% Hydrogen peroxide, 1% Triton X-100, 0.26% EDTA, 0.1% Peracetic acid, 4% Ethanol	0.25% Trypsin	40.25	SPEX	Pepsin	✓			Bioprinted Scaffold	✓	✓	✓	
Tan 2019 <sup>284</sup>	Porcine dermis	Triton X-100	Trypsin	ND	SPEX	Pepsin	✓			Injectable Hydrogel			✓	
Tang 2019 <sup>285</sup>	Porcine skin	3% Tween-20, 4% Sodium deoxycholate, 0.1% Peracetic acid	0.02% Trypsin	2	ND	Pepsin	✓			Injectable Hydrogel		✓	✓	
Won 2019 <sup>275</sup>	Porcine	0.5% SDS,	NU	6	NU	Pepsin	✓			Injectable Hydrogel			✓	
Zhang 2019 <sup>286</sup>	Porcine SIS	1:1 Methanol and Chloroform, 0.05% EDTA, 0.5% SDS, 0.9% NaCl, 0.1% Peracetic acid, 20% Ethanol	0.05% Trypsin	28.5	TissueLyser-24	Pepsin	✓			Bioprinted	✓	✓	✓	

**Table 8** (Continued)

Author/Year	Tissue Type	Decellularization Method			Homogenization Method		Material Composition			Biomaterial Type	Characterization Method			
		Chemical Decellularization Solutions	Enzymatic Digestion	Protocol Length (Total Hours)	Mechanical Method	Solubilization	dECM only	Synthetic Addition	Natural Addition		Structural	Mechanical	Biological	Animal Model
Bankoti 2020 <sup>28</sup>	Human placenta	N-ethylmaleimide N-lauryl sarcosine	NU	16	NU	Pepsin	✓			Injectable Hydrogel			✓	
Bo 2020 <sup>288</sup>	Human skin	70% Ethanol, 3% Hydrogen peroxide, 1% Triton X-100, 0.26% EDTA, 0.1% Peracetic acid, 4% Ethanol	0.25% Trypsin	40.25	ND Freezer mill	Pepsin			Fibrinogen	Bioprinted Scaffold		✓	✓	
Hshieh 2020 <sup>276</sup>	Porcine skin	Acetone, 10% NaCl, 1.92% Citrate buffer, 30% Formic acid	0.25% Trypsin	234	ND	Pepsin			Sacchachitin	Injectable Hydrogel	✓	✓	✓	✓
Jorgenson 2020 <sup>289</sup>	Porcine skin	1 M NaOH	0.25% Trypsin	17	Macrohomogenizer	Pepsin	✓			Injectable Hydrogel		✓	✓	
Lee 2020 <sup>290</sup>	Rat skin	Hypertonic NaCl, EDTA, Triton X-100, 1:1 Chloroform and Methanol	0.25% Trypsin	ND	ND Mechanical Milling	Pepsin			Chitosan	Injectable Hydrogel	✓	✓	✓	
Allbritton-King 2021 <sup>291</sup>	UBM	8 mM PIPES buffer, 1 M NaCl, 25 mM EDTA, 1.8 mM SDS	NU	23.5	JavaPresse Espresso Grinder	Pepsin	✓			Injectable Hydrogel		✓✓	✓	
Barthold 2021 <sup>292</sup>	Porcine skin, articular cartilage, and skeletal muscle	2% SDS	0.1% DNase	13–29	ND Freezer mill	NU		PEGDA	HA	Molded Scaffold	✓	✓	✓	✓
Cai 2021 <sup>293</sup>	Porcine skin	1% Triton X-100, 1% CH3(CH2)11SO4Na	NU	18	ND Milling Method	Pepsin	✓			Injectable Hydrogel	✓		✓	✓
Huang 2021 <sup>294</sup>	Porcine skin	Supercritical carbon dioxide, 25% Sodium Hydroxide	0.5 U/mL Papain	6	ND Homogenizer	Papain			Alginate	Molded Scaffold	✓			
Jin 2021 <sup>295</sup>	Porcine skin	1 M NaCl, 1% Triton X-100, 25 mM EDTA	0.25% Trypsin	>54	NU	Pepsin			GelMA	Bioprinted Scaffold	✓	✓	✓	✓
Wang 2021 <sup>296</sup>	Human placenta, umbilical cord, and amniotic membrane	1% SDS, 0.1% EDTA	600 U/mL DNase	115.5	ND	Pepsin	✓			Injectable Hydrogel	✓	✓	✓	✓
Xu 2021 <sup>297</sup>	Porcine skin	1 mM EDTA, 1% Triton X-100, 10% Isopropanol, 0.1% Peracetic acid, 4% Ethanol	0.25% Trypsin, 30 U/mL DNase	86	NU	Pepsin			Gelatin, chitosan	Molded Scaffold	✓	✓	✓	

### 3.2.9. Lung dECM TE

The lungs are a series of branching tubes that are made of cartilages, mucosa, and epithelial cilia lining. The alveoli are sacs at the tips of the bronchioles where oxygen exchange occurs. Chronic lung diseases such as pulmonary fibrosis and chronic obstructive pulmonary disease (COPD) are characterized by inflammation, fibrosis, and excessive mucus production that obstructs the distal airways and negatively affects gas exchange.<sup>300,313</sup> The innate regeneration of distal lung tissue is limited in patients with chronic lung disease. For early-stage COPD, only 30% per dose of existing drugs reach the affected areas due to the lung's branching structure, mucociliary clearance, and disease symptoms such as mucus hypersecretion and airway closure.<sup>298</sup> Surgical intervention through lung transplant is currently the only option for end stage COPD. However, this procedure is highly invasive and has a greater than 60% ten-year mortality rate.<sup>314</sup>

Lung TE has focused on two areas: total lung replacements and drug carriers for distal lung delivery.<sup>315,316</sup> For the latter, protein-based carriers are under development for drug delivery as proteins are cleared by the mucosal cilia more slowly than other drugs, but these methods are in early stages of development.<sup>300</sup> The development of effective treatments has been further complicated by the lack of effective experimental models for COPD progression and drug response and the persistent cyclic deformation under large strain during breathing.<sup>27</sup>

Aerosolized lung dECM has the potential to serve as both delivery vector and drug, as an agent for tissue remodeling.<sup>299</sup> The primary targets for distal lung remodeling via dECM are to reach a sufficient amount of nanoparticle deposition that will promote proliferation of alveolar epithelial cells in the affected distal lung region.<sup>299,300</sup> Ideally, the remodeled lung tissue would be able to restore the mechanics of lung tissue such as the Young's modulus (1–5 kPa).<sup>303</sup> Electrospun scaffolds and gelatinous nanoparticles from particulate lung dECM have been designed for modeling lung disease and remodeling the distal lung (**Table 9**).

#### 3.2.9.1. Injectable hydrogels in lung dECM TE

Lung dECM was crosslinked with photopolymerizable PEG using thiol-ene click chemistry to produce a hydrogel that enabled the study of lung fibrosis through control of the hydrogel's mechanical properties.<sup>303</sup> The hydrogel's Young's modulus was spatially tuned using light-initiated photopolymerization over a range of 3.5–15 kPa, characteristic of healthy lung tissue at the lower end and fibrotic at the upper. Notably, the photopolymerization step was performed after

cell seeding, enabling the response of fibroblasts to be monitored as their substrate stiffened. Myofibroblasts activation was found to occur through the increased production of CollA1 and  $\alpha$ SMA as the hydrogels stiffened.

#### *3.2.9.2. Bioprinted scaffolds in lung dECM TE*

A composite lung dECM-alginate was printed in the form of hollow tubes or branching structures, intended to replicate the blood vessels and airway of the human lung, respectively.<sup>306</sup> In a mouse model, the dECM-alginate hydrogel appeared to modulate the immune response, exhibiting a reduced foreign body response and increased polarization of macrophages toward constructive remodeling compared to alginate-only. The dECM-alginate hydrogel also induced angiogenesis and the formation of a vascular network, while vessels in the alginate only-scaffold were less numerous and immature. Additionally, human bronchial epithelial cells cultured on the dECM-alginate hydrogel with an air-liquid interface for 28 days formed a stratified epithelium. Cells within the stratified epithelium expressed markers indicating further differentiation towards goblet (MUC5AC) and ciliated (FOXJ1) phenotypes.

#### *3.2.9.3. Aerosols in lung dECM TE*

dECM nanoparticles for aerosol delivery were produced by sonicating pepsin solubilized lung dECM in saline.<sup>299</sup> At concentrations of 0.3–0.45 mg/mL, coatings of lung dECM nanoparticles reduced apoptosis of alveolar epithelial cells under 24 h of hyperoxic (95% oxygen) conditions compared to TCP. The dECM nanoparticles (at 3.2 mg/mL) were delivered to rats subjected to hyperoxic conditions. Apoptosis of lung epithelial cells and oxidative tissue damage was significantly reduced in rats treated with dECM nanoparticles compared to a saline control.

To enable a more uniform distribution of dECM nanoparticles within the bronchioles, Link et al. prepared nanoparticles with a small size distribution by electrospraying.<sup>300</sup> The group first solubilized dECM with acetic acid and then electrosprayed dECM droplets onto aluminum foil. When lyophilized, the nanoparticles could be stored in a desiccator. The nanoparticles possessed a smaller size distribution of  $225 \pm 67$  nm and higher zeta potential ( $-10 \pm 1.6$  mV), compared to those of cryomilled dECM ( $\sim 5$   $\mu$ m and  $-17 \pm 23$  mV). Over 48 h, both alveolar and bronchiolar epithelial cells cultured in dECM nanoparticle supplemented medium increased proliferation over non-supplemented controls. Given their physical size ( $<500$  nm) and negative charge, electrosprayed dECM nanoparticles would be less aggregation-prone than pepsin-solubilized dECM and could reach the alveolar region through nebulization. Altogether, these results show

potential for nebulized dECM nanoparticles in the regeneration of distal lung tissue.

#### *3.2.9.4. Future prospects*

dECM biomaterials hold great promise in advancing lung disease models and stimulating distal lung regeneration. However, several aspects of these investigations can be expanded. In addition to cell proliferation, other biological markers indicative of functional and mature alveolar and bronchiolar epithelial cells, e.g., excreted neo-ECM molecules, can be included in the analysis. For instance, modeling the transport of oxygen across an alveolar epithelial barrier developed within a scaffold in vitro. In animal models, the distribution and percent of the dose delivered to the distal lung should be tested a short time after delivery to ensure sufficient dose reaches the target regions. Treatment efficacy could be determined by investigating whether dECM nanoparticles help reduce mucus hyperexcretion or remodel fibrotic tissue.

dECM biomaterials could also be used to aid in the delivery of drugs to the distal lung, either through chemical conjugation or encapsulation within dECM nanoparticles.<sup>59</sup> This method could induce a synergistic effect, wherein dECM provides a delivery method and stimulates regeneration, while the drug reduces inflammation or clears excess mucus.

Bioprinted lung dECM scaffolds, such as the dECM-alginate scaffold, could function as temporary stents to aid in lung function while aiding in tissue regeneration. Biodegradable drug-eluting stents are under development for use in treating severe airway inflammatory diseases such as COPD or airway stenosis.<sup>317</sup> These stents help keep dilated airways open and stimulate tissue remodeling but have not yet achieved common use. Also, biodegradable stents aim to reduce complications of silicone stents such as stent migration and reduced mucociliary clearance.<sup>317</sup> At the same time, biodegradable airway stents in combination with PLLA and other synthetic polymers often require repeat surgical procedures. Bioprinted lung dECM stents could be designed match the mechanical properties of the healthy lung as well as the shape of an individual's airways. Together with the similarity of lung dECM composition to the patient's lung, these design factors could increase both fusion with native tissue and tissue remodeling, thereby reducing the need for secondary procedures.<sup>318</sup> Lung dECM biomaterials remain in the early stage of development but possess great potential for application to lung TE.

**Table 9. Summary of dECM Particles in Lung Tissue Engineering.** Structural characterization includes SEM, FTIR, Raman, NMR, crosslinking efficiency, porosity, and swelling ratio. Mechanical characterization includes AFM, rheology, tensile testing, compressive testing, and electrical conductivity. Biological characterization includes in vitro studies, gene and protein assays, histology, and degradation kinetics.

Author/Year	Tissue Type	Decellularization Method			Homogenization Method		Material Composition			Biomaterial Type	Characterization Method			
		Chemical Decellularization Solutions	Enzymatic Digestion	Protocol Length (Total Hours)	Mechanical Method	Solubilization	dECM only	Synthetic Addition	Natural Addition		Structural	Mechanical	Biological	Animal Model
Pouliot <sup>2016</sup> <sup>29</sup>	Porcine lung	0.1% Triton X-100, 2% Sodium deoxycholate	DNase	49	SPEX 6700	Pepsin	✓			Injectable Hydrogel	✓	✓	✓	✓
Wu <sup>2017</sup> <sup>299</sup>	Porcine lung	0.5% SDS	NU	72	ND Mechanical Milling	Pepsin	✓			Aerosol	✓	✓	✓	
Young <sup>2017</sup> <sup>27</sup>	Porcine lung	0.1% Triton X-100, 2% Sodium deoxycholate, 1 M NaCl	DNase	50	SPEX 6700	NU		PLLA		Electrospun Scaffold	✓	✓	✓	
Hernandez <sup>2018</sup> <sup>59</sup>	Porcine lung, myocardium, and skeletal muscle	0.1% or 1% SDS	NU	ND	ND	Pepsin			Extracellular vesicles, microRNA(en capsulated)	Injectable Hydrogel			✓	
Link <sup>2018</sup> <sup>300</sup>	Porcine lung	0.1% Triton X-100, 2% Sodium deoxycholate, 1 M NaCl	DNase	ND	ND Freezer Mill	Pepsin	✓			Aerosol	✓		✓	
Zhou <sup>2019</sup> <sup>301</sup>	Rat lung	0.1% SDS, 1% Triton X-100	NU	2.5	ND	Pepsin	✓			Injectable Hydrogel	✓		✓	✓
Hilster <sup>2020</sup> <sup>302</sup>	Porcine lung	6 M NaCl, 70% Ethanol, 1% SDS, 1% Triton X-100, 1% Sodium deoxycholate	0.05% Trypsin, DNase	168	Commercial blender and Ultra-Turrax	Pepsin	✓			Injectable Hydrogel		✓	✓	
Petrou <sup>2020</sup> <sup>303</sup>	Porcine lung	0.1% Triton X-100, 2% Sodium deoxycholate, 1 M NaCl, 0.1% Peracetic acid, 4% Ethanol	30 µg/mL DNase	35	Mincing and lyophilization	NU		PEG methacrylate		Injectable Hydrogel	✓	✓	✓	
Pouliot <sup>2020</sup> <sup>30</sup>	Porcine lung	0.1% Triton X-100, 2% SDS, 1 M NaCl	DNase	50	SPEX 6700	Pepsin	✓			Injectable Hydrogel	✓	✓	✓	
Dabaghi <sup>2021</sup> <sup>305</sup>	Human lung	0.1% Triton X-100, 2% Sodium deoxycholate, 1 M NaCl	NU	115.5	Mortar and pestle	Pepsin	✓			Bioprinted Scaffold	✓	✓	✓	
De Santis <sup>2021</sup> <sup>306</sup>	Human and mouse lung	0.1% Triton X-100,	30 µg/mL DNase	52	TissueLyser	Pepsin	✓			Bioprinted Scaffold		✓	✓	✓
Falcones <sup>2021</sup> <sup>307</sup>	Porcine lung	0.1% Triton X-100, 2% SDS, 1 M NaCl	DNase	50	SPEX 6755	Pepsin	✓			Bioprinted Scaffold	✓	✓	✓	
Jung <sup>2021</sup> <sup>308</sup>	Porcine lung	1% SDS	50 U/mL DNase	216	NU	Pepsin			HA	Injectable Hydrogel		✓	✓	
Noori <sup>2021</sup> <sup>309</sup>	Ovine lung	1% Sodium deoxycholate, 1 M NaCl, 70% Ethanol	NU	25	ND Milling Method	Pepsin	✓			Injectable Hydrogel			✓	
Park <sup>2021</sup> <sup>310</sup>	Porcine lung	0.1% SDS, 1% Triton X-100	30 µg/mL DNase	74	SPEX 6775	Pepsin			Collagen	Injectable Hydrogel	✓	✓	✓	
Ravindra <sup>2021</sup> <sup>311</sup>	Porcine trachea and UBM	0.25% Triton X-100, 0.25% Sodium deoxycholate, 15% Peracetic acid, 4% Ethanol	2000 KU/ mL DNase	240	ND	Pepsin	✓							✓
Song <sup>2021</sup> <sup>312</sup>	Rat lung	20 µM Camptothecin, 125 mM SB-10, 0.1% Triton X-100, 2% Sodium deoxycholate	75 U/mL DNase	82–93	NU	Pepsin	✓			Injectable Hydrogel			✓	✓

### 3.3. Progress in dECM TE of other tissue types

#### 3.3.1. Gastrointestinal dECM TE

Gastrointestinal (GI) dECM biomaterials have sought to modulate the chronic inflammation condition and stimulate neo-ECM deposition in damaged GI tracts from ulcerative colitis (UC) and radiation esophagitis (**Table 10**).<sup>319-322</sup> Major TE challenges for GI dECM materials include recapitulating the segment-specific mucosal and muscle layers as well as restoring the motility function for peristalsis of the gut's tract.

For repair of the colon mucosa in severe UC, an injectable colon dECM hydrogel was investigated in a rat model.<sup>320</sup> The colon dECM hydrogel adhered to the colon with comparable strength to native mucosa, together with reduced UC symptoms such as weight loss and bloody stools over 14 days. An increase in mucosal barrier function to levels comparable to a healthy mucosa was also demonstrated by dextran permeability assay, TEER, and a 50% increase in E-cadherin expression. Remodeling of colon mucosa was attributed to dECM-associated inflammation reduction and neo-ECM deposition.

For esophageal mucosa repair, a bioprinted porcine esophageal dECM-PCL stent was implanted in a radiation esophagitis rat model.<sup>322</sup> A static compression test showed that the stent possessed a radial force of 5.13–7.65 N, in the acceptable range (3.6–11.5 N) for esophageal stents. The dECM-PCL stent incurred no significant plastic deformation after twenty cycles in cyclic three-point bending tests, indicating an ability to withstand the muscle contractions of peristalsis. One week after catheter-loading into the rat model, explants of dECM-PCL stents contained about 35% neutrophils and 15% macrophages of total cells. Irradiated, untreated mucosa contained around 51% neutrophils and 30% macrophages. Macrophages within the dECM-PCL stent were also predominantly polarized to the anti-inflammatory M2 phenotype. These results demonstrated the dECM-PCL stent has potential to reduce inflammation in irradiated esophageal mucosa.

To replicate a segment of the esophagus, a bioprinted cylindrical scaffold with layered esophageal muscle and mucosal dECM was developed.<sup>323</sup> dECM was printed into a porous PCL frame with “wrinkled” structures on the inner edges to mimic the structure of the two layers. The esophageal smooth muscle cells cultured within the muscle layer were elongated and expressed significantly greater  $\alpha$ -SMA than a Col I-PCL control after 7 days. Within the mucosal layer, esophageal epithelial cells adopted the round morphology of native mucosal cells and expressed greater E-

cadherin than the control. The ultimate tensile strength of the scaffold (6.85–8.45 MPa) was significantly higher than of native muscle (0.6 MPa) or mucosa (2.14 MPa) that may be capable of withstanding physiological peristalsis.

Finally, the complex roles of the bacteria in the GI microbiome remain incompletely understood.

<sup>324</sup> Damage to mucosal and epithelial barriers can result from depopulation or imbalance (dysbiosis) of the microbiome related to chronic disease, invasion by pathogenic bacteria, or uncontrolled antibiotic treatments. Biomaterial research into the microbiome is currently geared towards developing functional models of bacteria-mammalian gut cell interactions in platforms such as organoids and organ-on-a-chip. <sup>325</sup> dECM could provide a more physiologically relevant substrate for cell culture and influence bacteria activity. Biomaterial-mediated delivery of probiotic drugs is also hypothesized to improve probiotic bacteria survival and delivery to target regions in the intestines. <sup>326</sup> Investigating the ability of a probiotic-loaded dECM biomaterial to stimulate microbiome repopulation or delivery of probiotic bacteria would be an intriguing route for future GI dECM TE research.



**Table 10. Summary of dECM Particles in Gastrointestinal Tissue Engineering.** Structural characterization includes SEM, FTIR, Raman, NMR, crosslinking efficiency, porosity, and swelling ratio. Mechanical characterization includes AFM, rheology, tensile testing, compressive testing, and electrical conductivity. Biological characterization includes in vitro studies, gene and protein assays, histology, and degradation kinetics.

Author/Year	Tissue Type	Decellularization Method			Homogenization Method		Material Composition			Biomaterial Type	Characterization Method			
		Chemical Decellularization Solutions	Enzymatic Digestion	Protocol Length (Total Hours)	Mechanical Method	Solubilization	dECM only	Synthetic Addition	Natural Addition		Structural	Mechanical	Biological	Animal Model
Keane 2015 <sup>320</sup>	Porcine SIS	0.1% Peracetic acid	NU	2	SPEX 6700	Pepsin	✓			Injectable Hydrogel	✓		✓	✓
Keane 2015 <sup>319</sup>	Porcine SIS	2:1 Chloroform and methanol, 100%, 90%, 70% and, 4% Ethanol, 0.05% EDTA, 4% Sodium deoxycholate 0.1% Peracetic acid	0.02% Trypsin	60	Wiley Mini Mill	Pepsin				Injectable Hydrogel			✓	✓
Kim 2015 <sup>32</sup>	Porcine SIS, esophagus, and UBM	0.05% EDTA, 1 M Sucrose, 3% Triton X-100, 0.1% Peracetic acid, 4% Ethanol	1% Trypsin	5	Wiley Mini Mill	Pepsin	✓			Injectable Hydrogel	✓	✓	✓	✓
Keane 2017 <sup>321</sup>	Porcine SIS	0.1% Peracetic acid, 4% Ethanol	NU	2	Wiley Mini Mill	Pepsin	✓			Injectable Hydrogel		✓	✓	✓
Ha 2020 <sup>322</sup>	Porcine esophagus	1% Triton X-100, 1% SDS, 0.1% Peracetic acid, 4% Ethanol	100 U/mL DNase	134	ND Milling Method	Pepsin		PCL		Bioprinted Scaffold	✓		✓	✓
Kim 2020 <sup>328</sup>	Porcine SIS	0.1% Peracetic acid	NU	2	SPEX 6800	Acetic acid			Collagen	Bioprinted Scaffold	✓	✓	✓	
Nam 2020 <sup>323</sup>	Porcine esophagus and muscle	1% Triton X-100, 1% SDS, 0.1% Peracetic acid, 4% Ethanol	50 U/mL DNase	194	ND	Pepsin	✓			Bioprinted Scaffold		✓	✓	
Naranjo 2020 <sup>329</sup>	Porcine esophagus	0.05% EDTA, 1 M Sucrose, 3% Triton X-100, 0.1% Peracetic acid, 4% Ethanol	1% Trypsin	5	ND	Pepsin	✓			Injectable Hydrogel		✓		✓
Han 2021 <sup>330</sup>	Porcine colon	70% and 4% Ethanol, 1% SDS, 1% Triton X-100, 0.1% Peracetic Acid	10 U/mL DNase	50	NU	Pepsin	✓			Bioprinted Scaffold		✓	✓	
Kang 2021 <sup>76</sup>	Porcine heart, liver, and colon	70% and 4% Ethanol, 1% SDS, 1% Triton X-100, 0.1% Peracetic Acid	10 U/mL DNase	50	NU	Pepsin	✓			Bioprinted Scaffold		✓	✓	
Kim 2021 <sup>331</sup>	Porcine gastric tissue	1% SDS, 1% Triton X-100, 0.1% Peracetic acid	NU	73	ND	Pepsin			Cellulose Nanoparticles	Bioprinted Scaffold	✓	✓	✓	
Saldin 2021 <sup>332</sup>	Rat and human small intestinal submucosa, Porcine UBM	0.05% EDTA, 1 M NaCl, 0.1% Peracetic acid	0.25% Trypsin, 50 U/mL DNase	76	ND Milling Method	Pepsin	✓			Injectable Hydrogel	✓		✓	

### 3.3.2. Corneal dECM TE

Corneal dECM biomaterials have endeavoured to replicate the differential structural organization and density of collagen fibers in the layers of the cornea, and as well as modulate the phenotype of corneal keratocytes and maintain optical transparency and viscoelasticity (**Table 11**).<sup>333,334</sup> In the cornea, scarring and clouding commonly result from disruptions of the corneal shape and ECM structure, making ECM organization a significant target for corneal regeneration.<sup>335</sup>

To replicate the dense fiber structure and mechanical properties of the corneal stroma, a corneal dECM-Col I molded scaffold was fabricated by first gelling the composite, then compressing it to the desired thickness.<sup>336</sup> While the macroscale Young's modulus of a 100% Col I scaffold was 0.42–0.62 MPa, the Young's modulus of a 50% dECM composite was 0.26–0.32 MPa, comparable to the average in the native stroma (0.27 MPa). Furthermore, transmittance of the dECM-Col I scaffold was approximately 80% at 600 nm, closer to the 94% transmission of the native cornea than 100% Col I hydrogel (~65%). Compared to those of Col-I only hydrogel, the expression of functional keratocyte gene markers increased by 100-fold in the dECM-Col I composite. However, the dECM-Col I composite was indicated only for partial thickness corneal replacement.

Electrospinning was proposed to enhance the structural biomimicry of corneal dECM biomaterials.<sup>337</sup> To promote cell migration, a collector with a central pin and surrounding cup was used to generate electrospun fibers in a radial direction. To mimic the fiber alignment in corneal stroma, another collector with perpendicularly oriented pins was used to generate electrospun fibers in a perpendicular orientation. Scaffolds with randomly deposited fibers were used as a control. On both radial and perpendicular scaffolds, cells bridged across multiple fibers and produced processes, like the native morphology of corneal stromal keratocytes. Cells migrated across significantly greater areas within the radial (8.5–14 mm<sup>2</sup>) and perpendicular (7–21 mm<sup>2</sup>) dECM-PCL scaffolds than the random scaffolds (3–7 mm<sup>2</sup>). However, the cells only penetrated into 1–2 layers into the electrospun scaffold and thus further product improvement is required to improve cellular infiltration for use in corneal TE.

Electrospun and bioprinted corneal dECM scaffolds could be suitable for producing multi-layered structures that replicate the whole cornea.<sup>338</sup> Creating the layered structure would require layer by layer replication of the mechanical properties unique to each layer as well as heterogeneous cell types including keratocytes, epithelial cells, and endothelial cells. In electrospinning, different collectors could aid in producing differentially oriented fibers for each layer. For instance, the pin and cup method of generating radial fibers was suggested to stimulate epithelial cell migration. Bioprinting has been used to pattern keratocytes within a dECM scaffold for stroma replication. This method could be extended to pattern cells within the multiple corneal layers with built in curvature.

**Table 11. Summary of dECM Particles in Corneal Tissue Engineering.** Structural characterization includes SEM, FTIR, Raman, NMR, crosslinking efficiency, porosity, and swelling ratio. Mechanical characterization includes AFM, rheology, tensile testing, compressive testing, and electrical conductivity. Biological characterization includes in vitro studies, gene and protein assays, histology, and degradation kinetics.

Author/Year	Tissue Type	Decellularization Method			Homogenization Method		Material Composition			Biomaterial Type	Characterization Method			
		Chemical Decellularization Solutions	Enzymatic Digestion	Protocol Length (Total Hours)	Mechanical Method	Solubilization	dECM only	Synthetic Addition	Natural Addition		Structural	Mechanical	Biological	Animal Model
Ahearne 2015 <sup>335</sup>	Human and porcine corneal stromal tissue	NU	10 U/mL DNase, 10 U/mL RNase	103	SPEX SamplePrep	Pepsin	✓			Injectable Hydrogel	✓	✓	✓	
Ahearne 2016 <sup>339</sup>	Human and porcine corneal stromal tissue	NU	10 U/mL DNase, 10 U/mL RNase	103	SPEX SamplePrep	Pepsin	✓			Molded Scaffold	✓	✓	✓	
Hong 2019 <sup>336</sup>	Bovine cornea	19 mM Ammonium hydroxide, 0.5% Triton X-100, 10 mM Tris-HCl, 1% Triton X-100, 1% Peracetic Acid, 50% Ethanol	NU	62	ND Freezer Mill	Pepsin				Collagen Molded Scaffold		✓	✓	
Kim 2019 <sup>340</sup>	Bovine cornea	20 mM Ammonium hydroxide, 0.5% Triton X-100, 10 mM Tris-HCl, 1% Triton X-100, 1% Peracetic Acid, 50% Ethanol	NU	62	ND Freezer Mill	Pepsin				Collagen Bioprinted Scaffold	✓	✓	✓	✓
Fernandez- Perez 2020 <sup>337</sup>	Porcine cornea	NU	10 U/mL DNase, 10 U/mL RNase	103	SPEX 6770	NU		PCL		Electrospun Scaffold	✓	✓	✓	
Wang 2020 <sup>341</sup>	Porcine cornea	0.5% Sodium lauroylglutamate	500 U/mL recombinant endonuclease	3	TissueLyser II	Pepsin	✓			Injectable Hydrogel	✓	✓	✓	✓
Chameetachal 2021 <sup>342</sup>	Bovine cornea	1.5 M Sodium Chloride	NU	144	Mortar and Pestle	Pepsin	✓			Injectable Hydrogel	✓		✓	
Yazdanpanah 2021 <sup>343</sup>	Porcine cornea and human placenta	20 mM Ammonium hydroxide, 0.5% Triton X-100, 10 mM Tris-HCl, 1% Triton X-100, 1% Peracetic Acid, 50% Ethanol	7.5 U/mL deoxyribonuclease	118	SPEX 6700	Pepsin	✓			Injectable Hydrogel	✓	✓	✓	
Yazdanpanah 2021 <sup>344</sup>	Porcine cornea and human placenta	20 mM Ammonium hydroxide, 0.5% Triton X-100, 10 mM Tris-HCl, 1% Triton X-100, 1% Peracetic Acid, 50% Ethanol	7.5 U/mL deoxyribonuclease	118	SPEX 6701	Pepsin	✓			Injectable Hydrogel				✓

### 3.3.3. Kidney dECM TE

In kidney TE, imperative challenges are to improve existing in vitro modeling of kidney growth and diseases as well as to develop regenerative biomaterials for functional kidney tissue replacements.<sup>345,346</sup> dECM biomaterials have been developed to better replicate the microenvironment of the kidney parenchyma's complex structure including a million nephron filters (**Figure 7A**), waste processing-related molecular signals, and extensive vasculature for both in vitro models and tissue repair (**Table 12**).<sup>347</sup>

To produce an artificial renal filtration barrier, a scaffold was electrospun in a random pattern from kidney dECM and PCL.<sup>348</sup> Electrospun fibers provided intrinsic physical and molecular cues from dECM for the formation of epithelial linings with functional tight junctions (**Figure 7B**). When proximal tubule kidney epithelial cells were co-cultured with HUVECs on a dECM scaffold, epithelial linings formed after 7 days. Cells cultured on scaffolds containing dECM formed ZO-1 expressing tight junctions, but not in PCL-only controls. Additionally, epithelial monolayers on dECM-PCL scaffolds produced significantly higher TEER measurements over 14-days, indicating the epithelial monolayer possessed integrity and permeability comparable to the native nephron.

For regeneration of vascularized renal tissue, dECM and magnesium hydroxide (Mg(OH)<sub>2</sub>), an anti-inflammatory drug were incorporated into a molded PLGA scaffold.<sup>346</sup> (**Figure 7C**) In a partial nephron excision mouse model, the number of glomeruli increased within both dECM-PLGA and Mg(OH)<sub>2</sub>-PLGA scaffolds four weeks after implantation. The increase was most significant for scaffolds containing both dECM and Mg(OH)<sub>2</sub>, with concurrent reduced fibrosis in the animals. Only the dECM-Mg(OH)<sub>2</sub>-PLGA scaffold approached healthy levels of blood urea nitrogen (BUN, 23.3 ± 0.8 mg/dL) and creatinine (1.89 ± 0.02 mg/dL) after 4 weeks, and reached healthy levels after 8 weeks. The combination of dECM and Mg(OH)<sub>2</sub> may create synergistic benefits toward nephron reconstruction.

In future work, kidney dECM TE could benefit from a more comprehensive replication of the kidney microenvironment. For instance, the epithelial lining formed on the electrospun artificial nephron lost integrity after 14 days under static culture conditions.<sup>348</sup> A dynamic perfusion protocol that more closely matches the native kidney environment could lead to the utility of an electrospun nephron for long-term in vitro models or direct nephron regeneration.<sup>349</sup> While renal defects were fully reconstructed in mice treated with the dECM-Mg(OH)<sub>2</sub>-PLGA scaffold, wound

healing in rodents is demonstrably different from humans.<sup>350</sup> Further in vitro studies on scaffold mechanics and cellular response as well as in vivo assessment with large animals can help ascertain the safety and efficacy of the kidney dECM biomaterials.

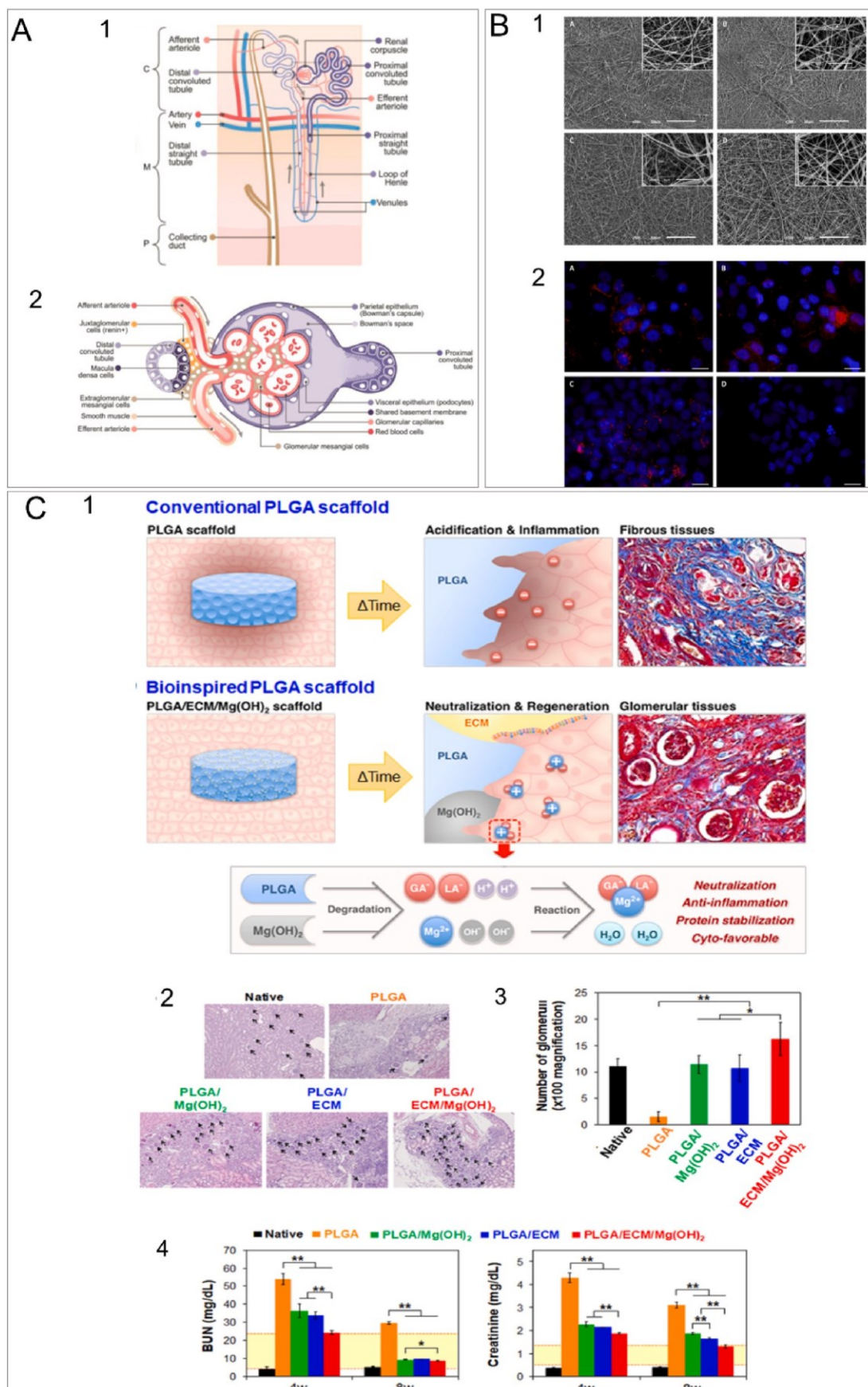


**Figure 7. Highlights of dECM Research in Kidney TE. A. Kidney Anatomy.** 1. Structures of the Nephron. 2. Structures and cells of the renal corpuscle, the nephron component responsible for blood filtration. **B. Electrospun dECM-PCL Artificial Renal Filtration Barrier.** 1. SEM images of electrospun scaffolds with dECM: PCL ratios of A. 70:30, B. 50:50, C. 30:70, and D. 0:100. Scale bar = 50  $\mu\text{m}$ , insert scale bar = 5  $\mu\text{m}$ . 2. Expression of the epithelial marker zona occludens-1 (red) by immortalized human kidney cortex/proximal tubule cells (HK-1) cultured on electrospun scaffolds with dECM: PCL ratios of A. 70:30, B. 50:50, C. 30:70, and D. 0:100. Nuclei stained with DAPI (blue). Scale bar = 20  $\mu\text{m}$ . **C. Molded dECM-PLGA Scaffold with Magnesium Hydroxide Nanoparticles for Glomerular Blood Vessel Regeneration.** 1. Diagram comparison of the effects of PLGA-only and dECM-PLGA scaffolds on glomerular regeneration and fibrosis. PLGA-only scaffolds cause the production of fibrotic tissue by creating an acidic, inflammatory environment. dECM-PLGA scaffolds stimulate the regeneration of glomerular blood vessels. The magnesium hydroxide nanoparticles interact with PLGA to prevent inflammation and maintain a neutral pH, while dECM promotes regeneration. 2. Response of a Partial Nephrectomy Mouse Model to the dECM-PLGA scaffold after 4 weeks. 3. Histological staining of scaffolds excised from sacrificed mice with hematoxylin and eosin. Regenerated blood vessels marked by black arrows. 4. Quantitative representation of regenerated glomerular blood vessels per unit area of 4860  $\mu\text{m}^2$ . Specifically, the dECM-PLGA scaffold containing nanoparticles produced  $16.29 \pm 3.15$  vessels, significantly more than native ( $11.14 \pm 1.35$ ), PLGA-only ( $1.58 \pm 0.98$ ), PLGA-only with nanoparticles ( $11.43 \pm 1.72$ ), or dECM-PLGA without nanoparticles ( $10.71 \pm 2.50$ ). **c. Renal function measured with BUN and creatinine levels after 4 and 8 weeks.** Normal levels indicated by the yellow box. Panel A is reproduced from Ref. <sup>351</sup>; Panel B. is reproduced from Ref. <sup>348</sup>; Panel C is reproduced from Ref. <sup>346</sup> with permissions.



**Table 12. Summary of dECM Particles in Kidney Tissue Engineering.** Structural characterization includes SEM, FTIR, Raman, NMR, crosslinking efficiency, porosity, and swelling ratio. Mechanical characterization includes AFM, rheology, tensile testing, compressive testing, and electrical conductivity. Biological characterization includes in vitro studies, gene and protein assays, histology, and degradation kinetics.

Author/Year	Tissue Type	Decellularization Method			Homogenization Method		Material Composition			Biomaterial Type	Characterization Method			
		Chemical Decellularization Solutions (Surfactants, Salts, Acids, Bases)	Enzymatic Digestion	Protocol Length (Total Hours)	Mechanical Method	Solubilization	dECM only	Synthetic Addition	Natural Addition		Structural	Mechanical	Biological	Animal Model
Nagao 2016 <sup>345</sup>	Human kidney	1% SDS	NU	240	Polytron homogenizer	Pepsin			Collagen	Injectable Hydrogel		✓	✓	
Magno 2017 <sup>352</sup>	Porcine kidney	0.1% and 1% SDS	NU	120	Mortar and Pestle	Pepsin			Ficoll 400	Injectable Hydrogel	✓	✓	✓	
Su 2018 <sup>347</sup>	Porcine kidney	0.1% SDS	NU	96	Wiley Mini Mill	Pepsin	✓			Injectable Hydrogel	✓	✓	✓	
Ali 2019 <sup>353</sup>	Porcine kidney	1% SDS	NU	ND	ND	Pepsin		PCL		Electrospun Scaffold	✓	✓	✓	
Lih 2019 <sup>346</sup>	Porcine kidney	1% Triton X-100	30 µg/mL DNase	337	SPEX 6750	NU		PLGA		Molded Scaffold	✓	✓	✓	✓
Sobreiro-Almeida 2019 <sup>348</sup>	Porcine kidney	1% SDS	NU	ND	ND	Pepsin		PCL		Electrospun Scaffold	✓	✓	✓	
Sobreiro-Almeida 2020 <sup>354</sup>	Porcine kidney	1% SDS, 1% Triton X-100	NU	ND	ND	NU		PCL		Electrospun Scaffold	✓		✓	
Zhou 2020 <sup>355</sup>	Rat kidney	0.1% or 1% SDS, 1% Triton X-100	40 U/mL DNase, 2 U/mL RNase	20	Wiley Mini Mill	Pepsin	✓			Injectable Hydrogel	✓	✓	✓	
Sobreiro-Almeida 2021 <sup>356</sup>	Porcine kidney	1% SDS, 1% Triton X-100	NU	ND	SPEX SamplePrep	Pepsin	✓			Bioprinted Scaffold	✓	✓	✓	

#### 3.3.4. Pancreatic dECM TE

In pancreatic TE, design strategies aim to reproduce the pancreatic niche to preserve or replicate functional Islets of Langerhans for treatment of diabetes, particularly insulin-producing  $\beta$  cells (**Figure 8A**).<sup>357</sup> Pancreas dECM biomaterials have potential to reproduce an artificial pancreas microenvironment for islet preservation or  $\beta$ -cell differentiation (**Table 13**).<sup>357-359</sup>

To replicate the pancreatic microenvironment, human pancreatic islets were encapsulated with or without ECs in an injectable pancreas dECM hydrogel.<sup>357</sup> (**Figure 8B**) The indentation Young's modulus (1.1–1.3 kPa) was comparable to that of the native pancreas. Islet functionality was evaluated based on the production of insulin by islets in response to a range of glucose levels (3 mM and 11 mM). After 7 days, islets in the pancreas dECM hydrogel released greater quantities of insulin at both low (1070–1725 mU/L) and high (11,100–15,650 mU/L) glucose concentration than islets in suspension cultures (320–1200 mU/L at 3 mM, 5300–9100 mU/L at 11 mM). Additionally, ECs co-encapsulated with islets formed capillary-like structures within the dECM hydrogels, which is essential for long-term islet survival. After 80 days of culture, the encapsulated islets showed less agglomeration and apoptotic stress than islets in a suspension culture control. However, hydrogels demonstrated retraction by the 10-day mark, demonstrating a need for a more mechanically stable biomaterial structure.

With the goal of generating a vascularized pancreas biomaterial, islets and endothelial cells were patterned within a bioprinted scaffold.<sup>358</sup> (**Figure 8C**) The glucose-stimulated insulin secretion of islets in dECM was about 3.2, significantly greater than those in Col I (~1.8) and alginate (~2.0) controls. After 5 days, insulin secretion was significantly higher in the co-culture group compared to islets alone. The bioprinted scaffold also promoted the differentiation of iPSCs into insulin-producing cells that expressed insulin and PDX1, mature  $\beta$ -cell markers, over a Col I control. Insulin secretion was further tested by patterning single cells or spheroids in the scaffold in comparison to a 2D control. In general, spheroids are more similar in structure to native islets than single cells. While both 3D methods secreted more insulin than the 2D control, hypoxia was found in the spheroid models.

While mimicking the islets' microenvironment could increase the longevity and compatibility of islet transplants, this method does not overcome the risk of rejection inherent to using allogeneic islets. The use of autologous stem cells may be a possible solution. However, islet functionality depends on cell-cell interactions between multiple cell types in addition to  $\beta$ -cells, such as  $\alpha$  and

$\delta$ -cells. Future studies should investigate whether dECM aids in the differentiation of all cells found in the Islets of Langerhans. Additionally, spheroids are more similar in structure to native islets than 2D monolayer cultures that may also facilitate islet cell differentiations and move towards improved islet transplantations and pancreatic tissue replication.

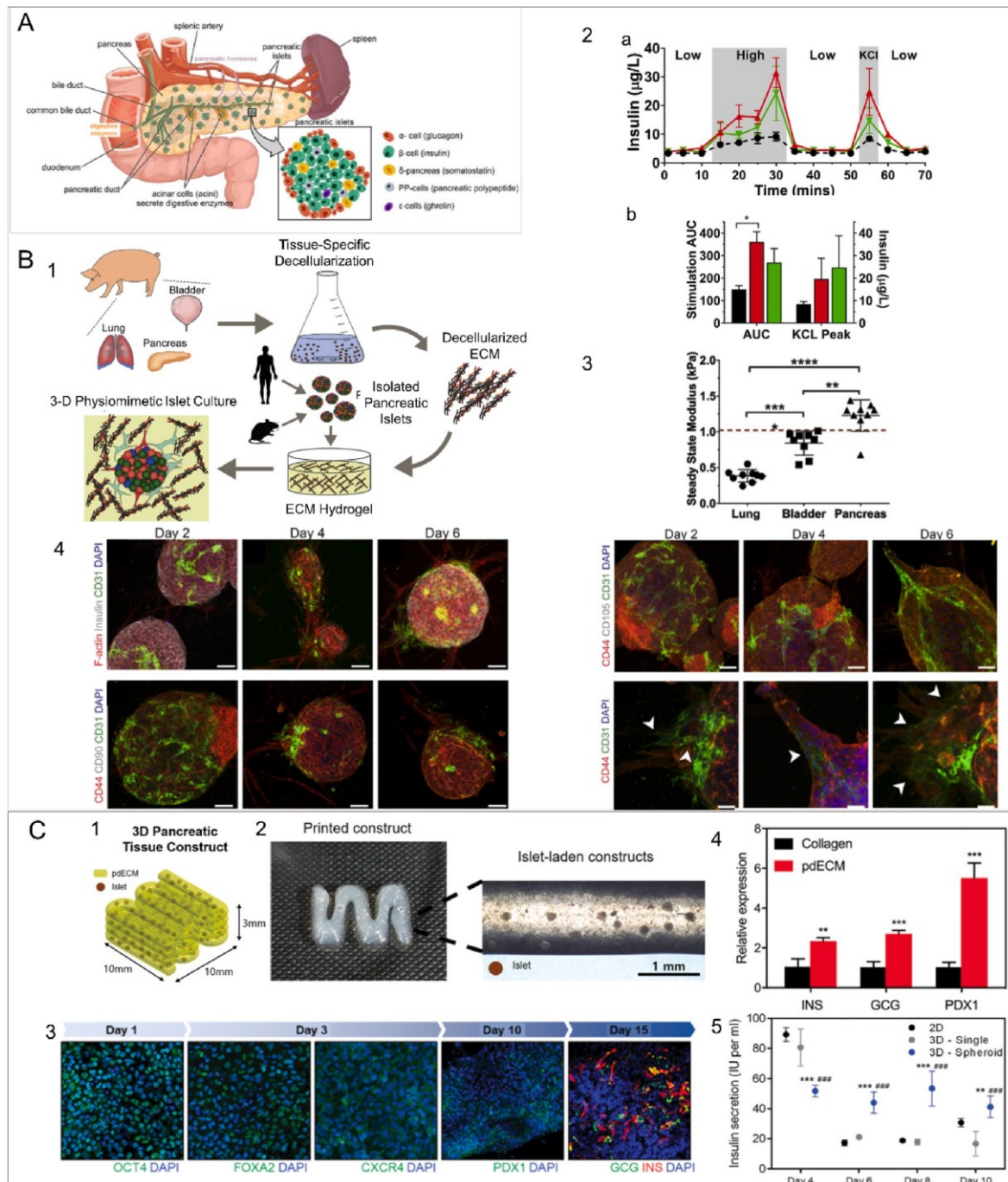


**Figure 8. Highlights of dECM Research in Pancreatic TE.** A. Anatomy of the pancreas with the cells that make up the islets and the hormones these cells produce. B. Pancreatic dECM hydrogel to replicate the pancreatic niche for islet culture. 1. Schematic of hydrogel production and islet encapsulation. 2. GSIR of rat islets cultured on dECM hydrogels. a. Islet function by dynamic perfusion with alternating low glucose, high glucose, and KCl solutions after 5 days of culture. b. Average stimulation area under curve (from a.) during high glucose period and peak insulin levels during KCl period. 3. Steady state modulus of hydrogels produced from lung, bladder, and pancreas. Dotted line represents the steady state modulus of the native human pancreas. 4. Islets stained and imaged after 2, 4 and 6 days of culture in dECM hydrogels for expression of genes characteristic of mature islets. Scale bar = 20  $\mu\text{m}$ . Arrows indicate CD31+ endothelial sprouts showing blood vessel outgrowth. C. Bioprinted pancreatic dECM scaffold for maintenance of islets. 1. Schematic of bioprinted scaffold with encapsulated islets. 2. Image of construct with encapsulated islets. 3. Culture of iPSC-derived insulin producing cells in the scaffold over 14 days, dyed for gene expression at each stage of maturation. 4. Expression of genes characteristic of mature beta cells (INS, GCG, PDX1) by insulin producing cells cultured in bioprinted dECM or Col I after 14 days. 5. Insulin production by insulin producing cells cultured in the dECM structure in 2D, 3D, or as 3D spheroids. Panel A. is reproduced from OpenStax (Open Access, Regents of University of Michigan Medical School © 2012); Panel B. is reproduced from Ref. <sup>357</sup>; Panel C. is reproduced from Ref. <sup>358</sup> with permissions.

**Table 13. Summary of dECM Particles in Pancreatic Tissue Engineering.** Structural characterization includes SEM, FTIR, Raman, NMR, crosslinking efficiency, porosity, and swelling ratio. Mechanical characterization includes AFM, rheology, tensile testing, compressive testing, and electrical conductivity. Biological characterization includes in vitro studies, gene and protein assays, histology, and degradation kinetics.

Author/ Year	Tissue Type	Decellularization Method			Homogenization Method		Material Composition			Biomaterial Type	Characterization Method			
		Chemical Decellularization Solutions (Surfactants, Salts, Acids, Bases)	Enzymatic Digestion	Protocol Length (Total Hours)	Mechanical Method	Solubilization	dECM only	Synthetic Addition	Natural Addition		Structural	Mechanical	Biological	Animal Model
Gaetani 2018 <sup>37</sup>	Porcine pancreas	0.34 M and 1.28 M NaCl, 0.1%, 0.5% or 1% SDS, 1% Triton x-10	NU	26.5	Wiley Mini Mill	Pepsin	✓			Injectable Hydrogel		✓	✓	
Sackett 2018 <sup>35</sup>	Human pancreas	2.5 mM Sodium deoxycholate	NU	93	ND Mechanical Milling	Pepsin	✓			Injectable Hydrogel	✓		✓	
Jiang 2019 <sup>357</sup>	Porcine pancreas, lung, and bladder	1.1% and 0.7% NaCl, 8 mM SDS, 70% Isopropanol, 1% Triton X-100, 0.1% Ammonium hydroxide	70 U/mL Benzonase	360	Retsch CryoMill	Pepsin	✓			Injectable Hydrogel	✓	✓	✓	
Kim 2019 <sup>358</sup>	Porcine pancreas	0.5% SDS, 1% Triton X-100, 0.1% Peracetic Acid	NU	38	ND Mechanical Milling	Pepsin	✓			Bioprinted Scaffold		✓	✓	
Wang 2020 <sup>391</sup>	Human adipose	NU (centrifugation)	NU	0.75	Phillips blender	Pepsin			Alginate	Injectable Hydrogel		✓	✓	
Zhu 2020 <sup>392</sup>	Porcine pancreas	1% Triton X-100, 0.1% Ammonia	NU	ND	ND Mechanical Milling	NU			Silk fibroin	Electrospun Scaffold	✓		✓	
Idasek 2021 <sup>393</sup>	Porcine Pancreas	1% Triton X-100	NU	ND	ND Cryomill	NU			Alginate	Bioprinted Scaffold		✓	✓	
Hwang 2021 <sup>394</sup>	Porcine pancreas	1% Triton X-100, Isopropanol, 0.1% Peracetic acid, 4% Ethanol	NU	ND	ND	Pepsin		PCL		Bioprinted Scaffold	✓	✓	✓	✓

### 3.3.5. Vocal fold dECM TE

Vocal fold tissue has a unique multi-layer anatomical structure that enables stretching by up to 50% during high-frequency oscillations.<sup>2,360-363</sup> The developments of injectable hydrogels with permanent regenerative function and minimal need for re-injection are a primary challenge in regenerating vocal folds (VF).<sup>364-366</sup> dECM-based hydrogels have been proposed as a method for repairing defects and restoring the VF oscillatory capacity by stimulating and guiding the intrinsic wound healing process (**Table 14**).

The proteomic composition of native VF was compared to VF dECM particles and pepsin-solubilized dECM pre-gels to determine how decellularization affected the specific VF ECM composition.<sup>367</sup> Though collagens were retained in bovine dECM hydrogels, elastin, which contributes to VF viscoelasticity, was absent after solubilization. When injected into scarred rabbit VF, a greater reduction of the scarred tissue contraction was noted in the VF dECM hydrogel group compared to saline injection sham controls 3 months after injection. The thickness of the treated VF reached 70% of its original thickness prior to injury compared to 54% thickness for the control. However, histological analyses showed that amounts of HA and sulfated GAGs, which provides an insulating effect against VF oscillation, were comparable in dECM-treated and sham VF.

In another proteomic analysis, a higher concentration of LTBP4, which binds and sequesters TGF- $\beta$ 1, was identified in VF dECM powder in comparison to UBM.<sup>368</sup> Binding of TGF- $\beta$ 1 by LTBP4 could downregulate fibrotic TGF- $\beta$ 1-mediated fibroblast activity. Gene expression associated with TGF- $\beta$ 1-mediated fibroblast activation (Col1A1, ACTA2) was upregulated and downregulated in human VF fibroblasts cultured on Col I and VF-dECM hydrogels respectively. Compared to VF dECM, cells on UBM expressed comparable levels of ACTA2 but higher levels of Col1A, indicating that the VF dECM may possess greater anti-fibrotic capacity. A notable limitation was that the Young's Modulus of VF-derived dECM (118–187 Pa), UBM hydrogels (120–154 Pa), and Col I (108–178 Pa) were all below the range of the native VF (0.5–13 kPa).

While dECM hydrogels for VF TE show potential for stimulating VF regeneration with reduced scar formation, the regenerated tissue must also be structurally complete and mechanically functional to meet the dynamic mechanical demands of VF during phonation.<sup>369,370</sup> Chemically crosslinked dECM composites could retain the regenerative effects of dECM, while better mimicking the structure and mechanics of native VF. Composite dECM biomaterials could also

reduce the need for reinjection by allowing the degradation rate to be tuned to match dECM biomaterial-stimulated wound healing.

**Table 14. Summary of dECM Particles in Vocal Fold Tissue Engineering.** Structural characterization includes SEM, FTIR, Raman, NMR, crosslinking efficiency, porosity, and swelling ratio. Mechanical characterization includes AFM, rheology, tensile testing, compressive testing, and electrical conductivity. Biological characterization includes in vitro studies, gene and protein assays, histology, and degradation kinetics.

Author/Year	Tissue Type	Decellularization Method			Homogenization Method		Material Composition			Biomaterial Type	Characterization Method			
		Chemical Decellularization Solutions	Enzymatic Digestion	Protocol Length (Total Hours)	Mechanical Method	Solubilization	dECM only	Synthetic Addition	Natural Addition		Structural	Mechanical	Biological	Animal Model
Choi 2014 <sup>365</sup>	Porcine SIS	0.1% Peracetic Acid	NU	2	Freezer Mill	Pepsin	✓			Injectable Hydrogel			✓	✓
Huang 2016 <sup>364</sup>	Porcine SIS	dECM from Cook Biotech	NU	NA	NA	Pepsin			HA	Injectable Hydrogel			✓	
Xu 2019 <sup>367</sup>	Bovine Vocal Fold	3 M Sodium Chloride, 70% Ethanol	25 µg/mL DNase, 10 µg/mL RNase	96	SPEX Cryomill	Pepsin	✓			Injectable Hydrogel			✓	✓
Mora-Navarro 2020 <sup>368</sup>	Porcine Vocal Fold and UBM	4% Sodium Deoxycholate, 0.1% Peracetic Acid	273 K/mL DNase	8.5	Mortar and Pestle	and Pepsin	✓			Injectable Hydrogel	✓	✓	✓	



### *3.4. Future prospects in dECM biomaterials for TE*

The field of dECM biomaterials has greatly diversified and expanded over the past decade. Applications now range across a broad spectrum of tissues, and have branched from wound healing patches to scaffolds designed to repair a specific defect region by matching physicochemical properties and replicating entire organs. This expansion is continuing, with the recent addition of dECM biomaterial applications to the salivary glands, tongue, and several reproductive tissues.<sup>371-376</sup> Researchers have grasped the vast potential of dECM biomaterials to better replicate the structural and functional properties of native tissues, yet there remain limitations to be addressed. By reviewing over 15 tissue types of dECM application, we have identified links in the preparation of dECM and tissue-specific biomaterial design that could help overcome current limitations, and guide dECM biomaterials to achieve improved therapeutic efficacy (**Figure 9**).

#### *3.4.1. Methodology of tissue decellularization and preparation of dECM for biomaterial production*

Commonly used decellularization protocols frequently result in dECM with high batch to batch variation, unreliable gelation, and altered composition including the loss of GAGs and growth factors and modification of collagens.<sup>4,377</sup> While variation is expected due to its biological nature, dECM has been found to possess batch-to-batch variation beyond that of native tissue.<sup>377,378</sup> Decellularizing tissue that has been minced or homogenized prior to decellularization improves the consistency of exposure to decellularization agents across the tissue by increasing surface area, which can help to reduce both technical variation and exposure time required for satisfactory cellular removal.

Another source of batch-to-batch variation is that the preservation of native small molecules and ECM fiber organization is highly dependent on the choice of decellularization agents, which in turn result in variations in the biological activity and consistency of gelation of the dECM products.<sup>4,50</sup> Surfactants such as SDS and Triton X-10 are known as primary sources of ECM alteration during decellularization.<sup>4</sup> However, when the surfactants were constituted with 70% isopropanol instead of water, more VEGF (55-fold increase) and BMP-2 (4-fold increase) were preserved in the dECM samples from porcine skin.<sup>60</sup> Also, surfactant-free decellularization protocols have been developed to replace SDS and Triton X-100 with supercritical carbon dioxide, hypertonic salt, and/or nuclease solutions.<sup>50,367</sup> These surfactant-free protocols have been shown to achieve similar decellularization efficacy with reduced alteration of ECM composition.<sup>50,379</sup>

Additionally, lipid retention has been linked to inhibited fibrillogenesis of solubilized dECM and unreliable gelation.<sup>359</sup> In tissues such as adipose, bone, and pancreas, the addition of a delipidization step with isopropanol or chloroform/methanol solution has been shown to significantly improve the reliability of gelation.<sup>181,265,359</sup> The disadvantage of delipidization is that alcohols can crosslink collagens, reducing the availability of the soluble collagens that undergo fibrillogenesis for gelation.<sup>4</sup> However, evidence shows that lipid removal is a critical factor for effective gelation and therefore biomaterial reproducibility from batch-to-batch.

Variability in dECM biomaterials can also be caused by the lack of standardized, tissue-specific homogenization methods. Automated methods produce more uniform particles than hand grinding with a mortar and pestle or a commercial blender, while homogenization in a liquid medium risks alterations due to heat production.<sup>380,381</sup> Cryomills provide an automated method of dECM homogenization at a sub-zero temperature, resulting in uniform particles and reducing one potential source of batch-to-batch variation with protocols designed to suit specific tissues.

The solubilization process can also result in significant variation of dECM biomaterial products. Pepsin is the most common method of solubilization, but can cause degradation or denaturation of some dECM components, as well as weak mechanical properties when chemical crosslinking methods are not used.<sup>26</sup> In general, the dECM should be stirred in pepsin solution at a slow rate to produce a viscous liquid and kept on ice until neutralization to prevent premature gelation or particle agglomeration. Alternative methods such as urea extraction may be used to retain key proteins and growth factors for tissue-specific cellular activity, such as osteogenesis in bone.<sup>23</sup> However, the urea extraction process is time consuming and does not result in stronger biomaterial mechanics. While it is possible to fabricate a dECM biomaterial without solubilization, covalent crosslinking is required.<sup>26</sup> Ultimately, the most effective method of modulating network properties to produce tissue-specific dECM biomaterials is through the use of crosslinkers and composites.

#### *3.4.2. Missing links in tissue-specific dECM biomaterial design*

Future works should aim to address the tissue specific physicochemical properties to meet the structural, mechanical, and functional needs of the target tissue and modulate the immune response. For example, aerosol delivery of a biomaterial is unique, innovative, and organ specific to lung.<sup>299,300</sup> The design of aerosol delivery methods involved looking at the specific requirements of an organ, and seeking to construct a biomaterial that addresses those needs.

### 3.4.3. Structural considerations in dECM biomaterial design

The structure and cellular content differ greatly based on tissue type. dECM biomaterials should likewise seek to match these tissue-specific structures. For example, articular cartilage and the cornea each have layers with variable ECM network structures and pore sizes. Freezing drying, salt leaching, and crosslinking can be used to achieve specific physicochemical properties such as pore structures.<sup>382-384</sup> In addition, electrospinning deposition substrates and methodologies can be manipulated to optimize fiber diameters and network organization, or to form a bridge that guides the growth of new tissue across a defect.<sup>134,337</sup> For instance, electrospinning into a liquid bath rather than a metal collector decreases inter-fibril bonding, dispersing the fibers and resulting in scaffolds with larger pore sizes and improved cellular infiltration.<sup>101,385</sup>

However, traditional electrospinning has practical limitations including densely packed fibers that restrict cell infiltration, needle clogging, and dissolution of natural fibers like dECM in organic solution.<sup>386</sup> To improve cell infiltration, wet electrospinning by electrospraying aerosolized dECM onto electrospun synthetic fibers can help generate a looser structure with negligible change in pore size.<sup>195,385</sup> To prevent needle clogging, needleless electrospinning by using jets or nozzle spinnerets have been proposed for ECM scaffold fabrication.<sup>262,387</sup> To help preserve the dECM components by limiting contact with organic solutions, a co-axial technique with two nozzles like that used to electrospin gelatin in hydrophilic acetic acid solution concurrently with PCL in hydrophobic organic solution could be applied to electrospun dECM scaffolds.<sup>388</sup> In this technique, the hydrophilic and hydrophobic solutions repel each other, keeping dECM isolated from the organic solution. As electrospun dECM alone lacks the mechanical integrity to maintain its structure, such an approach would preserve the bioactivity while maintaining the structural framework of the electrospun scaffold provided by synthetic polymers.<sup>386</sup>

Highly complex organs like the liver kidney, GI tract, and pancreas have multiple parenchyma. The first steps toward replicating these complex structures using dECM biomaterials have been conducted for liver and GI application, but have yet to match the complexity of native tissue<sup>227,323</sup> Seeding stem cells or multiple cell types could aid in the development of tissues into layers and functional structures. For example, in an esophageal scaffold with muscle and mucosal layers, this method could aid in the stratification of the mucosal layer into mucosal and submucosal layers.

For most tissues with a thickness beyond 200  $\mu\text{m}$ , vascularization is a general requirement for cell

viability within the implants.<sup>389</sup> An extensive vascular network helps deliver the oxygen and nutrients necessary to perform the functions of healthy tissue and aid in wound healing. An exception is cartilage, an avascular tissue in which the delivery of oxygen and nutrients occurs by diffusion.<sup>112</sup> However, cartilage possesses slow, limited wound healing capacity as a result of its avascular nature. Vascularization is especially critical for biomaterials intended to treat VML due to the high requirement for oxygen in skeletal muscle.<sup>202</sup> Liver and pancreas also have blood vessel networks that are essential for cell function in these large, complex organs, yet vascularization has not yet been incorporated in dECM biomaterials for these applications. Organization of vasculature can also be tissue-specific, such as in the VF lamina propria, where capillaries lie parallel to the VF edge, aiding the tissue in withstanding oscillations.

Replicating the structures innate to specific tissues and organs could ultimately be useful in the production of artificial organs or partial organ replacement, and more immediately in creating models with greater physiological models for understanding organ function.

#### *3.4.4. Mechanical considerations in dECM biomaterial design*

Improved design of dECM biomaterials could stem from choosing key mechanical properties and seeking to replicate them. For example, cartilage has high load bearing requirements with varying compression across its layers, muscles undergo frequent contraction, and VF stretch repetitively at high strain.<sup>90,223,366</sup> Specific mechanical properties such as these can be achieved through the use of composites and crosslinkers. Composites are particularly useful for enhancing the dECM stability over time, which has been noted as a critical shortcoming in pancreas dECM biomaterials.

Conventional crosslinkers such as carbodiimides, glutaraldehyde, and photocrosslinking can be used to modulate the mechanics of a biomaterial.<sup>26,339</sup> However, these crosslinkers frequently have detrimental side effects, such as toxic side products or interactions with cells that necessitate ex-situ fabrication. These conditions may be suitable for acellular scaffolds where impurities may be removed prior to implantation, such as for electrospun dECM nerve grafts or corneal replacements.

For injectables or cell-encapsulated scaffolds, bioorthogonal click chemistry presents an alternative.<sup>303</sup> Bioorthogonal click reactions like tetrazine ligation or alkene hydrothiolation are highly specific and produce only non-toxic side products, such as nitrogen gas.<sup>303,390</sup> These factors enable crosslinking in the presence of cells and in situ without a significant risk of cytotoxic

effects. Click dECM injectables could be injected into an irregular bone, muscle, or VF defect as a pre-gel, thereby forming a mechanically relevant scaffold that fills the entire defect. Click chemistry could also aid in achieving differential mechanical properties in cell-patterned bioprinted scaffolds with regions mimicking multiple parenchyma or layers, such as for liver, kidney, or cartilage applications. In addition to supporting dECM mechanically, composites and crosslinkers may contribute to functional outcome.

#### *3.4.5. Immune modulation considerations in dECM biomaterial design*

The immune system plays a key role in the integration of regenerative biomaterials in the host site. Immune cells detect and react to the presence of a foreign material in a pro- or anti-inflammatory fashion.<sup>2,395,396</sup> The pro-inflammatory immune response is characterized by M1 macrophages, neutrophil and t-lymphocyte activation and dendritic cell maturation.<sup>2</sup> Prolonged inflammation can result in macrophage fusion into foreign body giant cells that form fibrous capsules around the biomaterial, deposition of disorganized ECM, and abnormal adipogenesis, leading to poor outcomes.<sup>2,395,397</sup> In successful wound healing, an initial inflammatory immune response must be followed by an anti-inflammatory response, characterized by the polarization of M1 macrophages into a reconstructive M2 phenotype.<sup>398</sup> M2 macrophages release anti-inflammatory cytokines that help reduce swelling and scarring. The anti-inflammatory response helps to regulate the production of functional, organized ECM fibers by tissue-specific cells such as fibroblasts, osteoblasts, or stellate cells.<sup>2,398</sup>

Although whole dECM scaffolds were reported to induce varied immune responses in clinical trials, the cause is likely due to insufficient decellularization. The resulting residual inflammatory epitopes (Gal $\alpha$ 1,3Gal $\alpha$ 1) and disease-associated molecular patterns (DAMPs) impede successful wound healing.<sup>399</sup> On the other hand, substantial literature data also supports the idea that dECM itself is innately immunomodulatory. M2 polarization of macrophages has been demonstrated for skeletal muscle, UBM, SIS, gastrointestinal, and cardiac dECM biomaterials.<sup>25,34,321</sup>

The physicochemical properties of a dECM-based biomaterial can be further leveraged to aid in modulating the immune response in achieving favorable and consistent outcomes. For example, increasing material porosity can lead to increased M2 polarization of macrophages and reduced inflammatory activity by T-lymphocytes and dendritic cells.<sup>2</sup> Substrate stiffness is also a factor in

inflammation. For instance, in one study, molded scaffolds were produced from either solubilized or unsolubilized bone dECM particles.<sup>260</sup> The solubilized dECM scaffolds possessed a lower Young's modulus than the unsolubilized dECM scaffolds (0.5–8.3 kPa vs. 27.1–37.7 kPa). When implanted in a rat periodontal defect model, the softer solubilized dECM scaffolds were found to induce M2 polarization, while the stiffer unsolubilized dECM scaffolds induced M1 polarization.

When selecting potential materials for composites, it is critical to consider that both polymers and crosslinking may alter the response of immune cells.<sup>2,399</sup> The surface moieties of a biomaterial impact protein absorption depending on their hydrophobicity. Hydrophobic methyl groups trigger increased inflammatory immune cell recruitment by increasing protein absorption, while carboxyl groups reduce protein absorption.<sup>2</sup> Degradation byproducts from composite polymers like PEG as well as crosslinkers may be cytotoxic, which again leads to increased inflammation.<sup>2,399</sup> It is therefore critical to integrate material-driven immunomodulatory strategies in dECM biomaterial applications in tissue regeneration.

#### *3.4.6. Functional considerations in dECM biomaterial design*

Beyond inducing a cellular response, there is a need to ensure dECM biomaterials are capable of effectively stimulating both tissue function and repair. dECM biomaterials should therefore be adapted to their application. To achieve this goal, the capacity of a biomaterial to completely repair tissue should be assessed in contrast to existing materials and their functional outcomes should be compared to healthy, native tissue.

Functions vary by tissue type, and may include dynamic or stress-related mechanics, electrical conductivity, selective filtration or biomolecule production.<sup>24,65,348,366</sup> Design strategies can be chosen to achieve these functions. For instance, a composite scaffold of dECM and a conductive polymer may be designed to match the conductivity of cardiac or nerve tissue.

To develop biomaterials that achieve the full regenerative potential of dECM, the rapid degradation of dECM by native MMPs should also be regulated.<sup>153,400</sup> Degradation can be slowed by crosslinking, especially in a composite polymer. More slowly biodegradable composite polymers such as alginate can be selected such that the entire scaffold is ultimately replaced by regenerated tissue over time. With a reduced degradation rate, the long-term regenerative potential of dECM can then be more accurately assessed in relation to existing biomaterials.

Elements such as growth factor activity and extracellular vesicles (EVs) should also be considered

for dECM-based regenerative biomaterials. In addition to retaining native growth factors, the dECM itself can help to bind, sequester, distribute, and regulate the production of growth factors produced by local cells.<sup>401</sup> For example, local macrophages expressed higher levels of pro-angiogenic growth factors (e.g., VEGF, IL-6, TNF etc.) when cultured in dECM derived from vascularized cartilage dECM (i.e., the growth plate) than those of avascular cartilage (i.e., articular cartilage).<sup>402</sup> These findings show how dECM from vascular cartilage has the capacity to regulate growth factor production to promote angiogenesis.

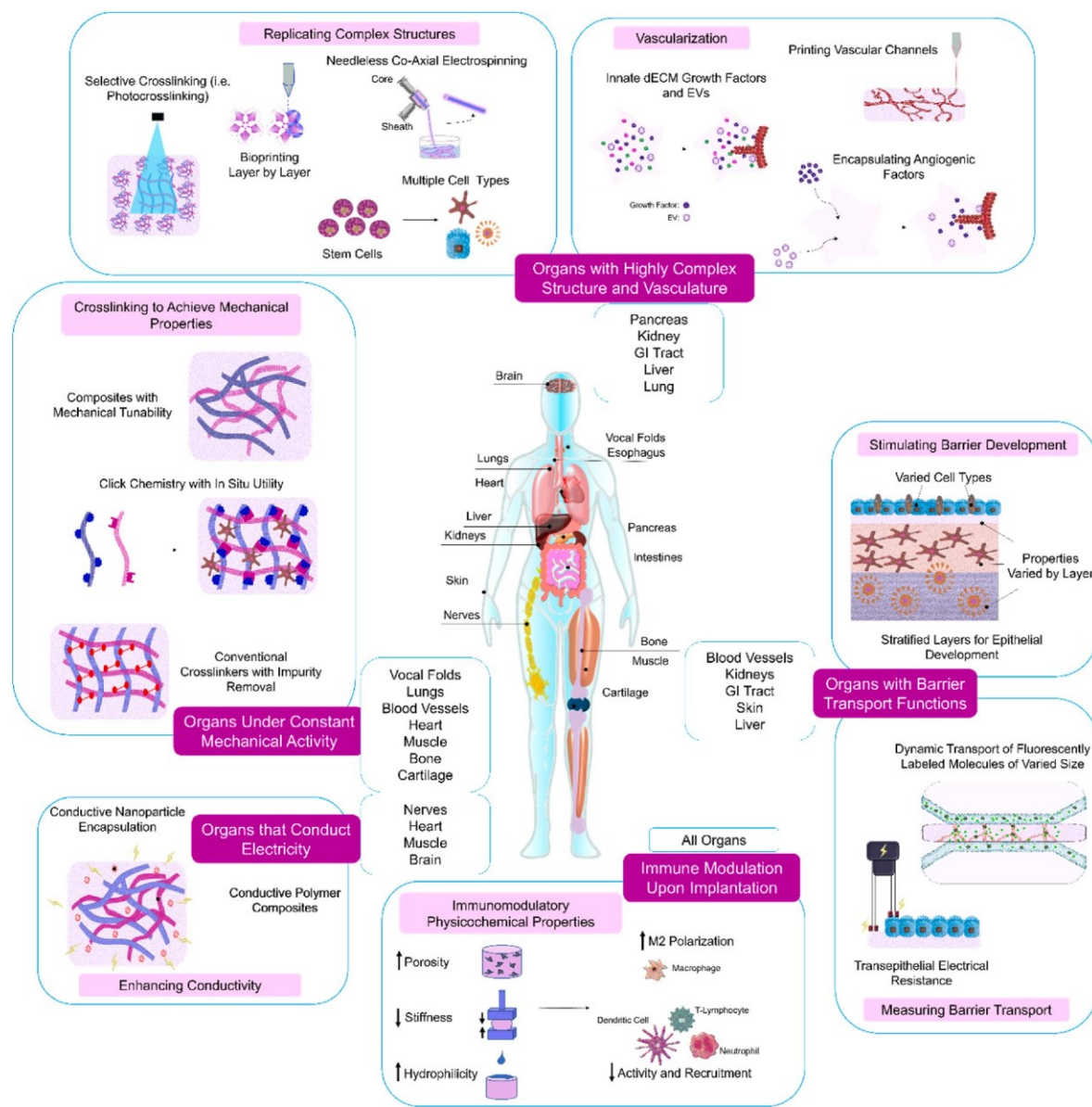


**Figure 9. Prospective Methodology for the Development of dECM Biomaterials.** Toward Effective Therapeutic Applications. The varied organs of the body require specific approaches. Approaches for organs with highly complex structure and vasculature include creating biomaterials with multiple structural elements and angiogenic capacity. For organs under constant mechanical activity, dECM biomaterials should be designed for mechanical performance. For organs that conduct electivity, conductivity should match the capacity of healthy tissue. Organs with barrier transport function require both barrier development, and functional barrier transport. dECM = Decellularized Extracellular Matrix. EV = Extracellular Vesicles.

Apart from endogenous small molecules, dECM with encapsulated growth factors produced by stem cells may have a synergetic regenerative effect over dECM or the growth factor alone.<sup>133</sup> For instance, TGF- $\beta$ 1 and BMP-2 encapsulated in bone dECM enhanced osteogenesis over dECM alone, though the quantity of endogenous growth factors was not quantified.<sup>130,133</sup> FGF-2 in spinal cord dECM-HP exhibited sustained release resulting in enhanced neuroregeneration and improved mobility over a HP control.<sup>133</sup> dECM slowed the release of FGF-2, with only 47% released from dECM-HP after 24 h, compared to 65% from the HP control. In other words, dECM can act as a reservoir for controlled release of the encapsulated growth factors.

Besides growth factors, EVs are another key element of the ECM as matrix bound nanovesicles.<sup>403,404</sup> EVs contain microRNA that contributes to the modulation of immune cell activity and ECM homeostasis. EV-related dECM studies originated with the identification of EVs bound to the collagen network of clinically approved whole dECM scaffolds including Cook Biotech's Biodesign(R), ACell's Matristem(R), and C.R. Bard's XenMatrix.<sup>404</sup>

Interestingly, subsequent studies on the dECM's innate EVs have continued to focus on whole dECM scaffolds, rather than in other forms of dECM biomaterials. One possible reason for the focus on whole dECM scaffolds is that pepsin is commonly used as part of the EV extraction process.<sup>404,405</sup> It is not yet clear how the pepsin solubilization step used in the majority of dECM particle-based scaffolds may impact EV retention and activity.<sup>19</sup> Due to the importance of EVs in regenerative functions, the possibility of EV depletion should be studied to determine the degree to which EVs are retained within solubilized dECM.

While the content of native EVs in dECM particle-based scaffolds remains unclear, a few studies



have combined exogenous EVs produced by stem cells with dECM hydrogels through encapsulation. One study showed that EVs encapsulated in cardiac dECM hydrogels bioactivity over 7 days, measured through stimulation of the ERK  $\frac{1}{2}$  central cell signaling pathway and anti-apoptotic effect.<sup>59</sup> However, the EV release profiles varied across samples of the same tissue type. Encapsulation in a composite cardiac dECM-PEG hydrogel was shown to enhance EV retention over dECM alone.<sup>74</sup> Despite these promising results, the heterogeneity and cell-derived nature of exogenous growth factors and EVs could complicate the clinical approval due to regulatory standards for standardized production and safety and efficacy profiles.<sup>406</sup>

Functionality should be measured beyond cell survival and phenotype. Biomaterial functionality can be monitored by multiple methods, including the production of and response to biomolecules. For instance, neo-ECM deposition is an important marker of a dECM biomaterial's ability to repair tissue and can be monitored by immunofluorescence or quantitative assays.<sup>407</sup> In tissues containing capillaries, barrier function is highly important, and can be measured by TEER or the dynamic, selective passage of molecules across layers.<sup>30,408</sup> In addition to capillary models, skin, lung, and GI can benefit from these studies for epidermal because skin and lung epidermis provides a protective layer against toxins from the outside world but also need to absorb beneficial molecules, while GI tract tissues must pass molecules across selectively during digestion.

### *3.5. Conclusions*

Biomaterials constructed from dECM particles present a promising prospect in TE applications, yet existing dECM biomaterials have several key limitations that will need to overcome by reducing variability and designing for tissue-specific applications. Selecting detergent-free decellularization protocols and milling methods that achieve homogenous particle size could lead to dECM preparation with lowered batch- to-batch variation. As a whole, designing dECM biomaterials with crosslinkers and composite polymer based on considerations for tissue structure, mechanics, and functionality could ultimately give rise to effective biomaterials that achieve the regenerative potential of dECM.

### **Author contribution**

**Mika Brown:** Investigation, Conceptualization, Writing – Original Draft, Writing – Review and Editing. Jianyu Li: Writing – Review and Editing. Christopher Moraes: Writing –

Review and Editing. Maryam Tabrizian: Supervision, Writing – Review and Editing. Nicole Y.K. Li-Jessen: Supervision, Conceptualization, Writing – Review and Editing.

### **Declaration of competing interest**

The authors declare that they have no known competing financial interests or personal relationships that could have appeared to influence the work reported in this paper.

### **Acknowledgements**

This review was supported by the National Sciences and Engineering Research Council of Canada (RGPIN-2018–03843 and ALLRP 548623- 19), Canada Research Chair research stipend (N.L.-J., J.L., C.M., M.T.) and the National Institutes of Health (R01 DC-018577-01A1). The presented content is solely the responsibility of the authors and does not necessarily represent the official views of the above funding agencies.

### 3.5. References

- 1 Chen, F. M. & Liu, X. Advancing biomaterials of human origin for tissue engineering. *Progress in Polymer Science* **53**, 86-168 (2016). <https://doi.org/10.1016/j.progpolymsci.2015.02.004>
- 2 Coburn, P. T., Li, X., Li, J., Kishimoto, Y. & Li-Jessen, N. Y. Progress in Vocal Fold Regenerative Biomaterials: An Immunological Perspective. *Advanced NanoBiomed Research*, 2100119 (2021).
- 3 Gattazzo, F., Urciuolo, A. & Bonaldo, P. Extracellular matrix: A dynamic microenvironment for stem cell niche. *Biochimica et Biophysica Acta* **1840**, 2506-2519 (2014). <https://doi.org/https://doi.org/10.1016/j.bbagen.2014.01.010>
- 4 Keane, T. J., Swinehart, I. T. & Badylak, S. F. Methods of Tissue Decellularization Used for Preparation of Biologic Scaffolds and In Vivo Relevance. *Methods* **84**, 25-34 (2015).
- 5 Chowdhury, C. (U.S. Food and Drug Administration, Center for Devices and Radiological Health, Maryland, 2020).
- 6 Krause, D. (U.S. Food and Drug Administration, Center for Devices and Radiological Health, 2017).
- 7 Krause, D. (U.S. Food and Drug Administration, Center for Devices and Radiological Health, 2018).
- 8 Liu, L. (U.S. Food and Drug Administration, Center for Devices and Radiological Health, 2019).
- 9 Wang, N. (U.S. Food and Drug Administration, Center for Devices and Radiological Health, Maryland, 2016).
- 10 Chang, C. (U.S. Food and Drug Administration, Center for Devices and Radiological Health, 2018).
- 11 Howell, R. S. *et al.* Paraesophageal Hiatal Hernia Repair With Urinary Bladder Matrix Graft. *Journal of the Society of Laparoscopic & Robotic Surgeons* **22** (2018). <https://doi.org/10.4293/JSL.S.2017.00100>
- 12 Sasse, K., Ackerman, E. & Brandt, J. J. O. S. Complex wounds treated with MatriStem xenograft material: case series and cost analysis. *OA Surgery* **1**, 3 (2013).
- 13 Washington, M. J., Hodde, J. P., Cohen, E. & Cote, L. Biologic staple line reinforcement for laparoscopic sleeve gastrectomy: A case series. *International Journal of Surgery* **17**, 1-4 (2019).
- 14 Brown-Etris, M., Milne, C. T. & Hodde, J. P. An extracellular matrix graft (Oasis® wound matrix) for treating full-thickness pressure ulcers: A randomized clinical trial. *Journal of Tissue Viability* **28**, 21-26 (2019). <https://doi.org/https://doi.org/10.1016/j.jtv.2018.11.001>
- 15 Badylak, S. F. *et al.* The use of extracellular matrix as an inductive scaffold for the partial replacement of functional myocardium. *Cell Transplantation* **15**, 29-40 (2006).
- 16 Xu, C. C., Chan, R. W. & Tirunagari, N. A biodegradable, acellular xenogeneic scaffold for regeneration of the vocal fold lamina propria. *Tissue Eng Pt A* **13**, 551-566 (2007). <https://doi.org/10.1089/ten.2006.0169>
- 17 Masaeli, E., Karamali, F., Loghmani, S., Eslaminejad, M. B. & Nasr-Esfahani, M. H. Bio-engineered electrospun nanofibrous membranes using cartilage extracellular matrix particles. *Journal of Materials Chemistry B* **5**, 765-776 (2017). <https://doi.org/10.1039/c6tb02015a>
- 18 Claudio-Rizo, J. A. *et al.* Influence of residual composition on the structure and properties

- of extracellular matrix derived hydrogels. *J Materials Science Engineering: C* **79**, 793-801 (2017).
- 19 Saldin, L. T., Cramer, M. C., Velankar, S. S., White, L. J. & Badylak, S. F. Extracellular matrix hydrogels from decellularized tissues: Structure and function. *Acta Biomaterialia* **49**, 1-15 (2017). <https://doi.org/10.1016/j.actbio.2016.11.068>
  - 20 Sutherland, A. J., Converse, G. L., Hopkins, R. A. & Detamore, M. S. The Bioactivity of Cartilage Extracellular Matrix in Articular Cartilage Regeneration. *Advanced Healthcare Materials* **4**, 29-39 (2015). <https://doi.org/10.1002/adhm.201400165>
  - 21 Yu, C., Kornmuller, A., Brown, C., Hoare, T. & Flynn, L. E. Decellularized adipose tissue microcarriers as a dynamic culture platform for human adipose-derived stem/stromal cell expansion. *Biomaterials* **120**, 66-80 (2017). <https://doi.org/10.1016/j.biomaterials.2016.12.017>
  - 22 Grant, R., Hallett, J., Forbes, S., Hay, D. & Callanan, A. Blended Electrospinning with Human Liver Extracellular Matrix for Engineering New Hepatic Microenvironments. *Scientific Reports* **9**, 6293 (2019). <https://doi.org/10.1038/s41598-019-42627-7>
  - 23 Kusuma, G. D. *et al.* Transferable Matrixes Produced from Decellularized Extracellular Matrix Promote Proliferation and Osteogenic Differentiation of Mesenchymal Stem Cells and Facilitate Scale-Up. *Acs Biomater Sci Eng* **4**, 1760-1769 (2018). <https://doi.org/10.1021/acsbiomaterials.7b00747>
  - 24 Das, S. *et al.* Decellularized extracellular matrix bioinks and the external stimuli to enhance cardiac tissue development in vitro. *Acta Biomaterialia* **95**, 188-200 (2019). <https://doi.org/10.1016/j.actbio.2019.04.026>
  - 25 Zhu, Y. *et al.* Injectable, porous, biohybrid hydrogels incorporating decellularized tissue components for soft tissue applications. *Acta Biomaterialia* **73**, 112-126 (2018). <https://doi.org/10.1016/j.actbio.2018.04.003>
  - 26 Beachley, V. *et al.* Extracellular matrix particle–glycosaminoglycan composite hydrogels for regenerative medicine applications. *Journal of Biomedical Materials Research Part A* **106**, 147-159 (2018).
  - 27 Young, B. M. *et al.* Electrospun decellularized lung matrix scaffold for airway smooth muscle culture. *Acs Biomater Sci Eng* **3**, 3480-3492 (2017).
  - 28 Pati, F. *et al.* Printing three-dimensional tissue analogues with decellularized extracellular matrix bioink. *Nat Commun* **5**, 3935 (2014). <https://doi.org/10.1038/ncomms4935>
  - 29 Gao, G. *et al.* Tissue engineered bio-blood-vessels constructed using a tissue-specific bioink and 3D coaxial cell printing technique: a novel therapy for ischemic disease. *Advanced functional materials* **27**, 1700798 (2017).
  - 30 Kim, B. S. *et al.* 3D cell printing of in vitro stabilized skin model and in vivo pre-vascularized skin patch using tissue-specific extracellular matrix bioink: a step towards advanced skin tissue engineering. *Biomaterials* **168**, 38-53 (2018).
  - 31 Mitragotri, S. & Lahann, J. Physical Approaches to Biomaterial Design. *Nature Materials* **8**, 15-23 (2009). <https://doi.org/10.1038/nmat2344>
  - 32 Hussey, G. S., Dziki, J. L. & Badylak, S. F. Extracellular matrix-based materials for regenerative medicine. *Nature Reviews Materials* **3**, 159-173 (2018).
  - 33 Benjamin, E. J. *et al.* Heart Disease and Stroke Statistics—2019 Update: A Report From the American Heart Association. *American Heart Association* **139**, e56-e528 (2019). <https://doi.org/doi:10.1161/CIR.0000000000000659>
  - 34 Becker, M. *et al.* Towards a Novel Patch Material for Cardiac Applications: Tissue-

- Specific Extracellular Matrix Introduces Essential Key Features to Decellularized Amniotic Membrane. *International Journal of Molecular Science* **19**, 1032 (2018). <https://doi.org/10.3390/ijms19041032>
- 35 Fujita, K. *et al.* Modulation of the mechanical properties of ventricular extracellular matrix hydrogels with a carbodiimide crosslinker and investigation of their cellular compatibility. *AIMS Materials Science* **5**, 54-74 (2018). <https://doi.org/10.3934/matricsci.2018.1.54>
- 36 Wilhelm, M. J. Long-term outcome following heart transplantation: current perspective. *Thoracic Disease* **7**, 549-551 (2015). <https://doi.org/10.3978/j.issn.2072-1439.2015.01.46>
- 37 Bejleri, D. *et al.* A Bioprinted Cardiac Patch Composed of Cardiac-Specific Extracellular Matrix and Progenitor Cells for Heart Repair. *Advanced healthcare materials* **7**, 1800672 (2018).
- 38 Rodrigues, I. C. P., Kaasi, A., Maciel Filho, R., Jardini, A. L. & Gabriel, L. P. Cardiac tissue engineering: current state-of-the-art materials, cells and tissue formation. *Einstein* **16**, eRB4538-eRB4538 (2018). <https://doi.org/10.1590/S1679-45082018RB4538>
- 39 Vunjak-Novakovic, G. *et al.* Challenges in cardiac tissue engineering. *Tissue engineering Part B Reviews* **16**, 169-187 (2010). <https://doi.org/10.1089/ten.TEB.2009.0352>
- 40 Pok, S., Benavides, O. M., Hallal, P. & Jacot, J. G. Use of Myocardial Matrix in a Chitosan-Based Full-Thickness Heart Patch. *Tissue Eng Pt A* **20**, 1877-1887 (2014). <https://doi.org/10.1089/ten.tea.2013.0620>
- 41 Curley, C. J. *et al.* An injectable alginate/extra cellular matrix (ECM) hydrogel towards acellular treatment of heart failure. *Drug Delivery and Translational Research* **9**, 1-13 (2019). <https://doi.org/10.1007/s13346-018-00601-2>
- 42 Baghalishahi, M. *et al.* Cardiac extracellular matrix hydrogel together with or without inducer cocktail improves human adipose tissue-derived stem cells differentiation into cardiomyocyte-like cells. *Biochemical biophysical research communications* **502**, 215-225 (2018).
- 43 Zhang, Y. *et al.* Novel preparation of Au nanoparticles loaded Laponite nanoparticles/ECM injectable hydrogel on cardiac differentiation of resident cardiac stem cells to cardiomyocytes. *Photochemistry and Photobiology B* **192**, 49-54 (2019). <https://doi.org/10.1016/j.jphotobiol.2018.12.022>
- 44 Jang, J. *et al.* 3D printed complex tissue construct using stem cell-laden decellularized extracellular matrix bioinks for cardiac repair. *Biomaterials* **112**, 264-274 (2017). <https://doi.org/10.1016/j.biomaterials.2016.10.026>
- 45 Camelliti, P. *et al.* Adult human heart slices are a multicellular system suitable for electrophysiological and pharmacological studies. *Journal of Molecular and Cellular Cardiology* **51**, 390-398 (2011). <https://doi.org/https://doi.org/10.1016/j.yjmcc.2011.06.018>
- 46 Janssen, P. M., Lehnart, S. E., Prestle, J. & Hasenfuss, G. Preservation of contractile characteristics of human myocardium in multi-day cell culture. *Journal of Molecular and Cellular Cardiology* **31**, 1419-1427 (1999). <https://doi.org/10.1006/jmcc.1999.0978>
- 47 Arbogast, K. B., Thibault, K. L., Pinheiro, B. S., Winey, K. I. & Margulies, S. S. A high-frequency shear device for testing soft biological tissues. *Journal of Biomechanics* **30**, 757-759 (1997). [https://doi.org/10.1016/s0021-9290\(97\)00023-7](https://doi.org/10.1016/s0021-9290(97)00023-7)
- 48 Kim, T. H., Jung, Y. & Kim, S. H. Nanofibrous Electrospun Heart Decellularized Extracellular Matrix-Based Hybrid Scaffold as Wound Dressing for Reducing Scarring in Wound Healing. *Tissue Eng Pt A* **24**, 830-848 (2018).

- <https://doi.org/10.1089/ten.tea.2017.0318>
- 49 Wang, W. *et al.* Preparation and Characterization of Pro-Angiogenic Gel Derived from Small Intestinal Submucosa. *Acta Biomaterialia* **29**, 135-148 (2016).  
<https://doi.org/10.1016/j.actbio.2015.10.013>
  - 50 Seo, Y., Jung, Y. & Kim, S. H. Decellularized heart ECM hydrogel using supercritical carbon dioxide for improved angiogenesis. *Acta Biomaterialia* **67**, 270-281 (2018).  
<https://doi.org/10.1016/j.actbio.2017.11.046>
  - 51 Grover, G. N., Rao, N. & Christman, K. L. Myocardial matrix–polyethylene glycol hybrid hydrogels for tissue engineering. *Nanotechnology* **25**, 014011 (2013).
  - 52 Golob, M., Moss, R. L. & Chesler, N. C. Cardiac tissue structure, properties, and performance: a materials science perspective. *Ann Biomed Eng* **42**, 2003-2013 (2014).  
<https://doi.org/10.1007/s10439-014-1071-z>
  - 53 Ghadiri, M. *et al.* Physico-chemical, mechanical and cytotoxicity characterizations of Laponite®/alginate nanocomposite. *Applied Clay Science* **85**, 64-73 (2013).  
<https://doi.org/https://doi.org/10.1016/j.clay.2013.08.049>
  - 54 Oropeza, B. P., Adams, J. R., Furth, M. E., Chessa, J. & Boland, T. Bioprinting of decellularized porcine cardiac tissue for large-scale aortic models. *Frontiers in Bioengineering and Biotechnology* **10**, 855186 (2022).
  - 55 Bavishi, C. *et al.* Intravascular ultrasound–guided vs angiography-guided drug-eluting stent implantation in complex coronary lesions: meta-analysis of randomized trials. *American heart journal* **185**, 26-34 (2017).
  - 56 Istanbulu, O. B. & Akdogan, G. Influences of stent design on in-stent restenosis and major cardiac outcomes: a scoping review and meta-analysis. *Cardiovascular Engineering and Technology* **13**, 147-169 (2022).
  - 57 Zong, J. *et al.* Advances in the development of biodegradable coronary stents: A translational perspective. *Materials Today Bio* **16**, 100368 (2022).
  - 58 Lee, C. *et al.* Concise review: Human articular cartilage repair: Sources and detection of cytotoxicity and genotoxicity in photo-crosslinkable hydrogel bioscaffolds. *Stem Cells and Regenerative Medicine* (2019).
  - 59 Hernandez, M. J. *et al.* Decellularized Extracellular Matrix Hydrogels as a Delivery Platform for MicroRNA and Extracellular Vesicle Therapeutics. *Advanced therapeutics* **1**, 1800032 (2018).
  - 60 Ventura, R. D., Padalhin, A. R. & Lee, B. T. In-vitro and in-vivo evaluation of hemostatic potential of decellularized ECM hydrogels. *Materials Letters* **232**, 130-133 (2018).
  - 61 Bai, R. *et al.* Combining ECM hydrogels of cardiac bioactivity with stem cells of high cardiomyogenic potential for myocardial repair. **2019** (2019).
  - 62 Fu, W. *et al.* A hydrogel derived from acellular blood vessel extracellular matrix to promote angiogenesis. *J Biomater Appl* **33**, 1301-1313 (2019).  
<https://doi.org/10.1177/0885328219831055>
  - 63 Qiao, L. *et al.* Synergistic effects of adipose-derived stem cells combined with decellularized myocardial matrix on the treatment of myocardial infarction in rats. **239**, 116891 (2019).
  - 64 Reid, J. A. & Callanan, A. Influence of aorta extracellular matrix in electrospun polycaprolactone scaffolds. *Journal of Applied Polymer Science* **136**, 48181 (2019).  
<https://doi.org/https://doi.org/10.1002/app.48181>
  - 65 Roshanbinfar, K. *et al.* Carbon nanotube doped pericardial matrix derived



- electroconductive biohybrid hydrogel for cardiac tissue engineering. **7**, 3906-3917 (2019).
- 66 Liguori, G. R. *et al.* Molecular and biomechanical clues from cardiac tissue decellularized extracellular matrix drive stromal cell plasticity. **8** (2020).
- 67 Rajabi, S., Aghdami, N., Varzideh, F., Parchehbaf-Kashani, M. & Nobakht Lahrood, F. Decellularized muscle-derived hydrogels support in vitro cardiac microtissue fabrication. **108**, 3302-3310 (2020). <https://doi.org/10.1002/jbm.b.34666>
- 68 Reid, J. A. & Callanan, A. Hybrid cardiovascular sourced extracellular matrix scaffolds as possible platforms for vascular tissue engineering. **108**, 910-924 (2020). <https://doi.org/10.1002/jbm.b.34444>
- 69 Basara, G., Ozcebe, S. G., Ellis, B. W. & Zorlutuna, P. Tunable Human Myocardium Derived Decellularized Extracellular Matrix for 3D Bioprinting and Cardiac Tissue Engineering. *Gels* **7**, 70 (2021). <https://doi.org/10.3390/gels7020070>
- 70 Bejleri, D. *et al.* In vivo evaluation of bioprinted cardiac patches composed of cardiac-specific extracellular matrix and progenitor cells in a model of pediatric heart failure. *Biomater Sci-Uk* **10**, 444-456 (2022).
- 71 Diaz, M. D. *et al.* Injectable Myocardial Matrix Hydrogel Mitigates Negative Left Ventricular Remodeling in a Chronic Myocardial Infarction Model. *JACC Basic Transl Sci* **6**, 350-361 (2021). <https://doi.org/10.1016/j.jacbts.2021.01.003>
- 72 Du, P. *et al.* An injectable, self-assembled multicellular microsphere with the incorporation of fibroblast-derived extracellular matrix for therapeutic angiogenesis. *Mater Sci Eng C Mater Biol Appl* **113**, 110961 (2020). <https://doi.org/10.1016/j.msec.2020.110961>
- 73 Ercan, H., Elcin, A. E. & Elcin, Y. M. Preliminary assessment of an injectable extracellular matrix from decellularized bovine myocardial tissue. *Z Naturforsch C J Biosci* (2021). <https://doi.org/10.1515/znc-2021-0039>
- 74 Gómez-Cid, L. *et al.* Cardiac Extracellular Matrix Hydrogel Enriched with Polyethylene Glycol Presents Improved Gelation Time and Increased On-Target Site Retention of Extracellular Vesicles. **22**, 9226 (2021).
- 75 Guan, G. *et al.* Engineering hiPSC-CM and hiPSC-EC laden 3D nanofibrous splenic hydrogel for improving cardiac function through revascularization and remuscularization in infarcted heart. *Bioactive materials* **6**, 4415-4429 (2021).
- 76 Kang, B. *et al.* Facile bioprinting process for fabricating size-controllable functional microtissues using light-activated decellularized extracellular matrix-based bioinks. *Advanced Materials Technologies* **7**, 2100947 (2022).
- 77 Kim, H. *et al.* Light-Activated Decellularized Extracellular Matrix-Based Bioinks for Volumetric Tissue Analogs at the Centimeter Scale. *Advanced Functional Materials*, 2011252 (2021).
- 78 Kobayashi, M. *et al.* Elastic Modulus of ECM Hydrogels Derived from Decellularized Tissue Affects Capillary Network Formation in Endothelial Cells. *Int J Mol Sci* **21**, 6304 (2020). <https://doi.org/10.3390/ijms21176304>
- 79 Liguori, T. T. A., Liguori, G. R., van Dongen, J. A., Moreira, L. F. P. & Harmsen, M. C. Bioactive decellularized cardiac extracellular matrix-based hydrogel as a sustained-release platform for human adipose tissue-derived stromal cell-secreted factors. *Biomedical Materials* **16**, 025022 (2021). <https://doi.org/ARTN.02502210.1088/1748-605X/abcff9>
- 80 Mousavi, A., Mashayekhan, S., Baheiraei, N. & Pourjavadi, A. Biohybrid oxidized alginate/myocardial extracellular matrix injectable hydrogels with improved electromechanical properties for cardiac tissue engineering. *Int J Biol Macromol* **180**, 692-

- 708 (2021). <https://doi.org/10.1016/j.ijbiomac.2021.03.097>
- 81 Nishiguchi, A. & Taguchi, T. A pH-driven genipin gelator to engineer decellularized  
extracellular matrix-based tissue adhesives. *Acta Biomaterialia* **131**, 211-221 (2021).
- 82 Shin, Y. J. *et al.* 3D bioprinting of mechanically tuned bioinks derived from cardiac  
decellularized extracellular matrix. (2020).
- 83 Tsui, J. H. *et al.* Tunable electroconductive decellularized extracellular matrix hydrogels  
for engineering human cardiac microphysiological systems. *Biomaterials* **272**, 120764  
(2021). <https://doi.org/10.1016/j.biomaterials.2021.120764>
- 84 Wang, X. *et al.* Exogenous extracellular matrix proteins decrease cardiac fibroblast  
activation in stiffening microenvironment through CAPG. *Journal of Molecular Cellular  
Cardiology* (2021).
- 85 Zhu, D. *et al.* Minimally invasive delivery of therapeutic agents by hydrogel injection into  
the pericardial cavity for cardiac repair. *Nat Commun* **12**, 1412 (2021).
- 86 Klein, T. J., Malda, J., Sah, R. L. & Hutmacher, D. W. Tissue engineering of articular  
cartilage with biomimetic zones. *Tissue Engineering Part B Reviews* **15**, 143-157 (2009).  
<https://doi.org/10.1089/ten.TEB.2008.0563>
- 87 Wu, J. *et al.* An injectable extracellular matrix derived hydrogel for meniscus repair and  
regeneration. *Acta Biomaterialia* **16**, 49-59 (2015).  
<https://doi.org/10.1016/j.actbio.2015.01.027>
- 88 Liu, C., Jin, Z., Ge, X., Zhang, Y. & Xu, H. Decellularized Annulus Fibrosus  
Matrix/Chitosan hydrogels for annulus fibrous tissue engineering. *Tissue Eng Pt A* (2019).  
<https://doi.org/10.1089/ten.TEA.2018.0297>
- 89 Gao, S. *et al.* Fabrication and characterization of electrospun nanofibers composed of  
decellularized meniscus extracellular matrix and polycaprolactone for meniscus tissue  
engineering. *Journal of Materials Chemistry B* **5**, 2273-2285 (2017).  
<https://doi.org/10.1039/c6tb03299k>
- 90 Danso, E. K., Honkanen, J. T. J., Saarakkala, S. & Korhonen, R. K. Comparison of  
nonlinear mechanical properties of bovine articular cartilage and meniscus. *Journal of  
Biomechanics* **47**, 200-206 (2014).  
<https://doi.org/https://doi.org/10.1016/j.jbiomech.2013.09.015>
- 91 Rothrauff, B. B., Yang, G. & Tuan, R. S. Tissue-specific bioactivity of soluble tendon-  
derived and cartilage-derived extracellular matrices on adult mesenchymal stem cells. *Stem  
Cell Research and Therapy* **8**, 133 (2017). <https://doi.org/10.1186/s13287-017-0580-8>
- 92 Visser, J. *et al.* Crosslinkable hydrogels derived from cartilage, meniscus, and tendon  
tissue. *Tissue Eng Pt A* **21**, 1195-1206 (2015). <https://doi.org/10.1089/ten.TEA.2014.0362>
- 93 Rothrauff, B. B. *et al.* Efficacy of thermoresponsive, photocrosslinkable hydrogels derived  
from decellularized tendon and cartilage extracellular matrix for cartilage tissue  
engineering. *Tissue Engineering and Regenerative Medicine* **12**, e159-e170 (2018).  
<https://doi.org/10.1002/term.2465>
- 94 Basiri, A. *et al.* A silk fibroin/decellularized extract of Wharton's jelly hydrogel intended  
for cartilage tissue engineering. *Progress in Biomaterials* **8**, 31-42 (2019).
- 95 Benders, K. E. *et al.* Extracellular matrix scaffolds for cartilage and bone regeneration.  
*Trends in Biotechnology* **31**, 169-176 (2013). <https://doi.org/10.1016/j.tibtech.2012.12.004>
- 96 Huey, D. J., Hu, J. C. & Athanasiou, K. A. J. S. Unlike bone, cartilage regeneration remains  
elusive. **338**, 917-921 (2012).
- 97 Li, J. *et al.* Tough adhesives for diverse wet surfaces. **357**, 378-381 (2017).



- 98 Wang, D.-A. *et al.* Multifunctional chondroitin sulphate for cartilage tissue–biomaterial integration. *Nature materials* **6**, 385-392 (2007).
- 99 Sutherland, A. J. & Detamore, M. S. Bioactive Microsphere-Based Scaffolds Containing Decellularized Cartilage. *Macromol Biosci* **15**, 979-989 (2015). <https://doi.org/10.1002/mabi.201400472>
- 100 Kwon, J. S. *et al.* Injectable extracellular matrix hydrogel developed using porcine articular cartilage. *International journal of pharmaceutics* **454**, 183-191 (2013).
- 101 Garrigues, N. W., Little, D., Sanchez-Adams, J., Ruch, D. S. & Guilak, F. Electrospun cartilage-derived matrix scaffolds for cartilage tissue engineering. *J Biomed Mater Res A* **102**, 3998-4008 (2014). <https://doi.org/10.1002/jbm.a.35068>
- 102 Sutherland, A. J. *et al.* Decellularized cartilage may be a chondroinductive material for osteochondral tissue engineering. *J PloS one* **10**, e0121966 (2015).
- 103 Browe, D. C. *et al.* Glyoxal cross-linking of solubilized extracellular matrix to produce highly porous, elastic, and chondro-permissive scaffolds for orthopedic tissue engineering. **107**, 2222-2234 (2019). <https://doi.org/https://doi.org/10.1002/jbm.a.36731>
- 104 Lindberg, G. C. J. *et al.* Intact vitreous humor as a potential extracellular matrix hydrogel for cartilage tissue engineering applications. *Acta Biomaterialia* **85**, 117-130 (2019). <https://doi.org/https://doi.org/10.1016/j.actbio.2018.12.022>
- 105 Townsend, J. M. *et al.* Effects of tissue processing on bioactivity of cartilage matrix-based hydrogels encapsulating osteoconductive particles. *Biomedical Materials* **13**, 034108 (2018). <https://doi.org/10.1088/1748-605X/aaad77>
- 106 Bhattacharjee, M. *et al.* Preparation and characterization of amnion hydrogel and its synergistic effect with adipose derived stem cells towards IL1 $\beta$  activated chondrocytes. **10**, 1-15 (2020).
- 107 Bordbar, S. *et al.* Production and evaluation of decellularized extracellular matrix hydrogel for cartilage regeneration derived from knee cartilage. **108**, 938-946 (2020).
- 108 Chen, W. *et al.* 3D printing electrospinning fiber-reinforced decellularized extracellular matrix for cartilage regeneration. **382**, 122986 (2020).
- 109 Feng, B. *et al.* Engineering cartilage tissue based on cartilage-derived extracellular matrix cECM/PCL hybrid nanofibrous scaffold. *Materials & Design* **193**, 108773 (2020). <https://doi.org/https://doi.org/10.1016/j.matdes.2020.108773>
- 110 Ibsirlioglu, T., Elçin, A. E. & Elçin, Y. M. J. M. Decellularized biological scaffold and stem cells from autologous human adipose tissue for cartilage tissue engineering. **171**, 97-107 (2020).
- 111 Kim, H. S., Mandakhbayar, N., Kim, H.-W., Leong, K. W. & Yoo, H. S. J. B. Protein-reactive nanofibrils decorated with cartilage-derived decellularized extracellular matrix for osteochondral defects. 120214 (2020).
- 112 Visscher, D. O. *et al.* A photo-crosslinkable cartilage-derived extracellular matrix (ECM) bioink for auricular cartilage tissue engineering. *Acta Biomaterialia* (2020). <https://doi.org/https://doi.org/10.1016/j.actbio.2020.11.029>
- 113 Xu, Y. *et al.* Injectable photo-crosslinking cartilage decellularized extracellular matrix for cartilage tissue regeneration. *Materials Letters* **268**, 127609 (2020). <https://doi.org/https://doi.org/10.1016/j.matlet.2020.127609>
- 114 Yu, L. *et al.* Thermosensitive injectable decellularized nucleus pulposus hydrogel as an ideal biomaterial for nucleus pulposus regeneration. 0885328220921328 (2020).
- 115 Zhang, X. *et al.* Crosslinker-free silk/decellularized extracellular matrix porous bioink for

- 3D bioprinting-based cartilage tissue engineering. **118**, 111388 (2020).
- 116 Zhu, S. *et al.* 3D-Printed Extracellular Matrix/Polyethylene Glycol Diacrylate Hydrogel Incorporating the Anti-inflammatory Phytomolecule Honokiol for Regeneration of Osteochondral Defects. *The American Journal of Sports Medicine* **48**, 2808-2818 (2020). <https://doi.org/10.1177/0363546520941842>
- 117 Antich, C. *et al.* Development of a Biomimetic Hydrogel Based on Predifferentiated Mesenchymal Stem-Cell-Derived ECM for Cartilage Tissue Engineering. *Adv Healthc Mater* **10**, e2001847 (2021). <https://doi.org/10.1002/adhm.202001847>
- 118 Chae, S. *et al.* 3D cell-printing of biocompatible and functional meniscus constructs using meniscus-derived bioink. *Biomaterials* **267**, 120466 (2021).
- 119 Jeyakumar, V. *et al.* Decellularized Cartilage Extracellular Matrix Incorporated Silk Fibroin Hybrid Scaffolds for Endochondral Ossification Mediated Bone Regeneration. *Int J Mol Sci* **22**, 4055 (2021). <https://doi.org/10.3390/ijms22084055>
- 120 Kuang, W., Liu, C. & Xu, H. The application of decellularized nucleus pulposus matrix/chitosan with transforming growth factor  $\beta$ 3 for nucleus pulposus tissue engineering. *Cytotechnology* **73**, 447-456 (2021).
- 121 Li, H. *et al.* Nanofiber configuration affects biological performance of decellularized meniscus extracellular matrix incorporated electrospun scaffolds. *Biomedical Materials* **16**, 065013 (2021).
- 122 Masaeli, E. & Nasr-Esfahani, M. H. An in vivo evaluation of induced chondrogenesis by decellularized extracellular matrix particles. *J Biomed Mater Res A* **109**, 627-636 (2021). <https://doi.org/10.1002/jbm.a.37047>
- 123 Peng, Y. *et al.* Decellularized Disc Hydrogels for hBMSCs tissue-specific differentiation and tissue regeneration. *Bioact Mater* **6**, 3541-3556 (2021). <https://doi.org/10.1016/j.bioactmat.2021.03.014>
- 124 Ravari, M. K. *et al.* Fabrication and characterization of an injectable reinforced composite scaffold for cartilage tissue engineering: an in vitro study. *Biomed Mater* **16**, 045007 (2021). <https://doi.org/10.1088/1748-605X/abed97>
- 125 Setayeshmehr, M. *et al.* Bioprinting Via a Dual-Gel Bioink Based on Poly(Vinyl Alcohol) and Solubilized Extracellular Matrix towards Cartilage Engineering. *Int J Mol Sci* **22**, 3901 (2021). <https://doi.org/10.3390/ijms22083901>
- 126 Shojarazavi, N., Mashayekhan, S., Pazooki, H., Mohsenifard, S. & Baniasadi, H. Alginate/cartilage extracellular matrix-based injectable interpenetrating polymer network hydrogel for cartilage tissue engineering. *J Biomater Appl*, 8853282211024020 (2021). <https://doi.org/10.1177/08853282211024020>
- 127 Tian, G. *et al.* Cell-free decellularized cartilage extracellular matrix scaffolds combined with interleukin 4 promote osteochondral repair through immunomodulatory macrophages: in vitro and in vivo preclinical study. *Acta biomaterialia* **127**, 131-145 (2021).
- 128 Xia, B. *et al.* Development of a decellularized meniscus matrix-based nanofibrous scaffold for meniscus tissue engineering. *Acta Biomater* **128**, 175-185 (2021). <https://doi.org/10.1016/j.actbio.2021.03.074>
- 129 Yi, P. *et al.* Composite System of 3D-Printed Polymer and Acellular Matrix Hydrogel to Repair Temporomandibular Joint Disc. *Front Mater* **8** (2021). <https://doi.org/ARTN62141610.3389/fmats.2021.621416>
- 130 Zhang, X. *et al.* 3D Bioprinting of Biomimetic Bilayered Scaffold Consisting of Decellularized Extracellular Matrix and Silk Fibroin for Osteochondral Repair.

- 131 *International journal of bioprinting* **7**, 401 (2021). <https://doi.org/10.18063/ijb.v7i4.401>
- 132 Chen, C. C. *et al.* The Physicochemical Properties of Decellularized Extracellular Matrix-Coated 3D Printed Poly(epsilon-caprolactone) Nerve Conduits for Promoting Schwann Cells Proliferation and Differentiation. *Materials (Basel)* **11**, 1665 (2018). <https://doi.org/10.3390/ma11091665>
- 133 Ghuman, H. *et al.* ECM hydrogel for the treatment of stroke: Characterization of the host cell infiltrate. *Biomaterials* **91**, 166-181 (2016). <https://doi.org/10.1016/j.biomaterials.2016.03.014>
- 134 Xu, H. L. *et al.* Sustained-release of FGF-2 from a hybrid hydrogel of heparin-polyoxamer and decellular matrix promotes the neuroprotective effects of proteins after spinal injury. *International Journal of Nanomedicine* **13**, 681-694 (2018). <https://doi.org/10.2147/IJN.S152246>
- 135 Lin, T. *et al.* Hydrogel derived from porcine decellularized nerve tissue as a promising biomaterial for repairing peripheral nerve defects. *Acta biomaterialia* **73**, 326-338 (2018).
- 136 Cerqueira, S. R. *et al.* Decellularized peripheral nerve supports Schwann cell transplants and axon growth following spinal cord injury. *Biomaterials* **177**, 176-185 (2018). <https://doi.org/10.1016/j.biomaterials.2018.05.049>
- 137 Chen, S. *et al.* Promoting Neurite Growth and Schwann Cell Migration by the Harnessing Decellularized Nerve Matrix onto Nanofibrous Guidance. *ACS Applied Materials & Interfaces* **11**, 17167-17176 (2019). <https://doi.org/10.1021/acsami.9b01066>
- 138 Viswanath, A. *et al.* Extracellular matrix-derived hydrogels for dental stem cell delivery. *Biomedical Materials Research A* **105**, 319-328 (2017). <https://doi.org/10.1002/jbm.a.35901>
- 139 Madhusudan, P., Raju, G. & Shankarappa, S. Hydrogel systems and their role in neural tissue engineering. *Journal of the Royal Society Interface* **17**, 20190505 (2020).
- 140 Koči, Z. *et al.* Extracellular matrix hydrogel derived from human umbilical cord as a scaffold for neural tissue repair and its comparison with extracellular matrix from porcine tissues. *Tissue Engineering Part C Methods* **23**, 333-345 (2017).
- 141 Massensini, A. R. *et al.* Concentration-dependent rheological properties of ECM hydrogel for intracerebral delivery to a stroke cavity. *Acta Biomaterialia* **27**, 116-130 (2015). <https://doi.org/10.1016/j.actbio.2015.08.040>
- 142 Zou, J. L. *et al.* Peripheral nerve-derived matrix hydrogel promotes Remyelination and inhibits synapse formation. *Advanced Functional Materials* **28**, 1705739 (2018).
- 143 Tukmachev, D. *et al.* Injectable extracellular matrix hydrogels as scaffolds for spinal cord injury repair. *Tissue Eng Pt A* **22**, 306-317 (2016).
- 144 Li, R. *et al.* Heparin-Polyoxamer Thermosensitive Hydrogel Loaded with bFGF and NGF Enhances Peripheral Nerve Regeneration in Diabetic Rats. *Biomaterials* **168**, 24-37 (2018). <https://doi.org/10.1016/j.biomaterials.2018.03.044>
- 145 Wen, X. *et al.* Cauda equina-derived extracellular matrix for fabrication of nanostructured hybrid scaffolds applied to neural tissue engineering. *Tissue Eng Pt A* **21**, 1095-1105 (2015). <https://doi.org/10.1089/ten.TEA.2014.0173>
- 146 Trojaborg, W. Rate of recovery in motor and sensory fibres of the radial nerve: clinical and electrophysiological aspects. *Neurology, Neurosurgery, and Psychiatry* **33**, 625-638 (1970). <https://doi.org/10.1136/jnnp.33.5.625>
- 147 Rehfeld, A., Nylander, M. & Karnov, K. in *Compendium of Histology: A Theoretical and Practical Guide* (eds Anders Rehfeld, Malin Nylander, & Kirstine Karnov) 247-266

- (Springer International Publishing, 2017).
- 147 Baiguera, S. *et al.* Electrospun gelatin scaffolds incorporating rat decellularized brain extracellular matrix for neural tissue engineering. *Biomaterials* **35**, 1205-1214 (2014).
  - 148 Medberry, C. J. *et al.* Hydrogels derived from central nervous system extracellular matrix. *Biomaterials* **34**, 1033-1040 (2013). <https://doi.org/10.1016/j.biomaterials.2012.10.062>
  - 149 Ghuman, H. *et al.* Long-term retention of ECM hydrogel after implantation into a sub-acute stroke cavity reduces lesion volume. *Acta biomaterialia* **63**, 50-63 (2017).
  - 150 Prest, T. A. *et al.* Nerve-specific, xenogeneic extracellular matrix hydrogel promotes recovery following peripheral nerve injury. *J Biomed Mater Res A* **106**, 450-459 (2018). <https://doi.org/10.1002/jbm.a.36235>
  - 151 Thompson, R. E. *et al.* Effect of hyaluronic acid hydrogels containing astrocyte-derived extracellular matrix and/or V2a interneurons on histologic outcomes following spinal cord injury. *J Biomaterials* **162**, 208-223 (2018).
  - 152 Tatic, N., Rose, F. R. A. J., des Rieux, A. & White, L. J. Stem cells from the dental apical papilla in extracellular matrix hydrogels mitigate inflammation of microglial cells. *Scientific Reports* **9**, 14015 (2019). <https://doi.org/10.1038/s41598-019-50367-x>
  - 153 Výborný, K. *et al.* Genipin and EDC crosslinking of extracellular matrix hydrogel derived from human umbilical cord for neural tissue repair. *Scientific Reports* **9**, 10674 (2019). <https://doi.org/10.1038/s41598-019-47059-x>
  - 154 Hong, J. Y. *et al.* Decellularized brain matrix enhances macrophage polarization and functional improvements in rat spinal cord injury. *Acta Biomaterialia* **101**, 357-371 (2020). <https://doi.org/https://doi.org/10.1016/j.actbio.2019.11.012>
  - 155 Xu, Y. *et al.* Understanding the Role of Tissue-Specific Decellularized Spinal Cord Matrix Hydrogel for Neural Stem/Progenitor Cell Microenvironment Reconstruction and Spinal Cord Injury. 120596 (2020).
  - 156 Qiu, S. *et al.* Decellularized nerve matrix hydrogel and glial-derived neurotrophic factor modifications assisted nerve repair with decellularized nerve matrix scaffolds. **14**, 931-943 (2020). <https://doi.org/https://doi.org/10.1002/term.3050>
  - 157 Rao, Z. *et al.* Decellularized Nerve Matrix Hydrogel Scaffolds with Longitudinally Oriented and Size-Tunable Microchannels for Peripheral Nerve Regeneration. *Materials Science and Engineering: C*, 111791 (2020). <https://doi.org/https://doi.org/10.1016/j.msec.2020.111791>
  - 158 Seo, Y. *et al.* Development of an Anisotropically Organized Brain dECM Hydrogel-Based 3D Neuronal Culture Platform for Recapitulating the Brain Microenvironment in Vivo. *Acs Biomater Sci Eng* **6**, 610-620 (2020). <https://doi.org/10.1021/acsbiomaterials.9b01512>
  - 159 Ghuman, H. *et al.* ECM hydrogel improves the delivery of PEG microsphere-encapsulated neural stem cells and endothelial cells into tissue cavities caused by stroke. *Brain Res Bull* **168**, 120-137 (2021). <https://doi.org/10.1016/j.brainresbull.2020.12.004>
  - 160 Kong, J. S. *et al.* Promoting long-term cultivation of motor neurons for 3D neuromuscular junction formation of 3D in vitro using central-nervous-tissue-derived bioink. *Advanced healthcare materials* **10**, 2100581 (2021).
  - 161 Li, R. *et al.* Facilitate angiogenesis and neurogenesis by growth factors integrated decellularized matrix hydrogel. *Tissue Eng Pt A* **27**, 771-787 (2021).
  - 162 Ozudogru, E. *et al.* Decellularized spinal cord meninges extracellular matrix hydrogel that supports neurogenic differentiation and vascular structure formation. *Journal of Tissue Engineering and Regenerative Medicine* **15**, 948-963 (2021).



- 163 Simsa, R. *et al.* Brain organoid formation on decellularized porcine brain ECM hydrogels. *PLoS One* **16**, e0245685 (2021). <https://doi.org/10.1371/journal.pone.0245685>
- 164 Zhang, F. *et al.* Decellularized nerve extracellular matrix/chitosan crosslinked by genipin to prepare a moldable nerve repair material. *Cell Tissue Bank* **22**, 419-430 (2021). <https://doi.org/10.1007/s10561-020-09889-2>
- 165 Choi, Y. C. *et al.* Decellularized extracellular matrix derived from porcine adipose tissue as a xenogeneic biomaterial for tissue engineering. *Tissue Engineering Part C: Methods* **18**, 866-876 (2012).
- 166 Francis, M. P. *et al.* Electrospinning adipose tissue-derived extracellular matrix for adipose stem cell culture. *Journal of biomedical materials research Part A* **100**, 1716-1724 (2012).
- 167 Turner, A. E. & Flynn, L. E. Design and characterization of tissue-specific extracellular matrix-derived microcarriers. *Tissue Engineering Part C Methods* **18**, 186-197 (2012). <https://doi.org/10.1089/ten.TEC.2011.0246>
- 168 Turner, A. E., Yu, C., Bianco, J., Watkins, J. F. & Flynn, L. E. The performance of decellularized adipose tissue microcarriers as an inductive substrate for human adipose-derived stem cells. *Biomaterials* **33**, 4490-4499 (2012).
- 169 Cheung, H. K. *et al.* Composite hydrogel scaffolds incorporating decellularized adipose tissue for soft tissue engineering with adipose-derived stem cells. *Biomaterials* **35**, 1914-1923 (2014). <https://doi.org/10.1016/j.biomaterials.2013.11.067>
- 170 Brown, C. F. *et al.* Effect of decellularized adipose tissue particle size and cell density on adipose-derived stem cell proliferation and adipogenic differentiation in composite methacrylated chondroitin sulphate hydrogels. *Biomedical Materials* **10**, 045010 (2015). <https://doi.org/10.1088/1748-6041/10/4/045010>
- 171 Pati, F. *et al.* Biomimetic 3D tissue printing for soft tissue regeneration. *Biomaterials* **62**, 164-175 (2015). <https://doi.org/10.1016/j.biomaterials.2015.05.043>
- 172 Rijal, G. *et al.* Robust tissue growth and angiogenesis in large-sized scaffold by reducing H<sub>2</sub>O<sub>2</sub>-mediated oxidative stress. *Biofabrication* **9**, 015013 (2017). <https://doi.org/10.1088/1758-5090/9/1/015013>
- 173 Zhao, Y., Fan, J. & Bai, S. Biocompatibility of injectable hydrogel from decellularized human adipose tissue in vitro and in vivo. *Biomedical Materials Research B Applied Biomaterials* **107**, 1684-1694 (2019). <https://doi.org/10.1002/jbm.b.34261>
- 174 van Dongen, J. A. *et al.* Adipose tissue-derived extracellular matrix hydrogels as a release platform for secreted paracrine factors. *Tissue Engineering and Regenerative Medicine* **13**, 973-985 (2019).
- 175 Lin, M. *et al.* Biochemical and biomechanical comparisons of decellularized scaffolds derived from porcine subcutaneous and visceral adipose tissue. **10**, 2041731419888168 (2019).
- 176 Martin, P. M., Grant, A., Hamilton, D. W. & Flynn, L. E. Matrix composition in 3-D collagenous bioscaffolds modulates the survival and angiogenic phenotype of human chronic wound dermal fibroblasts. *Acta biomaterialia* **83**, 199-210 (2019).
- 177 Mohiuddin, O. A. *et al.* Human Adipose-Derived Hydrogel Characterization Based on In Vitro ASC Biocompatibility and Differentiation. **2019** (2019).
- 178 Shridhar, A., Amsden, B. G., Gillies, E. R., Flynn, L. E. J. F. i. b. & biotechnology. Investigating the effects of tissue-specific extracellular matrix on the adipogenic and osteogenic differentiation of human adipose-derived stromal cells within composite hydrogel scaffolds. **7**, 402 (2019).

- 179 Getova, V. E., van Dongen, J. A., Brouwer, L. A. & Harmsen, M. C. Adipose tissue-derived ECM hydrogels and their use as 3D culture scaffold. *J Artificial cells, nanomedicine, biotechnology* **47**, 1693-1701 (2019).
- 180 Mohiuddin, O. A. *et al.* Characterization And Proteomic Analysis Of Decellularized Adipose Tissue Hydrogels Derived From Lean And Overweight/Obese Human Donors. **4**, 2000124 (2020).
- 181 Nguyen, M. T. N., Tran, H. L. B. J. J. o. S. A. M. & Devices. Fabrication of an injectable acellular adipose matrix for soft tissue regeneration. (2020).
- 182 Nyambat, B. *et al.* New insight into natural extracellular matrix: Genipin cross-linked adipose-derived stem cell extracellular matrix gel for tissue engineering. **21**, 4864 (2020).
- 183 Chen, Z. *et al.* Human decellularized adipose matrix derived hydrogel assists mesenchymal stem cells delivery and accelerates chronic wound healing. *J Biomed Mater Res A* **109**, 1418-1428 (2021). <https://doi.org/10.1002/jbm.a.37133>
- 184 Cho, W. W. *et al.* Flexible Adipose-Vascular Tissue Assembly Using Combinational 3D Printing for Volume-Stable Soft Tissue Reconstruction. *Advanced Healthcare Materials* **10**, 2001693 (2021).
- 185 Leclerc, C. J. *et al.* Decellularized adipose tissue scaffolds guide hematopoietic differentiation and stimulate vascular regeneration in a hindlimb ischemia model. *Biomaterials* **274**, 120867 (2021). <https://doi.org/10.1016/j.biomaterials.2021.120867>
- 186 Lee, S. *et al.* Enhanced Regeneration of Vascularized Adipose Tissue with Dual 3D-Printed Elastic Polymer/dECM Hydrogel Complex. *Int J Mol Sci* **22**, 2886 (2021). <https://doi.org/10.3390/ijms22062886>
- 187 Liu, P. C. *et al.* Hydrogel from acellular porcine adipose tissue promotes survival of adipose tissue transplantation. *Biomedical Materials* **16**, 045015 (2021). <https://doi.org/ARTN 045015>
- 10.1088/1748-605X/abf982
- 188 Pu, W., Han, Y. & Yang, M. Human decellularized adipose tissue hydrogels as a culture platform for human adipose-derived stem cell delivery. *Journal of Applied Biomaterials Functional Materials* **19**, 2280800020988141 (2021).
- 189 Gir, P. *et al.* Fat grafting: evidence-based review on autologous fat harvesting, processing, reinjection, and storage. *Plastic Reconstructive Surgery* **130**, 249-258 (2012). <https://doi.org/10.1097/PRS.0b013e318254b4d3>
- 190 Simonacci, F., Bertozzi, N., Grieco, M. P., Grignaffini, E. & Raposio, E. Procedure, applications, and outcomes of autologous fat grafting. *Ann Med Surg (Lond)* **20**, 49-60 (2017). <https://doi.org/10.1016/j.amsu.2017.06.059>
- 191 Iivarinen, J. T., Korhonen, R. K. & Jurvelin, J. S. Experimental and numerical analysis of soft tissue stiffness measurement using manual indentation device—significance of indentation geometry and soft tissue thickness. *Skin Research Technology* **20**, 347-354 (2014).
- 192 Hong, Y. *et al.* An elastomeric patch electrospun from a blended solution of dermal extracellular matrix and biodegradable polyurethane for rat abdominal wall repair. *Tissue Eng Part C Methods* **18**, 122-132 (2012). <https://doi.org/10.1089/ten.TEC.2011.0295>
- 193 Chainani, A. *et al.* Multilayered electrospun scaffolds for tendon tissue engineering. *Tissue Eng Pt A* **19**, 2594-2604 (2013).
- 194 DeQuach, J. A. *et al.* Injectable skeletal muscle matrix hydrogel promotes neovascularization and muscle cell infiltration in a hindlimb ischemia model. *European*

- Cells and Materials* **23**, 400-412; discussion 412 (2012).  
<https://doi.org/10.22203/ecm.v023a31>
- 195 Takanari, K. *et al.* Abdominal wall reconstruction by a regionally distinct biocomposite of  
 extracellular matrix digest and a biodegradable elastomer. *Tissue Engineering and  
 Regenerative Medicine* **10**, 748-761 (2013). <https://doi.org/10.1002/term.1834>
- 196 Farnebo, S. *et al.* Design and characterization of an injectable tendon hydrogel: a novel  
 scaffold for guided tissue regeneration in the musculoskeletal system. *Tissue Eng Part A*  
**20**, 1550-1561 (2014). <https://doi.org/10.1089/ten.TEA.2013.0207>
- 197 Choi, Y. J. *et al.* 3D cell printing of functional skeletal muscle constructs using skeletal  
 muscle-derived bioink. *Advanced Healthcare Materials* **5**, 2636-2645 (2016).
- 198 Fu, Y. *et al.* Decellularization of porcine skeletal muscle extracellular matrix for the  
 formulation of a matrix hydrogel: a preliminary study. *Journal of Cellular and Molecular  
 Medicine* **20**, 740-749 (2016). <https://doi.org/https://doi.org/10.1111/jcmm.12776>
- 199 Ungerleider, J. L. *et al.* Extracellular Matrix Hydrogel Promotes Tissue Remodeling,  
 Arteriogenesis, and Perfusion in a Rat Hindlimb Ischemia Model. *JACC Basic  
 Translational Science* **1**, 32-44 (2016). <https://doi.org/10.1016/j.jacbts.2016.01.009>
- 200 Rao, N. *et al.* Engineering an injectable muscle-specific microenvironment for improved  
 cell delivery using a nanofibrous extracellular matrix hydrogel. *ACS Nano* **11**, 3851-3859  
 (2017).
- 201 Toprakhisar, B. *et al.* Development of Bioink from Decellularized Tendon Extracellular  
 Matrix for 3D Bioprinting. *Macromol Biosci* **18**, e1800024 (2018).  
<https://doi.org/10.1002/mabi.201800024>
- 202 Choi, Y.-J. *et al.* A 3D cell printed muscle construct with tissue-derived bioink for the  
 treatment of volumetric muscle loss. *Biomaterials* **206**, 160-169 (2019).  
<https://doi.org/https://doi.org/10.1016/j.biomaterials.2019.03.036>
- 203 Lee, H. *et al.* Effect of Hierarchical Scaffold Consisting of Aligned dECM Nanofibers and  
 Poly(lactide-co-glycolide) Struts on the Orientation and Maturation of Human Muscle  
 Progenitor Cells. *ACS Applied Materials & Interfaces* **11**, 39449-39458 (2019).  
<https://doi.org/10.1021/acsami.9b12639>
- 204 Smoak, M. M. *et al.* Fabrication and Characterization of Electrospun Decellularized  
 Muscle-Derived Scaffolds. *Tissue Engineering Part C Methods* **25**, 276-287 (2019).  
<https://doi.org/10.1089/ten.TEC.2018.0339>
- 205 Patel, K. H. *et al.* Aligned nanofibers of decellularized muscle ECM support myogenic  
 activity in primary satellite cells in vitro. *Biomed Mater* **14**, 035010 (2019).  
<https://doi.org/10.1088/1748-605X/ab0b06>
- 206 Hernandez, M. J., Zelus, E. I., Spang, M. T., Braden, R. L. & Christman, K. L. Dose  
 optimization of decellularized skeletal muscle extracellular matrix hydrogels for improving  
 perfusion and subsequent validation in an aged hindlimb ischemia model. *Biomater Sci-Uk*  
**8**, 3511-3521 (2020). <https://doi.org/10.1039/C9BM01963D>
- 207 Lee, H. *et al.* A novel decellularized skeletal muscle-derived ECM scaffolding system for  
 in situ muscle regeneration. *Methods* **171**, 77-85 (2020).  
<https://doi.org/https://doi.org/10.1016/j.ymeth.2019.06.027>
- 208 Moreno-Manzano, V. *et al.* Injectable Gel Form of a Decellularized Bladder Induces  
 Adipose-Derived Stem Cell Differentiation into Smooth Muscle Cells In Vitro. **21**, 8608  
 (2020).
- 209 Raj, R., Sobhan, P. K., Pratheesh, K. V. & Anilkumar, T. V. A cholecystic extracellular

- matrix-based hybrid hydrogel for skeletal muscle tissue engineering. **108**, 1922-1933 (2020). <https://doi.org/https://doi.org/10.1002/jbm.a.36955>
- 210 Boso, D. *et al.* Porcine decellularized diaphragm hydrogel: a new option for skeletal muscle malformations. *Biomedicines* **9**, 709 (2021).
- 211 Gaffney, L., Davis, Z., Mora-Navarro, C., Fisher, M. B. & Freytes, D. O. Extracellular Matrix Hydrogels Promote Expression of Muscle-Tendon Junction Proteins. *Tissue Eng Part A* (2021). <https://doi.org/10.1089/ten.TEA.2021.0070>
- 212 Kim, W. *et al.* A bioprinting process supplemented with in situ electrical stimulation directly induces significant myotube formation and myogenesis. *Advanced Functional Materials* **31**, 2105170 (2021).
- 213 Lee, H. *et al.* Self-aligned myofibers in 3D bioprinted extracellular matrix-based construct accelerate skeletal muscle function restoration. *Appl Phys Rev* **8**, 021405 (2021). <https://doi.org/10.1063/5.0039639>
- 214 Liu, Z. N., Liu, J. J., Liu, N., Zhu, X. Q. & Tang, R. Tailoring electrospun mesh for a compliant remodeling in the repair of full-thickness abdominal wall defect-The role of decellularized human amniotic membrane and silk fibroin. *Mat Sci Eng C-Mater* **127**, 112235 (2021). <https://doi.org/ARTN 11223510.1016/j.msec.2021.112235>
- 215 Ning, L. J. *et al.* Enhancement of Migration and Tenogenic Differentiation of Macaca Mulatta Tendon-Derived Stem Cells by Decellularized Tendon Hydrogel. *Front Cell Dev Biol* **9**, 651583 (2021). <https://doi.org/10.3389/fcell.2021.651583>
- 216 Smoak, M. M., Hogan, K. J., Grande-Allen, K. J. & Mikos, A. G. Bioinspired electrospun dECM scaffolds guide cell growth and control the formation of myotubes. *Sci Adv* **7**, eabg4123 (2021). <https://doi.org/10.1126/sciadv.abg4123>
- 217 Yang, D., Fang, Z., Kang, R. & Liu, K. Composite electrospun scaffold containing decellularized amniotic matrix for pelvic organ prolapse. *Materials & Design* **210**, 110106 (2021). <https://doi.org/https://doi.org/10.1016/j.matdes.2021.110106>
- 218 Zhao, F. *et al.* Comparison of three different acidic solutions in tendon decellularized extracellular matrix bio-ink fabrication for 3D cell printing. *Acta Biomaterialia* **131**, 262-275 (2021).
- 219 Zhu, M., Qin, B., Yi, Y., Yang, J. & Gu, L. TGFβ1 Improves the Proliferation of Decellularized and Aligned Skeletal Muscle in Extracellular Matrix Hydrogels by m6A Modification-Mediated Integrin Through Inducing ERK Phosphorylation. (2021).
- 220 Squire, J. M. Architecture and function in the muscle sarcomere. *Current Opinion in Structural Biology* **7**, 247-257 (1997). [https://doi.org/https://doi.org/10.1016/S0959-440X\(97\)80033-4](https://doi.org/https://doi.org/10.1016/S0959-440X(97)80033-4)
- 221 Gilbert-Honick, J. & Grayson, W. Vascularized and Innervated Skeletal Muscle Tissue Engineering. *Advanced Healthcare Materials* **9**, e1900626 (2020). <https://doi.org/10.1002/adhm.201900626>
- 222 Morrow, D. A., Haut Donahue, T. L., Odegard, G. M. & Kaufman, K. R. Transversely isotropic tensile material properties of skeletal muscle tissue. *Journal of the Mechanical Behavior of Biomedical Materials* **3**, 124-129 (2010). <https://doi.org/https://doi.org/10.1016/j.jmbbm.2009.03.004>
- 223 Sato, M., Ito, A., Kawabe, Y., Nagamori, E. & Kamihira, M. Enhanced contractile force generation by artificial skeletal muscle tissues using IGF-I gene-engineered myoblast cells. *Journal of Bioscience and Bioengineering* **112**, 273-278 (2011). <https://doi.org/https://doi.org/10.1016/j.jbiosc.2011.05.007>



- 224 Ma, X. *et al.* Rapid 3D bioprinting of decellularized extracellular matrix with regionally varied mechanical properties and biomimetic microarchitecture. *Biomaterials* **185**, 310-321 (2018). <https://doi.org/10.1016/j.biomaterials.2018.09.026>
- 225 Skardal, A. *et al.* Tissue specific synthetic ECM hydrogels for 3-D in vitro maintenance of hepatocyte function. *Biomaterials* **33**, 4565-4575 (2012). <https://doi.org/10.1016/j.biomaterials.2012.03.034>
- 226 Ijima, H., Nakamura, S., Bual, R. P. & Yoshida, K. Liver-specific extracellular matrix hydrogel promotes liver-specific functions of hepatocytes in vitro and survival of transplanted hepatocytes in vivo. *Bioscience and Bioengineering* **128**, 365-372 (2019). <https://doi.org/10.1016/j.jbiosc.2019.02.014>
- 227 Lewis, P. L. *et al.* Complex bile duct network formation within liver decellularized extracellular matrix hydrogels. *Scientific Reports* **8**, 1-14 (2018). <https://doi.org/ARTN1222010.1038/s41598-018-30433-6>
- 228 Bual, R., Kimura, H., Ikegami, Y., Shirakigawa, N. & Ijima, H. Fabrication of liver-derived extracellular matrix nanofibers and functional evaluation in in vitro culture using primary hepatocytes. *Materialia* **4**, 518-528 (2018).
- 229 Yeh, W. C. *et al.* Elastic modulus measurements of human liver and correlation with pathology. *Ultrasound in Medicine and Biology* **28**, 467-474 (2002). [https://doi.org/10.1016/s0301-5629\(02\)00489-1](https://doi.org/10.1016/s0301-5629(02)00489-1)
- 230 Lee, J. S. *et al.* Liver extracellular matrix providing dual functions of two-dimensional substrate coating and three-dimensional injectable hydrogel platform for liver tissue engineering. *Biomacromolecules* **15**, 206-218 (2014). <https://doi.org/10.1021/bm4015039>
- 231 Saheli, M. *et al.* Three-dimensional liver-derived extracellular matrix hydrogel promotes liver organoids function. *Cellular Biochemistry* **119**, 4320-4333 (2018). <https://doi.org/10.1002/jcb.26622>
- 232 Yu, C. *et al.* Scanningless and continuous 3D bioprinting of human tissues with decellularized extracellular matrix. *Biomaterials* **194**, 1-13 (2019). <https://doi.org/10.1016/j.biomaterials.2018.12.009>
- 233 Lee, H. *et al.* Development of Liver Decellularized Extracellular Matrix Bioink for Three-Dimensional Cell Printing-Based Liver Tissue Engineering. *Biomacromolecules* **18**, 1229-1237 (2017). <https://doi.org/10.1021/acs.biomac.6b01908>
- 234 Lewis, P. L., Yan, M., Su, J. & Shah, R. N. Directing the growth and alignment of biliary epithelium within extracellular matrix hydrogels. *Acta Biomaterialia* **85**, 84-93 (2019).
- 235 Deng, J. *et al.* Engineered Liver-on-a-Chip Platform to Mimic Liver Functions and Its Biomedical Applications: A Review. *Micromachines (Basel)* **10**, 676 (2019). <https://doi.org/10.3390/mi10100676>
- 236 Bao, J. *et al.* Enhanced hepatic differentiation of rat bone marrow-derived mesenchymal stem cells in spheroidal aggregate culture on a decellularized liver scaffold. *Int J Mol Med* **38**, 457-465 (2016). <https://doi.org/10.3892/ijmm.2016.2638>
- 237 Hiller, T. *et al.* Generation of a 3D Liver Model Comprising Human Extracellular Matrix in an Alginate/Gelatin-Based Bioink by Extrusion Bioprinting for Infection and Transduction Studies. *Int J Mol Sci* **19**, 3129 (2018). <https://doi.org/10.3390/ijms19103129>
- 238 Ijima, H., Nakamura, S., Bual, R., Shirakigawa, N. & Tanoue, S. Physical Properties of the Extracellular Matrix of Decellularized Porcine Liver. *Gels* **4**, 39 (2018). <https://doi.org/10.3390/gels4020039>
- 239 Lee, J. S. *et al.* Tissue Beads: Tissue-Specific Extracellular Matrix Microbeads to

- Potentiate Reprogrammed Cell-Based Therapy. *Advanced Functional Materials* **29**, 1807803 (2019).
- 240 Vafaei, S., Tabaei, S. R., Guneta, V., Choong, C. & Cho, N. J. Hybrid Biomimetic Interfaces Integrating Supported Lipid Bilayers with Decellularized Extracellular Matrix Components. *Langmuir* **34**, 3507-3516 (2018).  
<https://doi.org/10.1021/acs.langmuir.7b03265>
- 241 Ahmed, E. *et al.* Decellularized extracellular matrix-rich hydrogel–silver nanoparticle mixture as a potential treatment for acute liver failure model. **108**, 2351-2367 (2020).  
<https://doi.org/10.1002/jbm.a.36988>
- 242 Hussein, K. H. *et al.* Decellularized hepatic extracellular matrix hydrogel attenuates hepatic stellate cell activation and liver fibrosis. 111160 (2020).
- 243 Kim, M. K. *et al.* Decellularized extracellular matrix-based bio-ink with enhanced 3D printability and mechanical properties. **12**, 025003 (2020).
- 244 Mao, Q. *et al.* Fabrication of liver microtissue with liver decellularized extracellular matrix (dECM) bioink by digital light processing (DLP) bioprinting. *Materials Science and Engineering: C* **109**, 110625 (2020).  
<https://doi.org/10.1016/j.msec.2020.110625>
- 245 Asadi, M. *et al.* Hepatic cell-sheet fabrication of differentiated mesenchymal stem cells using decellularized extracellular matrix and thermoresponsive polymer. *Biomed Pharmacother* **134**, 111096 (2021). <https://doi.org/ARTN11109610.1016/j.biopha.2020.111096>
- 246 Chen, L., Ma, H. J., Li, K. M., Song, X. Q. & Zeng, X. S. Liver extracellular matrix hydrogel-based three-dimensional culture system of HepG2 cells to enhance cancer stem cell properties. *Mat Sci Eng C-Mater* **126**, 112119 (2021). <https://doi.org/ARTN11211910.1016/j.msec.2021.112119>
- 247 Choi, Y. S. *et al.* Immunomodulatory Scaffolds Derived from Lymph Node Extracellular Matrices. *ACS Appl Mater Interfaces* **13**, 14037-14049 (2021).  
<https://doi.org/10.1021/acsami.1c02542>
- 248 Janani, G. & Mandal, B. B. Mimicking Physiologically Relevant Hepatocyte Zonation Using Immunomodulatory Silk Liver Extracellular Matrix Scaffolds toward a Bioartificial Liver Platform. *Acs Applied Materials & Interfaces* **13**, 24401-24421 (2021).  
<https://doi.org/10.1021/acsami.1c00719>
- 249 Jeong, W., Kim, M. K. & Kang, H. W. Effect of detergent type on the performance of liver decellularized extracellular matrix-based bio-inks. *J Tissue Eng* **12**, 2041731421997091 (2021). <https://doi.org/10.1177/2041731421997091>
- 250 Li, S. *et al.* Tissue-Specific Hydrogels Ameliorate Hepatic Ischemia/Reperfusion Injury in Rats by Regulating Macrophage Polarization via TLR4/NF- $\kappa$ B Signaling. *Acs Biomater Sci Eng* **7**, 1552-1563 (2021).
- 251 Sawkins, M. J. *et al.* Hydrogels derived from demineralized and decellularized bone extracellular matrix. *Acta Biomaterialia* **9**, 7865-7873 (2013).  
<https://doi.org/10.1016/j.actbio.2013.04.029>
- 252 Gibson, M. *et al.* Tissue extracellular matrix nanoparticle presentation in electrospun nanofibers. *Biomedical Research International* **2014**, 469120 (2014).  
<https://doi.org/10.1155/2014/469120>
- 253 Ni, P. *et al.* Injectable thermosensitive PEG–PCL–PEG hydrogel/acellular bone matrix

- composite for bone regeneration in cranial defects. *Biomaterials* **35**, 236-248 (2014).
- 254 Smith, E. L. *et al.* Evaluation of skeletal tissue repair, part 1: assessment of novel growth-factor-releasing hydrogels in an ex vivo chick femur defect model. *Acta Biomaterialia* **10**, 4186-4196 (2014). <https://doi.org/10.1016/j.actbio.2014.06.011>
- 255 Smith, E. *et al.* Evaluation of skeletal tissue repair, part 2: enhancement of skeletal tissue repair through dual-growth-factor-releasing hydrogels within an ex vivo chick femur defect model. *Acta biomaterialia* **10**, 4197-4205 (2014).
- 256 Alom, N., Peto, H., Kirkham, G. R., Shakesheff, K. M. & White, L. J. Bone extracellular matrix hydrogel enhances osteogenic differentiation of C2C12 myoblasts and mouse primary calvarial cells. *Biomedical Materials Research B Applied Biomaterials* **106**, 900-908 (2018). <https://doi.org/10.1002/jbm.b.33894>
- 257 Kim, J. Y. *et al.* Synergistic Effects of Beta Tri-Calcium Phosphate and Porcine-Derived Decellularized Bone Extracellular Matrix in 3D-Printed Polycaprolactone Scaffold on Bone Regeneration. *Macromolecular Bioscience* **18**, e1800025 (2018). <https://doi.org/10.1002/mabi.201800025>
- 258 Carvalho, M. S. *et al.* Co-culture cell-derived extracellular matrix loaded electrospun microfibrillar scaffolds for bone tissue engineering. *Materials Science and Engineering C Materials Biological Applications* **99**, 479-490 (2019). <https://doi.org/10.1016/j.msec.2019.01.127>
- 259 Mohiuddin, O. A. *et al.* Decellularized Adipose Tissue Hydrogel Promotes Bone Regeneration in Critical-Sized Mouse Femoral Defect Model. **7** (2019). <https://doi.org/10.3389/fbioe.2019.00211>
- 260 Wu, R.-X. *et al.* Modulating macrophage responses to promote tissue regeneration by changing the formulation of bone extracellular matrix from filler particles to gel bioscaffolds. **101**, 330-340 (2019).
- 261 Black, C. *et al.* Characterisation and evaluation of the regenerative capacity of Stro-4+ enriched bone marrow mesenchymal stromal cells using bovine extracellular matrix hydrogel and a novel biocompatible melt electro-written medical-grade polycaprolactone scaffold. *Biomaterials* **247**, 119998 (2020). <https://doi.org/https://doi.org/10.1016/j.biomaterials.2020.119998>
- 262 Choi, E. *et al.* Characterization and intracellular mechanism of electrospun poly ( $\epsilon$ -caprolactone) (PCL) fibers incorporated with bone-dECM powder as a potential membrane for guided bone regeneration. *Journal of Industrial and Engineering Chemistry* (2020). <https://doi.org/https://doi.org/10.1016/j.jiec.2020.11.001>
- 263 Junka, R. & Yu, X. Polymer nanofibrous scaffolds laden with cell-derived extracellular matrix for bone regeneration. *Materials Science and Engineering: C* **113**, 110981 (2020). <https://doi.org/https://doi.org/10.1016/j.msec.2020.110981>
- 264 Luciana Aurora Soares do Amaral, D. *et al.* Induction of osteogenic differentiation by demineralized and decellularized bovine extracellular matrix derived hydrogels associated with barium titanate. *Biologicals* **66**, 9-16 (2020). <https://doi.org/https://doi.org/10.1016/j.biologicals.2020.06.003>
- 265 Obregon-Miano, F. *et al.* Injectable porcine bone demineralized and digested extracellular matrix—PEGDA hydrogel blend for bone regeneration. **31**, 21 (2020).
- 266 Datta, S. *et al.* Decellularized bone matrix/oleoyl chitosan derived supramolecular injectable hydrogel promotes efficient bone integration. *Mat Sci Eng C-Mater* **119**, 111604 (2021). <https://doi.org/ARTN11160410.1016/j.msec.2020.111604>

- 267 Dong, L. *et al.* The effect of collagen hydrogels on chondrocyte behaviors through  
restricting the contraction of cell/hydrogel constructs. *Regenerative Biomaterials* **8**,  
rbab030 (2021). <https://doi.org/10.1093/rb/rbab030>
- 268 Kim, S. *et al.* Partially Digested Osteoblast Cell Line-Derived Extracellular Matrix Induces  
Rapid Mineralization and Osteogenesis. *Acs Biomater Sci Eng* **7**, 1134-1146 (2021).  
<https://doi.org/10.1021/acsbiomaterials.0c01349>
- 269 Parthiban, S. P. *et al.* BoneMA—synthesis and characterization of a methacrylated bone-  
derived hydrogel for bioprinting of in-vitro vascularized tissue constructs. **13**, 035031  
(2021).
- 270 Rho, J.-Y., Kuhn-Spearing, L. & Zioupos, P. Mechanical properties and the hierarchical  
structure of bone. *Medical Engineering & Physics* **20**, 92-102 (1998).  
[https://doi.org/https://doi.org/10.1016/S1350-4533\(98\)00007-1](https://doi.org/10.1016/S1350-4533(98)00007-1)
- 271 Yamashita, J., Furman, B. R., Rawls, H. R., Wang, X. & Agrawal, C. M. The use of  
dynamic mechanical analysis to assess the viscoelastic properties of human cortical bone.  
*Journal of Biomedical Materials Research* **58**, 47-53 (2001). [https://doi.org/10.1002/1097-4636\(2001\)58:1<47::Aid-jbm70>3.0.Co;2-u](https://doi.org/10.1002/1097-4636(2001)58:1<47::Aid-jbm70>3.0.Co;2-u)
- 272 Rahmoun, J., Auperrin, A., Delille, R., Naceur, H. & Drazetic, P. Characterization and  
micromechanical modeling of the human cranial bone elastic properties. *Mechanics  
Research Communications* **60**, 7-14 (2014).  
<https://doi.org/10.1016/j.mechrescom.2014.04.001>
- 273 Stojic, M. *et al.* in *Biomaterials for Skin Repair and Regeneration* (ed Elena García-  
Gareta) 59-99 (Woodhead Publishing, 2019).
- 274 Morris, A. H. *et al.* Tunable Hydrogels Derived from Genetically Engineered Extracellular  
Matrix Accelerate Diabetic Wound Healing. *ACS Applied Material Interfaces* **10**, 41892-  
41901 (2018). <https://doi.org/10.1021/acsami.8b08920>
- 275 Won, J.-Y. *et al.* A potential dermal substitute using decellularized dermis extracellular  
matrix derived bio-ink. *Artificial cells, nanomedicine, biotechnology* **47**, 644-649 (2019).
- 276 Hsieh, C.-M. *et al.* A Novel Composite Hydrogel Composed of Formic Acid-  
Decellularized Pepsin-Soluble Extracellular Matrix Hydrogel and Sacchachitin Hydrogel  
as Wound Dressing to Synergistically Accelerate Diabetic Wound Healing. *Pharmaceutics*  
**12**, 538 (2020).
- 277 Blacklow, S. *et al.* Bioinspired mechanically active adhesive dressings to accelerate wound  
closure. **5**, eaaw3963 (2019).
- 278 Nestle, F. O., Di Meglio, P., Qin, J. Z. & Nickoloff, B. J. Skin immune sentinels in health  
and disease. *Nat Rev Immunol* **9**, 679-691 (2009). <https://doi.org/10.1038/nri2622>
- 279 Wolf, M. T. *et al.* A hydrogel derived from decellularized dermal extracellular matrix.  
*Biomaterials* **33**, 7028-7038 (2012). <https://doi.org/10.1016/j.biomaterials.2012.06.051>
- 280 Wolf, M. T. *et al.* Polypropylene surgical mesh coated with extracellular matrix mitigates  
the host foreign body response. *Journal of Biomedical Materials Research Part A: An  
Official Journal of The Society for Biomaterials, The Japanese Society for Biomaterials,  
and The Australian Society for Biomaterials and the Korean Society for Biomaterials* **102**,  
234-246 (2014).
- 281 Lee, H., Yang, S., Kim, M. & Kim, G. A scaffold with a bio-mimetically designed  
micro/nano-fibrous structure using decellularized extracellular matrix. *RSC advances* **6**,  
29697-29706 (2016).
- 282 Ahn, J. *et al.* Investigation on vascular cytotoxicity and extravascular transport of cationic

- polymer nanoparticles using perfusable 3D microvessel model. *Acta Biomaterialia* **76**, 154-163 (2018). <https://doi.org/https://doi.org/10.1016/j.actbio.2018.05.041>
- 283 Shi, L. *et al.* Cryogenic free-form extrusion bioprinting of decellularized small intestinal submucosa for potential applications in skin tissue engineering. *Biofabrication* **11**, 035023 (2019). <https://doi.org/10.1088/1758-5090/ab15a9>
- 284 Tan, Q.-W. *et al.* Hydrogel from acellular porcine adipose tissue accelerates wound healing by inducing intradermal adipocyte regeneration. **139**, 455-463 (2019).
- 285 Tang, K.-C. *et al.* Human adipose-derived stem cell secreted extracellular matrix incorporated into electrospun poly (lactic-co-glycolic acid) nanofibrous dressing for enhancing wound healing. **11**, 1609 (2019).
- 286 Zhang, X., Xiao, S., Liu, B., Miao, Y. & Hu, Z. J. R. M. Use of extracellular matrix hydrogel from human placenta to restore hair-inductive potential of dermal papilla cells. **14**, 741-751 (2019).
- 287 Bankoti, K. *et al.* Dual Functionalized Injectable Hybrid Extracellular Matrix Hydrogel for Burn Wounds. *Biomacromolecules* (2020). <https://doi.org/10.1021/acs.biomac.0c01400>
- 288 Bo, Q. *et al.* Decellularized dermal matrix-based photo-crosslinking hydrogels as a platform for delivery of adipose derived stem cells to accelerate cutaneous wound healing. *Materials & Design* **196**, 109152 (2020). <https://doi.org/https://doi.org/10.1016/j.matdes.2020.109152>
- 289 Jorgensen, A. M. *et al.* Decellularized Skin Extracellular Matrix (dsECM) Improves the Physical and Biological Properties of Fibrinogen Hydrogel for Skin Bioprinting Applications. *Nanomaterials (Basel)* **10**, 1484 (2020). <https://doi.org/10.3390/nano10081484>
- 290 Lee, S. J., Lee, J. H., Park, J., Kim, W. D. & Park, S. A. Fabrication of 3D Printing Scaffold with Porcine Skin Decellularized Bio-Ink for Soft Tissue Engineering. *Materials (Basel, Switzerland)* **13**, 3522 (2020). <https://doi.org/10.3390/ma13163522>
- 291 Allbritton-King, J. D., Kimicata, M. & Fisher, J. P. J. o. B. M. R. P. A. Incorporating a structural extracellular matrix gradient into a porcine urinary bladder matrix-based hydrogel dermal scaffold. (2021).
- 292 Barthold, J. E. *et al.* Recellularization and Integration of Dense Extracellular Matrix by Percolation of Tissue Microparticles. 2103355 (2021).
- 293 Cai, D. *et al.* Construction of multifunctional porcine acellular dermal matrix hydrogel blended with vancomycin for hemorrhage control, antibacterial action, and tissue repair in infected trauma wounds. *Materials Today Bio* **12**, 100127 (2021).
- 294 Huang, C.-C. Characteristics and preparation of designed alginate-based composite scaffold membranes with decellularized fibrous micro-scaffold structures from porcine Skin. *Polymers* **13**, 3464 (2021).
- 295 Jin, R. *et al.* Three-dimensional bioprinting of a full-thickness functional skin model using acellular dermal matrix and gelatin methacrylamide bioink. *Acta biomaterialia* **131**, 248-261 (2021).
- 296 Wang, C. *et al.* Sulfated glycosaminoglycans in decellularized placenta matrix as critical regulators for cutaneous wound healing. *Acta Biomaterialia* **122**, 199-210 (2021). <https://doi.org/10.1016/j.actbio.2020.12.055>
- 297 Xu, J. *et al.* A biological functional hybrid scaffold based on decellularized extracellular matrix/gelatin/chitosan with high biocompatibility and antibacterial activity for skin tissue engineering. *International Journal of Biological Macromolecules* **187**, 840-849 (2021).



- 298 Pouliot, R. A. *et al.* Development and characterization of a naturally derived lung  
extracellular matrix hydrogel. *Biomedical Materials Research A* **104**, 1922-1935 (2016).  
<https://doi.org/10.1002/jbm.a.35726>
- 299 Wu, J., Ravikumar, P., Nguyen, K. T., Hsia, C. C. & Hong, Y. Lung protection by  
inhalation of exogenous solubilized extracellular matrix. *PLoS One* **12**, e0171165 (2017).  
<https://doi.org/10.1371/journal.pone.0171165>
- 300 Link, P. A. *et al.* Electrosprayed extracellular matrix nanoparticles induce a pro-  
regenerative cell response. *Tissue Engineering and Regenerative Medicine* **12**, 2331-2336  
(2018). <https://doi.org/10.1002/term.2768>
- 301 Zhou, J. *et al.* Lung tissue extracellular matrix-derived hydrogels protect against radiation-  
induced lung injury by suppressing epithelial–mesenchymal transition. **235**, 2377-2388  
(2020). <https://doi.org/https://doi.org/10.1002/jcp.29143>
- 302 de Hilster, R. H. J. *et al.* Human lung extracellular matrix hydrogels resemble the stiffness  
and viscoelasticity of native lung tissue. **318**, L698-L704 (2020).
- 303 Petrou, C. L. *et al.* Clickable decellularized extracellular matrix as a new tool for building  
hybrid-hydrogels to model chronic fibrotic diseases in vitro. *Journal of materials  
chemistry. B* **8**, 6814-6826 (2020). <https://doi.org/10.1039/d0tb00613k>
- 304 Pouliot, R. A. *et al.* Porcine Lung-Derived Extracellular Matrix Hydrogel Properties Are  
Dependent on Pepsin Digestion Time. (2020).
- 305 Dabaghi, M. *et al.* A Robust Protocol for Decellularized Human Lung Bioink Generation  
Amenable to 2D and 3D Lung Cell Culture. *Cells* **10**, 1538 (2021).  
<https://doi.org/10.3390/cells10061538>
- 306 De Santis, M. M. *et al.* Extracellular-Matrix-Reinforced Bioinks for 3D Bioprinting Human  
Tissue. *Adv Mater* **33**, e2005476 (2021). <https://doi.org/10.1002/adma.202005476>
- 307 Falcones, B. *et al.* Bioprintable lung extracellular matrix hydrogel scaffolds for 3D culture  
of mesenchymal stromal cells. *Polymers* **13**, 2350 (2021).
- 308 Jung, M., Han, Y., Woo, C. & Ki, C. S. Pulmonary tissue-mimetic hydrogel niches for  
small cell lung cancer cell culture. *J Mater Chem B* **9**, 1858-1866 (2021).  
<https://doi.org/10.1039/d0tb02609c>
- 309 Noori, A. *et al.* Decellularized lung extracellular matrix scaffold promotes human  
embryonic stem cell differentiation towards alveolar progenitors. *Cell Journal (Yakhteh)*  
**25**, 372 (2023).
- 310 Park, S., Kim, T. H., Kim, S. H., You, S. & Jung, Y. Three-Dimensional Vascularized  
Lung Cancer-on-a-Chip with Lung Extracellular Matrix Hydrogels for In Vitro Screening.  
*Cancers (Basel)* **13**, 3930 (2021). <https://doi.org/10.3390/cancers13163930>
- 311 Ravindra, A. *et al.* Human Bronchial Epithelial Cell Growth on Homologous Versus  
Heterologous Tissue Extracellular Matrix. *J Surg Res* **263**, 215-223 (2021).  
<https://doi.org/10.1016/j.jss.2021.01.040>
- 312 Song, Y. H. *et al.* Development of novel apoptosis-assisted lung tissue decellularization  
methods. *Biomater Sci* **9**, 3485-3498 (2021). <https://doi.org/10.1039/d1bm00032b>
- 313 Mannino, D. M. & Buist, A. S. Global burden of COPD: risk factors, prevalence, and future  
trends. *The Lancet* **370**, 765-773 (2007). [https://doi.org/https://doi.org/10.1016/S0140-6736\(07\)61380-4](https://doi.org/https://doi.org/10.1016/S0140-6736(07)61380-4)
- 314 Doryab, A., Amoabediny, G. & Salehi-Najafabadi, A. Advances in pulmonary therapy and  
drug development: Lung tissue engineering to lung-on-a-chip. *Biotechnology Advances* **34**,  
588-596 (2016). <https://doi.org/10.1016/j.biotechadv.2016.02.006>

- 315 Skolasinski, S. D. & Panoskaltsis-Mortari, A. Lung tissue bioengineering for chronic obstructive pulmonary disease: overcoming the need for lung transplantation from human donors. *Expert Reviews in Respiratory Medicine* **13**, 665-678 (2019). <https://doi.org/10.1080/17476348.2019.1624163>
- 316 Moztarzadeh, S., Mottaghy, K., Sefat, F., Samadikuchaksaraei, A. & Mozafari, M. in *Nanoengineered Biomaterials for Regenerative Medicine* (eds Masoud Mozafari, Jayakumar Rajadas, & David Kaplan) 305-323 (Elsevier, 2019).
- 317 Bellia-Munzon, G. *et al.* in *Seminars in Pediatric Surgery*. 151063 (Elsevier).
- 318 Sun, F., Lu, Y., Wang, Z. & Shi, H. Vascularization strategies for tissue engineering for tracheal reconstruction. *Regenerative Medicine* **16**, 549-566 (2021).
- 319 Keane, T. J. *et al.* Tissue-Specific Effects of Esophageal Extracellular Matrix. *Tissue Eng Pt A* **21**, 2293-2300 (2015). <https://doi.org/10.1089/ten.TEA.2015.0322>
- 320 Keane, T. J. *et al.* Preparation and Characterization of a Biologic Scaffold and Hydrogel Derived from Colonic Mucosa. *Biomedical Materials Research B Applied Biomaterials* **105**, 291-306 (2017). <https://doi.org/10.1002/jbm.b.33556>
- 321 Keane, T. J. *et al.* Restoring Mucosal Barrier Function and Modifying Macrophage Phenotype with an Extracellular Matrix Hydrogel: Potential Therapy for Ulcerative Colitis. *Journal of Crohns and Colitis* **11**, 360-368 (2017). <https://doi.org/10.1093/ecco-jcc/jjw149>
- 322 Ha, D.-H. *et al.* Therapeutic effect of decellularized extracellular matrix-based hydrogel for radiation esophagitis by 3D printed esophageal stent. *Biomaterials* **266**, 120477 (2021). <https://doi.org/https://doi.org/10.1016/j.biomaterials.2020.120477>
- 323 Nam, H. *et al.* Multi-layered Free-form 3D Cell-printed Tubular Construct with Decellularized Inner and Outer Esophageal Tissue-derived Bioinks. *Scientific Reports* **10**, 7255 (2020). <https://doi.org/10.1038/s41598-020-64049-6>
- 324 Krezalek, M. A. *et al.* The intestinal microbiome and surgical disease. *Current Problems in Surgery* **53**, 257-293 (2016). <https://doi.org/10.1067/j.cpsurg.2016.06.001>
- 325 Arnold, J. W., Roach, J. & Azcarate-Peril, M. A. Emerging Technologies for Gut Microbiome Research. *Trends in Microbiology* **24**, 887-901 (2016). <https://doi.org/10.1016/j.tim.2016.06.008>
- 326 Cook, M. T., Tzortzis, G., Charalampopoulos, D. & Khutoryanskiy, V. V. Microencapsulation of probiotics for gastrointestinal delivery. *Journal of Controlled Release* **162**, 56-67 (2012). <https://doi.org/https://doi.org/10.1016/j.jconrel.2012.06.003>
- 327 Kim, K. & Kim, M. S. An injectable hydrogel derived from small intestine submucosa as a stem cell carrier. **104**, 1544-1550 (2016). <https://doi.org/https://doi.org/10.1002/jbm.b.33504>
- 328 Kim, W. & Kim, G. H. An intestinal model with a finger-like villus structure fabricated using a bioprinting process and collagen/SIS-based cell-laden bioink. *Theranostics* **10**, 2495-2508 (2020). <https://doi.org/10.7150/thno.41225>
- 329 Naranjo, J. D. *et al.* Esophageal extracellular matrix hydrogel mitigates metaplastic change in a dog model of Barrett's esophagus. **6**, eaba4526 (2020). <https://doi.org/10.1126/sciadv.aba4526> %J Science Advances
- 330 Han, H. *et al.* A Bioprinted Tubular Intestine Model Using a Colon-Specific Extracellular Matrix Bioink. *Advanced Healthcare Materials* **11**, 2101768 (2022).
- 331 Kim, J., Jang, J. & Cho, D.-W. Controlling cancer cell behavior by improving the stiffness of gastric tissue-decellularized ECM bioink with cellulose nanoparticles. *Frontiers in Bioengineering and Biotechnology* **9**, 605819 (2021).

- 332 Saldin, L. T. *et al.* The effect of normal, metaplastic, and neoplastic esophageal extracellular matrix upon macrophage activation. *Journal of Immunology Regenerative Medicine* **13**, 100037 (2021).
- 333 Ma, J., Wang, Y., Wei, P. & Jhanji, V. Biomechanics and structure of the cornea: implications and association with corneal disorders. *Survey of Ophthalmology* **63**, 851-861 (2018). <https://doi.org/10.1016/j.survophthal.2018.05.004>
- 334 Eghrari, A. O., Riazuddin, S. A. & Gottsch, J. D. in *Progress in Molecular Biology and Translational Science* Vol. 134 (eds J. Fielding Hejtmancik & John M. Nickerson) 7-23 (Academic Press, 2015).
- 335 Ahearne, M. & Lynch, A. P. Early Observation of Extracellular Matrix-Derived Hydrogels for Corneal Stroma Regeneration. *Tissue Engineering Part C Methods* **21**, 1059-1069 (2015). <https://doi.org/10.1089/ten.TEC.2015.0008>
- 336 Hong, H. *et al.* Compressed collagen intermixed with cornea-derived decellularized extracellular matrix providing mechanical and biochemical niches for corneal stroma analogue. *Materials Science and Engineering C* **103**, 109837 (2019). <https://doi.org/https://doi.org/10.1016/j.msec.2019.109837>
- 337 Fernández-Pérez, J., Kador, K. E., Lynch, A. P. & Ahearne, M. Characterization of extracellular matrix modified poly( $\epsilon$ -caprolactone) electrospun scaffolds with differing fiber orientations for corneal stroma regeneration. *Materials Science and Engineering C* **108**, 110415 (2020). <https://doi.org/https://doi.org/10.1016/j.msec.2019.110415>
- 338 Ahearne, M., Fernández-Pérez, J., Masterton, S., Madden, P. W. & Bhattacharjee, P. J. A. F. M. Designing scaffolds for corneal regeneration. **30**, 1908996 (2020).
- 339 Ahearne, M. & Coyle, A. Application of UVA-riboflavin crosslinking to enhance the mechanical properties of extracellular matrix derived hydrogels. *Mechanical Behavior and Biomedical Materials* **54**, 259-267 (2016). <https://doi.org/10.1016/j.jmbbm.2015.09.035>
- 340 Kim, H. *et al.* Characterization of cornea-specific bioink: high transparency, improved in vivo safety. *Journal of Tissue Engineering* **10**, 2041731418823382 (2019). <https://doi.org/10.1177/2041731418823382>
- 341 Wang, F. *et al.* Decellularized porcine cornea-derived hydrogels for the regeneration of epithelium and stroma in focal corneal defects. *The Ocular Surface* **18**, 748-760 (2020). <https://doi.org/https://doi.org/10.1016/j.jtos.2020.07.020>
- 342 Chameettachal, S. *et al.* Prevention of corneal myofibroblastic differentiation in vitro using a biomimetic ECM hydrogel for corneal tissue regeneration. *ACS Applied Bio Materials* **4**, 533-544 (2020).
- 343 Yazdanpanah, G. *et al.* Fabrication, Rheological, and Compositional Characterization of Thermoresponsive Hydrogel from Cornea. *Tissue Eng Part C Methods* **27**, 307-321 (2021). <https://doi.org/10.1089/ten.TEC.2021.0011>
- 344 Yazdanpanah, G. *et al.* In-situ porcine corneal matrix hydrogel as ocular surface bandage. *The Ocular Surface* **21**, 27-36 (2021).
- 345 Nagao, R. J. *et al.* Decellularized Human Kidney Cortex Hydrogels Enhance Kidney Microvascular Endothelial Cell Maturation and Quiescence. *Tissue Eng Pt A* **22**, 1140-1150 (2016). <https://doi.org/10.1089/ten.TEA.2016.0213>
- 346 Lih, E. *et al.* A Bioinspired Scaffold with Anti-Inflammatory Magnesium Hydroxide and Decellularized Extracellular Matrix for Renal Tissue Regeneration. *ACS Central Science* **5**, 458-467 (2019). <https://doi.org/10.1021/acscentsci.8b00812>
- 347 Su, J., Satchell, S. C., Shah, R. N. & Wertheim, J. A. Kidney decellularized extracellular



- matrix hydrogels: Rheological characterization and human glomerular endothelial cell response to encapsulation. *Biomedical Materials Research A* **106**, 2448-2462 (2018). <https://doi.org/10.1002/jbm.a.36439>
- 348 Sobreiro-Almeida, R., Fonseca, D. R. & Neves, N. M. Extracellular matrix electrospun membranes for mimicking natural renal filtration barriers. *Materials Science and Engineering C Materials Biological Applications* **103**, 109866 (2019). <https://doi.org/10.1016/j.msec.2019.109866>
- 349 Irrera, P., Consolino, L., Cutrin, J. C., Zöllner, F. G. & Longo, D. L. J. N. i. B. Dual assessment of kidney perfusion and pH by exploiting a dynamic CEST-MRI approach in an acute kidney ischemia–reperfusion injury murine model. **33**, e4287 (2020).
- 350 Sami, D. G., Heiba, H. H. & Abdellatif, A. Wound healing models: A systematic review of animal and non-animal models. *Wound Medicine* **24**, 8-17 (2019). <https://doi.org/https://doi.org/10.1016/j.wndm.2018.12.001>
- 351 McMahon, A. P. in *Current Topics in Developmental Biology* Vol. 117 (ed Paul M. Wassarman) 31-64 (Academic Press, 2016).
- 352 Magno, V. *et al.* Macromolecular crowding for tailoring tissue-derived fibrillated matrices. *Acta Biomaterialia* **55**, 109-119 (2017). <https://doi.org/10.1016/j.actbio.2017.04.018>
- 353 Ali, M. *et al.* A Photo-Crosslinkable Kidney ECM-Derived Bioink Accelerates Renal Tissue Formation. **8**, 1800992 (2019). <https://doi.org/https://doi.org/10.1002/adhm.201800992>
- 354 Sobreiro-Almeida, R., Melica, M. E., Lasagni, L., Romagnani, P. & Neves, N. M. Co-cultures of renal progenitors and endothelial cells on kidney decellularized matrices replicate the renal tubular environment in vitro. *Acta Physiol (Oxf)* **230**, e13491 (2020). <https://doi.org/10.1111/apha.13491>
- 355 Zhou, C. *et al.* Kidney extracellular matrix hydrogel enhances therapeutic potential of adipose-derived mesenchymal stem cells for renal ischemia reperfusion injury. *Acta Biomaterialia* **115**, 250-263 (2020). <https://doi.org/https://doi.org/10.1016/j.actbio.2020.07.056>
- 356 Sobreiro-Almeida, R. *et al.* Decellularized kidney extracellular matrix bioinks recapitulate renal 3D microenvironment in vitro. *Biofabrication* **13**, 045006 (2021).
- 357 Jiang, K. *et al.* 3-D physiometric extracellular matrix hydrogels provide a supportive microenvironment for rodent and human islet culture. *Biomaterials* **198**, 37-48 (2019). <https://doi.org/10.1016/j.biomaterials.2018.08.057>
- 358 Kim, J. *et al.* 3D cell printing of islet-laden pancreatic tissue-derived extracellular matrix bioink constructs for enhancing pancreatic functions. *Materials Chemistry B* **7**, 1773-1781 (2019).
- 359 Sackett, S. D. *et al.* Extracellular matrix scaffold and hydrogel derived from decellularized and delipidized human pancreas. *Scientific Reports* **8**, 10452 (2018). <https://doi.org/10.1038/s41598-018-28857-1>
- 360 Kolosova, K. *et al.* Characterizing Vocal Fold Injury Recovery in a Rabbit Model With Three-Dimensional Virtual Histology. *The Laryngoscope* **131**, 1578-1587 (2021). <https://doi.org/https://doi.org/10.1002/lary.29028>
- 361 Kazarine, A. *et al.* Multimodal virtual histology of rabbit vocal folds by nonlinear microscopy and nano computed tomography. *Biomed. Opt. Express* **10**, 1151-1164 (2019). <https://doi.org/10.1364/BOE.10.001151>
- 362 Miri, A. K. Mechanical Characterization of Vocal Fold Tissue: A Review Study. *Journal*

- of Voice **28**, 657-667 (2014). <https://doi.org/10.1016/j.jvoice.2014.03.001>
- 363 Garg, A. *et al.* Towards a Physiological Scale of Vocal Fold Agent-Based Models of Surgical Injury and Repair: Sensitivity Analysis, Calibration and Verification. *Appl Sci (Basel)* **9**, 2974 (2019). <https://doi.org/10.3390/app9152974>
- 364 Huang, D., Wang, R. & Yang, S. Cogels of Hyaluronic Acid and Acellular Matrix for Cultivation of Adipose-Derived Stem Cells: Potential Application for Vocal Fold Tissue Engineering. *Biomedical Research International* **2016**, 6584054 (2016). <https://doi.org/10.1155/2016/6584054>
- 365 Choi, J. W. *et al.* Small intestine submucosa and mesenchymal stem cells composite gel for scarless vocal fold regeneration. *Biomaterials* **35**, 4911-4918 (2014). <https://doi.org/10.1016/j.biomaterials.2014.03.008>
- 366 Chan, R. W. Nonlinear viscoelastic characterization of human vocal fold tissues under large-amplitude oscillatory shear (LAOS). *J Rheol (N Y N Y)* **62**, 695-712 (2018). <https://doi.org/10.1122/1.4996320>
- 367 Xu, C. C. & Mau, T. A tissue-specific, injectable acellular gel for the treatment of chronic vocal fold scarring. *Acta Biomaterialia* (2019). <https://doi.org/10.1016/j.actbio.2019.08.025>
- 368 Mora-Navarro, C. *et al.* Porcine Vocal Fold Lamina Propria-Derived Biomaterials Modulate TGF- $\beta$ 1-Mediated Fibroblast Activation in Vitro. *Acs Biomater Sci Eng* **6**, 1690-1703 (2020).
- 369 Latifi, N. *et al.* A Flow Perfusion Bioreactor System for Vocal Fold Tissue Engineering Applications. *Tissue Eng Part C Methods* **22**, 823-838 (2016). <https://doi.org/10.1089/ten.tec.2016.0053>
- 370 Seekhao, N., Shung, C., JaJa, J., Mongeau, L. & Li-Jessen, N. Y. K. High-Performance Agent-Based Modeling Applied to Vocal Fold Inflammation and Repair. *Frontiers in physiology* **9**, 304 (2018). <https://doi.org/10.3389/fphys.2018.00304>
- 371 Shin, K. *et al.* Three-Dimensional Culture of Salivary Gland Stem Cell in Orthotropic Decellularized Extracellular Matrix Hydrogels. *Tissue Eng Pt A* (2019). <https://doi.org/10.1089/ten.TEA.2018.0308>
- 372 Lee, J. S. *et al.* Bio-artificial tongue with tongue extracellular matrix and primary taste cells. *Biomaterials* **151**, 24-37 (2018). <https://doi.org/10.1016/j.biomaterials.2017.10.019>
- 373 Bashiri, Z. *et al.* Artificial testis: a testicular tissue extracellular matrix as a potential bio-ink for 3D printing. **9**, 3465-3484 (2021).
- 374 Francés-Herrero, E. *et al.* Development of Decellularized Oviductal Hydrogels as a Support for Rabbit Embryo Culture. *J Reproductive Sciences* **28**, 1644-1658 (2021).
- 375 Hou, C. *et al.* Printing 3D vagina tissue analogues with vagina decellularized extracellular matrix bioink. *International Journal of Biological Macromolecules* **180**, 177-186 (2021).
- 376 López-Martínez, S. *et al.* A Natural Xenogeneic Endometrial Extracellular Matrix Hydrogel Toward Improving Current Human in vitro Models and Future in vivo Applications. *Frontiers in bioengineering* **9**, 156 (2021).
- 377 Gaetani, R. *et al.* Evaluation of different decellularization protocols on the generation of pancreas-derived hydrogels. *Tissue Engineering Part C Methods* **24**, 697-708 (2018). <https://doi.org/10.1089/ten.TEC.2018.0180>
- 378 Hill, R. C., Calle, E. A., Dzieciatkowska, M., Niklason, L. E. & Hansen, K. C. Quantification of extracellular matrix proteins from a rat lung scaffold to provide a molecular readout for tissue engineering. *Mol Cell Proteomics* **14**, 961-973 (2015).

<https://doi.org/10.1074/mcp.M114.045260>

- 379 Rossi, E. A., Quintanilha, L. F., Nonaka, C. K. V. & Souza, B. S. d. F. Advances in hepatic  
tissue bioengineering with decellularized liver bioscaffold. *Stem cells international* **2019**  
(2019).
- 380 Size, A., Sharon, A. & Sauer-Budge, A. An automated low cost instrument for  
simultaneous multi-sample tissue homogenization. *Robotics Computer-Integrated*  
*Manufacturing* **27**, 276-281 (2011).
- 381 Atwood, J. A. in *Sample Preparation Techniques for Soil, Plant, and Animal Samples* 69-  
84 (Springer, 2016).
- 382 Grenier, J. *et al.* Mechanisms of pore formation in hydrogel scaffolds textured by freeze-  
drying. *Acta Biomater* **94**, 195-203 (2019). <https://doi.org/10.1016/j.actbio.2019.05.070>
- 383 Coogan, K. R., Stone, P. T., Sempertegui, N. D. & Rao, S. S. J. E. P. J. Fabrication of  
micro-porous hyaluronic acid hydrogels through salt leaching. **135**, 109870 (2020).
- 384 Pan, T., Song, W., Cao, X., Wang, Y. & Technology. 3D bioplotting of gelatin/alginate  
scaffolds for tissue engineering: influence of crosslinking degree and pore architecture on  
physicochemical properties. *Journal of Materials Science* **32**, 889-900 (2016).
- 385 Wu, J. & Hong, Y. Enhancing cell infiltration of electrospun fibrous scaffolds in tissue  
regeneration. *Bioactive materials* **1**, 56-64 (2016).
- 386 Politi, S. *et al.* Smart ECM-Based Electrospun Biomaterials for Skeletal Muscle  
Regeneration. *Nanomaterials (Basel)* **10**, (2020). <https://doi.org/10.3390/nano10091781>
- 387 Li, S. *et al.* Development and fabrication of co-axially electrospun biomimetic periosteum  
with a decellularized periosteal ECM shell/PCL core structure to promote the repair of  
critical-sized bone defects. *Composites Part B: Engineering* **234**, 109620 (2022).  
<https://doi.org/https://doi.org/10.1016/j.compositesb.2022.109620>
- 388 Mashayekhan, S., Jahanshahi, M., Moghadam, S. & Research, B. Reinforcement of a  
decellularized extracellular matrix-derived hydrogel using nanofibers for cardiac tissue  
engineering. *J International Journal of Advanced Biological* **8**, 303-314 (2020).
- 389 Auger, F. A., Gibot, L. & Lacroix, D. The Pivotal Role of Vascularization in Tissue  
Engineering. *Annu Rev Biomed Eng* **15**, 177-200 (2013). <https://doi.org/10.1146/annurev-bioeng-071812-152428>
- 390 Desai, R. M., Koshy, S. T., Hilderbrand, S. A., Mooney, D. J. & Joshi, N. S. Versatile click  
alginate hydrogels crosslinked via tetrazine–norbornene chemistry. *Biomaterials* **50**, 30-37  
(2015).
- 391 Wang, J. K. *et al.* Interpenetrating Network of Alginate–Human Adipose Extracellular  
Matrix Hydrogel for Islet Cells Encapsulation. **41**, 2000275 (2020).
- 392 Zhu, Y. *et al.* Biomimetic hybrid scaffold of electrospun silk fibroin and pancreatic  
decellularized extracellular matrix for islet survival. *Journal of Biomaterials Science,*  
*Polymer Edition*, 1-15 (2020). <https://doi.org/10.1080/09205063.2020.1818018>
- 393 Idaszek, J. *et al.* Alginate-based tissue-specific bioinks for multi-material 3D-bioprinting  
of pancreatic islets and blood vessels: A step towards vascularized pancreas grafts.  
*Bioprinting* **24**, e00163 (2021).
- 394 Hwang, D. G. *et al.* A 3D bioprinted hybrid encapsulation system for delivery of human  
pluripotent stem cell-derived pancreatic islet-like aggregates. *Biofabrication* **14**, 014101  
(2021).
- 395 Sadtler, K. *et al.* Proteomic composition and immunomodulatory properties of urinary  
bladder matrix scaffolds in homeostasis and injury. *Seminars in Immunology* **29**, 14-23

- (2017). <https://doi.org/https://doi.org/10.1016/j.smim.2017.05.002>
- 396 Wolf, M. T. *et al.* A biologic scaffold–associated type 2 immune microenvironment  
inhibits tumor formation and synergizes with checkpoint immunotherapy. *Science*  
*translational medicine* **11**, eaat7973 (2019).
- 397 Estrellas, K. M. *et al.* Biological scaffold–mediated delivery of myostatin inhibitor  
promotes a regenerative immune response in an animal model of Duchenne muscular  
dystrophy. *Journal of Biological Chemistry* **293**, 15594-15605 (2018).
- 398 Smigiel, K. S. & Parks, W. C. Macrophages, wound healing, and fibrosis: recent insights.  
*Current rheumatology reports* **20**, 1-8 (2018).
- 399 Li, C. *et al.* Design of biodegradable, implantable devices towards clinical translation.  
*Nature Reviews Materials* **5**, 61-81 (2020).
- 400 Wassenaar, J. W., Braden, R. L., Osborn, K. G. & Christman, K. L. Modulating In Vivo  
Degradation Rate of Injectable Extracellular Matrix Hydrogels. *J Mater Chem B* **4**, 2794-  
2802 (2016). <https://doi.org/10.1039/C5TB02564H>
- 401 Kim, J. & Ma, T. Autocrine fibroblast growth factor 2-mediated interactions between  
human mesenchymal stem cells and the extracellular matrix under varying oxygen tension.  
*J Journal of cellular biochemistry* **114**, 716-727 (2013).
- 402 Mahon, O. R. *et al.* Extracellular matrix scaffolds derived from different musculoskeletal  
tissues drive distinct macrophage phenotypes and direct tissue-specific cellular  
differentiation. *Journal of Immunology and Regenerative Medicine* **12**, 100041 (2021).  
<https://doi.org/https://doi.org/10.1016/j.regen.2021.100041>
- 403 Al Halawani, A., Mithieux, S. M., Yeo, G. C., Hosseini-Beheshti, E. & Weiss, A. S.  
Extracellular Vesicles: Interplay with the Extracellular Matrix and Modulated Cell  
Responses. *J International Journal of Molecular Sciences* **23**, 3389 (2022).
- 404 Huleihel, L. *et al.* Matrix-bound nanovesicles within ECM bioscaffolds. *J Science*  
*advances* **2**, e1600502 (2016).
- 405 van der Merwe, Y. *et al.* Matrix-bound nanovesicles prevent ischemia-induced retinal  
ganglion cell axon degeneration and death and preserve visual function. *Scientific reports*  
**9**, 3482 (2019).
- 406 Allan, D., Tieu, A., Lalu, M. & Burger, D. Mesenchymal stromal cell-derived extracellular  
vesicles for regenerative therapy and immune modulation: Progress and challenges toward  
clinical application. *Stem Cells Translational Medicine* **9**, 39-46 (2019).  
<https://doi.org/10.1002/sctm.19-0114> %J Stem Cells Translational Medicine
- 407 Zhu, M. *et al.* In vivo engineered extracellular matrix scaffolds with instructive niches for  
oriented tissue regeneration. *Nat Commun* **10**, 4620 (2019).  
<https://doi.org/10.1038/s41467-019-12545-3>
- 408 van Duinen, V. *et al.* 96 perfusable blood vessels to study vascular permeability in vitro.  
*Scientific Reports* **7**, 18071 (2017). <https://doi.org/10.1038/s41598-017-14716-y>

## Preface to Chapter 4

As reviewed in Chapter 3, tissue-specific dECM is commonly reported to stimulate a preferential regenerative response in the target tissue over dECM derived from other sources. However, the use of VF dECM presents challenges for scale up and outcome consistency due to their small size and variation in tissue composition and properties between animals.

Other soft tissues like SIS can be derived in significantly larger quantities from a single animal, are already available on a commercial scale. As reviewed in Chapter 2, SIS-based biomaterials have been reported to induce regenerative responses in animal models. We hypothesized that SIS-based injectable dECM hydrogels would stimulate a comparable regenerative response to VF dECM hydrogels due to similarity in tissue composition and reduced variation between samples.

In Chapter 4, we proposed the use of SIS dECM hydrogels as a scalable substitute for tissue-specific VF dECM hydrogels in VF applications. First, we compared the composition of porcine SIS and VF dECMs to native porcine VF through comprehensive analyses of proteomic data obtained by mass spectroscopy. We then compared the response of human vocal fold fibroblasts (HVFF) cultured on SIS dECM, VF dECM, and collagen and glass controls through viability and neo-ECM deposition assays. Overall, we showed that SIS dECM has potential as a sufficiently similar substitute for VF dECM in VF applications.

This work was published in *Advanced NanoBiomed Research* in 2023:

Mika Brown, Shirley Zhu, Lorne Taylor, Maryam Tabrizian, and Nicole YK Li-Jessen. "Unraveling the Relevance of Tissue-Specific Decellularized Extracellular Matrix Hydrogels for Vocal Fold Regenerative Biomaterials: A Comprehensive Proteomic and In Vitro Study." *Advanced NanoBiomed Research* 3, no. 4 (2023): 2200095.

## **Chapter 4. Unraveling the Relevance of Tissue-Specific Decellularized Extracellular Matrix Hydrogels for Vocal Fold Regenerative Biomaterials: A Comprehensive Proteomic and In Vitro Study**

### *Abstract*

Decellularized extracellular matrix (dECM) is a promising material for tissue engineering applications. Tissue-specific dECM is often seen as a favorable material that recapitulates a native-like microenvironment for cellular remodeling. However, the minute quantity of dECM derivable from small organs like the vocal fold (VF) hampers manufacturing scalability. Small intestinal submucosa (SIS), a commercial product with proven regenerative capacity, may be a viable option for VF applications. This study aims to compare dECM hydrogels derived from SIS or VF tissue with respect to protein content and functionality using mass spectrometry-based proteomics and in vitro studies.

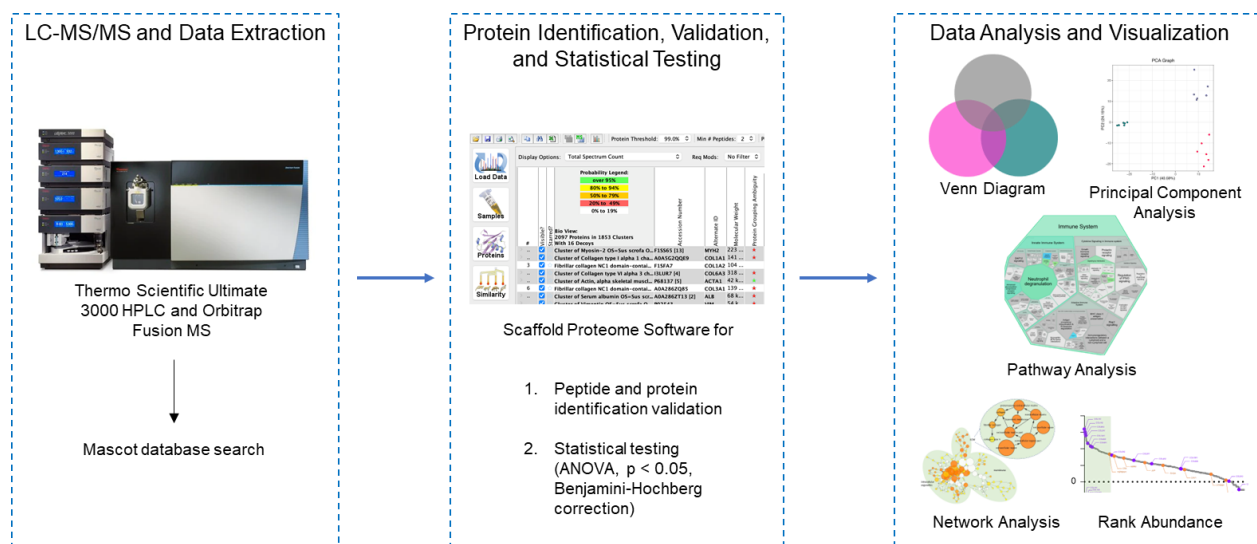
Proteomic analysis reveals that VF and SIS dECM share 75% of core matrisome proteins. Although VF dECM proteins have greater overlap with native VF, SIS dECM shows less cross-sample variability. Following decellularization, significant reductions of soluble collagen (61%), elastin (81%), and hyaluronan (44%) are noted in VF dECM. SIS dECM contains comparable elastin and hyaluronan but 67% greater soluble collagen than VF dECM. Cells deposit more neo-collagen on SIS than VF-dECM hydrogels, whereas neo-elastin (~50 µg/scaffold) and neo-hyaluronan (~ 6 µg/scaffold) are comparable between the two hydrogels.

Overall, SIS dECM possesses reasonably similar proteomic profile and regenerative capacity to VF dECM. SIS dECM is considered a promising alternative for dECM-derived biomaterials for VF regeneration.

### *Table of Contents*

Decellularized Extracellular Matrix (dECM) derived from the same source as the target tissue is thought to augment regeneration, but limited dECM is obtained from small organs like vocal folds (VF). VF dECM and a commercial alternative, Small Intestinal Submucosa (SIS) possess similar proteomic content. Additionally, hydrogels from SIS and VF dECM stimulate deposition of the ECM components comparable levels.





#### 4.1. Introduction

Decellularized extracellular matrix (dECM) has become a major naturally derived biomaterial in tissue engineering and regeneration. Depending on the application, dECM-based biomaterials are manufactured in forms of injectables, bioinks, and electrospun scaffolds.<sup>1-3</sup> With dECM materials, cells and immunogenic molecules are largely removed that minimize adverse host response. Meanwhile, structural, core-matrisome proteins [e.g., collagen, proteoglycans, glycoproteins], macromolecules [e.g., glycosaminoglycans (GAGs) etc.] and matrisome-associated proteins [e.g., ECM-affiliated proteins, ECM-Regulators] are mostly preserved in the dECM materials.<sup>4,5</sup> These preserved ECM structural and signaling molecules are essential to provide a native-like, tissue-specific microenvironment for local cell functions in tissue repair.<sup>6,7</sup>

Mammalian vocal folds (VF) have unique ECM-structural and mucosa-immunological profiles that likely benefits from a tissue-specific regenerative approach like dECM.<sup>8-10</sup> Mass spectrometry has aided in profiling the proteome of organs of interest through measuring the mass to charge ratio ( $m/z$ ) of fragmented proteins in the sample. For complex ECM profiles like VF, proteomic analyses are imperative to generate a deep understanding of the interaction between biological systems and biomaterials for bioengineering applications.<sup>11,12</sup>

In VF tissue engineering, mass spectrometry was used to identify and compare proteins in native and decellularized human VF mucosa to determine which extent dECM preserved a niche for cellular attachment and infiltration.<sup>13</sup> The 219 proteins that remained in dECM included those

involved in wound healing activities such as ECM production and organization. Although traditional histology did not identify antigenic cellular proteins in the VF dECM, mass spectrometry found residual antigenic proteins including Prxs1, 2 and 4, CuZnSOD and GPx3. These results indicated a possible source of varied immune responses to dECM biomaterials *in vivo*.

Proteomic analysis was also applied to evaluate the variability of VF dECM samples during manufacturing. Conventional decellularization protocols at the bench scale produce highly varied batches of dECM due to manual reagent changes and biological variation between animals.<sup>14</sup> Customized bioreactors have been designed to reduce variability between dECM hydrogels through automation and aid in scale-up manufacturing. Mass spectrometry was implemented to compare conventionally produced VF dECM with dECM produced using the bioreactor.<sup>14</sup> In this study, 2430 unique proteins were identified, including 84 core matrisome proteins. Bioreactor-VF dECM contained a greater overall number of protein types by 10-fold compared to the conventional dECM protocol.

While the general biomimetic benefit of dECM is well-acknowledged, manufacturing VF-specific dECM biomaterials at the commercial scale is almost impossible because only very minute amounts of matrix material can be derived from the small human VF with sizes ranging between 240 and 2400 mm<sup>3</sup>.<sup>15</sup> To address this scalability challenge, large organs such as Small Intestinal Submucosa (SIS) or Urinary Bladder Matrix (UBM) have been used for extraction of dECM in developing VF regenerative biomaterials.<sup>8,16</sup> The larger size of porcine SIS can generate a larger volume of material from a single batch for testing and gel production. Several dECM-derived scaffolds are already clinically approved including Cook Biotech's Biodesign® from Small Intestinal Submucosa (SIS) and ACELL's Matristem UBM®.<sup>17,18</sup>

To date, only limited studies provided data regarding the importance of tissue-specific dECM for VF tissue regenerative biomaterials. In one *in vitro* study, mass spectrometry was used to compare the proteomes of dECM extracted from porcine VF and UBM tissues.<sup>19</sup> Compared to that of UBM, dECM from VF tissue contained a higher concentration of the TGF- $\beta$ 1 sequestering protein, LTBP4. The presence of this molecule may help reduce TGF- $\beta$ 1-mediated fibrotic activity. When Human Vocal Fold Fibroblasts (HVFF) were cultured on VF dECM, UBM, or collagen hydrogels, fibrosis-associated genes Coll1A1 and ACTA2 were found downregulated on VF dECM hydrogels.



However, neo-ECM production by HVFF as functions of dECM tissue sources were not evaluated and therefore the overall regenerative efficacy could not be confirmed. In an animal study, MSCs encapsulated in SIS dECM hydrogels and MSCs alone were injected to scarred rabbit VF.<sup>20</sup> Compared to MSC-only controls, more neo-hyaluronan and neo-collagen was found in scarred VF at Week 8 post-injection. Improved glottal function was also identified in the SIS-MSC group, indicating the SIS provided a niche for MSCs to regenerate functional tissue. As a VF dECM group was not included in this study, whether SIS dECM possessed comparable regenerative capacity to VF dECM remained to be confirmed.

The primary goal of this study was to compare the protein components, biocompatibility and functional features between VF and SIS-dECM biomaterials using a combination of mass spectrometry-based proteomics and in vitro studies. Molecular components and pathways related to ECM, angiogenesis and immune systems were the focus of these analyses. VF dECM was hypothesized to contain target tissue-specific bioactive molecules, while SIS dECM was hypothesized to fulfill the fabrication challenge of supply and accessibility.

## 4.2. Results

### 4.2.1. Efficacy of Decellularization Protocols for Porcine Vocal Folds

We first tested seven dECM protocols of their efficacy in removing cells and their residual DNA from porcine VF. (**Figure 1A**). In selecting a protocol, we used a literature value of < 50 ng DNA/mg tissue.<sup>21</sup> While higher levels of DNA have been suggested to be acceptable, standard levels for DNA removal in dECM products have not yet been designated.<sup>1</sup> 50 ng is a widely adopted and stringent target for decellularization protocols.<sup>18,21-25</sup> We sought to achieve a comparable level of decellularization with reduced heat exposure time and consequent protein degradation by minimizing nuclease incubation time. We also sought to increase efficacy of gelation by using isopropanol to delipidize the tissue.

Protocol 3, which used 18 total hours of nuclease incubation in 6 h cycles, was sufficient to reduce the residual DNA concentration to <50 ng DNA/mg tissue (**Figure 1B**). The residual DNA in Protocol 3 was significantly less than Protocol 2 where two 6 h cycles were used, and Protocol 5 where a single 24 h cycle was used ( $43.4 \pm 5.9$  ng DNA/mg tissue v/s  $127 \pm 35$  ng DNA/mg tissue and  $118 \pm 35$  ng DNA/mg tissue respectively,  $p < 0.0001$ ). While protocols 4, 6, and 7 also reduced

DNA content below the 50-ng/mg target, Protocol 3 was selected for subsequent experiments as the dECM protocol that met the 50 ng/mg DNA target with the shortest incubation time.

The commercially produced dECM from Cook Biotech that we used for comparison to our VF dECM throughout our research is produced from porcine SIS. The DNA content of their powdered SIS dECM is not publicly accessible. However, Cook Biotech's Oasis®, which is produced using the same peracetic acid and ethanol-based methods, has been reported to contain  $0.42 \pm 0.01$  ng DNA/mg dry tissue.<sup>26</sup>

The peracetic acid and ethanol method alone, while highly effective for decellularization of SIS, does not achieve sufficient penetration for effective decellularization of VF. To decellularize VF, peracetic acid has been used in combination with sodium deoxycholate and nucleases.<sup>[27]</sup> However, peracetic acid can damage collagen structure with exposure of longer than 1-2 hours, while sodium deoxycholate also damages ECM components.<sup>4</sup> In our pilot work, a protocol involving exposure to sodium deoxycholate for 2 h, nucleases for 48 h, and peracetic acid for 1 h was required to achieve comparable levels of decellularization to our Protocol 3.<sup>28</sup> Hydrogel gelation was noted to be inconsistent, which hampered the reproducibility of experiments and potential for scaleup in manufacturing.

#### *4.2.2. Hydrogel Formation and Characterization*

To form hydrogels, 20 mg/mL VF dECM produced using Protocol 3 was solubilized in pepsin in hydrochloric acid. Once neutralized, diluted to a concentration of 16 mg/mL, and incubated at 37 °C, hydrogels formed within 30 minutes. Both SIS dECM and VF dECM hydrogels could be manipulated with a spatula without losing integrity. Time sweeps were performed to evaluate gelation kinetics and viscoelasticity. 2 mg/mL collagen I hydrogels were used as controls. All hydrogels possessed storage moduli ( $G'$ ) greater than loss moduli ( $G''$ ) throughout the experiment, and reached a plateau in under 30 minutes. This confirmed our observations of the time to gelation. The plateau, or final  $G'$  for SIS dECM ( $178 \pm 47$  Pa) and VF dECM ( $144 \pm 59$  Pa) hydrogels were comparable and not significantly greater than that of the collagen hydrogels ( $25.53 \pm 13.75$  Pa). No significant difference was identified between groups ( $p = 0.21$ ) (**Figure 1D**).

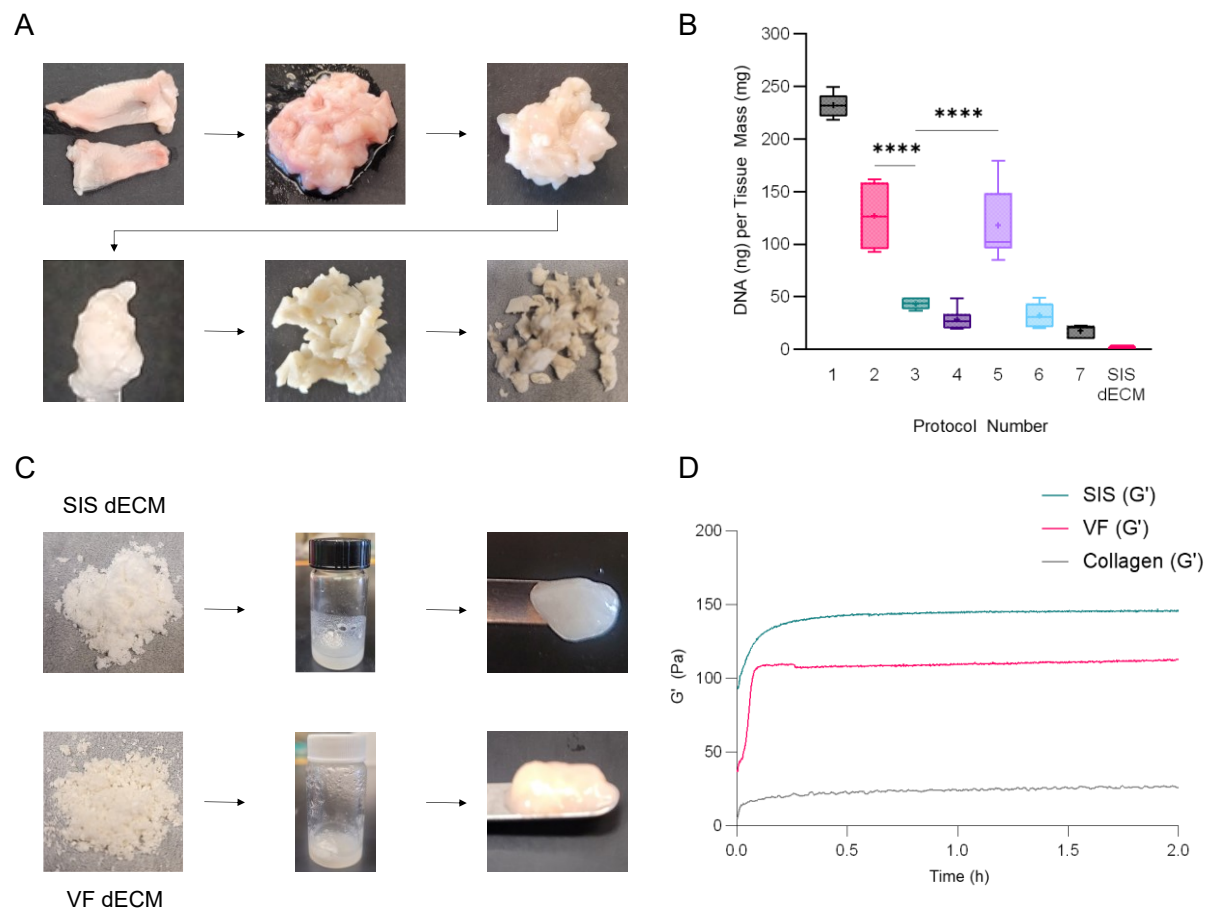


**Figure 1. A.** Decellularization Process of Porcine Vocal Folds. VF were dissected from a porcine larynx, then minced to increase surface area. Cell lysis was performed for 24 h in 3M sodium chloride at 4°C. Incubation was performed with nucleases at 37 °C for 6 hours breaks down DNA, Delipidization in Isopropanol for 24 h at 4 °C, followed by additional nuclease incubation cycles to maximize DNA removal. A 6-hour incubation cycle is repeated twice in the selected protocol. Homogenization by cryomilling produces a white powder. **B.** Nanograms Residual DNA for Each Decellularization Protocol. Incubation cycles lasted either 6 or 24 h. \*\*\*\*  $p < 0.0001$  **C.** Formation of VF and SIS dECM Hydrogels. 20 mg/ML dECM Powder is suspended in 2 mg/mL pepsin in 0.05 M HCl for 48 h while stirring at a 30 rpm for 48 h. The solution is neutralized with 1 M NaOH and 10X PBS, diluted to 16 mg/mL, and incubated at 37 °C to induce gelation. **D.** Storage Modulus of 16 mg/mL SIS dECM and VF dECM hydrogels, and 2 mg/mL Collagen I hydrogel controls over 2 h.

**Table 1.** Table of Decellularization Protocols and Residual DNA Averages for VF dECM and SIS dECM (if data available). Nucleases are not used in the decellularization of Cook Biotech’s SIS dECM, and complete details of the protocol are not available due to propriety.

Protocol Number	Total Nuclease Incubation Time (h)	Length of Each Incubation Cycle (h)	Number of Incubation Cycles	Residual DNA content (ng)
1	6	6	1	232 ± 12
2	12	6	2	127 ± 35
3	18	6	3	43.4 ± 5.9
4	24	6	4	28.4 ± 10
5	24	24	1	118 ± 35
6	48	24	2	32.3 ± 13
7	72	24	3	12.6 ± 6.2
SIS dECM	N/A	N/A	N/A	0.42 ± 0.01

#### 4.2.3. Protein Identification, Gene Ontology Enrichment, and Analysis

We then performed mass spectrometry-based proteomics on the three sample types: native VF tissue, VF dECM produced using Protocol 3, and Cook Biotech’s SIS dECM. Using Venn Diagrams, we determined the number of proteins in common and unique to each tissue type (**Figure 2A**). A total of 620 proteins were identified from the Native VF samples. Of these proteins, 63% (391/620) were shared between VF dECM and SIS dECM. A further 29% (182/620) were shared with only VF dECM, and 6% (36/620) with only SIS dECM. 2% of proteins (11/620) were unique to Native VF, 9% of proteins (36/411) to SIS dECM, and 3% of proteins (17/614) to VF dECM. A total of 24 proteins were shared by the two dECM types (6% of SIS dECM v/s 4% of VF dECM), but not identified in native VF. The decellularization process eliminates abundant proteins (i.e., albumin) that in native tissues serve to “block” the signal of less abundant proteins. This dynamic range issue results in hidden proteins in the native samples.

Principle component analysis enables a more detailed look at variability between samples, as well as sources of variability. From principal component analysis (**Figure 2B**), 40.59% and 24.15% of variability were attributed to PC1 and PC2 respectively. To gain further insights into how content of specific proteins impacts observed variability between samples, a protein loadings plot was generated. The proteins that contributed most strongly to PC1 and PC2 was based on the magnitude of loading scores (-1 to 1) from the origin. For instance, ALB and MYH2 had strong contributions and positive correlation with PC1 and PC2, respectively. While ALB had a log<sub>10</sub> abundance greater than 2 in all sample types, it was most abundant in native VF, leading to the high loading score. MYH2 had the highest log<sub>10</sub> abundance of all proteins in native VF (3.37) and VF dECM (3.22), but was much lower in SIS dECM (0.81). This difference caused its high PC2 loading score. Likewise, the loading score of BPIFB1, which also had a high log<sub>10</sub> abundance in native VF and VF dECM but was absent in SIS dECM, showed a strong negative correlation with PC1. In contrast, COL6A3 was negatively correlated with both PC1 and PC2, and had high but differing log<sub>10</sub> abundance in native VF (2.71), VF dECM (2.97), and SIS dECM (2.9). The protein loadings plot allows us to tie our variability data more directly from PCA to notable differences between sample types.

Samples of native VF and VF dECM demonstrated a high degree of similarity based on the first principal component, PC1, with the majority of variability introduced between the VF tissues and SIS. However, PC2 indicated variation between native VF and VF dECM. Based on sample distribution, the highest degree of similarity was noted in the SIS dECM samples, which originated from two bulk lots produced using standardization procedures. In contrast, high in-group sample variability was observed within Native VF and VF dECM. The greater in-group similarity identified in SIS dECM samples is beneficial for product consistency in scale-up for manufacturing. Overall, these analyses showed that while our VF dECM is more similar to Native VF, the majority of proteins are also shared with SIS dECM decellularized with peracetic acid and ethanol.

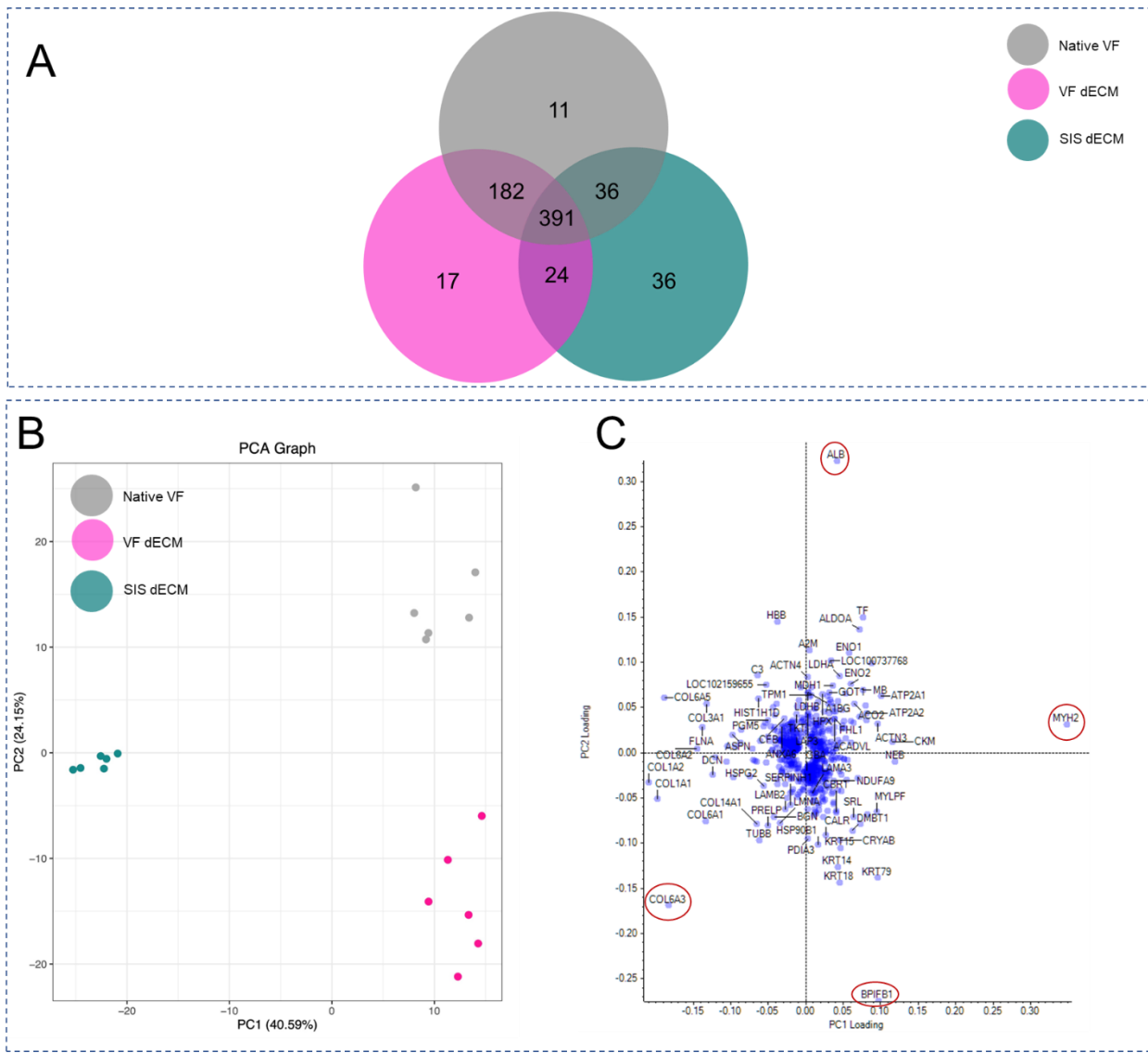


**Figure 2.** Comparison of identified proteins in Native VF, VF dECM, and SIS dECM **A.** Total identified proteins produced using Functional Enrichment Analysis Tool (FunRICH). **B.** Principal component analysis (PCA) of the proteomics data for each tissue sample (n = 6 per tissue type). The PCA graph depicts in group variation for Principal component 1 (PC1) and Principal component 2 (PC2). PC1 accounts for 40.59% of variation between the tissue samples and PC2 accounts for 24.15%. **C.** Protein loadings plot. The protein loadings plot describes the degree to which specific proteins contribute to PC1 and PC2. Circles indicate proteins with relatively high loading scores discussed in text.

#### 4.2.3.1. Comparison of Matrisome and Matrisome-Associated Proteins by Tissue Type

Core matrisome proteins represent the main structural and mechanical components of the ECM and include collagens, glycoproteins, and proteoglycans.<sup>5</sup> Matrisome-associated proteins include ECM-affiliated proteins, ECM Regulators, and secreted factors, which have roles in directing cell behavior toward wound healing. Venn Diagrams were used to identify which specific core matrisome and matrisome-associated proteins overlapped or were distinctively present in native VF, VF dECM from Protocol 3 and Cook Biotech's SIS dECM (**Figure 3A**). Respective abundance curves were also created to rank the top 100 collagens and VEGF-signaling associated proteins and provide a representation of the shifts in protein abundance between sample types (**Figure 4**). The purpose of these analyses was to provide a deeper comparison of core matrisome and matrisome-associated proteins between sample types and to evaluate their roles in regeneration.

With respect to the core matrisome proteins, a total of 13 collagen types were common in all sample types. Seven of these 13 collagens were in the top 100 protein abundance in native VF, 8 in VF dECM, and 10 in SIS dECM. Specifically, COL1A1, COL1A2, COL5A1 and COLA2 are key to the formation of neo-collagen fibers.<sup>5</sup> The COL6 family and COL14A1 are involved in fibrillogenesis, or self-assembly of the collagen network.<sup>29,30</sup> COL3A1, a collagen essential to the elasticity of healthy VF tissue that is replaced by Collagen 1 in scar tissue, was also identified in all sample types.<sup>31,32</sup> A total of 18 glycoproteins were shared across the three sample types. Several of these proteins (EMILIN1, FBLN1, FBLN5, FBN1) contribute to elastic fiber formation, an essential process repaired VF to regain elasticity.<sup>33-36</sup> Laminins, involved in basement membrane formation, integrin binding, and cell signaling were identified in all sample types (LAMA4, LAMB1, LAMB2, LAMC1), native VF only (LAMA3), or VF dECM only (LAMB3, LAMC2).<sup>5,36</sup> Seven proteoglycans were identified across all sample types. Among them, ASPN and LUM are involved in collagen binding,<sup>37,38</sup> whereas BGN, DCN, and HSPG2 are involved in angiogenesis and ECM binding.<sup>39-42</sup> HAPLN1 and VCAN were found only in native VF and VF dECM, which are involved in the regulation of cellular adhesion and hyaluronan binding.<sup>[43,44]</sup> A sample-by-sample comparison of core matrisome protein abundance using hierarchical clustering analysis is available in **Figure S1**.

Among the matrisome-associated proteins, a total of 9 ECM-affiliated proteins were noted across all sample types (**Figure 3B**). Annexins (ANXA1, ANXA2, ANXA5, ANXA6, ANXA8, ANXA11) are involved in angiogenesis, adoption of cellular morphology, and immune

modulation.<sup>45-47</sup> LMAN1, which regulates blood clot formation, was shared only by native VF and VF dECM. LGALS1, a protein related to cellular adhesion and signaling, is unique to VF dECM.<sup>48,49</sup> In addition, five proteins were unique to SIS dECM that are involved in angiogenesis (GREM1) or cellular adhesion, migration, and signaling (C1QA, GPC6, LGALS2, LGALS4).<sup>50-53</sup> Ten ECM-regulator proteins were shared by all three sample types that have roles in regulating angiogenesis and blood clots such as fibrin clot formation, heparin binding, and blood coagulation.<sup>54,55</sup> Other roles include growth factor binding (A2M, F2).<sup>56,57</sup> Of the ECM-regulators unique to native VF and SIS dECM, AGT, plays a role in angiogenesis.<sup>58</sup> Other secreted growth factors, cytokines, and chemokines are usually difficult to detect by mass spectrometry.<sup>59</sup> As expected, only one secreted factor was detected in all tissue types (S100A1), and one by native VF and VF dECM (S100A14).

Proteins involved in angiogenesis, an important process in VF repair, were identified using a rank abundance curve for proteins in the VEGF-signaling pathway. The three most abundant VEGF signaling-associated proteins in all three sample types were HSP90AA1, HSPB1, and CRK. These proteins regulate VEGF binding, endothelial cell outgrowth, and endothelial cell migration, respectively.<sup>60-62</sup> HSP90AA1 and CRK were ranked in the top 100 in SIS dECM. On the other hand, HSPB1 (76<sup>th</sup>) and HSP90AA1 (100<sup>th</sup>) were in the top 100 of VF dECM. These proteins were all ranked >100<sup>th</sup> in native VF.

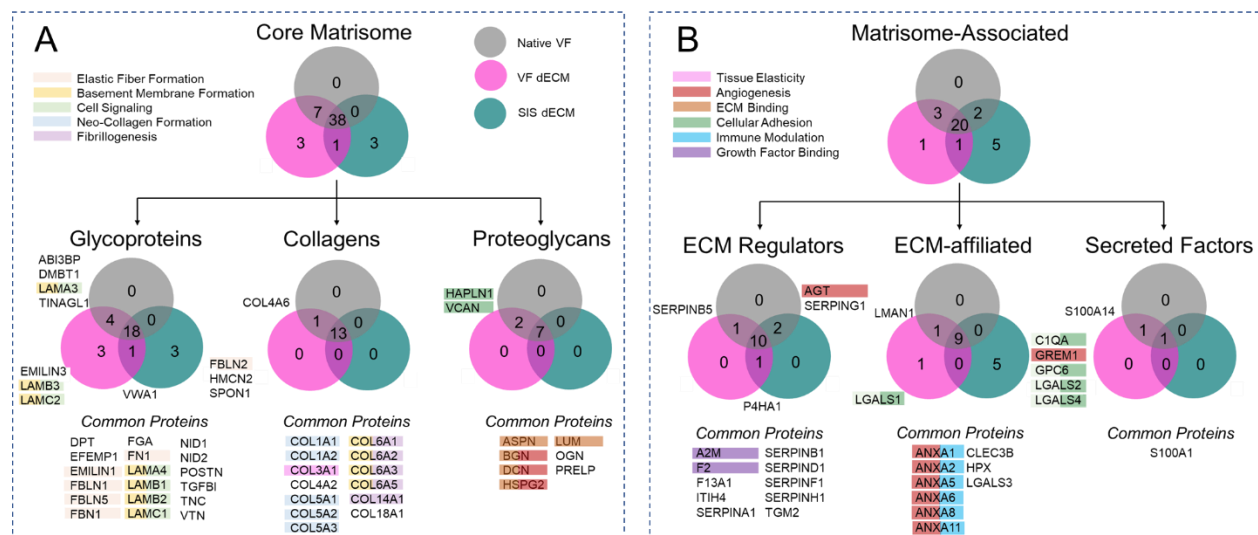




**Figure 3.** Venn diagram of identified **A.** core matrisome and **B.** matrisome-associated proteins. Selected pathways (e.g., elastic fiber formation, angiogenesis, etc.) in which these proteins play a role are highlighted.

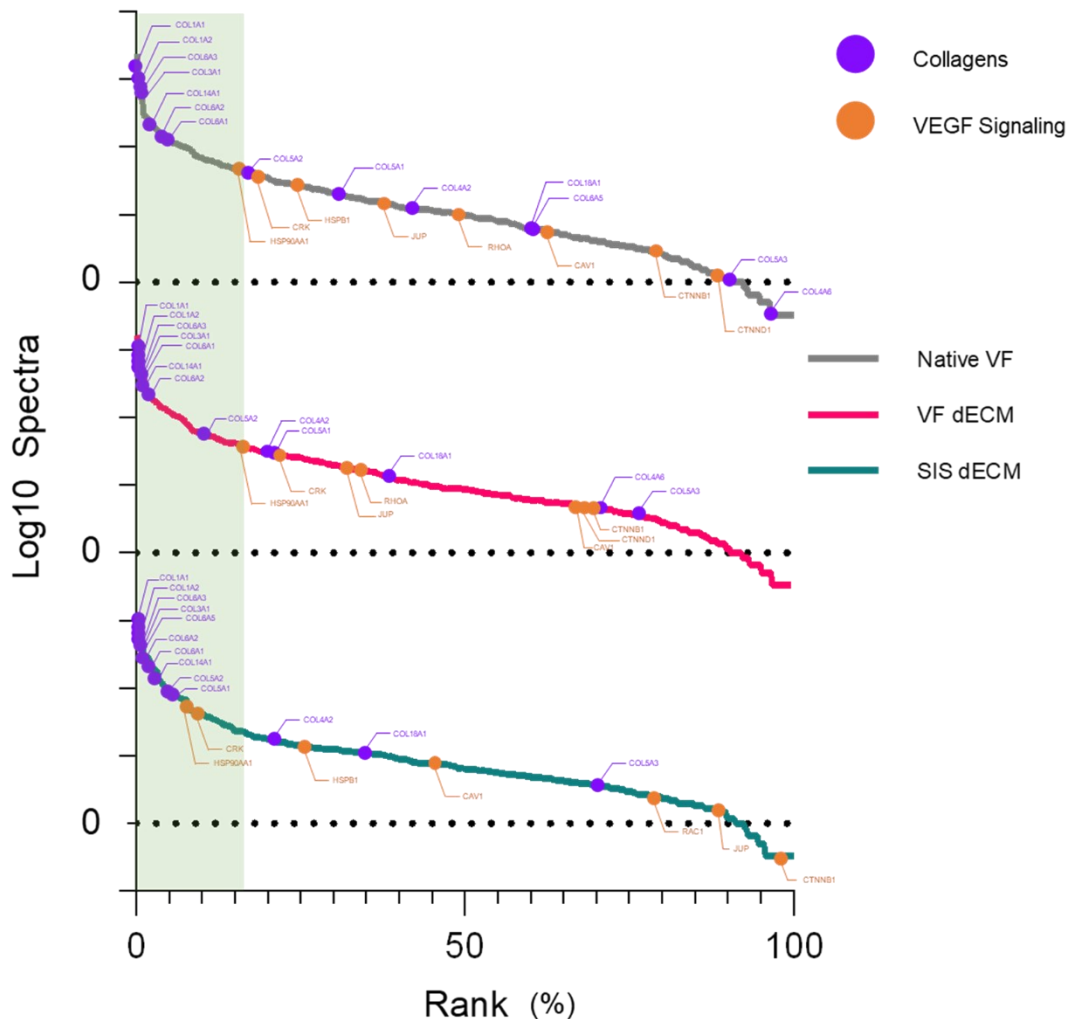


**Figure 4.** Rank abundance curve highlighting identified collagens and proteins involved in Reactome's VEGF signaling pathway. The green-shaded area represents the top 100 proteins. Only collagens and VEGF-related proteins are highlighted in this figure, not all proteins in the samples.

#### 4.2.3.2. Pathway and Network Enrichment Analyses

ECM organization and Immune pathways were highlighted in Voronoi Diagrams generated using Reactome. In ECM organization, the sub-pathway laminin interactions and sub-sub pathway anchoring of fibers in collagen formation were overrepresented for VF dECM from Protocol 3 in

comparison to native VF and Cook Biotech's SIS dECM (**Figure 4A-C**). Voronoi diagrams visually showed the comparative overrepresentation of ECM organization pathways in the dECMs compared to native VF, i.e. laminin interactions in VF dECM and fibronectin matrix formation in SIS dECM. Signaling by receptor tyrosine kinases includes pathways associated with angiogenesis including signaling by VEGF and PDGF. In our analyses, VEGFR-mediated vascular permeability, a process involved in inducing angiogenesis, was represented at comparable levels between sample types.<sup>63</sup> Signaling by PDGF was more highly represented in VF and SIS dECM compared to native VF. This pathway involves the recruitment of smooth muscle cells or pericytes and is therefore instrumental in neo-blood vessel stabilization.<sup>64</sup> MET signaling, while not as commonly associated with angiogenesis, also plays a role by stimulating VEGF release and endothelial cell motility, as well as regulating blood vessel permeability.<sup>[65]</sup> MET signaling was overrepresented in VF dECM compared to our other samples, notably with respect to the MET promotes cell motility pathway. In contrast, immune system pathways such as neutrophil degranulation and signalling by interleukins were overrepresented in native VF compared to either SIS or VF dECM source. This visualization provides an overview of information upon which we based more in-depth analysis of immune system pathways in our tissue sources.



**Figure 5.** Voronoi Diagrams of signaling by receptor tyrosine kinases, extracellular matrix organization, and immune system pathways generated using Reacfoam pathway analysis in Reactome of log10 total spectra for **A.** Native VF **B.** VF dECM and **C.** SIS dECM. Pathway enrichment is shown as a spectrum from dark blue (underrepresented) to yellow (overrepresented). Overview Voronoi Diagrams of all pathways identified in Reactome are available in **Figures S1-S3**.

In our further analyses on statistically significant proteins involved in the innate immune system, 17 abundant proteins were allocated to the neutrophil degranulation pathway, 14 of which (AHSG, PMG1, CCT2, CBR1, CCT8, PGAM1, SERPINB1, AP2A2, GPI, HBB, SERPIN1, STOM) were exclusively found in this pathway (**Table 2**). Neutrophil degranulation, a pathway involved in inflammatory disease in the VF, was also found to be overrepresented in the native VF.<sup>66</sup> Of proteins involved in neutrophil degranulation, CRISP3 was found exclusively in native VF, MME in both native VF and VF dECM, and RAC1 exclusively in SIS dECM. Among statistically significant proteins in the adaptive immune system, four proteins were allocated to the MHC II adaptive immune response, of which one, CAPZ8 was not found in VF dECM (**Table 3**). The interleukins pathway in cytokine signaling contained 13 proteins, two of which (SOD1 and CA1) were identified exclusively in native VF, while CA2 was found in native VF and SIS dECM.

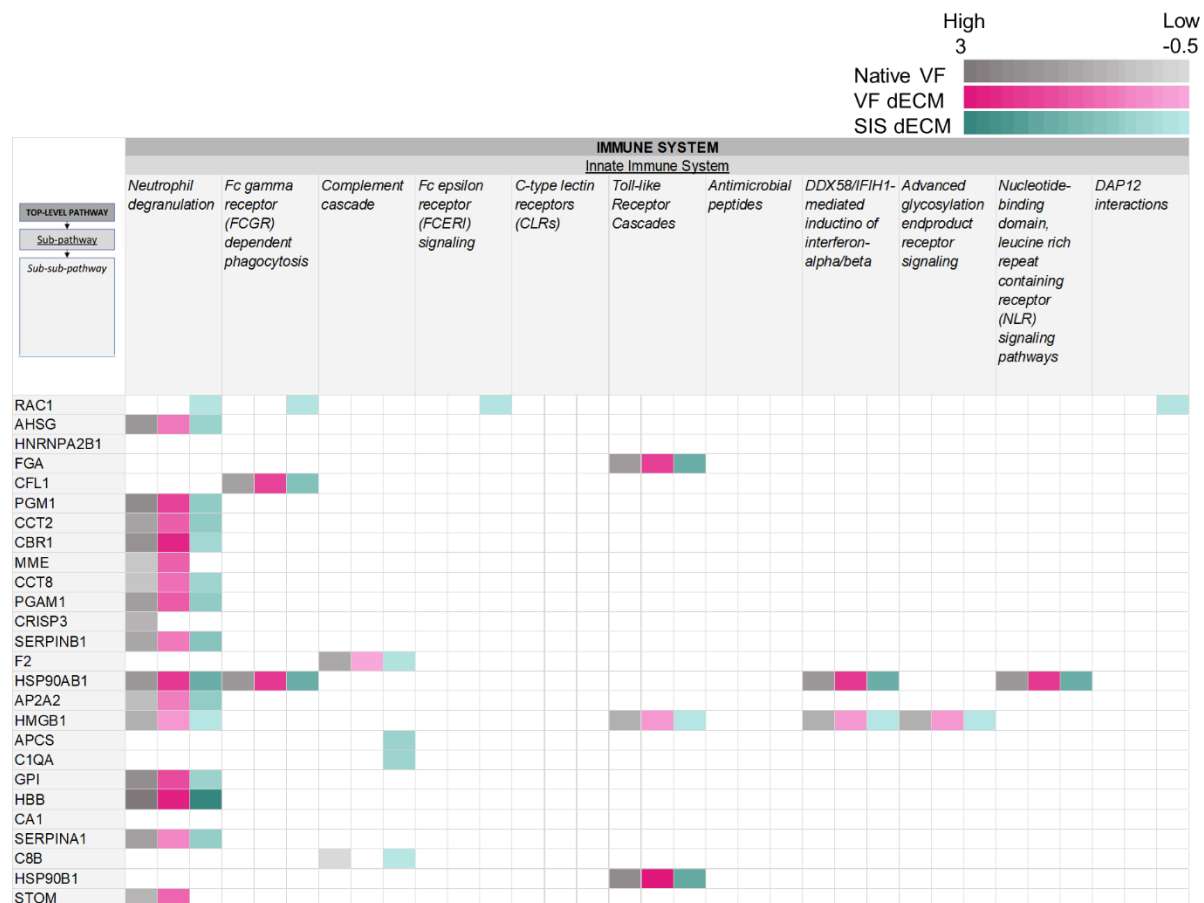


**Table 2.** Alternate IDs of proteins with statistical significance ( $p < 0.01583$ ) assigned to the “Innate Immune System” sub-pathway via Reactome. Color intensity correlates to the log10 spectra of protein abundance.

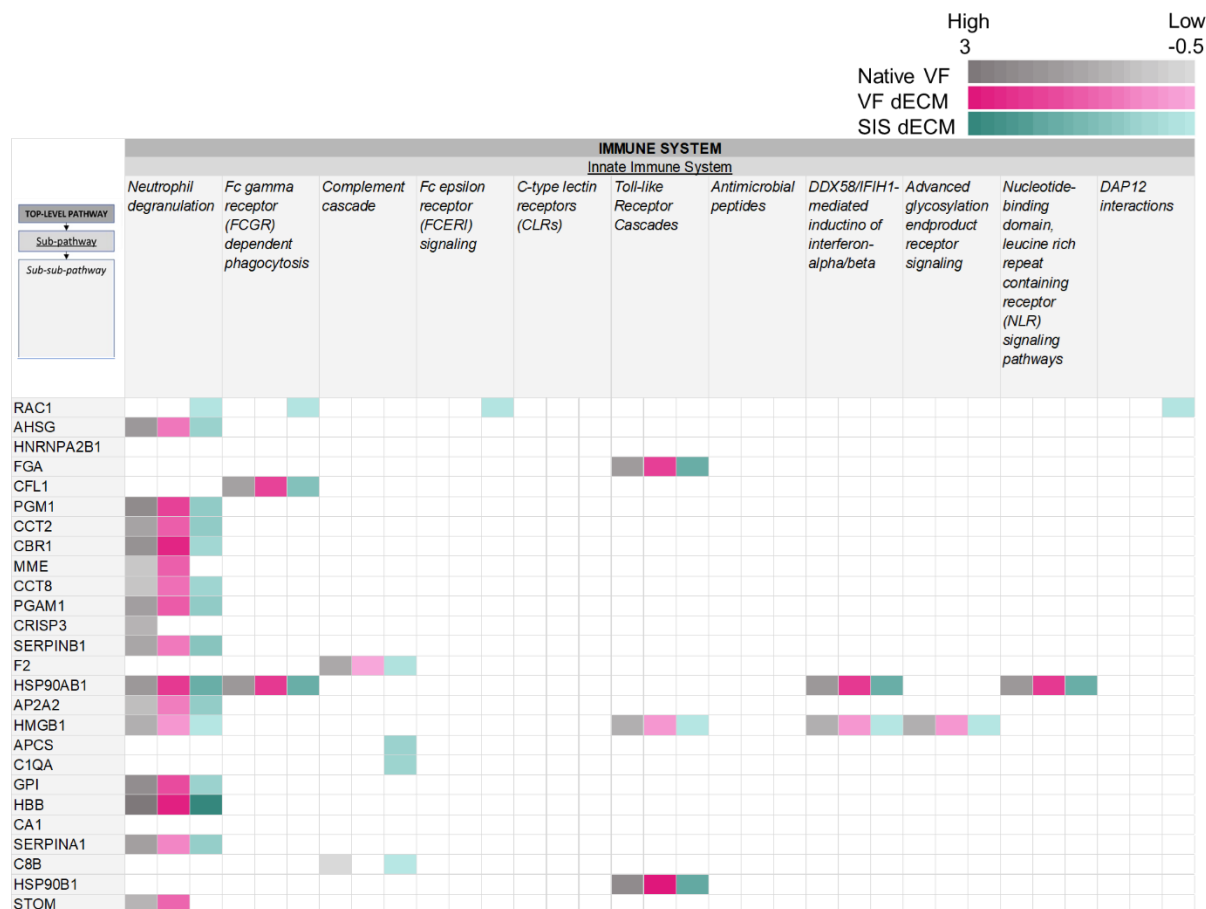


**Table 3.** Alternate IDs of proteins with statistical significance ( $p < 0.01583$ ) assigned to the “Adaptive Immune System” and “Cytokine Signaling in Immune System” sub-pathways via Reactome. Color intensity correlates to the log10 spectra of protein abundance.

Gene Ontology (GO) term enrichment analysis of overrepresented proteins in Cytoscape helps to produce results that are more consistent and reproducible. The average number of proteins involved in ECM-related (**Figure 6A**), angiogenesis-related (**Figure 6B**), and immune related (**Figure 6C**) GO terms were identified in the biological process category.

ECM-related GO terms (**Figure 6A**) showed that SIS dECM contained comparable numbers of proteins with VF dECM, but significantly greater than native VF in the “extracellular matrix organization” ( $17.2 \pm 0.75$  v/s  $17.0 \pm 0.63$  v/s  $15.7 \pm 1.0$  proteins) and “collagen fibril organization” ( $6.8 \pm 0.41$  v/s  $6.2 \pm 0.41$  v/s  $6.0 \pm 0.0$  proteins) terms. Significantly greater protein number involved in cell-matrix adhesion were identified in VF dECM ( $10.0 \pm 0.0$  proteins) compared to SIS dECM ( $5.8 \pm 2.9$  proteins), with no significant difference with native VF ( $8.5 \pm 1.4$  proteins).

Proteins involved in two processes were only identified in SIS dECM: collagen biosynthetic process ( $2.5 \pm 1.2$  proteins) and collagen metabolic process ( $3.3 \pm 1.6$  proteins). Cell adhesion was only identified in native VF and VF dECM. Comparable protein numbers were found for all sample types for integrin activation, integrin-mediated signaling pathway, and calcium-independent cell-matrix adhesion. No significant difference in protein number was identified between native VF and VF dECM ECM-related terms.

For angiogenesis-related biological process GO terms (**Figure 6B**), while comparable protein numbers were identified for “negative regulation of angiogenesis” in native VF, VF dECM, and SIS dECM (v/s  $2.3 \pm 3.6$  v/s  $2.0 \pm 3.1$  proteins), these terms were predominantly identified in SIS dECM. Proteins were only found in SIS dECM for the term “response to hypoxia” ( $6.7 \pm 3.3$ ). This biological processes was key to initiation of angiogenesis.

Regarding immune-related biological processes (**Figure 6C**), more GO terms were identified in SIS dECM, with a particularly high number of proteins in “cellular response to stimulus”. The highest number of proteins identified in all three tissue types were related to “regulation of cell migration” (native VF:  $15.5 \pm 11.9$ ; VF dECM:  $23.2 \pm 2.3$ ; SIS dECM:  $23 \pm 0.89$  proteins). SIS dECM contained a significantly higher number of proteins than VF dECM in “innate immune response” ( $14.8 \pm 0.9$  v/s  $2.8 \pm 5.3$  proteins) and “regulation of wound healing” ( $11.5 \pm 0.4$  v/s  $9.0 \pm 0.9$  proteins). Compared to native VF, VF dECM had comparable proteins in “innate immune response” ( $11.8 \pm 6.0$  proteins) but significantly less proteins for “regulation of wound healing” ( $11.2 \pm 0.4$  proteins). Interestingly, only SIS dECM contained proteins involved in “regulation of acute inflammatory response” ( $3.3 \pm 1.6$  proteins), and “humoral immune response mediated by circulating immunoglobulin” ( $4.0 \pm 0.0$  proteins), while native VF and VF dECM had significantly more GO terms in “mucosal immune response”. In general, VF dECM, contained significantly less proteins associated with immune processes such as “regulation of wound healing”, and “regulation of cell migration”, and no proteins in “acute inflammatory response”. Although the presence of these proteins may create an adverse foreign body response, the complete absence of these immune-related proteins may also deter the initiation of effective wound healing.<sup>67</sup>

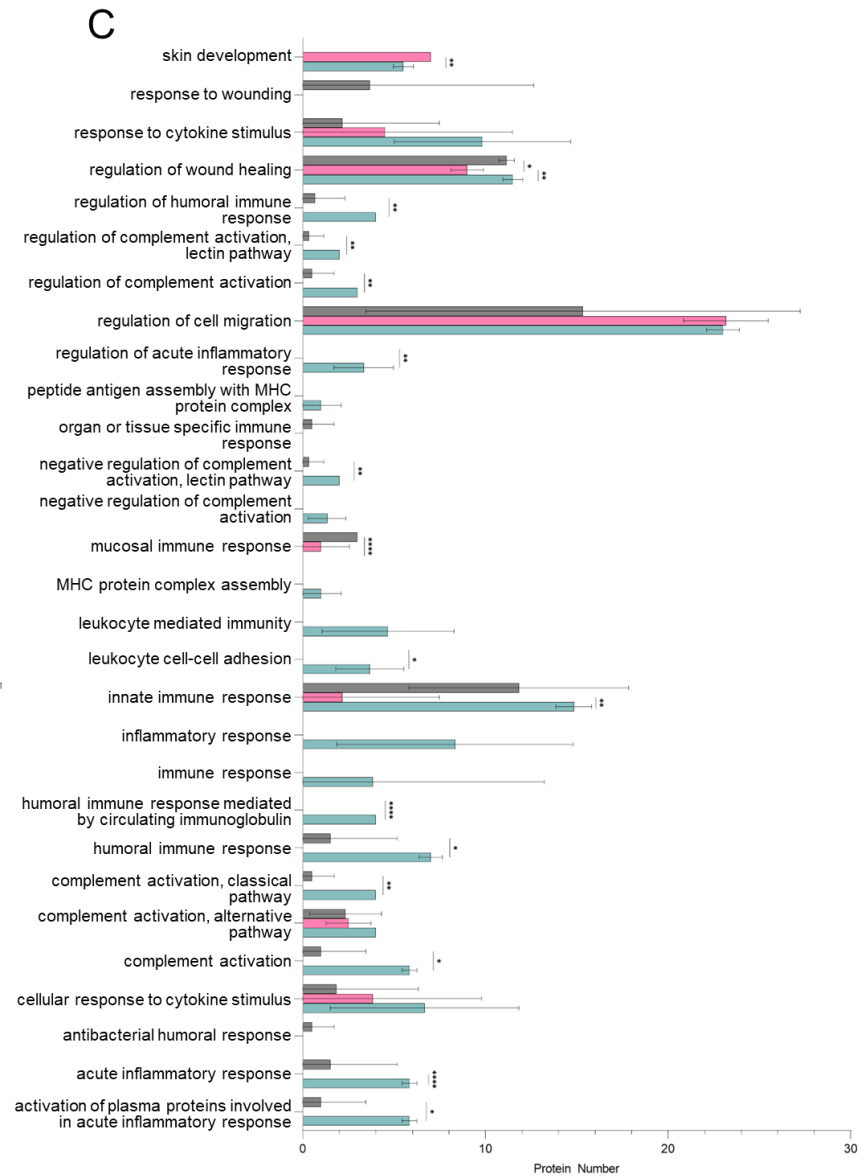
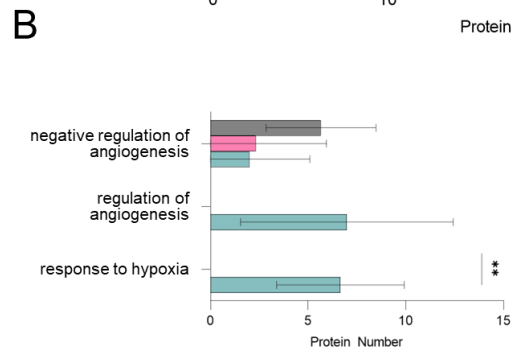
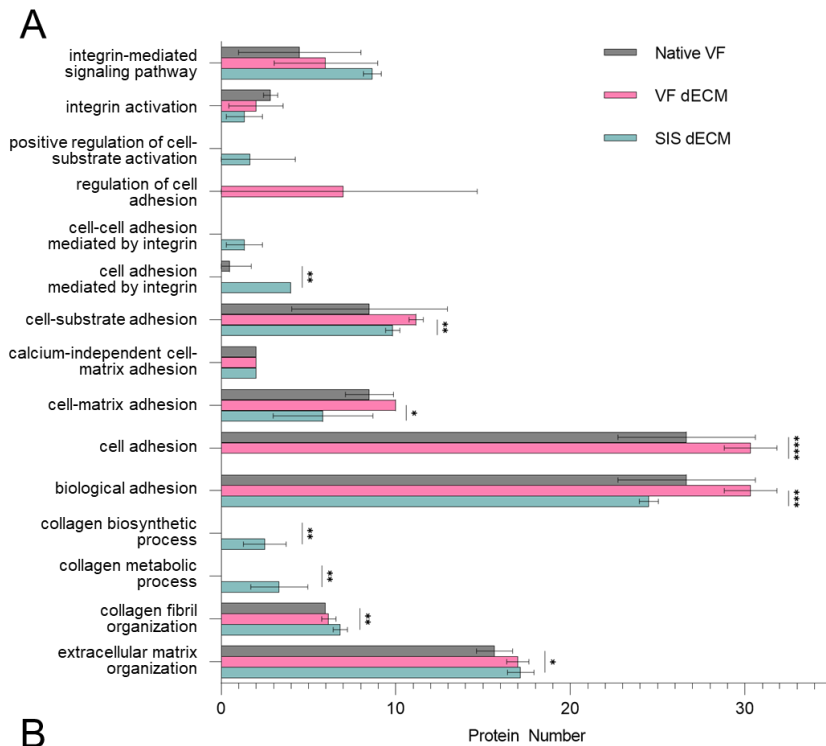




**Figure 6.** Gene ontology of biological process terms using BiNGO Cytoscape plug-in. **A.** ECM-related terms. **B.** Angiogenesis related terms **C.** Immune-related terms. The number of proteins involved in each term identified in SIS dECM, VF dECM, and Native VF samples (n = 6/ group) was determined. Statistical analysis was performed by ANOVA with post-hoc Tukey Tests. \*p< 0.05, \*\* p< 0.01, \*\*\* p < 0.001, \*\*\*\* p < 0.0001. These terms are represented in an interaction diagram in **Figure S4**.

To link Gene Ontology (GO) term enrichment to specific proteins, a table of the top 35 proteins identified in three categories of biological processes was generated for each sample type (**Table 4**). This analysis identified the comparative roles of top proteins in regeneration between tissue types. One biological process, muscle cell development, was exclusively linked to VF dECM in our analyses. Three biological processes, collagen biosynthetic process, cellular response to stimulus, and response to wounding, were identified only in the SIS dECM network. The process response to coagulation was linked to only native VF and SIS dECM, while the process extracellular structure organization was linked to only native VF and VF dECM. The remaining nine selected biological processes were common to all three tissue types.

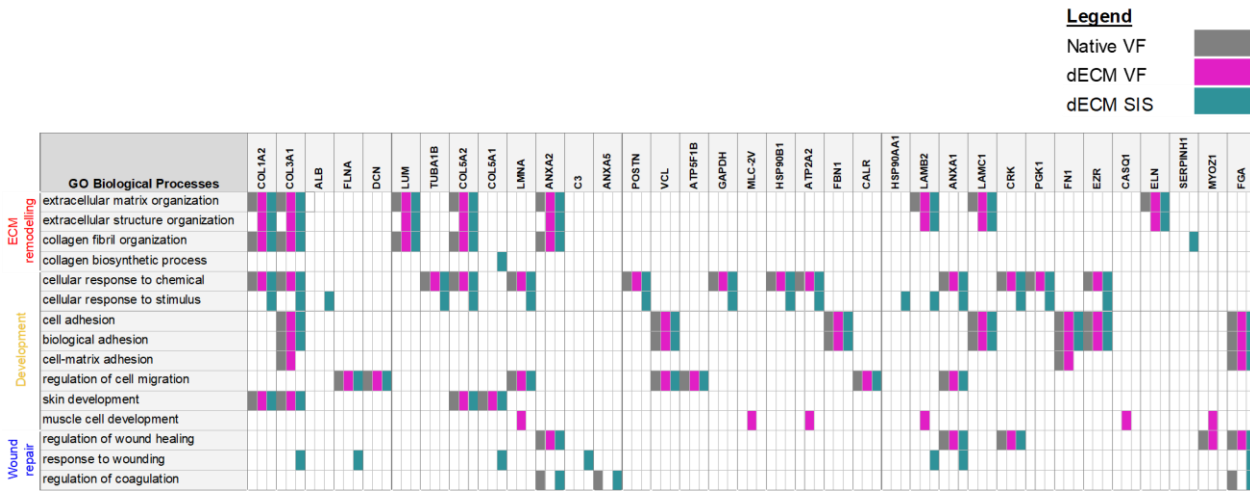


**Table 4.** Proteins associated with Biological Process Gene Ontology terms identified in Cytoscape.

#### 4.2.4. Quantitative Comparison of Key Vocal Fold ECM Components by Tissue Source

To complement the mass spectrometry data, biochemical assays were performed to quantitatively compare the major ECM components collagen, elastin, and hyaluronan in native VF to our VF dECM and Cook Biotech’s SIS dECM. Total collagen by dry mass of samples (**Figure 7A**) was greatest in the VF dECM samples ( $237 \pm 26 \mu\text{g}/\text{mg}$ ), significantly greater than native VF ( $204 \pm 40 \mu\text{g}/\text{mg}$ ) and SIS dECM ( $167 \pm 15 \mu\text{g}/\text{mg}$ ). The quantity of total collagen by mass was greater in VF dECM than native VF because native VF contained mass from intra-cellular content while VF dECM contained ECM alone. Content of soluble collagen was significantly reduced in VF dECM ( $59 \pm 3 \mu\text{g}/\text{mg}$ ) compared to native VF ( $150 \pm 19 \mu\text{g}/\text{mg}$ ), with SIS dECM ( $98 \pm 19 \mu\text{g}$ ) between the two (**Figure 7B**).

Following decellularization, elastin content was significantly reduced by 5-fold (native VF v/s VF dECM:  $13 \pm 1.7 \mu\text{g}/\text{mg}$  v/s  $2.5 \pm 0.54 \mu\text{g}/\text{mg}$ ) (**Figure 7C**). Interestingly, VF dECM and SIS dECM ( $2.4 \pm 0.54 \mu\text{g}/\text{mg}$ ) contained comparable quantities of elastin.

Hyaluronan content was also significantly reduced by almost 2-fold after decellularization (native VF:  $14 \pm 2.6 \mu\text{g}/\text{mg}$  v/s  $7.8 \pm 0.95 \mu\text{g}/\text{mg}$  in VF dECM) (**Figure 7D**). Hyaluronan content of VF dECM and SIS dECM were not significantly different. The values of ECM component content are compiled in **Table 5**.

**Table 5.** Summary of Quantitative Comparison of Key Vocal Fold ECM Components.

	Native VF	VF dECM	SIS dECM
Soluble Collagen ( $\mu\text{g}$ )	$150 \pm 19$	$59 \pm 3$	$98 \pm 19$
Total Collagen ( $\mu\text{g}$ )	$204 \pm 40$	$237 \pm 26$	$167 \pm 15$
Elastin ( $\mu\text{g}$ )	$13 \pm 1.7$	$2.5 \pm 0.40$	$2.4 \pm 0.54$
Hyaluronan ( $\mu\text{g}$ )	$14 \pm 2.6$	$7.8 \pm 0.95$	$8.9 \pm 1.4$

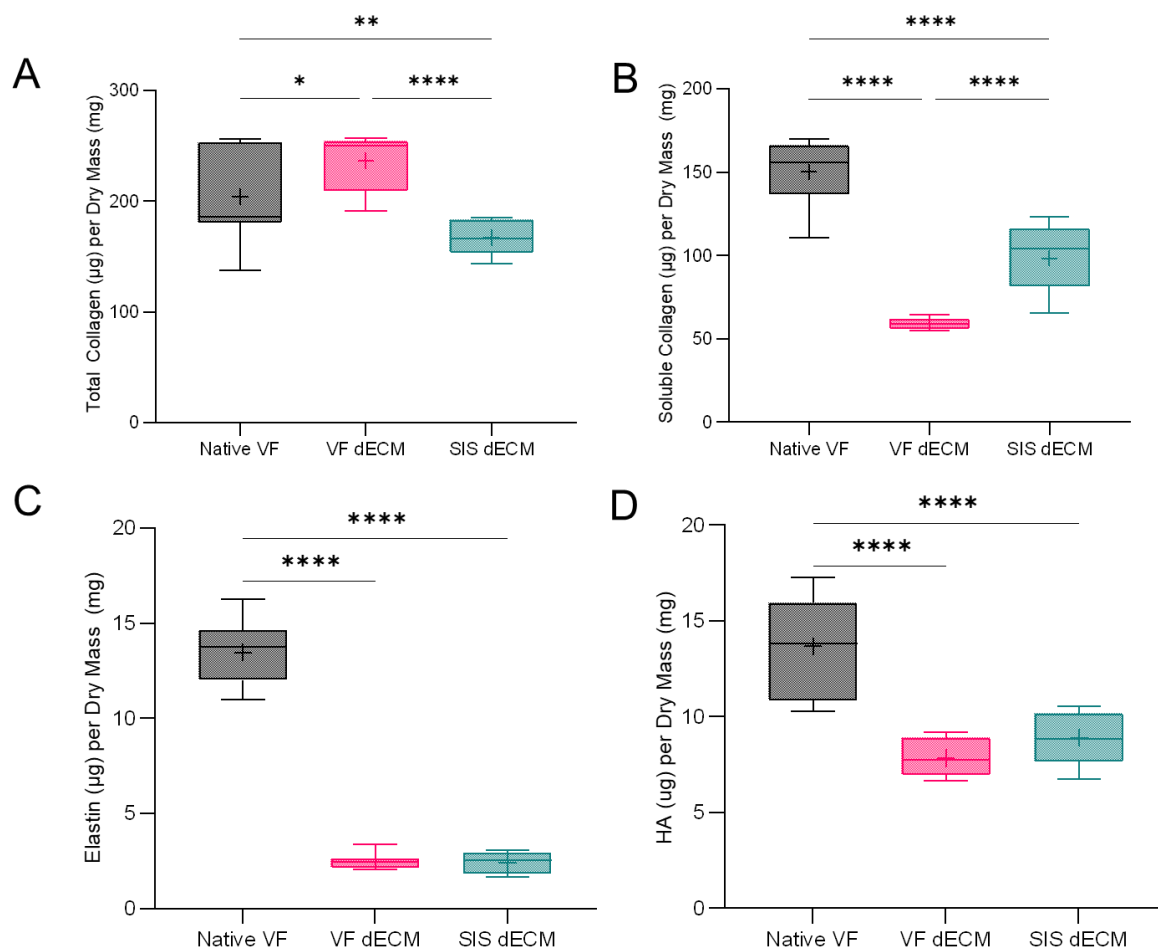


**Figure 7.** Quantitative Comparison of Key Vocal Fold ECM Components by Tissue Source **A.** Total Collagen Content (μg/mg tissue) **B.** Soluble Collagen Content (μg/mg tissue) **C.** Elastin Content (μg/mg tissue) **D.** Hyaluronan Content (μg/mg tissue). Statistical Analysis was performed by ANOVA with post-hoc Tukey Tests. \* $p < 0.05$ , \*\*  $p < 0.01$ , \*\*\*\*  $p < 0.0001$

#### 4.2.5 Viability and Cytotoxicity of Human Vocal Fold Fibroblasts

HVFF were cultured on VF and SIS dECM hydrogels as well as gelatin-coated glass and collagen I hydrogel controls to ensure the biocompatibility of our dECM hydrogels. HVFF exhibited greater than 90% viability on all substrates (**Figure 8A**). Between day 1 and 14, active proliferation of HVFF was observed as indicated by a significant increase in cellular density across substrates (**Figure 8B**). On day 1, cellular density was comparable on all substrates. On day 7, the HVFF density on gelatin-coated glass ( $175 \pm 23$  cells/mm<sup>2</sup>) was significantly greater than all other groups. By day 14, the cellular density on both collagen and glass groups were comparable ( $160 \pm 26$

cells/mm<sup>2</sup> v/s  $185 \pm 20$  cells/mm<sup>2</sup>). Unexpectedly, proliferation was significantly lower on VF dECM ( $77 \pm 4.7$  cells/mm<sup>2</sup>) or SIS dECM ( $83 \pm 5$  cells/mm<sup>2</sup>). No significant difference was identified between cellular density of HVFF cultured on VF and SIS dECM across all time points.

#### *4.2.6 Deposition of Neo-ECM by HVFF on dECM Hydrogels*

Neo-ECM assays were performed to evaluate the impact of dECM sources on HVFF functions. Soluble collagen, the form in which neo-collagens are deposited, was detected in initial cell-free “Day 0” samples at substantial quantities, but lost the majority of their soluble collagen by day 14. Soluble collagen content of cell-free SIS dECM, VF dECM and collagen hydrogels significantly decreased from  $351 \pm 22$  µg/scaffold to  $2.99 \pm 0.35$  µg/scaffold, from  $171 \pm 3.0$  µg/scaffold to  $6.63 \pm 0.11$  µg/scaffold from  $224 \pm 40$  µg/scaffold to  $9.16 \pm 0.42$  µg/scaffold, respectively.

The only significant increase in deposited collagen content identified within a sample type over time was for the collagen control between day 7 ( $168 \pm 49$  µg/scaffold) and day 14 ( $211 \pm 39$  µg/scaffold) (**Figure 8C**). A significant decrease in VF neo-collagen content was observed between day 7 ( $169 \pm 42$  µg/scaffold) and day 14 ( $125 \pm 28$  µg/scaffold). On the glass control, only small amounts of collagen were deposited after 14 days. The quantity of deposited soluble collagen after 14 days on collagen hydrogels, VF dECM hydrogels, and SIS dECM hydrogels ( $279 \pm 50$  µg/scaffold) were significantly greater than on glass. The quantity of deposited soluble collagen on SIS dECM hydrogels was significantly higher than VF dECM at all three time points, but not significantly different from collagen hydrogels on day 7 and day 14.

Negligible quantities of elastin and hyaluronan were identified in the initial “Day 0” hydrogels, due to the lower quantity of these components in the dECM, indicating that the presence of these ECM components at later time points was likely attributed to de novo production by HVFF. Neo-elastin was reliably detectable after 3 days on VF dECM, SIS dECM, and collagen samples and after 7 days on glass (**Figure 8D**). After 14 days, the quantity of neo-elastin deposited on VF dECM ( $46 \pm 6.4$  µg/scaffold) and SIS dECM ( $57 \pm 10$  µg/scaffold) was significantly greater than on collagen ( $33 \pm 7.9$  µg/scaffold). HVFF on glass produced the lowest quantity of neo-elastin ( $22 \pm 4.2$  µg/scaffold). No significant difference was identified between the two dECM types.

Neo-hyaluronan deposition was reliably detectable on VF dECM and SIS dECM samples after 3 days of HVFF culture, collagen samples after 7 days, and glass after 14 days (**Figure 8E**). Significantly greater quantities of neo-hyaluronan were produced by HVFF on VF dECM ( $5.6 \pm$

0.76  $\mu\text{g}/\text{scaffold}$ ) and SIS dECM ( $6.7 \pm 1.1 \mu\text{g}/\text{scaffold}$ ), compared to collagen ( $2.3 \pm 0.76 \mu\text{g}/\text{scaffold}$ ) and glass ( $1.5 \pm 0.59 \mu\text{g}/\text{scaffold}$ ). No significant difference in deposition of neo-hyaluronan was found between the two dECM sources, or between collagen and glass.

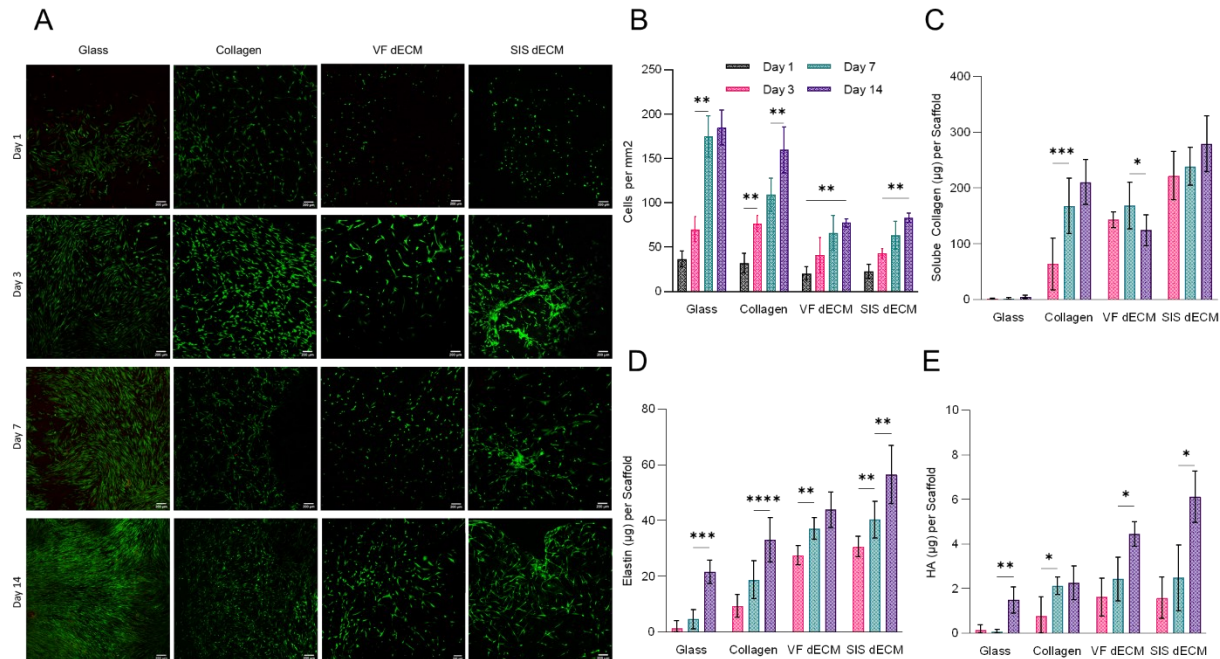


**Figure 8.** Viability and Cytotoxicity of Human Vocal Fold Fibroblasts A. Fluorescent imaging of HVFF on Glass, Collagen, SIS dECM, or VF dECM over 14 days. B. Count of HVFF (cells/mm<sup>2</sup>). C. Neo-Collagen Deposited per Scaffold D. Micrograms Neo-Elastin Deposited per Scaffold (in  $\mu\text{g}$ ). E. Neo-Hyaluronan Deposited per Scaffold (in  $\mu\text{g}$ ). Statistical Analysis was performed by Two-Way ANOVA with post-hoc Tukey Tests. \* $p < 0.05$ , \*\*  $p < 0.01$

### 4.3. Discussion

The present study aimed to investigate the differences in proteomic composition between porcine VF dECM and SIS dECM, and the impact of tissue source on the production of neo-ECM in vitro to evaluate SIS dECM as a potential scalable alternative to VF dECM. In this study, a decellularization protocol for VF tissues was optimized to reduce nuclease incubation time and produce more stable, reliably gelling VF dECM hydrogels through delipidization.<sup>14,68</sup>

#### 4.3.1 Proteomic Insights into Tissue Specificity

Comparing the homogenized VF dECM and commercially produced SIS dECM powders with the composition of native VF, we found that VF dECM preserved many of the same processes based

on GO term enrichment as native VF. The majority of these ECM-related processes were also present in SIS dECM. When abundance levels were taken into account, VF dECM was more similar to native VF than SIS dECM as expected, but SIS samples exhibited lower variability between samples.

Variability observed between VF dECM, and native VF could be partially accounted for by the removal of cellular proteins during decellularization. Conversely, the most probable reason that proteins were identified in VF dECM, but not native VF is that proteins present at low levels became detectable when more abundant cellular proteins were removed through decellularization.<sup>69</sup> Differences in decellularization protocols could also cause differences in protein abundances between the two dECMs. While VF dECM is tissue-specific, the increased scalability and decreased variability of SIS dECM could provide practical advantages for application. In future work, additional proteomic analyses following cell culture would provide a comprehensive picture of variation in regenerative response due to tissue source, as Leng *et al* demonstrated in evaluating the response of epidermal cells to decellularized skin scaffolds.<sup>5</sup>

Core matrisome proteins were largely preserved following our decellularization protocol. This includes collagens necessary to the durability of VF, glycoproteins involved in elastic fiber deposition and angiogenesis, and proteoglycans involved in angiogenesis and ECM binding. ECM regulators and soluble factors are largely lost during decellularization due to their solubility, but proteins involved in stimulating their secretion remain.<sup>5</sup> These proteins are often expressed at low levels under healthy conditions, and secreted in response to injury.<sup>5</sup>

However, pathway and GO term analyses indicated that decellularization caused an overall depletion of immune-related proteins in VF dECM prepared using Protocol 3 compared to native tissue. The overrepresentation of immune system pathways in native VF compared to VF and SIS dECMs likely represents the removal of inflammatory proteins from decellularization. That being said, certain proteins involved in inflammatory processes such as neutrophil degranulation were preserved in both dECMs. Neutrophil degranulation is an immune pathway that helps prevent infection, but overexpression is associated with inflammatory disease in the VF, such as laryngeal papilloma.<sup>8,56</sup> Decreased expression of neutrophil degranulation and other inflammatory immune pathways in dECM biomaterials may contribute to improved regenerative responses. The lower

abundance levels of proteins involved in the immune response in dECM compared to native VF could help prevent deleterious levels of inflammation.

Decellularization protocols do not necessarily remove all antigenic proteins.<sup>13</sup> In a previous proteomic study on Bovine VF, Welham et al. listed proteins identified in their samples that are associated with processes that may cause deleterious responses to the xenogeneic dECM.<sup>13</sup> These processes were identified from the biological process category of GO term enrichment and included: leukocyte-mediated immunity, oxidative stress response, cell killing, and biotic stimuli response.

In our GO term enrichment analyses, these processes were not identified as overexpressed. However, we did identify some of the proteins overlapped with those reported by Welham et al. in our samples (**Table 5**). The observed difference could be due to a combination of tissue source (porcine VF and SIS vs bovine VF), decellularization protocol, and differing extraction and analysis techniques during mass spectroscopy.

While some researchers have suggested that all immunogenic proteins should be selectively removed from dECM biomaterials, this approach may prove a double-edged sword and undermine the immunomodulatory potential of dECM.<sup>13</sup> For instance, we have identified proteins on this list such as annexins (ANXA1, 2, 5, and 11) as involved in immune mediation and angiogenesis. Additionally proteins that can cause severe, deleterious immune responses, such as those containing xenogeneic  $\alpha$ -Gal epitopes, may be reduced to tolerable levels with existing decellularization techniques.<sup>71,72</sup>

**Table 5.** Comparison of Antigenic Proteins Reported from Previous VF dECM Literature<sup>13</sup> in Native VF, VF dECM, and SIS dECM Samples. ✕ indicates the presence of the protein. Nil indicates the protein was not identified in samples.

Antigenic Proteins	Native VF	VF dECM	SIS dECM
HMGB1	✕	✕	✕
LMNB2	✕	✕	✕
PRDX1	✕	✕	✕



<b>PRDX2</b>	×	×	×
<b>PRDX4</b>	×	×	×
<b>SOD1</b>	×	Nil	Nil
<b>GPX3</b>	×	×	×
<b>LYSC</b>	Nil	Nil	Nil
<b>DEF1</b>	Nil	Nil	Nil
<b>LPO</b>	Nil	Nil	Nil
<b>ALB</b>	×	×	×
<b>C4BPA</b>	Nil	Nil	Nil
<b>HP</b>	×	×	×
<b>ANXA1</b>	×	×	×
<b>ANXA2</b>	×	×	×
<b>ANXA5</b>	×	×	×
<b>ANXA11</b>	×	×	×
<b>ENO1</b>	×	×	×
<b>LMNA</b>	×	×	×

Several dECM sources have been reported to induce pro-regenerative immune responses, including SIS decellularized using a peracetic acid-ethanol method.<sup>73-76</sup> The presence of the MHC II pathway may indicate that VF dECM is also capable of inducing a pro-regenerative response, though further validation is required. Proteomic analysis of macrophage response to VF dECM could be used to explore this possibility.<sup>73</sup> Macrophages in the VF may polarize to inflammatory phenotypes that contribute to scar formation or anti-inflammatory phenotypes that contribute to tissue reconstruction. The induction of macrophage polarization towards the M2 phenotype would

provide key evidence toward the applicability of VF dECM hydrogels toward VF repair.<sup>8,77</sup> Rather than solely relying on proteomic analyses and the presence of remnant immunogenic proteins, these results should be used in combination with *in vivo* studies to predict the immune response.

With respect to angiogenesis, our abundance curve analysis identified HSP90AA1, HSPB1, and CRK as the most abundant proteins in the VEGF signaling pathways across all three sample types. Interestingly, our GO term analysis showed that SIS dECM contained the greatest number of proteins involved in response to hypoxia. VEGF signaling is involved in the sprouting of new blood vessels, and is an essential step in VF defect regeneration that has not been extensively explored for VF biomaterials.<sup>78</sup> Our evidence suggests that dECM biomaterials possess intrinsic capacity to modulate VF endothelial cells for capillary regeneration, but functional assays are required for confirmation.

Taken together, the stimulation of regenerative processes including ECM production, immune modulation, and angiogenesis can lead to effective tissue regeneration in the VF. The similar proteomic profiles of SIS and VF dECM with respect to the aforesaid processes, indicate a potential for comparable VF-specific regenerative outcomes, which were partially verified with our subsequent functional analyses.

#### *4.3.2. Validation of Proteomic Analyses through ECM Component Quantification*

The use of quantitative and functional analyses is often needed to confirm the results of proteomic analysis in various aspects. For instance, proteomic analysis cannot quantify the ratio between total collagen versus the uncrosslinked, soluble collagens that contribute to hydrogel formation. The availability of soluble collagen is expected to affect the consistency of hydrogel formation and the production of healthy tissue when applied *in vivo*.<sup>29,79</sup> Greater amounts of soluble, uncrosslinked collagen is associated with production of organized collagen and decreased scar formation, as in fetal skin, compared to lower amounts of soluble collagen.<sup>79</sup> Our Sircol-based biochemical assay identified a reduction in soluble collagen content from native VF to VF dECM. The most likely cause was crosslinking during the isopropanol step.<sup>4,80</sup> However, delipidization has been shown to generate more stable dECM hydrogels in a pancreas dECM hydrogel study, an important factor for scale-up to manufacture.<sup>80</sup>

Based on biochemical analyses, elastin and hyaluronan levels were reduced following decellularization. However, the quantitative levels were comparable between VF dECM and SIS.

The reduction from VF decellularization is expected from literature, as elastin may be lost during exposure to salts.<sup>81,82</sup> As anticipated, hyaluronan quantities were significantly reduced in VF dECM samples. The primary reason is that hyaluronan, as a GAG bound to cell membranes, is often lost with cell removal, and GAG loss has been shown to increase with higher DNase concentrations.<sup>83,84</sup>

Despite the reduction in elastin and hyaluronan quantities, core matrisome proteins involved in the elastin formation and hyaluronan binding processes were identified by our proteomic analyses. We therefore predicted that these proteins in the dECM scaffolds would stimulate production of elastin and hyaluronan by local cells, even after they were lost during decellularization.

#### *4.3.3. In vitro Validation of Neo-ECM Production by dECM Hydrogels*

The production of neo-ECM is an essential component in the repair of defects in soft tissues such as VF.<sup>85</sup> Our proteomic analyses indicated overrepresentation of proteins and pathways involved in the production of neo-ECM components including collagen, elastin, and hyaluronan. In vitro neo-ECM deposition assays were used to determine whether these identified core matrisome proteins were bioactive.

While significant increases of elastin and hyaluronan were identified on scaffolds after 14 days, results of the neo-collagen assay were inconclusive. The hydrolysis-based control used in this study does not account for collagen degradation by MMPs and may not be sufficient to account for all collagen that is degraded over the culture period, skewing the amount of collagen deposited.<sup>5,86-89</sup> The significant increase in quantity of elastin and hyaluronan partially validated the hypothesis that SIS and VF dECM stimulated de novo ECM production by HVFF.

However, further analyses such as histology and quantitative polymerase chain reaction (QPCR) are needed to support the regenerative potential of dECM hydrogels for VF tissue engineering. Virtual histology with the use of advanced imaging techniques such as nonlinear laser-scanning microscopy can visualize remodeled tissue and determine whether ECM organization is characteristic of healthy or scarred tissue.<sup>10,90-91</sup> QPCR can be used to determine whether HVFF adopt an inflammatory or anti-inflammatory phenotype when cultured on SIS and VF dECM hydrogels by expression of markers such as ACTA2.<sup>19</sup>

#### 4.3.4. Future Directions

In our proteomic and biochemical analyses, some key ECM proteins were found to be significantly reduced in decellularized tissues compared to native VF. A strategic replenishment of depleted ECM components in dECM biomaterials may help boost its regenerative capacity for VF tissue engineering.

Native elastin is difficult to isolate and purify, limiting its utility in tissue engineering. In recent years elastin-like peptides (ELPs) have been synthesized from recombinant elastin genes *in vitro* with properties that may replicate the mechanical and biological functions of native elastin.<sup>[92,93]</sup> For instance, ELP coatings on an electrospun TecoFlex™ scaffolds upregulated production of neo-elastin and collagen III by HVFF after 7 days.<sup>[92]</sup> If necessary, ELPs could be incorporated into the hydrogel formulation, through the incorporation of crosslinkable residues in the recombinant protein, though these methods remain challenging.<sup>93</sup>

Replenishment of hyaluronan and other GAGs has also been suggested to improve the efficacy of dECM scaffolds.<sup>94,95</sup> Hyaluronan is commonly used as a scaffold on its own and crosslinked with other materials. In its uncrosslinked form, hyaluronan degrades rapidly *in vivo*. Thiol-modified hyaluronan has been crosslinked with porcine UBM scaffolds, and induced increased contractility of smooth muscle cells and matrix remodeling over 28 days compared to UBM scaffolds without replenished hyaluronan.<sup>96</sup> A hydrogel produced from methacrylated lung dECM and hyaluronan was found to increase cell proliferation and possess rheological mechanical properties comparable to native lung tissue.<sup>97</sup> Hyaluronan-based biomaterials are already widely developed for VF biomaterials with encouraging outcomes.<sup>98</sup> Therefore, the integration of hyaluronan to dECM scaffolds should be highly feasible.

Additionally, collagen loss to media from the control VF and SIS dECM hydrogels during the neo-ECM deposition experiments reflects a shortcoming common to existing VF injectables: rapid degradation. Degradation of VF biomaterials without compete tissue regeneration leads to a need for repeated reinjection.<sup>99</sup> Crosslinking the dECM with itself or another naturally derived biomaterial could aid in biomaterial stability, resulting in a biomaterial that degrades as native tissue regenerates.<sup>100</sup>

Beyond the ability to stimulate deposition of three key ECM components, further *in vitro* and *in vivo* assays would help to verify the bioactivity of the VF and SIS dECM hydrogels, and determine

their applicability toward VF regeneration. The ability of VF and SIS dECM hydrogels to stimulate angiogenesis could be investigated through 3D tube formation assays and immunostaining for lumen development markers such as PECAM-1 and Actin. The immune response could be investigated through in vitro macrophage polarization experiments, and in animal models to evaluate the foreign body response. In both cases, QPCR and RNA-seq could be used to gain a more comprehensive outlook into the gene transcripts for a broad panel of angiogenic and pro-/anti-inflammatory markers.

#### *4.4. Conclusions*

Mass-spectrometry based proteomics have contributed to identifying the base proteomic composition of the dECM, as well as, examining the impact of composition on ECM regeneration. We demonstrated that VF dECM possesses greater similarity to native VF than SIS dECM, pointing toward tissue specific effects. However, SIS dECM stimulated the production of key VF neo-ECM components, elastin and hyaluronan, at comparable levels to VF dECM with less variation between samples. These results indicated that SIS dECM may prove a viable, more scalable alternative to tissue-specific VF dECM. As development of dECM hydrogels progresses toward applications in VF repair, we recommend further proteomic analyses with respect to functional response to the VF and SIS dECM hydrogels. This study demonstrated a direct link between proteomic content of dECM and the production of neo-ECM in the VF that will guide and help to optimize selection of dECM tissue source and evaluation methodology.

#### *4.5. Experimental Section*

##### *4.5.1. Materials*

Porcine larynges were sourced from a local farm and abattoir (Ferme Co-op Point du Jour, Bury, QC, Canada). Powder ECM from small intestinal submucosa was generously donated from Cook Biotech (West Lafayette, IN, USA). Ribonuclease A (RNase) was from Roche Diagnostics GmbH (Mannheim, Germany). Pepsin from porcine gastric mucosa (2500 U/mg protein), Deoxyribonuclease I (DNase) from Bovine Pancreas (400 KU/mg protein), Gelatin from bovine skin type B, Papain from papaya latex (10 U/mg protein), Fetal Bovine Serum, and Penicillin-Streptomycin (10,000 U/mL) were purchased from Sigma-Aldrich (St. Louis, MO, USA). 3 mg/mL Collagen I from Rat Tail, Gibco® Cell Dissociation Buffer, and Phosphate Buffered Saline was bought from Gibco (Grand Island, NY, USA). Sodium Chloride and Thermo Scientific™

Nunc™ Lab-Tek™ II Chamber Slide™ System Slides were from Fisher Scientific (Saint-Laurent, QC, Canada). Phenylmethylsulfonyl fluoride (PMSF) and the Quant-IT™ PicoGreen DNA assay kit (P7589) were from Thermo Fisher Scientific (Waltham, MA, USA). The Fastin™ Elastin Assay (F2000), Sircol™ Soluble Collagen Assay (S5000), Hyaluronan Purple-Jelley Assay (H1000), Denatured Collagen Standard 1mg/ml (S2010), and Fragmentation Reagent (SFRAG) were from Biocolor Life Science Assays (Carrickfergus, UK). Dulbecco's modified Eagle medium was purchased from Life Technologies, Inc. (Burlington, ON). The Live/Dead Viability/Cytotoxicity Kit (L3224) was purchased from Invitrogen (Eugene, OR, USA).

Powder ECM from SIS was generously donated from Cook Biotech (West Lafayette, IN, USA). SIS dECM was produced according to Cook Biotech's standard manufacturing protocols.<sup>102</sup> The submucosa of the porcine small intestine was first mechanically separated from the other intestinal layers. Samples were washed in water and stored at -80 °C until additional processing. Defrosted SIS was then disinfected and decellularized in peracetic acid and ethanol. Rinses with high-purity water were used to remove the solution. The SIS dECM was then lyophilized into sheets and comminuted into powder. Terminal sterilization was performed with ethylene oxide gas under standard temperatures, pressures, and durations.

#### *4.5.2. Decellularization of Porcine Vocal Folds*

Porcine larynges were stored at -80 °C in PBS until use. A decellularization protocol was adapted from a previously developed protocol.<sup>68</sup> Larynges were thawed in PBS overnight prior to dissection. VF were removed, washed to remove blood, and minced with a scalpel to increase surface area for decellularization. Minced VF were first agitated in 3 M sodium chloride on a shaker plate at 4 °C for 24 h to lyse cells.

The existing protocol used 24-hour enzymatic incubation steps. However, nucleases lose activity over time, and longer incubation times can damage the protein content of the ECM.<sup>101,103</sup> Frequent enzyme changes, dubbed “cycles”, were predicted to decrease the total incubation time. Seven nuclease incubation protocols with varying incubation time, length of incubation cycle and number of incubation cycles were thus tested in this study. Nuclease Incubation was performed at 37 °C in 25 µg/mL DNase and 10 µg/mL RNase for 6 or 24 h under constant agitation to break down DNA in the tissue samples.

Delipidization was performed after the first incubation cycle by agitating minced VF in isopropanol for 24 h at 4 °C. The inclusion of a delipidization has been reported to enhance gelation kinetics and integrity.<sup>[80]</sup> For Protocols 2, 3, 4, 6 and 7, additional nuclease incubation cycles followed delipidization. 1% Penicillin-Streptomycin and 1 U/mL PMSF were used in all steps to prevent bacterial growth and protease activity.

Between all steps, the minced tissue was washed under running water in a Falcon® 100 µm cell strainer with evenly spaced nylon pores to remove reagents. The lyophilized tissue was homogenized into powder using a SPEX SamplePrep 6775 Freezer Mill.

#### *4.5.3. DNA Quantification*

DNA quantification was performed according to established methods to identify a decellularization protocol that effectively reduced the DNA content of VF in the minimum total nuclease incubation time.<sup>4,27,104</sup> Selection of a final protocol was based on reduction of DNA content to less than 50 ng per milligram of tissue.<sup>4</sup> Decellularized VF powder from each decellularization protocol was digested in 250 µg/mL papain in 1X TE buffer (10 mM Tris-HCL, 1 mM EDTA, pH 7.5) at 60 °C for 16 h.<sup>27</sup> Each dECM sample was produced from a mixture of VF (N=4), with three biological replicates and two technical replicates. After digestion 100 µL of PicoGreen® Reagent was added to 100 µL of the digests and fluorescence measured at 520 nm in a SpectraMax i3x Multimode Plate Reader from Molecular Devices (San Jose, CA, USA).

#### *4.5.4. Hydrogel Formation and Characterization*

To prepare dECM pre-gels, 20 mg/mL SIS dECM or VF dECM powder was slowly stirred in a sterile filtered solution of 1 mg/mL pepsin and 0.05 M HCl. After 48 hours, the solution pH and salt concentration were neutralized with sterile filtered 1 M NaOH and 10X PBS respectively and diluted to 8 mg/mL with ddH<sub>2</sub>O. Collagen I pre-gels were similarly prepared by pH and salt neutralization of the 3 mg/mL solution with 1 M NaOH and 10X PBS and diluted to 2 mg/mL with ddH<sub>2</sub>O. After neutralization, the solutions were incubated at 37 °C for 30 min to form hydrogels. The gelation kinetics and viscoelastic properties of the hydrogels were analyzed using 2 h time sweeps on a TA Instruments Discovery HR-2 Rheometer.

#### *4.5.5. Mass Spectrometry*

Proteomics analysis was performed by the Clinical Proteomics Platform, Research Institute of the McGill University Health Centre, Montréal, Canada. Samples of native porcine VF, VF dECM, and SIS dECM powder (N = 6 for each group) were submitted for analysis. The native VF were

homogenized using the same process described in **Section 5.2**, without undergoing decellularization and used as a control for the dECM.

At the Clinical Proteomics Platform, tissue lysates for each sample were loaded onto a single stacking gel band to remove lipids, detergents and salts. The single gel band containing all proteins was reduced with DTT, alkylated with iodoacetic acid and digested with trypsin. 2 ug of extracted peptides were re-solubilized in 0.1% aqueous formic acid and loaded onto a Thermo Acclaim Pepmap (Thermo, 75uM ID X 2cm C18 3uM beads) precolumn and then onto an Acclaim Pepmap Easyspray (Thermo, 75uM X 15cm with 2uM C18 beads) analytical column separation using a Dionex Ultimate 3000 uHPLC at 250 nL/min with a gradient of 2-35% organic (0.1% formic acid in acetonitrile) over 3 hours. Peptides were analyzed using a Thermo Orbitrap Fusion mass spectrometer operating at 120,000 resolution (FWHM in MS1) with HCD sequencing (15,000 resolution) at top speed for all peptides with a charge of 2+ or greater.

#### *4.5.6. Bioinformatic Data Processing of Mass Spectrometry Data*

Mascot database search, data validation and statistical testing in Scaffold Proteome Software, and data analysis were performed following data acquisition (**Figure 9**). The raw data were converted into \*.mgf format (Mascot generic format) by Proteome Discoverer 2.1 for searching using the Mascot 2.6.2 search engine (Matrix Science, London, UK; version 2.6.2) against porcine protein sequences (Uniprot 2020; 49571 entries). Assuming the digestion enzyme trypsin, Mascot was searched with a fragment ion mass tolerance of 0.100 Da and a parent ion tolerance of 5.0 PPM. Carboxymethyl of cysteine was specified in Mascot as a fixed modification. Deamidation of asparagine and glutamine as well as oxidation of methionine and proline were specified in Mascot as variable modifications. A maximum of 1 missed cleavage was also used and a decoy search was performed. The mass spectrometry proteomics data have been deposited to the ProteomeXchange Consortium via the PRIDE [1] partner repository with the dataset identifier PXD033621.



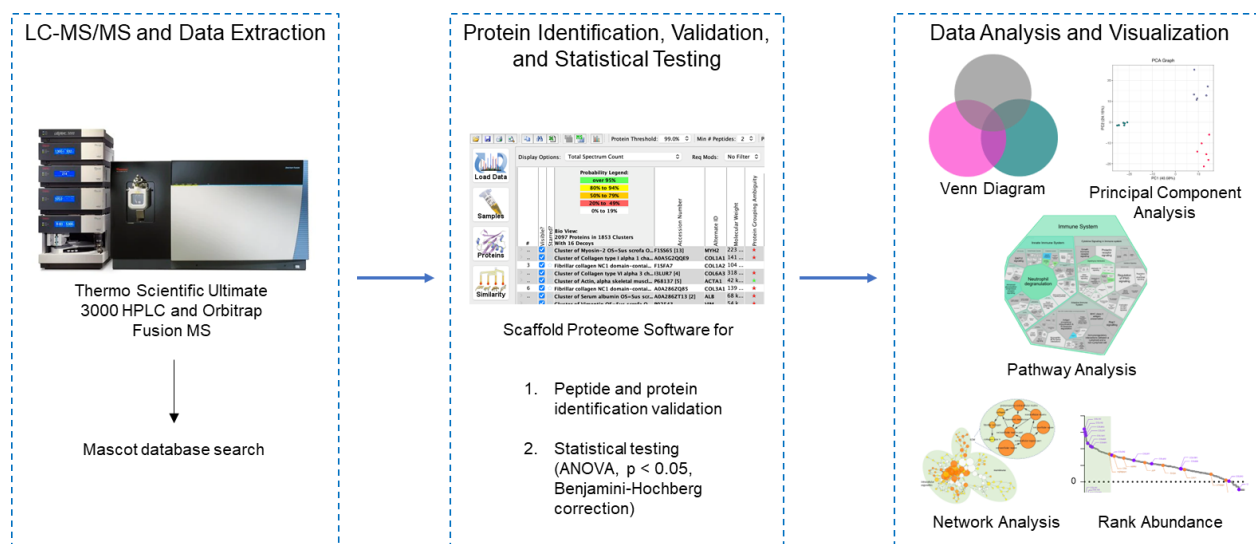


**Figure 9.** Illustrated workflow of the proteomics data analysis pipeline. The image of the LC-MS/MS equipment, a Thermo Scientific Ultimate 3000 HPLC and Orbitrap Fusion MS: Quadrupole-Orbitrap-Linear ion trap hybrid, was taken from the Thermo Fisher Scientific website.

The database search results were loaded onto Scaffold Q+ Scaffold\_4. (11.0, Proteome Software Inc., Portland, OR, USA) to validate MS/MS based peptide and protein identifications and to perform statistical tests.<sup>105</sup> Peptide identifications were accepted if they could be established at greater than 95.0% probability by the Scaffold Local FDR algorithm. Protein identifications were accepted if they could be established at greater than 99.0% probability and contained at least 2 identified peptides. Protein probabilities were assigned by the Protein Prophet algorithm.<sup>106</sup> Proteins that contained similar peptides and could not be differentiated based on MS/MS analysis alone were grouped to satisfy the principles of parsimony. Proteins sharing significant peptide evidence were grouped into clusters. Decoy peptide false discovery rate (FDR) was determined to be 0.08% and decoy protein FDR was 0.8%. The statistical significance of the data were determined with ANOVA test,  $p$ -value  $< 0.05$ , and Benjamini-Hochberg correction, resulting in a corrected  $p$ -value  $< 0.02177$ . The data were also normalized.

All protein duplicates as well as proteins with incomplete identification information, including missing names and alternate IDs, were removed. The total spectra of the remaining 698 proteins were then log10 transformed.

The principal component analysis graph and corresponding scree plot were also created using the R programming language. A PCA loadings plot was generated in Markerview (SCIEX, v. 1.3.1)

using Pareto scaling. Total area sums were used for data normalization with no weighting in order to visualize how each protein contributed to the corresponding principal components.

Pathway enrichment analysis was performed on the data using open-source Reactome pathway browser v3.7 and Reactome database v76.<sup>36</sup> A list of protein alternate IDs and their corresponding log10 transformed total spectra was entered into the Reactome “Analysis Tools” feature for pathway identifier mapping, over-representation, and expression analysis. Pathways mapped to inputted proteins were highlighted in color. Yellow represents a relatively higher p-value of the overrepresentation statistical test, or weak overrepresentation of the pathway, and blue represents a relatively lower p-value of the overrepresentation statistical test, or strong overrepresentation of the pathway. These pathways were then displayed as Voronoi diagrams to present the p-value of the statistical test for over-represented molecular pathways, especially those related to the immune system and ECM organization.<sup>107</sup>

Large-scale topological information molecular pathway network analysis was performed on the data using open-source bioinformatics software platform Cytoscape with plugin BiNGO 3.0.3 to calculate Gene Ontology (GO) term enrichment for the biological process, cellular component, and molecular function category.<sup>108-110</sup> A hypergeometric test, Benjamini-Hochberg False Discovery Rate (FDR) correction, and a p-value threshold of 0.01 were implemented as statistical testing. Protein alternate IDs were used as input data and evaluated against a custom database of a porcine GO Annotation File (GAF) downloaded from Gene Ontology.<sup>111,112</sup> The proteins were annotated to GO terms shown as nodes (circles) whose area was proportional to the number of genes in the data categorized to that node. Overrepresented GO terms were highlighted were highlighted in colour, with yellow representing a relatively higher adjusted p-value of the overrepresentation statistical test, or weak overrepresentation of the GO term, and orange representing a relatively lower adjusted p-value of the overrepresentation statistical test, or strong overrepresentation. White nodes represented those with no significant overrepresentation. For all 6 biological replicates of each tissue type (SIS dECM, VF dECM, and Native VF), the number of proteins annotated to each biological process GO term was determined for ECM, immune, and angiogenesis-related terms. The mean number of proteins and standard deviation were calculated for the GO terms of interest in each tissue type.

#### 4.5.7. Quantitative Verification of dECM Components

ECM Quantification Assays were performed according to manufacturer instructions. For each assay, three replicates of 4-6 mg of dry, homogenized native VF, VF dECM, and SIS dECM powders were used. Native VF and VF dECM samples were produced from a mixture of VF (N=6) with samples selected from three decellularization batches.

*Sircol™ Soluble Collagen Assay.* Samples were prepared for the Sircol™ Soluble Collagen Assay by overnight incubation in 1mL of 0.1 mg/mL pepsin in 0.5 M HCl at 4 °C. Digestion was halted with the addition of 100 µL acid neutralization reagent. To this solution, 200 µL Collagen Isolation and Concentration reagent was added and incubated again at 4 °C overnight. Concentrated collagen solutions were centrifuged at 12000 rpm and the supernatant aliquoted. Samples were prepared with 50 µL concentrated collagen solution and made up to 100 µL. Standards were prepared in the range of 0-45 µg. 1 mL Sircol Dye Reagent was added to each tube, and incubated at room temperature under gentle agitation for 30 min. The dye solution was centrifuged, and the supernatant removed, with tubes drained onto paper towels. Acid Salt Wash was added, and pellets centrifuged again to remove excess dye. After draining samples onto paper towels, 1000 µL Alkali Reagent was added and samples vortexed to release dye. Absorbance was measured at 555 nm.

*Sircol™ Insoluble Collagen Assay.* Insoluble collagen was assayed by incubating samples in 50 µL fragmentation reagent per 1 mg tissue for 2 hours at 65 °C. Fragmented collagen was then assayed as in the soluble collagen protocol, from the dye step forward. Denatured collagen standards of 0-60 ug were used. Absorbance was measured at 555 nm. In analysis, a 2.2X conversion factor was used to account for the 45% binding affinity of denatured collagen.

*Fastin™ Elastin Assay.* Elastin was extracted in 0.25 M Oxalic acid for 1 h at 100 °C to. After cooling to room temperature, samples were centrifuged at 10,000 rpm for 10 min. Supernatants were removed from samples, and the extraction process repeated on residual tissue. Samples were prepared from 100 µL with the first and second rounds assayed as separate samples. Standards were prepared containing 0-50 µg α-elastin. An equal volume of Elastin Precipitating Reagent was added to each sample and standard and vortexed. After 15 minutes, samples were centrifuged for 10 min, and supernatant discarded. 1 mL Fastin Dye Reagent was added to each tube. The precipitate was dispersed by vortexing, and samples were incubated at room temperature under gentle agitation for 90 min. Samples were centrifuged again and drained of dye before the addition of 250 µL Dye Dissociation Reagent. Samples were vortexed to release dye immediately and after

a 10 min incubation period. Samples from round 1 of extraction were diluted at a 1:2 ratio, and samples from round 2 were not diluted. Absorbance was measured at 513 nm.

*Purple-Jelley Hyaluronan Assay.* Tissue samples were digested in 400  $\mu$ L Tris-HCl and 20  $\mu$ L Proteinase at 65 °C for 3 h. After centrifuging at 12000 rpm for 10 min, supernatants were transferred to new microcentrifuge tubes mixed with 1 mL GAG precipitation reagent. After 15 min, samples were centrifuged, and supernatants discarded. Residues were extracted in 360  $\mu$ L water for 15 min with intermittent vortexing before the addition of concentrated NaCl and Cetylpyridinium Chloride. Samples were left undisturbed for 30 min without mixing, then centrifuged, and residues discarded. The entire process was repeated from the GAG precipitation step once. GAG Precipitation Reagent was added a third time, but 500  $\mu$ L 98% ethanol was added to residues after centrifugation rather than water and centrifuged again without mixing. Supernatant was removed and tubes dried by draining onto paper towels. The remaining pellet contained isolated HA, which was extracted with 100  $\mu$ L water for 30 min using intermittent vortexing. Standards were prepared from 0-3  $\mu$ g HA. 20  $\mu$ L from each standard and sample was mixed with 200  $\mu$ L Dye Reagent, and the absorbance measured at 655 nm.

#### *4.5.8. Culture of Human Vocal Fold Fibroblasts*

Human Vocal Fold Fibroblasts (HVFF) were generously supplied by Prof. Susan Thibeault (Department of Surgery, University of Wisconsin-Madison, USA). HVFF were cultured in T-75 flasks in a solution of Dulbecco's modified Eagle medium (DMEM), 10%v/v fetal bovine serum, and 1%v/v penicillin/ streptomycin under conditions of 5% CO<sub>2</sub> atmosphere and 37 °C. Media changes were performed every 3 days. Passages were performed when cells reached approximately 70% confluency using Gibco® Cell Dissociation Buffer. Dissociated HVFF were centrifuged, suspended in fresh DMEM, and plated onto to fresh T-75 flasks. HVFF were used between passages 9 and 14 for this study.

#### *4.5.9. Cellular Viability and Cytotoxicity*

SIS dECM, VF dECM, and collagen I pre-gels were prepared as described in **Section 5.4**. On day 0 of cell experiments, 70  $\mu$ L of SIS, VF dECM, and Collagen I pre-gels were pipetted into four wells for each time point. Pre-gels were incubated for at least 1 hr prior to cell seeding to form hydrogels with approximately 1 mm thickness.

Glass control wells were pre-coated with 0.1 mg/mL gelatin and incubated overnight prior to seeding. A total of sixteen 8-well chamber slides were used for each experiment, i.e. 4 replicates.

HVFF were seeded in each chamber well at a concentration of 10,000 cells per well. Additional media was then added for a total volume of 300  $\mu$ L per well. HVFF were cultured under conditions of 5% CO<sub>2</sub> atmosphere and 37 °C over 14 days, with media changes performed every 2-3 days.

At each time point (1, 3, 7, or 14 days) media was removed from samples in randomly selected chamber slides and the HVFF and hydrogels were washed twice with PBS. 100  $\mu$ L Calcein AM and Ethidium Homodimer solution was added to each well and incubated at room temperature while protected from light for 30 min. The dye solution was removed and each sample washed two additional times with PBS. A final 100  $\mu$ L of PBS was added to keep samples hydrated, and all samples were imaged on a Zeiss LSM 800 Confocal Microscope the same day. Each image covered a region of 3 mm x 3 mm, and z-stacks were used to ensure imaging of all cells in the imaging region. Cell counting was performed using ImageJ.<sup>113</sup>

#### *4.5.10. Deposition of Neo-ECM Components*

Chamber slides were prepared as described in **Section 5.8**. However, two chamber slides were set aside without cell seeding for immediate “0 day” analysis. Cells were seeded on the remaining 14 chamber slides as described in section 5.9 and cultured for up to 14 days. Chamber slides were randomly selected for analysis on days 3, 7, and 14. This cell culture procedure was followed for both deposition of neo-Elastin and neo-Hyaluronan ECM Quantification assays. Three technical replicates were used for each assay.

*Sircol™ Soluble Collagen Assay:* The assay was performed as described in Section 5.6 with slight modifications in sample preparation. Volumes in the sample preparation step were reduced by half to ensure collagen would be detectable across all samples. Collagen content of control hydrogels incubated in DMEM without cells was measured at each time point to account for collagen degradation over time. For the assay, 100  $\mu$ L samples were used.

*Fastin™ Elastin Assay:* To prepare samples for the Fastin™ Elastin Assay, hydrogels were removed from wells and transferred to 1.5 mL microcentrifuge tubes. Cells were removed from glass controls using Gibco® Cell Dissociation Buffer and centrifuged in PBS. The Fastin™ Elastin was then performed as described in **Section 5.6**, with no dilution prior to the measurement of absorbance to account for the lower concentrations compared to tissue.

*Purple-Jelley Hyaluronan Assay:* Samples were prepared for the Purple-Jelley™ Hyaluronan Assay and the assay performed as described in **Section 5.6**.

#### *4.5.11 Statistical Analysis*

Statistical Analyses were performed using GraphPad Prism 9 (GraphPad Software, Inc., USA). Data was analyzed using one or two-way ANOVA followed by Tukey's post-hoc test. Data values are presented as mean  $\pm$  SD. Values of  $p < 0.05$  were deemed statistically significant.

#### **Acknowledgements**

This study was supported by the National Sciences and Engineering Research Council of Canada (RGPIN-2018-03843 and ALLRP 548623-19), Canada Research Chair research stipend (N.L.-J., MT)) and the National Institutes of Health (R01 DC-018577-01A1). Cryomilling was performed in the Dr. Christopher Moraes' Cellular Microenvironment Design Lab at McGill University, with technical support from Prabu Karthick Parameshwar. Microscopic imaging for this manuscript was performed in the McGill University Life Sciences Complex Advanced BioImaging Facility (ABIF). Rheology was performed in Dr. Luc Mongeau's Biomechanics laboratory at McGill University. Mass Spectrometry Analysis was performed in the Proteomics Platform at the Research Institute of the McGill University Health Center (RI-MUHC). We would also like to acknowledge the generous donation of HVFF by Prof. Susan Thibeault's laboratory (University of Wisconsin-Madison). The presented content is solely the responsibility of the authors and does not necessarily represent the official views of the above funding agencies.

#### **Conflict of Interest**

Powder Extracellular Matrix was provided by Cook Biotech through a Material Transfer Agreement at the cost of shipping. The authors hold no financial interest in Cook Biotech and declare no additional conflicts of interest.

#### **Author Contributions**

**Mika Brown:** Conceptualization (lead), Investigation (lead), Formal Analysis (equal), Writing – original draft (lead). **Shirley Zhu:** Formal Analysis (equal), Data Curation (lead), Writing – original draft (supporting). **Lorne Taylor:** Investigation (supporting), Formal Analysis (supporting), Writing – review and editing (supporting). **Maryam Tabrizian:** Supervision (supporting), Writing – review and editing (supporting). **Nicole Li-Jessen:** Supervision (lead), Conceptualization (supporting), Funding Acquisition (lead), Resources (lead), Writing – review and editing (lead).

**Data Availability Statement**

The mass spectrometry proteomics data have been deposited to the ProteomeXchange Consortium via the PRIDE [1] partner repository with the dataset identifier PXD033621. All other data that support the findings of this study are available from the corresponding author upon reasonable request.

#### 4.6. References

- 1 Chen, S. *et al.* Promoting Neurite Growth and Schwann Cell Migration by the Harnessing Decellularized Nerve Matrix onto Nanofibrous Guidance. *ACS Applied Material Interfaces* **11**, 17167-17176 (2019). <https://doi.org/10.1021/acsami.9b01066>
- 2 Ali, M. *et al.* A Photo-Crosslinkable Kidney ECM-Derived Bioink Accelerates Renal Tissue Formation. **8**, 1800992 (2019). <https://doi.org/10.1002/adhm.201800992>
- 3 Brown, M., Li, J., Moraes, C., Tabrizian, M. & Li-Jessen, N. Y. K. Decellularized extracellular matrix: New promising and challenging biomaterials for regenerative medicine. *Biomaterials* **289**, 121786 (2022). <https://doi.org/10.1016/j.biomaterials.2022.121786>
- 4 Keane, T. J., Swinehart, I. T. & Badylak, S. F. Methods of Tissue Decellularization Used for Preparation of Biologic Scaffolds and In Vivo Relevance. *Methods* **84**, 25-34 (2015).
- 5 Leng, L. *et al.* Comprehensive proteomic atlas of skin biomatrix scaffolds reveals a supportive microenvironment for epidermal development. *J Tissue Eng* **11**, 2041731420972310 (2020). <https://doi.org/10.1177/2041731420972310>
- 6 Beachley, V. *et al.* Extracellular matrix particle–glycosaminoglycan composite hydrogels for regenerative medicine applications. *Journal of Biomedical Materials Research Part A* **106**, 147-159 (2018).
- 7 Xu, Y. *et al.* Understanding the Role of Tissue-Specific Decellularized Spinal Cord Matrix Hydrogel for Neural Stem/Progenitor Cell Microenvironment Reconstruction and Spinal Cord Injury. 120596 (2020).
- 8 Coburn, P. T., Li, X., Li, J., Kishimoto, Y. & Li-Jessen, N. Y. Progress in Vocal Fold Regenerative Biomaterials: An Immunological Perspective. *Advanced NanoBiomed Research*, 2100119 (2021).
- 9 Garg, A. *et al.* Towards a Physiological Scale of Vocal Fold Agent-Based Models of Surgical Injury and Repair: Sensitivity Analysis, Calibration and Verification. *Appl Sci (Basel)* **9**, 2974 (2019). <https://doi.org/10.3390/app9152974>
- 10 Kazarine, A. *et al.* Multimodal virtual histology of rabbit vocal folds by nonlinear microscopy and nano computed tomography. *Biomed. Opt. Express* **10**, 1151-1164 (2019). <https://doi.org/10.1364/BOE.10.001151>
- 11 Zhang, Y., Fonslow, B. R., Shan, B., Baek, M.-C. & Yates, J. R., 3rd. Protein analysis by shotgun/bottom-up proteomics. *Chemical reviews* **113**, 2343-2394 (2013). <https://doi.org/10.1021/cr3003533>
- 12 Othman, Z., Cillero Pastor, B., van Rijt, S. & Habibovic, P. Understanding interactions between biomaterials and biological systems using proteomics. *Biomaterials* **167**, 191-204 (2018). <https://doi.org/10.1016/j.biomaterials.2018.03.020>
- 13 Welham, N. V., Chang, Z., Smith, L. M. & Frey, B. L. Proteomic analysis of a decellularized human vocal fold mucosa scaffold using 2D electrophoresis and high-resolution mass spectrometry. *Biomaterials* **34**, 669-676 (2013). <https://doi.org/10.1016/j.biomaterials.2012.09.050>
- 14 Mora-Navarro, C. *et al.* Monitoring decellularization via absorbance spectroscopy during the derivation of extracellular matrix scaffolds. *Biomedical Materials* **17**, 015008 (2021). <https://doi.org/10.1088/1748-605x/ac361f>
- 15 Miri, A. K. Mechanical Characterization of Vocal Fold Tissue: A Review Study. *Journal of Voice* **28**, 657-667 (2014). <https://doi.org/10.1016/j.jvoice.2014.03.001>



- 16 Branski, R. C., Verdolini, K., Sandulache, V., Rosen, C. A. & Hebda, P. A. Vocal Fold Wound Healing: A Review for Clinicians. *Journal of Voice* **20**, 432-442 (2006). <https://doi.org/https://doi.org/10.1016/j.jvoice.2005.08.005>
- 17 Chowdhury, C. (U.S. Food and Drug Administration, Center for Devices and Radiological Health, Maryland, 2020).
- 18 Cramer, M. C. & Badylak, S. F. Extracellular Matrix-Based Biomaterials and Their Influence Upon Cell Behavior. *Ann Biomed Eng* **48**, 2132-2153 (2020). <https://doi.org/10.1007/s10439-019-02408-9>
- 19 Mora-Navarro, C. *et al.* Porcine Vocal Fold Lamina Propria-Derived Biomaterials Modulate TGF- $\beta$ 1-Mediated Fibroblast Activation in Vitro. *Acs Biomater Sci Eng* **6**, 1690-1703 (2020).
- 20 Choi, J. W. *et al.* Small intestine submucosa and mesenchymal stem cells composite gel for scarless vocal fold regeneration. *Biomaterials* **35**, 4911-4918 (2014). <https://doi.org/10.1016/j.biomaterials.2014.03.008>
- 21 Crapo, P. M., Gilbert, T. W. & Badylak, S. F. An overview of tissue and whole organ decellularization processes. *Biomaterials* **32**, 3233-3243 (2011). <https://doi.org/10.1016/j.biomaterials.2011.01.057>
- 22 Sawkins, M. J. *et al.* Hydrogels derived from demineralized and decellularized bone extracellular matrix. *Acta Biomaterialia* **9**, 7865-7873 (2013). <https://doi.org/10.1016/j.actbio.2013.04.029>
- 23 Fu, Y. *et al.* Decellularization of porcine skeletal muscle extracellular matrix for the formulation of a matrix hydrogel: a preliminary study. *Journal of Cellular and Molecular Medicine* **20**, 740-749 (2016). <https://doi.org/https://doi.org/10.1111/jcmm.12776>
- 24 Lee, M. S. *et al.* Biofabrication and application of decellularized bone extracellular matrix for effective bone regeneration. *Journal of Industrial and Engineering Chemistry* **83**, 323-332 (2020). <https://doi.org/https://doi.org/10.1016/j.jiec.2019.12.005>
- 25 Pati, F. *et al.* Printing three-dimensional tissue analogues with decellularized extracellular matrix bioink. *Nat Commun* **5**, 3935 (2014). <https://doi.org/10.1038/ncomms4935>
- 26 Gilbert, T. W., Freund, J. M. & Badylak, S. F. Quantification of DNA in Biologic Scaffold Materials. *Journal of Surgical Research* **152**, 135-139 (2009). <https://doi.org/https://doi.org/10.1016/j.jss.2008.02.013>
- 27 Wrona, E. A. *et al.* Derivation and characterization of porcine vocal fold extracellular matrix scaffold. *Laryngoscope* **126**, 928-935 (2016). <https://doi.org/10.1002/lary.25640>
- 28 Brown, M. *Decellularized extracellular matrix (dECM) microparticle based hydrogels for vocal fold tissue engineering.* (McGill University (Canada), 2019).
- 29 Ansorge, H. L. *et al.* Type XIV Collagen Regulates Fibrillogenesis\*. *Journal of Biological Chemistry* **284**, 8427-8438 (2009). <https://doi.org/https://doi.org/10.1074/jbc.M805582200>
- 30 Gelse, K., Pöschl, E. & Aigner, T. Collagens—structure, function, and biosynthesis. *Advanced Drug Delivery Reviews* **55**, 1531-1546 (2003). <https://doi.org/https://doi.org/10.1016/j.addr.2003.08.002>
- 31 Pessin, A. B. B., Martins, R. H. G., Gushiken, L. F. S. & Pellizzon, C. H. Sectorial Analysis of the Fibrous Matrix of Vocal Folds in the Elderly. *Journal of Voice* (2020). <https://doi.org/https://doi.org/10.1016/j.jvoice.2020.07.003>
- 32 Svistushkin, M. V. *et al.* Collagen fibrillar structures in vocal fold scarring and repair using stem cell therapy: a detailed histological, immunohistochemical and atomic force

- microscopy study. *Journal of Microscopy* **274**, 55-68 (2019).  
<https://doi.org/https://doi.org/10.1111/jmi.12784>
- 33 Fitoussi, R., Beauchef, G., Guéré, C., André, N. & Vié, K. Localization, fate and interactions of Emilin-1 in human skin. *International Journal of Cosmetic Science* **41**, 183-193 (2019). <https://doi.org/https://doi.org/10.1111/ics.12524>
- 34 Spitalieri, P. *et al.* Effects of Simulated Microgravity on Wild Type and Marfan hiPSCs-Derived Embryoid Bodies. *Cellular and Molecular Bioengineering* **14**, 613-626 (2021). <https://doi.org/10.1007/s12195-021-00680-1>
- 35 Choi, J. *et al.* Analysis of dermal elastic fibers in the absence of fibulin-5 reveals potential roles for fibulin-5 in elastic fiber assembly. *Matrix Biology* **28**, 211-220 (2009). <https://doi.org/https://doi.org/10.1016/j.matbio.2009.03.004>
- 36 Jassal, B. *et al.* The reactome pathway knowledgebase. *Nucleic acids research* **48**, D498-d503 (2020). <https://doi.org/10.1093/nar/gkz1031>
- 37 Kalamajski, S., Aspberg, A., Lindblom, K., Heinegård, D. & Oldberg, A. Asporin competes with decorin for collagen binding, binds calcium and promotes osteoblast collagen mineralization. *The Biochemical journal* **423**, 53-59 (2009). <https://doi.org/10.1042/bj20090542>
- 38 Neame, P. J., Kay, C. J., McQuillan, D. J., Beales, M. P. & Hassell, J. R. Independent modulation of collagen fibrillogenesis by decorin and lumican. *Cellular and molecular life sciences : CMLS* **57**, 859-863 (2000). <https://doi.org/10.1007/s000180050048>
- 39 Berendsen, A. D. *et al.* Biglycan modulates angiogenesis and bone formation during fracture healing. *J Matrix Biology* **35**, 223-231 (2014).
- 40 Buraschi, S. *et al.* Decorin causes autophagy in endothelial cells via Peg3. *Proc Natl Acad Sci U S A* **110**, E2582-2591 (2013). <https://doi.org/10.1073/pnas.1305732110>
- 41 Chen, X. D. Extracellular matrix provides an optimal niche for the maintenance and propagation of mesenchymal stem cells. *J Birth Defects Research Part C: Embryo Today: Reviews* **90**, 45-54 (2010).
- 42 Wright, S. *et al.* Perlecan domain V inhibits  $\alpha 2$  integrin-mediated amyloid- $\beta$  neurotoxicity. *Neurobiology of aging* **33**, 1379-1388 (2012). <https://doi.org/10.1016/j.neurobiolaging.2010.10.018>
- 43 Frischknecht, R. & Seidenbecher, C. I. The crosstalk of hyaluronan-based extracellular matrix and synapses. *Neuron Glia Biol* **4**, 249-257 (2008). <https://doi.org/10.1017/S1740925X09990226>
- 44 Zimmermann, D. R. & Ruoslahti, E. Multiple domains of the large fibroblast proteoglycan, versican. *The EMBO journal* **8**, 2975-2981 (1989).
- 45 D'Acquisto, F., Perretti, M. & Flower, R. J. Annexin-A1: a pivotal regulator of the innate and adaptive immune systems. *British Journal of Pharmacology* **155**, 152-169 (2008). <https://doi.org/https://doi.org/10.1038/bjp.2008.252>
- 46 Munoz, L. E. *et al.* The role of annexin A5 in the modulation of the immune response against dying and dead cells. *Curr Med Chem* **14**, 271-277 (2007). <https://doi.org/10.2174/092986707779941131>
- 47 Aitkenhead, M. *et al.* Identification of Endothelial Cell Genes Expressed in an in Vitro Model of Angiogenesis: Induction of ESM-1,  $\beta$ ig-h3, and NrCAM. *Microvascular Research* **63**, 159-171 (2002). <https://doi.org/https://doi.org/10.1006/mvre.2001.2380>
- 48 Nichols, W. C. *et al.* Mutations in the ER-Golgi intermediate compartment protein ERGIC-53 cause combined deficiency of coagulation factors V and VIII. *Cell* **93**, 61-70 (1998).

- [https://doi.org/10.1016/s0092-8674\(00\)81146-0](https://doi.org/10.1016/s0092-8674(00)81146-0)
- 49 Ruvolo, P. P. *et al.* LGALS1 acts as a pro-survival molecule in AML. *Biochimica et Biophysica Acta (BBA) - Molecular Cell Research* **1867**, 118785 (2020). <https://doi.org/https://doi.org/10.1016/j.bbamcr.2020.118785>
  - 50 Xiang, Q. *et al.* Overexpression of Gremlin1 in Mesenchymal Stem Cells Improves Hindlimb Ischemia in Mice by Enhancing Cell Survival. *Journal of Cellular Physiology* **232**, 996-1007 (2017). <https://doi.org/https://doi.org/10.1002/jcp.25578>
  - 51 Yiu, G. K., Kaunisto, A., Chin, Y. R. & Toker, A. NFAT promotes carcinoma invasive migration through glypican-6. *The Biochemical journal* **440**, 157-166 (2011). <https://doi.org/10.1042/bj20110530>
  - 52 Leigh, L. E. *et al.* C1q-mediated chemotaxis by human neutrophils: involvement of gC1qR and G-protein signalling mechanisms. *The Biochemical journal* **330** ( Pt 1), 247-254 (1998). <https://doi.org/10.1042/bj3300247>
  - 53 Barondes, S. H. J. G., Hoboken, NJ: Wiley. Stumbling on galectins. 1-8 (2008).
  - 54 Olson, S. T., Richard, B., Izaguirre, G., Schedin-Weiss, S. & Gettins, P. G. Molecular mechanisms of antithrombin–heparin regulation of blood clotting proteinases. A paradigm for understanding proteinase regulation by serpin family protein proteinase inhibitors. *J Biochimie* **92**, 1587-1596 (2010).
  - 55 van Gent, D., Sharp, P., Morgan, K. & Kalsheker, N. Serpins: structure, function and molecular evolution. *Int J Biochem Cell Biol* **35**, 1536-1547 (2003). [https://doi.org/10.1016/s1357-2725\(03\)00134-1](https://doi.org/10.1016/s1357-2725(03)00134-1)
  - 56 Gavish, H. *et al.* Human alpha 2-macroglobulin is an osteogenic growth peptide-binding protein. *Biochemistry* **36**, 14883-14888 (1997). <https://doi.org/10.1021/bi971670t>
  - 57 Stefansson, S., Lawrence, D. A. & Argraves, W. S. Plasminogen activator inhibitor-1 and vitronectin promote the cellular clearance of thrombin by low density lipoprotein receptor-related proteins 1 and 2. *The Journal of biological chemistry* **271**, 8215-8220 (1996). <https://doi.org/10.1074/jbc.271.14.8215>
  - 58 Lehtonen, J. Y., Daviet, L., Nahmias, C., Horiuchi, M. & Dzau, V. J. Analysis of functional domains of angiotensin II type 2 receptor involved in apoptosis. *Molecular endocrinology (Baltimore, Md.)* **13**, 1051-1060 (1999). <https://doi.org/10.1210/mend.13.7.0303>
  - 59 Naba, A., Hoersch, S. & Hynes, R. O. Towards definition of an ECM parts list: an advance on GO categories. *Matrix Biol* **31**, 371-372 (2012). <https://doi.org/10.1016/j.matbio.2012.11.008>
  - 60 Endo, A., Fukuhara, S., Masuda, M., Ohmori, T. & Mochizuki, N. Selective Inhibition of Vascular Endothelial Growth Factor Receptor-2 (VEGFR-2) Identifies a Central Role for VEGFR-2 in Human Aortic Endothelial Cell Responses to VEGF. *Journal of Receptors and Signal Transduction* **23**, 239-254 (2003). <https://doi.org/10.1081/RRS-120025567>
  - 61 Le Boeuf, F., Houle, F. & Huot, J. Regulation of vascular endothelial growth factor receptor 2-mediated phosphorylation of focal adhesion kinase by heat shock protein 90 and Src kinase activities. *The Journal of biological chemistry* **279**, 39175-39185 (2004). <https://doi.org/10.1074/jbc.M405493200>
  - 62 Benn, A. *et al.* Role of bone morphogenetic proteins in sprouting angiogenesis: differential BMP receptor-dependent signaling pathways balance stalk vs. tip cell competence. *The FASEB Journal* **31**, 4720-4733 (2017). <https://doi.org/https://doi.org/10.1096/fj.201700193RR>
  - 63 Nathan, J. & Ramachandran, A. Efficacy of marine biomolecules on angiogenesis by

- targeting hypoxia inducible factor/vascular endothelial growth factor signaling in zebrafish model. *J Biochem Mol Toxicol* **36**, e22954 (2022). <https://doi.org/10.1002/jbt.22954>
- 64 Sarkar, B. *et al.* Angiogenic Self-Assembling Peptide Scaffolds for Functional Tissue Regeneration. *Biomacromolecules* **19**, 3597-3611 (2018). <https://doi.org/10.1021/acs.biomac.8b01137>
- 65 Gallo, S., Sala, V., Gatti, S. & Crepaldi, T. Cellular and molecular mechanisms of HGF/Met in the cardiovascular system. *Clinical Science* **129**, 1173-1193 (2015). <https://doi.org/10.1042/CS20150502>
- 66 Sobti, A. *et al.* Immune delineation of laryngeal papilloma reveals enhanced neutrophil associated gene profile. *European Journal of Immunology* **51**, 2535-2539 (2021). <https://doi.org/https://doi.org/10.1002/eji.202149202>
- 67 Babensee, J. E. in *Biomaterials Science (Fourth Edition)* (eds William R. Wagner, Shelly E. Sakiyama-Elbert, Guigen Zhang, & Michael J. Yaszemski) 737-746 (Academic Press, 2020).
- 68 Xu, C. C. & Mau, T. A tissue-specific, injectable acellular gel for the treatment of chronic vocal fold scarring. *Acta Biomaterialia* (2019). <https://doi.org/10.1016/j.actbio.2019.08.025>
- 69 Gessel, M., Spraggins, J. M., Voziyan, P., Hudson, B. G. & Caprioli, R. M. Decellularization of intact tissue enables MALDI imaging mass spectrometry analysis of the extracellular matrix. *Journal of Mass Spectrometry* **50**, 1288-1293 (2015). <https://doi.org/https://doi.org/10.1002/jms.3696>
- 70 Griffiths, L. G., Choe, L. H., Reardon, K. F., Dow, S. W. & Christopher Orton, E. Immunoproteomic identification of bovine pericardium xenoantigens. *Biomaterials* **29**, 3514-3520 (2008). <https://doi.org/https://doi.org/10.1016/j.biomaterials.2008.05.006>
- 71 Xu, C. C., Chan, R. W. & Tirunagari, N. A biodegradable, acellular xenogeneic scaffold for regeneration of the vocal fold lamina propria. *Tissue Eng Pt A* **13**, 551-566 (2007). <https://doi.org/10.1089/ten.2006.0169>
- 72 Hashimoto, Y. *et al.* Alteration of the extracellular matrix and alpha-gal antigens in the rat lung scaffold reseeded using human vascular and adipogenic stromal cells. *J Tissue Eng Regen Med* **13**, 2067-2076 (2019). <https://doi.org/10.1002/term.2923>
- 73 Sadtler, K. *et al.* Proteomic composition and immunomodulatory properties of urinary bladder matrix scaffolds in homeostasis and injury. *Seminars in Immunology* **29**, 14-23 (2017). <https://doi.org/https://doi.org/10.1016/j.smim.2017.05.002>
- 74 Dziki, J. L., Sicari, B. M., Wolf, M. T., Cramer, M. C. & Badylak, S. F. Immunomodulation and Mobilization of Progenitor Cells by Extracellular Matrix Bioscaffolds for Volumetric Muscle Loss Treatment. *Tissue Eng Part A* **22**, 1129-1139 (2016). <https://doi.org/10.1089/ten.TEA.2016.0340>
- 75 Dziki, J. L. *et al.* Solubilized extracellular matrix bioscaffolds derived from diverse source tissues differentially influence macrophage phenotype. *J Biomed Mater Res A* **105**, 138-147 (2017). <https://doi.org/10.1002/jbm.a.35894>
- 76 Yang, L. *et al.* Surface modified small intestinal submucosa membrane manipulates sequential immunomodulation coupled with enhanced angio- and osteogenesis towards ameliorative guided bone regeneration. *Materials Science and Engineering: C* **119**, 111641 (2021). <https://doi.org/https://doi.org/10.1016/j.msec.2020.111641>
- 77 Coburn, P. T., Herbay, A. C., Berrini, M. & Li-Jessen, N. Y. K. An in vitro assessment of the response of THP-1 macrophages to varying stiffness of a glycol-chitosan hydrogel for

- vocal fold tissue engineering applications. *J Biomed Mater Res A* **109**, 1337-1352 (2021). <https://doi.org/10.1002/jbm.a.37125>
- 78 Eichmann, A. & Simons, M. VEGF Signaling Inside Vascular Endothelial Cells and Beyond. *Curr Opin Cell Biol* **24**, 188-193 (2012). <https://doi.org/10.1016/j.ceb.2012.02.002>
- 79 Namazi, M. R., Fallahzadeh, M. K. & Schwartz, R. A. Strategies for prevention of scars: what can we learn from fetal skin? *International journal of dermatology* **50**, 85-93 (2011).
- 80 Sackett, S. D. *et al.* Extracellular matrix scaffold and hydrogel derived from decellularized and delipidized human pancreas. *Scientific Reports* **8**, 10452 (2018). <https://doi.org/10.1038/s41598-018-28857-1>
- 81 Daly, A. B. *et al.* Initial Binding and Recellularization of Decellularized Mouse Lung Scaffolds with Bone Marrow-Derived Mesenchymal Stromal Cells. *Tissue Eng Pt A* **18**, 1-16 (2011). <https://doi.org/10.1089/ten.tea.2011.0301>
- 82 Pérez, M. L. *et al.* Fast protocol for the processing of split-thickness skin into decellularized human dermal matrix. *Tissue and Cell* **72**, 101572 (2021). <https://doi.org/https://doi.org/10.1016/j.tice.2021.101572>
- 83 Simsa, R. *et al.* Effect of fluid dynamics on decellularization efficacy and mechanical properties of blood vessels. *PLoS One* **14**, e0220743 (2019). <https://doi.org/10.1371/journal.pone.0220743>
- 84 Wang, Z. *et al.* Rapid Preparation Method for Preparing Tracheal Decellularized Scaffolds: Vacuum Assistance and Optimization of DNase I. *ACS Omega* **6**, 10637-10644 (2021). <https://doi.org/10.1021/acsomega.0c06247>
- 85 Latifi, N., Asgari, M., Vali, H. & Mongeau, L. A tissue-mimetic nano-fibrillar hybrid injectable hydrogel for potential soft tissue engineering applications. *Scientific Reports* **8**, 1047 (2018). <https://doi.org/10.1038/s41598-017-18523-3>
- 86 Sanjurjo-Rodríguez, C. *et al.* Differentiation of human mesenchymal stromal cells cultured on collagen sponges for cartilage repair. *Histol Histopathol* **31**, 1221-1239 (2016).
- 87 Terada, S. *et al.* Hydrogel optimization for cultured elastic chondrocytes seeded onto a polyglycolic acid scaffold\*. *Journal of Biomedical Materials Research Part A* **75A**, 907-916 (2005). <https://doi.org/https://doi.org/10.1002/jbm.a.30505>
- 88 Minor, A. J. & Coulombe, K. L. K. Engineering a collagen matrix for cell-instructive regenerative angiogenesis. *Journal of Biomedical Materials Research Part B: Applied Biomaterials* **108**, 2407-2416 (2020). <https://doi.org/https://doi.org/10.1002/jbm.b.34573>
- 89 Capella-Monsonís, H., Coentro, J. Q., Graceffa, V., Wu, Z. & Zeugolis, D. I. An experimental toolbox for characterization of mammalian collagen type I in biological specimens. *Nature Protocols* **13**, 507-529 (2018). <https://doi.org/10.1038/nprot.2017.117>
- 90 Seekhao, N., Shung, C., JaJa, J., Mongeau, L. & Li-Jessen, N. Y. K. High-Performance Agent-Based Modeling Applied to Vocal Fold Inflammation and Repair. *Frontiers in physiology* **9**, 304 (2018). <https://doi.org/10.3389/fphys.2018.00304>
- 91 Kolosova, K. *et al.* Characterizing Vocal Fold Injury Recovery in a Rabbit Model With Three-Dimensional Virtual Histology. *The Laryngoscope* **131**, 1578-1587 (2021). <https://doi.org/https://doi.org/10.1002/lary.29028>
- 92 Hughes, L. A., Gaston, J., McAlindon, K., Woodhouse, K. A. & Thibeault, S. L. Electrospun fiber constructs for vocal fold tissue engineering: Effects of alignment and elastomeric polypeptide coating. *Acta Biomaterialia* **13**, 111-120 (2015). <https://doi.org/https://doi.org/10.1016/j.actbio.2014.10.039>

- 93 Shirzaei Sani, E. *et al.* Engineering Adhesive and Antimicrobial Hyaluronic Acid/Elastin-like Polypeptide Hybrid Hydrogels for Tissue Engineering Applications. *Acs Biomater Sci Eng* **4**, 2528-2540 (2018). <https://doi.org/10.1021/acsbiomaterials.8b00408>
- 94 Brown, A. L., Srokowski, E. M., Shu, X. Z., Prestwich, G. D. & Woodhouse, K. A. Development of a Model Bladder Extracellular Matrix Combining Disulfide Cross-Linked Hyaluronan with Decellularized Bladder Tissue. *Macromolecular Bioscience* **6**, 648-657 (2006). <https://doi.org/https://doi.org/10.1002/mabi.200600052>
- 95 Uhl, F. E. *et al.* Functional role of glycosaminoglycans in decellularized lung extracellular matrix. *Acta Biomaterialia* **102**, 231-246 (2020). <https://doi.org/https://doi.org/10.1016/j.actbio.2019.11.029>
- 96 Brown, B., Lindberg, K., Reing, J., Stolz, D. B. & Badylak, S. F. The basement membrane component of biologic scaffolds derived from extracellular matrix. *Tissue Eng* **12**, 519-526 (2006). <https://doi.org/10.1089/ten.2006.12.519>
- 97 Jung, M., Han, Y., Woo, C. & Ki, C. S. Pulmonary tissue-mimetic hydrogel niches for small cell lung cancer cell culture. *J Mater Chem B* **9**, 1858-1866 (2021). <https://doi.org/10.1039/d0tb02609c>
- 98 Walimbe, T., Panitch, A. & Sivasankar, P. M. A Review of Hyaluronic Acid and Hyaluronic Acid-based Hydrogels for Vocal Fold Tissue Engineering. *J Voice* **31**, 416-423 (2017). <https://doi.org/10.1016/j.jvoice.2016.11.014>
- 99 Seo, K. K. in *Facial Volumization with Fillers* 29-83 (Springer, 2021).
- 100 Jang, J. *et al.* Tailoring mechanical properties of decellularized extracellular matrix bioink by vitamin B2-induced photo-crosslinking. *Acta Biomaterialia* **33**, 88-95 (2016). <https://doi.org/https://doi.org/10.1016/j.actbio.2016.01.013>
- 101 Swartjes, J. J. T. M. *et al.* A Functional DNase I Coating to Prevent Adhesion of Bacteria and the Formation of Biofilm. *Advanced Functional Materials* **23**, 2843-2849 (2013). <https://doi.org/https://doi.org/10.1002/adfm.201202927>
- 102 Record Ritchie, R. D., Salmon, S. L., Hiles, M. C. & Metzger, D. W. Lack of immunogenicity of xenogeneic DNA from porcine biomaterials. *Surgery Open Science* **10**, 83-90 (2022). <https://doi.org/https://doi.org/10.1016/j.sopen.2022.07.005>
- 103 Yang, D., Fang, Z., Kang, R. & Liu, K. Composite electrospun scaffold containing decellularized amniotic matrix for pelvic organ prolapse. *Materials & Design* **210**, 110106 (2021). <https://doi.org/https://doi.org/10.1016/j.matdes.2021.110106>
- 104 Wrona, E. A., Peng, R., Amin, M. R., Branski, R. C. & Freytes, D. O. Extracellular Matrix for Vocal Fold Lamina Propria Replacement: A Review. *Tissue Eng Part B Rev* **22**, 421-429 (2016). <https://doi.org/10.1089/ten.TEB.2016.0015>
- 105 Elias, J. E. & Gygi, S. P. Target-decoy search strategy for increased confidence in large-scale protein identifications by mass spectrometry. *Nature Methods* **4**, 207-214 (2007). <https://doi.org/10.1038/nmeth1019>
- 106 Nesvizhskii, A. I., Keller, A., Kolker, E. & Aebersold, R. A Statistical Model for Identifying Proteins by Tandem Mass Spectrometry. *Analytical Chemistry* **75**, 4646-4658 (2003). <https://doi.org/10.1021/ac0341261>
- 107 Weigand, M., Hauck, S. M., Deeg, C. A. & Degroote, R. L. Deviant proteome profile of equine granulocytes associates to latent activation status in organ specific autoimmune disease. *Journal of Proteomics* **230**, 103989 (2021). <https://doi.org/https://doi.org/10.1016/j.jpro.2020.103989>
- 108 Maere, S., Heymans, K. & Kuiper, M. BiNGO: a Cytoscape plugin to assess

- overrepresentation of gene ontology categories in biological networks. *Bioinformatics (Oxford, England)* **21**, 3448-3449 (2005). <https://doi.org/10.1093/bioinformatics/bti551>
- 109 Wu, X., Hasan, M. A. & Chen, J. Y. Pathway and network analysis in proteomics. *J Theor Biol* **362**, 44-52 (2014). <https://doi.org/10.1016/j.jtbi.2014.05.031>
- 110 Chisanga, D., Keerthikumar, S., Mathivanan, S. & Chilamkurti, N. in *Proteome Bioinformatics* (eds Shivakumar Keerthikumar & Suresh Mathivanan) 177-197 (Springer New York, 2017).
- 111 Ashburner, M. *et al.* Gene ontology: tool for the unification of biology. The Gene Ontology Consortium. *Nat Genet* **25**, 25-29 (2000). <https://doi.org/10.1038/75556>
- 112 The Gene Ontology resource: enriching a GOld mine. *Nucleic acids research* **49**, D325-d334 (2021). <https://doi.org/10.1093/nar/gkaa1113>
- 113 Schindelin, J. *et al.* Fiji: an open-source platform for biological-image analysis. *Nat methods* **9**, 676-682 (2012). <https://doi.org/10.1038/nmeth.2019>

## Preface to Chapter 5

In Chapter 4, a proteomic study was combined with functional assays to evaluate the utility of hydrogels derived from two tissue sources, SIS and VF dECM, for use as an injectable VF biomaterial. This study found that SIS dECM may serve as an alternative tissue source for VF applications due to its reduced batch to batch variability and comparable functional outcomes in terms of neo-ECM deposition by HVFF.

Despite favorable outcomes in terms of neo-ECM deposition, dECM-only hydrogels derived from both SIS and VF exhibited mechanical properties that did not match native VF and exhibited poor stability. In particular, we observed that the majority of soluble collagen was lost from hydrogels over the first three days of a 14-day experiment. While soluble collagen did not comprise the total collagen of the hydrogels, we also observed the hydrogel size decreasing over the culture period. In general, hydrogel contraction alters the structure of the hydrogel by increasing fibril density and provide a favorable environment for myofibroblast activity, leading to a risk of increased fibrosis, demonstrating a need for improved stability in dECM hydrogels.

In Chapter 5, we proposed that improving the stability dECM hydrogels and mimicking the VF mechanical properties through the use of a crosslinked composite would provide a critical benefit for effective VF regeneration. Specifically, the use of tetrazine ligation to create supportive alginate linkages within the dECM hydrogel structure was hypothesized to retain the bioactive and structural features that make dECM favorable for regeneration. This click hydrogel would achieve mechanical properties comparable to the VF and slow degradation without negatively impacting biocompatibility. To evaluate this hypothesis, we carried out a series of tests evaluating mechanical properties, degradability, cell behavior *in vitro*, and *in vivo* biocompatibility.

We demonstrated that the click dECM hydrogels retained an ECM-like structure and achieved mechanical properties characteristic of native human VF. The click hydrogels exhibited slowed degradation by both hydrolysis and enzymatic methods, resisted contraction by encapsulated HVFF, and preferentially stimulated tubule formation by encapsulated human umbilical vein endothelial cells. We confirmed that the click dECM hydrogels were injectable and biocompatible upon *in situ* gelation in a subcutaneous rat model, showing initial formation of a fibrotic capsule followed by integration with surrounding tissue. Throughout these experiments, click SIS



hydrogels generated comparable responses overall to click VF hydrogels. Overall, we validated the potential of SIS and VF-mimicking click composite hydrogels for VF regeneration.

This work is in preparation for submission to ***Biomaterials***:

Mika Brown, Hideaki Okuyama, Ling Li, Jianyu Li, Zhen Yang, Maryam Tabrizian, Nicole YK Li-Jessen. “The Puzzle of Complete Tissue Regeneration: Click Decellularized Extracellular Matrix Hydrogels for Vocal Fold Tissue Engineering.” ***Biomaterials***. (In Preparation) (2024).

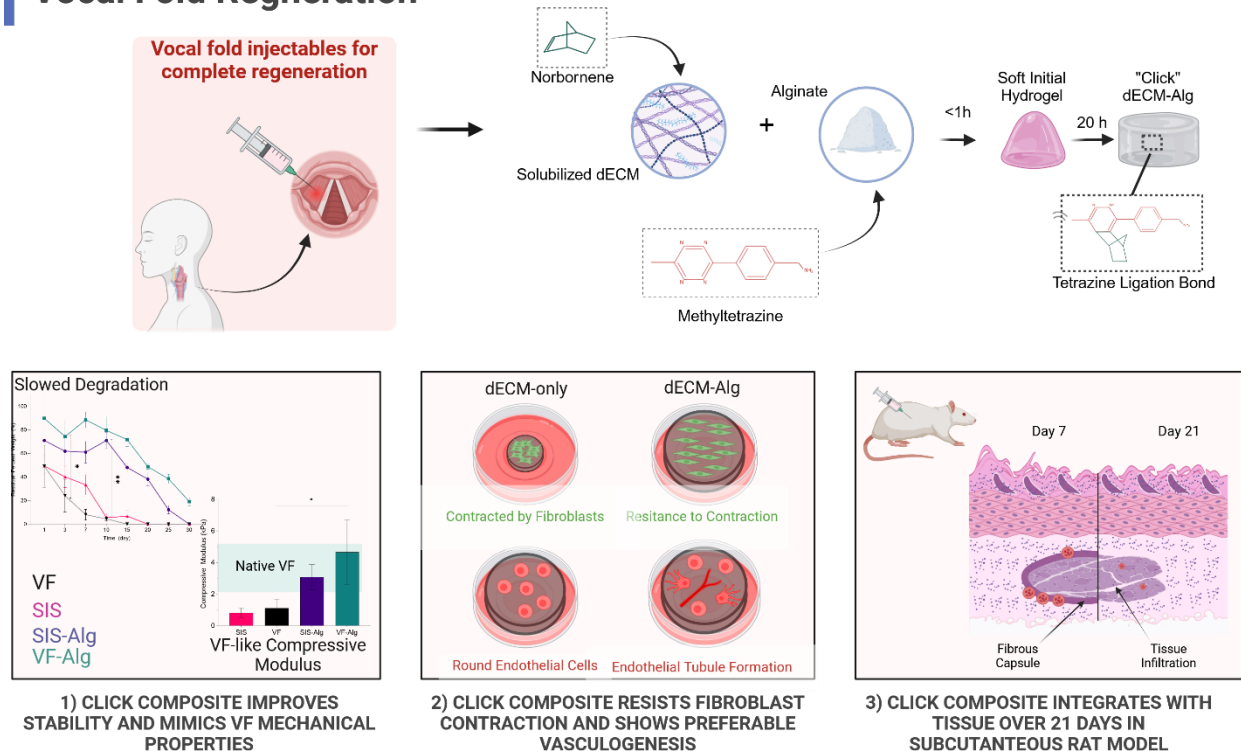
## **Chapter 5. The Puzzle of Complete Tissue Regeneration: Click Decellularized Extracellular Matrix Hydrogels for Vocal Fold Tissue Engineering**

### *Abstract*

Vocal folds are soft tissues in the larynx that vibrate at very high frequencies for sound production. Current vocal fold biomaterial treatments suffer from fast degradation and require frequent re-injection. Decellularized extracellular matrix (dECM) hydrogels are a tissue-derived, injectable biomaterial with intrinsic regenerative capacity. However, dECM hydrogels often exhibit mechanical instability and share the same problems with degradation as existing vocal fold biomaterials. In this work, we developed a composite dECM-alginate hydrogel with bioorthogonal click tetrazine ligation with improved stability, biocompatibility and regenerative capacity. dECM was extracted from two sources: tissue-specific vocal fold mucosa and scalable small intestinal submucosa for comparative analysis. Click dECM hydrogels from both sources were tunable and matched mechanical properties of native human vocal folds. The click dECM hydrogels showed capacity to resist contraction by fibroblasts and stimulate vasculogenesis by endothelial cells. When injected subcutaneously into rats, both gels exhibit a strong initial immune response, followed by integration with the surrounding tissue by day 21. Overall, our click dECM hydrogels showed improved stability over previous dECM hydrogels and their regenerative performance were independent of tissue source.

## Graphical Abstract.

### Click dECM-Alginate Hydrogels for Complete Vocal Fold Regeneration



#### 5.1. Introduction

Human vocal folds (VF) are responsible for voice production and contribute to airway protection, playing vital roles in human health and communication in daily life.<sup>1</sup> As many as 1 in 13 adults annually experience VF disorders in the United States, with only 10% seeking treatment.<sup>2</sup> Severe VF disorders such as sulcus vocalis, VF atrophy and VF scars can result from aging, heavy voice use, or surgical resection, leading to functional disability in speaking, swallowing, or breathing.<sup>3</sup>

Biomaterial injection is commonly used for treating severe VF disorders.<sup>4-8</sup> These injectables serve as primary fillers to augment the bulk of VF and improve its closure for phonation.<sup>5,7,9</sup> Several natural materials have been used routinely in clinics but unpredictable degradation ranging from one month to over a year remains an unresolved challenge.<sup>9,10</sup> For instance, hyaluronan-based Restylane and Juvederm are well tolerated in 97% of patients but efficacy varies from 3-9 months.<sup>11-13</sup> Autologous fat is subject to unpredictable resorption by 20-60% within 2 months and can cause inflammation and necrosis.<sup>5,13-15</sup> Calcium hydroxyapatite may last as long as 2 years but

may form deposits in the lamina propria that impede VF function or cause deleterious inflammation.<sup>16,17</sup>

Unpredictable outcomes and disruption of the LP result in substantial time and financial costs for the healthcare system and in severe cases, life-threatening inflammatory responses may require emergency surgery.<sup>14,17,18</sup> To address these challenges, we sought to develop a biocompatible, injectable hydrogel that would match the mechanical properties of VF mucosa as a short-term filler while possessing bioactivity for effective tissue regeneration in the longer term. In particular, we focused on leveraging the technology of decellularized extracellular matrix (dECM), which has been shown to provide substantial benefits for tissue regeneration in skin, tendon, bone, and muscle in the clinic.<sup>19</sup> Promising results have been achieved with dECM for VF applications in preclinical models.<sup>20-22</sup>

dECM is a natural biomaterial derived from human or animal tissue by removing the immunogenic cells.<sup>23</sup> dECM retains the host tissue's ECM proteins, polysaccharides and membrane-bound biomolecules that circumvent the need for exogenous factors to induce vascularization and tissue regeneration.<sup>23-26</sup> Manufacturing VF-specific dECM at the commercial scale is almost impossible because only minute amounts of matrix can be derived from the small size of VF. On the other hand, porcine Small Intestinal Submucosa (SIS) enables generation of a larger volume of material from a single batch for testing and gel production. SIS has already been used in a variety of applications including skin, muscle, cardiac, gastrointestinal, and VF regeneration.<sup>23</sup>

In our previous work, we compared the proteomic composition of dECM from VF and SIS sources and analyzed their ability to stimulate neo-ECM deposition by human vocal fold fibroblasts (HVFF).<sup>27</sup> While VF dECM proteins had greater overlap with native VF, SIS had less cross-sample variability and comparable quantities of neo-ECM molecules were deposited on both hydrogels.<sup>27</sup> Based on these results, we concluded that continuing the comparison of SIS to VF dECM could provide evidence for the use of SIS dECM in VF applications.

Beyond the issue of scale up in manufacturing, the mechanical instability and rapid degradation of dECM hydrogels remain major challenges in dECM biomaterial design. For instance, previously reported VF dECM hydrogels possess Young's moduli of 120-180 Pa, which were significantly lower than that of physiological range (1-14 kPa).<sup>20,28</sup> dECM-only hydrogels from soft tissues also

degrade rapidly *in vivo* without achieving complete regeneration, falling short of the goal of repairing defects in a single treatment.<sup>22,29</sup>

Composites, a mixture of two or more distinct materials, can be used to grant mechanical tunability and improve stability of dECM hydrogels, resulting in more precise control over interactions between the scaffold and surrounding tissue.<sup>24</sup> Alginate is a favorable composite materials for VF injectables because it is highly biocompatible, mechanically tunable, and degrades slowly *in vivo*.<sup>30,31</sup> These effects can lengthen the retention of ECM-derived biomaterials in the VF and better enable regeneration.

Click chemistry is an advantageous method for fabricating composites for *in situ* gelling injectables. Click chemistry allows stereospecific and chemoselective reactions with high product yield.<sup>32</sup> Compared to traditional crosslinkers like carbodiimides, bioorthogonal click chemistry can be performed *in vivo* without cytotoxic effects.<sup>33-35</sup> Click chemistry with Thiol-Michael and Strain-promoted Azide-Alkyne Cycloaddition (SPAAC) reactions have been used to fabricate several hyaluronan-based VF injectables, though these reactions require catalysts that may cause side reactions and have low yield, respectively.<sup>36-43</sup> Tetrazine ligation through inverse electron demand Diels-Alder cycloaddition is a click reaction between tetrazines and strained alkenes that does not require a catalyst and produces only non-toxic nitrogen gas as a side product. Tetrazine ligation has thus far only been applied to engineer an *in vitro* model of studying VF mucosa maturation by manipulating the stiffness of HA-based hydrogels.<sup>44</sup>

In this study, we proposed to develop a click dECM-alginate composite hydrogel from both VF dECM and SIS dECM sources. We first comprehensively characterized the properties of the click dECM hydrogels in comparison to dECM-only controls in terms of gelation rate, mechanical properties, and stability. *In vitro* testing was then used to confirm the cytocompatibility of the click dECM hydrogels and characterize their potential regenerative capacity. An *in vivo* biocompatibility study was performed to assess the local immune response, particularly in terms of fibrotic capsule formation and macrophage polarization, in a rat subcutaneous model. This work validated the use of a biocompatible click dECM composite that can mimic VF mechanical properties and improve the stability of ECM-based hydrogels, as well as the potential use of SIS dECM as a clinically relevant, scalable substitute for tissue-specific VF dECM. Specific design targets and parameters

as well as respective characterization methods of this novel click dECM hydrogel system are summarized in **Supplementary Table 1**.

## 5.2. Results

### 5.2.1. Click Chemistry Enables the Synthesis of dECM Hydrogels

Click dECM hydrogels were fabricated using tetrazine ligation between norbornene (Nb) and methyltetrazine (MTz) (**Figure 1A**). SIS and VF dECM were functionalized with Nb-N-hydroxysuccinimide (NHS).<sup>45</sup> Functionalization was confirmed in both SIS-Nb and VF-Nb samples using solid state <sup>13</sup>C NMR, with norbornene peaks identified at 130, 140, and 155 ppm (**Figure S1**). These peaks were preserved in the functionalized dECM following ethylene oxide sterilization. Fluoraldehyde assay showed no significant differences in the degree of substitution (DOS) between dECM types (SIS-Nb:  $26 \pm 6.6\%$  v/s VF-Nb:  $31 \pm 12\%$ ,  $p = 0.19$ ), confirming comparable amine substitution for both dECM sources.

For the functionalization of alginate, methyltetrazine amine was substituted to the carboxyl groups to form alginate-methyltetrazine (Alg-Tz) via carbodiimide chemistry.<sup>46-48</sup> Liquid state <sup>1</sup>H NMR confirmed the presence of methyltetrazine peaks to the spectra of Alg-Tz at 7.5 and 8.5 ppm, and the DOS was between 12% and 15% (**Figure S2**).

Click SIS-Alg and VF-Alg hydrogels were formed by mixing 2% dECM-Nb and 2% Alg-Tz solutions at a 4:1 ratio at 37 °C. Gelation kinetics were determined based on the turbidity, or cloudiness, of the solution, which increases during fibrillogenesis (**Figure 1B**).<sup>49,50</sup> SIS-Alg hydrogels took about 24 min to reach 50% gelation while the other three (VF-Alg, SIS-only, and VF-only) took less time, between 11 and 13 min on average (**Table 1**). To reach 95% gelation, the average required time was significantly shorter for gels derived from VF (VF-only: 16 min, VF-Alg: 23 min) than SIS-Alg (68 min) but comparable with SIS-only gels (52 min).

In contrast to dECM-only hydrogels, both SIS-Alg and VF-Alg continued stiffening over a longer period as the click reaction proceeded, crosslinking alginate to the dECM network. This observation was supported by spectral transmittance analysis of tetrazine and norbornene powders, in which the tetrazine peak progressively decreased in size over 12 hours and was absent at the 24 h time point (**Figure S3**).

### 5.2.2. Click dECM Hydrogels Mimic the Mechanical Properties of Native Vocal Folds

The mechanically active nature of VF creates a need for biomaterials capable of mimicking the native tissue's mechanical properties and withstanding repetitive mechanical loading. We performed rheological time sweeps over 20 h to confirm gelation kinetics and determine the plateau storage modulus ( $G'$ ) of the hydrogels as tetrazine ligation goes to completion in the click hydrogels (**Table 1 and S2, Figure 1C**). For all sample types, the storage modulus was greater than the loss modulus throughout the testing period. The storage modulus plateaued in less than 30 min for SIS-only ( $142 \pm 76$  Pa) and VF-only gels ( $150 \pm 40$  Pa). Interestingly, the storage moduli of SIS-Alg ( $860 \pm 355$  Pa) and VF-Alg gels ( $1129 \pm 227$  Pa) continued to increase, reaching a significantly greater plateau value around the 16 h mark. In terms of stiffness, the average plateau storage moduli of all hydrogels were within the range of native VF, between 0.3 – 1.2 kPa.

Amplitude sweeps were performed to determine the yield point – the strain that the hydrogel can withstand without destroying the structure, or the limit of linear behavior (**Figure 1D**). All four hydrogels exhibited similar yield points that were greater than or equal to 7%. The linear viscoelastic region of native human VF by amplitude sweep is 3-7%, above which the VF adopt a nonlinear regime.<sup>45,46</sup> As such, our gels likely withstand shear strains generated from daily phonation.

Atomic force nanoindentation microscopy was used to measure the microscale Young's modulus of the hydrogels (**Figure 1E**).<sup>51,52</sup> For dECM-only samples, the Young's modulus of SIS-only and VF-only hydrogels were not significantly different ( $59 \pm 50$  Pa vs.  $39 \pm 25$  Pa). Click crosslinking significantly increased the Young's modulus to  $1045 \pm 841$  Pa for SIS-Alg and  $1508 \pm 1032$  Pa for VF-Alg, which were, again, within the range of healthy native VF, i.e., between 500 Pa and 6000 Pa.<sup>53,54</sup>

To measure the bulk response to loads, hydrogel samples with 1.5 cm diameter and 1.2 mm thickness were compressed at a rate of 0.02 mm/s (**Figure 1F**).<sup>55</sup> Compressive moduli were calculated from the linear region of the stress-strain curve, between 0 and 10% strain. The compressive moduli of VF and SIS-only samples were similar,  $1.1 \pm 0.58$  kPa and  $0.82 \pm 0.30$  kPa respectively ( $p = 0.92$ ). VF-Alg hydrogels exhibited significantly greater compressive moduli than dECM-only samples ( $p < 0.05$ ), similar to that of SIS-Alg ( $4.6 \pm 2.0$  kPa vs.  $3.1 \pm 0.79$  kPa,  $p = 0.31$ ) The compressive modulus of the VF-Alg hydrogel was in the range of the native VF medial

surface cover's compressive modulus (3.9-5.4 KPa), while SIS-Alg hydrogels were in the range of the superior surface cover (2.7-3.2 kPa).<sup>56</sup>

Cyclic stress-relaxation and recovery tests were also performed, alternating between 5% strain, which normal VF may be expected to withstand, and recovery at 0.01% strain (**Figure 1G**).<sup>57</sup> The relaxation time for VF-only hydrogels (8.2-10.2 s) was significantly less than SIS-Alg (11.6-12.4 s) and VF-Alg (10.2-11.6 s) for several intermediary cycles, but not across all cycles (**Figure S4A**). In samples with similar relaxation times, stress relaxation amplitude has been shown to modulate cellular behavior. Stress relaxation amplitude was significantly greater for SIS-Alg (4.5-8.4 Pa) and SIS-only hydrogels (2.7-4.3 Pa), compared to VF-only hydrogels (0.37-1.2 Pa) at all six cycles (**Figure S4B**). VF-Alg showed significant greater amplitude (3.6-7.9 Pa) than VF-only hydrogels at cycles for the final four cycles.

Based on these mechanical evaluations, the click dECM hydrogels showed mechanical properties including Young's modulus, compressive modulus, and response to strain that were comparable to native VF on a micro- and macroscopic level.



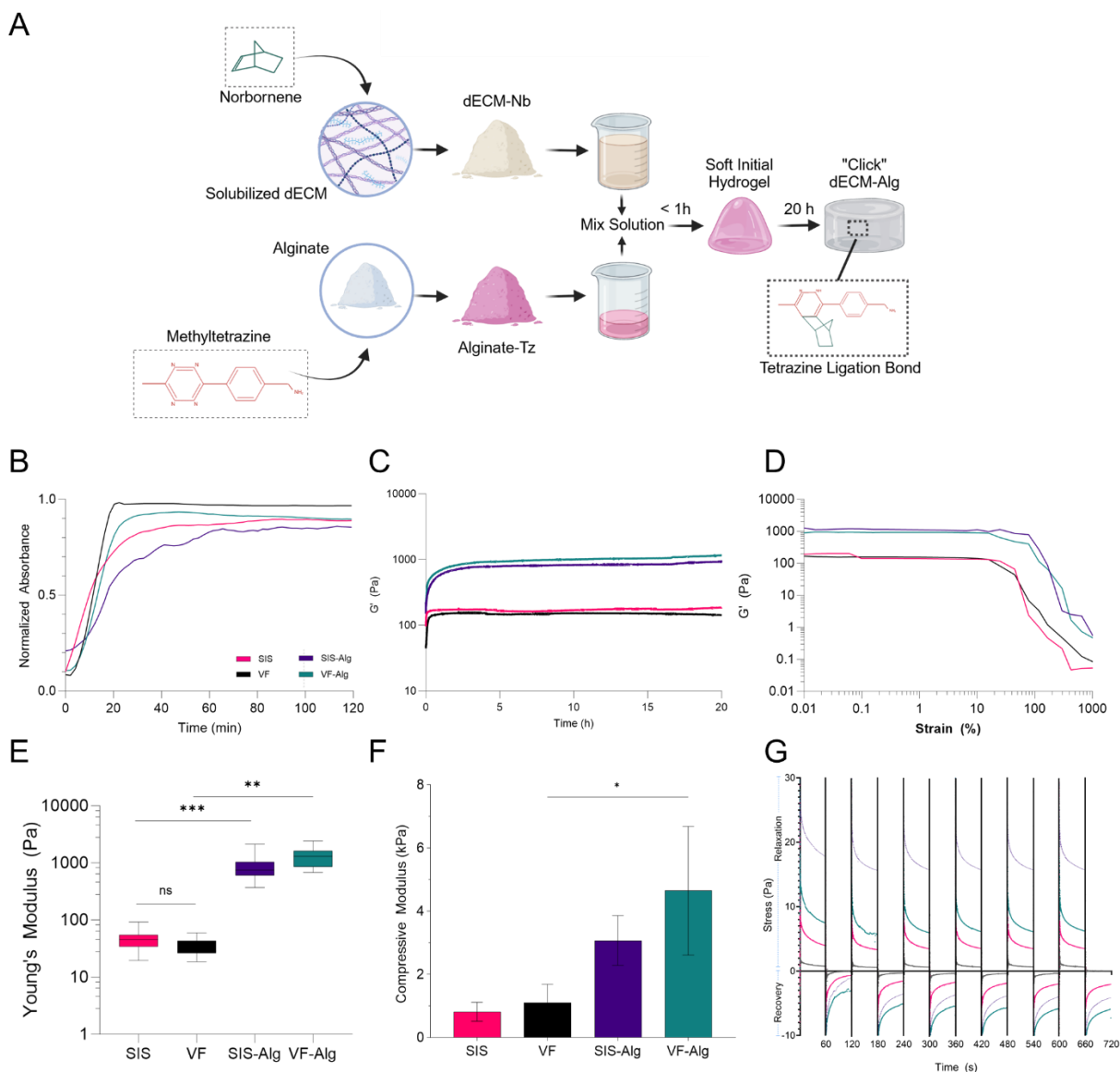


**Figure 1.** Mechanical Characterization of Click dECM-Alginate and dECM-only Hydrogels. **A)** Schematic of dECM-Alg Hydrogel Fabrication Process **B)** Turbidimetric Gelation Kinetics. **C)** Time Dependent Viscoelastic Behavior over 20 h. **D)** Oscillation Amplitude Dependent Viscoelastic Behavior. **E)** Average Young's Moduli by Nanoindentation. **F)** Average Compressive Moduli. **G)** Stress Relaxation and Recovery Tests. Analysis was performed by One-Way ANOVA with post-hoc Tuckey Tests. For D, the log normal transform of the data and Nested ANOVA was used for statistical analysis. For all, ● SIS-only ● VF-only ● SIS-Alg ● VF-Alg.  $p < 0.05$ , \*\* $p < 0.01$ , \*\*\* $p < 0.001$ , \*\*\*\* $p < 0.0001$ , ns is not significant. Error bars represent standard deviation.

**Table 1.** Comparison of Hydrogel Mechanical Properties to Native Human VF.

Property	Human VF	SIS-only	VF-only	SIS-Alg	VF-Alg
<b>Time to Half Gelation (<math>t_{1/2}</math>, min)</b>	-	$12 \pm 10$	$11 \pm 0.8$	$24 \pm 7.9$	$13 \pm 4.3$
<b>Time to 95% gelation (<math>t_{95}</math>, min)</b>	-	$52 \pm 42$	$16 \pm 1.8$	$68 \pm 33$	$23 \pm 8.9$
<b>Lag Time (min)</b>		$3.7 \pm 4.5$	$7.8 \pm 1.2$	$6.3 \pm 2.9$	$9.5 \pm 3.1$
<b>Gelation Rate (S, <math>\text{min}^{-1}</math>)</b>		$2.5 \pm 0.88$	$8.9 \pm 3.4$	$3.5 \pm 1.4$	$4.9 \pm 2.8$
<b>Plateau Storage Modulus (Pa)</b>	300-1200 Pa <sup>58-60</sup>	$199 \pm 110$	$144 \pm 103$	$880 \pm 354$	$1129 \pm 227$
<b>Yield Point (% Strain)</b>	3-7% <sup>61</sup>	$8.7 \pm 1.7$ 95% CI [5.2, 12]	$14 \pm 6.9$ 95% CI [-0.3, 27]	$26 \pm 7.8$ 95% CI [11, 42]	$27 \pm 12$ 95% CI [3.7, 51]
<b>Average Young's Modulus (Pa)</b>	1000-14000 Pa <sup>121</sup>	$59 \pm 50$	$39 \pm 25$	$1045 \pm 841$ Pa	$1508 \pm 1032$ Pa
<b>Average Compressive Modulus (kPa)</b>	Medial Surface Cover: 3900 – 5400 Pa <sup>56</sup> Superior Surface Cover: 2700 – 3200 Pa <sup>56</sup> Muscle: 1300-2700 Pa	$0.8 \pm 0.3$	$1.1 \pm 0.6$	$3.1 \pm 0.8$	$4.6 \pm 2.0$

Statistical comparisons are listed in Table S2.

### 5.2.3. Click Chemistry with Alginate Improves the Stability of dECM Hydrogels

Stability of click hydrogels and dECM-only hydrogels was assessed under hydrolytic and enzymatic degradation conditions up to 30 days (**Figure 2A-B**, **Table S3-S4**). Under hydrolytic conditions, dECM-only samples lost ~50% of their original mass on day 1 and continued to slowly degrade over the 30-day experiment. The significant initial drop-off was not observed for click dECM hydrogels. Under enzymatic conditions with collagenase, dECM-only gels lost their mass and structural integrity progressively and completely dissolved around day 15 (VF-only) and 20 (SIS-only). In contrast, click hydrogels showed significantly slower degradation. On day 30, trace amounts of SIS-Alg remained, while VF-Alg retained 15-22% weight.

Scanning electron microscopy was performed on cross sections of the hydrogels to visualize how the structure changed over time during the degradation experiment (**Figure 2C**). At day 0, all hydrogels possessed porous network structures upon gelation. Under hydrolytic conditions, SIS-

Alg and VF-Alg hydrogels largely maintained their structure over 20 days without a significant increase in pore density. (**Figure 2D**). In SIS-only and VF-only hydrogels, the structure loosened with many individual fibers becoming visible over 20 days and a significant increase in the number of pores, indicative of the loss of material to solution. Under enzymatic degradation, these two hydrogels also had a significantly greater number of pores than click dECM hydrogels on day 7.

Compared to hydrolytic degradation, degradation tests using collagenase induced greater structural changes in click dECM hydrogels. The hydrogel structure of SIS-Alg and VF-Alg gels showed a structural deterioration by day 20 with a corresponding significant increase in the number of pores.

The improved physical stability of click dECM hydrogels over dECM-only hydrogels was further supported by their resistance to contractile fibroblasts. SIS-Alg, VF-Alg, and SIS-only gels encapsulated with human vocal fold fibroblasts (HVFF) showed more than 90% viability across 14 days. A significant increase in cell number was observed in SIS-Alg hydrogels from day 1 to 3, and VF-only hydrogels from day 1 to 7. The viability of HVFF in VF-only maintained ~80% at the end point of the study (**Figure 3A and B**). On day 14, both dECM-only hydrogels no longer covered the entire confocal imaging area of  $1800 \times 1800 \mu\text{m}^2$ , indicating contraction over the culture period (**Figure 3A**).

Scanning Electron Microscopy was used to evaluate the HVFF morphology (**Figure 3C**). In day 1 samples, HVFF displayed a predominantly round morphology in all samples. From day 3 onwards, cells displayed elongated fibroblast morphology, i.e., presumed contractile phenotypes, for all sample types. While the VF and SIS-only hydrogels exhibited up to 90% contraction by day 14, click dECM hydrogels did not visibly contract (**Figure 3D**).

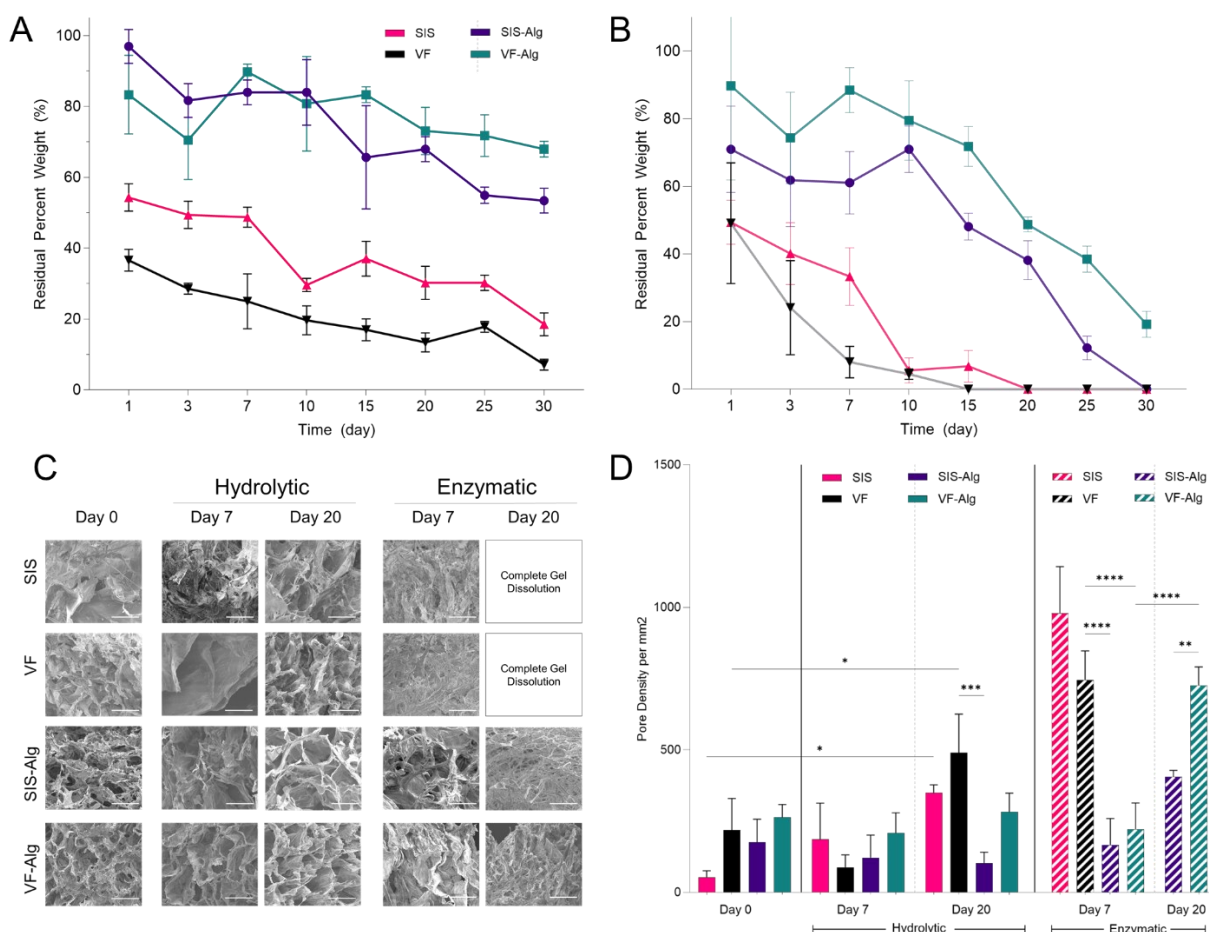


**Figure 2.** Click dECM and dECM-only Hydrogel Viability, Stability, and Degradation **A)** Hydrolytic degradation of hydrogels in PBS over 30 days. **B)** Enzymatic degradation of hydrogels in PBS with 2 U/mL collagenase over 30 days.  $\blacktriangle$  SIS-only  $\blacktriangledown$  VF-only  $\bullet$  SIS-Alg  $\blacksquare$  VF-Alg. **C)** Structure of hydrogels degraded in PBS and collagenase over 30 days at 500X magnification. Scale bar: 50  $\mu$ m. **D)** Pore density per micron squared quantified from SEM images at 100X and 500X.  $\bullet$  SIS-only  $\bullet$  VF-only  $\bullet$  SIS-Alg  $\bullet$  VF-Alg. Solid bars represent hydrolytic degradation, striped represent enzymatic degradation. \* $p < 0.05$ , \*\*\* $p < 0.001$ , \*\*\*\* $p < 0.0001$ . Error bars represent standard deviation.

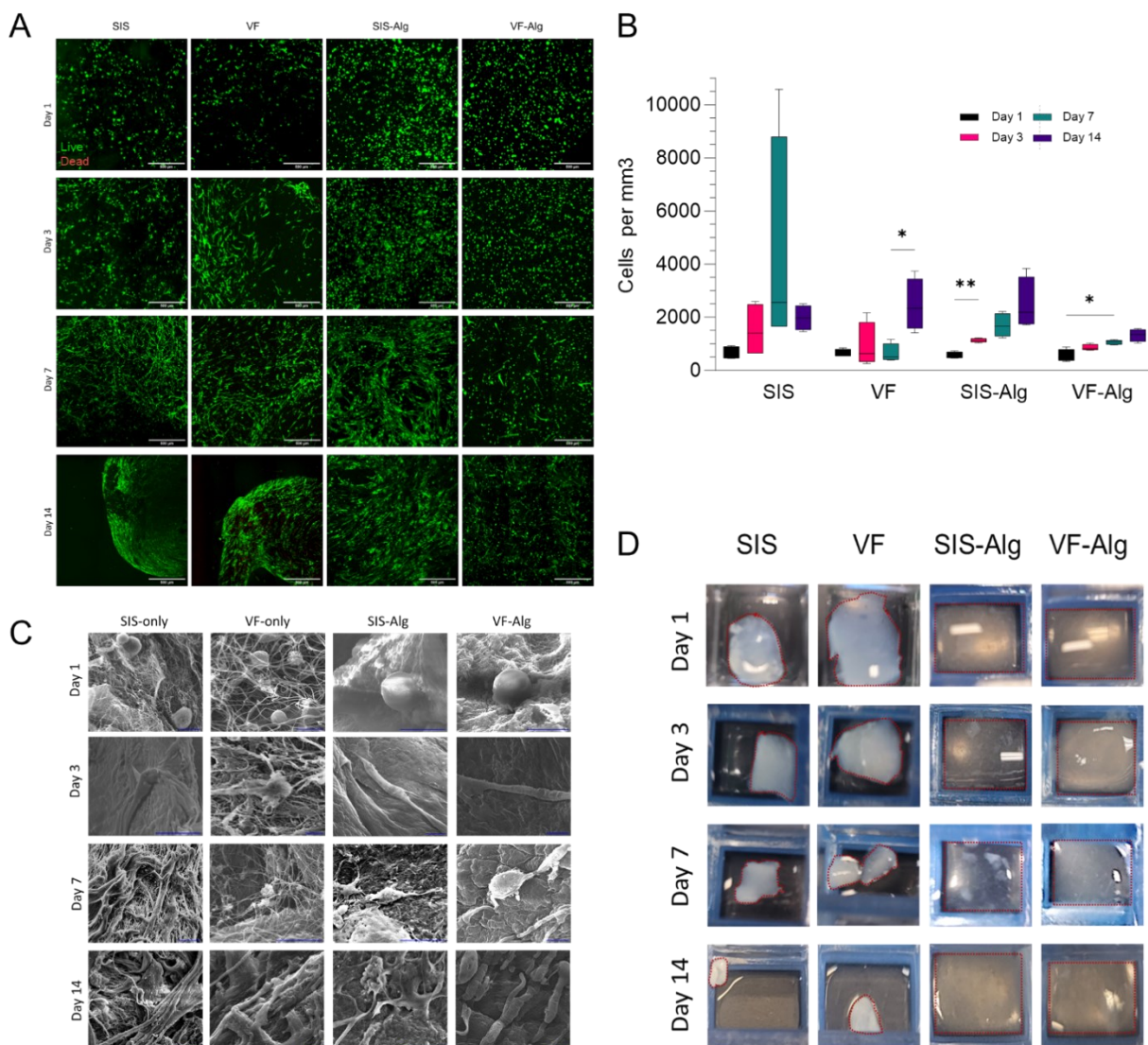


**Figure 3.** Click dECM and dECM-only Hydrogel Viability, Stability, and Degradation **A)** Live/Dead Viability/Toxicity of HVFF. 10X Magnification, Scale Bar: 200  $\mu$ m. ● Live ● Dead **B)** Count of Live HVFF per millimeter squared. **C)** Cellular Morphology of HVFF by SEM. Scale Bar = 5  $\mu$ m. **D)** Contraction of Hydrogels by HVFF. ● Day 1 ● Day 3 ● Day 7 ● Day 14. \* $p < 0.05$ , \*\*\* $p < 0.001$ , \*\*\*\* $p < 0.0001$ . Error bars represent standard deviation.

#### 5.2.4 Click dECM Hydrogels Stimulate Vasculogenesis over dECM-only Hydrogels

Culture experiments with human umbilical vein endothelial cells (HUVECs) were used to evaluate the intrinsic capacity of the gels in vasculogenesis, or the formation of de novo blood vessels, and angiogenesis, or the sprouting of new blood vessels. In addition to dECM gels, collagen gels were

included in this experiment because collagen is commonly used in vascularization studies, including as a control for dECM-based biomaterials.<sup>62,63</sup>

Vascular endothelial growth factor (VEGF) is a key regulator of blood vessel formation and is typically added to media as an exogenous factor to stimulate sprouting by endothelial cells.<sup>64-67</sup> To test whether the gels have innate vasculogenic capacity, encapsulated HUVECs were cultured in standard Endothelial Growth Medium (EGM-2) medium (+VEGF) or in EGM-2 without VEGF (-VEGF).

On day 3, HUVECs in click dECM and collagen hydrogels began to change from a round to elongated morphology, which is an indicator of blood vessel formation.<sup>68</sup> By day 14, network-like structures were observed in both click dECM hydrogels and the collagen control, with or without VEGF (**Figure 4A**). In contrast, dECM-only hydrogels formed only short linkages between adjacent cells in both +VEGF and -VEGF conditions.

Quantitative analysis on the number and length of tubule-like structures (in tubules/mm<sup>3</sup>) showed the effect of VEGF was minimal across sample types but click gels seem to stimulate the formation of tubule-like structures (**Figure S5**). On day 14 under -VEGF conditions, the total number of tubules in both click gels (SIS-Alg: -VEGF 653 ± 380; VF-Alg: -VEGF 803 ± 211) were comparable to collagen -VEGF: 807 ± 495) but significantly greater than dECM-only gels (SIS-only: -VEGF 54 ± 36; VF-only: -VEGF: 59 ± 15) (**Figure 4B**).

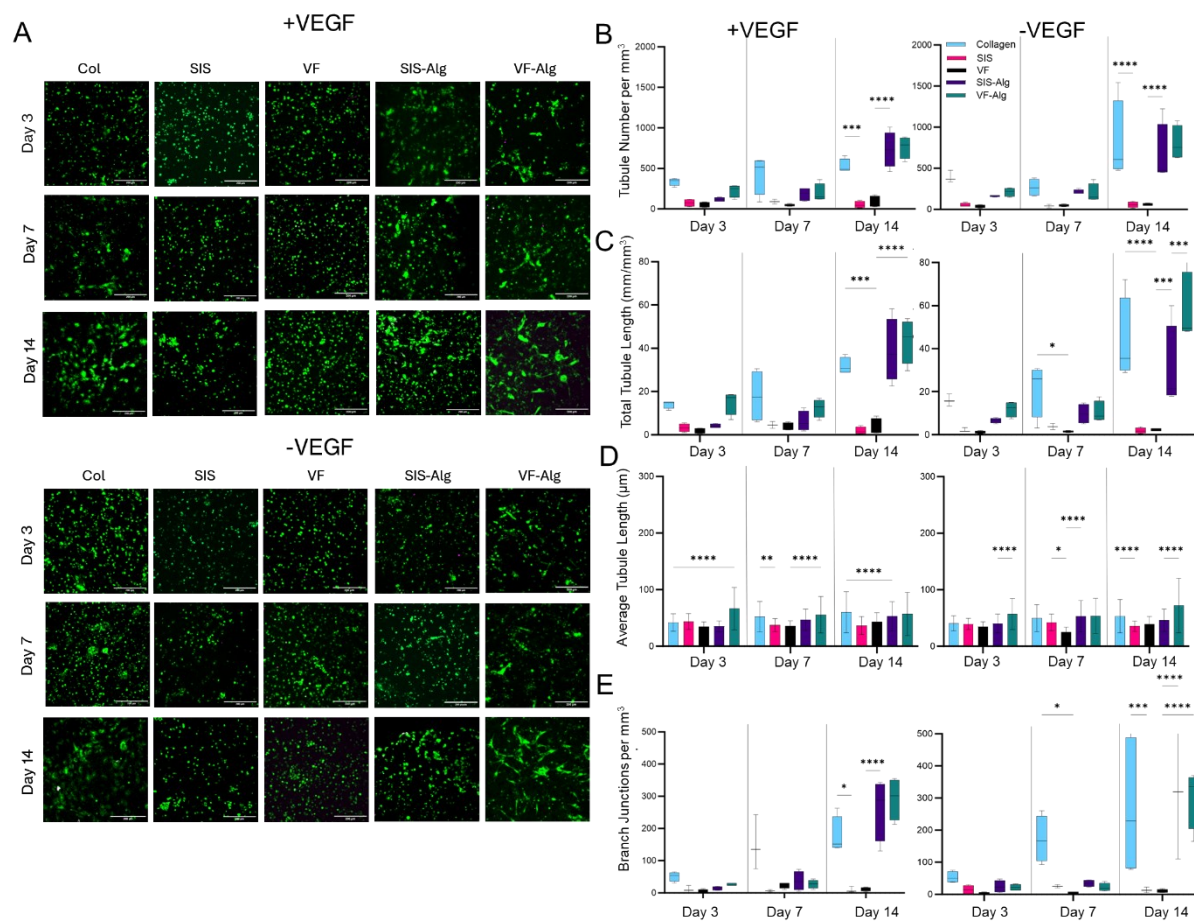
Significant differences in total tubule length (mm/mm<sup>3</sup>) were observed between click dECM and collagen hydrogels in comparison to dECM-only hydrogels on day 14 (**Figure 4C**). On day 14 under -VEGF conditions, the total tubule length in both click gels (VF-Alg: 58 ± 18; SIS-Alg: 30 ± 20) were comparable to the total tubule length in collagen gels (43 ± 20) and significantly greater than dECM-only gels (SIS-only: 1.9 ± 1.4; VF-only: 2.3 ± 0.6).

Regarding average tubule length (μm), all samples showed similar length over time, indicating that the network was not highly developed (**Figure 4D**). This result can be attributed to the lack of growth factor supplementation above the standard concentration of EGM-2 in our +VEGF conditions.






Tubule branching is also expected as vessels develop and sprouting occurs off existing vessels.<sup>69</sup> The number of tubule branch junctions (/mm<sup>3</sup>) on day 14 followed the same pattern as tubule



number and total tubule length (**Figure 4E**). For -VEGF conditions, the number of branch junctions in click dECM gels (VF-Alg:  $301 \pm 93$ ; SIS-Alg:  $319 \pm 295$ ) were not significantly different from collagen controls ( $266 \pm 220$ ). The click dECM and collagen hydrogels likewise contained a significantly greater number of branch junctions than dECM-only gels (SIS-only:  $13 \pm 8.8$ ; VF-only:  $10 \pm 5.4$ ). Together, these results provide quantitative evidence for the preferential formation of tubule-like structures by HUVECs in click dECM hydrogels over dECM-only hydrogels.



**Figure 4.** Vasculogenesis in Click dECM and dECM-only Hydrogels. **A)** Live/Dead Viability/Cytotoxicity of encapsulated HUVECs over 14 days in EGM-2 medium with and without VEGF. ● Live ● Dead 10X Magnification, Scale Bar: 200 μm. **B)** Tubule number per cubic millimeter. **C)** Total Tubule Length. **D)** Average Tubule Length. **E)** Number of Branch Junctions per cubic

millimeter.  Collagen  SIS-only  VF-only  SIS-Alg  VF-Alg. \* $p < 0.05$ , \*\*\* $p < 0.001$ , \*\*\*\* $p < 0.0001$ . Error bars represent standard deviation.

#### *5.2.5 Click dECM hydrogels form an initial fibrous capsule followed by integrating into surrounding tissue over time*

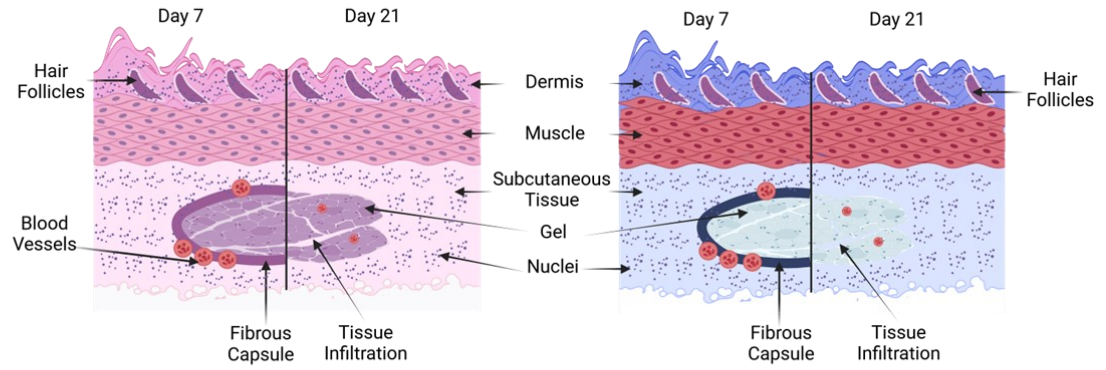
To evaluate in vivo biocompatibility, SIS-Alg, VF-Alg, and PBS were injected into the back of Sprague-Dawley rats. Click dECM hydrogels were identifiable as a lump beneath the skin on day 7. Hydrogels remained visible within the excised tissue on day 21 (**Figure S5**). Staining with Hematoxylin and Eosin (H&E) revealed that the hydrogels were present in all rats after day 7 and 21, except SIS-Alg in one animal at day 21 (**Figure 6A**). This sample was excluded from the subsequent analysis as the gel area could not be identified under the skin. A strong immune response was observed at day 7 for both gels, as indicated by a dense border area with nuclei around the hydrogels. On day 21, the dense cell border was absent, while cells accumulated near the center of the gel area for all click dECM hydrogel samples. The presence of blood vessels clustered around the edges of the hydrogel area was also identified in both click gel samples at day 7, and the presence of capillaries within the hydrogel area at day 21.

Based on Masson's Trichrome (MT) stains, the borders of both click gels consisted of dense collagen, characteristic of a fibrous capsule on day 7 (**Figure 5B**). However, the fibrous capsule was no longer evident around the click dECM hydrogels by day 21, and regions of organized collagenous ECM infiltrated the gel area.

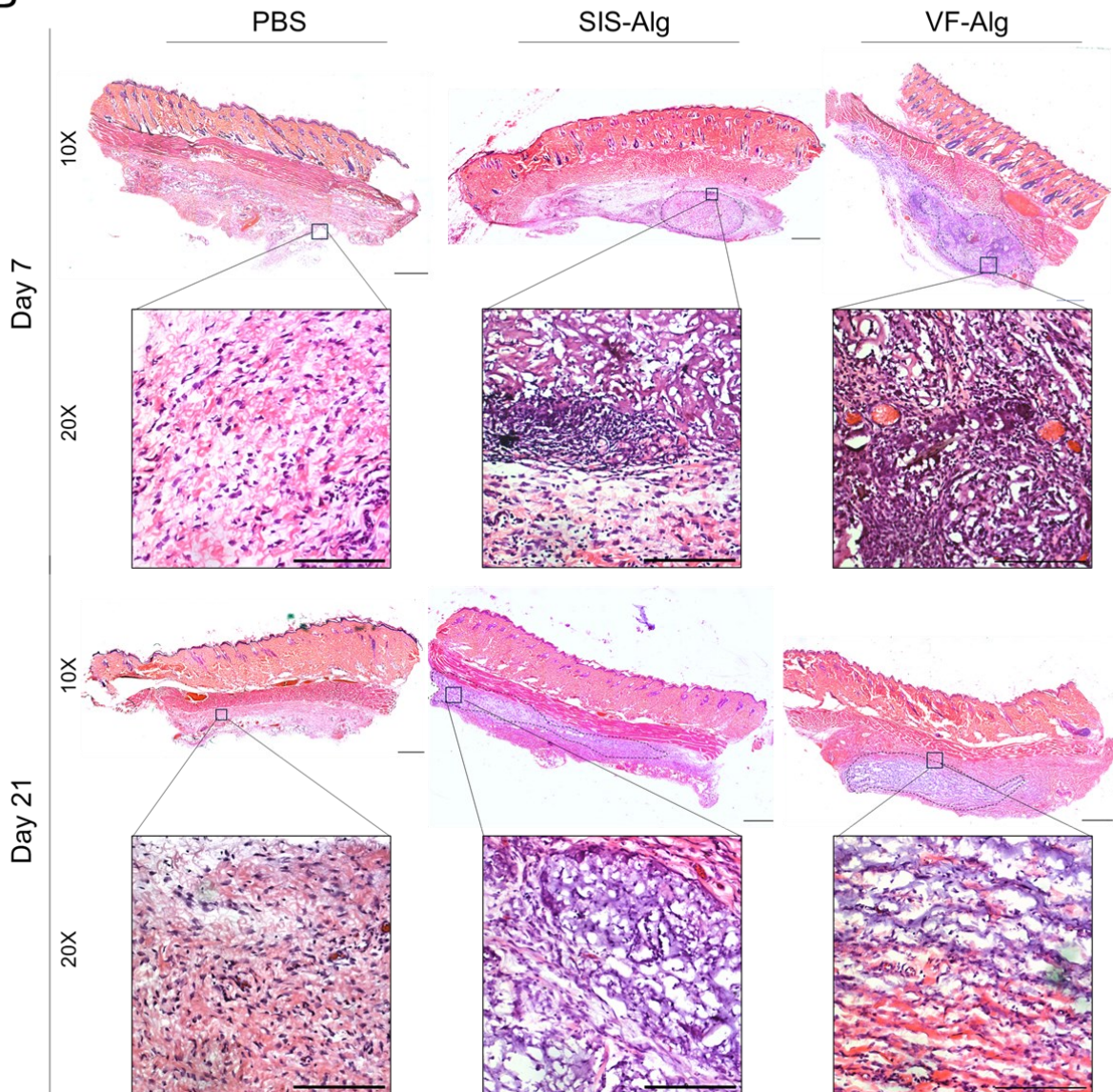
Scanning electron microscopy on cross sections of the hydrogel explants identified distinct borders at the interface between the hydrogel and surrounding subcutaneous tissue (**Figure 6**). The structure of both click gels had a smooth appearance broken up by pores. The day 21 samples showed evidence of the click dECM hydrogels integrating with surrounding tissue, with less defined borders. The interior of SIS-Alg hydrogels adopted a more fibrous structure, while the structure of VF-Alg hydrogels remained more homogenous with some fibrous structures.



**A**



**B**



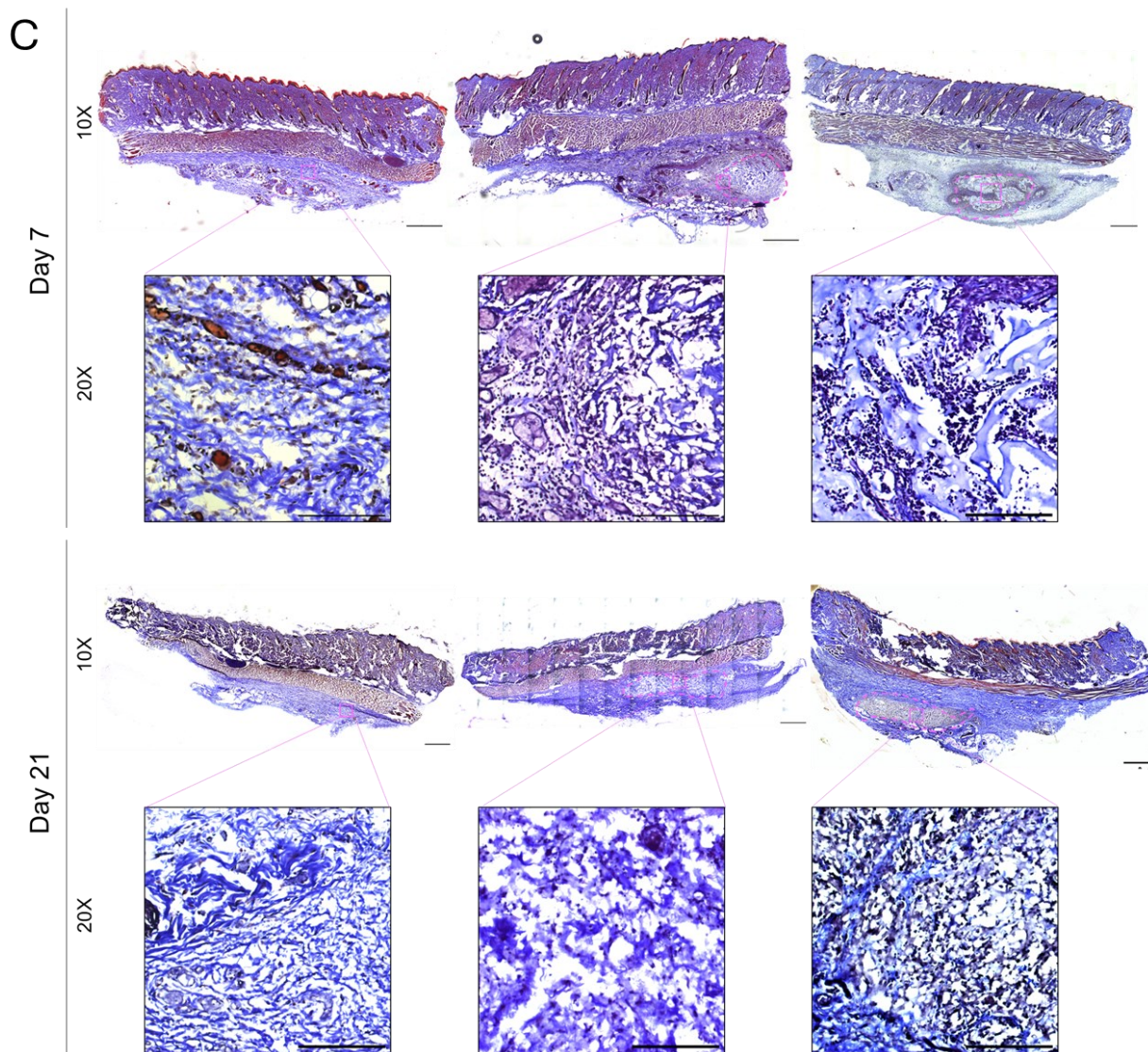


**Figure 5.** Representative Histological Staining of Rat Skin Injected with Click dECM Hydrogels or PBS. **A)** Representative schematic of samples stained with Hematoxylin and Eosin (Left) and Masson's Trichrome (Right) **B)** Hematoxylin and Eosin Stains at 10X, 20X, and 40X magnification. Click dECM hydrogels stained purple due to the presence of alginate. **C)** Masson's Trichrome Stains at 10X, 20X, and 40X magnification. Scale Bars: 10X = 1 mm, 20X = 200  $\mu$ m, 40X = 100  $\mu$ m. Click dECM hydrogels stained a lighter blue than surrounding tissue due to the presence of alginate.



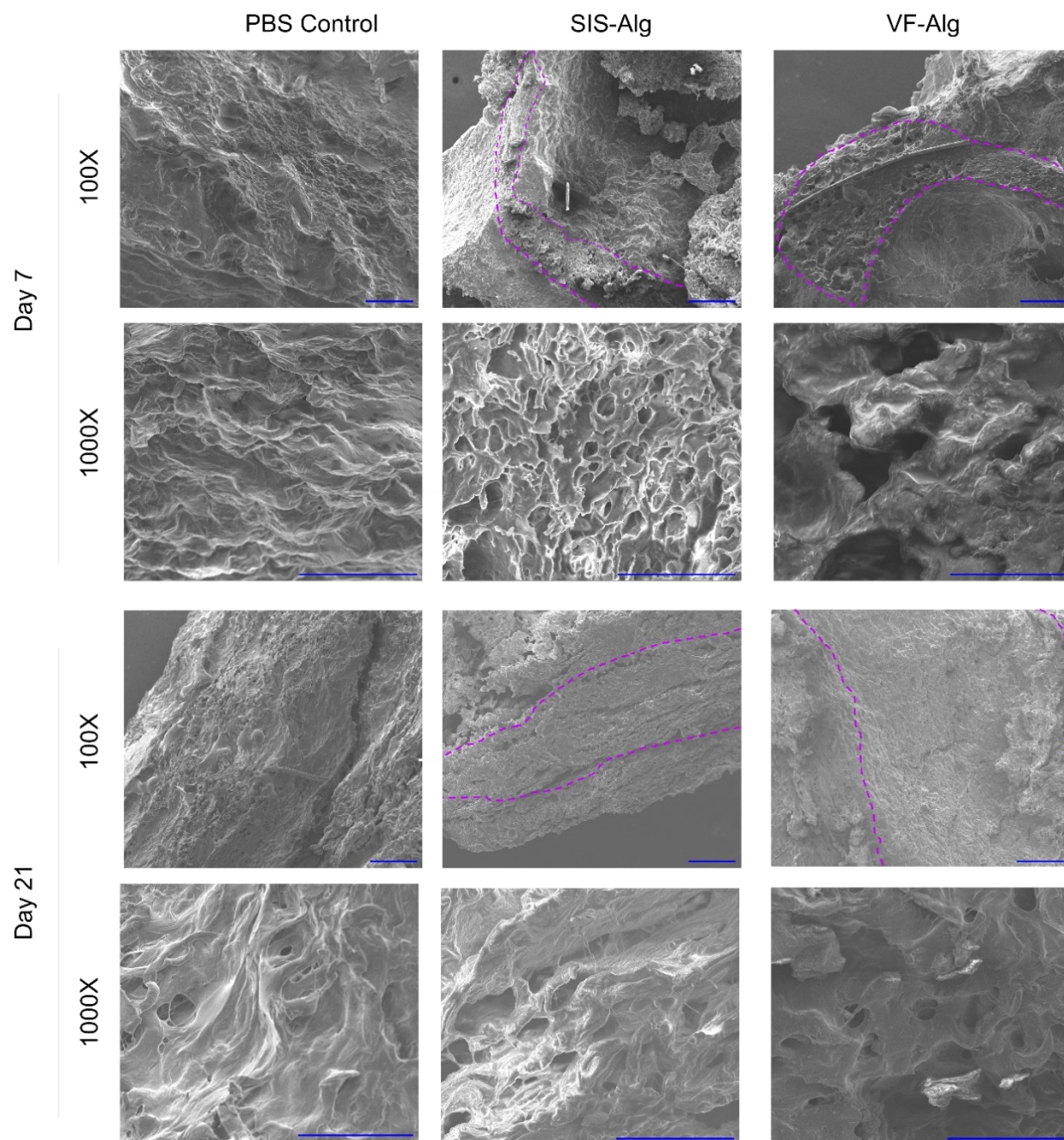


**Figure 6.** Scanning Electron Microscopy on Cross Sections of Click dECM Hydrogels Embedded in Tissue Explants and the PBS Control. 500X magnification, Scale Bar = 50  $\mu$ m. Dotted lines represent the hydrogel borders.

#### *5.2.6. Click dECM hydrogels induce an elevated macrophage response with an M2 response predominating in SIS-Alg hydrogels*

Immunocytochemistry was performed to detect the expression of two macrophage markers, the pan macrophage marker CD68, and M2 macrophage marker CD206 (**Figure 7A-B**). The number of cells per area ( $\text{cells}/\text{mm}^2$ ) were computed within the hydrogel (i.e., interior) and outside the hydrogel border (i.e., exterior). This methodology evaluates the type and quantity of cells infiltration the hydrogel, as well as their impact on surrounding tissue.

Robust clustering of CD68<sup>+</sup> macrophages was observed around the edges and within SIS-Alg hydrogels on Day 7 (interior:  $1410 \pm 896$ , exterior:  $2786 \pm 1262$ ) (**Figure 7C**). A significant decrease in the density of CD68<sup>+</sup> macrophages in the exterior of SIS-Alg hydrogels ( $916 \pm 362$ ) was observed on Day 21. A proportion of macrophages expressing CD206 were found on the exterior and interior of SIS-Alg (interior:  $716 \pm 402$ , exterior:  $1386 \pm 247$ ) (**Figure 7D**). In the exterior of the SIS-Alg hydrogels, a decrease in CD206<sup>+</sup> macrophages was observed from Day 7 to Day 21 ( $530 \pm 199$ ).

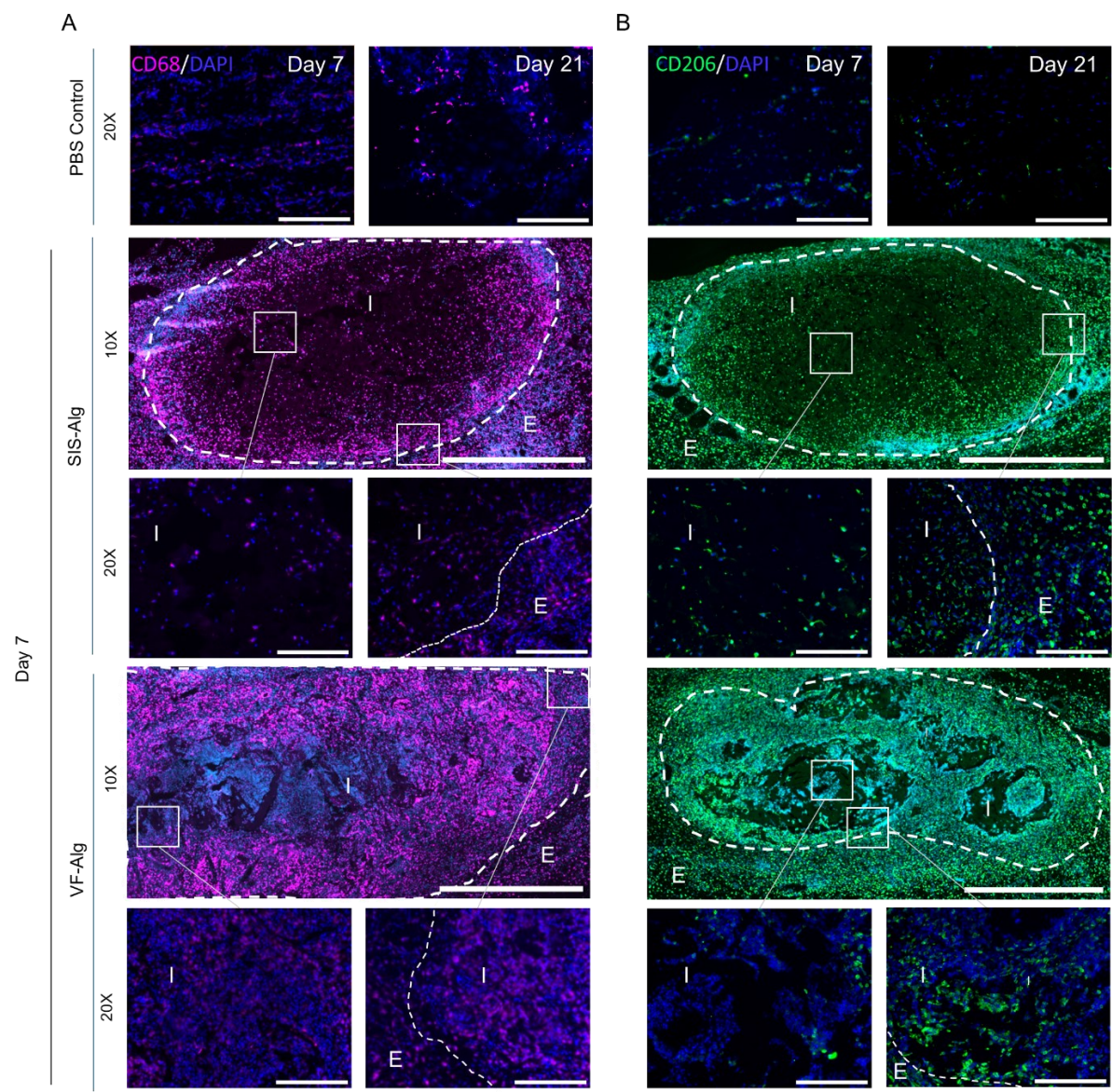
For VF-Alg hydrogels, CD68<sup>+</sup> macrophages were likewise found in the hydrogel interior and clustered around the edges of the hydrogel on Day 7 (interior:  $1967 \pm 787$ , exterior:  $2750 \pm 809$ ). On Day 21, the density of CD68<sup>+</sup> macrophages on the interior and exterior of VF-Alg hydrogels (interior:  $881 \pm 93$ , exterior:  $857 \pm 307$ ) significantly decreased from Day 7. CD206<sup>+</sup> macrophages were also identified on the exterior and interior of VF-Alg (interior:  $732 \pm 421$ , exterior:  $1097 \pm 300$ ). A significant decrease in CD206<sup>+</sup> macrophage density was observed in the exterior of VF-Alg hydrogels on Day 21 ( $351 \pm 154$ ).

For the ratio between CD206<sup>+</sup>/CD68<sup>+</sup> macrophages, the only significant difference was between the PBS control and VF-Alg interior (**Figure 7E**). The average CD206<sup>+</sup>/CD68<sup>+</sup> ratio was approximately 0.6 for both the exterior and interior of SIS-Alg, meaning the majority of macrophages exhibited M2 polarization, while the average ratio for VF-Alg was 0.47 for the exterior and 0.38 for the interior.

The decreases in CD206<sup>+</sup> macrophage density should be taken in context with the corresponding decrease in CD68<sup>+</sup> macrophages. High variability within regions of the same sample and between animals precluded identification of significant differences. However, the mean CD206<sup>+</sup>/CD68<sup>+</sup>

ratio for all SIS-Alg samples remained 0.6 or above on Day 21, while the ratios for VF-Alg samples remained below 0.5.

In comparison to the PBS controls, VF-Alg and SIS-Alg hydrogels showed higher density of CD68<sup>+</sup> (Day 7:  $588 \pm 291$ , Day 21:  $344 \pm 160$ ) and CD206<sup>+</sup> (Day 7:  $348 \pm 124$ , Day 21:  $172 \pm 61$ ) macrophages in both exterior and interior regions, suggesting that the macrophage response remained elevated at the end point of the experiment.





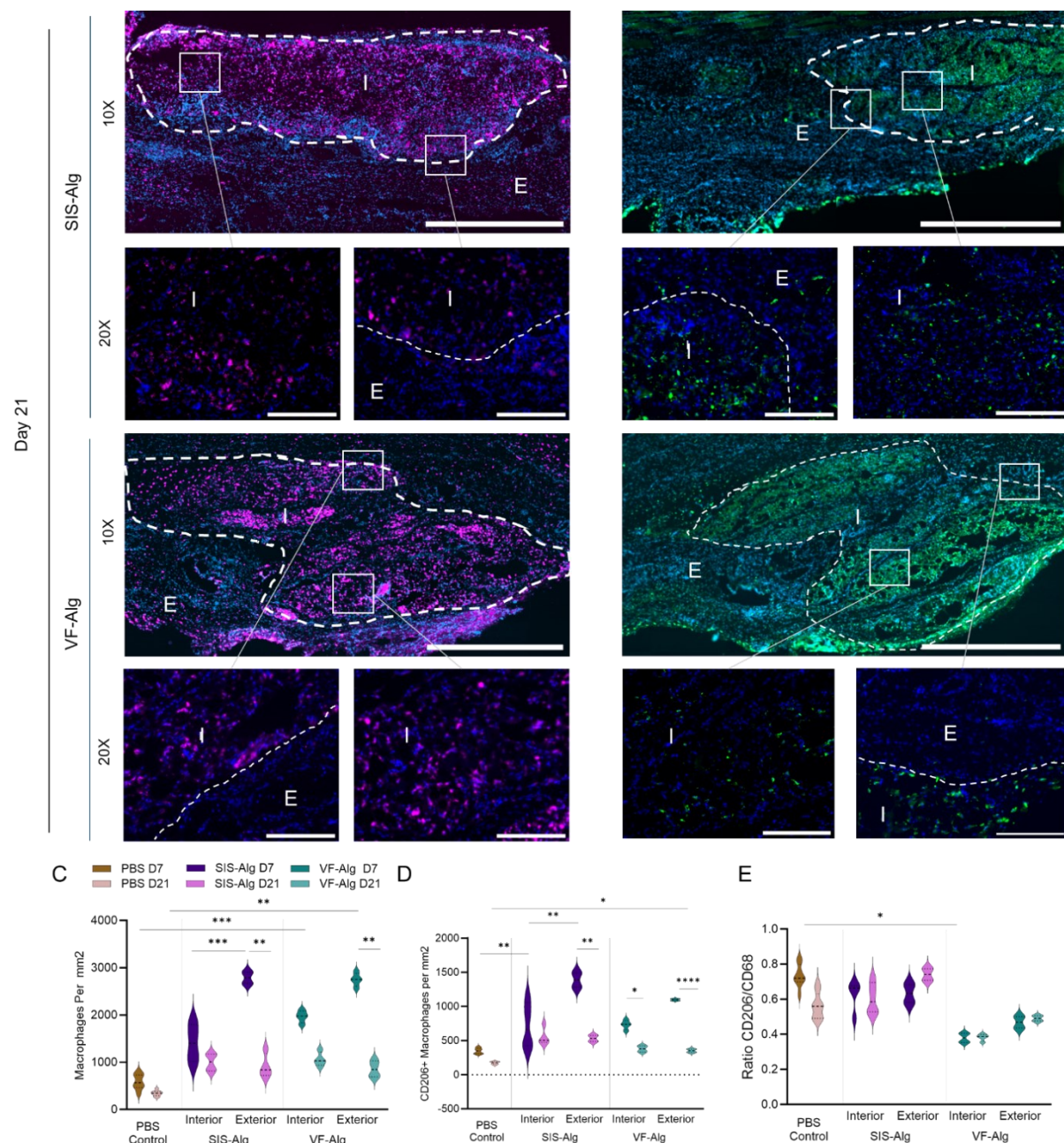


**Figure 7.** Macrophage Infiltration and Polarization in Click dECM Hydrogels in Subcutaneous Rat Tissue. **A)** Immunofluorescence of pan-macrophage marker CD68 at 10X and 20X magnification. ● DAPI ● CD68 **B)** Immunofluorescence of M2 macrophage marker CD206 at 10X and 20X magnification. 20X images show exterior and interior of hydrogel area. ● DAPI ● CD206 **C)** Total macrophages (CD68+) per square millimeter of tissue. **D)** CD206+ macrophages per square millimeter of tissue. **E)** Ratio of CD206+ macrophages to total CD68+ macrophages. E

= Exterior of Hydrogel; I = Interior of Hydrogel. PBS Control ● Day 7 ● Day 21; SIS-Alg ● Day 7 ● Day 21; VF-Alg ● Day 7 ● Day 21. \* $p < 0.05$ , \*\* $p < 0.01$ , \*\*\* $p < 0.001$ , \*\*\*\* $p < 0.0001$ . Error bars represent standard deviation.

#### *5.2.7. Click dECM hydrogels recruit B cells in the initial immune response that decrease in density over time*

To evaluate the B cell response to the click dECM hydrogels, tissue sections were stained with the CD45R isoform B220, a pan-B cell marker (**Figure 8A**). On day 7, B cells were identified at both the interior and exterior of SIS-Alg hydrogels (interior  $223 \pm 240$ , exterior:  $196 \pm 170$ ). B cell density on the interior and exterior of SIS-Alg hydrogels did not significantly decrease from Day 7 to Day 21 (interior:  $141 \pm 71$ , exterior:  $55 \pm 41$ ).

In VF-Alg hydrogels, a high density of B cells were observed on the interior and exterior regions on Day 7 (interior:  $567 \pm 373$ , exterior:  $257 \pm 253$ ). The quantity of B cells on the interior of VF-Alg significantly decreased by day 21 ( $122 \pm 121$ ), while B cells on the exterior did not significantly decrease (interior:  $122 \pm 121$ , exterior:  $54 \pm 33$ ).

Low quantities of B cells (B220+ cells/mm<sup>2</sup>) were identified in PBS control samples (Day 7:  $27 \pm 29$ , Day 21:  $19 \pm 16$ ) and were significantly lower than B cell levels on the interior of SIS-Alg and VF-Alg at both time points (**Figure 8B**). B cell density on the exterior of the click dECM hydrogels was elevated compared to PBS controls on Day 7, and not significantly different from PBS controls on Day 21.

In terms of the total number of nuclei, the density of cells surrounding both click dECM hydrogels was elevated compared to PBS controls on day 7, but equalized on day 21, which is consistent with the disappearance of the fibrous capsule observed in histology (**Figure 8C**). Together, these results indicate that inflammation related to the acute immune response decreased between day 7 to 21 in the region surrounding the click dECM hydrogels but had not yet fully resolved.



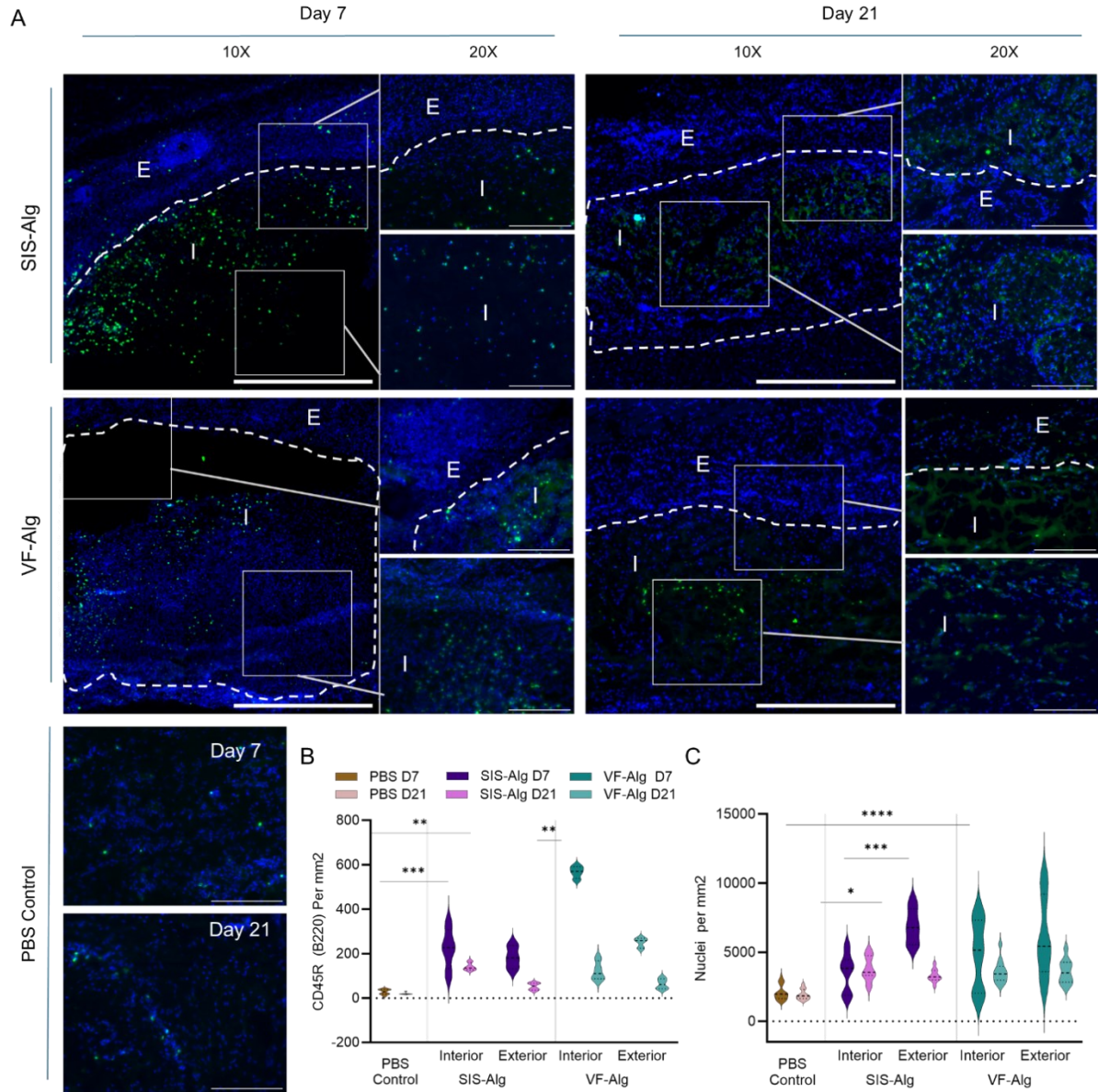


**Figure 8.** B-Cell and Total Cellular Infiltration in Click dECM Hydrogels in Subcutaneous Rat Tissue. **A)** Immunofluorescence of B-Cell marker CD45R/B220 at 10X and 20X magnification. 20X images show exterior and interior of hydrogel area. **B)** B220+ lymphocytes per square millimeter. ● DAPI ● CD45R/B220. **C)** Total Cellular Infiltration determined from the average number of nuclei per square millimeter in all immunofluorescence stains. E = Exterior of Hydrogel; I = Interior of Hydrogel. PBS Control ● Day 7 ● Day 21; SIS-Alg ● Day 7 ● Day 21; VF-Alg ● Day 7 ● Day 21. \* $p < 0.05$ , \*\* $p < 0.01$ , \*\*\* $p < 0.001$ , \*\*\*\* $p < 0.0001$ . Error bars represent standard deviation.

### 5.3. Discussion

The aim of the present study was to develop a novel, injectable dECM hydrogel to overcome the limits of rapid degradation, poor mechanical properties, and lack of scalability of VF-derived dECM hydrogels for VF tissue engineering. Using a click composite with alginate, we developed a click dECM hydrogel with improved stability and mechanical properties that resists contraction by fibroblasts.

#### *5.3.1. Fibrillogenesis followed by bioorthogonal click tetrazine ligation produces hydrogels with ECM-like structure*

Use of tetrazine ligation was selected for the development of the click dECM-Alg hydrogels for its bioorthogonal nature, enabling in situ gelation without toxic byproducts or side reactions with cells. Functionalization of dECM for tetrazine ligation also required selection of reagents to avoid nonspecific reactions. For instance, carbodiimide chemistry is useful in fabricating dECM scaffolds intended for implantation, such as for tailoring the viscoelasticity and Young's modulus of a dECM hydrogel to mimic that of the naïve human ventricle.<sup>70</sup> In conventional carbodiimide chemistry, 1-ethyl-3-(3-dimethylaminopropyl)-carbodiimide hydrochloride (EDC) is used to attach NHS to carboxyl groups, forming an intermediate that reacts with primary amines to form a zero-length amide bond crosslink.<sup>71</sup> However, EDC is not suitable for our functionalization of dECM.

As the primary component of dECM is collagen, which contains both carboxyl groups in aspartic and glutamic acid residues and amine groups in (hydroxy-)lysine residues, conventional carbodiimide chemistry crosslinks dECM to itself.<sup>23,72</sup> The result is a solid material with non-specific substitution that would not be suitable as an injectable, or for reproducible click chemistry with tetrazine. Pre-modification of norbornene with NHS is therefore critical for successful dECM functionalization. Norbornene-NHS enabled the reaction with primary amine groups in dECM without exposing dECM to EDC.

For the functionalization of alginate, methyltetrazine amine was substituted to the carboxyl groups using carbodiimide chemistry to form alginate-methyltetrazine (Alg-Tz).<sup>46-48</sup> Methyltetrazine amine is a tetrazine analogue with high aqueous stability, albeit a slow reaction rate with norbornene relative to unmodified tetrazine, by about 15-fold.<sup>46</sup> Spectral transmittance measurements in one study showed that the reaction between hyaluronan functionalized with

norbornene and methylphenyltetrazine goes to completion in 8 h.<sup>73</sup> However, tetrazines that react more rapidly have also been shown to have low aqueous stability, with about 40% or less remaining after 10 h, or even precipitation in under 2 h.<sup>46</sup>

While the slow rate of the click reaction would be a disadvantage if it was the only method of gelation, turbidimetric assay confirmed that SIS-Alg and VF-Alg gelled in an average of 60 min and 30 min, consistent with their respective dECM-only hydrogels. Fibrillogenesis therefore remained the primary method of gelation for the click dECM-Alg hydrogels. The combination of the rheological time sweeps and kinetic spectral transmittance measurements showed that the click tetrazine ligation reaction continued to proceed after initial gel formation, linking supportive alginate bridges within the existing dECM structure. This fabrication methodology resulted in a gel with a microstructure similar to dECM-only hydrogels as confirmed by our SEM imaging, while achieving the VF-like mechanical properties of alginate.

### *5.3.2 Tissue-mimicking mechanical property correlates with functional regeneration*

Stiffness that matches native tissue on both a macro and micro level is favorable for guiding functional wound repair and regeneration.<sup>74</sup> To meet the demands of phonation, VF tissue possesses unique material and structural properties capable of withstanding strong physical contact and deformation.<sup>75-78</sup> Mimicking the microscale Young's modulus and the compressive modulus suggests that our click dECM-Alg hydrogels have potential to withstand the mechanical stress and activity of the native VF.

In general, the microscale Young's modulus reflects the collagen structure and crimping, a pattern of fibril organization that enables stretching in the VF.<sup>53,54</sup> Higher Young's moduli indicate dense collagen packing and fibrosis, while measurements lower than the native range would be expected to exhibit a loose, weak collagen structure and fail to meet the mechanical demands of the VF.<sup>53</sup>

Compression testing measures the material's bulk response to the application of loads, and biomaterials that match the compressive response of VF may aid in limiting further damage to the tissue. In this study, we found that the click composite SIS-Alg and VF-Alg gels better mimicked the native VF compared to the weak properties of VF-only and SIS-only gels with respect to the microscale Young's modulus and compressive modulus.

In materials with the same polymeric composition and approximately equivalent Young's moduli, higher viscoelasticity has been found to enhance cellular migration, spreading, and proliferation.<sup>79-81</sup> Higher stress relaxation amplitude and shorter relaxation times correlate with increased viscoelasticity. Consistency of the stress relaxation response is also important for predicting the cellular response and ability to withstand normal stresses of biomaterials for use in soft tissues that undergo repetitive strains.<sup>57,82</sup> Based on dynamic cyclic stress relaxation testing, SIS-Alg, VF-Alg, and SIS-only hydrogels exhibited an increased stress relaxation amplitude that would be predicted to aid in cellular elongation, migration, and proliferation in 3D hydrogels, and favoring matrix remodeling.<sup>79,80</sup>

In this study, the cyclic stress-relaxation tests were performed at 5% strain, which is within the limit of linear behavior of the VF.<sup>61-83</sup> During phonation, the VF repetitively undergo significantly higher strains as they elongate by up to 50%, exhibit nonlinear behavior, and recover rapidly from this deformation.<sup>28,83</sup> Therefore, the behavior of the click dECM hydrogels under repetitive deformation characteristic of normal human phonation remains to be evaluated in future work.

The chemical crosslinks in the click dECM hydrogels may pose a risk of breaking at high strains, resulting in the loss of mechanical stability.<sup>84,85</sup> However, the physical crosslinks of dECM provide shear-thinning characteristics that may help improve fatigue resistance and enable recovery following application of high strains.<sup>84,86</sup> To aid in further validating the applicability of the click dECM hydrogels for VF applications, large amplitude oscillatory shear rheometry can be used to evaluate the behavior of the click dECM-Alg hydrogels under cyclic conditions of high strain and frequency.<sup>83</sup>

The mechanical properties of a biomaterial may change in response to cellular activity.<sup>39</sup> For instance, the contraction of the dECM-only hydrogels by HVFF would be expected to increase the hydrogel stiffness.<sup>87,88</sup> In this study, mechanical testing on the click dECM hydrogels has only been performed in a cell-free environment, i.e., with no HVFF.

To mechanically test cell-encapsulated materials, AFM with surface mapping is an effective methodology. Future work can focus on assessing the impact of fibroblast activity on hydrogel structure and mechanics over time with relevance to fibrosis. Specifically, AFM with surface mapping is capable of revealing differences in collagen distribution, stiffness, and adhesion properties between samples.<sup>89,90</sup> A particular benefit of AFM is that it can be performed in a

hydrated environment without destroying the sample, enabling analysis of samples containing live cells.<sup>76,91</sup> In future work, the click dECM structure and mechanical properties could be tested using AFM mapping to determine whether the hydrogel properties remain consistent with human VF after culture with HVFF.<sup>89,90</sup>

#### *5.3.3. Resistance to contractility may correspond to improved reliability of injectables*

Gel contraction is typical when fibroblasts are cultured on or encapsulated in collagen-based hydrogels.<sup>87,92,93</sup> High contractility by fibroblasts is associated with the adoption of a myofibroblast phenotype that can result in deposition of disorganized collagen, leading to fibrosis and limiting regeneration of functional tissue. Additionally, existing VF injectables such as autologous fat are frequently over or under injected due to their high swelling ratio and subsequent contraction.<sup>14</sup> Thanks to the higher stiffness achieved by crosslinking, the click dECM hydrogels demonstrated resistance to fibroblast contraction. The combination of increased resistance to degradation and fibroblast contraction as well as increased maintenance of hydrogel structure confirms that click dECM hydrogels exhibit improved stability compared to dECM-only hydrogels.

Vascularization is a necessity for infiltration and maintenance of cells in biomaterials greater than 100-200  $\mu\text{m}$  thick.<sup>67</sup> The VF average 3-6 mm in thickness and are extensively vascularized, with capillaries that are organized with a specific orientation that enables them to withstand vibration without rupture during phonation.<sup>56,94,95</sup> Previous studies have proposed that the innate growth factors of dECM may stimulate vascularization. In our study, click dECM hydrogels provided a preferential environment for vasculogenic tubule formation compared to dECM-only hydrogels but did not show formation of an extensive vessel network. These results indicate a need for in vivo assessment of blood vessels to determine whether supplementation with exogenous growth factors is necessary for vascularization in live VF mucosal tissues.<sup>26</sup>

#### *5.3.4. Click dECM hydrogel stability and cellular infiltration*

One of the goals of the present study was to produce a click dECM hydrogel that degrades at a slower rate than dECM-only hydrogels, an effect that was confirmed from both of *in vitro* degradation and animal study. Notably, the click dECM hydrogels remained present within the rat subcutaneous tissue till the study endpoint, i.e., 21 days.

Reports for the time to complete degradation of dECM-only hydrogels from soft tissue *in vivo* typically vary between 7 days to 3 months, depending on the target tissue, implantation sites, and decellularization method.<sup>22,29,96</sup> For instance, dermal dECM and UBM hydrogels both degraded by day 35 in a rat abdominal wall defect. UBM degraded more rapidly between the two. Likewise, a composite of SIS with gelatin, PLLA, and chitosan degraded significantly by day 14. Only a few small fragments remained in the tissue at day 28.<sup>97,98</sup>

Our animal study further showed that the click dECM hydrogels induced a fibrous capsule after 7 days, but the capsule was absent at 21 days, with signs of integration with surrounding tissue. SIS-only hydrogels have been found to decrease or inhibit fibrous capsule formation.<sup>26</sup> Fibrous capsule formation is typical of alginate hydrogels and may last 8 weeks or more. There are no enzymes present in native tissue capable of digesting alginate, and the breakdown of standard alginate hydrogels formed with calcium ions largely occurs through the loss of ions to the environment.<sup>99</sup> This detrimental effect may be averted by modifying alginate to degrade by partial oxidation of the polymer backbone prior to MTz functionalization, increasing susceptibility to hydrolysis.<sup>47,48</sup> The drawback is that this modification may increase the degradation rate by an undesirable degree. However, given the integration of the click dECM hydrogels with surrounding tissue over time, alginate modification may not be necessary.

The absence of a fibrous capsule on day 21 could be due to continuous tissue remodeling by the local matrix metalloproteinases (MMPs), loosening the hydrogel structure and enabling effective cellular infiltration.<sup>47,48</sup> This observation corresponds with the near-complete degradation of SIS-Alg in our *in vitro* experiments. Similar responses have been observed in other dECM-composite hydrogels, such as dECM and laponite clay for vascular regeneration.<sup>100</sup> The longer retention of alginate as dECM breaks down and neo-ECM is deposited may help support VF mechanical function during the wound healing period.

#### 5.3.5. Click dECM-Alg hydrogels are biocompatible with SIS-Alg exhibiting M2 Polarization

As one of the promoted benefits of click chemistry is its lack of side reactions and toxic byproducts, it was important to evaluate the response of macrophages to the click dECM hydrogels. The pan macrophage population remained elevated in our samples after 21 days, though a significant decrease was observed in the exterior of the hydrogels. Notably, the ratio of CD206+ M2 polarized macrophages was above 0.5 in SIS-Alg samples, but below 0.5 in VF-Alg samples, implicating a

more favorable anti-inflammatory and regenerative macrophage response to hydrogels produced from SIS.

Reports of macrophage response in dECM tissue engineering have largely pointed toward induction of an M2 phenotype.<sup>23,101,102</sup> For instance, lymph node dECM hydrogels induced strong CD206+ M2 polarization in a murine model of volumetric muscle loss after 10 days. However, varied outcomes were reported in literature.<sup>103,104</sup> One study showed that less than 50% of macrophages in SIS expressed CD206, but when supplemented with the anti-inflammatory compound epigallocatechin gallate, approximately 75% were CD206+.<sup>105</sup> Recent studies have shown that decellularization with nucleases or surfactants that linger after washing can impact the composition of dECM and trigger inflammation.<sup>106,107</sup> As nucleases are used in our VF decellularization protocol but not Cook Biotech's SIS decellularization protocol, this may be associated with the low proportion of CD206 expression.

B cells are part of the adaptive immune response and are responsible for antibody production.<sup>25,108</sup> Activation of B cells may be associated with properties of the biomaterial, including surface chemistry, such as the hydroxyl and carboxyl groups of alginate, porosity, topography, and more.<sup>109</sup> While B cell infiltration of biomaterials is part of the wound healing process, prolonged presence of B cells is associated with deleterious fibrotic responses and hampers wound healing as the body recognizes the biomaterial as a foreign substance and produces antibodies against it.

An initial elevated B cell response followed by a decrease to day 21 can be considered consistent with some literature reports for SIS dECM. For instance, an SIS dECM scaffold was found to induce an elevated B cell response on day 7 compared to a volumetric muscle loss (VML) injury control and a PCL scaffold, but a significantly decreased response on day 21.<sup>108</sup> It should be noted that B220+ B cell response to dECM biomaterials are varied in literature. In a murine VML model, very low levels of B cells were localized within UBM hydrogels on day 7. In contrast, up to 70% of the total cell population were B220+ B cells when SIS dECM powder was injected to the porcine peritoneal cavity.<sup>25,110</sup> The B cell response to our click dECM hydrogels can therefore be considered favorable in comparison to other dECM biomaterials.

The results of these experiments confirm the biocompatibility of the click dECM hydrogels through the integration of the hydrogels with surrounding tissue. Overall, the click dECM hydrogels showed a similar early immune response to those of other dECM hydrogels in literature.

The SIS-Alg hydrogel better maintained the anti-inflammatory M2 macrophage phenotype over time compared to the VF-Alg hydrogel. We also show that the hydrogels from both SIS dECM and VF dECM induce similar local immune responses. Remodeling of dECM in the click dECM hydrogels demonstrated increased cellular infiltration and replacement with neo-ECM in a manner supported by the remaining hydrogel.

#### 5.3.6. Conclusions

The retention and integration of the click dECM hydrogels in our biocompatibility study does not guarantee that hydrogels will have a sufficient residence period in VF defects for complete regeneration. While SIS-Alg produced comparable results to VF-Alg overall, it degraded more quickly in our enzymatic degradation assay. Crosslinking dECM and alginate with transcyclooctene (TCO) could aid in further slowing the degradation rate. As the reaction rate between tetrazine and TCO is faster, this would decrease the time necessary for the click dECM hydrogels to reach their final stiffness but may have the practical limitation of shortening the amount of time prior to injection that the dECM and alginate components of the pre-gel can be mixed.

Beyond *in vitro* studies, the next step would be a VF-specific *in vivo* study with larger animals that allow testing of the long-term effect of phonation on hydrogel retention and integrity. Also, skin models were used to evaluate biomaterial compatibility in this study. However, skin tissue and vocal folds differ in their local immune environment as well as the remodeling dynamics driven by MMPs and tissue inhibitors of metalloproteinases (TIMPs). These factors would dictate the eventual integration of biomaterial into the target tissue.<sup>111-113</sup> For instance, a stronger pro-inflammatory immune response and faster degradation may be observed in sensitive target sites such as the VF or cardiovascular system compared to the subcutaneous response.<sup>111,113</sup>

To further characterize the type of immune response, staining for M1 macrophage markers such as CD86 or iNOS would help elucidate the effect of the click dECM hydrogel on macrophage polarization. Given the formation of the fibrous capsule on day 7 in our subcutaneous rat study, a strong initial expression of M1 inflammatory markers that decreases by day 21 might be predicted.

Overall, click tetrazine ligation of dECM with the slower degrading natural polymer alginate can improve the mechanical properties and stability of dECM hydrogels while retaining biocompatibility and stimulating the vasculogenesis. To achieve an effective VF biomaterial, key



considerations include mimicking mechanical properties to support function while stimulating VF-specific regeneration and degradation at a rate that matches functional tissue repair. For VF tissue engineering therapeutics, this approach to biomaterial design will support progress toward long-term voice restoration, which will reduce the burden of repeated treatments on the medical system and increase quality of life for patients.

#### *5.4. Methods*

##### *5.4.1. Production of Powder ECM from Small Intestinal Submucosa*

Powder ECM from porcine SIS was produced according to Cook Biotech's (West Lafayette, IN, USA) standard manufacturing protocols and supplied as a generous donation.<sup>114</sup> Mechanical delamination was performed to separate the submucosa from other intestinal layers, washed in water, and stored at -80 °C. Decellularization and disinfection of defrosted SIS was performed using peracetic acid and ethanol. The residual solution was removed by rinsing with high-purity water. Sheets of SIS dECM were then lyophilized and homogenized into powder. Terminal sterilization was performed with ethylene oxide gas under standard temperatures, pressures, and durations at the McGill Animal Resources Center.

##### *5.4.2. Decellularization of Porcine Vocal Folds*

Porcine vocal folds were dissected from larynges and decellularized as previously described.<sup>27</sup> In brief, larynges stored at -80 °C were thawed overnight and dissected to remove VF. VF were minced to increase surface area and decellularized in a series of steps using 3M sodium chloride, nuclease solution (25 µg/mL DNase, 10 µg/mL RNase), and isopropanol (**Table S1**). All decellularization solutions contained 1% Penicillin-Streptomycin and 1 U/mL PMSF. Lyophilized VF dECM was comminuted into powder using a SPEX SamplePrep 6775 Freezer Mill.

##### *5.4.3. Functionalization of Decellularized Extracellular Matrices*

VF and SIS dECM were functionalized with Nb by adapting a protocol used for the functionalization of gelatin.<sup>45</sup> The dECMs were first solubilized with pepsin. 60 mg Nb-NHS per 100 mg dECM and 10 µL/mL N,N-diisopropylethylamine were then added to the solution and the reaction allowed to proceed for 24 h (**Table S5**). The resulting product was dialyzed for 4 days in a Spectra/Por™ 4 12-14 kD MWCO dialysis membrane to remove impurities and lyophilized.

Functionalization was confirmed using solid-state nuclear magnetic resonance (NMR). All spectra were recorded on a Bruker Avance III HD spectrometer operating at a field of 9.4 T with corresponding  $^{13}\text{C}$  and  $^1\text{H}$  Larmor frequencies of 100.6 and 400.1 MHz, using a double resonance 4 mm Magic-Angle Spinning probe. The  $^{13}\text{C}$  spectra are obtained at room temperature with a Magic-Angle Spinning frequency of 10 kHz using a 2 ms long 30% ramped  $^1\text{H}$  to  $^{13}\text{C}$  cross polarization. A 30 kHz spectral width was used. 16384 transients were added with 20 ms acquisition time and a recycle delay of 3 s for a total experimental time of 14 hours. High-power  $^1\text{H}$  TPPM decoupling was applied during the acquisition. The applied radio-frequency fields were 75 kHz and 85 kHz for  $^{13}\text{C}$  and  $^1\text{H}$ . All spectra were externally referenced to TMS (0 ppm) by setting the unshielded CH<sub>2</sub> resonance of adamantane to 38.48 ppm.

Degree of substitution was determined by fluoroldehyde assay according to manufacturer protocols with BSA (0-25  $\mu\text{g/mL}$ ) as a standard.<sup>115,116</sup> Functionalized dECM (SIS-Nb, VF-Nb) and the base material (SIS-only, VF-only) were suspended at 10  $\mu\text{g/mL}$  in PBS and mixed with fluoroldehyde at a 1:10 ratio. Fluorescence was measured at 450 nm with an excitation wavelength of 360 nm using a SpectraMax i3x Multimode Plate Reader from Molecular Devices (San Jose, CA, USA).

#### 5.4.4. Functionalization of Alginate

Alginate was functionalized with MTz by modifying a previously described method.<sup>47</sup> First, 0.67% wt alginate was dissolved overnight in a buffer consisting of 0.1 M MES, 0.3 M NaCl at pH 6.5. EDC and NHS were added to solution at 5X molar excess to the carboxyl groups of alginate and incorporated (**Table S6**). MTz was then added at 2.5 mmol/g alginate and the reaction solution was stirred for 24 h under a nitrogen atmosphere. The reaction was quenched with hydroxylamine in 5X molar excess to the carboxyl groups of alginate and dialyzed for 4 days in a Spectra/Por™ 4 12-14 kD MWCO dialysis membrane against a decreasing salt gradient (150 mM-0 mM). The Alg-Tz product was then treated with activated charcoal and sterile filtered through a 0.22  $\mu\text{m}$  PES membrane before lyophilization.

Functionalization was confirmed using liquid-state nuclear magnetic resonance. NMR experiments were recorded on a Varian INOVA 500 MHz NMR with room temperature HCN probe equipped with Z-axis gradients. 1D proton spectra were recorded at 25°C with a single pulse experiment, 2s acquisition time, 1.5s d1, 32768 points, 8000 Hz sweep width. If the residual water

signal interfered with the signals of interest a 1D proton spectrum with water suppression by presaturation or excitation sculpting was employed.

#### 5.4.5. Fabrication of Click dECM-Alg Hydrogels

To fabricate click dECM-Alg hydrogels, 20 mg/mL dECM-Nb was solubilized again in pepsin-HCl for 24-48 h and neutralized with 10X PBS and sodium hydroxide. Alg-Tz was dissolved overnight at a concentration of 20 mg/mL and mixed with neutralized dECM-Nb at a 1:4 ratio (**Table S7**). VF and SIS-only hydrogels were prepared by solubilization in pepsin-HCl, neutralized with sodium hydroxide and 10X PBS, and diluted to a concentration of 16 mg/mL. Both click dECM-Alg and dECM-only pre-gel solutions were incubated at 37 °C for at least 30 min to form hydrogels. To determine the time to completion of tetrazine ligation, spectral transmittance was measured from 300-800 nm 0, 1, 2, 5, 10, and 24 hours after mixing of methyltetrazine and norbornene solutions.<sup>73</sup>

#### 5.4.6. Turbidimetric Gelation Kinetics and Tetrazine Ligation Reaction Kinetics

To determine turbidimetric gelation kinetics, 200 µL of each sample (N = 4) was added to a pre-chilled 96 well plate before starting the experiment in a UV-vis spectrometer pre-heated to 37 °C.<sup>49,50</sup> Absorbance was measured at 405 nm over 2 hours. Absorbance values were normalized according to Equation 1:

$$N_A = \frac{A - A_{min}}{A_{max} - A_{min}} \quad \text{Equation 1}$$

Where  $N_A$  represents the normalized absorbance,  $A$  is the absorbance at each time point,  $A_{max}$  is the maximum absorbance, and  $A_{min}$  is the minimum absorbance. Time to half gelation ( $t_{1/2}$ ), time to 95% gelation ( $t_{95}$ ) were determined based on the times at which the normalized absorbance reached 50% and 95% respectively. Gelation rate ( $S$ ) was determined from the maximum slope of the curve, and lag time ( $t_{lag}$ ) as the time at which the normalized absorbance intercepted the x-axis.

#### 5.4.7. Rheological Analysis

Rheological properties were evaluated on a TA Instruments Discovery HR-2 Rheometer with 20 mm parallel geometry. Time sweeps were performed over 20 h by adding pre-gels to a plate kept at 4 °C. The temperature was rapidly raised to 37 °C upon commencing the time sweep with constant strain (0.01%) and frequency (1 Hz). Strain sweeps were performed from 0-1000% strain

at 1 Hz frequency on the same samples to determine the linear viscoelastic range and failure point. Cyclic stress-relaxation tests were performed using six cycles of stress-relaxation and recovery with strain alternating between 0.1% and 5% at constant frequency (1 Hz). Nonlinear regression with the one-phase decay least-squares fit in Graphpad Prism 9 was used to identify the change in plateau stress and relaxation time between cycles.

#### *5.4.8. Atomic Force Microscopy*

Atomic Force microscopy (JPK NanoWizard 3, Berlin, Germany) was performed using a polystyrene particle (25  $\mu\text{m}$ ) probe tip on a rectangular silicon cantilever with a 0.6 N/m spring constant (Novasan, IA, USA).<sup>51,52</sup> A thermal noise method was used to determine the spring constant before each experiment. Indentations were made at 20 locations across each sample surface (N=3). During experiments, samples were covered in PBS to maintain hydration. Microscale Young's Moduli were determined using the Hertzian Contact Model.

#### *5.4.9. Compression Testing*

An Instron Machine Model 5965 was used to perform compression testing on click hydrogels and dECM-only controls with 1.5 cm diameter and 1.2 mm thickness. The hydrogels were compressed at a fixed rate of 0.02 mm/s with a 10 N loading cell while the force and displacement were recorded. Compressive moduli were calculated based on the slope of the linear region.

#### *5.4.10. Hydrogel Stability, and Degradation*

SIS-only, VF-only, VF-Alg, and SIS-Alg pre-gels were prepared as previously described in **Section 4.5**. Following neutralization, hydrogels were incubated at 37°C to ensure solid gel formation for 24 h.

For degradation tests, hydrogels were suspended in PBS or 2 U/mL collagenase in PBS. Samples were then incubated under gentle agitation at 37°C. The incubation solution was changed regularly, as if for cell culture. At intervals over 30 days, 3 replicates of each sample type were lyophilized and weighed to determine residual mass.

Samples were mounted on SEM stages and coated with platinum in a Leica Microsystem EM ACE600 High-Resolution Sputter Coater. Images were taken on a FEI Quanta 450 Environmental Scanning Electron Microscope under high vacuum at 100 Pa chamber pressure, 5 kV and a spot of 2.5. For quantitative analysis, pore size was measured in ImageJ from 100X and 500X images.

The scale bar was used to calibrate measurements. Circles were positioned within each pore, and measurements of the circle area were used to determine the pore diameter.

#### *5.4.11. Cell Culture*

Immortalized Human Vocal Fold Fibroblasts (HVFF) were generously supplied by Prof. Susan Thibeault (Department of Surgery, University of Wisconsin-Madison, USA).<sup>117</sup> HVFF were cultured in a solution of Dulbecco's modified Eagle medium (DMEM), 10%v/v fetal bovine serum, and 1%v/v penicillin/ streptomycin under conditions of 5% CO<sub>2</sub> atmosphere and 37 °C (**Table S4**). HVFF were stably transduced with green fluorescent protein (GFP). Myr-GFP Cut and switch restriction enzyme cloning was used to replace mRFP in pCAG:myr-mRFP. The Myr-GFP plasmid was cloned into a pHIV blasticidin lentiviral vector. HVFF were infected with the lentivirus and selected for stable GFP expression by Molly Shen in the lab of Dr. Peter Seigel (McGill University, Canada).<sup>118</sup> GFP-HVFF were cultured in DMEM supplemented with blasticidin to select GFP-positive cells across passages. Human Umbilical Vein Endothelial Cells (HUVECs, Lonza C2519AS) were cultured in Endothelial Growth Medium EGM<sup>TM</sup>-2 BulletKit<sup>TM</sup> (CC-3162).

Media changes were performed every 2-3 days for all cell types. Passages were performed using Gibco® Cell Dissociation Buffer when cells reached approximately 70% confluency for HVFF and 90% confluency for HUVECs. For this study, HVFF were used between passages 9 and 20, GFP-HVFF between passages 3 and 9, and HUVECs between passages 3 and 8.

#### *5.4.12. Human Vocal Fold Fibroblast Viability and Morphology*

SIS-only, VF-only, VF-Alg, and SIS-Alg pre-gels were prepared as previously described in **Section 4.5**. Following neutralization, HVFF were seeded by encapsulation at a concentration of 1 million cells/mL. 70 µL of SIS-only, VF-only, VF-Alg, and SIS-Alg pre-gels with encapsulated HUVECs were pipetted into each well of 8-well chamber slides for each time point with a total of 4 replicates per sample type. Hydrogels were incubated for a minimum of 1 h to ensure hydrogels formation before the addition of 200 µL media per well. HVFF were cultured under conditions of 5% CO<sub>2</sub> atmosphere and 37 °C over 14 days. Media changes were performed every 2-3 days.

At each time point (1, 3, 7, or 14 days) media was removed from samples in randomly selected chamber slides and the HVFF-encapsulated hydrogels were washed twice with PBS. Live/Dead

Staining was performed with calcein AM and ethidium homodimer prior to imaging on a Zeiss LSM 800 Confocal Microscope. The number of live and dead cells was analyzed using ImageJ.<sup>119</sup>

Samples from each time point were dehydrated in graded ethanol and critical point dried in a Leica Microsystems EM CPD030. Cross sections were mounted on SEM stages and coated with platinum in a Leica Microsystem EM ACE600 High-Resolution Sputter Coater. Images were taken on a FEI Quanta 450 Environmental Scanning Electron Microscope under high vacuum.

#### *5.4.13. Human Umbilical Vein Endothelial Cell Viability and Network Formation Analyses*

HUVECs encapsulated in SIS-only, VF-only, VF-Alg, and SIS-Alg pre-gels at a concentration of 2 million cells/mL. Collagen hydrogel controls were also used for this experiment. Collagen pre-gels were prepared by neutralizing 3 mg/mL stock solution and dilution to a final 2 mg/mL solution prior to HUVEC encapsulation. Pre-gel solutions were added to 8-well chamber slides and incubated for a minimum of 1 h before the addition of 200  $\mu$ L media. Standard EGM-2 was added to half the samples, and EGM-2 without VEGF to the remaining samples. Media changes were performed every 2-3 days.

At each time point (3, 7, or 14 days) media was removed from samples in randomly selected chamber slides and the HUVEC-encapsulated hydrogels and stained with Calcein AM and Ethidium Homodimer solution as previously described. Following Live/Dead staining, the cells were fixed by incubation with 4% paraformaldehyde (PFA) for 10 min, then stained with 100  $\mu$ L DAPI for 10 min prior to imaging with a Zeiss LSM 800 Confocal Microscope. ImageJ was used to analyze HUVEC network formation in terms of length, number, and branching.

#### *5.4.14 Evaluation of the Local Fibrotic and Immune Response in Subcutaneous Rat Model*

Animal experimental procedures were approved by the McGill University Animal Compliance Office (Protocol MCGL-8275). A total of 10 Sprague-Dawley rats, 5-20 weeks old (100-500 g) were used in the study. For subcutaneous injection, animals were anesthetized with isoflurane and subcutaneously injected in four places along the back with SIS-Alg and VF-Alg pre-gels with a 21-gauge needle. Pepsin solubilization of SIS-Nb and VF-Nb commenced two days in advance, and the solutions were neutralized on ice and mixed with Alg-Tz immediately prior to injection. The remaining two injections were 200  $\mu$ L 1X PBS. At each of the one- and three-week endpoints of the study, animals were euthanized by CO<sub>2</sub> asphyxiation (N=5 for each time point) while under

anesthesia and skin from the injection areas was immediately excised. Excised skin samples were fixed with 4% paraformaldehyde followed by cryoprotection with 30% sucrose. Slices of skin tissue with 2 µm thickness were taken from each hydrogel and PBS sample and lyophilized for 24 hours. These samples were sputter coated with platinum and imaged using scanning electron microscopy as previously described.

#### *5.4.15 Histology and Immunohistochemistry*

Excised skin samples were fixed with 4% paraformaldehyde followed by cryoprotection with 30% sucrose. 10 µm cryosections were made on a cryostat for hemotoxylin and eosin staining, and immunofluorescence (**Table S5**). 5 µm cryosections were made for Masson's Trichrome staining. Sections were stained with Hemotoxylin and Eosin or Masson's Trichrome and mounted with Permount™. Staining for immunofluorescence was performed following permeabilization with 0.2% Triton X-100, and blocked with 5% goat serum (CD68, CD206) for 1 h or 1% BSA for 40 min (CD45R). Macrophages were stained by incubating sections overnight at 4 °C with rabbit anti-CD68 (1:500 dilution, Invitrogen PA5-78996), rabbit anti-CD206 (1:200 dilution, Proteintech 18704-1) in 5% goat serum. The next day, sections were incubated for 1 h with DAPI and secondary antibodies, Alexa Fluor® 488 or Alexa Fluor® 647 Goat anti-rabbit IgG (1:1000) in 5% goat serum. B cells were stained overnight with HIS24 mouse anti-rat CD45R (B220) (1:50 dilution, eBioscience 11-0460-82). The next day, sections were washed for 1 h with 1% BSA, then stained with DAPI in 1% BSA for 1 h. Immunofluorescence samples were mounted with Fluoromount-G™. Both brightfield and fluorescent imaging was performed on a Zeiss Axio Observer 3, and analysis performed using ImageJ.

#### *5.4.16 Statistical Analysis*

Statistical Analyses were performed using GraphPad Prism 9 (GraphPad Software, Inc., USA). For most experiments, data were analyzed using one or two-way ANOVA followed by Tukey's post-hoc test. Data values are presented as mean ± SD except in the case of best-fit curves, where 95% confidence intervals are reported. Values of  $p < 0.05$  were deemed statistically significant.

### **Acknowledgements**

This study was supported by the National Sciences and Engineering Research Council of Canada (RGPIN-2018-03843, RGPIN-2024-04235 and ALLRP 548623-19), Canada Research Chair

research stipend (J.Y.L, M.T. and N.Y.K.L.-J.) and the National Institutes of Health (R01 DC-018577-01A1). Cryomilling was performed in the Dr. Christopher Moraes' Cellular Microenvironment Design Lab at McGill University, with technical support from Prabu Karthick Parameshwar. Microscopic imaging for this manuscript was performed in the McGill University Life Sciences Complex Advanced BioImaging Facility (ABIF). Rheology was performed in Dr. Luc Mongeau's Biomechanics laboratory at McGill University. Compression testing was performed with Zhen Yang in Jianyu Li's laboratory at McGill University. Animal work was carried out in the Comparative Medicine and Animal Resources Center at McGill University. We would also like to acknowledge the generous donation of HVFF by Prof. Susan Thibeault's laboratory (University of Wisconsin-Madison). The presented content is solely the responsibility of the authors and does not necessarily represent the official views of the above funding agencies.

### **Conflict of Interest**

Powder Extracellular Matrix was provided by Cook Biotech through a Material Transfer Agreement at the cost of shipping. The authors hold no financial interest in Cook Biotech and declare no additional conflicts of interest.

### **Author Contributions**

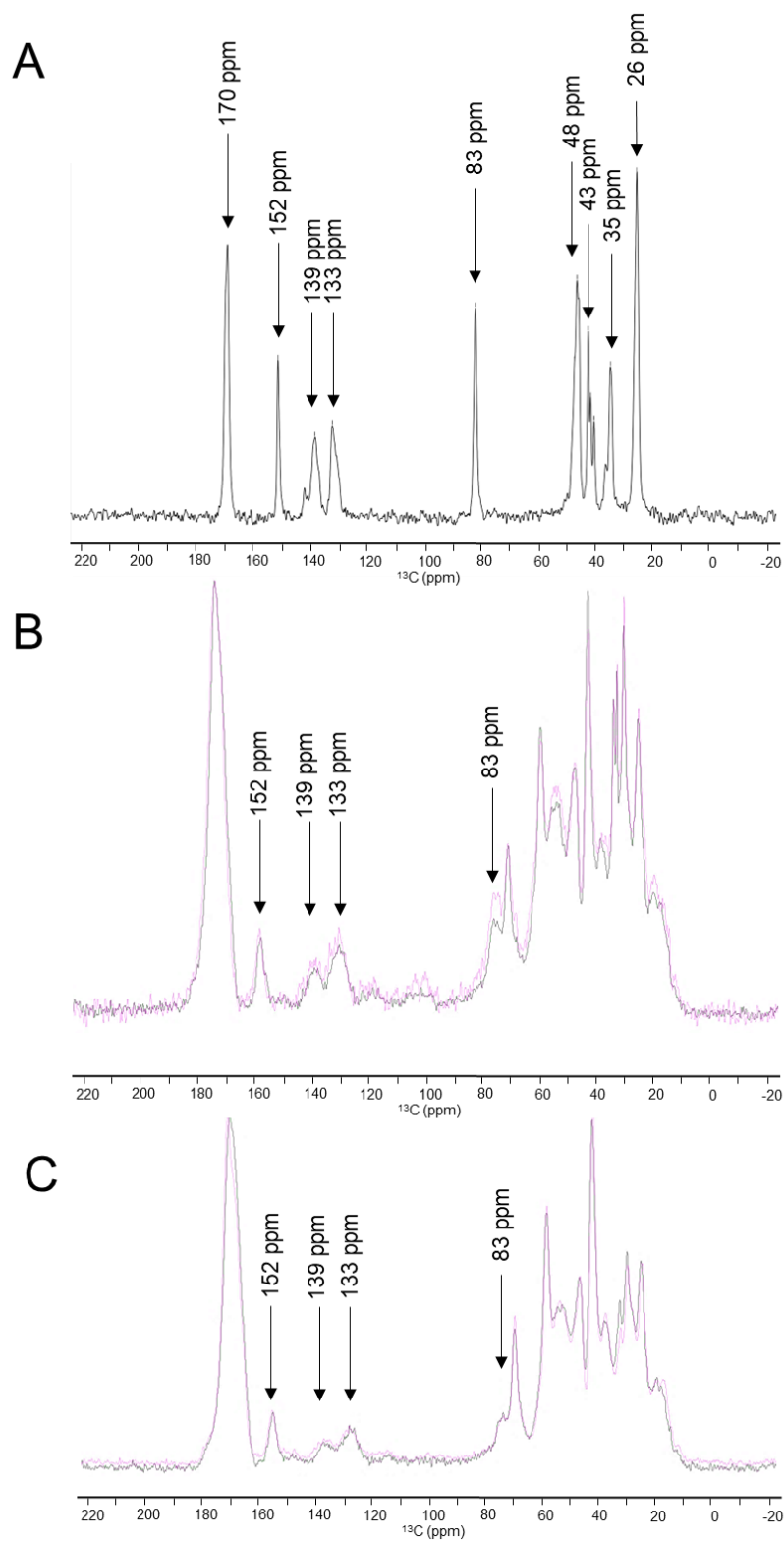
**Mika Brown:** Conceptualization (lead), Investigation (lead), Data Analysis (lead), Writing – original draft (lead). **Hideaki Okuyama** Investigation (supporting) **Ling Li** Investigation (supporting) **Zhen Yang** Investigation (supporting), Writing – review and editing (supporting), **Jianyu Li:** Conceptualization (supporting), Writing – review and editing (supporting), **Maryam Tabrizian:** Supervision (supporting), Writing – review and editing (supporting), **Nicole Li-Jessen:** Supervision (lead), Conceptualization (supporting), Funding Acquisition (lead), Resources (lead), Writing – review and editing (lead).

### **Data Availability Statement**

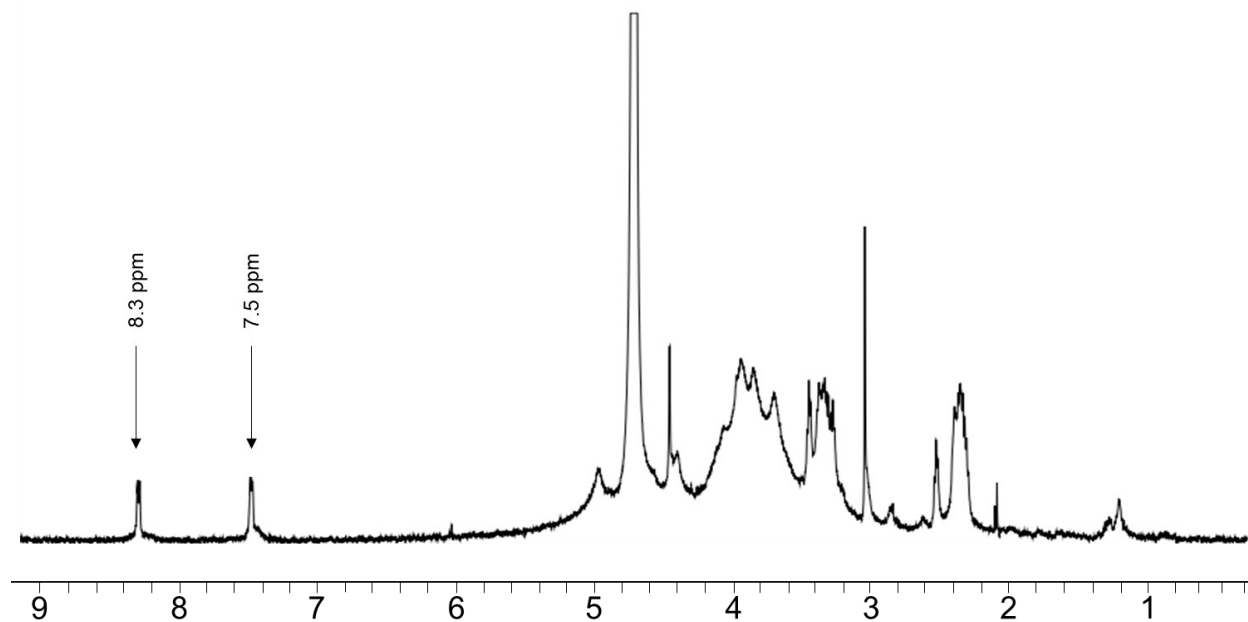
All data that support the findings of this study are available from the corresponding author upon reasonable request.



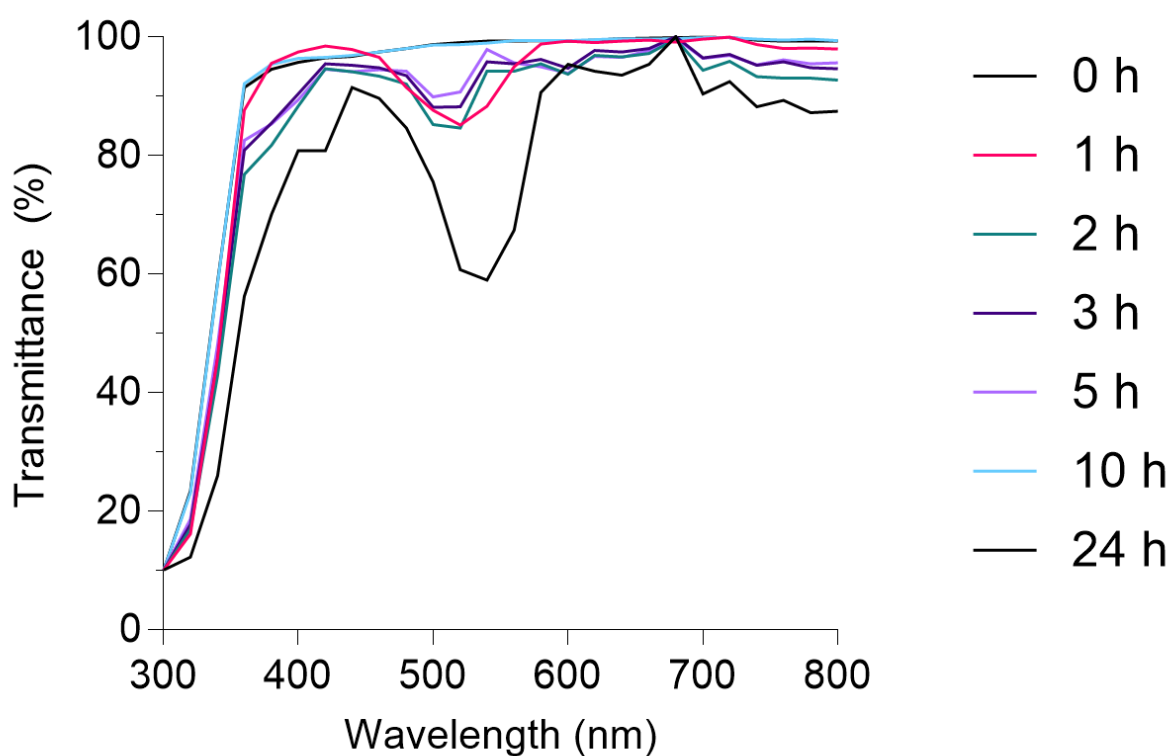
### 5.5. Supplementary Information



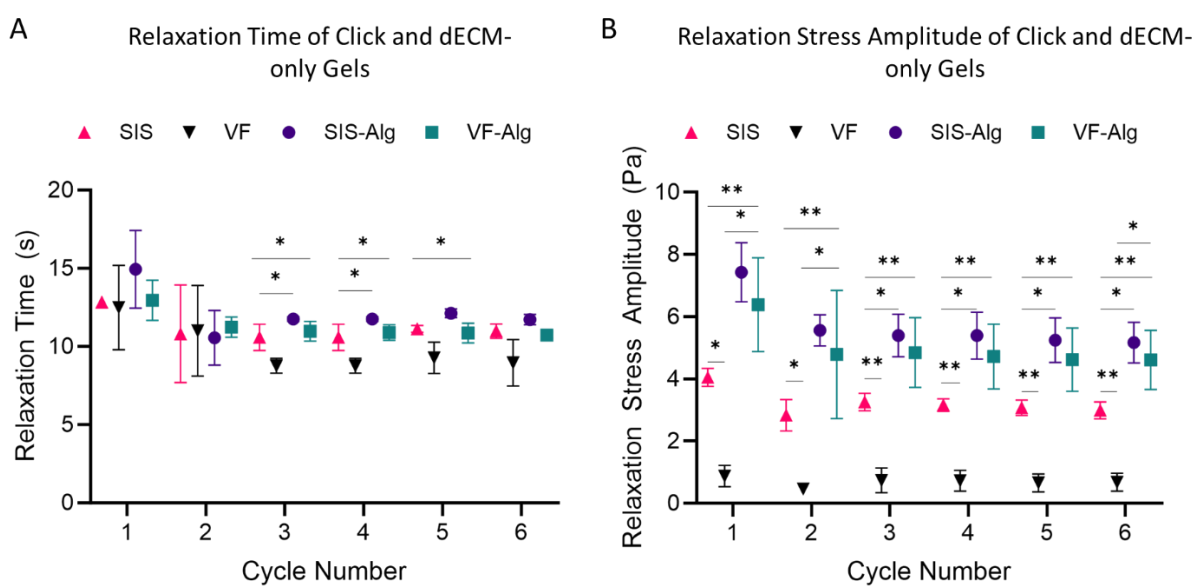
**Supplementary Figure 1.**  $^{13}\text{C}$  Solid NMR of Nb-NHS and Functionalized dECM: **A)** Nb-NHS **B)** VF-Nb and **C)** SIS-Nb with overlay of Non-Sterile (● line) and EtO sterilized (● line) samples. Nb peaks were identified in Functionalized dECM at 83, 133, 139, and 152 ppm.



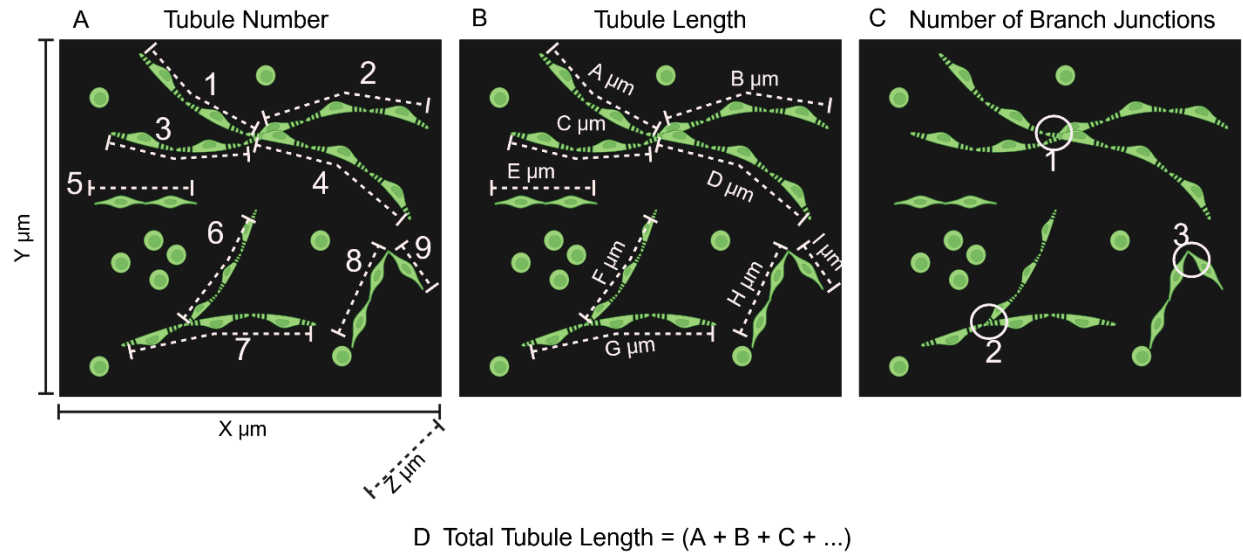
**Supplementary Figure 2.** Liquid NMR spectrum of alginate functionalized with MTz. MTz peaks were identified at 7.5 and 8.3 ppm.<sup>47,48</sup>



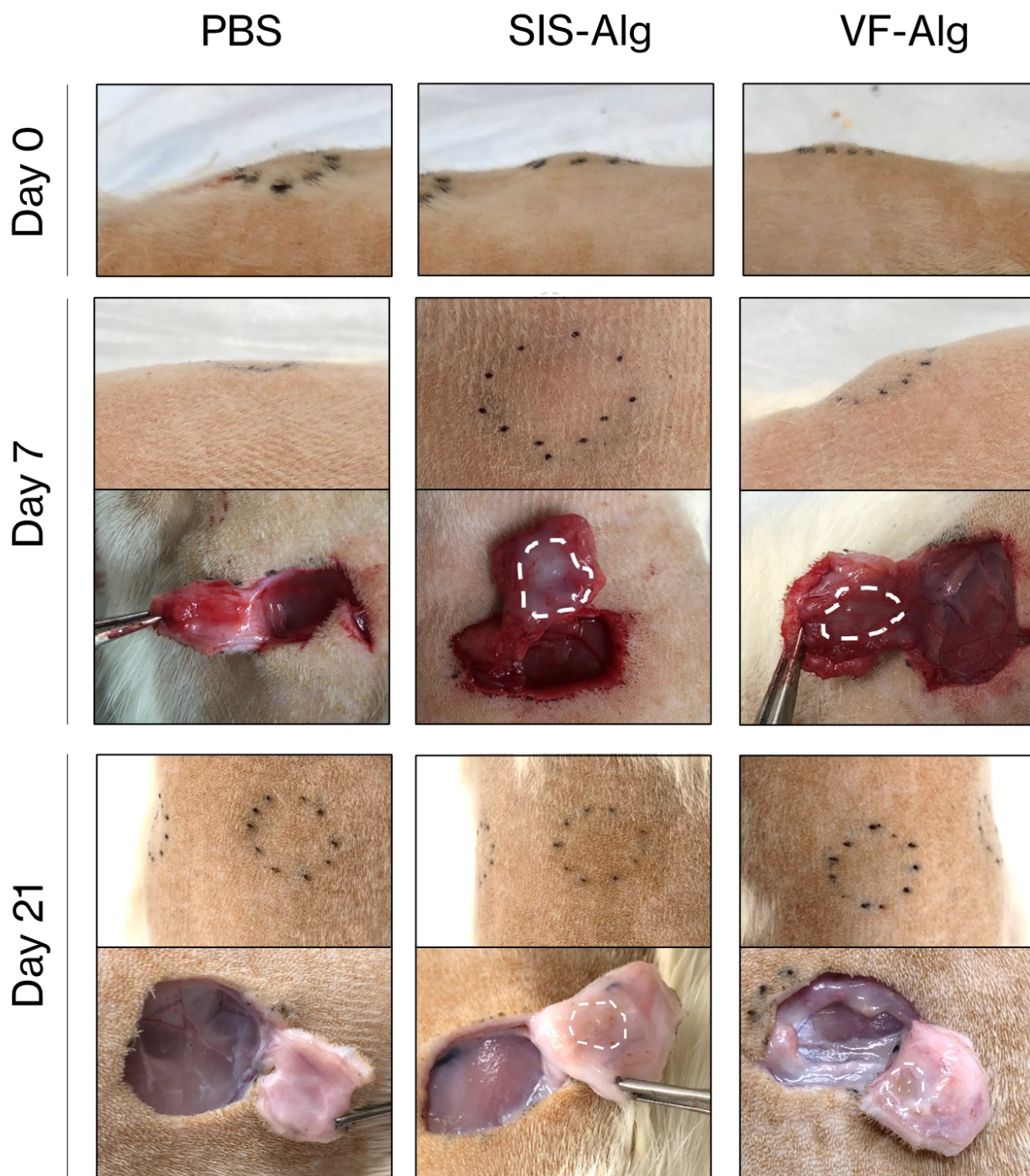
**Supplementary Figure 3.** Determination of tetrazine ligation rate by spectral transmittance. The tetrazine peak is found at 520 nm and shrinks as tetrazine ligation proceeds.



**Supplementary Figure 4.** Stress-Relaxation Quantification of click and dECM-only gels over six cycles alternating between 0.01% and 5% strain in terms of **A)** Relaxation time and **B)** Relaxation Stress Amplitude. ▲ SIS-only ▼ VF-only ● SIS-Alg ■ VF-Alg. \* $p < 0.05$ , \*\* $p < 0.01$ . Error bars represent standard deviation.



**Supplementary Figure 5.** Vasculogenesis Tubule Measurement Methodology. 2D projections of stacks were used to measure structures formed by linked cells to find **A)** Tubule number **B)** Tubule length **C)** Number of branch junctions and **D)** Total tubule length. Tubule number, total tubule length, and number of branch junctions are reported as a function of volume, from the length (X), height (Y), and depth (Z) of the imaging area. Average tubule length was reported as the mean of tubule lengths.



**Supplementary Figure 6.** Monitoring of Subcutaneous Injection Site in Sprague-Dawley Rats over 21 Days. No severe symptoms of inflammation were observed. Hydrogels were identified by palpation and as white masses within the subcutaneous tissue upon sacrifice and excision at Day 7. At Day 21, hydrogels were not identifiable by palpation, but possible gel areas were visually identified, subsequently confirmed by H&E staining. Dotted lines indicate area of injection.

**Supplementary Table 1. Design Targets and Parameters of Proposed Click dECM Hydrogel**

	Target Properties	Evaluation Methodology
<b>Mechanical Properties</b>	VF Mechanical Mimicry	Series of mechanical tests to reflect known ranges of properties.
Storage Modulus	Adult Male (>39 years): 363-1323 Pa <sup>120</sup>  Adult Female (>42 years): 280-954 Pa <sup>120</sup>	Linear shear rheology on cylindrical tissue samples punched from both VF of deceased adult patients. No significant differences were identified based on age or gender.
Microindentation Young's Modulus	Adult female (>70 years): 4000-14000 Pa <sup>121</sup>  Adult male: (>45 years): 1000-8000 Pa	Indentation with a microscale probe to generate force curves at multiple points.  Six adult human cadaveric samples. Significant differences in age and gender not reported.
Bulk Compressive Modulus	Medial Surface Cover: 3900 – 5400 Pa <sup>56</sup>  Superior Surface Cover: 2700 – 3200 Pa  Inferior Medial Cover: 7000 – 7900 Pa  Muscle: 1300 – 2700 Pa	Bulk or macroscale indentation of a cylindrical area.  Three adult human cadaveric samples (Female: Age 19; Male: Age 30 and 49). Measurements were performed dissected on dissected VF lamina propria and thyroarytenoid muscle. <sup>56</sup>
Linear Stress-Strain Response Region	3-7% (>53 years) <sup>61</sup>	Response to increasing strain with frequency held steady.

	<10% at low strain (>53 years) <sup>83</sup>	Seven adult human cadaveric samples, two female and five male. Differences in age and gender not reported. <sup>61</sup>  Eight adult human cadaveric samples. Four female and four male. Differences in age and gender not reported.
Response to Cyclic Deformation	Recovery when subjected to repeated stresses. <sup>57</sup>  Resilience to strain within the standard human speaking range (100-300 Hz) <sup>122,123</sup>	Exposure to repetitive strains to determine cyclic stress-relaxation behavior
Nonlinearity	Recovery from deformation under high strain and elongation by 50% <sup>28,83</sup>	Not evaluated
<b>Physical Properties</b>	Increased stability under physiological conditions	Qualitative and quantitative structural and degradation testing.
Biodegradation	Slowed breakdown by hydrolysis and matrix metalloproteinases compared to dECM hydrogels	Hydrolytic and enzymatic degradation assays to determine degradation rate
ECM-Mimicking	Basket-like structure of collagen I, collagen III, and elastin	Scanning electron microscopy to determine comparability of structure to ECM

	Structure comparable to dECM-Hydrogel	
Swelling Properties	Low swelling ratio of <10% to ensure predictability of response and prevent airway blockage <sup>38,124</sup>	Analysis of swelling kinetics
<b>Bioactivity Properties</b>	Pro-regenerative response	In-vitro and In-vivo viability and biocompatibility assays
Downregulation of Myofibroblast activity	Resistance to collagen contraction by fibroblasts  Reduced expression of myofibroblast markers such as Il-6	3D culture of human vocal fold fibroblasts
Stimulation of Angiogenesis	Innate vasculogenic capacity stimulates capillary formation	3D culture of HUVECs and quantification of formation of tubule-like structures
Neo-ECM Production	Remodeling and deposition of neo-tissue.	Hydrogel integration with surrounding tissue by histological staining
Macrophage Polarization	Promotion of an M2 Macrophage phenotype	Immunofluorescence of CD68 and CD206 to determine ratio of CD206+ macrophages to pan CD68+ macrophages

**Supplementary Table 2.** Statistical Comparisons of Hydrogel Mechanical Properties. Analysis was performed by One-Way ANOVA with post-hoc Tuckey Tests. \*p<0.05, \*\*p < 0.01, \*\*\*p < 0.001, \*\*\*\*p < 0.0001



	F Value	Overall P Value	SIS vs. VF	SIS vs. SIS-Alg	SIS vs. VF-Alg	VF vs. SIS-Alg	VF vs. VF-Alg	SIS-Alg vs. VF-Alg
<b>Time to Half Gelation (t1/2, min)</b>	5.8	0.004**	0.99	0.0143*	>0.99	0.007**	0.96	0.02*
<b>Time to 95% gelation (t95, min)</b>	5.4	0.006**	0.09	0.2414	0.72	0.97	0.009**	0.03*
<b>Lag Time (min)</b>	4.3	0.01*	0.0002 ***	0.24	0.84	0.02*	0.001**	0.69
<b>Gelation Rate (S, min-1)</b>	10.0	0.0002***	0.10	0.01*	0.44	0.75	0.80	0.24
<b>Plateau Storage Modulus (Pa)</b>	14.3	0.001**	0.99	0.03*	0.004**	0.02*	0.003**	0.49
<b>Yield Point (% Strain)</b>	8.8	0.006**	0.90	0.40	0.01*	0.19	0.007**	0.15
<b>Average Young's Modulus (Pa)</b>	28.3	0.0001***	0.90	0.003**	0.0007 ***	0.001**	0.0004 ***	0.65
<b>Average Compressive Modulus (kPa)</b>	7.5	0.01*	0.99	0.15	0.01*	0.23	0.02*	0.39

**Supplementary Table 3.** Statistical Comparisons of Hydrolytic Degradation of Hydrogels. Analysis was performed by Two-Way ANOVA with post-hoc Tuckey Tests. \*p<0.05, \*\*p < 0.01, \*\*\*p < 0.001, \*\*\*\*p < 0.0001

Time	SIS vs. VF	SIS vs. SIS- Alg	SIS vs. VF- Alg	VF vs. SIS- Alg	VF vs. VF- Alg	SIS-Alg vs. VF- Alg
<b>Day 1</b>	0.01*	0.001**	0.09	0.0005***	0.04*	0.38
<b>Day 3</b>	0.02*	0.003**	0.18	0.004**	0.05	0.50

<b>Day 7</b>	0.06	0.0008***	0.0002***	0.005**	0.007**	0.24
<b>Day 10</b>	0.10	0.02*	0.05	0.007**	0.03*	0.98
<b>Day 15</b>	0.02*	0.17	0.003**	0.06	<0.0001****	0.38
<b>Day 20</b>	0.03*	0.002**	0.004**	0.002**	0.004**	0.67
<b>Day 25</b>	0.006**	0.0006***	0.009**	0.0002***	0.007**	0.07*
<b>Day 30</b>	0.04*	0.0008***	0.0003***	0.001**	<0.0001****	0.02*
<b>Time</b>	<b>SIS</b>	<b>VF</b>	<b>SIS-Alg</b>	<b>VF-Alg</b>		
<b>Day 1 to 3</b>	0.75	0.16	0.12	0.82		
<b>Day 1 to 7</b>	0.56	0.46	0.15	0.94		
<b>Day 1 to 10</b>	0.01*	0.04*	0.52	>0.99		
<b>Day 1 to 15</b>	0.07*	0.01*	0.25	>0.99		
<b>Day 1 to 20</b>	0.02*	0.005**	0.01*	0.83		
<b>Day 1 to 25</b>	0.01*	0.02*	0.006**	0.74		
<b>Day 1 to 30</b>	0.002**	0.005**	0.003**	0.50		
<b>Day 3 to 7</b>	>0.99	0.98	0.99	0.36		
<b>Day 3 to 10</b>	0.03*	0.24	>0.99	0.95		
<b>Day 3 to 15</b>	0.19	0.06	0.66	0.62		
<b>Day 3 to 20</b>	0.04*	0.018*	0.12	>0.99		
<b>Day 3 to 25</b>	0.03*	0.009**	0.02*	>0.99		
<b>Day 3 to 30</b>	0.004**	0.0006***	0.01*	>0.99		
<b>Day 7 to 10</b>	0.009**	0.93	>0.99	0.90		
<b>Day 7 to 15</b>	0.19	0.71	0.56	0.16		
<b>Day 7 to 20</b>	0.049*	0.45	0.04*	0.18		

<b>Day 7 to 25</b>	0.009**	0.76	0.004**	0.12
<b>Day 7 to 30</b>	0.002**	0.22	0.004**	0.002**
<b>Day 10 to 15</b>	0.45	0.97	0.64	>0.99
<b>Day 10 to 20</b>	>0.99	0.49	0.36	0.97
<b>Day 10 to 25</b>	>0.99	0.99	0.12	0.93
<b>Day 10 to 30</b>	0.07	0.12	0.10	0.73
<b>Day 15 to 20</b>	0.68	0.78	>0.99	0.43
<b>Day 15 to 25</b>	0.52	>0.99	0.86	0.29
<b>Day 15 to 30</b>	0.06	0.10	0.81	0.009**
<b>Day 20 to 25</b>	>0.99	0.41	0.06	>0.99
<b>Day 20 to 30</b>	0.18	0.20	0.05	0.87
<b>Day 25 to 30</b>	0.06	0.009**	0.99	0.93

**Supplementary Table 4.** Statistical Comparisons of Enzymatic Degradation of Hydrogels. Analysis was performed by Two-Way ANOVA with post-hoc Tuckey Tests. \*p<0.05, \*\*p < 0.01, \*\*\*p < 0.001, \*\*\*\*p < 0.0001

<b>Time</b>	<b>SIS vs. VF</b>	<b>SIS vs. SIS- Alg</b>	<b>SIS vs. VF- Alg</b>	<b>VF vs. SIS- Alg</b>	<b>VF vs. VF- Alg</b>	<b>SIS-Alg vs. VF- Alg</b>
<b>Day 1</b>	>0.99	0.22	0.30	0.42	0.30	0.73
<b>Day 3</b>	0.45	0.26	0.08	0.09	0.04*	0.70
<b>Day 7</b>	0.06	0.06	0.004**	0.01**	0.0005***	0.05
<b>Day 10</b>	0.96	0.002**	0.01*	0.007**	0.02*	0.72
<b>Day 15</b>	0.29	0.001**	0.0005***	0.006**	0.006**	0.02*
<b>Day 20</b>	-	0.02*	0.0004***	0.0004***	0.02*	0.19

<b>Day 25</b>	-	0.06	0.009**	0.06	0.009**	0.003**
<b>Day 30</b>	-	-	0.03*	-	0.03*	0.03*
<b>Time</b>	<b>SIS</b>	<b>VF</b>	<b>SIS-Alg</b>	<b>VF-Alg</b>		
<b>Day 1 to 3</b>	0.81	0.60	0.98	0.97		
<b>Day 1 to 7</b>	0.36	0.22	0.93	>0.99		
<b>Day 1 to 10</b>	0.01*	0.20	>0.99	>0.99		
<b>Day 1 to 15</b>	0.009**	0.17	0.34	0.92		
<b>Day 1 to 20</b>	0.02*	0.17	0.16	0.46		
<b>Day 1 to 25</b>	0.02*	0.17	0.05	0.33		
<b>Day 1 to 30</b>	0.02*	0.17	0.045*	0.19		
<b>Day 3 to 7</b>	0.96	0.63	>0.99	0.73		
<b>Day 3 to 10</b>	0.07	0.48	0.94	>0.99		
<b>Day 3 to 15</b>	0.07	0.36	0.72	>0.99		
<b>Day 3 to 20</b>	0.07	0.36	0.37	0.31		
<b>Day 3 to 25</b>	0.07	0.36	0.09	0.17		
<b>Day 3 to 30</b>	0.07	0.36	0.07	0.07		
<b>Day 7 to 10</b>	0.09	0.87	0.79	0.91		
<b>Day 7 to 15</b>	0.10	0.36	0.51	0.21		
<b>Day 7 to 20</b>	0.09	0.36	0.18	0.03*		
<b>Day 7 to 25</b>	0.09	0.36	0.03*	0.008**		
<b>Day 7 to 30</b>	0.09	0.36	0.03*	0.003**		
<b>Day 10 to 15</b>	>0.99	0.16	0.08	0.94		
<b>Day 10 to 20</b>	0.44	0.16	0.03*	0.18		
<b>Day 10 to 25</b>	0.44	0.16	0.006**	0.09		
<b>Day 10 to 30</b>	0.44	0.16	0.01*	0.04*		

<b>Day 15 to 20</b>	0.46	-	0.41	0.06
<b>Day 15 to 25</b>	0.46	-	0.003**	0.02*
<b>Day 15 to 30</b>	0.46	-	0.01*	0.004**
<b>Day 20 to 25</b>	-	-	0.03*	0.15
<b>Day 20 to 30</b>	-	-	0.03*	0.007**
<b>Day 25 to 30</b>	-	-	0.11	0.03*

**Supplementary Table 5.** Materials for Decellularization of Porcine Vocal Folds

<b>Item</b>	<b>Company</b>	<b>Location</b>	<b>Additional Details</b>
Porcine larynges	Ferme Co-op Point du Jour	Bury, QC, Canada	-
Ribonuclease A	Roche Diagnostics GmbH	Mannheim, Germany	50 U/mg
Deoxyribonuclease I from bovine pancreas	Sigma-Aldrich	St. Louis, MO, USA	400 KU/mg
Penicillin-Streptomycin	Sigma-Aldrich	St. Louis, MO, USA	10000 U/mL
Sodium chloride	Fisher Scientific	Saint-Laurent, QC, Canada	
Isopropanol	Fisher Scientific	Saint-Laurent, QC, Canada	
Phenylmethylsulfonyl fluoride	ThermoFisher Scientific	Waltham, MA, USA	

**Supplementary Table 6.** Materials for Functionalization of Alginate

Item	Company	Location	Additional Details
High MW Alginate	KIMICA Corporation	Tokyo, Japan	150 kDA, carboxyl group number 0.338/g
Methyltetrazine-amine	Click Chemistry Tools	Scottsdale, AZ, USA	
1-ethyl-3-(3-dimethylaminopropyl)-carbodiimide hydrochloride	Sigma-Aldrich	St. Louis, MO, USA	-
N-hydroxysuccinimide	Sigma-Aldrich	St. Louis, MO, USA	
2-(N-morpholino)ethanesulfonic acid	Sigma-Aldrich	St. Louis, MO, USA	
Hydroxylamine	Sigma-Aldrich	St. Louis, MO, USA	
Spectrum™ Spectra/Por™ 4 Dialysis Membranes	Fisher Scientific	Saint-Laurent, QC, Canada	12-14 kD MWCO

**Supplementary Table 7.** Materials for Functionalization of dECM

Item	Company	Location	Additional Details
Norbornene-NHS	Iris Biotech GmbH	Marktredwitz, Germany	
Pepsin from porcine gastric mucosa	Sigma-Aldrich	St. Louis, MO, USA	2500 U/mg

Powder Extracellular Matrix from porcine small intestinal submucosa	Cook Biotech	West Lafayette, IN, USA	
Hydrochloric Acid	VWR	Radnor, PA, USA	
Sodium Hydroxide	Sigma-Aldrich	St. Louis, MO, USA	
N,N-diisopropylethylamine	Sigma-Aldrich	St. Louis, MO, USA	
Fluoraldehyde™ o-Phthaldialdehyde Reagent Solution	ThermoFisher Scientific	Waltham, MA, USA	

**Supplementary Table 8.** Materials for Cell Culture Experiments

Item	Company	Location	Additional Details
Human Vocal Fold Fibroblasts	Thibeault Lab, Department of Surgery, University of Wisconsin-Madison	Madison, WI, USA	
Human Umbilical Vein Endothelial Cells	Lonza	Basel, Switzerland	C2519AS
Dulbecco's Modified Eagle Medium	Life Technologies, Inc.	Burlington, ON, Canada	
Fetal Bovine Serum	Sigma-Aldrich	St. Louis, MO, USA	

Endothelial Growth Medium EGMTM-2 BulletKit™	Lonza	Basel, Switzerland	CC-3162
Phosphate Buffered Saline	Gibco	Grand Island, NY, USA	
Phosphate Buffered Saline Tablets	Bioshop Canada	Burlington, ON, Canada	
Gibco® Cell Dissociation Buffer	Gibco	Grand Island, NY, USA	
Thermo Scientific™ Nunc™ Lab- Tek™ II Chamber Slide™ System Slides	Fisher Scientific	Saint- Laurent, QC, Canada	
Live/Dead Viability/Cytotoxicity Kit (L3224)	Invitrogen	Eugene, OR, USA	
Paraformaldehyde	Fisher Scientific	Saint- Laurent, QC, Canada	
DAPI Staining Solution	Abcam	Cambridge, UK	ab228549

**Supplementary Table 9.** Materials for Animal Experiments

Item	Company	Location	Additional Details
------	---------	----------	--------------------



Hemotoxylin and Eosin Staining Kit	Abcam	Cambridge, UK	ab245880
Masson's Trichrome Staining Kit	Abcam	Cambridge, UK	ab150686
Bovine Serum Albumin	Sigma-Aldrich	St. Louis, MO, USA	
Triton X-100	Sigma-Aldrich	St. Louis, MO, USA	
NormalGoat Serum	Abcam	Cambridge, UK	ab7481
Rabbit Anti-CD68	Invitrogen	Eugene, OR, USA	PA5-78996, 1:500 dilution
Rabbit anti-CD206	Proteintech	Rosemont, IL, USA	18704-1, 1:200 dilution
Goat anti-rabbit IgG Alexa Fluor 488®	Invitrogen	Eugene, OR, USA	A11034, 1:1000 dilution
HIS24 mouse anti-rat CD45R (B220)	eBioscience	San Diego, CA	11-0460-82, 1:50 dilution
Permout™	Fisher Scientific	Saint-Laurent, QC, Canada	
Fluoromount-G	Invitrogen	Eugene, OR, USA	

## 5.6. References

- 1 Lungova, V., Chen, X., Wang, Z., Kendzierski, C. & Thibeault, S. L. Human induced pluripotent stem cell-derived vocal fold mucosa mimics development and responses to smoke exposure. *Nat Commun* **10**, 4161 (2019). <https://doi.org/10.1038/s41467-019-12069-w>

- 2     Bhattacharyya, N. The prevalence of voice problems among adults in the United States. *The Laryngoscope* **124**, 2359-2362 (2014).
- 3     Kim, J.-S. *et al.* Effect of Occupational Noise Exposure on the Prevalence of Benign Vocal Fold Lesions: A Nationwide Population-Based Study. *Clin Exp Otorhinolaryngol* **16**, 87-94 (2023). <https://doi.org/10.21053/ceo.2022.01298>
- 4     Bhatt, N. K. *et al.* Treatments for Age-related Vocal Atrophy: A Systematic Review. *The Laryngoscope* **n/a** (2023). <https://doi.org/https://doi.org/10.1002/lary.30653>
- 5     Chang, W.-D., Chen, S.-H., Tsai, M.-H. & Tsou, Y.-A. Autologous Fat Injection Laryngoplasty for Unilateral Vocal Fold Paralysis. *Journal of Clinical Medicine* **10** (2021).
- 6     Rapoport, S. K., Alnouri, G., Sataloff, R. T., Woo, P. & Laryngology. Acute vocal fold paresis and paralysis after COVID-19 infection: a case series. *J Annals of Otolary, Rhinology and Laryngology* **131**, 1032-1035 (2022).
- 7     Švejsová, A. *et al.* Injection laryngoplasty with hyaluronic acid for glottal insufficiency in unilateral vocal fold paralysis: a systematic review of the literature. *European Archives of Oto-Rhino-Laryngology* **279**, 5071-5079 (2022). <https://doi.org/10.1007/s00405-022-07437-0>
- 8     Almothahbi, A. *et al.* Evaluating Interventions for Sulcus Vocalis or Vocal Fold Scar: A Systematic Review and Meta-analysis. *Journal of Voice* (2024). <https://doi.org/https://doi.org/10.1016/j.jvoice.2023.11.026>
- 9     Liu, A. Q., Ji, Y. & Hu, A. Do patients regret having in-office vocal fold injections for glottic insufficiency? *Journal of Otolaryngology - Head & Neck Surgery* **52**, 33 (2023). <https://doi.org/10.1186/s40463-023-00643-8>
- 10    Misono, S. & Merati, A. L. Evidence-Based Practice: Evaluation and Management of Unilateral Vocal Fold Paralysis. *Otolaryngologic Clinics of North America* **45**, 1083-1108 (2012). <https://doi.org/https://doi.org/10.1016/j.otc.2012.06.011>
- 11    Seo, K. K. in *Facial Volumization with Fillers* 29-83 (Springer, 2021).
- 12    Cheung, H. K. *et al.* Composite hydrogel scaffolds incorporating decellularized adipose tissue for soft tissue engineering with adipose-derived stem cells. *Biomaterials* **35**, 1914-1923 (2014). <https://doi.org/10.1016/j.biomaterials.2013.11.067>
- 13    Rosen, C. A. & Simpson, C. B. in *Operative Techniques in Laryngology* 147-152 (Springer, 2024).
- 14    Lin, Y.-H., Wang, C.-T. J. A. o. O., Rhinology & Laryngology. Salvage Treatments for Poor Voice Outcomes Following Autologous Fat Injection Laryngoplasty. 00034894221140777 (2022).
- 15    Sanderson, J. D. & Simpson, C. B. Laryngeal complications after lipoinjection for vocal fold augmentation. *The Laryngoscope* **119**, 1652-1657 (2009).
- 16    Henriques, D. P., Martins, R. H. G. & Cataneo, A. J. M. Efficacy of Injectable Laryngoplasty With Hyaluronic Acid and/or Calcium Hydroxyapatite in the Treatment of Glottic Incompetence. Systematic Review and Meta-analysis. *Journal of Voice* (2023).
- 17    DeFatta, R. A., Chowdhury, F. R. & Sataloff, R. T. Complications of injection laryngoplasty using calcium hydroxylapatite. *Journal of voice* **26**, 614-618 (2012).
- 18    Adkins, D. M. & Fritz, M. A. Airway Complications Following Vocal Fold Injection Augmentation: A Case Series and Review of Literature. *Journal of Voice* (2024). <https://doi.org/https://doi.org/10.1016/j.jvoice.2024.02.019>
- 19    Capella-Monsonís, H., Crum, R. J., Hussey, G. S. & Badylak, S. F. Advances, challenges, and future directions in the clinical translation of ECM biomaterials for regenerative

- medicine applications. *Advanced Drug Delivery Reviews* **211**, 115347 (2024).  
<https://doi.org/https://doi.org/10.1016/j.addr.2024.115347>
- 20 Mora-Navarro, C. *et al.* Porcine Vocal Fold Lamina Propria-Derived Biomaterials Modulate TGF- $\beta$ 1-Mediated Fibroblast Activation in Vitro. *Acs Biomaterials Science & Engineering* **6**, 1690-1703 (2020).
  - 21 Hu, J.-J. *et al.* Scarless healing of injured vocal folds using an injectable hyaluronic acid-waterborne polyurethane hybrid hydrogel to tune inflammation and collagen deposition. *ACS Applied Materials & Interfaces* **14**, 42827-42840 (2022).
  - 22 Xu, C. C. & Mau, T. A tissue-specific, injectable acellular gel for the treatment of chronic vocal fold scarring. *Acta Biomaterialia* (2019).  
<https://doi.org/10.1016/j.actbio.2019.08.025>
  - 23 Brown, M., Li, J., Moraes, C., Tabrizian, M. & Li-Jessen, N. Y. K. Decellularized extracellular matrix: New promising and challenging biomaterials for regenerative medicine. *Biomaterials* **289**, 121786 (2022).  
<https://doi.org/https://doi.org/10.1016/j.biomaterials.2022.121786>
  - 24 Chen, F. M. & Liu, X. Advancing biomaterials of human origin for tissue engineering. *Progress in Polymer Science* **53**, 86-168 (2016).  
<https://doi.org/10.1016/j.progpolymsci.2015.02.004>
  - 25 Sadtler, K. *et al.* Proteomic composition and immunomodulatory properties of urinary bladder matrix scaffolds in homeostasis and injury. *Seminars in Immunology* **29**, 14-23 (2017). <https://doi.org/https://doi.org/10.1016/j.smim.2017.05.002>
  - 26 Wang, W. *et al.* Preparation and Characterization of Pro-Angiogenic Gel Derived from Small Intestinal Submucosa. *Acta Biomaterialia* **29**, 135-148 (2016).  
<https://doi.org/10.1016/j.actbio.2015.10.013>
  - 27 Brown, M., Zhu, S., Taylor, L., Tabrizian, M. & Li-Jessen, N. Y. K. Unraveling the Relevance of Tissue-Specific Decellularized Extracellular Matrix Hydrogels for Vocal Fold Regenerative Biomaterials: A Comprehensive Proteomic and In Vitro Study. *Advanced NanoBiomed Research* **3**, 2200095 (2023).  
<https://doi.org/https://doi.org/10.1002/anbr.202200095>
  - 28 Miri, A. K. Mechanical characterization of vocal fold tissue: a review study. *Journal of Voice* **28**, 657-667 (2014).
  - 29 Wolf, M. T. *et al.* A hydrogel derived from decellularized dermal extracellular matrix. *Biomaterials* **33**, 7028-7038 (2012). <https://doi.org/10.1016/j.biomaterials.2012.06.051>
  - 30 Kim, Y. M. *et al.* Adipose-derived stem cell-containing hyaluronic acid/alginate hydrogel improves vocal fold wound healing. *The Laryngoscope* **124**, E64-E72 (2014).
  - 31 Choi, J.-S., Heang Oh, S., Kim, Y.-M. & Lim, J.-Y. Hyaluronic Acid/Alginate Hydrogel Containing Hepatocyte Growth Factor and Promotion of Vocal Fold Wound Healing. *Tissue Engineering and Regenerative Medicine* **17**, 651-658 (2020).  
<https://doi.org/10.1007/s13770-020-00280-6>
  - 32 Mayer, S. V., Murnauer, A., von Wrisberg, M. K., Jokisch, M. L. & Lang, K. Photo-Induced and Rapid Labeling of Tetrazine-Bearing Proteins via Cyclopropanone-Caged Bicyclononynes. *Angew Chem Int Ed Engl* (2019). <https://doi.org/10.1002/anie.201908209>
  - 33 Hermanson, G. T. in *Bioconjugate Techniques (Third Edition)* (ed Greg T. Hermanson) 229-258 (Academic Press, 2013).
  - 34 Hermanson, G. T. in *Bioconjugate Techniques (Third Edition)* (ed Greg T. Hermanson) 757-785 (Academic Press, 2013).

- 35 Reddy, N., Reddy, R. & Jiang, Q. Crosslinking biopolymers for biomedical applications. *Trends Biotechnol* **33**, 362-369 (2015). <https://doi.org/10.1016/j.tibtech.2015.03.008>
- 36 Luo, Y. *et al.* Injectable hyaluronic acid-dextran hydrogels and effects of implantation in ferret vocal fold. *J Biomed Mater Res B Appl Biomater* **93**, 386-393 (2010). <https://doi.org/10.1002/jbm.b.31593>
- 37 King, R. E. *et al.* Biocompatibility and Viscoelastic Properties of Injectable Resilin-Like Polypeptide and Hyaluronan Hybrid Hydrogels in Rabbit Vocal Folds. *Regenerative Engineering and Translational Medicine* **5**, 373-386 (2019). <https://doi.org/10.1007/s40883-019-00094-6>
- 38 Walimbe, T., Calve, S., Panitch, A. & Sivasankar, M. P. Incorporation of types I and III collagen in tunable hyaluronan hydrogels for vocal fold tissue engineering. *Acta Biomaterialia* **87**, 97-107 (2019). <https://doi.org/10.1016/j.actbio.2019.01.058>
- 39 Tindell, R. K. *et al.* Trilayered Hydrogel Scaffold for Vocal Fold Tissue Engineering. *Biomacromolecules* **23**, 4469-4480 (2022). <https://doi.org/10.1021/acs.biomac.1c01149>
- 40 Zhang, D., Dumont, M.-J. & Cherestes, A. An efficient strategy for the synthesis of 5-hydroxymethylfurfural derivative based poly ( $\beta$ -thioether ester) via thiol-Michael addition polymerization. *J RSC advances* **6**, 83466-83470 (2016).
- 41 Hunckler, M. D. *et al.* Linkage Groups within Thiol–Ene Photoclickable PEG Hydrogels Control In Vivo Stability. *Advanced Healthcare Materials* **8**, 1900371 (2019). <https://doi.org/10.1002/adhm.201900371>
- 42 Pirota, V., Benassi, A. & Doria, F. Lights on 2,5-diaryl tetrazoles: applications and limits of a versatile photoclick reaction. *Photochemical & Photobiological Sciences* **21**, 879-898 (2022). <https://doi.org/10.1007/s43630-022-00173-8>
- 43 Mueller, E., Poulin, I., Bodnaryk, W. J. & Hoare, T. Click Chemistry Hydrogels for Extrusion Bioprinting: Progress, Challenges, and Opportunities. *Biomacromolecules* **23**, 619-640 (2022). <https://doi.org/10.1021/acs.biomac.1c01105>
- 44 Zou, X. *et al.* Modeling the Maturation of the Vocal Fold Lamina Propria Using a Bioorthogonally Tunable Hydrogel Platform. *Advanced Healthcare Materials* **n/a**, 2301701 (2023). <https://doi.org/10.1002/adhm.202301701>
- 45 Carthew, J., Frith, J., Forsythe, J. & Truong, V. Polyethylene glycol–gelatin hydrogels with tuneable stiffness prepared by horseradish peroxidase-activated tetrazine–norbornene ligation. *Materials Chemistry B* **6**, 1394-1401 (2018).
- 46 Karver, M. R., Weissleder, R. & Hilderbrand, S. A. Synthesis and evaluation of a series of 1,2,4,5-tetrazines for bioorthogonal conjugation. *Bioconjug Chem* **22**, 2263-2270 (2011). <https://doi.org/10.1021/bc200295y>
- 47 Desai, R. M., Koshy, S. T., Hilderbrand, S. A., Mooney, D. J. & Joshi, N. S. Versatile click alginate hydrogels crosslinked via tetrazine–norbornene chemistry. *Biomaterials* **50**, 30-37 (2015).
- 48 Lueckgen, A. *et al.* Hydrolytically-degradable click-crosslinked alginate hydrogels. *Biomaterials* **181**, 189-198 (2018). <https://doi.org/10.1016/j.biomaterials.2018.07.031>
- 49 Claudio-Rizo, J. A. *et al.* Influence of residual composition on the structure and properties of extracellular matrix derived hydrogels. *J Materials Science Engineering: C* **79**, 793-801 (2017).
- 50 Jeong, W., Kim, M. K. & Kang, H. W. Effect of detergent type on the performance of liver decellularized extracellular matrix-based bio-inks. *J Tissue Eng* **12**, 2041731421997091

- (2021). <https://doi.org/10.1177/2041731421997091>
- 51 Mohammadi, S., Ravanbakhsh, H., Taheri, S., Bao, G. & Mongeau, L. Immunomodulatory Microgels Support Proregenerative Macrophage Activation and Attenuate Fibroblast Collagen Synthesis. *Advanced Healthcare Materials* **11**, 2102366 (2022). <https://doi.org/https://doi.org/10.1002/adhm.202102366>
  - 52 Ma, Z. *et al.* Bioinspired tough gel sheath for robust and versatile surface functionalization. *Science Advances* **7**, eabc3012 <https://doi.org/10.1126/sciadv.abc3012>
  - 53 Svistushkin, M. V. *et al.* Collagen fibrillar structures in vocal fold scarring and repair using stem cell therapy: a detailed histological, immunohistochemical and atomic force microscopy study. *Journal of Microscopy* **274**, 55-68 (2019). <https://doi.org/https://doi.org/10.1111/jmi.12784>
  - 54 Heris, H. K., Miri, A. K., Tripathy, U., Barthelat, F. & Mongeau, L. Indentation of poroviscoelastic vocal fold tissue using an atomic force microscope. *Journal of the Mechanical Behavior of Biomedical Materials* **28**, 383-392 (2013). <https://doi.org/https://doi.org/10.1016/j.jmbbm.2013.05.026>
  - 55 Taheri, S. *Injectable and Functionalized Tough Porous Hydrogels for Vocal Fold Repair*. (McGill University (Canada), 2022).
  - 56 Chhetri, D. K., Zhang, Z. & Neubauer, J. Measurement of Young's Modulus of Vocal Folds by Indentation. *Journal of Voice* **25**, 1-7 (2011). <https://doi.org/https://doi.org/10.1016/j.jvoice.2009.09.005>
  - 57 Hui, E., Gimeno, K. I., Guan, G. & Caliri, S. R. Spatiotemporal Control of Viscoelasticity in Phototunable Hyaluronic Acid Hydrogels. *Biomacromolecules* **20**, 4126-4134 (2019). <https://doi.org/10.1021/acs.biomac.9b00965>
  - 58 Chan, R. W. & Titze, I. R. Viscoelastic shear properties of human vocal fold mucosa: measurement methodology and empirical results. *J Acoust Soc Am* **106**, 2008-2021 (1999).
  - 59 Goodyer, E., Hemmerich, S., Muller, F., Kobler, J. B. & Hess, M. The shear modulus of the human vocal fold, preliminary results from 20 larynxes. *Eur Arch Otorhinolaryngol* **264**, 45-50 (2007). <https://doi.org/10.1007/s00405-006-0133-8>
  - 60 Goodyer, E., Muller, F., Licht, K. & Hess, M. In vivo measurement of the shear modulus of the human vocal fold: interim results from eight patients. *Eur Arch Otorhinolaryngol* **264**, 631-635 (2007). <https://doi.org/10.1007/s00405-006-0239-z>
  - 61 Chan, R. W. & Rodriguez, M. L. A simple-shear rheometer for linear viscoelastic characterization of vocal fold tissues at phonatory frequencies. *Journal of the Acoustical Society of America* **124**, 1207-1219 (2008). <https://doi.org/10.1121/1.2946715>
  - 62 Comperat, L. *et al.* Harnessing Human Placental Membrane-Derived Bioinks: Characterization and Applications in Bioprinting and Vasculogenesis. *Advanced Healthcare Materials* **n/a**, 2303370 (2023). <https://doi.org/https://doi.org/10.1002/adhm.202303370>
  - 63 Bist, S. *et al.* in *Regenerative Medicine: Emerging Techniques to Translation Approaches* (eds Nishant Chakravorty & Praphulla Chandra Shukla) 143-180 (Springer Nature Singapore, 2023).
  - 64 Moccia, F., Negri, S., Shekha, M., Faris, P. & Guerra, G. Endothelial Ca<sup>2+</sup> Signaling, Angiogenesis and Vasculogenesis: Just What It Takes to Make a Blood Vessel. *International Journal of Molecular Sciences* **20** (2019).
  - 65 Payne, S., Neal, A. & De Val, S. Transcription factors regulating vasculogenesis and angiogenesis. *Developmental Dynamics* **n/a** (2023).

- <https://doi.org/https://doi.org/10.1002/dvdy.575>
- 66 Ribatti, D. The discovery of the fundamental role of VEGF in the development of the vascular system. *Mechanisms of Development* **160**, 103579 (2019). <https://doi.org/https://doi.org/10.1016/j.mod.2019.103579>
  - 67 Omorphos, N. P., Gao, C., Tan, S. S. & Sangha, M. S. Understanding angiogenesis and the role of angiogenic growth factors in the vascularisation of engineered tissues. *Mol Biol Rep* **48**, 941-950 (2021). <https://doi.org/10.1007/s11033-020-06108-9>
  - 68 Tsuji-Tamura, K. & Ogawa, M. Morphology regulation in vascular endothelial cells. *Inflammation and regeneration* **38**, 1-13 (2018).
  - 69 Herbert, S. P. & Stainier, D. Y. R. Molecular control of endothelial cell behaviour during blood vessel morphogenesis. *Nature Reviews Molecular Cell Biology* **12**, 551-564 (2011). <https://doi.org/10.1038/nrm3176>
  - 70 Fujita, K. *et al.* Modulation of the mechanical properties of ventricular extracellular matrix hydrogels with a carbodiimide crosslinker and investigation of their cellular compatibility. *AIMS Materials Science* **5**, 54-74 (2018). <https://doi.org/10.3934/matricsci.2018.1.54>
  - 71 Fujita, K. *et al.* Modulation of the mechanical properties of ventricular extracellular matrix hydrogels with a carbodiimide crosslinker and investigation of their cellular compatibility. *AIMS Materials Science*
  - 72 van Wachem, P. B. *et al.* In vivo biocompatibility of carbodiimide-crosslinked collagen matrices: Effects of crosslink density, heparin immobilization, and bFGF loading. *Journal of Biomedical Materials Research* **55**, 368-378 (2001). [https://doi.org/https://doi.org/10.1002/1097-4636\(20010605\)55:3<368::AID-JBM1025>3.0.CO;2-5](https://doi.org/https://doi.org/10.1002/1097-4636(20010605)55:3<368::AID-JBM1025>3.0.CO;2-5)
  - 73 Delplace, V. *et al.* Nonswelling, Ultralow Content Inverse Electron-Demand Diels–Alder Hyaluronan Hydrogels with Tunable Gelation Time: Synthesis and In Vitro Evaluation. **30**, 1903978 (2020).
  - 74 Li, X. *et al.* Designing regenerative bioadhesives for tissue repair and regeneration. *Advanced Therapeutics* **7**, 2300139 (2024).
  - 75 Cochereau, T. *et al.* Mechanics of human vocal folds layers during finite strains in tension, compression and shear. *Journal of Biomechanics* **110**, 109956 (2020). <https://doi.org/https://doi.org/10.1016/j.jbiomech.2020.109956>
  - 76 Li, N. Y., Heris, H. K. & Mongeau, L. Current Understanding and Future Directions for Vocal Fold Mechanobiology. *J Cytol Mol Biol* **1**, 001 (2013). <https://doi.org/10.13188/2325-4653.1000001>
  - 77 Li, N. Y. *et al.* Biosimulation of acute phonotrauma: an extended model. *Laryngoscope* **121**, 2418-2428 (2011). <https://doi.org/10.1002/lary.22226>
  - 78 Taheri, S. *et al.* Injectable, pore-forming, perfusable double-network hydrogels resilient to extreme biomechanical stimulations. *Advanced Science* **9**, 2102627 (2022).
  - 79 Hazur, J., Endrizzi, N., Schubert, D. W., Boccaccini, A. R. & Fabry, B. Stress relaxation amplitude of hydrogels determines migration, proliferation, and morphology of cells in 3-D culture. *Biomater Sci-Uk* **10**, 270-280 (2022).
  - 80 Yu, W. *et al.* Gradual Stress-Relaxation of Hydrogel Regulates Cell Spreading. *International Journal of Molecular Sciences* **23** (2022).
  - 81 Liu, Y. *et al.* Viscoelastic hydrogels regulate adipose-derived mesenchymal stem cells for nucleus pulposus regeneration. *Acta Biomaterialia* **180**, 244-261 (2024).
  - 82 Sumey, J. L., Johnston, P. C., Harrell, A. M. & Caliar, S. R. Hydrogel mechanics regulate

- fibroblast DNA methylation and chromatin condensation. *J Biomaterials Science* **11**, 2886-2897 (2023).
- 83 Chan, R. W. Nonlinear viscoelastic characterization of human vocal fold tissues under large-amplitude oscillatory shear (LAOS). *Journal of Rheology* **62**, 695-712 (2018). <https://doi.org/10.1122/1.4996320>
- 84 Miller, B., Hansrisuk, A., Highley, C. B. & Caliri, S. R. Guest–Host Supramolecular Assembly of Injectable Hydrogel Nanofibers for Cell Encapsulation. *ACS Biomaterials Science & Engineering* **7**, 4164-4174 (2021). <https://doi.org/10.1021/acsbiomaterials.1c00275>
- 85 Li, W. *et al.* Preparation, mechanical properties, fatigue and tribological behavior of double crosslinked high strength hydrogel. *Journal of the Mechanical Behavior of Biomedical Materials* **126**, 105009 (2022). <https://doi.org/https://doi.org/10.1016/j.jmbbm.2021.105009>
- 86 Wong, J. H. M. *et al.* Injectable hybrid-crosslinked hydrogels as fatigue-resistant and shape-stable skin depots. *Biomacromolecules* **23**, 3698-3712 (2022).
- 87 Zhang, Q. *et al.* Collagen gel contraction assays: From modelling wound healing to quantifying cellular interactions with three-dimensional extracellular matrices. *European journal of cell biology* **101**, 151253 (2022).
- 88 Scott, R. A., Robinson, K. G., Kiick, K. L. & Akins, R. E. Human Adventitial Fibroblast Phenotype Depends on the Progression of Changes in Substrate Stiffness. *Adv Healthc Mater* **9**, e1901593 (2020). <https://doi.org/10.1002/adhm.201901593>
- 89 Raspanti, M. *et al.* The extracellular matrix of the human aortic wall: ultrastructural observations by FEG-SEM and by tapping-mode AFM. *Micron* **37**, 81-86 (2006).
- 90 Peñuela, L. *et al.* Atomic force microscopy for biomechanical and structural analysis of human dermis: A complementary tool for medical diagnosis and therapy monitoring. *Experimental Dermatology* **27**, 150-155 (2018).
- 91 Norman, M. D., Ferreira, S. A., Jowett, G. M., Bozec, L. & Gentleman, E. Measuring the elastic modulus of soft culture surfaces and three-dimensional hydrogels using atomic force microscopy. *Nature Protocols* **16**, 2418-2449 (2021).
- 92 Lotz, C. *et al.* Cross-linked Collagen Hydrogel Matrix Resisting Contraction To Facilitate Full-Thickness Skin Equivalents. *ACS Applied Materials & Interfaces* **9**, 20417-20425 (2017). <https://doi.org/10.1021/acsaami.7b04017>
- 93 Dong, L. *et al.* The effect of collagen hydrogels on chondrocyte behaviors through restricting the contraction of cell/hydrogel constructs. *Regenerative Biomaterials* **8**, rbab030 (2021). <https://doi.org/10.1093/rb/rbab030>
- 94 Sato, K. in *Pericyte Biology-Novel Concepts* 79-93 (Springer, 2018).
- 95 Mobashir, M. K., Mohamed, A. E. R. S., Quriba, A. S., Anany, A. M. & Hassan, E. M. Linear Measurements of Vocal Folds and Laryngeal Dimensions in Freshly Excised Human Larynges. *Journal of Voice* **32**, 525-528 (2018). <https://doi.org/https://doi.org/10.1016/j.jvoice.2017.08.024>
- 96 Wu, J. *et al.* An injectable extracellular matrix derived hydrogel for meniscus repair and regeneration. *Acta Biomaterialia* **16**, 49-59 (2015). <https://doi.org/10.1016/j.actbio.2015.01.027>
- 97 Liao, J., Li, X., He, W., Guo, Q. & Fan, Y. A biomimetic triple-layered biocomposite with effective multifunction for dura repair. *Acta Biomaterialia* **130**, 248-267 (2021). <https://doi.org/https://doi.org/10.1016/j.actbio.2021.06.003>

- 98 Dearth, C. L. *et al.* The effect of terminal sterilization on the material properties and in vivo remodeling of a porcine dermal biologic scaffold. *Acta Biomaterialia* **33**, 78-87 (2016). <https://doi.org/https://doi.org/10.1016/j.actbio.2016.01.038>
- 99 Barceló, X., Eichholz, K. F., Garcia, O. & Kelly, D. J. Tuning the Degradation Rate of Alginate-Based Bioinks for Bioprinting Functional Cartilage Tissue. *Biomedicines* **10** (2022). <https://doi.org/10.3390/biomedicines10071621>
- 100 Hu, J. *et al.* Bioactive-Tissue-Derived Nanocomposite Hydrogel for Permanent Arterial Embolization and Enhanced Vascular Healing. *Advanced Materials* **32**, 2002611 (2020). <https://doi.org/https://doi.org/10.1002/adma.202002611>
- 101 Wolf, M. T. *et al.* A biologic scaffold–associated type 2 immune microenvironment inhibits tumor formation and synergizes with checkpoint immunotherapy. *Science translational medicine* **11**, eaat7973 (2019).
- 102 Choi, Y. S. *et al.* Immunomodulatory Scaffolds Derived from Lymph Node Extracellular Matrices. *ACS Appl Mater Interfaces* **13**, 14037-14049 (2021). <https://doi.org/10.1021/acsami.1c02542>
- 103 Zhang, Q.-Y. *et al.* Acceleration of wound healing by composite small intestinal submucosa hydrogels through immunomodulation. *Composites Part B: Engineering* **254**, 110550 (2023). <https://doi.org/https://doi.org/10.1016/j.compositesb.2023.110550>
- 104 Keane, T. J. *et al.* Preparation and Characterization of a Biologic Scaffold and Hydrogel Derived from Colonic Mucosa. *Biomedical Materials Research B Applied Biomaterials* **105**, 291-306 (2017). <https://doi.org/10.1002/jbm.b.33556>
- 105 Nie, R. *et al.* EGCG modified small intestine submucosa promotes wound healing through immunomodulation. *Composites Part B: Engineering*, 111005 (2023). <https://doi.org/https://doi.org/10.1016/j.compositesb.2023.111005>
- 106 Keane, T. J., Swinehart, I. T. & Badylak, S. F. Methods of Tissue Decellularization Used for Preparation of Biologic Scaffolds and In Vivo Relevance. *Methods* **84**, 25-34 (2015).
- 107 Long, J., Qin, Z., Chen, G., Song, B. & Zhang, Z. Decellularized extracellular matrix (d-ECM): the key role of the inflammatory process in pre-regeneration after implantation. *Biomater Sci-Uk* **11**, 1215-1235 (2023). <https://doi.org/10.1039/D2BM01204A>
- 108 Moore, E. M. *et al.* Biomaterials direct functional B cell response in a material-specific manner. *Science Advances* **7**, eabj5830 <https://doi.org/10.1126/sciadv.abj5830>
- 109 Coburn, P. T., Li, X., Li, J., Kishimoto, Y. & Li-Jessen, N. Y. Progress in Vocal Fold Regenerative Biomaterials: An Immunological Perspective. *Advanced NanoBiomed Research*, 2100119 (2021).
- 110 DeStefano, S. *et al.* Conserved and tissue-specific immune responses to biologic scaffold implantation. *bioRxiv : the preprint server for biology* (2023). <https://doi.org/10.1101/2023.08.15.553390>
- 111 Luttikhuisen, D. T. *et al.* The correlation between difference in foreign body reaction between implant locations and cytokine and MMP expression. *Biomaterials* **27**, 5763-5770 (2006). <https://doi.org/https://doi.org/10.1016/j.biomaterials.2006.07.004>
- 112 Amer, L. D. & Bryant, S. J. The in vitro and in vivo response to MMP-sensitive poly (ethylene glycol) hydrogels. *Annals of biomedical engineering* **44**, 1959-1969 (2016).
- 113 Xu, M. *et al.* Inflammation-mediated matrix remodeling of extracellular matrix-mimicking biomaterials in tissue engineering and regenerative medicine. *Acta Biomaterialia* **151**, 106-117 (2022). <https://doi.org/https://doi.org/10.1016/j.actbio.2022.08.015>
- 114 Record Ritchie, R. D., Salmon, S. L., Hiles, M. C. & Metzger, D. W. Lack of



- immunogenicity of xenogeneic DNA from porcine biomaterials. *Surgery Open Science* **10**, 83-90 (2022). <https://doi.org/https://doi.org/10.1016/j.sopen.2022.07.005>
- 115 Pápay, Z. E. *et al.* Optimization and Development of Albumin–Biopolymer Bioconjugates with Solubility-Improving Properties. *Biomedicines* **9** (2021).
- 116 Muñoz, Z., Shih, H. & Lin, C.-C. Gelatin hydrogels formed by orthogonal thiol–norbornene photochemistry for cell encapsulation. *Biomater Sci-Uk* **2**, 1063-1072 (2014). <https://doi.org/10.1039/C4BM00070F>
- 117 Gaston, J., Quinchia Rios, B., Bartlett, R., Berchtold, C. & Thibeault, S. L. The response of vocal fold fibroblasts and mesenchymal stromal cells to vibration. *PLoS One* **7**, e30965 (2012). <https://doi.org/10.1371/journal.pone.0030965>
- 118 Kort-Mascort, J. *et al.* Bioprinted cancer-stromal in-vitro models in a decellularized ECM-based bioink exhibit progressive remodeling and maturation. *Biomedical Materials* **18**, 045022 (2023). <https://doi.org/10.1088/1748-605X/acd830>
- 119 Schindelin, J. *et al.* Fiji: an open-source platform for biological-image analysis. *Nat Methods* **9**, 676-682 (2012). <https://doi.org/10.1038/nmeth.2019>
- 120 Teller, S. S. *et al.* High-frequency viscoelastic shear properties of vocal fold tissues: implications for vocal fold tissue engineering. *Tissue Engineering Part A* **18**, 2008-2019 (2012).
- 121 Kelleher, J. E., Siegmund, T., Du, M., Naseri, E. & Chan, R. W. Empirical measurements of biomechanical anisotropy of the human vocal fold lamina propria. *Biomechanics and modeling in mechanobiology* **12**, 555-567 (2013).
- 122 Heris, H. K., Latifi, N., Vali, H., Li, N. & Mongeau, L. Investigation of chitosan-glycol/glyoxal as an injectable biomaterial for vocal fold tissue engineering. *Procedia Engineering* **110**, 143-150 (2015).
- 123 Latifi, N. *et al.* A flow perfusion bioreactor system for vocal fold tissue engineering applications. *Tissue Engineering Part C: Methods* **22**, 823-838 (2016).
- 124 Reyes Valenzuela, A. *et al.* Polymeric microspheres containing human vocal fold fibroblasts for vocal fold regeneration. *The Laryngoscope* **131**, 1828-1834 (2021).

## Chapter 6. Discussion

This thesis proposed the use of click chemistry to fabricate a regenerative, scalable dECM hydrogel suitable as an injectable VF biomaterial with ECM-like microstructure, VF-mimicking mechanical properties, and a slowed degradation rate. The novel click dECM hydrogel has introduced practical scale-up considerations to the conversation of dECM tissue-specificity, expanded material design options for *in situ* gelling biomaterials, and shown potential for improving predictability of VF injection outcomes. However, limitations of the proposed click dECM hydrogel remain that require further development and validation for successful application to VF regeneration in humans. Herein, we discuss strategies for the further work on the novel click dECM hydrogel including hydrogel optimization, additional functional analysis of regenerative properties, and requirements for clinical translation.

### 6.1. Tissue Specificity and Choice of Tissue Source

The first of the dual aims of this thesis was to evaluate the importance of tissue specific dECM for regeneration in contrast to practicality for scale up, in the context of VF tissue engineering applications. Varied sources in literature report that use of tissue-specific dECM leads corresponds to improved regenerative outcomes in the target tissue over non-tissue-specific sources.<sup>40</sup> For instance, bone dECM has been shown to most effectively induce osteogenesis, skeletal muscle dECM to preferentially generate striated muscle ECM and myotubes, and neural tissue sources to stimulate regeneration of functional neurons and stem cell differentiation into neural-lineage cells.<sup>9,10,41-43</sup>

Decellularization methodology impacts retention and alteration of proteins and GAGs. Historically, research into dECM tissue-specificity has lacked a standardized decellularization protocol, though recent efforts have sought to overcome this challenge. In an effort to produce a standardized protocol, eight types of tissue including VF were decellularized with sodium deoxycholate, DNase, and peracetic acid.<sup>44</sup> The number of proteins identified following decellularization varied greatly based on tissue type, but primary component analysis revealed that of the tissues tested, the composition of VF dECM was most similar to other dECMs from other respiratory (salivary gland, lung) and soft tissues (skin). Likewise, tendon and cartilage dECMs showed high similarity in proteomic profile. In studies of tissue-specificity, dECM from tissues within the same lineage, i.e., another musculoskeletal, respiratory, or nervous tissue, has been

shown to promote a more similar regenerative response than more distant sources. For instance, cartilage dECM has been found to promote osteogenesis over lung dECM.<sup>9,10,40</sup>

In this thesis, the decellularization protocols used to produce VF and SIS dECMs were different. More stringent decellularization methods are reported for VF than the ethanol and peracetic acid used for SIS dECM.<sup>11,45,46</sup> A notable difference between protocols was that nucleases were used in the VF dECM decellularization protocol, but not SIS dECM. Long-term exposure to nucleases, as was required for effective VF decellularization in this thesis, can disrupt ECM structure.<sup>47</sup> When residual nucleases remain in the dECM, the immune response may be altered and cellular attachment may be impeded.<sup>47,48</sup>

The composition, physical and mechanical characteristics, and functional outcomes measures of VF dECM and our proposed alternative, SIS dECM, were compared throughout the thesis. Although our findings confirmed that VF dECM is more similar to native VF, SIS dECM had less variability between batches and showed similar outcomes in terms of neo-ECM deposition. In our continued comparison between dECM tissue sources with the click dECM hydrogels, mechanics and biological response were overall comparable between the SIS and VF dECM materials. This finding was anticipated based on our proteomic analyses, wherein we found similar levels of proteins associated with extracellular matrix organization and remodeling, as well as cell-substrate adhesion.<sup>45</sup>

However, we identified one difference between the click hydrogels. Specifically, the macrophage response in the subcutaneous rat model was more indicative of a constructive immune response to SIS-Alg than VF-Alg. Proteomic analyses showed differences in immune related protein content, with SIS dECM showing a significantly larger number of proteins involved in regulation of cell migration, wound healing, and the acute inflammatory response, as well as cellular response to stimulus than VF dECM.<sup>45</sup> SIS dECM may therefore have a greater immunomodulatory capacity than VF dECM, possibly associated with decellularization method. Overall, it is reasonable to conclude that the similarity between SIS and VF dECM combined with reduced batch to batch variation and less intensive decellularization protocol used for SIS indicate its potential utility as an effective VF biomaterial.

To further validate outcomes from this thesis, future work can include additional high-throughput and functional assays comparing the response of VF-relevant cell types to the environment

provided by SIS and VF derived click dECM hydrogels. Including dECM derived from disparate sources (i.e. cartilage, bone) and another soft tissue dECM (i.e. skin) in the experiments could be used to confirm SIS as a sufficiently similar alternative to VF dECM. Specifically, multiplex protein analyses of secretions can be performed on click gels with encapsulated fibroblasts, endothelial cells, and macrophages to identify tissue-specific differences in the production of neo-ECM and inflammatory proteins.<sup>49,50</sup>

VF dECM hydrogels have previously been found to downregulate fibroblast-myofibroblast transdifferentiation compared to collagen and UBM hydrogels. HVFF showed decreased expression of COL1A1 and  $\alpha$ SMA when stimulated with TGF- $\beta$ .<sup>11</sup> In our neo-collagen deposition assay, we found a decrease in the total soluble collagen content. Additionally, our proteomic data showed overrepresentation of proteins associated with ECM organization in VF dECM, potentially indicating that VF dECM specifically promotes organization of healthy, rather than fibrotic, neo-ECM. This hypothesis requires further testing. One approach is to evaluate the role VF vs SIS dECM play in modulating VF fibrosis. By stimulating HVFF encapsulated in VF and SIS click dECM gels with fibrotic molecules (i.e. TGF- $\beta$ ), this comparative study would help further delineate the modulatory effect of both click dECM hydrogels on fibroblast-myofibroblast transdifferentiation.<sup>11,51,52</sup>

Besides HVFF, macrophage polarization in response to a biomaterial is a critical determining factor in VF fibrosis.<sup>12,53</sup> In the animal study of this thesis, the ratio of cells expressing the M2 marker CD206 to the pan macrophage marker CD68 was used to evaluate the polarization of anti-inflammatory M2 macrophages. In reality, macrophage polarization is a spectrum of phenotypes. Macrophages may simultaneously express a mixture of the markers classically used to identify M1 and M2 macrophages with markers of immunofluorescence.<sup>54-57</sup> Instead, flow cytometry is recommended for future validation with respect to the complexity of the macrophage response.

Flow cytometry allows a larger panel of markers to be profiled simultaneously, enabling more accurate distinction between basal, M1, M2, and mixed macrophage phenotypes.<sup>54,58</sup> These comparative experiments will help assess the relevance of SIS-derived hydrogels for VF applications on a more comprehensive level. In the next section, we discuss how performing subsequent assays in a VF-specific environment with integrated repetitive mechanical loading would increase applicability to predicting efficacy for wound healing.

## 6.2. Mechanical Property Mimicry

In developing a click dECM composite hydrogel as the second aim of this thesis, we sought to mimic the mechanical properties of native VF to enhance the performance of treated tissue and support functional regeneration.

The click hydrogels developed in this thesis consist of dECM hydrogels reinforced with alginate linkages between a pre-existing ECM-like network. A major advantage of dECM hydrogels is the replication of both tissue composition and microstructure.<sup>59</sup> However, these hydrogels are typically weaker than the original tissue, resulting in a mechanical mismatch.<sup>60</sup> VF biomaterials require specific mechanical characteristics to withstand repetitive high strain and compression, as well as to stimulate regeneration of the characteristic VF tissue.<sup>61-64</sup>

Composites can strengthen the dECM hydrogels and better mimic the mechanical properties of native tissue but crosslinking methods may cause deleterious side effects.<sup>62,65-68</sup> Our methodology of reinforcing the more quickly forming dECM hydrogel with slower, *in situ* click crosslinking results in the overall retention of ECM structure while mimicking VF mechanical properties on both a micro and macroscale.

The click dECM hydrogels also exhibit improved stability, slowed degradation, and resistance to contraction. Contraction, swelling, or material degradation are factors that may lead to difficulty in predicting outcomes in VF injectables.<sup>69-72</sup> This unpredictability can cause unfavorable results such as airway blockage due to overinjection, a potential deleterious side-effect of autologous fat injection, or failure to sufficiently restore the glottal wave during phonation.<sup>73</sup> Hyaluronan injectables are associated with rapid degradation, high swelling ratio, frequent reinjection, and a 17.8% discontinuation rate due to adverse effects.<sup>70,71</sup> Collagen-based hydrogels, which includes both dECM and autologous fat, are commonly associated with high levels of fibroblast-based contraction.<sup>74,75</sup> Consistent with our findings, contraction, swelling, and degradation of collagen-based hydrogels may be mitigated by use of composites and crosslinking.<sup>34,75,76</sup>

However, several limitations to the evaluation of the mechanical properties and stability of the click dECM hydrogels exist. In this thesis, mechanical tests were performed on hydrogels alone and the degradation studies were performed under cell-free conditions. Also, cyclic stress relaxation testing was performed under a maximum of 5% strain. Culture with cells can change the properties of a biomaterial, and cell-free, enzyme-based degradation assays do not perfectly

replicate the *in vivo* degradation process.<sup>36,77,78</sup> Besides, native human VF exhibit nonlinear behavior above 10% at low frequencies, and above 50% at higher frequencies (>125 Hz).<sup>79</sup> When subjected to high strains beyond the linear range of the VF, biomaterials must therefore be able to resist fatigue from deformation and repeatedly recover.<sup>64,79</sup>

The ability of click dECM hydrogels to recovery under repetitive deformation at high strain and in the nonlinear regime has not yet been tested. Of potential concern is that chemically crosslinked biomaterials may lack fatigue resistance under high strains.<sup>80-82</sup> Chemical crosslinks break permanently at high strains and do not recover. However, the shear-thinning capability of physical crosslinks in the click dECM hydrogels combined with the higher stiffness afforded by click chemistry may enable improved fatigue resistance under high strain in the nonlinear regime of VF.<sup>79,80,82</sup> Prior to further animal studies, click dECM hydrogels with encapsulated HVFF could be cultured in a VF bioreactor to assess resilience to vibration-induced fatigue and changes in mechanical properties due to remodeling by HVFF.

VF bioreactors are designed to simulate the tissue-specific structural and mechanical environment of the vocal fold. Thanks to their integration of controllable frequency and displacement with cell cultures, VF bioreactors can be used to model VF mechanobiology and phonatory oscillation at a realistic scale. VF bioreactors have been successfully applied for testing cellular response and biomaterial efficacy *in vitro*.<sup>83</sup> For instance, hydrogels with weak mechanical properties ( $G' \sim 100$  Pa) have been shown to fragment and degrade in bioreactors at phonatory frequencies, showing a lack of suitability for injectable VF applications and the importance of VF mimicry in biomaterial development<sup>64</sup>

Culture of cells in VF bioreactors under vibratory stimulation at frequencies in the typical speaking range of human phonation (100-300Hz) has also been shown to alter expression of inflammatory and neo-ECM markers in a manner dependent on material composition and stiffness.<sup>83,84</sup> As such, performing biomechanical analysis in VF bioreactors would aid in evaluating the mechanical stability and cellular response to click dECM hydrogels in a VF-specific environment.<sup>85-87</sup>

Subsequently, mechanical properties and stability could be tested in a long-term rabbit model of VF injury. Currently, animal models remain the gold standard as a final step for preclinical biomaterial assessment, as the response to biomaterials is more complex than can be recapitulated *in vitro* with the monocultures used in VF bioreactors.<sup>15,88</sup> When injected *in vivo*, the hydrogels

undergo continuous remodeling involving immune cells and matrix metalloproteinases as part of the tissue regeneration process that impacts biomaterial mechanical properties.<sup>41,89</sup> Mechanical testing including atomic force microscopy, compression, and cyclic stress relaxation could also be performed on tissue explants in comparison to a healthy control at different time points.<sup>90,91</sup> Mechanical testing on cell-laden click dECM hydrogels cultured in a VF bioreactor with subsequent evaluation in a VF-specific animal model will help to ensure both durability under VF-specific mechanical loading and maintenance of VF-mimicking properties in the presence of cells and the complex environment of the native VF.

### *6.3. Sufficiency of dECM-based Regeneration*

For our application, the most critical factor in developing a dECM-based click hydrogel was to validate its ability to induce a regenerative response. Click hydrogels provided a favorable environment for HVFF, which adopted fibroblast morphology and maintained greater than 90% viability without contraction. In our proteomics assays, we found that both VF and SIS dECM stimulate neo-ECM deposition. However, these dECM-only hydrogels contract by up to 90% in response to HVFF and consequently exhibit a decrease in viability over time. As previously stated, collagen-hydrogels exhibited high levels of contraction, resulting in outcome uncertainty in VF applications and reduced cellular viability, with crosslinking and composite materials enabling stabilization.<sup>34,74,75</sup> The click dECM hydrogels developed in this thesis achieved resistance to contraction through the use of a fully bioorthogonal crosslinking method.

The click hydrogels also promoted vasculogenesis over dECM-only and at similar levels to collagen through the formation of tubule-like structures, partly attributed to the proteins involved in angiogenesis-associated pathways identified from our proteomic analyses. These pathways included VEGFR-mediated vascular permeability and signaling by PDGF, while proteins in gene ontology terms for regulation of angiogenesis and response to hypoxia were specifically identified in SIS.

Vasculogenesis can be influenced by the density, stiffness, and viscoelasticity of the hydrogel.<sup>92</sup> A high concentration of dECM (20 mg/mL) was used, resulting in high density hydrogels, while the collagen hydrogels (2 mg/mL) were more permissive. High density combined with the low mechanical properties of the dECM-only hydrogels may have contributed to lack of vessel formation.<sup>92</sup> The tissue-mimicking mechanical properties of click dECM hydrogels may have

provided better support for tubule formation. *In vitro* dECM vasculogenesis assays in literature have typically used 2D culture or growth factor supplementation above the standard content of endothelial growth medium.<sup>93-95</sup> While the networks formed in these assays were more extensive, the results of this thesis indicate that it is possible to fabricate dECM hydrogels with some innate vasculogenic capacity.

In future work, stimulating HUVECs encapsulated in click dECM hydrogels with angiogenic molecules (i.e. VEGF) could aid in further demonstrating vasculogenic potential. Specifically, monitoring and monitoring angiogenic growth factor production and angiogenic marker expression (i.e. CD105) in addition to tubule and network formation would give a more comprehensive outlook on vasculogenic functionality<sup>11,96,97</sup>

While the click dECM hydrogels were biocompatible and exhibited a low foreign body response, a fibrotic capsule formed around the click hydrogel during the acute phase of the immune response. The fibrotic capsule was replaced with integrating tissue over time. However, the macrophage and B cell populations decreased but remained elevated compared to PBS controls at the 21-day end point of the study. dECM is generally thought to be immunomodulatory based on findings in tissues including gastrointestinal, muscle, and cardiac sources with particular emphasis given to stimulation of macrophage polarization toward an anti-inflammatory, regenerative M2 phenotype.<sup>8,98-101</sup> That being said, the literature reported impacts on immune cell recruitment and macrophage polarization, which may be associated with decellularization method<sup>19,102-104</sup> Additionally, this thesis did not directly compare the immune response to click dECM hydrogels to dECM-only hydrogels or an established commercial VF injectable to reduce animal use in the subcutaneous biocompatibility study.

To effectively evaluate sufficiency of VF wound healing by the click dECM hydrogels, commercial VF injectables (Juvederm®, Radiesse®) can be included as a benchmark in a VF-specific animal model as a benchmark. On a reconstructive level, structural changes in the injectables and production of neo-ECM can be evaluated using immunohistochemistry and quantitative polymerase chain reaction. Specifically, quantifying the ratio of collagen III to collagen I is a common measure of VF wound healing. In the VF, collagen I provides tensile strength while collagen III is critical for tissue compliance and elasticity. Excessive deposition of collagen I with



lower levels of collagen III are often observed in fibrotic VF.<sup>33</sup> Monitoring the ratio of collagen I to collagen III could aid in determining how the click dECM hydrogels remodel VF tissue.

On a functional level, videolaryngeal stroboscopy could be used to evaluate the degree to which the click dECM hydrogels restore the glottal wave and VF oscillatory functions upon injection to injured rabbit VF.<sup>36,105</sup> Determining whether VF function is maintained over the long term, as the hydrogels degrade, would effectively establish whether the click dECM hydrogels reduce the need for reinjection compared to commercial VF injectables.

#### *6.4. Future Prospectives*

Based on the findings of this thesis in relation to (1) the utility of dECM derived from a non-tissue specific source and (2) the regenerative and functional potential of a click dECM-alginate hydrogel, this thesis implicates broad horizons for the further development of injectable dECM-based click hydrogels within VF applications and beyond.

##### *6.4.1. Harnessing the Potential of Click Chemistry: Hydrogel Optimization*

Click chemistry has flexible utilities, and the hydrogel developed in this thesis may be adapted for use in broad applications in the VF as well as other tissues. The functionalization method used in this thesis links norbornene to any available primary amine in dECM, which is non-specific and can block the active site.<sup>106</sup> Metabolic glycoengineering enables the insertion of chemical reporter molecules into glycan structures within the dECM.<sup>106,107</sup> This approach has previously been used to incorporate alkene-modified polysaccharides within dECM for tetrazine ligation, which showed no cytotoxic effect on adipose stem cells. Specifically functionalizing glycan structures in dECM would improve repeatability and consistency in hydrogel fabrication.

The composition of the click dECM hydrogels could be readily modified for use in other tissues using dECM sources from the appropriate lineage as discussed in section 6.1. Additionally, the appropriate mechanical properties for application in the target tissue could be achieved by the degree of crosslinking to tune both mechanics and degradation rate. Methods for altering the degree of crosslinking include: (1) adjusting the ratio of dECM to alginate and (2) modifying the degree of substitution.

The ratio of norbornene to tetrazine affects the crosslink density. For instance, the Mooney lab achieved varied stiffness and swelling ratio by adjusting the ratio of Alginate-Tz to Alginate-Nb

from 0.5:1 to 4:1.<sup>108</sup> Altering the ratio of dECM to alginate can alter the stiffness, porosity, swelling kinetics and degradation rate of the hydrogel. A higher ratio of dECM to alginate would be expected to be softer and possess a higher swelling ratio, but possess a higher porosity and contain more sites for cellular adhesion.<sup>109</sup> While a high swelling ratio is contraindicated for use in the VF due to risk of airway obstruction, it can be favorable for gastric applications.<sup>110</sup> In contrast, an increased ratio of alginate to dECM would be expected to achieve a higher degree of crosslinking and exhibit increased stiffness and slower degradation kinetics for applicability in harder tissues, such as cartilage or bone.<sup>111</sup>

Also, altering the degree of substitution on the polymers could increase the availability of sites for crosslinking. The benefit of this strategy is that the biomaterial properties can be tuned while preserving the cellular adhesion sites of a majority-dECM hydrogel structure. Higher degrees of substitution are associated with increased stiffness, reduced swelling ratios, and slower degradation rates.<sup>112,113</sup> The degree of substitution may also be used to alter the reaction rate, with tetrazine ligation proceeding more rapidly at higher degrees of substitution.<sup>112</sup> In our study, we achieved a 14% degree of substitution for Alginate-MTz. We achieved this higher degree of substitution by doubling the mass of MTz per 100 mg alginate, compared to a prior protocol developed by the Mooney lab, who reported a 5% degree of substitution.<sup>108</sup> Degree of substitution may also be impacted by reaction time, the concentration of reagents such as EDC, and pH.<sup>114</sup> Overall, altering crosslink density can aid in modulating mechanical and physical properties, and has potential to further modulate the degradation rate for longer-lasting material residency in the host tissue.

The similarity of the click dECM hydrogels to the structure and mechanical properties of the native VF make them potential candidates for use in vocal fold bioreactors and mechanical modeling.<sup>61,64</sup> In a hyaluronan-based click hydrogel study, the hydrogel was initially formed by tetrazine ligation with norbornene, and subsequently stiffened by secondary crosslinking with transcyclooctene.<sup>39</sup> This click hydrogel was used to simulate mechanical conditions favorable for differentiation of MSCs into VF fibroblasts in an *in vitro* model of VF maturation. With the initial formation of the dECM hydrogel followed by click crosslinking, this technique could be harnessed *in vivo* to influence stem cell behavior and differentiation.

Further *in vitro* optimization could be performed in a microfluidic model of the VF. Microfluidic

devices are an effective method of investigating the impact of biomaterials and drugs on cellular activity under dynamic conditions using human cells in a microenvironment approximately representative of the target tissue. Once established, microfluidic models can be used to carry out high-throughput assays and evaluate experimental variables such as cell type, biomaterial composition, and mechanics under consistent, biologically relevant conditions.<sup>115</sup> Biomaterials in microfluidics devices may be evaluated for their ability to stimulate cellular infiltration, expression of regenerative genes, and neo-capillary formation.<sup>116,117</sup> While VF-specific *in vitro* models have largely been confined to bioreactors in 2D or transwell conditions, microfluidic devices create a more biologically representative environment and enable diverse testing of tissue functionality.<sup>12</sup> Large numbers of samples can be analyzed with high precision and only a small quantity of sample consumed at lower cost than animal models.<sup>118</sup>

Airway-on-a-chip microfluidic devices have been designed to mimic the mechanical stresses from respiration, as well as to test behavior of cells exposed to drugs or environmental hazards at interface of air and tissue.<sup>119</sup> These organ-on-a-chip platforms could be readily translated to mechanically active, *in vitro* optimization of click dECM hydrogels for VF applications and better predict their regenerative impact prior to use of animal models of VF injury.

#### 6.4.2. Translation to the Clinic for VF Applications

This thesis established the biocompatibility of the click dECM hydrogel, but there are additional steps necessary for successful clinical translation. For effective translation under current standards for VF biomaterials, the click dECM hydrogel would be injected into the thyroarytenoid muscle or paraglottic space.<sup>4,1006,120</sup> Unilateral VF paralysis or paresis are the most common indicators for VF injection laryngoplasty.<sup>121</sup> A long-term rabbit model of VF paralysis would therefore be favorable for assessing potential for translation to the clinic as an intramuscular injectable VF biomaterial intended to support VF function and stimulate regeneration at a rate comparable to biodegradation.

Rabbits are frequently chosen for VF small animal models because of the relatively larger size of the rabbit larynx compared to mice or rats that allows stroboscopic exams for experimentally induced phonation.<sup>122</sup> In this rabbit model of VF injury, the glottal wave and swallowing function in live animals could be evaluated when the click dECM hydrogel is injected to the VF deep muscle or lamina propria. Mechanical testing, immune and neo-ECM marker analysis, and degradation

would be assessed using tissue explants following sacrifice. Evaluating the predictability of injection outcomes would begin in this stage and continue throughout the translation process. Before moving to the first stage of human trials, evaluation of the click dECM hydrogel in a canine model would also provide beneficial data, particularly in functional evaluation of the glottal wave.

As a longer-term goal, we propose to evaluate the applicability of the click dECM hydrogel for intramucosally injection into the VF lamina propria. Intramucosal injection of biomaterials has historically been hampered by failure to effectively remodel scar tissue and disruption of the glottal wave.<sup>72,88,123-125</sup> However, anti-fibrotic remodeling stimulated by dECM has previously been suggested for repair of scars in the VF lamina propria, with promising intramucosal results in rabbits.<sup>11,33</sup> In combination with novel technologies like sub-surface ablation that use laser surgery to remove the existing scar and create a space for localized hydrogel injection, we hypothesize that the click dECM hydrogel will restore glottal sufficiency with predictable injection volume and limit fibrosis in the VF lamina propria.<sup>126</sup> While we present this biomaterial in a cell-free context, delivery with encapsulated stem cells could produce an enhanced response consistent with the improved regenerative and immunomodulatory outcomes caused by SIS dECM with urinary stem cells.<sup>33</sup>

#### *6.4.3. Personalized Medicine: Stem Cell-derived dECM*

dECM from xenogeneic sources largely averts adverse immunogenic responses. However, the ideal source of dECM is the patient's own body. An emerging technology within the field of dECM biomaterials is the fabrication of cell-derived dECM, which may be obtained from culture of undifferentiated stem cells, or directly from differentiated cells such as fibroblasts.<sup>127-129</sup> These cells may be obtained directly from a patient and cultured with supplements like ascorbate or macromolecular crowding to stimulate ECM production in order to produce patient-specific ECM *in vitro*.<sup>127,129</sup> For instance, cell-derived ECM produced by fibroblasts from different donors has been used *in vitro* to identify differences in collagen III produced by healthy donors and patients with Ehlers Danlos syndrome, a group of connective tissue disorders.<sup>130</sup>

Another major advantage of cell-derived dECM is that it can be produced with greater consistency between batches and tuned to produce specific components.<sup>127</sup> Cells may be genetically engineered or stimulated to produce specific proteins. Upon decellularization, this dECM can be used in the

fabrication of dECM biomaterials and help to overcome challenges in scale up, particularly batch-to-batch variation.

However, cell-derived dECM is prone to poor mechanical properties and has been mostly used as coatings for synthetic materials to induce osteogenesis or chondrogenesis so far.<sup>127,128</sup> Nevertheless, cell-derived dECM may be used to produce hydrogels following the same methods as standard injectable dECM hydrogels.<sup>131</sup> In composite with soft materials such as collagen and fibrin, cell-derived dECM lowered the Young's modulus, but the cell-derived dECM and fibrin composite promoted angiogenesis over a fibrin hydrogel alone in a microfluidic model of angiogenesis.<sup>132</sup> We propose that this limitation can possibly be overcome when used in a click composite biomaterial as polymer composites like alginate offer greater opportunities for mechanical tunability, leading to the possibility of click dECM hydrogels for personalized medicine.

## Chapter 7. Conclusions

The motivation guiding this thesis was derived from the challenges in developing regenerative, long-term VF injectable biomaterials to provide long-term augmentation. To this end, this thesis focused on (1) the practicalities vs. regenerative functionality of dECM for scale up and (2) step-by-step development of a novel, VF-mimicking injectable click dECM-alginate hydrogel using tissue engineering strategies.

In this thesis, we conducted a comprehensive comparison of tissue-specific VF dECM with commercially available SIS dECM through proteomic analyses and functional ECM deposition assays. On a preliminary level, we determined that SIS dECM may present a viable, scalable alternative to VF dECM in the fabrication of injectable VF biomaterials. While continuing this comparison with further assays, we harnessed click chemistry to produce a hydrogel from dECM and alginate that consists of an ECM-like structure with supportive alginate linkages. These click dECM hydrogels match the mechanical properties of native human VF and possess improved stability over dECM-only hydrogels. We demonstrated that when cultured with encapsulated human VF fibroblasts, these click dECM hydrogels resist contraction and improve cellular viability. Additionally, click dECM hydrogels stimulate preferential vasculogenic tubule formation by encapsulated HUVECs. Finally, we show the biocompatibility of the novel click dECM hydrogel in subcutaneous rat tissue through the lessening of the initial acute immune response and integration of the hydrogel with surrounding tissue.

Overall, we demonstrate the potential equivalency of SIS dECM in the fabrication of click dECM hydrogels for injectable VF biomaterials and present a novel, biocompatible biomaterial with potential to overcome the poor stability and rapid degradation of existing injectable VF biomaterials. We proposed the choice of biomaterial to be based on both regenerative potential and scalability, developed an injectable hydrogel with a novel fabrication mechanism capable of mimicking ECM structure and tissue mechanics, and took the first steps toward translating a novel biomaterial toward clinical regenerative medicine.

The hydrogels developed in this thesis are a step on the path toward permanent voice restoration, and on a broader level, toward developing effective methodologies for producing injectable biomaterials for vocal fold tissue regeneration.

## References

- 1     Bhattacharyya, N. The prevalence of voice problems among adults in the United States. *The Laryngoscope* **124**, 2359-2362 (2014).
- 2     Kim, J.-S. *et al.* Effect of Occupational Noise Exposure on the Prevalence of Benign Vocal Fold Lesions: A Nationwide Population-Based Study. *Clin Exp Otorhinolaryngol* **16**, 87-94 (2023). <https://doi.org/10.21053/ceo.2022.01298>
- 3     Cohen, S. M., Kim, J., Roy, N., Asche, C. & Courey, M. Direct health care costs of laryngeal diseases and disorders. *The Laryngoscope* **122**, 1582-1588 (2012). <https://doi.org/https://doi.org/10.1002/lary.23189>
- 4     Tam, S. *et al.* Medialization thyroplasty versus injection laryngoplasty: a cost minimization analysis. *Journal of Otolaryngology - Head & Neck Surgery* **46**, 14 (2017). <https://doi.org/10.1186/s40463-017-0191-5>
- 5     Henriques, D. P., Martins, R. H. G. & Cataneo, A. J. M. Efficacy of Injectable Laryngoplasty With Hyaluronic Acid and/or Calcium Hydroxyapatite in the Treatment of Glottic Incompetence. Systematic Review and Meta-analysis. *Journal of Voice* (2023).
- 6     Mallur, P. S. & Rosen, C. A. Vocal fold Injection: Review of Indications, Techniques, and Materials for Augmentation. *Clinical experimental otorhinolaryngology* **3**, 177 (2010).
- 7     Chen, F. M. & Liu, X. Advancing biomaterials of human origin for tissue engineering. *Progress in Polymer Science* **53**, 86-168 (2016). <https://doi.org/10.1016/j.progpolymsci.2015.02.004>
- 8     Sadtlir, K. *et al.* Proteomic composition and immunomodulatory properties of urinary bladder matrix scaffolds in homeostasis and injury. *Seminars in Immunology* **29**, 14-23 (2017). <https://doi.org/https://doi.org/10.1016/j.smim.2017.05.002>
- 9     Beachley, V. *et al.* Extracellular matrix particle–glycosaminoglycan composite hydrogels for regenerative medicine applications. *Journal of Biomedical Materials Research Part A* **106**, 147-159 (2018).
- 10    Gibson, M. *et al.* Tissue extracellular matrix nanoparticle presentation in electrospun nanofibers. *Biomedical Research International* **2014**, 469120 (2014). <https://doi.org/10.1155/2014/469120>
- 11    Mora-Navarro, C. *et al.* Porcine Vocal Fold Lamina Propria-Derived Biomaterials Modulate TGF- $\beta$ 1-Mediated Fibroblast Activation in Vitro. *Acs Biomater Sci Eng* **6**, 1690-1703 (2020).
- 12    Coburn, P. T., Li, X., Li, J., Kishimoto, Y. & Li-Jessen, N. Y. Progress in Vocal Fold Regenerative Biomaterials: An Immunological Perspective. *Advanced NanoBiomed Research*, 2100119 (2021).
- 13    Branski, R. C., Verdolini, K., Sandulache, V., Rosen, C. A. & Hebda, P. A. Vocal Fold Wound Healing: A Review for Clinicians. *Journal of Voice* **20**, 432-442 (2006). <https://doi.org/https://doi.org/10.1016/j.jvoice.2005.08.005>
- 14    Chowdhury, C. (U.S. Food and Drug Administration, Center for Devices and Radiological Health, Maryland, 2020).
- 15    Cramer, M. C. & Badylak, S. F. Extracellular Matrix-Based Biomaterials and Their Influence Upon Cell Behavior. *Ann Biomed Eng* **48**, 2132-2153 (2020). <https://doi.org/10.1007/s10439-019-02408-9>
- 16    Wolf, M. T. *et al.* A hydrogel derived from decellularized dermal extracellular matrix. *Biomaterials* **33**, 7028-7038 (2012). <https://doi.org/10.1016/j.biomaterials.2012.06.051>

- 17 Xu, C. C. & Mau, T. A tissue-specific, injectable acellular gel for the treatment of chronic vocal fold scarring. *Acta Biomaterialia* (2019). <https://doi.org/10.1016/j.actbio.2019.08.025>
- 18 Wrona, E. A., Peng, R., Amin, M. R., Branski, R. C. & Freytes, D. O. Extracellular Matrix for Vocal Fold Lamina Propria Replacement: A Review. *Tissue Eng Part B Rev* **22**, 421-429 (2016). <https://doi.org/10.1089/ten.TEB.2016.0015>
- 19 Keane, T. J., Swinehart, I. T. & Badylak, S. F. Methods of Tissue Decellularization Used for Preparation of Biologic Scaffolds and In Vivo Relevance. *Methods* **84**, 25-34 (2015).
- 20 Miri, A. K. Mechanical Characterization of Vocal Fold Tissue: A Review Study. *Journal of Voice* **28**, 657-667 (2014). <https://doi.org/https://doi.org/10.1016/j.jvoice.2014.03.001>
- 21 Chhetri, D. K., Zhang, Z. & Neubauer, J. Measurement of Young's Modulus of Vocal Folds by Indentation. *Journal of Voice* **25**, 1-7 (2011). <https://doi.org/https://doi.org/10.1016/j.jvoice.2009.09.005>
- 22 Goodyer, E., Hemmerich, S., Muller, F., Kobler, J. B. & Hess, M. The shear modulus of the human vocal fold, preliminary results from 20 larynxes. *Eur Arch Otorhinolaryngol* **264**, 45-50 (2007). <https://doi.org/10.1007/s00405-006-0133-8>
- 23 Teller, S. S. *et al.* High-frequency viscoelastic shear properties of vocal fold tissues: implications for vocal fold tissue engineering. *Tissue Engineering Part A* **18**, 2008-2019 (2012).
- 24 Anseth, K. S. & Klok, H.-A. (ACS Publications, 2016).
- 25 Zhang, H. *et al.* Rapid Bioorthogonal Chemistry Turn-on through Enzymatic or Long Wavelength Photocatalytic Activation of Tetrazine Ligation. *J Am Chem Soc* **138**, 5978-5983 (2016). <https://doi.org/10.1021/jacs.6b02168>
- 26 Karver, M. R., Weissleder, R. & Hilderbrand, S. A. Synthesis and Evaluation of a Series of 1,2,4,5-Tetrazines for Bioorthogonal Conjugation. *Bioconjugate Chemistry* **22**, 2263-2270 (2011). <https://doi.org/10.1021/bc200295y>
- 27 Reyes Valenzuela, A. *et al.* Polymeric microspheres containing human vocal fold fibroblasts for vocal fold regeneration. *J The Laryngoscope* **131**, 1828-1834 (2021).
- 28 Deng, Y., Shavandi, A., Okoro, O. V. & Nie, L. Alginate modification via click chemistry for biomedical applications. *Carbohydrate Polymers* **270**, 118360 (2021). <https://doi.org/https://doi.org/10.1016/j.carbpol.2021.118360>
- 29 Zhang, J. *et al.* Influence of divalent cations on the biofouling behaviors of alginate hydrogels. **15**, 015003 (2019).
- 30 Oleksy, M., Dynarowicz, K. & Aebisher, D. Advances in Biodegradable Polymers and Biomaterials for Medical Applications—A Review. *Molecules* **28** (2023).
- 31 Lee, J. H. *et al.* Evaluation of the poly (lactic-co-glycolic acid)/pluronic F127 for injection laryngoplasty in rabbits. *Otolaryngology--Head and Neck Surgery* **151**, 830-835 (2014).
- 32 Pruett, L. J. *et al.* De novo tissue formation using custom microporous annealed particle hydrogel provides long-term vocal fold augmentation. *NPJ Regen Med* **8**, 10 (2023). <https://doi.org/10.1038/s41536-023-00281-8>
- 33 Hu, J.-J. *et al.* Scarless vocal fold regeneration by urine-derived stem cells and small intestinal submucosa hydrogel composites through enhancement of M2 macrophage Polarization, neovascularization and Re-epithelialization. *Smart Materials in Medicine* **3**, 339-351 (2022).
- 34 Walimbe, T., Calve, S., Panitch, A. & Sivasankar, M. P. Incorporation of types I and III collagen in tunable hyaluronan hydrogels for vocal fold tissue engineering. *Acta*



- 35 Pruet, L. *et al.* Development of a microporous annealed particle hydrogel for long-term vocal fold augmentation. *The Laryngoscope* **130**, 2432-2441 (2020).
- 36 Tindell, R. K. *et al.* Trilayered Hydrogel Scaffold for Vocal Fold Tissue Engineering. *Biomacromolecules* **23**, 4469-4480 (2022). <https://doi.org/10.1021/acs.biomac.1c01149>
- 37 Kwon, S. *et al.* In vivo vocal fold augmentation using an injectable polyethylene glycol hydrogel based on click chemistry. *Biomaterials Science* **9**, 108-115 (2021). <https://doi.org/10.1039/D0BM01155J>
- 38 Ravikrishnan, A., Zhang, H., Fox, J. M. & Jia, X. Core-Shell Microfibers via Bioorthogonal Layer-by-Layer Assembly. *ACS Macro Letters* **9**, 1369-1375 (2020). <https://doi.org/10.1021/acsmacrolett.0c00515>
- 39 Zou, X. *et al.* Modeling the Maturation of the Vocal Fold Lamina Propria Using a Bioorthogonally Tunable Hydrogel Platform. *Advanced Healthcare Materials* **n/a**, 2301701 (2023). <https://doi.org/10.1002/adhm.202301701>
- 40 Brown, M., Li, J., Moraes, C., Tabrizian, M. & Li-Jessen, N. Y. K. Decellularized extracellular matrix: New promising and challenging biomaterials for regenerative medicine. *Biomaterials* **289**, 121786 (2022).
- 41 Ungerleider, J. L., Dzieciatkowska, M., Hansen, K. C. & Christman, K. L. Tissue specific muscle extracellular matrix hydrogel improves skeletal muscle regeneration *in vivo* over non-matched tissue source. 2020.2006.2030.181164 (2020). <https://doi.org/10.1101/2020.06.30.181164> %J bioRxiv
- 42 Viswanath, A. *et al.* Extracellular matrix-derived hydrogels for dental stem cell delivery. *Biomedical Materials Research A* **105**, 319-328 (2017). <https://doi.org/10.1002/jbm.a.35901>
- 43 Zou, J. L. *et al.* Peripheral nerve-derived matrix hydrogel promotes Remyelination and inhibits synapse formation. *Advanced Functional Materials* **28**, 1705739 (2018).
- 44 Biehl, A. *et al.* Towards a standardized multi-tissue decellularization protocol for the derivation of extracellular matrix materials. *Biomater Sci-Uk* **11**, 641-654 (2023). <https://doi.org/10.1039/D2BM01012G>
- 45 Brown, M., Zhu, S., Taylor, L., Tabrizian, M. & Li-Jessen, N. Y. K. Unraveling the Relevance of Tissue-Specific Decellularized Extracellular Matrix Hydrogels for Vocal Fold Regenerative Biomaterials: A Comprehensive Proteomic and In Vitro Study. *Advanced NanoBiomed Research* **3**, 2200095 (2023). <https://doi.org/10.1002/anbr.202200095>
- 46 Wrona, E. A. *et al.* Derivation and characterization of porcine vocal fold extracellular matrix scaffold. *Laryngoscope* **126**, 928-935 (2016). <https://doi.org/10.1002/lary.25640>
- 47 Zhang, X. *et al.* Decellularized extracellular matrix scaffolds: Recent trends and emerging strategies in tissue engineering. *Bioactive Materials* **10**, 15-31 (2022). <https://doi.org/10.1016/j.bioactmat.2021.09.014>
- 48 Yam, G. H.-F. *et al.* Decellularization of human stromal refractive lenticles for corneal tissue engineering. *Scientific Reports* **6**, 26339 (2016). <https://doi.org/10.1038/srep26339>
- 49 Ferreira, S. A. *et al.* Neighboring cells override 3D hydrogel matrix cues to drive human MSC quiescence. *Biomaterials* **176**, 13-23 (2018). <https://doi.org/10.1016/j.biomaterials.2018.05.032>
- 50 Sawicki, L. A., Choe, L. H., Wiley, K. L., Lee, K. H. & Kloxin, A. M. Isolation and

- identification of proteins secreted by cells cultured within synthetic hydrogel-based matrices. *Acs Biomater Sci Eng* **4**, 836-845 (2018).
- 51 Karbiener, M. *et al.* Comparative proteomics of paired vocal fold and oral mucosa fibroblasts. *Journal of Proteomics* **155**, 11-21 (2017).  
<https://doi.org/https://doi.org/10.1016/j.jprot.2017.01.010>
- 52 Tarbit, E., Singh, I., Peart, J. N. & Rose'Meyer, R. B. Biomarkers for the identification of cardiac fibroblast and myofibroblast cells. *Heart failure reviews* **24**, 1-15 (2019).
- 53 Coburn, P. T., Herbay, A. C., Berrini, M. & Li-Jessen, N. Y. An in vitro assessment of the response of THP-1 macrophages to varying stiffness of a glycol-chitosan hydrogel for vocal fold tissue engineering applications. *Journal of Biomedical Materials Research Part A* **109**, 1337-1352 (2021).
- 54 Liu, L., Stokes, J. V., Tan, W. & Pruett, S. B. An optimized flow cytometry panel for classifying macrophage polarization. *J Immunol Methods* **511**, 113378 (2022).  
<https://doi.org/10.1016/j.jim.2022.113378>
- 55 Kosmac, K. *et al.* Immunohistochemical Identification of Human Skeletal Muscle Macrophages. *Bio Protoc* **8** (2018). <https://doi.org/10.21769/BioProtoc.2883>
- 56 Yu, T. *et al.* Enhanced activity of the macrophage M1/M2 phenotypes and phenotypic switch to M1 in periodontal infection. *Journal of periodontology* **87**, 1092-1102 (2016).
- 57 Wolf, M. T. *et al.* A biologic scaffold-associated type 2 immune microenvironment inhibits tumor formation and synergizes with checkpoint immunotherapy. *Science Translational Medicine* **11**, eaat7973 (2019). <https://doi.org/10.1126/scitranslmed.aat7973>
- 58 Misharin, A. V., Morales-Nebreda, L., Mutlu, G. M., Budinger, G. R. & Perlman, H. Flow cytometric analysis of macrophages and dendritic cell subsets in the mouse lung. *Am J Respir Cell Mol Biol* **49**, 503-510 (2013). <https://doi.org/10.1165/rcmb.2013-0086MA>
- 59 Girardeau-Hubert, S. *et al.* Impact of microstructure on cell behavior and tissue mechanics in collagen and dermal decellularized extra-cellular matrices. *Acta Biomaterialia* **143**, 100-114 (2022). <https://doi.org/https://doi.org/10.1016/j.actbio.2022.02.035>
- 60 Sasikumar, S., Chameettachal, S., Cromer, B., Pati, F. & Kingshott, P. Decellularized extracellular matrix hydrogels—cell behavior as a function of matrix stiffness. *Current Opinion in Biomedical Engineering* **10**, 123-133 (2019).  
<https://doi.org/https://doi.org/10.1016/j.cobme.2019.05.002>
- 61 Luizard, P. *et al.* Flow-induced oscillations of vocal-fold replicas with tuned extensibility and material properties. *Scientific Reports* **13**, 22658 (2023).  
<https://doi.org/10.1038/s41598-023-48080-x>
- 62 Song, J. *et al.* Matrix Adhesiveness Regulates Myofibroblast Differentiation from Vocal Fold Fibroblasts in a Bio-orthogonally Cross-linked Hydrogel. *ACS Applied Materials & Interfaces* **14**, 51669-51682 (2022). <https://doi.org/10.1021/acsami.2c13852>
- 63 Li, L. *et al.* Tissue Engineering-Based Therapeutic Strategies for Vocal Fold Repair and Regeneration. *Biomaterials* **108**, 91-110 (2016).  
<https://doi.org/10.1016/j.biomaterials.2016.08.054>
- 64 Latifi, N. *et al.* A Flow Perfusion Bioreactor System for Vocal Fold Tissue Engineering Applications. *Tissue Eng Part C Methods* **22**, 823-838 (2016).  
<https://doi.org/10.1089/ten.tec.2016.0053>
- 65 McKenzie, A. Glutaraldehyde: A review of its fixative effects on nucleic acids, proteins, lipids, and carbohydrates. (2019).
- 66 Moshnikova, A. B. *et al.* Cytotoxic activity of 1-ethyl-3-(3-dimethylaminopropyl)-

- carbodiimide is underlain by DNA interchain cross-linking. *Cellular and Molecular Life Sciences CMLS* **63**, 229-234 (2006). <https://doi.org/10.1007/s00018-005-5383-x>
- 67 Zhang, F. *et al.* Decellularized nerve extracellular matrix/chitosan crosslinked by genipin to prepare a moldable nerve repair material. *Cell Tissue Bank* **22**, 419-430 (2021). <https://doi.org/10.1007/s10561-020-09889-2>
- 68 Politi, S. *et al.* Smart ECM-Based Electrospun Biomaterials for Skeletal Muscle Regeneration. *Nanomaterials (Basel)* **10**, (2020). <https://doi.org/10.3390/nano10091781>
- 69 Chang, W.-D., Chen, S.-H., Tsai, M.-H. & Tsou, Y.-A. Autologous Fat Injection Laryngoplasty for Unilateral Vocal Fold Paralysis. *Journal of Clinical Medicine* **10** (2021).
- 70 Kharidia, K. M., Bensoussan, Y., Rosen, C. A., Johns III, M. M. & O'Dell, K. Variations in Practices and Preferences of Vocal Fold Injection Materials: A National Survey. *J The Laryngoscope* **133**, 1176-1183 (2023).
- 71 Nejati, S. & Mongeau, L. Injectable, pore-forming, self-healing, and adhesive hyaluronan hydrogels for soft tissue engineering applications. *Scientific Reports* **13**, 14303 (2023). <https://doi.org/10.1038/s41598-023-41468-9>
- 72 Hamdan, A. L., Yammine, Y., Hosri, J. & Mourad, M. Office-Based Cordotomy for the Release of Superficial Injection of Hyaluronic Acid: A Novel Approach. *OTO Open* **7**, e89 (2023). <https://doi.org/10.1002/oto2.89>
- 73 Lin, Y.-H., Wang, C.-T. J. A. o. O., Rhinology & Laryngology. Salvage Treatments for Poor Voice Outcomes Following Autologous Fat Injection Laryngoplasty. 00034894221140777 (2022).
- 74 Dong, L. *et al.* The effect of collagen hydrogels on chondrocyte behaviors through restricting the contraction of cell/hydrogel constructs. *Regenerative Biomaterials* **8**, rbab030 (2021). <https://doi.org/10.1093/rb/rbab030>
- 75 Lotz, C. *et al.* Cross-linked Collagen Hydrogel Matrix Resisting Contraction To Facilitate Full-Thickness Skin Equivalents. *ACS Applied Materials & Interfaces* **9**, 20417-20425 (2017). <https://doi.org/10.1021/acsami.7b04017>
- 76 Ng, W.-C. *et al.* In vitro evaluation of genipin-crosslinked gelatin hydrogels for vocal fold injection. *Scientific Reports* **13**, 5128 (2023). <https://doi.org/10.1038/s41598-023-32080-y>
- 77 Lueckgen, A. *et al.* Enzymatically-degradable alginate hydrogels promote cell spreading and in vivo tissue infiltration. *Biomaterials* **217**, 119294 (2019).
- 78 Wang, W. *et al.* Real-time and non-invasive fluorescence tracking of in vivo degradation of the thermosensitive PEGlyated polyester hydrogel. *Journal of Materials Chemistry B* **2**, 4185-4192 (2014).
- 79 Chan, R. W. Nonlinear viscoelastic characterization of human vocal fold tissues under large-amplitude oscillatory shear (LAOS). *Journal of Rheology* **62**, 695-712 (2018). <https://doi.org/10.1122/1.4996320>
- 80 Wong, J. H. M. *et al.* Injectable hybrid-crosslinked hydrogels as fatigue-resistant and shape-stable skin depots. *Biomacromolecules* **23**, 3698-3712 (2022).
- 81 Li, W. *et al.* Preparation, mechanical properties, fatigue and tribological behavior of double crosslinked high strength hydrogel. *Journal of the Mechanical Behavior of Biomedical Materials* **126**, 105009 (2022). <https://doi.org/https://doi.org/10.1016/j.jmbbm.2021.105009>
- 82 Miller, B., Hansrisuk, A., Highley, C. B. & Caliri, S. R. Guest–Host Supramolecular Assembly of Injectable Hydrogel Nanofibers for Cell Encapsulation. *ACS Biomaterials Science & Engineering* **7**, 4164-4174 (2021).

- <https://doi.org/10.1021/acsbiomaterials.1c00275>
- 83 Gracioso Martins, A. M., Biehl, A., Sze, D. & Freytes, D. O. Bioreactors for Vocal Fold Tissue Engineering. *Tissue Eng Part B Rev* **28**, 182-205 (2022).  
<https://doi.org/10.1089/ten.TEB.2020.0285>
  - 84 Latifi, N., Asgari, M., Vali, H. & Mongeau, L. A tissue-mimetic nano-fibrillar hybrid injectable hydrogel for potential soft tissue engineering applications. *Scientific reports* **8**, 1047 (2018).
  - 85 Titze, I. R., Palaparthi, A. & Mau, T. Vocal tradeoffs in anterior glottoplasty for voice feminization. *The Laryngoscope* **131**, 1081-1087 (2021).
  - 86 Heris, H. K., Latifi, N., Vali, H., Li, N. & Mongeau, L. Investigation of chitosan-glycol/glyoxal as an injectable biomaterial for vocal fold tissue engineering. *Procedia Engineering* **110**, 143-150 (2015).
  - 87 Biehl, A. *et al.* Scalable and High-Throughput In Vitro Vibratory Platform for Vocal Fold Tissue Engineering Applications. *Bioengineering* **10** (2023).
  - 88 Bouhabel, S. *et al.* Functional Analysis of Injectable Substance Treatment on Surgically Injured Rabbit Vocal Folds. *Journal of Voice* **37**, 829-839 (2023).  
<https://doi.org/https://doi.org/10.1016/j.jvoice.2021.06.001>
  - 89 Spang, M. T. & Christman, K. L. Extracellular matrix hydrogel therapies: In vivo applications and development. *Acta biomaterialia* **68**, 1-14 (2018).
  - 90 Hong, Y. *et al.* Mechanical properties and in vivo behavior of a biodegradable synthetic polymer microfiber–extracellular matrix hydrogel biohybrid scaffold. *Biomaterials* **32**, 3387-3394 (2011).
  - 91 Thorpe, A. A. *et al.* Thermally triggered hydrogel injection into bovine intervertebral disc tissue explants induces differentiation of mesenchymal stem cells and restores mechanical function. *Acta Biomaterialia* **54**, 212-226 (2017).  
<https://doi.org/https://doi.org/10.1016/j.actbio.2017.03.010>
  - 92 Crosby, C. O. & Zoldan, J. Mimicking the physical cues of the ECM in angiogenic biomaterials. *Regenerative Biomaterials* **6**, 61-73 (2019).  
<https://doi.org/10.1093/rb/rbz003>
  - 93 Wang, W. *et al.* Preparation and Characterization of Pro-Angiogenic Gel Derived from Small Intestinal Submucosa. *Acta Biomaterialia* **29**, 135-148 (2016).  
<https://doi.org/10.1016/j.actbio.2015.10.013>
  - 94 Magno, V. *et al.* Macromolecular crowding for tailoring tissue-derived fibrillated matrices. *Acta Biomaterialia* **55**, 109-119 (2017). <https://doi.org/10.1016/j.actbio.2017.04.018>
  - 95 Agarwal, T., Narayan, R., Maji, S., Ghosh, S. K. & Maiti, T. K. Decellularized caprine liver extracellular matrix as a 2D substrate coating and 3D hydrogel platform for vascularized liver tissue engineering. *Journal of tissue engineering and regenerative medicine* **12**, e1678-e1690 (2018).
  - 96 Ullah, I. *et al.* VEGF-supplemented extracellular matrix is sufficient to induce endothelial differentiation of human iPSC. *Biomaterials* **216**, 119283 (2019).
  - 97 Li, R. *et al.* Facilitate angiogenesis and neurogenesis by growth factors integrated decellularized matrix hydrogel. *Tissue Eng Pt A* **27**, 771-787 (2021).
  - 98 Becker, M. *et al.* Towards a Novel Patch Material for Cardiac Applications: Tissue-Specific Extracellular Matrix Introduces Essential Key Features to Decellularized Amniotic Membrane. *International Journal of Molecular Science* **19**, 1032 (2018).  
<https://doi.org/10.3390/ijms19041032>



- 99 Keane, T. J. *et al.* Restoring Mucosal Barrier Function and Modifying Macrophage Phenotype with an Extracellular Matrix Hydrogel: Potential Therapy for Ulcerative Colitis. *Journal of Crohns and Colitis* **11**, 360-368 (2017). <https://doi.org/10.1093/ecco-jcc/jjw149>
- 100 DeStefano, S. *et al.* Conserved and tissue-specific immune responses to biologic scaffold implantation. *bioRxiv : the preprint server for biology* (2023). <https://doi.org/10.1101/2023.08.15.553390>
- 101 Estrellas, K. M. *et al.* Biological scaffold-mediated delivery of myostatin inhibitor promotes a regenerative immune response in an animal model of Duchenne muscular dystrophy. *Journal of Biological Chemistry* **293**, 15594-15605 (2018).
- 102 Nie, R. *et al.* EGCG modified small intestine submucosa promotes wound healing through immunomodulation. *Composites Part B: Engineering*, 111005 (2023). <https://doi.org/https://doi.org/10.1016/j.compositesb.2023.111005>
- 103 Moore, E. M. *et al.* Biomaterials direct functional B cell response in a material-specific manner. *Science Advances* **7**, eabj5830 <https://doi.org/10.1126/sciadv.abj5830>
- 104 Dziki, J. L. *et al.* Solubilized extracellular matrix bioscaffolds derived from diverse source tissues differentially influence macrophage phenotype. *J Biomed Mater Res A* **105**, 138-147 (2017). <https://doi.org/10.1002/jbm.a.35894>
- 105 Zou, C.-Y. *et al.* A self-fused hydrogel for the treatment of glottic insufficiency through outstanding durability, extracellular matrix-inducing bioactivity and function preservation. *Bioactive Materials* **24**, 54-68 (2023). <https://doi.org/https://doi.org/10.1016/j.bioactmat.2022.12.006>
- 106 Nellinger, S., Rapp, M. A., Southan, A., Wittmann, V. & Kluger, P. J. An Advanced ‘clickECM’ That Can be Modified by the Inverse-Electron-Demand Diels-Alder Reaction. *ChemBioChem* **23**, e202100266 (2022). <https://doi.org/https://doi.org/10.1002/cbic.202100266>
- 107 Späte, A. K. *et al.* Exploring the Potential of Norbornene-Modified Mannosamine Derivatives for Metabolic Glycoengineering. *Chembiochem* **17**, 1374-1383 (2016). <https://doi.org/10.1002/cbic.201600197>
- 108 Desai, R. M., Koshy, S. T., Hilderbrand, S. A., Mooney, D. J. & Joshi, N. S. Versatile click alginate hydrogels crosslinked via tetrazine–norbornene chemistry. *Biomaterials* **50**, 30-37 (2015). <https://doi.org/https://doi.org/10.1016/j.biomaterials.2015.01.048>
- 109 Chen, Y.-W. *et al.* 3D-biofabricated chondrocyte-laden decellularized extracellular matrix-contained gelatin methacrylate auxetic scaffolds under cyclic tensile stimulation for cartilage regeneration. *Biofabrication* **15**, 045007 (2023).
- 110 Jin, X., Wei, C., Wu, C. & Zhang, W. Gastric fluid-induced double network hydrogel with high swelling ratio and long-term mechanical stability. *Composites Part B: Engineering* **236**, 109816 (2022). <https://doi.org/https://doi.org/10.1016/j.compositesb.2022.109816>
- 111 Lueckgen, A. *et al.* Dual alginate crosslinking for local patterning of biophysical and biochemical properties. *Acta Biomaterialia* **115**, 185-196 (2020).
- 112 George, O. J. *et al.* Tunable synthesis of hydrogel microfibers via interfacial tetrazine ligation. *Biomacromolecules* **23**, 3017-3030 (2022).
- 113 Distler, T. *et al.* Ionically and enzymatically dual cross-linked oxidized alginate gelatin hydrogels with tunable stiffness and degradation behavior for tissue engineering. *ACS Biomaterials Science & Engineering* **6**, 3899-3914 (2020).
- 114 Mushtaq, A., Li, L., A, A. & Grøndahl, L. Characterisation of products from EDC-mediated PEG substitution of chitosan allows optimisation of reaction conditions.

- International Journal of Biological Macromolecules* **221**, 204-211 (2022).  
<https://doi.org/https://doi.org/10.1016/j.ijbiomac.2022.08.179>
- 115 Ingber, D. E. J. A. S. Is it time for reviewer 3 to request human organ chip experiments  
 instead of animal validation studies? *7*, 2002030 (2020).
- 116 van Duinen, V. *et al.* 96 perfusable blood vessels to study vascular permeability in vitro.  
*Scientific Reports* **7**, 18071 (2017). <https://doi.org/10.1038/s41598-017-14716-y>
- 117 van Duinen, V. *et al.* Perfused 3D angiogenic sprouting. **22**, 77 (2019).
- 118 Aubry, G., Lee, H. J. & Lu, H. Advances in Microfluidics: Technical Innovations and  
 Applications in Diagnostics and Therapeutics. *Analytical Chemistry* **95**, 444-467 (2023).  
<https://doi.org/10.1021/acs.analchem.2c04562>
- 119 Preetam, S. *et al.* Emergence of microfluidics for next generation biomedical devices.  
*Biosensors and Bioelectronics: X* **10**, 100106 (2022).  
<https://doi.org/https://doi.org/10.1016/j.biosx.2022.100106>
- 120 Gao, W. Z. *et al.* Prospective> 12 Months Outcomes After Vocal Fold Injection  
 Medialization With Silk Microparticle-Hyaluronic Acid Material. *The Laryngoscope* **134**,  
 3679-3685 (2024).
- 121 Darweesh, M. E., El-Gazzar, A. F., Sarag, S. M. & Sheikhany, A.-A. R. Outcomes versus  
 complications in patients undergoing different modalities of injection laryngoplasty. *The  
 Egyptian Journal of Otolaryngology* **37**, 1-10 (2021).
- 122 Kolosova, K. *et al.* Characterizing Vocal Fold Injury Recovery in a Rabbit Model With  
 Three-Dimensional Virtual Histology. *The Laryngoscope* **131**, 1578-1587 (2021).  
<https://doi.org/https://doi.org/10.1002/lary.29028>
- 123 Nozawa, M. *et al.* Intracordal injection therapy for vocal fold scarring: Steroid versus basic  
 fibroblast growth factor. *Laryngoscope Investig Otolaryngol* **7**, 1465-1473 (2022).  
<https://doi.org/10.1002/lio2.881>
- 124 Jamal, N., Mundi, J. & Chhetri, D. K. Higher risk of superficial injection during injection  
 laryngoplasty in women. *American Journal of Otolaryngology* **35**, 159-163 (2014).  
<https://doi.org/https://doi.org/10.1016/j.amjoto.2013.09.002>
- 125 Tamura, E., Fukuda, H. & Tabata, Y. Intracordal injection technique: materials and  
 injection site. *Tokai J Exp Clin Med* **33**, 119-123 (2008).
- 126 Andrus, L. *et al.* Ultrafast laser surgery probe for sub-surface ablation to enable biomaterial  
 injection in vocal folds. *Scientific Reports* **12**, 20554 (2022).  
<https://doi.org/10.1038/s41598-022-24446-5>
- 127 Chan, W. W. *et al.* Towards Biomanufacturing of Cell-Derived Matrices. *International  
 Journal of Molecular Sciences* **22** (2021).
- 128 Guan, Y. *et al.* Cell-derived extracellular matrix materials for tissue engineering. *Tissue  
 Engineering Part B: Reviews* **28**, 1007-1021 (2022).
- 129 Assunção, M. *et al.* Cell-Derived Extracellular Matrix for Tissue Engineering and  
 Regenerative Medicine. *Frontiers in Bioengineering and Biotechnology* **8** (2020).  
<https://doi.org/10.3389/fbioe.2020.602009>
- 130 Doherty, E. L. *et al.* Patient-derived extracellular matrix demonstrates role of COL3A1 in  
 blood vessel mechanics. *Acta Biomaterialia* **166**, 346-359 (2023).  
<https://doi.org/https://doi.org/10.1016/j.actbio.2023.05.015>
- 131 Antich, C. *et al.* Development of a Biomimetic Hydrogel Based on Predifferentiated  
 Mesenchymal Stem-Cell-Derived ECM for Cartilage Tissue Engineering. *Adv Healthc  
 Mater* **10**, e2001847 (2021). <https://doi.org/10.1002/adhm.202001847>

- 132 Doherty, E. L. *et al.* Human Cell-derived Matrix Composite Hydrogels with Diverse Composition for Use in Vasculature-on-chip Models. *Advanced Healthcare Materials*, 2400192 (2024).